Molecular and Life Sciences

Fantastic Leaves and What's Inside Them: Chemistry and Biochemical Imaging of Natural Products in Western Australian Plants

Aswin Rajagopalan
0000-0002-2660-9987

This thesis is presented for the Degree of
Doctor of Philosophy
of
Curtin University

November 2021

Declaration

To the best of my knowledge and belief this thesis contains no material previously published by any other person except where due acknowledgement has been made. This thesis contains no material which has been accepted for the award of any other degree or diploma in any other university.

Signature: [redacted]

Date: 05/11/2021

Abstract

Plant secondary metabolites, commonly known as natural products, are ubiquitous and used in a wide variety of fields and industries, ranging from pharmaceuticals and cosmetics to agriculture. For plants in particular, the distribution of natural products has largely been localised to broad anatomical regions such as the leaves, stem, roots, bark and seeds. However, there is a scarcity of literature exploring the cellular or subcellular distribution of natural products, and the insights that may result. The spatial distribution of natural products have the potential to be spectroscopically mapped using vibrational spectroscopic methods, including FTIR and confocal Raman microscopy.

Western Australia is home to an incredible biodiversity of plant life, including a variety of plants in the Goodeniaceae and Sapindaceae families. The natural product composition of a variety of plants, including *Scaevola aemula*, *Scaevola albida*, Scaevola *striata*, *Scaevola caliptera*, *Scaevola nitida* and *Goodenia varia*, all of which were cultivated in Perth, Western Australia were investigated. Ursolic acid **110** was isolated from *Scaevola* and *Goodenia* species. A novel glycoside, α-bisabolol β-$_D$-ribofuranose **111**, was isolated from *Scaevola nitida*. Six beyerenes, four of which were novel, were isolated from *G. varia*.

The natural product composition of *Scaevola crassifolia* Labill. collected from its native environment in Port Beach, North Fremantle, Western Australia was investigated for comparison to the *S. crassifolia* collected from Curtin University in Perth, Western Australia. The natural product composition was very similar, with the addition of 12-hydroxycaryophyllene **60** and flavone **141**. However, 4-dihydroxy-α-bisabolol-2,10-diene **137** was not isolated from the leaf resin of the Port Beach sample.

The biosynthesis of the natural product birkenal **142** was explored using organic synthesis and spectroscopy. A mechanism for the formation of birkenal **142**, caryolan-1,3,4-triol **152** and 5,6-dihydroxycaryophyll-3,8-diene **154** from 6-hydroxycaryophyllene **1** was successfully developed (Figure 1). Longitudinal NMR and FTIR spectroscopic studies revealed that the formation of birkenal **142** and other aldehydes from 6-hydroxycaryophyllene **1** required an acidic environment. The auto-oxidation of compounds in the neutrals fraction of *S. crassifolia* leaf resin was found to be inhibited by the presence of phenolic compounds in the resin.

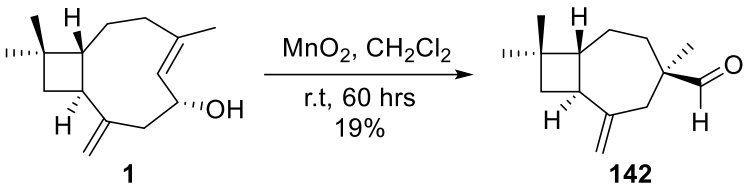

Figure 1. *Synthesis of birkenal* ***142*** *from 6-hydroxycaryophyllene* ***1*****.**

The abiotic factors influencing the cyclisation of chalcone **157** to form 8-prenylflavanone **138** and 6-prenylflavanone **139** in a 5:4 ratio was investigated synthetically and spectroscopically (Figure 2). The formation of 6-prenylflavanone **139** was favoured in the presence of a sterically bulky base, but cyclisation by photocatalysis led to polymerisation of chalcone **157**. Therefore, the formation of 8-prenylflavanone **138** and 6-prenylflavanone **139** in a 4:5 ratio was attributed to a natural bias in the enzymatic reaction.

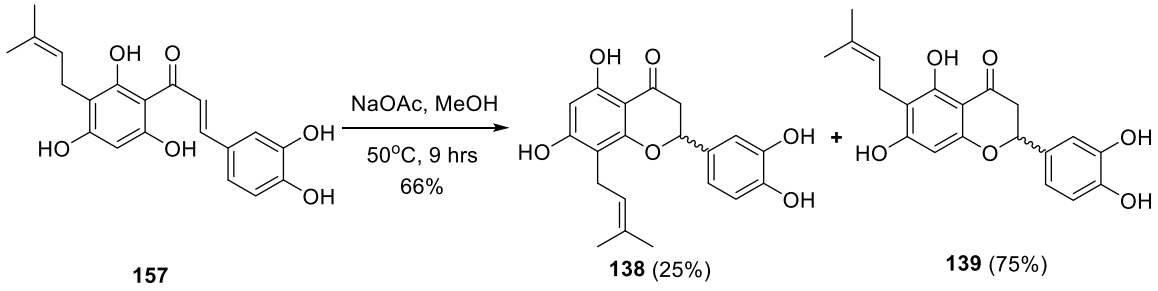

Figure 2. *Cyclisation of chalcone* ***157*** *into flavanones* ***138*** *and* ***139*** *using NaOAc.*

6-Hydroxycaryophyllenes are readily available from the leaf resin of *S. crassifolia* and the chemistry has been largely unexplored. The chemistry and reactivity of 6-hydroxycaryophyllenes was investigated. A variety of reactions were explored, including polyhydroxylation of the alkenes to synthesise amphipathic compounds, cationic rearrangements, functionalisation and oxidation of the allylic hydroxyl group and endocyclic alkene, and exploring the Diels-Alder chemistry of the endocyclic alkene (Figure 3).

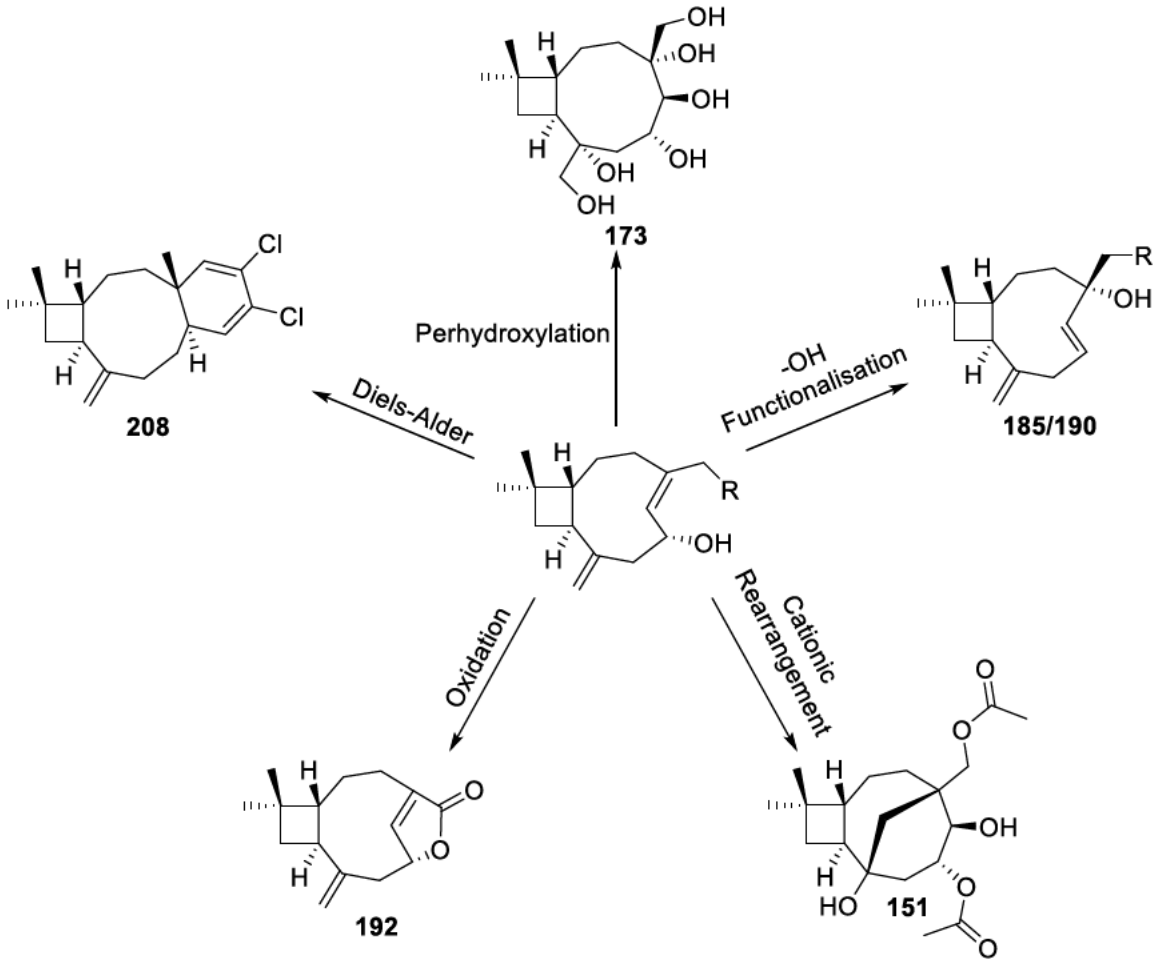

Figure 3. *Functionalisation and transformations of 6-hydroxycaryophyllenes.*

The strained alkene of caryophyllenes was a suitable chromophore for vibrational spectroscopic mapping. The distribution of caryophyllenes in the leaf resin of *S. crassifolia* could be mapped as a cross-section of the leaf using confocal Raman microscopy (Figure 4). The distribution of caryophyllenes was unable to be mapped in the plant cells, but the distribution of phenylalanine and fatty acids/lipids was spectroscopically imaged (Figure 4). A protocol was successfully developed to map the distribution of ligno-cellulose, phenylalanine and fatty acids/lipids using 3D Raman microscopy. The distribution of protein storage vacuoles in the leaf tissue was imaged using the infrared microscopy beamline at the Australian synchrotron (Figure 4).

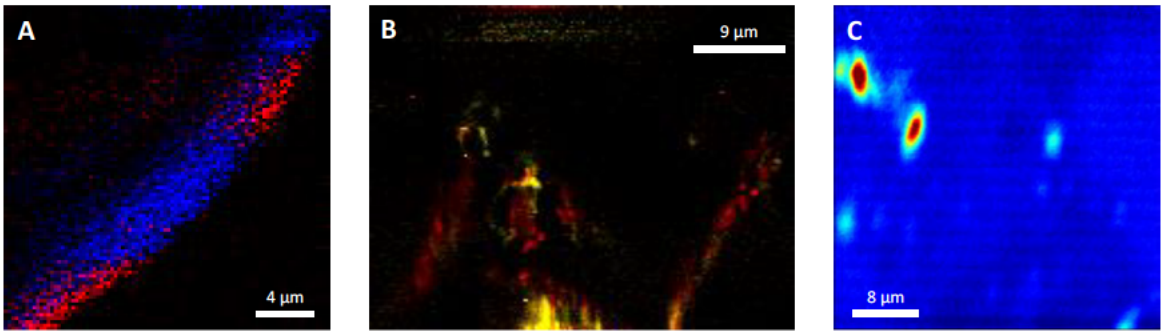

Figure 4. *Vibrational spectroscopy images (A-C). (A) Raman image of strained alkenes (red) and phenols (blue) in* S. crassifolia *leaf resin, (B) Raman image of phenylalanine (red) and fatty acids/lipids in* S. crassifolia *leaf cell, and (C) FTIR image of amine N-H stretching (3500-3600 cm^{-1}) in* S. crassifolia *leaf cell.*

Acknowledgements

I would like to start by thanking my primary supervisor, Dr Alan Payne. Thank you for sharing your knowledge and experience, encouraging me and providing generous feedback over the last several years. Also thank you for the tolerating my immediate office visits after sending you an email just to ensure that you were aware that I had sent it.

Thank you to my co-supervisor, Dr Mark Hackett. Thank you for taking me on as your student after coming from a humble synthetic organic chemistry background. Thank you for taking the time to help teach me and help me to develop my skills as a biospectroscopist and providing me with extensive feedback and guidance over these last few years. Finally, thank you for appreciating my plant puns and consistently having a positive attitude that made it a pleasure to be your student.

Thank you to everyone in Organic and Medicinal Research Group (OMG) and the Applied Biospectroscopy and Anaytical Chemistry using Synchrotron Science Group (ABACUSS) both past and present for all of the learning, feedback, food and laughter over the years. I would also like to acknowledge Associate Professor Mauro Mocerino and Dr Hendra Gunosewoyo for all of their help and support as well.

Thank you to Dr Ching Goh for his assistance with the NMR and promptly fixing the NMR after I repeatedly mess up the software. Thank you to Peter Chapman for assistance with the spectroscopic instrumentation and numerous times I've needed IT support over the years. Thank you to Dr Thomas Becker for his extensive assistance with the confocal Raman microscope and forgiving me whenever I smudged the objective lenses. Thank you to Dr Frankie Busetti of the ECU Science Analytical Facility for conducting the HRMS analysis.

Thank you to my dear friends. It's been a long road up to this point and your unconditional love and support has gotten me through. Thank you for the nonsensical conversations and arguments, memes, food, laughter and everything really. Words fail to describe how much you all mean to me and the impact that you have had on me, but know that I appreciate all of you.

Finally, to my family. To my mum and dad. Thank you for all of your unconditional love and support over the years as I continued my career as the perennial student. Thank you for taking care of me and nurturing me all these years to make me the person that I am today.

Thank you to my brother Eeshwar for your infinite support, a sympathetic ear and meaningful advice not just during my PhD, but my whole life. It is thanks to all of you that I have made it this far.

This research was supported by the Rowe Scientific HDR Top Up Scholarship and the Australian Government Research Training Program Scholarship.

Contents

List of Abbreviations

Ac	Acetyl
app	Apparent
ara	Arabinose
ATR-FTIR	Attenuated total reflection-Fourier transform infrared spectroscopy
BAIB	Bis(acetoxy)iodobenzene
BHT	2,6-di-*tert*-butyl-4-methylphenol
Bn	Benzyl
BPO	Benzoyl peroxide
br	Broad
Bz	Benzoyl
c	Concentration in g/mL
$CDCl_3$	Deuterated chloroform
CD_3CN	Deuterated acetonitrile
CHI	Chalcone isomerase
COSY	Homonuclear correlation spectroscopy
CSA	10-camphorsulfonic acid
d	Doublet
dd	Doublet of doublets
ddd	Doublet of doublet of doublets
dddd	Doublet of doublet of doublet of doublets
dquint	Doublet of quintets
dtd	Doublet of triplet of doublets
DEPT	Distortionless enhancement by polarisation transfer
DMAP	4-(*N*,*N*-Dimethylaminopyridine)
DMF	*N*,*N*-Dimethylformamide
DMS	Dimethylsulfide
DMSO	Dimethylsulfoxide
DTBMP	2,6-Di-*tert*-butyl-4-methylpyridine
Et	Ethyl
Glu/Glc	Glucose
HOD	Monodeuterated water (H_2O)
HMBC	Heteronuclear multiple bond correlation spectroscopy

HRMS	High resolution mass spectrometry
HSQC	Heteronuclear single quantum coherence/correlation spectroscopy
J	Coupling constant
LDA	Lithium *N*,*N*-diisopropylamide
m	Multiplet
$[M]^+$	Molecular ion
$[M+H]^+$	Protonated molecular ion
$[M+Na]^+$	Sodium adduct of molecular ion
m/z	Mass to charge ratio
m-CPBA	*Meta*-chloroperoxybenzoic acid
Me	Methyl
MOM	Methoxymethyl ether
NADI	Napthol and diamine
NBS	*N*-Bromosuccinimide
NMR	Nuclear magnetic resonance spectroscopy
NOESY	Nuclear Overhauser effect spectroscopy
[O]	Oxidation
OAc	Acetate
OCT	Optimum cutting temperature medium
OPP	Pyrophosphate
OTf	Triflate/Trifluoromethanesulfonate
Ph	Phenyl
Pr	Propyl
PS	Petroleum spirits 40-60ºC
Pyr	Pyridine
q	Quartet
quint	Quintet
Rha	Rhamnose
rib	Ribose
r.t	Room temperature
Rut	Rutinose
s	Singlet
SEMO	Trimethylsilylethoxymethyl

ssp.	Subspecies
t	Triplet
TBAI	Tetrabutylammonium iodide
t-Bu	*Tert*-Butyl
TCNE	Tetracyanoethylene
td	Triplet of doublets
TEMPO	(2,2,6,6-Tetramethylpiperidin-1-yl)oxyl
TES	Triethylsilyl ether
TFA	Trifluoroacetic acid
TFAA	Trifluoroacetic anhydride
THC	Tetrahydrocannabinol
THF	Tetrahydrofuran
TLC	Thin layer chromatography
tquint	Triplet of quintets
Ts	Tosyl/*para*-Toluenesulfonyl
UV-Vis	Ultraviolet-visible spectroscopy
δ	Chemical shift (ppm)
ν	Frequency
$[\alpha]_D^T$	Specific rotation

Chapter 1
Introduction

1.0 Introduction

Plants in the Goodeniaceae family, including *Scaevola* species, have been reported to possess a rich variety of natural products including terpenoids and flavonoids. *Scaevola crassifolia* Labill., commonly known as the thick-leaved fanflower, is a shrub native to Western Australia that is found along coastal sand dunes, plains and limestone cliffs (Figure 1.1). The leaves of the plant are covered in a thick, sticky resin. The natural product composition of the leaf resin was investigated during my Honours research project. Several compounds were isolated and identified in the resin, including 6-hydroxycaryophyllene **1**, 12-acetoxy-6-hydroxycaryophyllene **2** and 6,12-dihydroxycaryophyllene **3** (Figure 1.1). The preliminary investigation into the natural products composition found in *S. crassifolia* and exploration of the chemistry of the isolated compounds raised other research questions that warranted further investigation, such as:

- Do other plants in the Goodeniaceae family possess uncommon natural products?
- Can the spatial distribution of natural products such as caryophyllenes be mapped?
- Can organic synthesis and spectroscopy be used to improve our understanding of natural products biosynthesis and formation mechanisms?
- What chemistry do these molecules undergo?

These research questions ultimately served as the foundation of this PhD study.

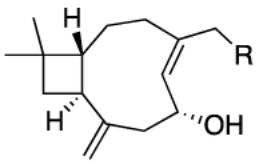

1 R = H
2 R = OAc
3 R = OH

Figure 1.1. S. crassifolia *and its natural products*

1.1 Plants growing in Western Australia

Australian plants are unique in the world due to the geographic isolation and harshness of the environment in which they inhabit. As of 2009, more than 21,000 species of plants have been described in Australia, of which more than 19,000 species are vascular plants alone.[1] Australian plants have been reported to possess an abundance of natural products and multiple studies have been conducted.[2] However, plants have been collected primarily from tropical regions in Australia, while arid and semi-arid regions compose 70% of mainland Australia have been neglected (Figure 1.2).[2] Plants that grow in these arid regions are exposed to different environmental stressors, such as low rainfall and high UV exposure, so novel natural products may be produced by these plants as a result. Western Australia is largely composed of arid and semi-arid regions and a number of native plant species have been shown to possess a heavy coating of leaf resin (Figure 1.2). The leaf resins have been shown to be abundant sources of polycyclic natural products and these compounds are believed to possess antifeedant or other protective properties.[3]

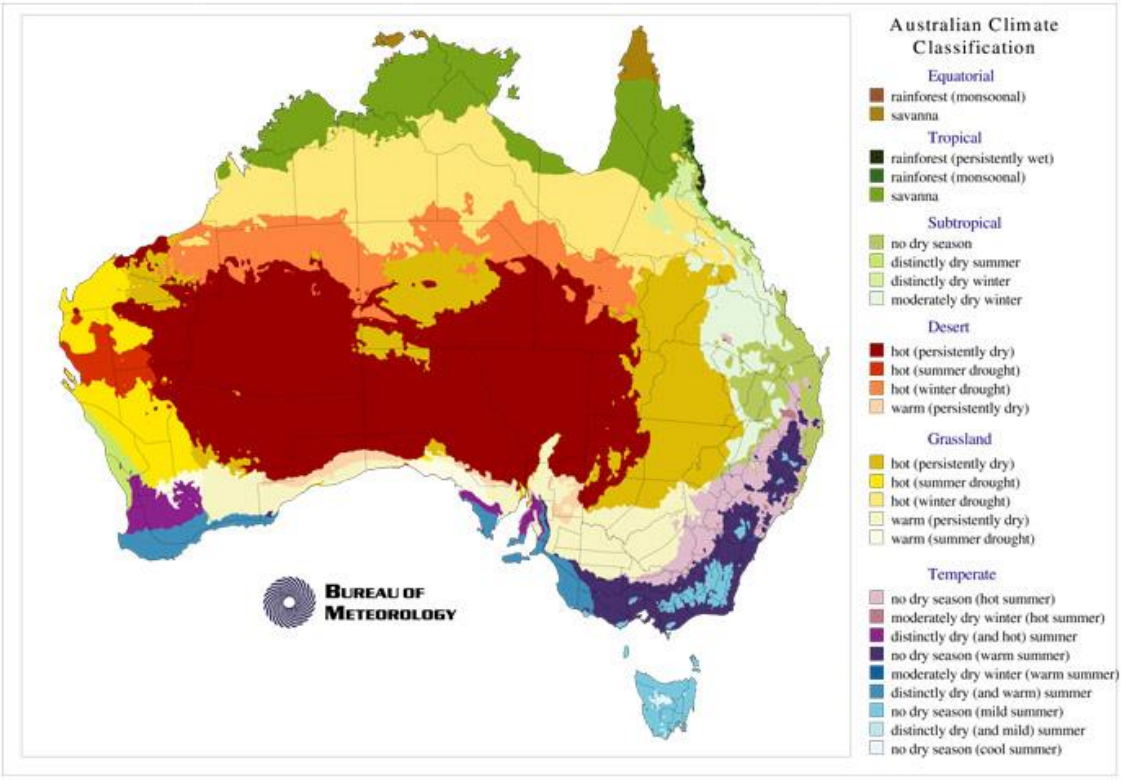

Figure 1.2. *Climate map of Australia created by the Bureau of Meteorology.*

Plants in the Goodeniaceae family have been reported to possess a number of novel natural products.[4] There are approximately 400 species of plants in the Goodeniaceae family, of

which 380 are found in Australia, with a majority being found in Western Australia.[4a, 5] There are 11 genera that have been reported in the Goodeniaceae family: *Anthotium*, *Coopernookia*, *Dampiera*, *Diaspasis*, *Goodenia*, *Lechenaultia*, *Pentapilon*, *Scaevola*, *Selleria*, *Velleia* and *Verreauxia*.[4a] The majority of these genera occur almost exclusively in Australia. However, plants in the *Scaevola* genus have been found outside of Australia in regions such as the tropical Americas, Africa and the Pacific Islands. Approximately, 40 out of 130 species in this genus have been found outside of Australia.[6] Species found in the *Scaevola* genus include *Scaevola crassifolia*, *Scaevola calliptera*, *Scaevola striata*, *Scaevola aemula*, *Scaevola albita*, and *Scaevola nitida*.

1.2 Natural products found in Goodeniaceae species

Plants in the Goodeniaceae family have been used for medicinal purposes by indigenous Australians. The extract of the leaves and twigs of *Goodenia ovata* have been reported to possess antidiabetic properties.[7] *Goodenia scaevolina* was used to relieve coughs by chewing the roots, which would release the juices that acted as treatment.[7] *Scaevola spiniscens* has been used for the treatment of several ailments. Stomach aches and urinary issues were treated by consuming a decoction of the roots. Boils, sores and rashes were treated with a decoction of the stems. Colds were treated by inhaling the fumes generated after burning the entire plant.[7]

The medicinal properties of plants are generally associated with the natural products. Natural products reported in Goodeniaceae species, and in particular in the *Scaevola* genus, include coumarins, fatty acids, flavonoids, glycosides and terpenoids (Figure 1.3).[4a] However, it is worth noting that research into the natural products found in Goodeniaceae plants in Western Australia is severely limited, and especially so with *Scaevola* species.

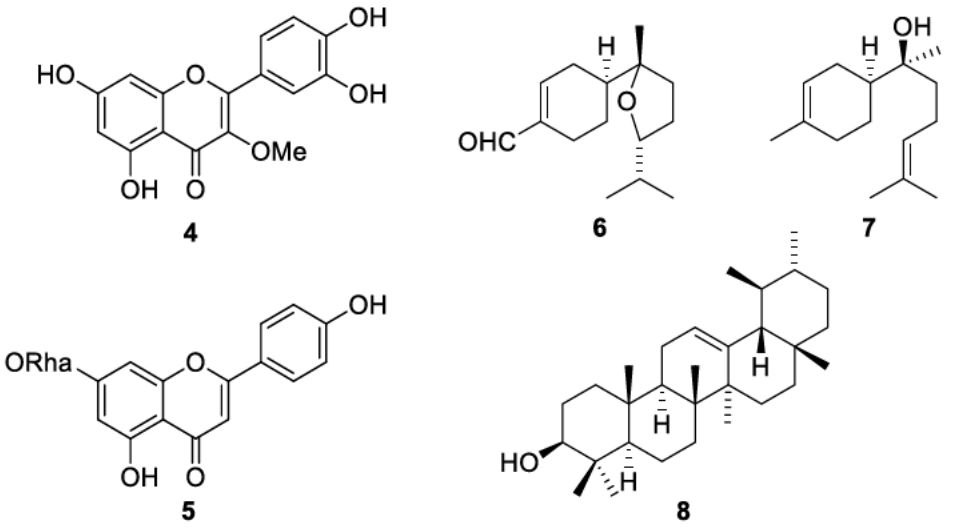

Figure 1.3. *Flavanol **4**, flavone **5**, and terpenoid (**6-8**) compounds isolated from Goodeniaceae species.*

Terpenes belong to a class of natural product where the compounds are composed of isoprene units, which are polyunsaturated 5-carbon compounds. Terpenoids refer to terpenes that contain an additional functional group, which is typically oxygen containing, and are also commonly referred to as isoprenoids. There are more than 30,000 known terpenes and terpenoids, which consists of 60% of known natural products. Terpenes and terpenoids play important roles in organisms, including antifeedant properties, disease resistance and attraction of pollinators.[8] Tepernoids have been used for the development of a number of medicines, including anti-inflammatory, antibacterial and anticancer drugs. For example, formestane **9** is an aromatse inhibitor used for the treatment of postmenopausal women with breast cancer, that can be synthesised from testosterone (Figure 1.4).[9] Another example is (-)-laulimalide **10**, which was first isolated from *Spongia mycofijiensis* by Chatgilialoglu *et al.* and is similarly used as an anticancer agent (Figure 1.4).[10]

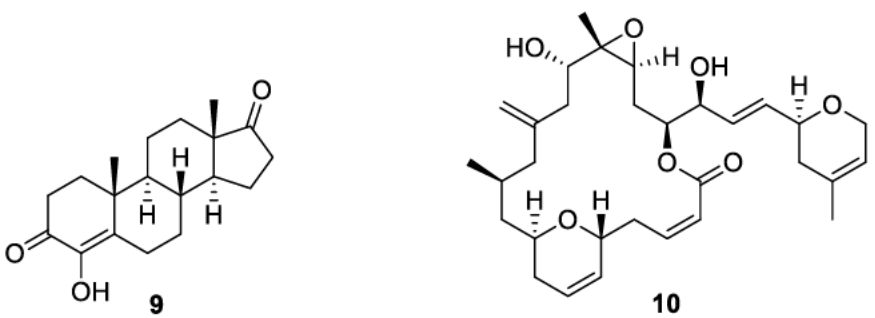

Figure 1.4. *Structures of formestane **9** and (-)-laulimalide **10**.*

Biosynthesis of terpenoids starts with the production of the precursor compounds isopentenyl pyrophosphate (IPP) and its allylic isomer, dimethylallyl pyrophosphate (DMAPP) (Scheme 1.1).[11] IPP and DMAPP are biosynthesised via the mevalonate or non-mevalonate pathways. The mevalonate pathway occurs in the cytoplasm, while the non-mevalonate pathway occurs in the plastid. Sesquiterpenes, polyprenols, squalene and triterpenes are synthesised via the mevalonate pathway, while monoterpenes, diterpenes, gibberellins, carotenoids and chlorophyll are synthesised via the non-mevalonate pathway. In both pathways, after the formation of IPP and DMAPP, geranyl pyrophosphate (GPP) is synthesised via the condensation of IPP and DMAPP via geranyl pyrophosphate synthase (GPPS) (Scheme 1.1). In the mevalonate pathway, GPP can be further reacted with IPP via a condensation reaction facilitated by farnesyl pyrophosphate synthase (FPPS) to afford farnesyl pyrophosphate (FPP). FPP is the precursor to a variety of compounds including sesquiterpenes, triterpenes, polyprenols, and squalene. In the non-mevalonate pathway, GPP can undergo further reactions to afford a variety of monoterpenoids or undergo a condensation reaction with another unit of GPP facilitated by geranylgeranyl pyrophosphate synthase (GGPPS) to afford geranylgeranyl pyrophosphate (GGPP).[11] GGPP can undergo further reactions to generate a variety of compounds including diterpenes, gibberellins, carotenoids and chlorophylls.

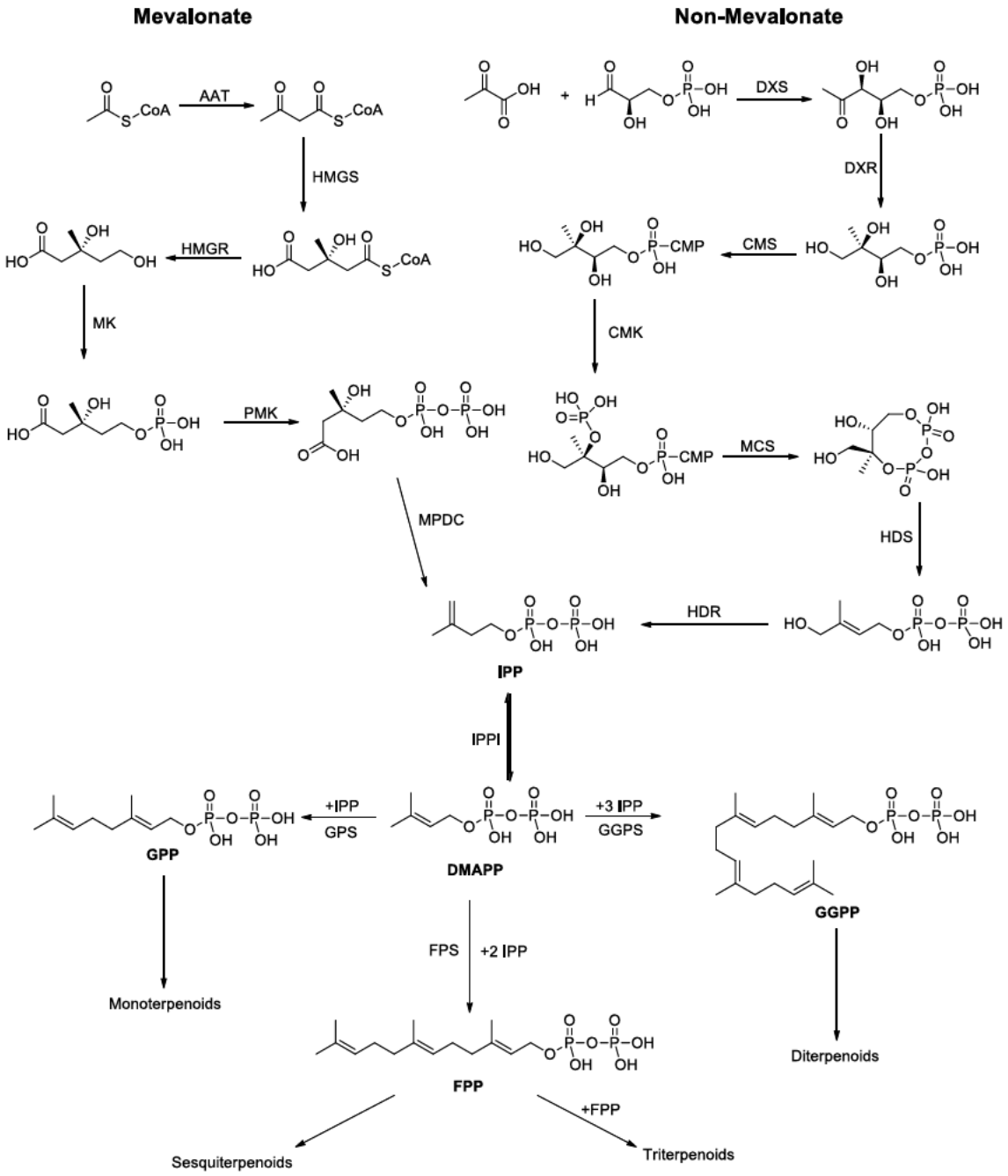

Scheme 1.1. *Biosynthesis of terpenoids by the mevalonate and non-mevalonate pathways.*

Terpenoids are present as part of the natural product composition for a variety of plants in the Goodeniaceae family. Kerr *et al*. screened the hexane and methanol extracts of *Scaevola spiniscens* and identified several terpenoid species including palmitic acid **11**, oleic acid **12**, xanthyletin **13**, hentriacontane **14**, (3β,22*E*)-stigmasta-5,22-dien-3-ol **15** and myricadiol **16** (Figure 1.5).[12]

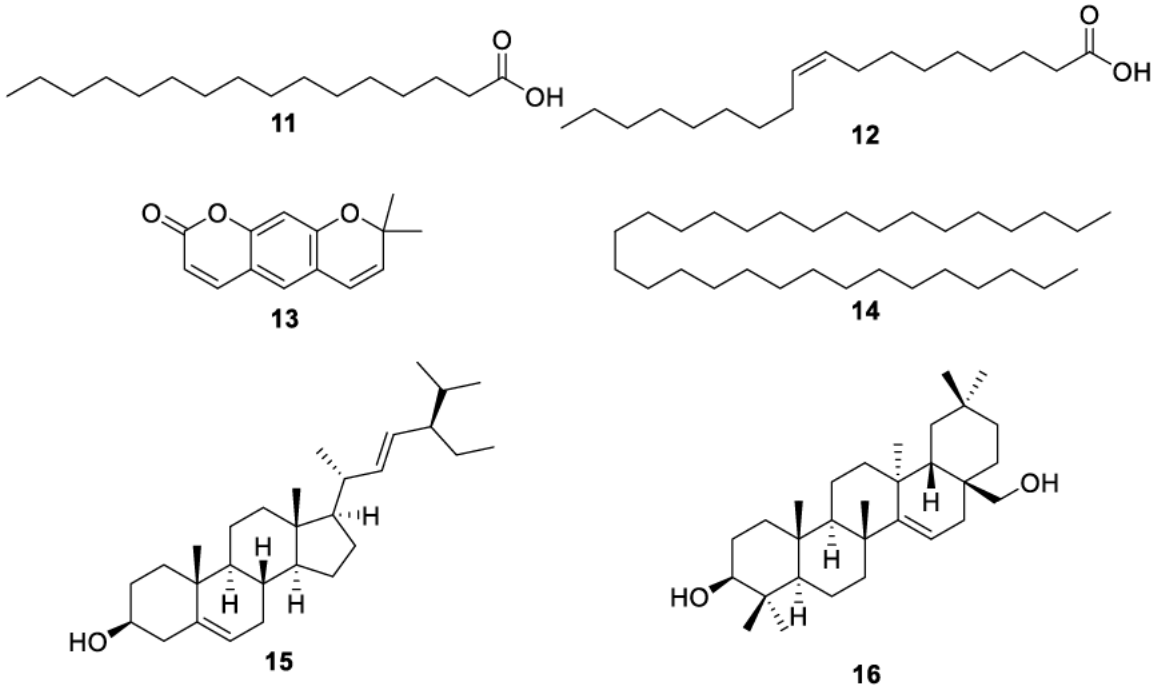

Figure 1.5. *Structures of palmitic acid* ***11****, oleic acid* ***12****, xanthyletin* ***13****, hentriacontane* ***14****, (3β, 22E)-stigmasta-5,22-dien-3-ol* ***15*** *and myricadiol* ***16*** *isolated from* Scaevola spiniscens *by Kerr et al.*

Cambie *et al*. isolated several triterpenoid compounds including δ-amyrin **17** and ursolic acid acetate **18** from *Scaevola floribunda* (Figure 1.6).[13]

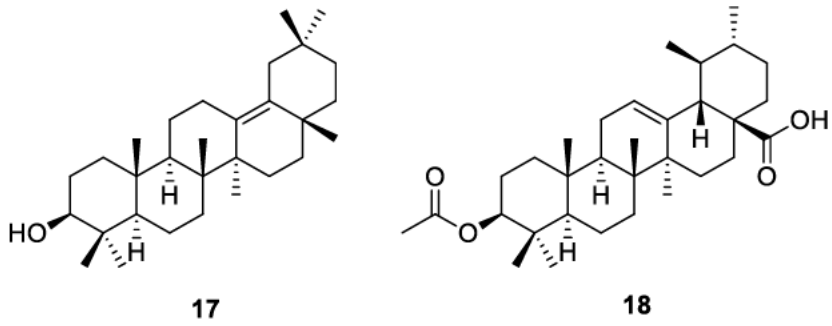

Figure 1.6. *Structures of δ-amyrin* ***17*** *and ursolic acid* ***18*** *isolated from* Scaevola floribunda *by Cambie et al.*

A number of iridoids have been isolated from *Scaevola* species to date, and are commonly found in the form of glycosides. Several iridoid compounds have been identified from *Scaevola montana* by Skaltsounis *et al*., including cantleyoside **19**, sylvestroside III **20** and loganin **21** (Figure 1.7).[14]

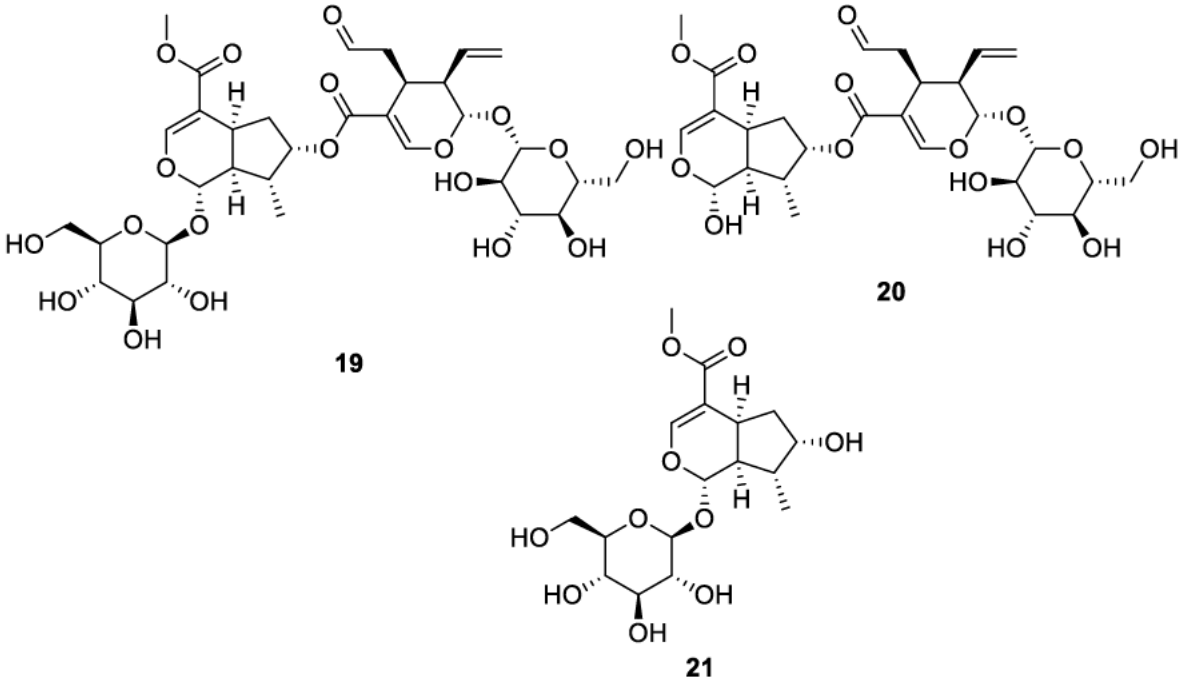

Figure 1.7. *Structures of cantleyoside* ***19****, sylvestroside III* ***20*** *and loganin* ***21*** *isolated from* Scaevola montana *by Skalsounis et al.*

Similarly, Skaltsounis *et al*. isolated a variety of iridoids from *Scaevola racemigera*, including scaevoloside **22** and loganic acid **23**, which were seemingly absent in *Scaevola montana* (Figure 1.8).[15] Cambie *et al*. also isolated the iridoid floribundal **24** from *Scaevola floribunda*.[13]

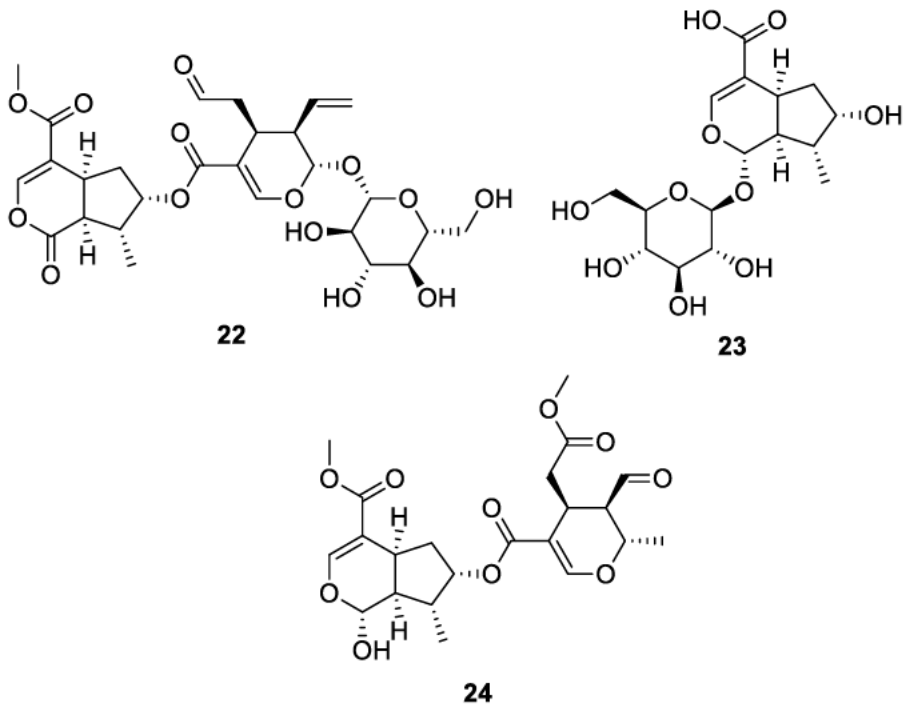

22 **23** **24**

Figure 1.8. *Structures of scaevoloside* ***22****, loganic acid* ***23*** *and floribundal* ***24*** *isolated from* Scaevola montana *and* Scaevola floribunda.

Coumarins have been reported to possess a large variety of valuable medicinal properties including, antioxidant, anti-inflammatory, anxiolytic, analgesic, neuroprotective, cardioprotective, antidiabetic and anticancer activity.[16] For example, 12-methoxyinophyllum P **25** was isolated from the leaves of *Rhizophora mucronata* by Taniguchi *et al*. and showed anticancer activity, with an IC_{50} of 3.8 μM for HeLa cells (cervical cancer cells) and 12.9 μM for HL-60 cells (myeloid leukemia cells). (Figure 1.9).[17]

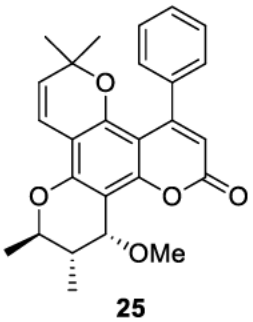

25

Figure 1.9. *Structure of 12-methoxyinophyllum P* ***25*** *isolated by Taniguchi et al.*

A number of coumarin compounds have been isolated from plants in the Goodeniaceae family. Bohlmann *et al*. isolated angenomalin **26** and isoangenomalin **27** from South

African *Scaevola lobelia*, and the absolute stereochemistry was later confirmed by Yamaguchi *et al*.[18] The enantiomer of isoangenomalin **27**, ammirin **28**, was isolated from *Scaevola frutescens*/*Scaevola taccada* along with xanthyletin **13** and its hydroxy acetate **29**.[19] Seselin **30** and nodakenetin **31** or its enantiomer marmesin **32** were isolated from *Scaevola spiniscens* by Kerr *et al*., along with xanthyletin **13**, and isoangenomalin **27** or ammirin **28** (Figure 1.10).[12]

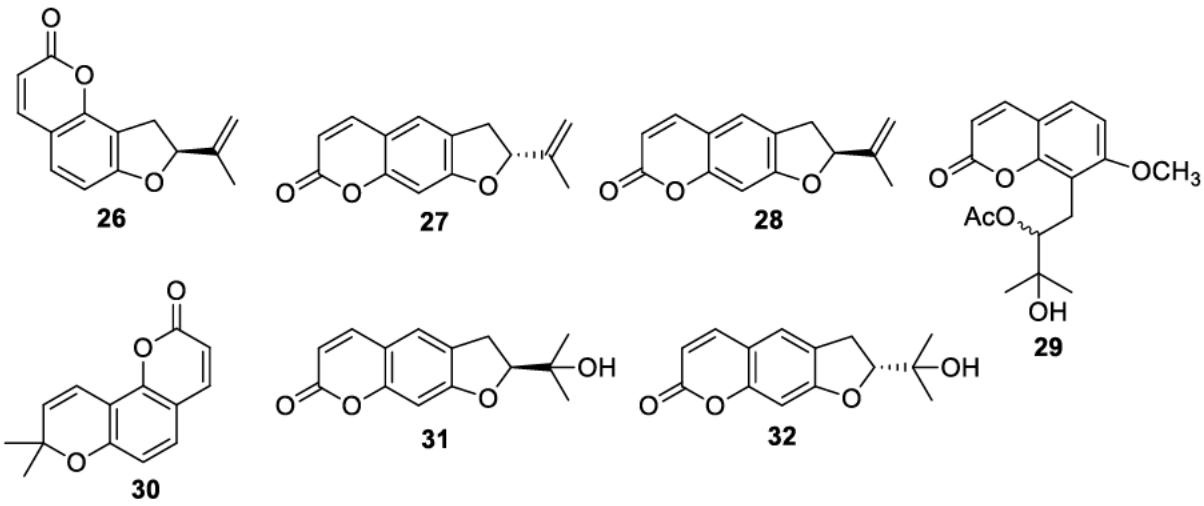

Figure 1.10. *Structures of angenomalin* ***26****, isoangenomalin* ***27****, ammirin* ***28*** *and the hydroxyl acetate of xanthyletin* ***29****, seselin* ***30****, nodakenetin* ***31*** *and marmesin* ***32****.*

Flavonoids are known to serve a variety of biological functions in plants including UV protection and contributing to the colour and aroma of flowers and fruits to aid in attracting pollinators.[20] They have also been reported to demonstrate many beneficial effects for human health including antioxidant, anti-inflammatory, anti-mutagenic and anti-carcinogenic effects.[21] Flavonoids are found in various parts of plants including the leaves, roots and fruit. Flavonoids that are found in food and beverages are known as dietary flavonoids, and includes fruits, vegetables, tea, cocoa and wine.[21b] Flavonoids can be classified into different types depending on the degree of oxidation and unsaturation of the C ring and the carbon of the C ring to which the B ring is attached. Types of flavonoids that have been reported included flavones **33**, flavanols **34**, flavanonols **35**, flavonols **36**, isoflavones **37** and flavanones **38** (Figure 1.11).

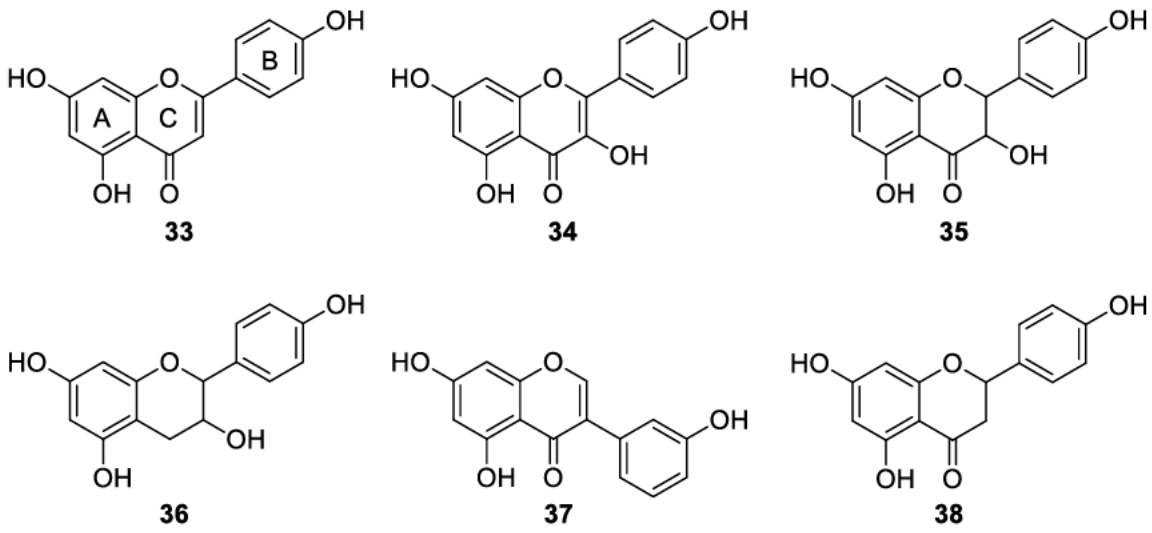

Figure 1.11. *Structures of flavones* ***33****, flavanols* ***34****, flavanonols* ***35****, flavonols* ***36****, isoflavones* ***37*** *and flavanones* ***38****.*

Flavanoids have been isolated from Goodeniaceae species. Several flavones consisting of glycosides of apigenin **39** and quercetin **40-45** were isolated from eight Hawaiian *Scaevola* species by Patterson.[22] Luteolin-7-*O*-glucoside **46** has been previously isolated from *Scaevola spiniscens* by Nobbs.[23] Saito *et al.* isolated 7-polyacylated delphinidin 3,7-diglucoside **47** from the blue flowers of *Leschenaultia* cv. Violet Lena (Figure 1.12).

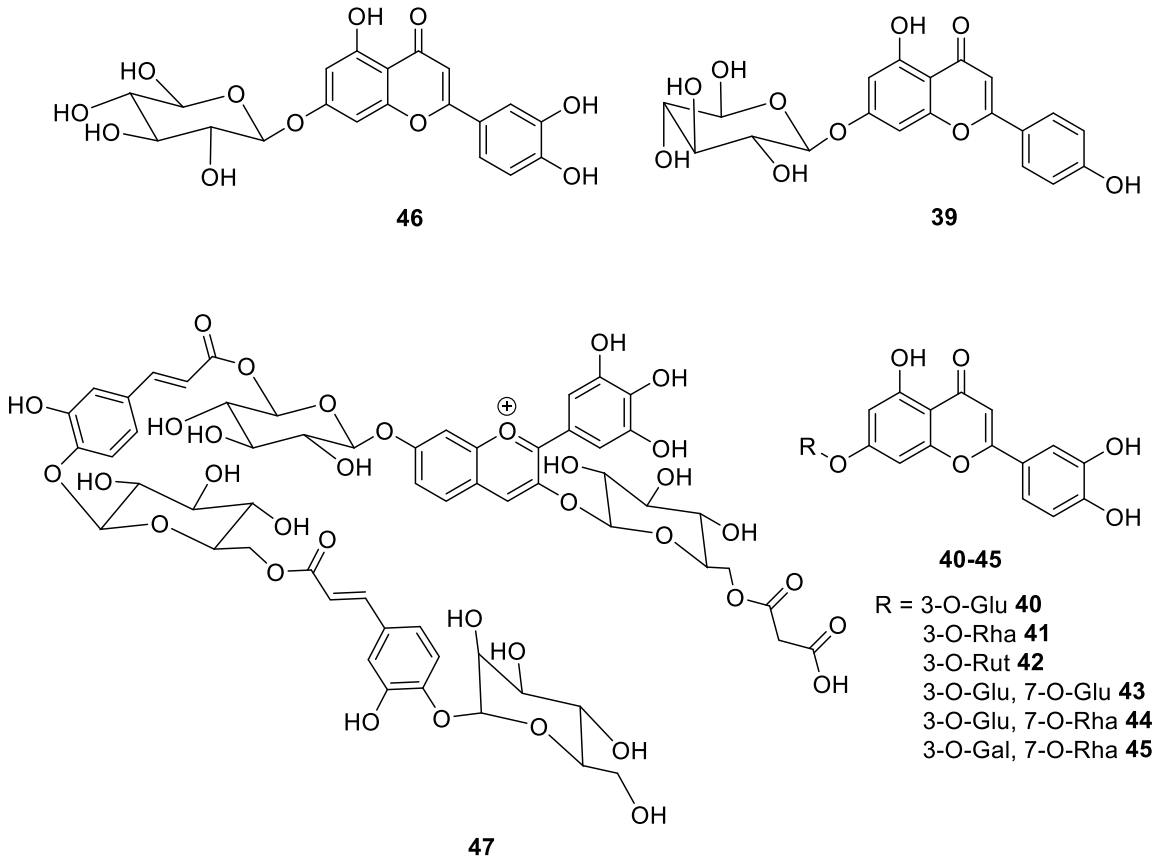

Figure 1.12. *Structures of luteolin-7-O-glucoside* ***46*** *apigenin rhamnoside* ***39*** *and quercetin glycosides* ***40-45****, and 7-polyacylated delphinidin 3,7-diglucoside* ***47****.*

Alkaloids are a class of natural products that typically refers to nitrogen containing compounds. Alkaloids have been isolated from Western Australian plants, but few examples are present in the Goodeniaceae family. Aplin *et al.* tested for the presence of alkaloids in a number of Western Australian plants, and only a handful of plants in the Goodeniaceae family gave a strongly or moderately positive response for the presence of alkaloids.[24] In particular *S. crassifolia* and *Scaevola striata* both tested negative for the presence of alkaloids. Interestingly, *Scaevola racemigera* collected in New Caledonia yielded nine alkaloids derived from iridoid glycosides, such as cantleyine **48**, tetrahydrocantleyine **49** and the lactam strychnovoline **50** (Figure 1.13).[15]

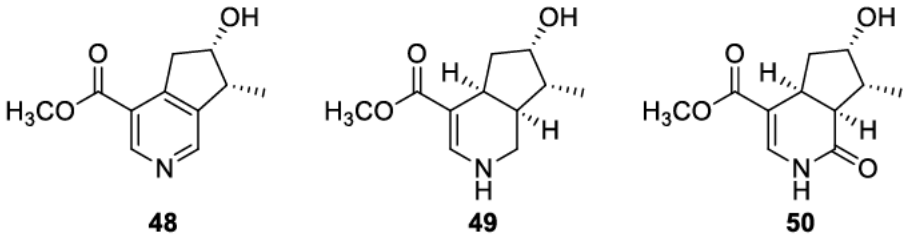

Figure 1.13. *Structures of cantleyine* ***48****, tetrahydrocantleyine* ***49*** *and strychnovoline* ***50*** *isolated from* Scaevola racemigera *by Skaltsounis et al.*

1.3 Conventional methods used in natural products research

A variety of techniques have been conventionally used for the isolation and analysis of natural products. Natural products have been isolated through the bulk extraction of compounds from various sections of the plants. The extractions are typically undertaken using aqueous or organic solvents, depending on the chemical properties of the compounds.[25] For example, the indole and flavonoid constituents of *Wrightia tinctoria*, *W. tomentosa* and *W. coccinea* were extracted from the leaves using $CHCl_3$ and MeOH.[26] Different sections of a plant can extracted for natural products depending on where the natural products may be located within the plant. The aerial components of plants refers to sections of the plant that are above the ground and exposed to the atmosphere, such as the leaves, stems, bark, flowers and buds. The aerial parts of the plant are generally renewable and can be harvested from the plant for extraction of natural products without killing the plant. The underground components of plants primarily consists of roots and underground stems, including bulbs, rhizomes and tubers. Analysis of natural products from the underground components of plants can result in the death of the plant, because harvesting of roots or undergrounds stems can kill the plant in the process.

The constituents of plant extracts are then typically separated into different classes of compounds using partitioning techniques.[27] Two main types of partitioning are used for the separation of compounds: acid-base partitioning and polarity partitioning. Acid-base partitioning is reliant on the acid-base properties of the compounds and through the selective protonation and deprotonation of different classes of molecules, they can be partitioned between aqueous and organic phases and separated in this manner (Figure 1.14).

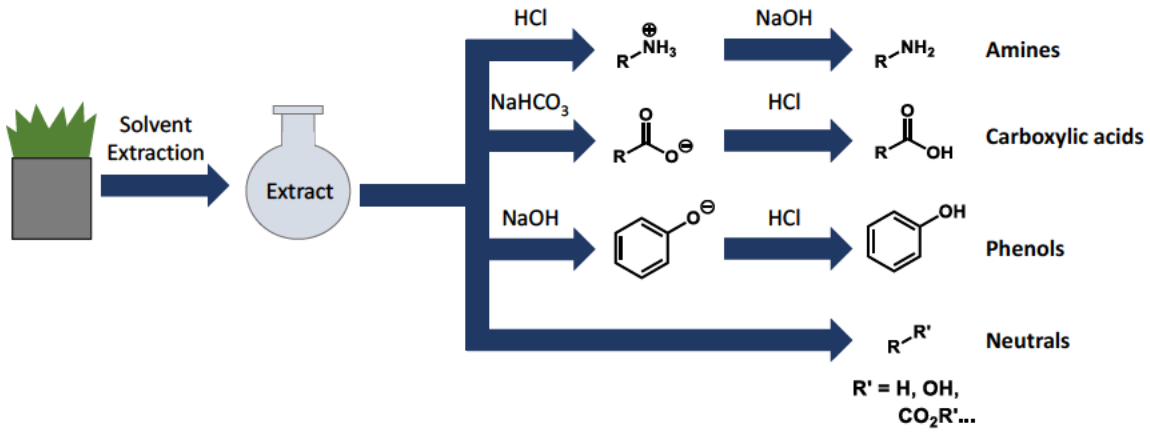

Figure 1.14. *Workflow for acid-base partitioning of natural products.*

Polarity partitioning is based on the relative polarities of the compounds. Solvents of varying polarities are used to extract different compounds, with the polarities of the solvents being increased or decreased as required. One example is the use of polarity partitioning by Moustafa *et al.* to separate the constituents of the ethanol extract of *C. procera* using PS, $CHCl_3$, EtOAc and 1-butanol (Figure 1.15).[28]

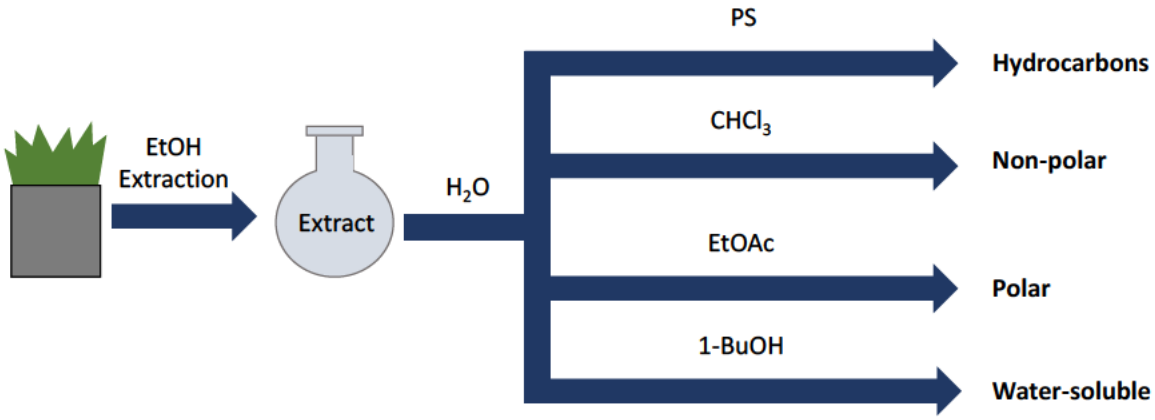

Figure 1.15. *Workflow for polarity partitioning of natural products based on work by Moustafa et al.*[28]

After partitioning of the crude extract, individual compounds are then usually isolated and purified using chromatography, such as high performance liquid chromatography (HPLC), or recrystallisation.[27] Purification of the crude plant extract without partitioning is also possible, but can be dependent on chemical composition of the extract. For example, Moussa *et al.* purified the crude ether extract of *Dodonaea ceratocarpa* leaves using flash chromatography to isolate a new clerodane diterpene.[29]

Isolated compounds are then characterised using techniques such as nuclear magnetic resonance (NMR) spectroscopy, Fourier transform infrared (FTIR) spectroscopy, ultraviolet-visible (UV-Vis) spectroscopy, polarimetry and mass spectrometry (MS). The use of NMR and MS for characterisation is highlighted in the characterisation of the toxin mycolactone **54** by George *et al*. (Figure 1.16).[30]

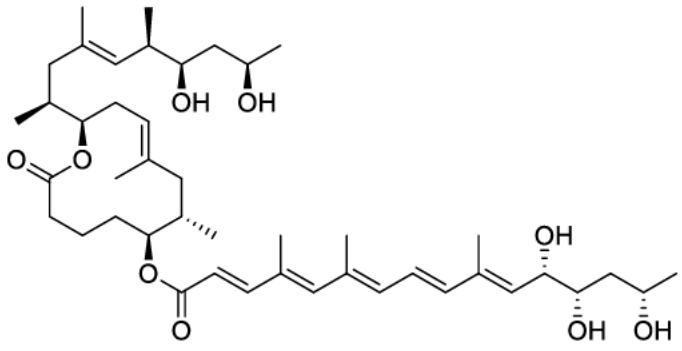

51

Figure 1.16. *Structure of mycolactone* ***51*** *isolated by George et al.*[30]

1.4. Techniques used for the characterisation and localisation of small molecules

Conventional isolation and characterisation are effective for the identification of individual natural products. However, compounds can be lost or altered during the isolation stage and the presence of specific compounds cannot be confirmed until the isolation process has been completed. The spatial distribution of natural products is also lost upon bulk extraction of the compounds from the plant. The distribution of natural products in plants has primarily been localised to broad anatomical locations such as the leaves, roots, stem and leaves. However, only limited work has been conducted to localise natural products with greater specificity to a cellular or subcellular level. A variety of chemical, spectroscopic and spectrometric techniques exist for the localisation of small molecules in biological tissue.

1.4.1. Histochemical methods

Histological stains are a chemical technique which typically use chemical reagents to react or bind with particular molecules, resulting in a visible colour change or fluoresce to show the molecular distribution. Common plant histological stains include phloroglucinol-HCl for staining lignin, toluidine blue for staining chromosomes and NADI for staining terpenes.[31] For example, Pomar *et al.* used phloroglucinol-HCl staining to stain for lignin

in plant species including *Zinnia elegans* L., *Capsicum annuum* var. *annuum*, *Populus alba* L., and *Pinus halepensis* L. (Figure 1.17).[32] Histological stains can be used to map the distribution of different molecules, but lack chemical specificity beyond broad chemical classes such as terpenes or flavonoids. Chemical staining can also lead to artefacts in biological tissue.[33]

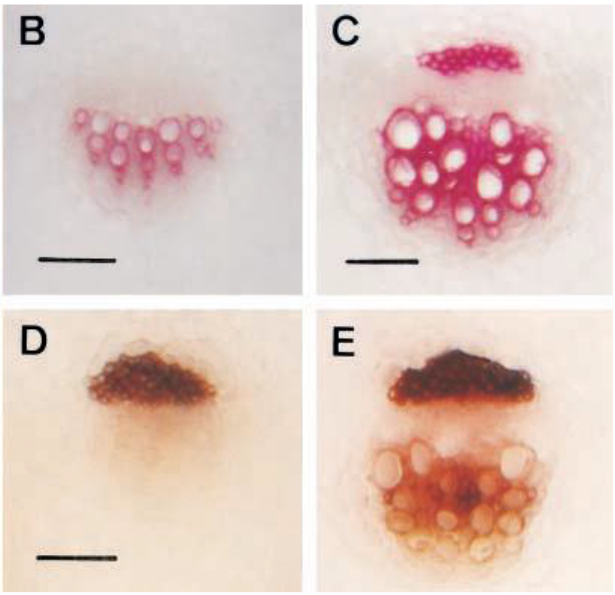

Figure 1.17. *Phloroglucinol-HCl stained* Zinnia elegans *stems (B) 5 days and (C) 10 days after appearance of first true leaves and* Zinnia elegans *hypocotyls (D) 10 days and (E) 15 days after the appearance of first true leaves. Scale bars are 100 µm. Figure and caption from work by Pomar et al.*[32]

1.4.2. Mass spectrometry imaging methods

Imaging mass spectrometry has traditionally been used to map the distribution of biomolecules such as proteins and lipids in animal samples, but has increasingly been used to map the distribution of natural products.[34] The primary mass spectrometry imaging techniques are Matrix-Assisted Laser Desorption/Ionisation (MALDI), Desorption Electrospray Ionisation (DESI) and Secondary Ion Mass Spectrometry (SIMS).

1.4.2.1 Matrix-Assisted Laser Desorption/Ionisation (MALDI)

MALDI mass spectrometry involves the use of a matrix to assist in desorption of the analytes from the sample surface. Evaporation of the matrix results in crystallisation of the matrix with the analytes embedded within the crystals. The sample is then irradiated with a laser, resulting in laser ablation of the crystals and desorption of the analytes and matrix materials. Finally, the desorbed analytes are ionised and can be detected by the mass

spectrometer. MALDI mass spectrometry is an accessible technique that can be used with a wide variety of samples, but ionisation must be conducted under vacuum. Shroff *et al.* used MALDI to map the distribution of glucosinolates in the leaves of *Arabidopsis thaliana* (Figure 1.18).[35]

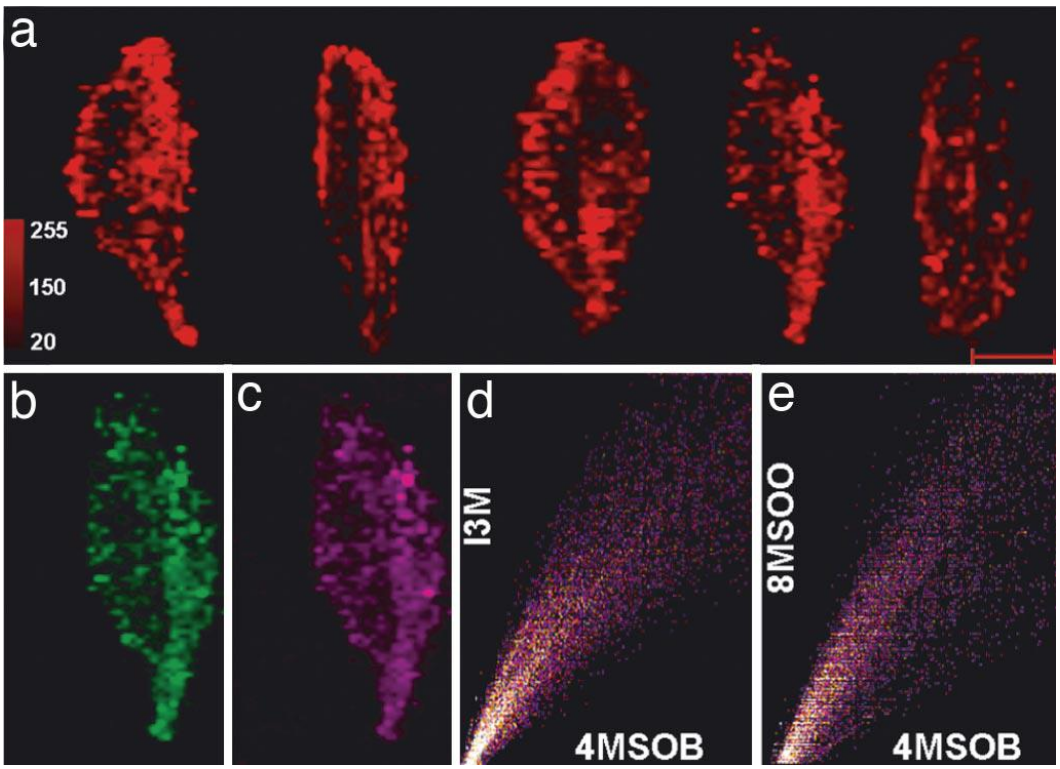

Figure 1.18. *MALDI-MS images of* Arabidopsis thaliana *leaves showing the uneven distribution of glucosinolates throughout the leaves by Shroff et al.*[35]

1.4.2.2 Desorption Electrospray Ionisation (DESI)

DESI mass spectrometry is based on the use of a stream of charged solvent at an angle to the sample surface to desorb analytes from the sample surface. The desorbed analytes are then propelled towards the mass spectrometer to be analysed. A significant advantage of DESI mass spectrometry is that the desorption of the sample is conducted under ambient conditions in open air and is a comparatively gentle ionisation technique relative to MALDI mass spectrometry. The set-up for DESI mass spectrometry is highly specialised, however, and typically requires assistance from mass spectrometry specialists. Lane *et al.* used DESI mass spectrometry to map the distribution of bromophycolides **52** and **53** on algal surfaces, showing that the distribution of the compounds was heterogenous (Figures 1.19 and 1.20).[36]

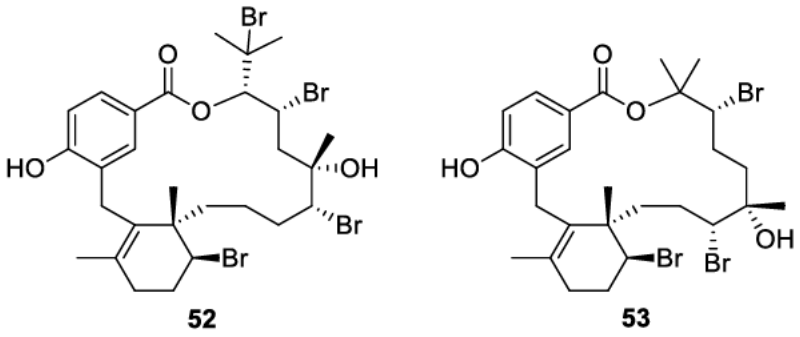

Figure 1.19. *Structures of bromophycolide A* ***52*** *and bromophycolide B* ***53****.*

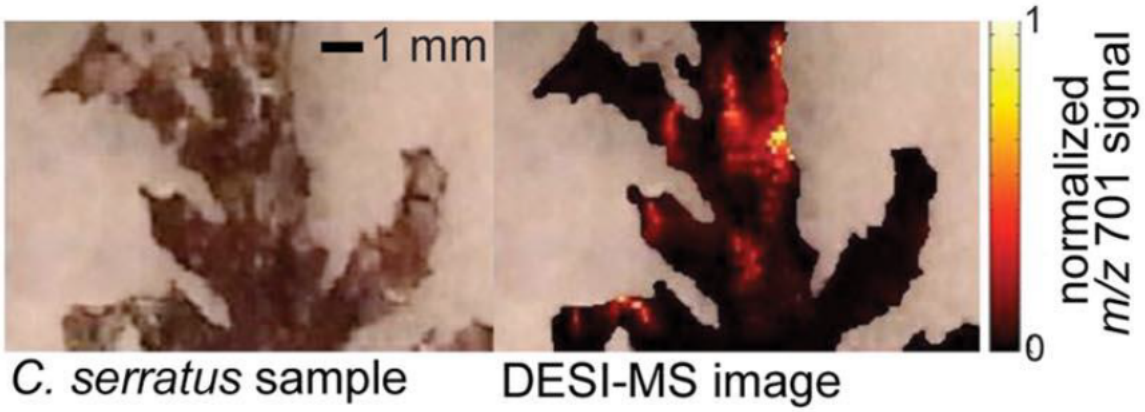

Figure 1.20. *DESI-MS images showing the distribution of the chloride adducts of bromophycolides A and B,* ***52*** *and* ***53****, in the algae* Callophycus serratus *by Lane et al.*[36]

1.4.2.3. Secondary Ion Mass Spectrometry (SIMS)

SIMS uses a focused ion beam to ionise the sample surface and results in the ejection of secondary ions, which are analysed in the mass spectrometer. SIMS mass spectrometry has better spatial resolution than both MALDI and DESI mass spectrometry, but like MALDI, it must be conducted under ultra-high vacuum. Saito *et al.* used TOF-SIMS mass spectrometry to distinguish between sapwood and heartwood in discoloured ancient wood by mapping the distribution of hinokinin **54**, hinokiresinol **55**, hinokione **56** and hinokiol **57** (Figures 1.21 and 1.22).[37]

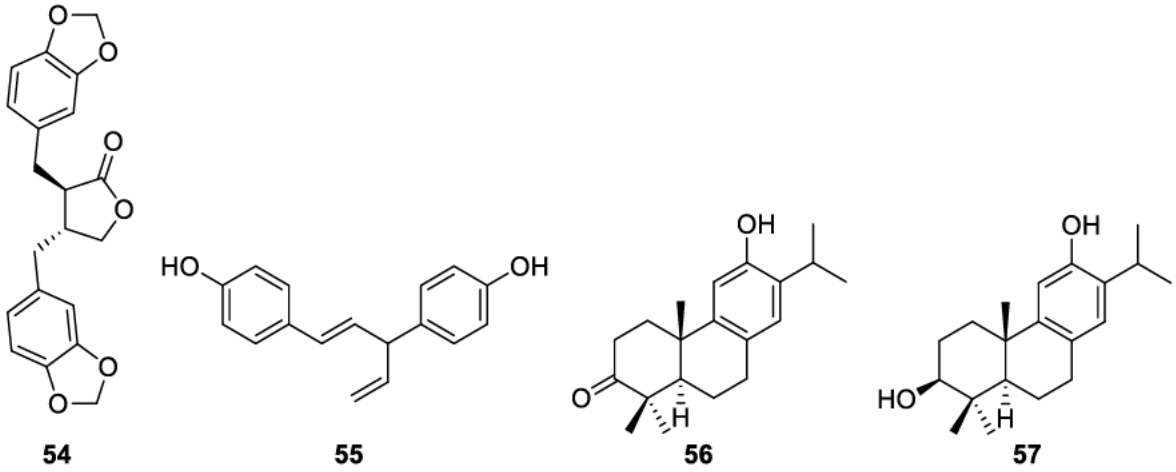

Figure 1.21. *Structures of hinokinin* ***54****, hinokiresinol* ***55****, hinokione* ***56*** *and hinokiol* ***57****.*

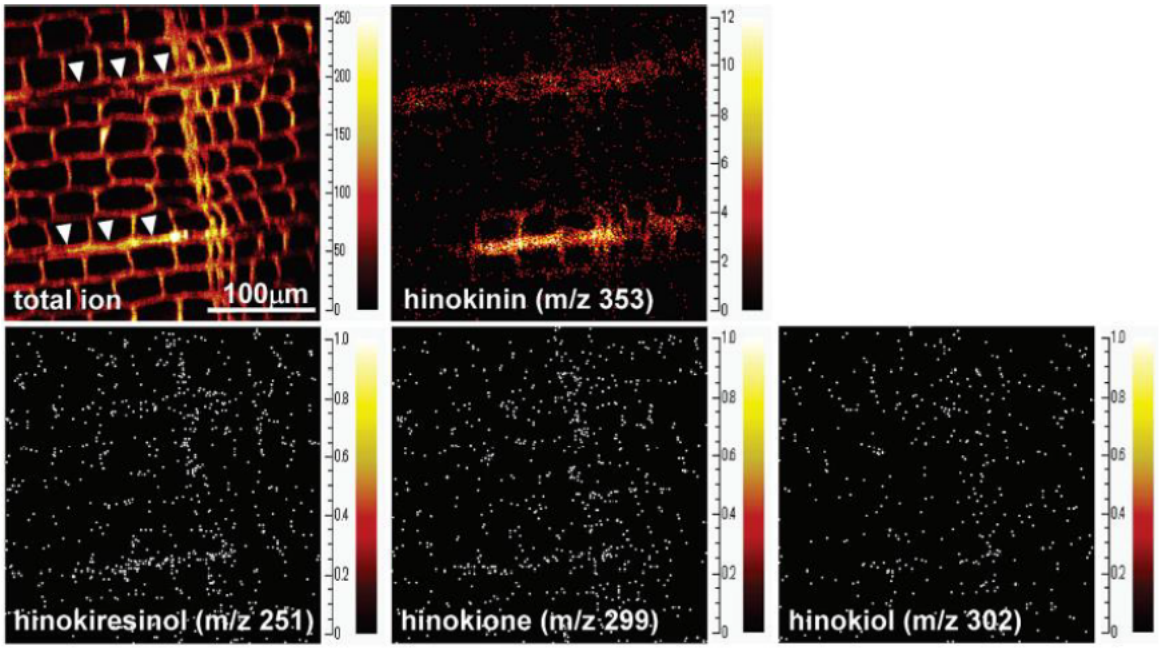

Figure 1.22. *TOF-SIMS positive ion image of the transverse section of ancient Hinoki Cyprus wood showing the total ion distribution, and distribution of selected ions of hinokiresinol* ***55****, hinokione* ***56*** *and hinokiol* ***57*** *by Saito et al.*[37]

1.4.3. Vibrational spectroscopic methods

Natural products and other chemical compounds can be localised in biological samples through the use of vibrational spectroscopy. Vibrational spectroscopy refers to the use of light to obtain chemical information about molecules through changes in the vibrational energy levels of the molecule.[38] Vibrational spectroscopic techniques include FTIR spectroscopy and Raman spectroscopy. Both spectroscopic techniques are non-destructive and can provide extensive chemical information about a given sample.

FTIR spectroscopy involves the use of infrared light to obtain chemical information about the sample. All molecules possess molecular vibrations, with 3N-6 vibrational modes for a given molecule (3N-5 for linear molecules), where N is the number of atoms in the molecule.[38] When the sample is exposed to infrared light, the light will be absorbed by the molecule and the low energy infrared light will be absorbed by particular molecular vibrations (Figure 1.26). Absorption of the infrared light results in a change in the dipole moment of the molecule, and the transmitted radiation is detected.[38] FTIR spectroscopy can be used for chemical mapping, known as FTIR imaging. FTIR imaging has an excellent signal-to-noise ratio but on a benchtop instrument, has a poorer spatial resolution in the range of 5 µm to 20 µm. FTIR imaging is also water-sensitive, so air purging is required before imaging.

The poor spatial resolution of benchtop FTIR imaging can be mitigated through the use of a synchrotron light source (Figure 1.23). A synchrotron generates high intensity light through the acceleration of high energy electrons in a circular orbit using magnetic fields. The light generated by the synchrotron covers a wide spectrum, ranging from infrared to hard x-rays, and is tuneable, allowing for any wavelength within that range to be selected. The infrared microscopy (IRM) beamline at the Australian synchrotron allows for high signal-to-noise ratios at diffraction-limited spatial resolutions between 3-8 µm, which is suitable for imaging of plant cells.[39]

Figure 1.23. *Aerial view of the Australian synchrotron.*[40]

Raman spectroscopy is a complementary technique to FTIR spectroscopy that uses light in the near-infrared, visible or near-ultraviolet region as opposed to infrared light.[38] For Raman spectroscopy, when the incident light interacts with the molecule, one of three types of light scattering can occur. The electrons can be excited to a virtual electronic state and then relax back down to the ground state in a single step, known as Rayleigh scattering (Figure 1.24). The electrons can be excited to a virtual electronic state and relax back down

to a higher vibrational energy level than the ground state, releasing photons of a lower energy and longer wavelength, known as Stokes scattering (Figure 1.24). Finally, the electrons can be excited to a virtual electronic state from the ground state and relax back down to a lower energy vibrational level, releasing photons of a higher energy and shorter wavelength, known as Anti-Stokes scattering (Figure 1.26). Stokes and Anti-Stokes scattering are the signals measured for Raman spectroscopy, but are weak scattering effects in comparison to Rayleigh scattering.[38]

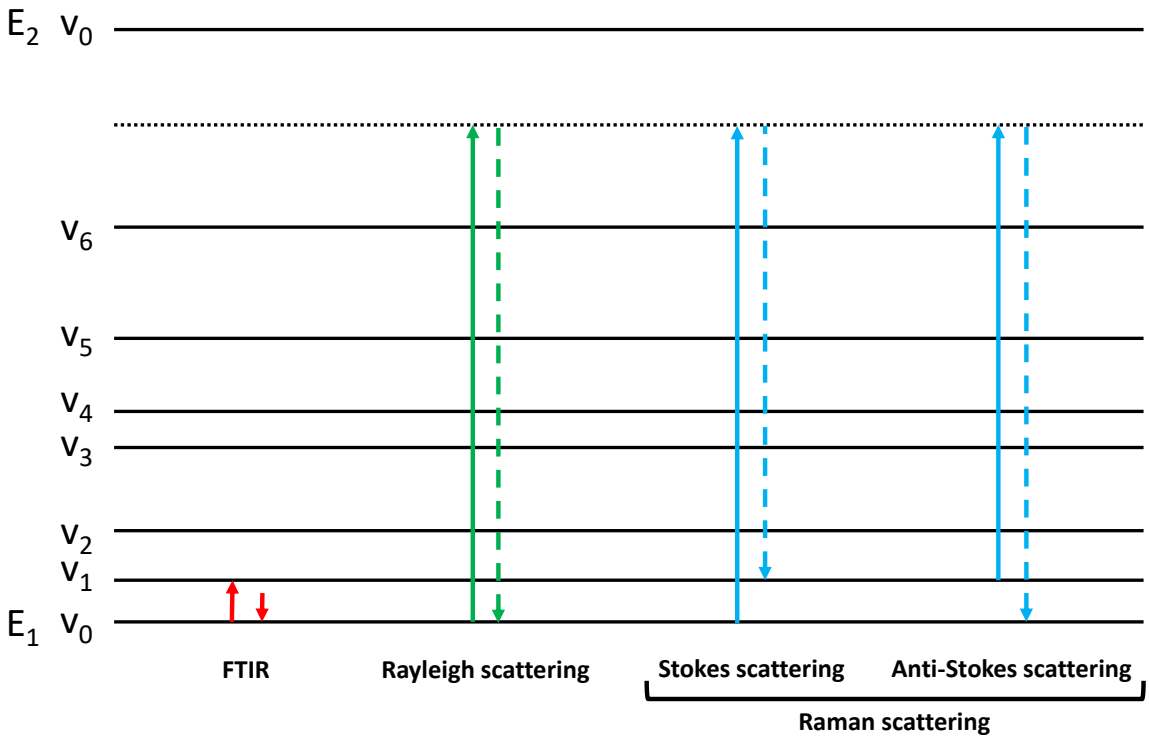

Figure 1.24. *Jablonski diagram showing FTIR and Raman scattering effects.*

Similar to FTIR imaging, Raman spectroscopy can also be used for chemical mapping, known as Raman microscopy. The signal-to-noise ratio of Raman microscopy is significantly worse than FTIR imaging, because Raman scattering is a very weak effect. The spatial resolution of Raman microscopy is substantially improved relative to that of FTIR imaging, with values in the sub-micromolar range. Raman microscopy is not water-sensitive and can provide greater chemical specificity than FTIR imaging, such as providing information about the expansion and contraction of rings in cyclic and polycyclic molecules.

Vibrational spectroscopy has been used for the characterisation of natural products such as essential oils in plants from Turkey.[41] However, the compounds were not characterised *in*

situ and instead characterisation was achieved with essential oils that had been extracted from the plant. *In situ* characterisation of natural products was conducted by Sanchez *et al*. to differentiate between hemp, cannabidiol-rich hemp and cannabis using a handheld Raman spectrometer. However, the measurements were of a single point on the plants and did not provide any information about the spatial resolution of compounds like cannabidiol or tetrahydrocannabinol (THC)[42]

Biospectroscopy refers to the use of vibrational spectroscopy, such as FTIR imaging and Raman microscopy, to directly obtain chemical information *in situ* about biological systems.[43] Furthermore, biospectroscopy can spatially resolve molecules, which has been successfully applied previously for the imaging of protein aggregates that are thought to be linked to Alzheimer's disease.[44] Similarly, biospectroscopy has been used extensively for the chemical analysis of plant cells and plant material. For example, lignin is a polyphenolic polymer used for structural reinforcement in plant cells and changes in lignin composition and distribution can provide valuable information about plant anatomy. The changes in the distribution of lignin in the cell walls of *Populus trichocarpa* has been previously mapped using Raman microscopy (Figure 1.25).[45] Raman spectroscopy has also been used to gain more structural information about the polymer and how the structures change upon milling and chemical treatment of wood.[46] Natural product distribution has also been mapped using Raman microscopy. The distribution of flavonoids, along with other compounds such as suberin, lignin and ferulate, has been mapped using a combination of fluorescence microscopy and Raman microscopy.[47] Flavonoids were localised to the epidermal cell lumens through the use of staining and extraction of compounds from the pine needles.

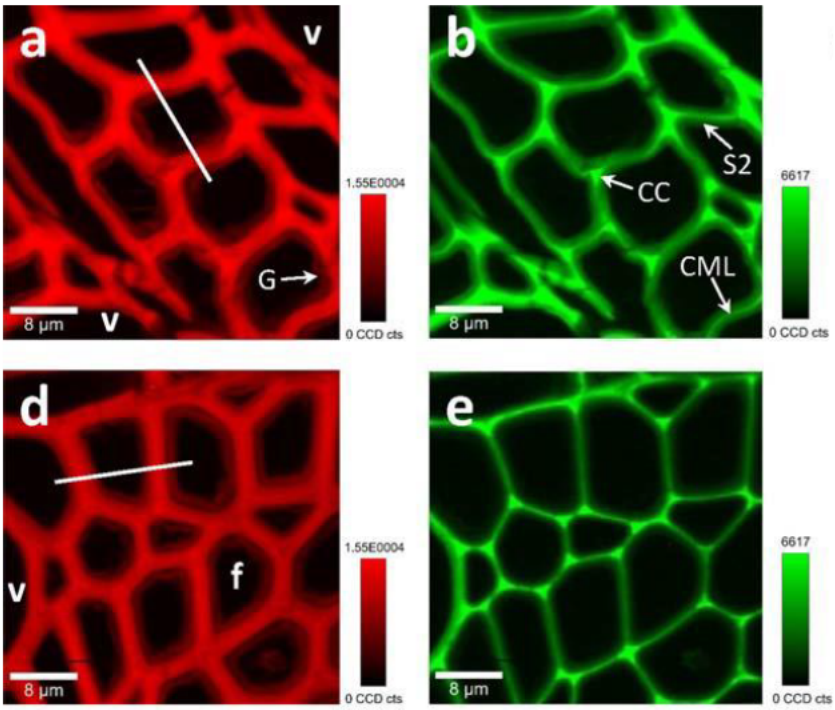

Figure 1.25. *False colour Raman images based on composite C-H stretching bands (red) and lignin distribution (green) for wild type (a) and as4CL-12* Populus trichocarpa *by Schmidt et al.*[45]

1.5 Chemistry of caryophyllenes

Unlike any other plants in the Goodeniaceae family, caryophyllenes have been isolated from the surface leaf resin of *S. crassifolia* Caryophyllenes are characterised by a bicyclic core consisting of a cyclobutane fused in a *trans* conformation to a nine-membered ring. The nine-membered ring contains an endocyclic alkene in the *E* confirmation in the C4 position and a terminal exocyclic alkene in the C8 position (Figure 1.26).

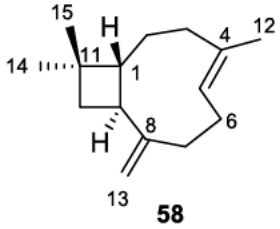

58

Figure 1.26. *General structure and numbering of caryophyllenes.*

β-Caryophyllene **58** is the most common of the caryophyllenes, but a variety of oxygenated derivatives of β-caryophyllene **58** have also been identified. Oxygenated caryophyllenes that have been previously identified include 6-hydroxycaryophyllene **1**, 14-

hydroxycaryophyllene **59**, 12-hydroxycaryophyllene **60** and caryophyllene **61** (Figure 1.27).[48a]

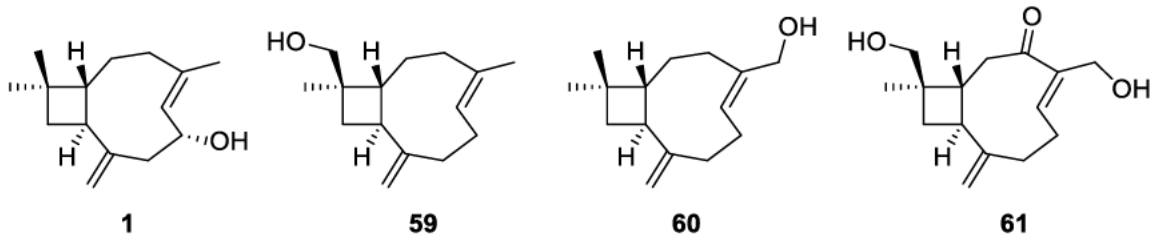

1 **59** **60** **61**

Figure 1.27. *Structures of 6-hydroxycaryophyllene **1**, 14-hydroxycaryophyllene **59**, 12-hydroxycaryophyllene **60** and compound **61**.*

Caryophyllenes are found in several species of plants and fungi, including the clove tree *Eugenia caryophyllata* and fungi in the *Naematoloma* genus.[48a, 49] β-Caryophyllene **58** has also been shown to exhibit interesting bioactivity within the endocannabinoid system, acting as an agonist for the anti-inflammatory CB_2 receptor.[50] β-Caryophyllene **58** has also been reported to aid in wound healing by improving cell proliferation and cell migration, both of which are associated with enhanced wound healing.[51]

Caryophyllenes are chemically interesting compounds because the *E* conformation of the endocyclic alkene results in the alkene being highly strained. Consequently, the endocyclic alkene is significantly more reactive than the exocyclic alkene, allowing for a huge variety of structural rearrangements to be facilitated. Caryophyllenes have been reported to have a number of conformers. β-Caryophyllene **58** has four different conformers: αα, αβ, βα and ββ (Figure 1.28).[52] However, only two conformers have been detected in 12-hydroxycaryophyllene **60**, on an NMR timescale, βα and ββ. 6-Hydroxycaryophyllene **1** possesses only the ββ conformer.[48b, 52a] The different conformers of caryophyllenes impact the reactivity of the caryophyllene, where some conformers may be unsuitable for particular reactions.

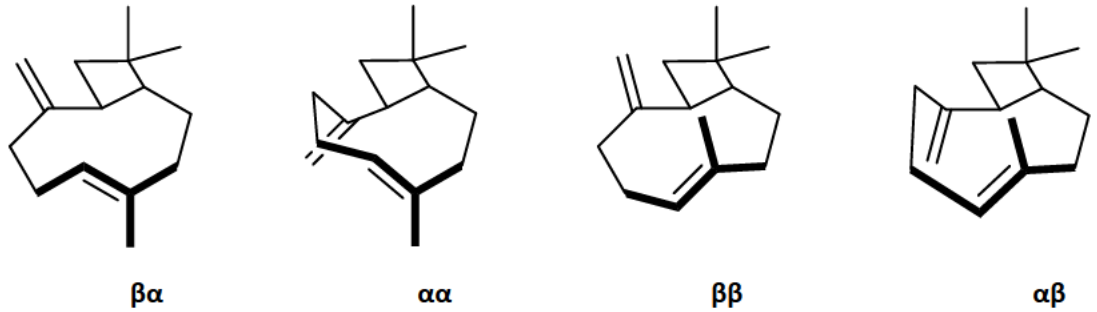

Figure 1.28. *Conformers of β-caryophyllene **58**.*

Cyclisations of caryophyllenes, and β-caryophyllene **58** in particular, have been thoroughly investigated. Treatment of β-caryophyllene **58** with H_2SO_4 in Et_2O at 0-20ºC for 30 mins initially afforded a mixture of 14 hydrocarbons and 4 alcohols, but after 3 days, three major products dominated the mixture: caryolan-1-ol **62**, clov-2-ene **63** and α-neoclovene **64**.[53] Compounds **62**, **63** and **64** were formed through protonation of the endocyclic alkene of the βα conformer (Scheme 1.2). In contrast, compounds **65**, **66** and **67** were formed through protonation of the exocyclic alkene of the βα conformer (Scheme 1.2).[53]

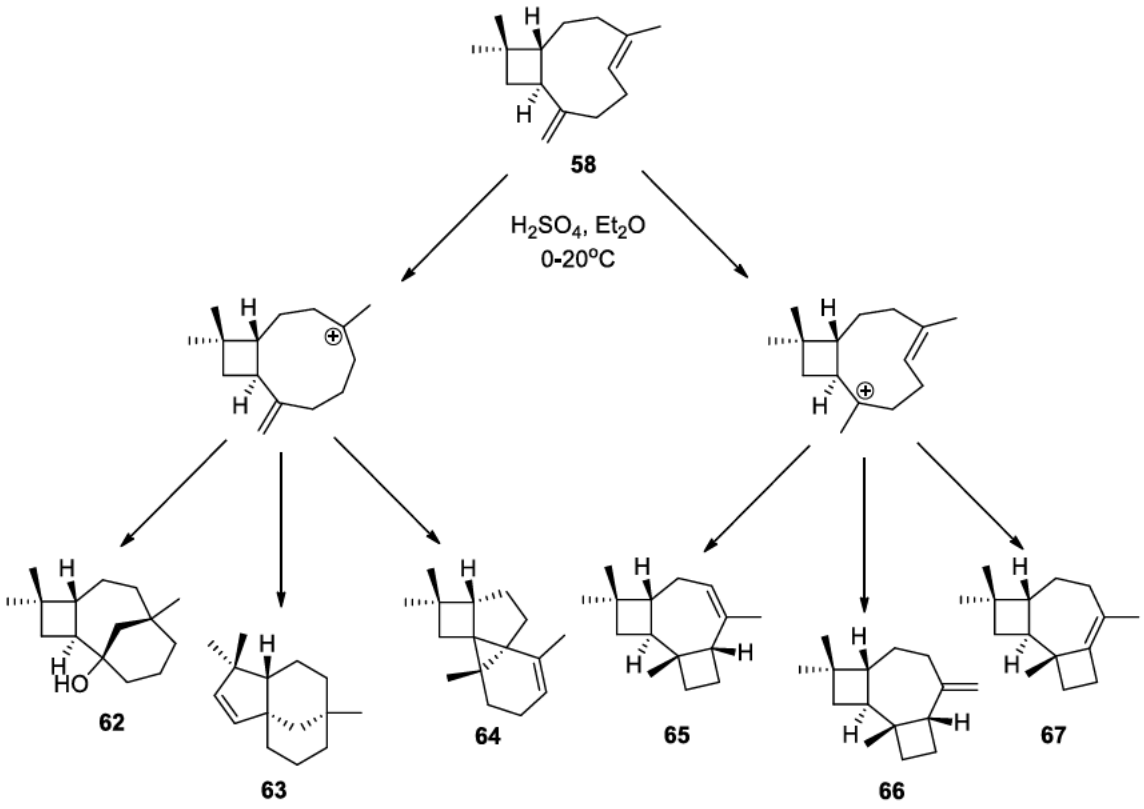

Scheme 1.2. *Cationic rearrangement products of β-caryophyllene **58** in the presence of H_2SO_4.*

The different skeletal products produced by the cyclization reactions highlights the varying reactivities of the different conformers of β-caryophyllene **58**.[54] Formation of the clov-2-ene skeleton, such as with compound **63**, can be attributed to cyclisation on the lower face of the molecule in the αα conformation along with a ring expansion of the four membered ring. The cyclisation affords the new six membered ring and generates a 3° carbocation on C8. Ring expansion by rearrangement of the C1-C9 bond generates a bridgehead alkene in a nine-membered ring. Nucleophilic addition of the alkene to the newly formed 2° carbocation forms the fused five and six membered rings of clove-2-ene **63**. Finally, the bridgehead alkene of clov-2-ene **63** is formed through an elimination reaction, regenerating the acid catalyst (Scheme 1.3).

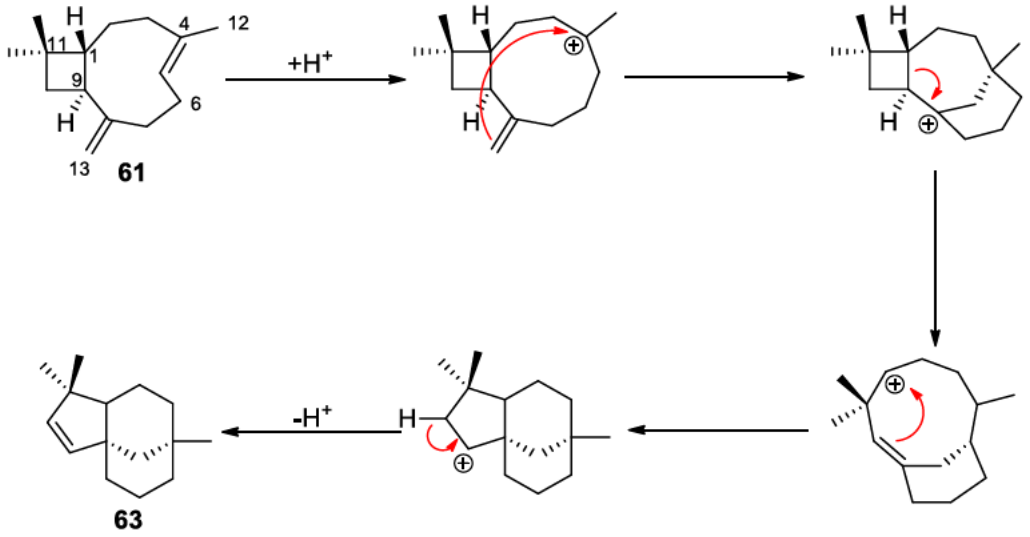

Scheme 1.3. *Mechanism for the formation of clov-2-ene **63** from β-caryophyllene **58**.*

In contrast, the formation of the caryolan-1-ol type skeleton, such as with compound **62**, can be attributed to cyclisation occurring on the β-face of the molecule in the ββ conformation. Protonation of the endocyclic and/or exocyclic alkenes can also lead to the generation of double bond isomers **68**, **69**, **70** and **71** (Figure 1.29).[55]

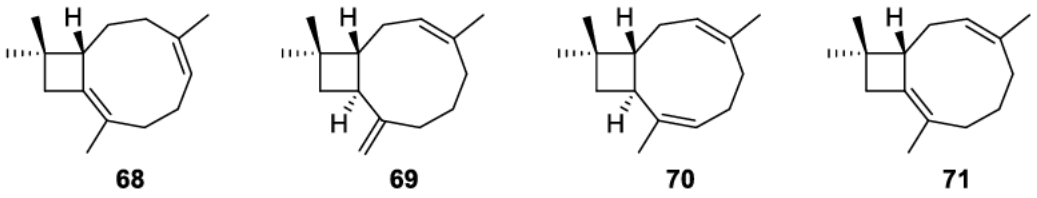

Figure 1.29. *Structures of compounds **68**, **69**, **70** and **71**.*

Isocaryophyllene **72** is the *Z* isomer of β-caryophyllene **58**, and has not been as extensively studied as its *E* relative. Treatment of isocaryophyllene **72** with H_2SO_4 in Et_2O at 0°C afforded compounds **73** and **74** in 34% and 46% yields respectively (Scheme 1.4).[56]

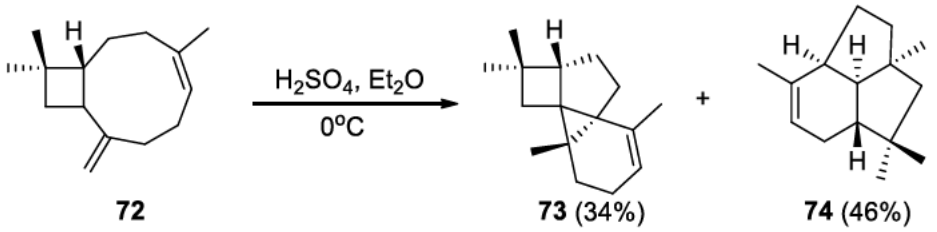

Scheme 1.4. *Cationic rearrangement products of isocaryophyllene 72 in the presence of H_2SO_4.*

The formation of compound **74** highlights the complexity of the skeletal rearrangements that caryophyllenes can undergo. The rearrangement of isocaryophyllene **72** can be rationalised through the mechanism proposed by Collado *et al.* (Scheme 1.5).[57] The exocyclic alkene is first protonated to form a 3° carbocation. A ring expansion of the cyclobutane then occurs to afford a fused cyclopentane-cyclooctene ring system. A nucleophilic addition of the endocyclic alkene to the newly formed 2° carbocation generates the five- and six membered rings of compound **74**. Finally, an elimination occurs to generate the new endocyclic alkene to afford compound **74**.

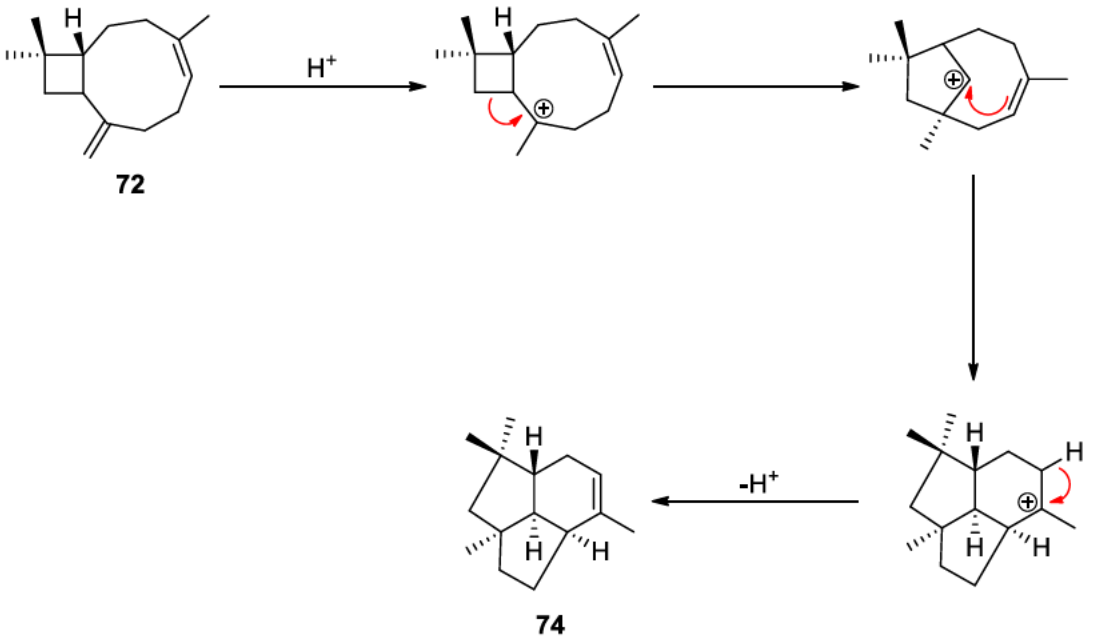

Scheme 1.5. *Mechanism for the formation of compound 74 from isocaryophyllene 72.*

Further exploration of the reactivity of isocaryophyllene **72** was pursued by Collado *et al*. Isocaryophyllene **72** was reacted with $FeCl_3$ supported on silica to afford compounds **73** and **74** in 10% and 60% yields respectively (Scheme 1.6). Chlorinated compound **75** was also isolated in small quantities.[57]

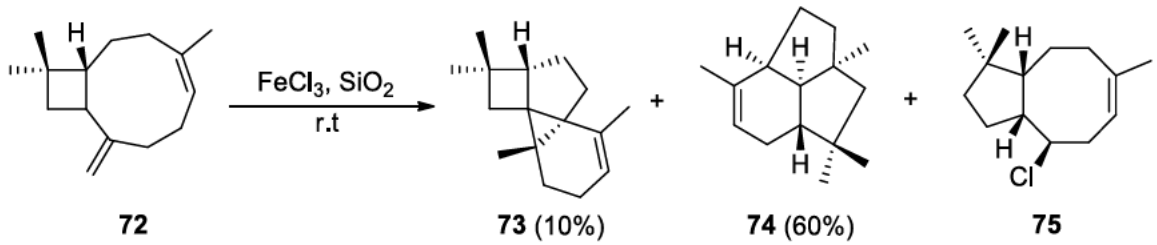

Scheme 1.6. *Cationic rearrangement products of isocaryophyllene **72** in the presence of $FeCl_3$.*

Alkenes can be hydroxylated using a variety of techniques, such as oxymercuration. The difference in reactivity between the endocyclic and exocyclic alkenes of caryophyllenes allows for selective reactivity of one alkene over the other. Oxymercuration and reductive demercuration of β-caryophyllene **58** afforded a mixture of compounds consisting of β-panasinsene **76**, clove-2-ene **63**, caryophyllene-4,8-oxides **77** and **78**, caryolan-1-ol **62**, caryophyllen-4-ols **79** and **80** (Scheme 1.7).[58]

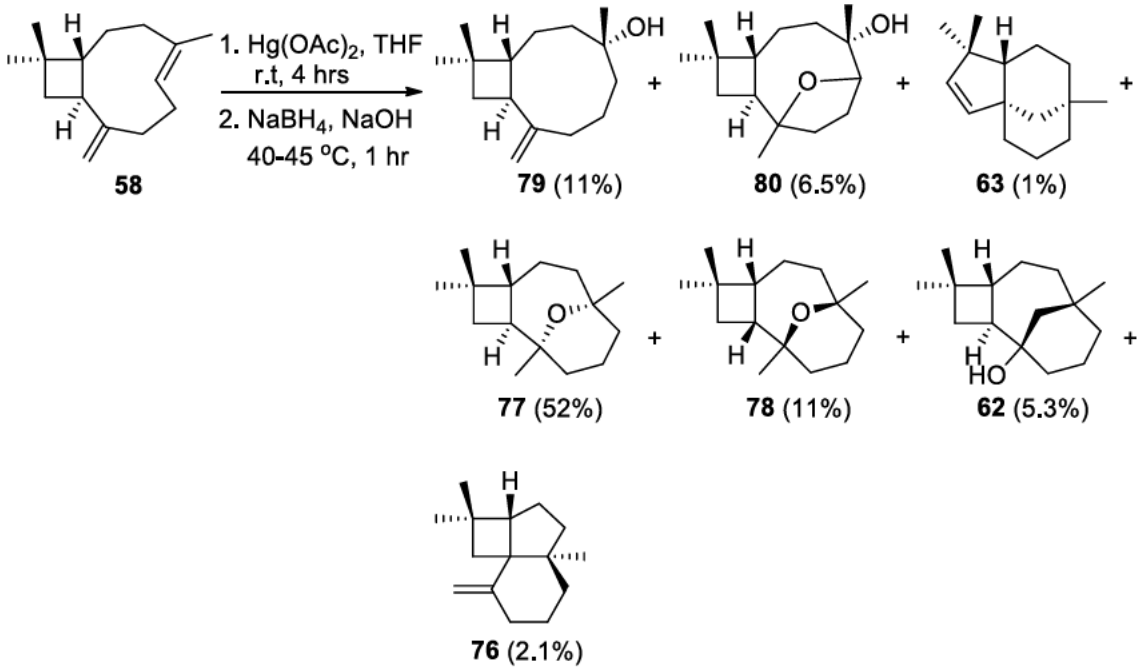

Scheme 1.7. *Mercuration-reductive mercuration of β-caryophyllene **58**.*

The different reactivities of the endocyclic and exocyclic alkenes of β-caryophyllene **58** similarly allow for epoxidation of either only the endocyclic alkene, or both alkenes.

Treatment of β-caryophyllene **58** with monoperphthalic acid in Et_2O generates 4β,5α-epoxycaryophyll-8(13)-ene **81** and 4α,5β-epoxycaryophyll-8(13)-ene **82** (Scheme 1.8).[59]

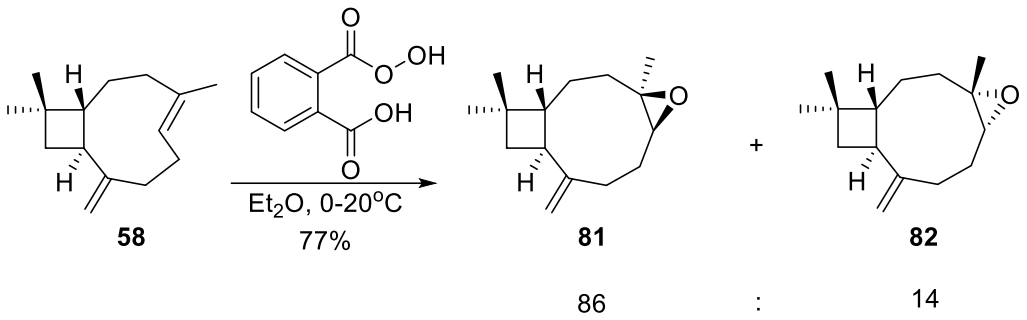

Scheme 1.8. *Epoxidation of β-caryophyllene **58** using monoperphthalic acid.*

Similar to the parent molecule β-caryophyllene **58**, treatment of caryophyllene oxide **81** using a Brønsted-Lowry or Lewis acid can result in a variety of structural rearrangements occurring. Treatment of caryophyllene oxide **81** using H_2SO_4 in Et_2O primarily afforded cloven-2β, 9α-ol **83** along with nine other products (Scheme 1.8).[54]

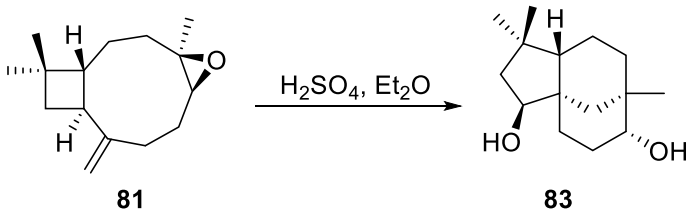

Scheme 1.9. *Cationic rearrangement of caryophyllene oxide **81** in the presence of H_2SO_4.*

Treatment of caryophyllene oxide **81** with tetracyanoethylene (TCNE), a mild Lewis acid, in MeOH afforded 2β-methoxyclovan-9α-ol **84**, along with 4β-methoxycaryophyllen-5α-ol **85** and elimination product **86** (Scheme 1.10).[60]

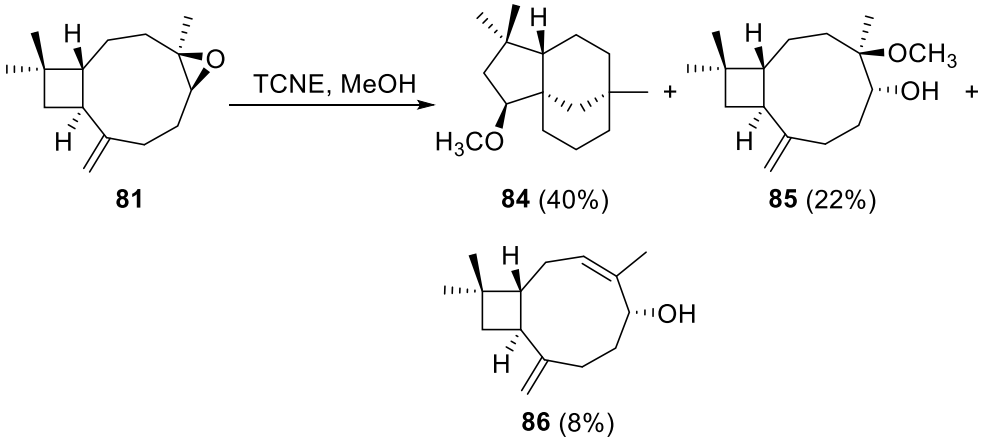

Scheme 1.10. *Cationic rearrangement of caryophyllene oxide* ***81*** *in the presence of TCNE in MeOH.*

Caryophyllene oxide **81** can be converted into kobusone **87** through ozonolysis of the exocyclic alkene, as reported by Amigo *et al*. (Scheme 1.11).[61]

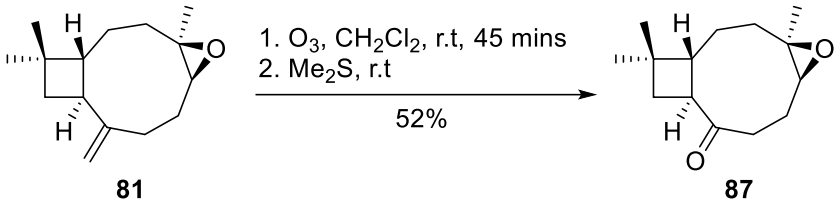

Scheme 1.11. *Ozonolysis of caryophyllene oxide* ***81***.

Caryophyllene oxide **81** is remarkably stable under basic conditions, but kobusone **87** rearranges under strongly basic conditions. Amigo *et al*. reported that the treatment of kobusone **87** with boiling methanolic KOH affords compounds **88** and **89** in 66% and 14% yields respectively (Scheme 1.12).[61]

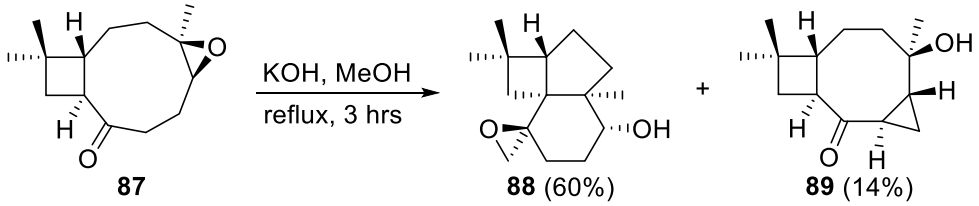

Scheme 1.12. *Base catalysed rearrangement of kobusone* ***87*** *in the presence of KOH.*

Thermal rearrangements of β-caryophyllene **58** have also been previously explored. Ohloff *et al.* reported that the pyrolysis at >240 ºC of β-caryophyllene **58** afforded isocaryophyllene **72** in 82% yield (Scheme 1.13).[62] It is proposed that the structural change occurred via multiple [3+3] sigmatropic rearrangements (Cope rearrangements) of the 1,5-diene (Scheme 1.13).

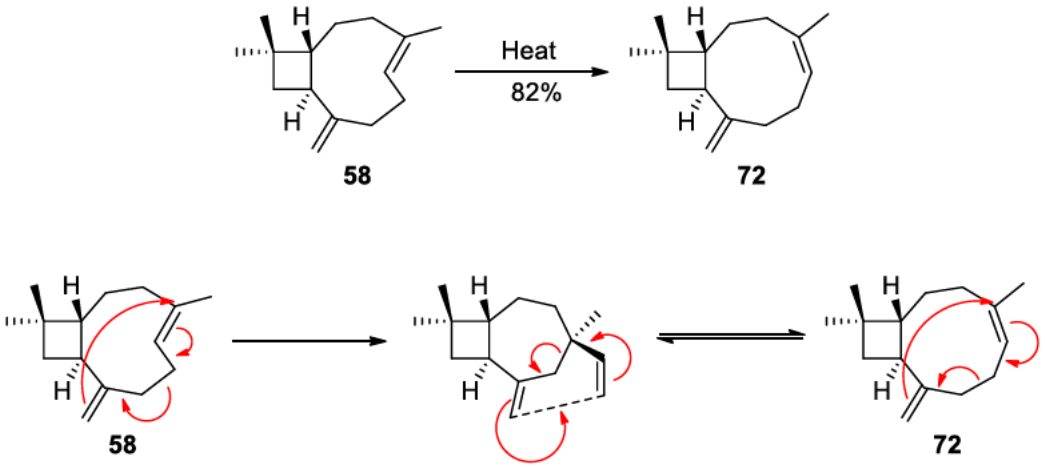

Scheme 1.13. *Thermal rearrangement of β-caryophyllene* ***58****.*

The biological activity of hydrocarbons can be modified and potentially improved through the addition of heteroatoms such as nitrogen or sulfur.[63] The reduction of azides to amines is a commonly used method for the introduction of amines into molecules. Karimov *et al.* reported the late stage azidation of caryophyllene oxide **81** using $Fe(OAc)_2$ and 1-azido-1,2-benziodoxol-3(1*H*)-one **90** to afford 8-azidocaryophyllene oxide **91** (Scheme 1.14).[64] Catalytic hydrogenation of the azide with Pd/C as the catalyst afforded 8-aminocaryophyllene oxide **92**.[64]

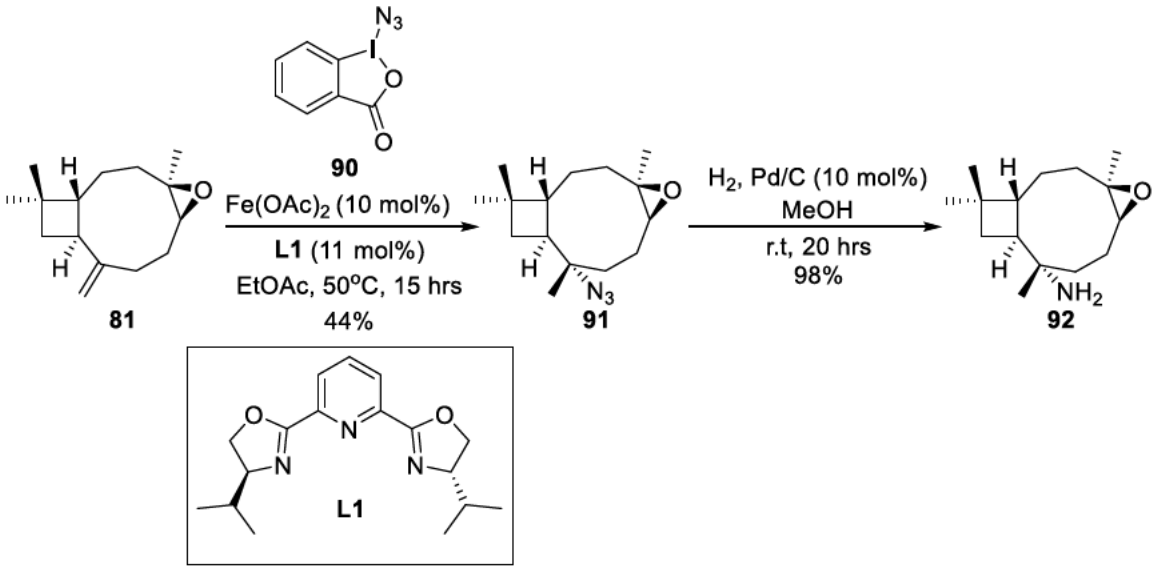

Scheme 1.14. *Prepataion of 8-aminocaryophyllene oxide* ***92*** *from caryophyllene oxide* ***81****.*

Nitrogen can also be introduced into molecules through a condensation reaction of a ketone with an amine or hydroxylamine to form an imine or oxime. Gyrdymova *et al.* synthesised the oxime of kobusone **87**, by condensation of kobusone **87** with $NH_2OH{\cdot}HCl$ (Scheme

1.15).[65] The condensation afforded the expected oxime **93** and two additional epoxide ring opened products **94** and **95** (Scheme 1.15).

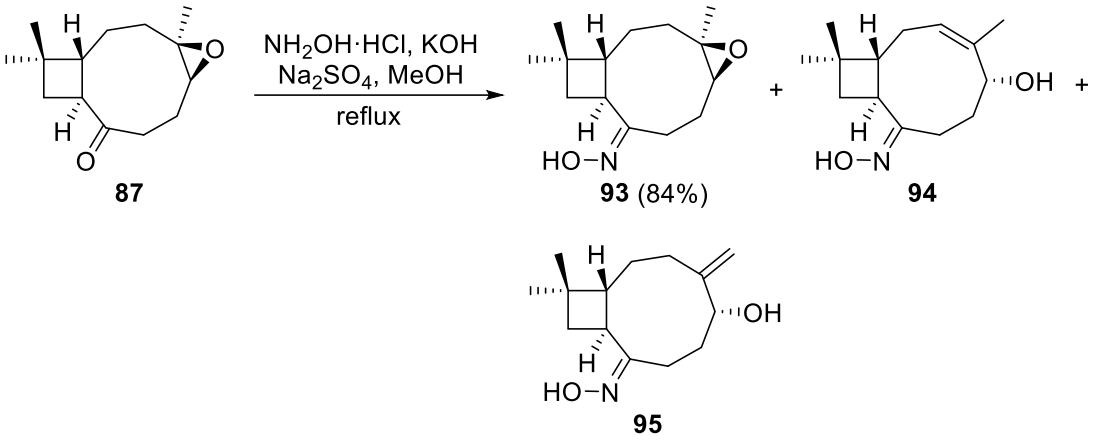

Scheme 1.15. *Oximation of kobusone **87** using $NH_2OH.HCl$.*

Sulfur can also be integrated into caryophyllene scaffolds in the form of sulfides and thiols. Saiz-Urra *et al.* reported the $BF_3{\cdot}Et_2O$ catalysed one pot rearrangement and nucleophilic addition of ethane-1,2-dithiol to caryophyllene oxide **81** to generate the thiol **96** (Scheme 1.16).[66]

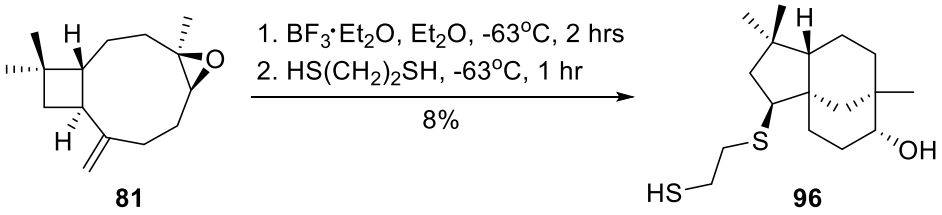

Scheme 1.16. *Lewis acid catalysed one pot formation of thiol **96**.*

The incorporation of thiols can be similarly accomplished through the use of thiols as a nucleophile in 1,4-conjugate additions with α,β-unsaturated carbonyl systems, such as enones. Gyrdymova *et al.* explored the incorporation of thiols via 1,4-conjugate additions using betulenone **97**. Betulenone **97** was prepared in two steps from caryophyllene oxide **81**. Firstly, an elimination using LDA in THF to afford allylic alcohol **98**, followed by a TEMPO oxidation to generate the betulenone **97** (Scheme 1.17).[67] The addition of different thiol compounds was then facilitated using Cs_2CO_3 and TBAI to afford the target sulfides **99**-**105** (Scheme 1.18).[67]

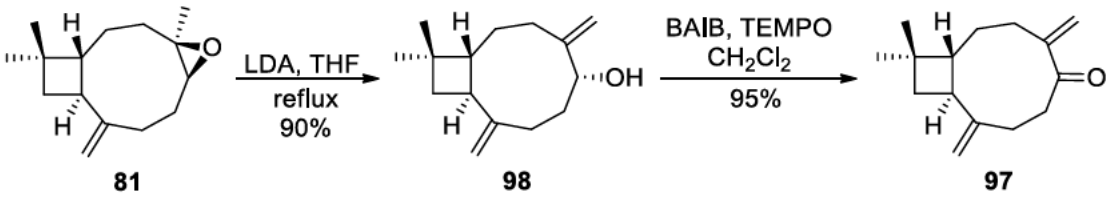

Scheme 1.17. *Preparation of betulenone* ***97*** *from caryophyllene oxide* ***81****.*

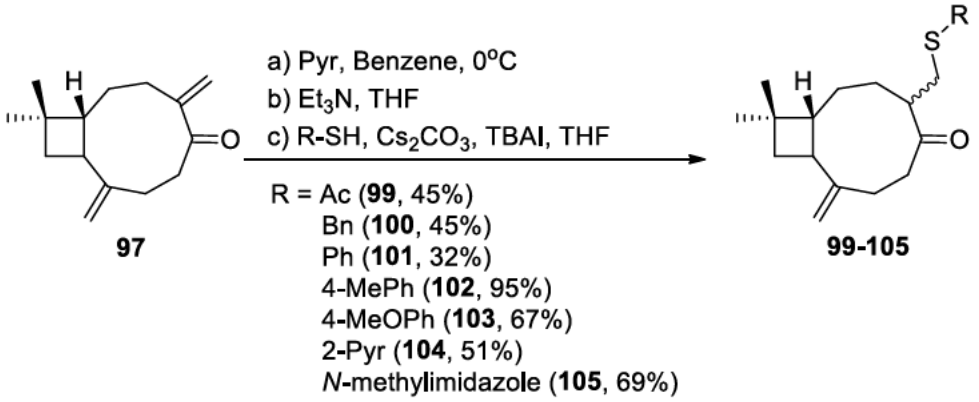

Scheme 1.18. *Preparation of sulfides* ***99-105*** *from betulenone* ***97****.*

The strained endocyclic alkene of β-caryophyllene **58** can act as a dienophile that participates in pericyclic reactions, including Diels-Alder reactions. Lam *et al.* used β-caryophyllene **58** as a dienophile for the biomimetic synthesis of hyperjapones B and D, **106** and **107**. (Scheme 1.19).[68]

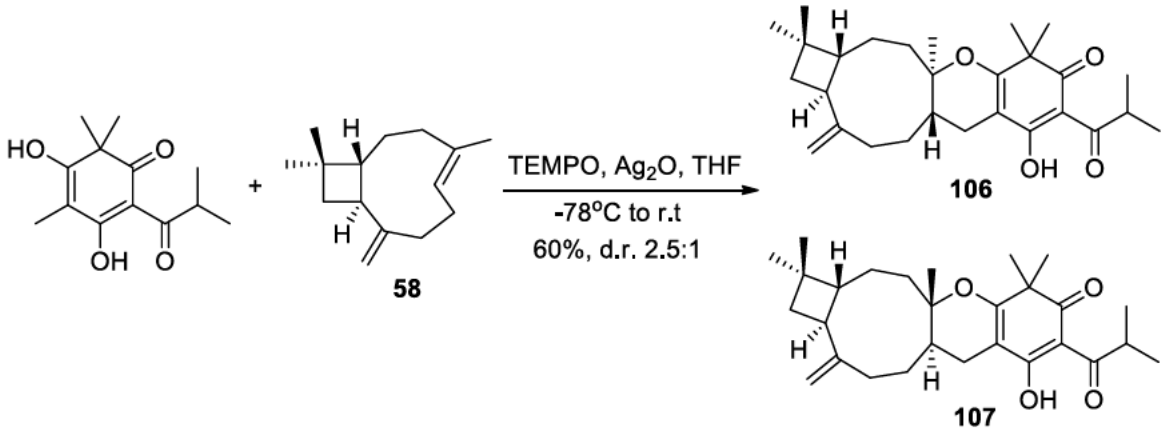

Scheme 1.19. *Biomimetic synthesis of hyperjapones B and D,* ***106*** *and* ***107****.*

Similarly, Wu *et al.* reported the use of hydroxylated β-caryophyllene **108** as a handle for tetrazine ligation for the labelling of proteins (Scheme 1.20).[69]

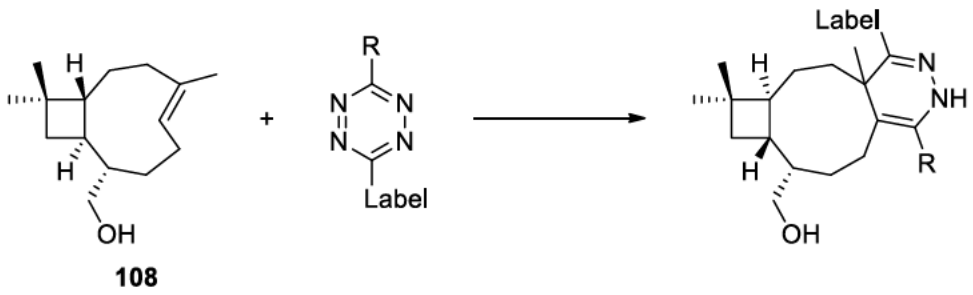

Scheme 1.20. *Tetrazine ligation of 13-hydroxy-β-caryophyllene* ***108****.*

Despite the extensive body of literature exploring the chemistry of β-caryophyllene **58**, very limited work has been conducted on the chemistry of 6-hydroxycaryophyllenes beyond simple esterification reactions. Clericuzio *et al.* esterified 6-hydroxycaryophyllene **1** using BzCl to generate the benzoate **109** (Scheme 1.21).[48a]

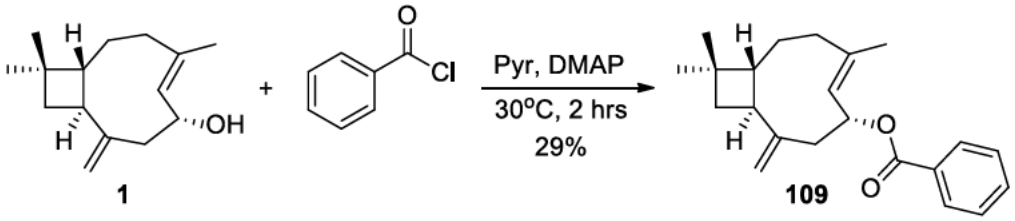

Scheme 1.21. *Benzoylation of 6-hydroxycaryophyllene* ***1****.*

1.6 Project aims

Aim 1

The natural products composition of *S. crassifolia* and other plants in the Goodeniaceae family will be explored:

- The natural products composition of *S. crassifolia* isolated from a coastal environment will be determined for comparison to plants growing on the grounds of Curtin University, Bentley campus.
- The natural products composition of other plants in the Goodeniaceae family will then be explored, with a particular focus on *Scaevola* species (Figure 1.30). Compounds of particular interest will include highly functionalised or oxygenated natural products, or compounds that could act as potential chromophores for FTIR and Raman spectroscopy.

Aim 2

The next part of the project will explore the use of vibrational spectroscopy to investigate the biosynthesis of natural products. The distribution of natural product chromophores will

be mapped used FTIR and confocal Raman microscopy in plant tissue, including the leaves, stem and roots. Mapping will initially be conducted using plant leaves, because leaves are a renewable part of the plant that can be collected without long term harm to the plant.

- A method for the preparation of plant tissue for spectroscopic mapping will first be developed, including investigation of various factors such as thickness of plant tissue sections, types of embedding media and viability of tissue fixation methods (Figure 1.30).
- Once a sample preparation has been developed, initial spectroscopic mapping will then be conducted using model 6-hydroxycaryophyllenes as the spectroscopic marker in *S. crassifolia*, because the strained endocyclic alkene has been reported as a unique spectroscopic marker in Raman spectra.[70]
- The surface leaf resin will be mapped first, because it will contain the highest caryophyllene concentration.
- After successful mapping of the surface leaf resin, the internal plant tissue will then be mapped in an attempt to map the distribution of caryophyllenes at a sub-micromolar spatial resolution (Figure 1.30).

Aim 3

In parallel, the biosynthesis of natural products will be mimicked in synthetic chemistry:

- The transformation of β-caryophyllene **58** into a variety of natural products has been extensively explored, but limited work has been conducted on the transformation of 6-hydroxycaryophyllenes. Rearrangements of 6-hydroxycaryophyllenes will be explored through exposure to acidic and basic conditions and/or oxidative conditions to explore how 6-hydroxycaryophyllenes may transform under a variety of abiotic conditions into other existing natural products (Figure 1.30).
- The biosynthesis of additional isolated natural products, such as flavonoids, will be similarly explored to investigate the impact of abiotic factors on natural products (Figure 1.30).

Aim 4

Finally, the chemistry of 6-hydroxycaryophyllenes will be further explored with the intention of developing unique molecular scaffolds for use in medicinal chemistry:

- The chemistry of 6-hydroxycaryophyllenes has been largely neglected, so a large number of areas are available for exploration within this class of compounds.
    - The chemistry of the *endo*- and *exo*cyclic alkenes will be further explored, such as structural rearrangements under acidic and basic conditions, or oxidation of the alkenes (Figure 1.30).
    - The pericyclic chemistry of the endocyclic alkene of 6-hydroxycaryophyllenes will also be investigated further, such as the Diels-Alder chemistry or use as a dipolarophile.
    - Oxidation of the allylic hydroxyl group would afford an α,β-unsaturated ketone which could be used for 1,4-conjugate additions or as a dienophile in hetero Diels-Alder reactions (Figure 1.30).
- Novel compounds that are synthesised in sufficient quantities will be sent for biological testing against a variety of targets, including Human African Trypanosomiasis (HAT) and malaria.

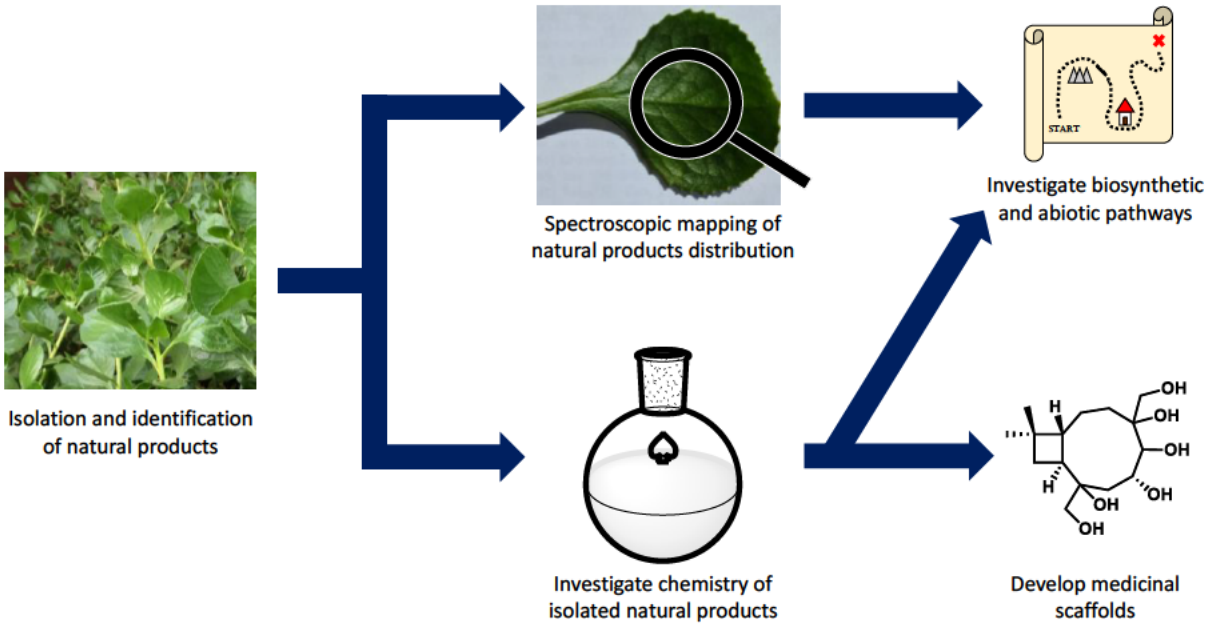

Figure 1.30. *Project aims for the PhD study.*

Chapter 2
Isolation and identification of natural products from Western Australian plants

S. crassifolia afforded interesting compounds, so the natural products composition of other plants in the Goodeniaceae family were screened to determine if other viable chromophores or unique scaffolds similar to caryophyllenes could be isolated. The aerial parts of *Scaevola striata*, *Scaevola caliptera*, *Scaevola nitida "*Aussie Spirit", *Scaevola aemula*, and *G. varia* were analysed. The plants were obtained from Kings Park (botanic garden) plant sales and Bunnings.

2.1 Scaevola nitida "Aussie Spirit"

S. nitida "Aussie Spirit" is a shrub native to Western Australia. It is typically found along coastal regions in Perth, Peel, the Wheatbelt and the South-West. The plant can grow to be between 0.3 and 3.0 m in height. The shrub typically flowers from August to December and the colours of the flowers range from blue to purple (Figure 2.1).[71]

Figure 2.1. S. nitida *"Aussie Spirit" growing in Perth, Western Australia.*

S. nitida "Aussie Spirit" was purchased from Bunnings and cultivated in Perth from March 2019 to January 2021. Fresh leaves were collected directly from the plant and steeped in diethyl ether for 20 minutes. The ether extract was filtered to remove detritus and the filtrate was concentrated under reduced pressure to afford a yellow powder-like solid in 0.64% w/w yield. The ^{1}H NMR spectrum of the crude solid showed multiple compounds. The poor solubility of the crude solid in $CDCl_3$ suggested that trituration could be used for purification. A portion of the crude extract was triturated with methanol to afford a white solid in 0.37% w/w yield. The FTIR spectrum contained a broad absorbance at 3424 cm^{-1}, which was characteristic of an alcohol and a strong carbonyl peak at 1687 cm^{-1}, which indicated the presence of a carboxylic acid. The ^{13}C NMR spectrum contained at least 30 signals. A signal at 180.5 ppm indicated the presence of a carboxylic acid and the two signals at 126.2 and 139.8 ppm suggested that the compound contained an alkene. The ^{1}H NMR spectrum contained a vinylic triplet at 5.52 ppm and seven signals at 1.27, 1.26, 1.09, 1.05, 1.03, 0.98 and 0.92 ppm, which was characteristic of a triterpene. The vinylic signal integrated for 1H, which, along with the multiplicity, indicated the presence of a trisubstituted alkene. A multiplet at 3.48 ppm that integrated for 1H suggested that the compound contained a secondary alcohol. The doublets at 0.98 and 1.03 ppm each integrated for 3H, meaning that the molecule contained two secondary methyl groups. The HMBC and COSY spectra indicated that the two secondary methyl groups were adjacent to each other. The FTIR, ^{1}H, ^{13}C, and 2D NMR spectra indicated that the compound was ursolic acid **110** and the NMR data was consistent with the literature (Figure 2.2).[72]

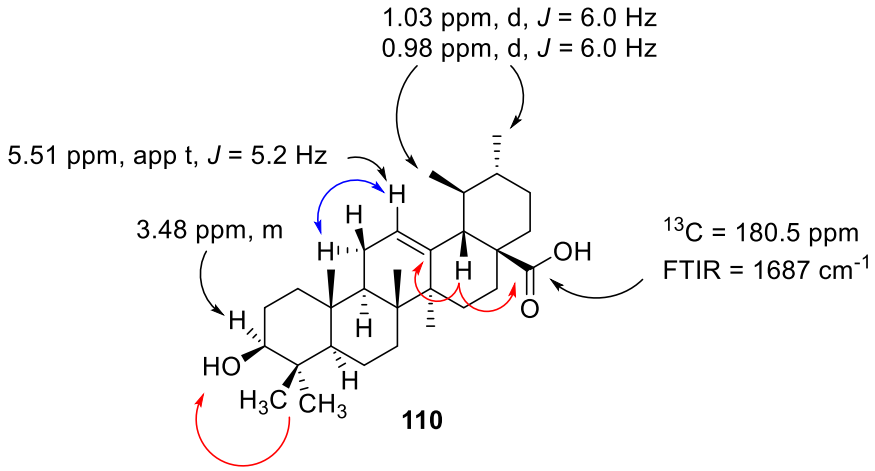

Figure 2.2. *Analysis of ursolic acid* ***110****. Red lines are HMBC correlations. Blue lines are COSY correlations.*

The methanol soluble component was concentrated under reduced pressure to afford a yellow-white oil in 0.27% w/w yield. The crude oil was purified by column chromatography to afford two compounds. The first was afforded as a white, waxy solid in 0.17% yield. The ^{1}H NMR spectrum was consistent with that of ursolic acid that has been previously isolated from the plant. The second compound was afforded as a yellow oil in 0.07% yield.

The ^{13}C NMR spectrum contained 23 signals. The molecular formula was confirmed by HRMS as having exact mass of 425.1786 *m/z* which was consistent with the $[M+H]^{+}$ molecular ion of $C_{22}H_{40}O_6$. The FTIR spectrum showed a broad stretch at 3401 cm^{-1}, which was characteristic of an alcohol, and a carbonyl stretch at 1732 cm^{-1} that was indicative of an ester. The ^{1}H NMR spectrum showed a singlet and a triplet at 5.06 and 5.34 ppm, respectively, that each integrated for 1H, which were indicative of the presence of alkenes in the compound. Three singlets at 1.60, 1.63 and 1.67 ppm each integrated for 3H each, which indicated the presence of three methyls in the compound. The two vinylic signals in combination with three methyl signals above 1.50 ppm was similar to the ^{1}H NMR spectrum of α-bisabolol, reported by Cerceau *et al*.[73] Six signals between 3.0 and 5.0 ppm that each integrated for 1H indicated the presence of hydrogens adjacent to an oxygen, and the high number of signals suggested that a sugar was attached to the molecule. The carbon signal at 94.4 ppm confirmed the presence of a sugar, as the chemical shift between 90-100 ppm was characteristic of the anomeric carbon of a sugar. The signal at 82.6 ppm correlated to a quaternary carbon and could be attributed to the tertiary alcohol of α-bisabolol. However, the tertiary alcohol was likely forming a glycosidic bond with the sugar in this molecule. The other five signals were present between 60 and 100 ppm in the ^{13}C NMR spectrum, which indicated that the compound was likely a pentose. The signal for the anomeric carbon correlated to the quaternary carbon of α-bisabolol in the HMBC spectrum, indicating that the glycosidic bond was formed by the anomeric alcohol. Analysis of the coupling constants between the protons of the sugar indicated that the sugar was likely D-ribofuranose, and the sugar was attached to α-bisabolol by a β-glycosidic linkage. A singlet at 2.12 ppm in the ^{1} integrated for 3H, which was characteristic of an acetate. The acetate was likely bonded to the exocyclic hydroxymethyl of the D-ribofuranose, because the other hydroxyl groups were likely to be too sterically hindered. Analysis of the FTIR, ^{1}H, ^{13}C, COSY, HSQC and HMBC NMR spectra allowed the sugar to be tentatively assigned as α-bisabolol β-D-ribofuranose **111** (Figure 2.3).

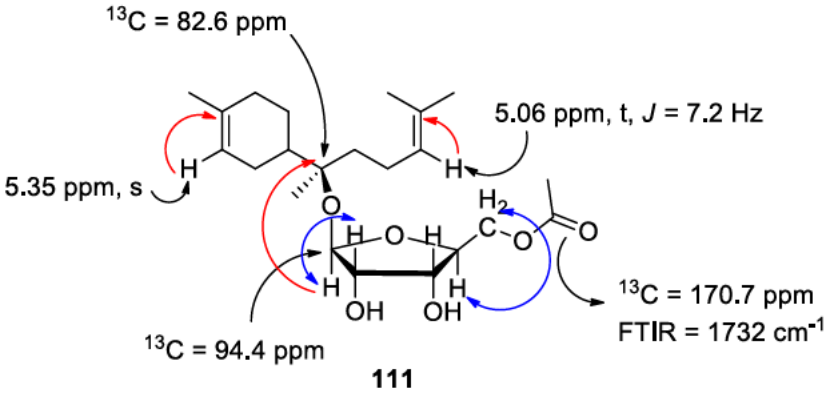

Figure 2.3. *Analysis of α-bisabolol β-D-ribofuranose **111**. Red lines are HMBC correlations. Blue lines are COSY correlations.*

Other glycosides of α-bisabolol have been synthesised by Piochon *et al.*, but the ^{13}C NMR spectral data for α-bisabolol β-D-ribofuranose **111** was not consistent with the ^{13}C NMR values reported for α-bisabolol β-D-fucopyranose **112** or α-bisabolol β-D-xylopyranose **113** (Figure 2.4).[74] Therefore, it appears that α-bisabolol β-D-ribofuranose **111** has not been previously reported by Piochon and no matches were observed using databases such as SciFinder.

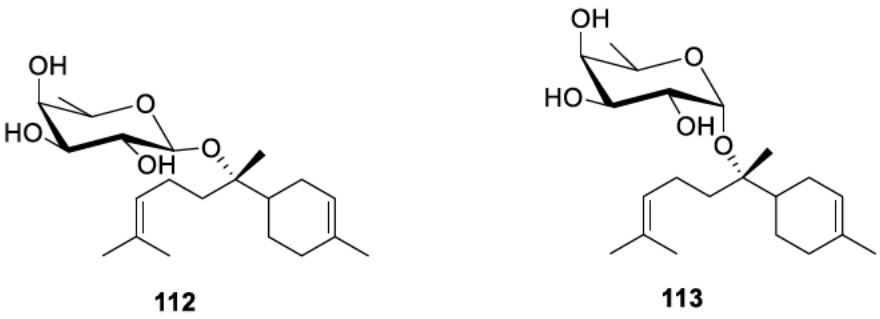

Figure 2.4. *Structures of α-bisabolol β-D-fucopyranose **112** and α-bisabolol β-D-xylopyranose **113**.*

Ribose glycosides are rare relative to other sugars such as glucose and galactose, but have been previously isolated. Shao *et al.* and Wang *et al.* both isolated triterpene ribose glycosides from *Clematis chinensis* and *Anemone hupehensis* respectively (Figure 2.5).[75].

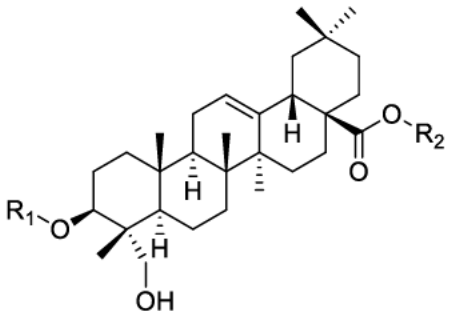

Saponin 114: R_1 = rib(1-->3)rha(1-->2)ara
R_2 = rha(1-->4)glu(1-->6)glu(1-->3)rha(1-->4)glu(1-->6)glu
Saponin 115: R_1 = rib(1-->3)rha(1-->2)ara
R_2 = glu(1-->6)rha(1-->4)glu(1-->6)glu(1-->3)rha(1-->4)glu(1-->6)glu

Figure 2.5. *Examples of triterpene saponins,* ***114*** *and* ***115****, isolated by Wang et al. from* Anemone hupehensis.[75b]

2.2 Scaevola striata

S. striata is a shrub native to Western Australia and is typically found in the Perth, Peel, South-West and Great Southern regions. It grows to up 0.3 m in height and is found in sand, sandplains and ridges, and swampy areas. Its flowers range in colour from blue to purple and it normally flowers between August and December (Figure 2.6).[76]

Figure 2.6. Scaevola striata *growing in Perth, Western Australia.*

S. striata was purchased from Kings Park and cultivated in Perth, Western Australia from March 2019 to January 2021. Fresh leaves were collected directly from the plant and steeped in Et_2O for 20 minutes. The ether extract was filtered to remove detritus and the filtrate was concentrated under reduced pressure to afford a white, waxy oil in a 0.15% w/w yield. The ^1H NMR spectrum indicated that the oil was primarily composed of one compound. The crude oil was purified by flash chromatography to afford a white, waxy oil.

The ^{1}H NMR spectrum was consistent with that of ursolic acid **110**, which had been previously isolated from *S. nitida* "Aussie Spirit" (Figure 2.7).

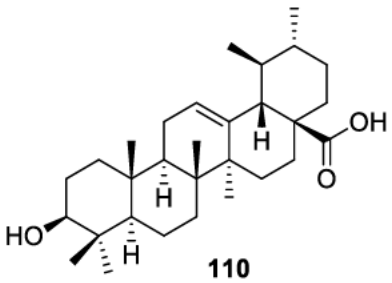

110

Figure 2.7. *Structure of ursolic acid* ***110****.*

2.3 Scaevola caliptera

S.caliptera is a shrub similar in appearance to *S. striata* commonly found in the Perth, Peel, South-West and Great Southern regions. It grows to between 0.1 and 0.4 m in height and is found in sand, lateritic ridges and sandplains. It flowers from September to December or January and the colours of the flowers range from blue to purple (Figure 2.8).[77]

Figure 2.8. S. caliptera *growing in Perth, Western Australia.*

S. caliptera was purchased from Kings Park and cultivated in Perth from March 2019 to January 2021. Fresh leaves were collected directly from the plant and steeped in Et_2O for 20 minutes. The ether extract was filtered to remove detritus and the filtrate was concentrated under reduced pressure to afford a white waxy oil in 0.17% w/w yield. The ^{1}H NMR spectrum indicated that the oil was primarily composed of one compound. The primary compound in the ^{1}H NMR spectrum had signals consistent with that of ursolic acid **111**. The presence of a vinylic triplet at 5.29 ppm next to the ursolic acid triplet at 5.25 ppm in a 1:2 ratio indicated that another triterpene was also present in the mixture. The vinylic triplet at 5.25 ppm and the doublet at 2.82 ppm that each integrated for 1H were

characteristic of oleanolic acid **116** (Figure 2.9).[78] Ursolic acid **110** and oleanolic acid **116** have been found together in many plants [79]

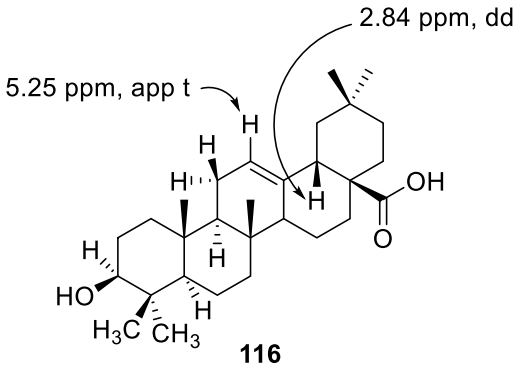

Figure 2.9. *Analysis of oleanolic acid* ***116.***

2.4 Scaevola aemula

S. aemula, commonly known as the Fairy Fan-flower, is a low-lying shrub native to southern Australia, including Western Australia, South Australia, New South Wales and Victoria. Several cultivars of *S. aemula* exist, but in general the plants do not exceed 0.5 m in height. They typically have blue, white or purple flowers that bloom from August to December or January to March (Figure 2.10). *S. aemula*, *S. aemula* Purple Fandancer and *S. aemula* Mauve Clusters are all cultivars of *S. aemula* and the natural products compositions of the surface leaf resin was analysed for each plant. [80]

Figure 2.10. S. aemula *growing in Perth, Western Australia.*

S. aemula was purchased from Bunnings and cultivated in Perth from March 2019 to July 2021. Fresh leaves were collected directly from the plant and steeped in Et_2O for 20 mins. The ether extract was filtered to remove detritus and the filtrate was concentrated under

reduced pressure to afford a white waxy oil in 0.25% yield. The ^{1}H NMR spectrum of the crude oil indicated that the oil contained several different compounds and further purification was required. The presence of multiple signals between 3 and 5 ppm indicated that glycosides were likely present in the oil. The crude oil was partitioned into neutrals, carboxylic acids and phenols.

The neutrals fraction was purified by column chromatography to afford a white solid in 11% yield of the neutrals mass. The ^{1}H NMR indicated that it contained a mixture of triterpenes, including ursolic acid **110** and oleanolic acid **116**, which had been previously isolated from other *Scaevola* species. Similarly, purification of the phenols fraction by column chromatography afforded a mixture of ursolic and oleanolic acid. The carboxylic acids fraction was afforded as a complex mixture and was not purified further.

S. aemula "Bondi Blue" was purchased from Bunnings and cultivated in Perth from September 2019 to August 2020. Fresh leaves were collected directly from the plant and steeped in Et_2O for 20 mins. The ether extract was filtered to remove detritus and the filtrate was concentrated under reduced pressure to afford a white waxy oil in 0.09% yield. The ^{1}H NMR spectrum of the crude oil indicated that multiple compounds were present, including ursolic acid **110**. However, the lack of signals between 3-5 ppm suggested that fewer glycosides were present on the leaves.

S. aemula "Purple Fandancer" was purchased from Bunnings and cultivated in Perth from September 2019 to January 2021 (Figure 2.11). Fresh leaves were collected directly from the plant and steeped in Et_2O for 20 mins. The ether extract was filtered to remove detritus and the filtrate was concentrated under reduced pressure to afford a white waxy oil in 0.10% yield. The ^{1}H NMR spectrum of the crude oil was similar to that of *S. aemula "*Bondi Blue" and indicated that multiple compounds were present, including ursolic acid **110** and oleanolic acid **116**. The spectrum was almost identical to that of "Bondi Blue", with some variation in the relative quantity of some compounds.

Figure 2.11. S. aemula *"Purple Fandancer" growing in Perth, Western Australia.*

2.5 Scaevola albida "White Carpet"

S. albida "White Carpet" is a cultivar of *Scaevola albida* and is a low-lying shrub that closely resembles *S. aemula*. *S. albida* is commonly found in Queensland, New South Wales, Victoria and Tasmania.[81] It is a ground cover plant that grows between 0.1 to 0.2 m in height. It typically flowers in spring or early summer with small white flowers (Figure 2.12).[4a]

Figure 2.12. S. albida "*White Carpet" growing in Perth, Western Australia.*

*S. albida "*White Carpet" was purchased from Bunnings and cultivated in Perth from March 2019 to July 2021. Fresh leaves were collected directly from the plant and steeped in Et_2O for 20 minutes. The ether extract was filtered to remove detritus and the filtrate was concentrated under reduced pressure to afford a yellow powder-like solid in 0.26% yield. The ^{1}H NMR spectrum of the crude oil was almost identical to that of *S. aemula*, containing a multitude of compounds. The crude oil was purified by column chromatography to afford a white solid. The ^{1}H NMR indicated that it was a mixture of ursolic acid **110** and oleanolic acid **116** like that found in *Scaevola aemula*.

S. aemula and *S. albida* "White Carpet" both had a similar leaf shape and size, with the primary difference being that *Scaevola aemula* had purple flowers while *S. albida* White Carpet had white flowers. The similarity in the leaf shape and size seemed to be reflected in the natural products composition of the leaf surfaces (Figure 2.13).

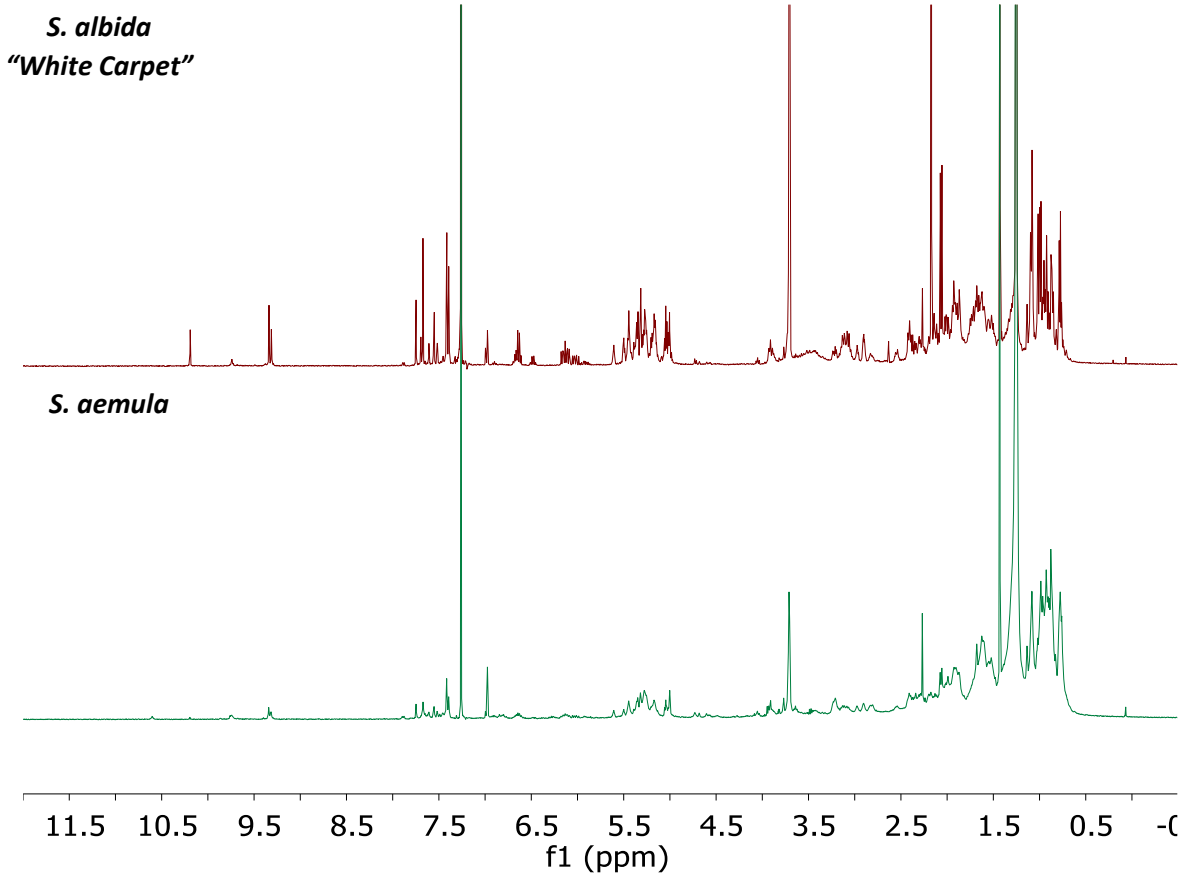

Figure 2.13. *^{1}H NMR spectra of* Scaevola aemula *and* Scaevola albida *"White Carpet".*

In contrast, the leaf shape and size of *Scaevola aemula "*Bondi Blue" and *Scaevola aemula "*Purple Fandancer" were similar to each other, but differed significantly from that of *Scaevola aemula* and *Scaevola albida* "White Carpet". The natural product composition of

"Bondi Blue" and "Purple Fandancer" reflected this difference, containing primarily triterpenes with a substantially reduced quantity of glycosides visible in the ^{1}H NMR spectra (Figure 2.14). Therefore, differences in the leaf shape and size of plant species or cultivars have a greater impact on the natural products composition of the plant leaves than differences in the flower colour.

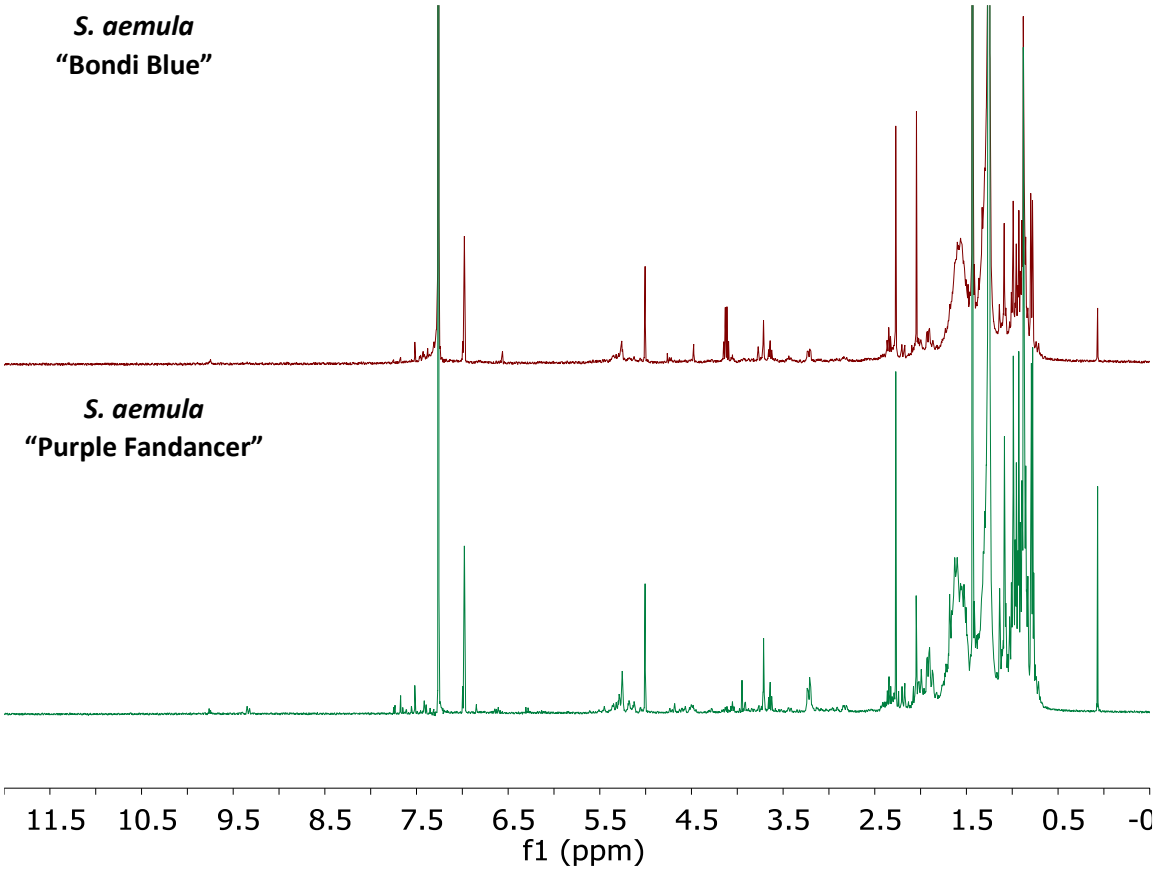

Figure 2.14. *^{1}H NMR spectra of* S. aemula *"Bondi Blue" and* S. aemula *"Purple Fandancer".*

2.6 Goodenia varia

G. varia is a shrub native to southern Western Australia. It is typically found along coastal cliffs, in sand and in sand dunes. The plant can grow to a height of 1.0 m and has yellow flowers that bloom from October to November (Figure 2.15).[82] *G. varia* has been reported to have been used by First Nations people for medicinal purposes. Mothers used the leaves of the plant to put their children to sleep on long journeys. The leaves of the plant were rubbed on the fingers and under the fingernails of the children, so when the children sucked on their fingers, they would fall asleep, allowing them to be carried more easily.[4a]

Figure 2.15. G. varia *growing in Perth, Western Australia.*

G. varia was purchased from Kings Park and cultivated in Perth from March 2019 to July 2021. Fresh leaves were collected directly from the plant and steeped in Et_2O for 20 minutes. The ether extract was filtered to remove detritus and the filtrate was concentrated under reduced pressure to afford a white solid in 1.5% yield. The ^{1}H NMR spectrum of the crude product contained multiple products. The presence of signals between 5.00 and 6.00 ppm and indicated the presence of vinylic hydrogens and signals located between 3.00 and 4.50 ppm suggested that polar functional groups were present in the compounds. The crude solid was triturated with ethyl acetate to afford an off-white solid. The ^{1}H NMR of the solid was consistent with that of ursolic acid **110**.

The filtrate was then partitioned using acid-base chemistry to separate the components of the crude extract into carboxylic acids, phenols and neutral compounds. The ^{1}H NMR spectrum of the carboxylic acids fraction indicated that one main compound **117** was present in reasonably high purity. Further purification would provide greater clarity, but purification of carboxylic acids using silica gel flash chromatography can result in significant yield loss due to acid-base interactions between carboxylic acids and silica gel. To minimise yield loss, the carboxylic acids fraction was esterified using diazomethane to afford the methyl ester **118** which would act as a protected carboxylic acid.

Diazomethane is a selective method of generating methyl esters from carboxylic acids. Other esterification methods, such as using MeI, possess selectivity issues if the compound contains other nucleophilic functional groups such as amines or alcohols that can be methylated. Diazomethane can be generated through decomposition of *N*-nitroso-*N*-methylurea in the presence of a strong base like KOH in Et_2O. Upon addition to the

carboxylic acid, the carboxylic acid esterified following the mechanism shown in Scheme 2.1.

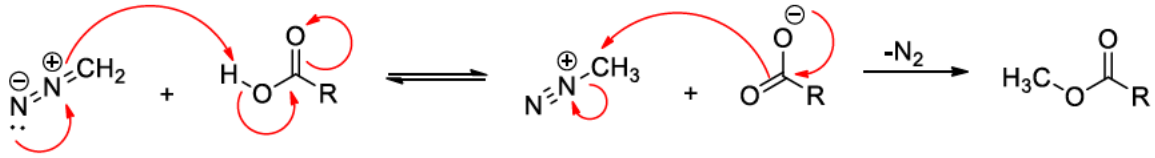

Scheme 2.1. *Mechanism of esterification using diazomethane.*

The methyl ester was purified by flash chromatography to afford the pure methyl ester in 17% yield as a colourless oil. The ^{1}H NMR spectrum of the pure oil showed the characteristic methyl ester singlet at 3.68 ppm that integrated for 3H, indicating that the esterification was successful and the starting material had contained a carboxylic acid. The FTIR spectrum showed a broad stretch at 3437 cm^{-1} that is characteristic of –OH stretching and overlapping carbonyl stretches at 1736 and 1752 cm^{-1}, which is characteristic of ester carbonyl stretching. The ^{13}C NMR spectrum contained 24 signals, indicating that the compound had 23 carbons excluding the methyl from the methyl ester. The compound was therefore likely a functionalised diterpene. The presence of two quaternary signals at 166.8 and 167.2 ppm indicated that the compound contained two ester carbonyls, including the known methyl ester. A singlet at 3.38 ppm integrated for 2H and in the HMBC spectrum correlated only to the two ester carbonyl signals. Similarly, the methyl ester singlet at 3.75 ppm correlated with both ester carbonyl signals in the HMBC spectrum, suggesting that a malonate ester was present in the molecule. Two methylene signals at 68.5 and 68.8 ppm indicated that the methylenes were bonded to oxygen. Two doublets at 3.96 and 4.35 ppm each integrated for 1H corresponded to the methylene at 68.5 ppm. Therefore, the signal at 68.8 ppm corresponded to a primary alcohol, as a –OH stretch was present in the FTIR spectrum, and the carboxylic acid had been esterified. The methylene bonded to the malonate ester exhibited an AB splitting pattern, indicating that the methylene hydrogens were diastereotopic. Two singlets in the ^{1}H NMR spectrum at 0.75 and 0.95 ppm each integrated for 3H, which was characteristic of methyl groups. The HSQC and HMBC spectra indicated that the methyl at 0.95 ppm and the methylene bonded to the malonate ester were both bonded to the same quaternary carbon at 37.5 ppm (Figure 2.16).

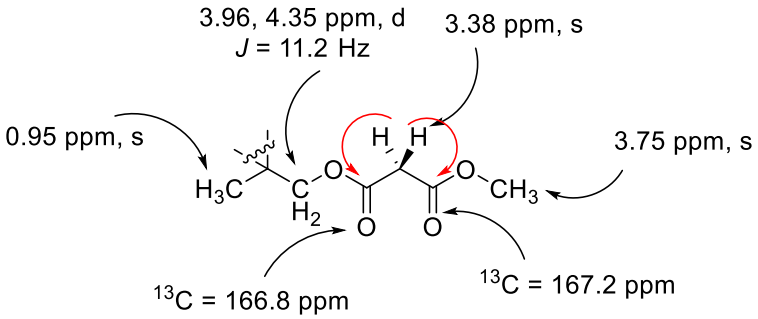

Figure 2.16. *Analysis of malonate component of compound* ***118****.*

Two signals at 132.2 and 137.1 ppm in the ^{13}C NMR spectrum were characteristic of vinylic carbons. Two doublets at 5.51 and 5.72 ppm in the ^{1}H NMR spectrum that each integrated for 1H and correlated to the signals at 132.2 and 137.1 ppm respectively in the HSQC spectrum suggested that the compound contained a di-substituted alkene. Both vinylic hydrogens correlated to multiple other carbon signals in the HMBC spectrum, indicating that it was an endocyclic alkene. The HSQC and HMBC spectra suggested that the primary alcohol was in close proximity of the alkene. The molecular formula was confirmed by HRMS as having an exact mass of 405.2631 *m/z* which was consistent with the $[M+H]^+$ molecular ion of $C_{24}H_{36}O_5$, which indicated that the compound had seven degrees of unsaturation. The alkene and two ester carbonyl groups accounted for three degrees of unsaturation, indicating that the compound contained four rings. Based on the ^{1}H NMR, ^{13}C NMR and FTIR spectra, the compound was tentatively assigned as *ent*-17-hydroxybeyer-15-ene methyl malonate **118** (Figure 2.17).

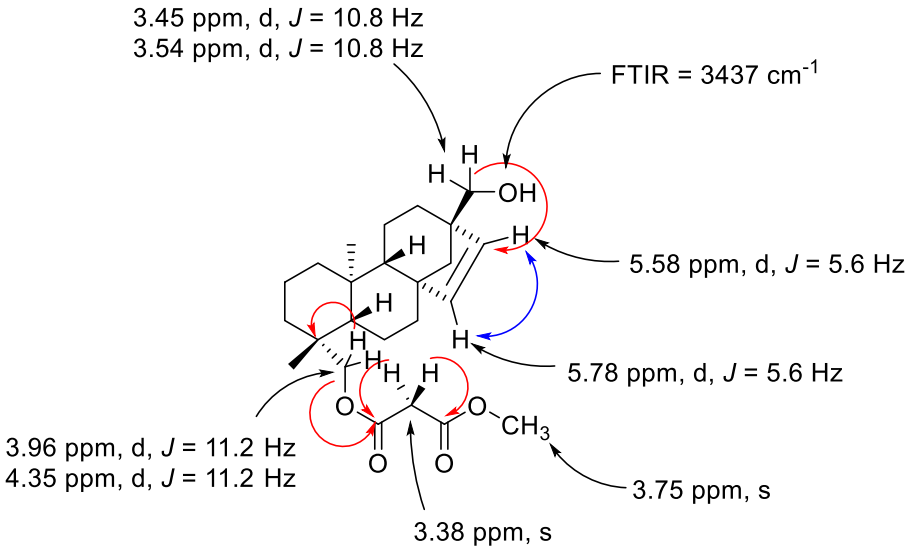

118

Figure 2.17. *Analysis of malonate ester beyerene* ***118****. Red lines are HMBC correlations. Blue lines are COSY correlations.*

The structure of the precursor malonic acid ester of beyerene **117** could then characterised based on the structural information from beyerene **118** (Figure 2.18). The stereochemistry of the malonic acid ester was confirmed through a comparison with the literature. Quaglio *et al*. reported the *S* configuration of the malonic acid ester of erythroxylol A **119** and the spectral data of the malonic acid moiety differed from that of proposed malonic acid ester beyerene **117 (**Figures 2.18 and 2.19**).**[83] Malonate esters occur less frequently in nature than succinate esters, so the occurrence of the malonic acid ester is intriguing and may serve a biological purpose.

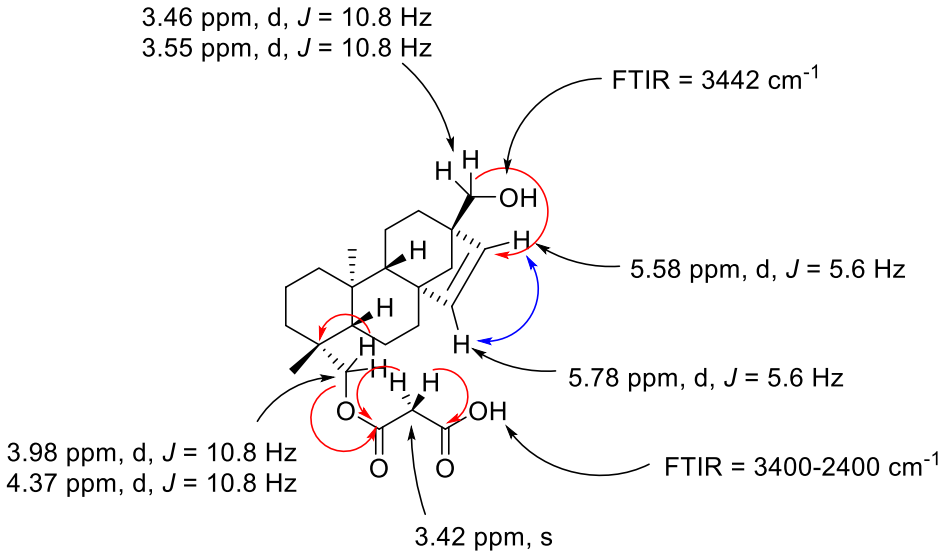

Figure 2.18. *Analysis of malonic acid ester beyerene* ***117****. Red lines are HMBC correlations. Blue lines are COSY correlations.*

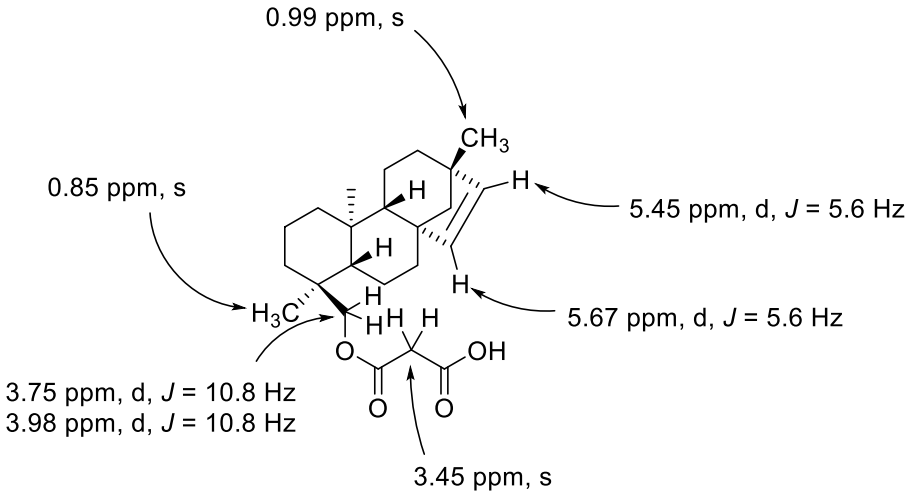

119

Figure 2.19. *Analysis of erthroxylol A malonic acid ester* ***119*** *synthesised by Quaglio et al.*

The neutrals fraction was purified by flash chromatography to afford four different compounds. The first compound was isolated as a colourless oil. The ^{13}C NMR spectrum contained 22 signals. The molecular formula was confirmed by HRMS as having an exact mass of 347.2581 *m/z*, which was consistent with the $[M+H]^+$ molecular ion of $C_{22}H_{34}O_3$. The ^{1}H NMR spectrum was similar to that of the beyerene **118**, except the malonate ester signals were absent. An extra singlet at 2.03 ppm was also present that integrated for 3H. The FTIR spectrum showed a two overlapping ester carbonyl peaks at 1720 and 1737 cm^{-1}, and a broad absorbance at 3414 cm^{-1}, characteristic of an alcohol. The spectral signals were consistent with an acetate group bonded to a methylene (CH_2OCOCH_3). The HMBC showed that the methyl group at 2.03 ppm was attached to the carbonyl carbon, confirming the presence of an acetate. The HMBC spectrum showed that methylene bonded to the acetate was attached to the same quaternary carbon as the methyl signal at 0.94 ppm. A combination of FTIR, ^{1}H NMR and ^{13}C NMR spectroscopy suggested that compound **120** was the acetate analogue of beyerene **117** (Figure 2.20). Acetate beyerene **120** has not been previously identified.

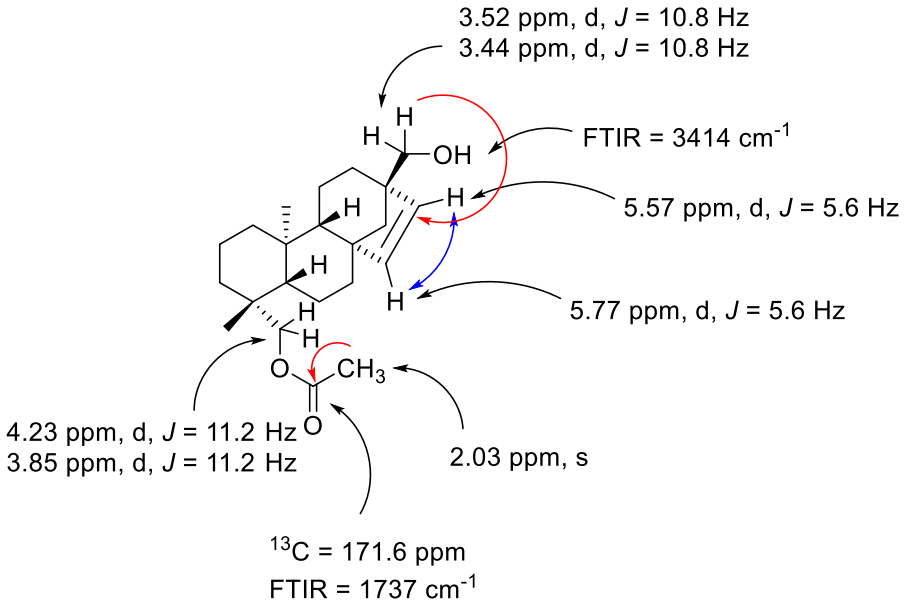

Figure 2.20. *Analysis of acetate beyerene* ***120****. Red lines are HMBC correlations. Blue lines are COSY correlations.*

The next compound was isolated as a white solid. The ^{13}C NMR spectrum contained 20 carbon signals. The molecular formula was confirmed by HRMS as having an exact mass of 305.2471 *m/z* which was consistent with the $[M+H]^+$ molecular ion of $C_{20}H_{32}O_2$. The FTIR spectrum showed a broad absorbance at 3363 cm^{-1} which is characteristic of an alcohol, and no carbonyl peaks were visible in the spectrum. The ^1H NMR spectrum looked similar to that of beyerenes **118** and **120**, except the signals associated with the malonate ester or acetate were absent. An AB splitting pattern at 3.44 and 3.77 ppm indicated the presence of a primary alcohol adjacent to an asymmetric centre. The HMBC spectrum showed that the methylene of the primary alcohol was bonded to the same quaternary carbon as the methyl at 0.97 ppm. A combination of FTIR, ^1H NMR and ^{13}C NMR spectroscopy suggested that compound **121** was the diol derivative of beyerenes **117** and **122** (Figure 2.21). Abad *et al*. reported the synthesis of the enantiomer of the proposed structure for beyerene **122**, erythroxydiol A, showing almost identical NMR shifts.[84] However, the specific rotation reported for erythroxydiol A was -14.0º ($CHCl_3$, 0.7 c), while for beyerene **121** it was +38.7º ($CHCl_3$, 0.9 c), indicating that the diol beyerene **121** was likely the enantiomer of erythroxydiol A. It is worth noting that the diol beyerene **121** is potentially an artefact of isolation produced by hydrolysis of the acetate beyerene **120** or the malonic acid ester beyerene **117**.

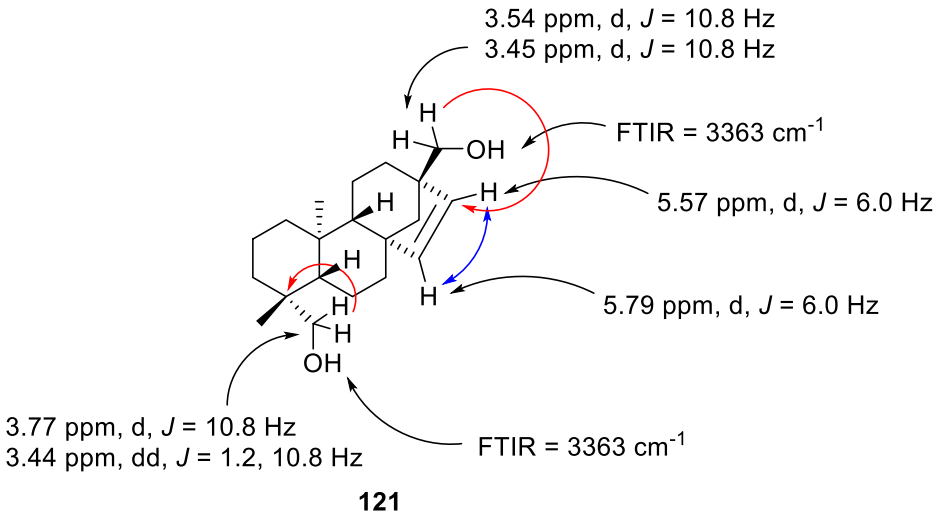

Figure 2.21. *Analysis of diol beyerene* ***121****. Red lines are HMBC correlations. Blue lines are COSY correlations.*

A mixture of two compounds was isolated from the column chromatography and further chromatography afforded two products. Sufficient material could only be isolated from the column for ^{1}H NMR spectroscopy and HRMS. Compound **122** was isolated as a colourless oil. The FTIR spectrum showed a broad absorbance at 3357 cm^{-1} that was characteristic of an alcohol. The molecular formula was confirmed by HRMS as having an exact mass of 289.2524 *m/z* which was consistent with the $[M+H]^{+}$ molecular ion of $C_{20}H_{32}O$. The ^{1}H NMR spectrum was similar to that of diol beyerene **121**. One AB splitting pattern, characteristic of a primary alcohol, was absent and an extra methyl group was present. An AB splitting pattern at 3.77 and 3.44 ppm was similar to that of the typical C19 hydroxyl group, suggesting that the C17 hydroxyl group was absent. The extra methyl group is likely in the C17 position instead. The compound was tentatively assigned as erthyroxylol A **122** (Figure 2.22).[85]

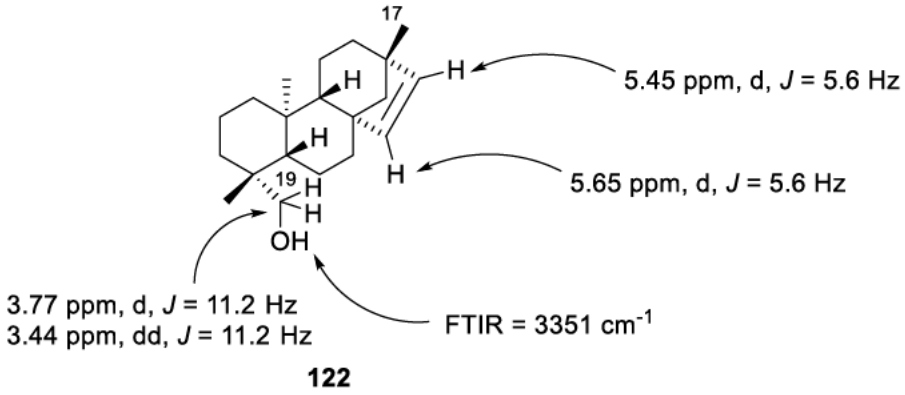

Figure 2.22. *Analysis of erthyroxylol A* ***122****.*

Compound **123** was also isolated as a colourless oil. The FTIR spectrum showed a broad absorbance between 3400 cm^{-1} and 2400 cm^{-1}, and a carbonyl stretch at 1692 cm^{-1}, which were characteristic of a carboxylic acid. The molecular formula was confirmed by HRMS as having an exact mass of 303.2319 *m/z*, which was consistent with the $[M+H]^+$ molecular ion of $C_{20}H_{30}O_2$. The ^1H NMR spectrum was similar to erthyroxylol A **122**, except the doublet signals of the primary alcohol were absent. Based on the ^1H NMR and FTIR spectra the compound was tentatively assigned as *ent*-beyer-15-en-19-oic acid **123** (Figure 2.22). The ^1H NMR data was confirmed by a comparison of the ^1H NMR data to the compound isolated by Tennakoon *et al.*[85]

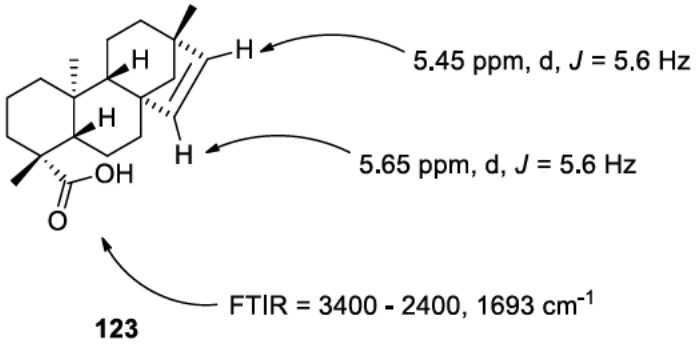

Figure 2.23. *Analysis of* ent*-beyer-15-en-19-oic acid* ***123****.*

The ^1H NMR spectrum of the crude phenols fractions showed a mixture of compounds, with at least two major products. The phenols fraction was purified by flash chromatography to afford the major product compound **124** as a colourless oil. The FTIR spectrum showed a broad absorbance spectrum at 3371 cm^{-1} that extended to 2400 cm^{-1}, indicating the presence of a carboxylic acid and potentially an alcohol. A carbonyl peak at 1692 cm^{-1} further supported the presence of a carboxylic acid. The ^{13}C NMR spectrum

contained 20 carbon signals. The molecular formula was confirmed by HRMS as having an exact mass of 319.2269 *m/z* which was consistent with the $[M+H]^+$ molecular ion of $C_{20}H_{30}O_3$. The ^1H NMR spectrum was similar to that of beyerenes **120** and **123**. Only one set of doublet signals was present between 3.0 and 4.0 ppm, indicating that either the C17 or C19 primary alcohol was absent. Two singlets at 0.68 and 1.25 ppm that each integrated for 3H showed that only two methyl signals were present in the molecule. The absence of a third methyl signal suggested that neither the C17 or C19 positions were a methyl like in beyerenes **122** and **123**. A signal at 68.8 ppm in the ^{13}C NMR and DEPT135 spectra confirmed the presence of a primary alcohol. The HSQC and HMBC spectra showed that the primary alcohol was in close proximity to the endocyclic alkene, indicating that the alcohol was in the C17 position. The HMBC spectrum showed that the methyl at 1.25 ppm correlated to the carboxylic acid carbonyl signal at 183.7 ppm, suggesting that the carboxylic acid was located in the C19 position. Therefore, based on the FTIR, ^1H and ^{13}C NMR spectroscopic data, the structure was assigned as *ent*-17-hydroxybeyer-15-en-19-oic acid **124** (Figure 2.24). Beyerene **124** has not been previously identified.

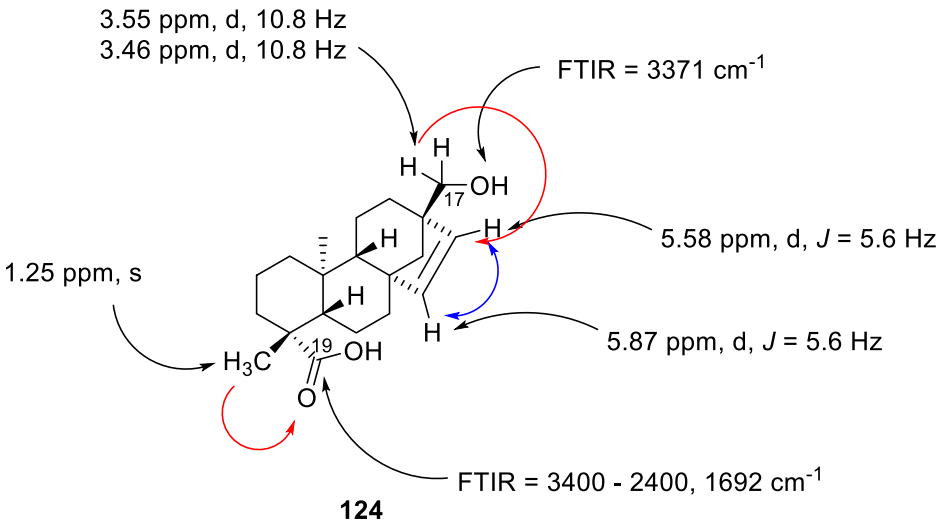

Figure 2.24. *Analysis of* ent*-17-hydroxybeyer-15-en-19-oic acid* ***124****. Red lines are HMBC correlations. Blue lines are COSY correlations.*

2.7 Conclusions

The natural product composition of the leaves of several plants from the *Scaevola* and *Goodenia* genera were investigated. Ursolic acid **110** and oleanolic acid **116** were found in all *Scaevola* and *Goodenia* plants that were investigated, indicating that it was a common compound produced by the plants. The natural product composition of the leaves in *S. aemula* cultivars and *S. albida* was heavily influenced by the leaf shape and size. *S. aemula* and *S. albida* "White Carpet" differed primarily by flower colour, and possessed highly similar natural products compositions. In contrast, *S. aemula* "Bondi Blue" and *S. aemula "*Purple Fandancer", which possessed similar leaves, had leaves of a different shape and size to *S. aemula* and *S. albida* "White Carpet" and this difference was reflected in the natural products composition. The novel glycoside α-bisabolol β-$_D$-ribofuranose **111** was isolated from *S. nitida* "Aussie Spirit". Six *ent*-beyerene species were isolated from the leaf resin of *G. varia* including the three novel compounds beyerenes **117**, **120** and **124**.

Chapter 3
Development and application of vibrational spectroscopic methods to investigate natural products in the leaf surface resin of *Scaevola* and *Dodonaea* species

Vibrational spectroscopic techniques such as FTIR imaging and Raman microscopy have been increasingly used in the plant sciences, particularly to study chemical and biophysical characteristics of biopolymers (e.g., cellulose, lignin). Vibrational spectroscopy techniques are well suited to study biopolymers in the plant sciences as they provide direct, *in situ*, reagent free, and spatially resolved chemical analysis. Such capability allows study of biological molecules in, or as close as possible to, their native state, drastically reducing artefact formation or specimen damage. Despite the immense potential of vibrational spectroscopy for analyses in the plant science, few studies have extended application beyond biopolymers. However, the same capabilities that make vibrational spectroscopy well suited to study biopolymers, also lend the technique to analysis of other chemical components in plant tissues, e.g. natural products on leaf surfaces. This chapters explores the development and application of vibrational spectroscopy methodology for eventual application to natural products in the plant sciences, specifically to study the surface resin of *Scaevola* and *Dodonaea* species.

3.1 General considerations for the preparation of biological samples

The ultimate goal for all bioanalytical analysis is measurement and detection of analytes in the *in vivo* state, with no sample preparation or perturbation of the biological system. Unfortunately, this is almost always unachievable or impractical, and therefore, some form of sample preparation is required prior to analysis. This is particularly true when using various forms of microscopy to analyse biological tissues. The type of sample preparation varies depending on the analysis type and the analyte being investigated. Vibrational microscopy techniques such as FTIR imaging and Raman microscopy are advantageous, as

they can be routinely conducted under ambient conditions and do not require extensive sample preparation, or the addition of reagents to stain the tissue.

Conventionally, sample preparation for optical microscopy analysis involves two main steps: embedding and fixation. Embedding refers to the medium used to hold a specimen in place allowing for sectioning of the specimen. Fixation refers to treatment of the specimen to prevent degradation of the specimen due to factors such as exposure to oxygen, or enzymatic activity. Many fixation techniques involve chemical treatment however, which can lead to artefacts in biological specimens, so chemical fixation was avoided.[33]

A number of embedding media are available for use with plant tissue, including paraffin and polyester waxes, epoxy resins and optimal cutting temperature medium (OCT). Paraffin and polyester wax embedding are common embedding medium, with paraffin wax likely the most common. Wax embedding allows for simultaneous fixation and embedding of the specimen, and greatly simplifies the sectioning process, which can be undertaken with a high degree of precision at room temperature. For example, Santi *et al*. uses paraffin embedding for laser microdissection of grapevine leaves to investigate phloem infected by stolbur.[86] Paraffin embedding poses a number of issues. Paraffin wax is composed of lipophilic long chain hydrocarbons, so a transitional fluid is required to allow penetration into much more hydrophilic biological tissues. Transitional fluids, such as toluene and xylene, can be used, but this may result in leaching of lipophilic compounds from the tissue, including natural products.[87] Paraffin embedding must also be done at high temperatures (60 C) due to the higher melting point of paraffin wax, which would likely cause the degradation of many natural products. Polyester waxes are an alternative to paraffin waxes and are composed of fatty acid esters of polyethylene glycol. Polyester waxes have a lower melting point than paraffin wax (40ºC) and transitional fluids are unnecessary because the wax is soluble in ethanol. However, for both paraffin and polyester wax embedding methods, dehydration of the specimen using ethanol is necessary. Ethanol will solubilise and leach many natural products from plant tissue, and is therefore, unsuitable for investigation of natural products.

Similar to paraffin and polyester waxes, epoxy resins can be used as an embedding medium. Epoxy resins typically consist of three components: an epoxy resin solution, a hardening agent and an accelerator.[87] The epoxy resin consists of an aliphatic or aromatic epoxide. The hardening agent is a reagent that forms a hard cross-linked polymer upon heating. The

accelerator is used to decrease curing times and temperatures. Epoxy resins are commonly used in light and transmission electron microscopy. Many epoxy resins do not require as a transitional solvent and are soluble in ethanol or acetone.[87] However, similar to polyester waxes, the use of a solution of epoxy resin in solvents such as ethanol and acetone will result in leaching of natural products. Consequently, epoxy resins are unsuitable as an embedding medium for the purposes of natural products microscopy. A recent example was seen with McDonald, using epoxy resin embedding for the analysis of cryofixed biological specimens.[88]

OCT is an embedding medium composed of polyvinyl alcohol, polyethylene glycol and other non-reactive ingredients.[89] OCT is used for cryosectioning of specimens, because it solidifies at temperatures below -10ºC, allowing for embedding of the specimen. OCT provides the advantage of not dulling microtome blades and does not leave residue if specimen fixation is required.

Many biological tissues/samples have sufficient thickness to be opaque to the microscopy measurement of choice, which either impedes analysis or degrades image resolution. Therefore, another important consideration with respect to sample preparation for microscopy analysis is the thickness of tissue sections. Plant cells are typically larger than animal cells, ranging from 10 to 100 μm in size. Therefore, section thickness should be below the plant cell size to allow for visualisation of the internal plant cell (e.g. 50 μm).

3.2 Optimisation of sample preparation methods

Preliminary investigation of *S. crassifolia* involved mapping the distribution of natural products in the surface leaf resin as a cross section of the plant. Specimen preparation of *S. crassifolia* leaves was conducted using OCT and a cryomicrotome at -18ºC, because paraffin and polyester wax, and epoxy embedding mediums were unsuitable. The top of the leaves were removed so that the stem and a small part of the leaf body remained (Figure 3.1). The cut leaf was flash frozen using liquid nitrogen and then the stem was embedded in OCT for sectioning. The leaves were flash frozen to ensure the leaves were rigid enough to be sectioned. The whole leaf was not embedded in OCT to ensure that the surface leaf resin remained undisturbed and was not at risk of leaching by OCT. Sections of 10 μm thickness were prepared to allow for visualisation and analysis of the surface leaf resin.

Figure 3.1. S. crassifolia *leaf with top half cut off in preparation for sectioning.*

Flash freezing of *S. crassifolia* leaves in liquid nitrogen and embedding of the stem in OCT was effective for analysis of the surface leaf resin, but was unsuitable for analysis of whole plant cells. Plant cells contain vacuoles that occupy a large volume of the cell. The vacuoles serve several purposes, including storage, waste disposal and maintaining the turgor pressure of the cell. The vacuoles contain large quantities of water and flash freezing of plant tissue causes the water in the cells to freeze. The rapid formation of ice (and associated expansion) causes the cells to rupture, leading to the destruction of the cells upon thawing and loss of the cell structure.[90]

Room temperature sectioning was a potential alternative to cryosectioning, which would prevent ice damage to the plant tissue. Manual sectioning of plant leaves using a razor blade was attempted. Sectioning of the plant leaf was possible, but the section thickness were variable and the inconsistency made the sections unsuitable for use with microscopy analysis. Sectioning at room temperature can also be conducted using a standard microtome. Sectioning leaves without use of an embedding medium was unsuccessful due to the flexibility of the fresh leaves. Traditional embedding media such as paraffin and polyester waxes or epoxy resins are unsuitable for natural products research, so an alternative was required. The Commonwealth Scientific and Industrial Research Organisation (CSIRO) reported a method for the use of carrot as a pseudo-embedding medium for sectioning.[91] Leaf tissue sections were placed within a wedge cut into a section of carrot to hold the leaf in place. The leaf was then sectioned while embedded in the carrot. The sectioning technique was partially successful, but difficulties were encountered due to the difference in rigidity between the carrot and the leaf (Figure 3.2). The leaf was more flexible than the carrot, so would section less effectively than the surrounding carrot. Carrot juice also leeched into the leaf sections, resulting in contamination of the leaf tissue with compounds such as β-carotene.

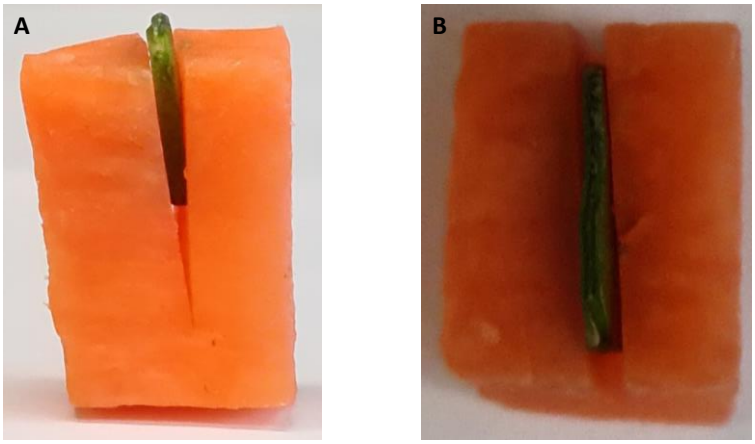

Figure 3.2. S. crassifolia *leaf embedded in a carrot (A-B). (A) Side view and (B) top down view.*

Room temperature sectioning of plant leaves resulted in inconsistent section thickness and contamination, so an alternative method using OCT was explored. A small section of plant leaf was embedded in OCT orthogonal to the chuck and allowed to solidify. Additional layers of OCT are applied to the leaf section until the whole leaf section is embedded in OCT. The layering approach allows for a more gradual cooling of the plant leaf and provides a solid support which reduces the likelihood of the leaf crumbling during sectioning. The thickness of sections greatly impacted the ease of sectioning. Stability of sections of 20 μm or below was low and easily disintegrated upon sectioning. Sections that had a thickness of 30 μm or more were substantially more stable and were sectioned more easily. A thickness of 50 μm provided the most stable sections, but some difficulties were encountered with curling of the tissue sections due to the thickness of the tissue section.

3.3 Investigation of the capability of Raman microscopy for sub-cellular biochemical imaging

Confocal Raman microscopy allows for the non-destructive spectroscopic mapping of biological samples, providing extensive spatially resolved biochemical information. The sub-micron spatial resolution achieved by confocal Raman microscopy is well suited to analysis of the subcellular distribution of biomolecules. The onion epidermis has been used extensively as a plant model in biology and spectroscopy.[92] In particular, onion epidermis has been used as a model specimen for surface enhanced Raman spectroscopy, such as the work by He *et al*. and Palanco *et al*.[92b, 92c] The ease of sample preparation and low

autofluorescence due to lack of chlorophyll makes the onion epidermis the ideal candidate for procedure development and validation.

The onion epidermis was manually peeled from fresh white onions using forceps and was directly applied to a glass microscope slide for analysis by confocal Raman microscopy. A green excitation wavelength of 532 nm was utilised, because it is highly advantageous for biological samples with the Raman scattering strength increasing as a function of the fourth power of laser frequency. The pectin C-O-C skeletal mode was detected with confocal Raman mapping at 856 cm^{-1}, revealing that pectin was primarily localised within the cell walls (Figure 3.3).[70] The symmetric ring breathing mode of tryptophan was also observed at 1457 cm^{-1} in highly localised regions, suggesting that there may be tryptophan enriched regions, such as in proteins, in the onion epidermal cells (Figure 3.3).[70] Imaging of the pectin and tryptophan distribution in the white onion epidermal cells successfully demonstrated that spectral mapping at a sub-micron spatial resolution using confocal Raman microscopy was viable.

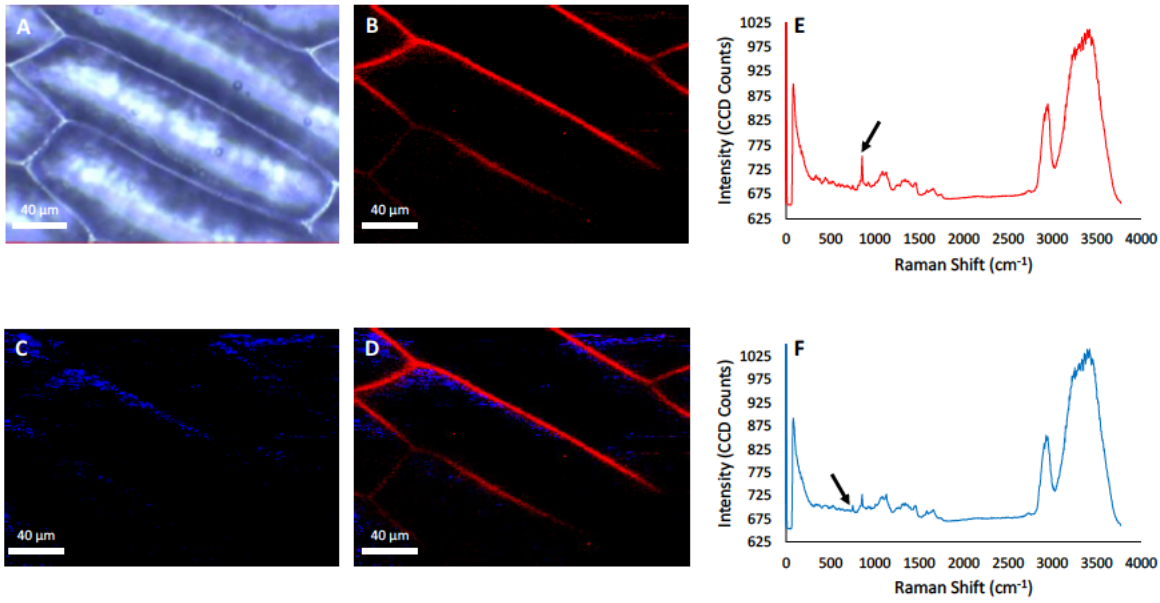

Figure 3.3. *Raman spectroscopic imaging (A-D) of white onion epidermal cells. (A) Bright field image of white onion epidermal cells, (B) Raman spectroscopic map of the pectin distribution (area under the curve skeletal C-O-C stretching band centred at 856 cm^{-1}), (C) Raman spectroscopic map of the tryptophan distribution (area under the curve ring breathing mode, centred at 753 cm^{-1}), (D) Composite Raman spectroscopic map of pectin and tryptophan distribution, (E) Representative Raman spectrum of pectin, (F) Representative Raman spectrum of fatty tryptophan. Black arrows indicate key peaks. Scale bars are 40 µm.*

3.4 Preliminary investigation of spectroscopic markers of natural products using vibrational spectroscopy

Raman spectroscopic markers for natural products found on the surface of the leaves of a variety of plants were investigated. The surface of *S. crassifolia* leaves were analysed first, due to the presence of high quantities of caryophyllenes. Schulz *et al*. reported that the caryophyllene strained alkene C=C stretching band was visible at 1671 cm^{-1} in Raman spectra along with the exocyclic alkene C=C stretching band at 1632 cm^{-1}.[70] The 1671 cm^{-1} C=C stretching band would then be suitable as a Raman spectroscopic marker, because it is suitably removed from the carbonyl region at ~1700 cm^{-1} and the standard alkene C=C region at 1630 cm^{-1}.[70]

The green 532 nm excitation was used again for analysis. Autofluorescence poses a significant issue for excitation wavelengths in the green colour range (514.5 to 550.0 nm). Chlorophyll, phenols and a variety of other compounds fluoresce in the green colour range, resulting in the occurrence of significant autofluorescence. This was most obvious when attempting to analyse the leaf surface of *S. crassifolia.* Attempts at minimising autofluorescence were made, and are described separately in Section 3.8. Very few distinct peaks were visible in the Raman spectrum due to the overwhelming autofluorescence. However, some peaks were visible at 1522, 1158 and 1007 cm^{-1}, which corresponded to C=C stretching, C-C stretching and C-C in-plane rocking, respectively, of carotenoids (Figure 3.4).[70] Carotenoids are a type of tetraterpene, with more than 1100 different compounds reported to date.[93] They are commonly found as pigments in a variety of plants and fungi, with the most well-known example being β-carotene **125** (Figure 3.5). The strained alkene signal of caryophyllenes was not visible in the Raman spectrum collected directly from the surface of intact leaves, due to autofluorescence from endogenous fluorophores, so direct imaging of the leaf surface was not a viable detection method.

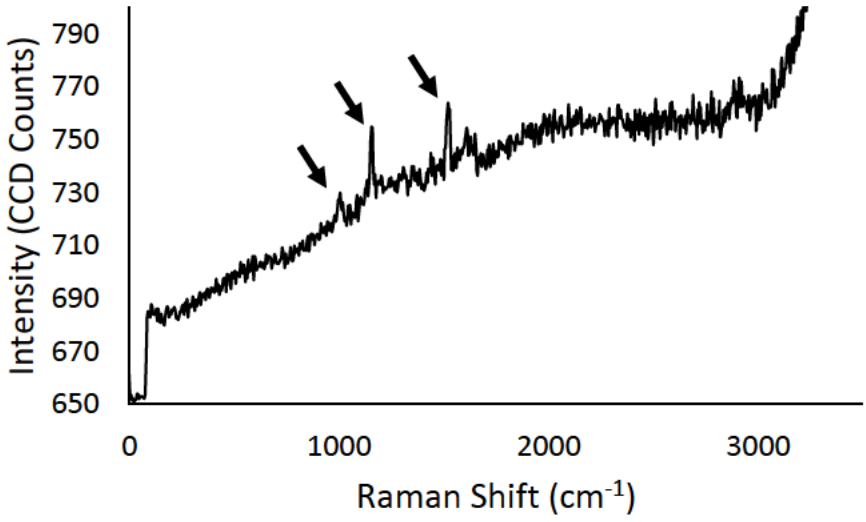

Figure 3.4. *Representative Raman spectrum of* S. crassifolia *leaf surface. Carotenoid peaks indicated by black arrows.*

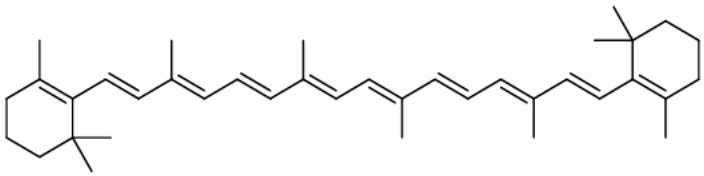

125

Figure 3.5. *Structure of β-carotene* ***125****.*

In addition to caryophyllenes, furans are another potential Raman spectroscopic marker of natural products in *Dodonaea* species. Kim *et al*. analysed a variety of furan species, including furan **126**, furfuryl alcohol **127** and hydroxymethylfurfural **128**, using Raman spectroscopy (Figure 3.6).[94] A strong signal at 1500 cm^{-1}, associated with the $C_1=C_2/C_3=C_4$ stretching was visible, which was a viable Raman spectroscopic marker that was removed from carbonyl stretching and typical alkene C=C stretching bands.

126 **127** **128**

Figure 3.6*. Structures of furan* ***126****, furfuryl alcohol* ***127*** *and hydroxymethylfurfural* ***128****.*

Analysis of the leaf surfaces with confocal Raman microscopy of *D. viscosa* subsp *angustissima* and *D. viscosa* subsp *purpurea* revealed similar peaks to that of *S. crassifolia* (Figure 3.7). The carotenoid peaks at approximately 1520, 1160 and 1005 cm^{-1} indicated

that carotenoids are found in plants in both genera and in sufficient quantities to exhibit a Raman scattering effect despite the autofluorescence.

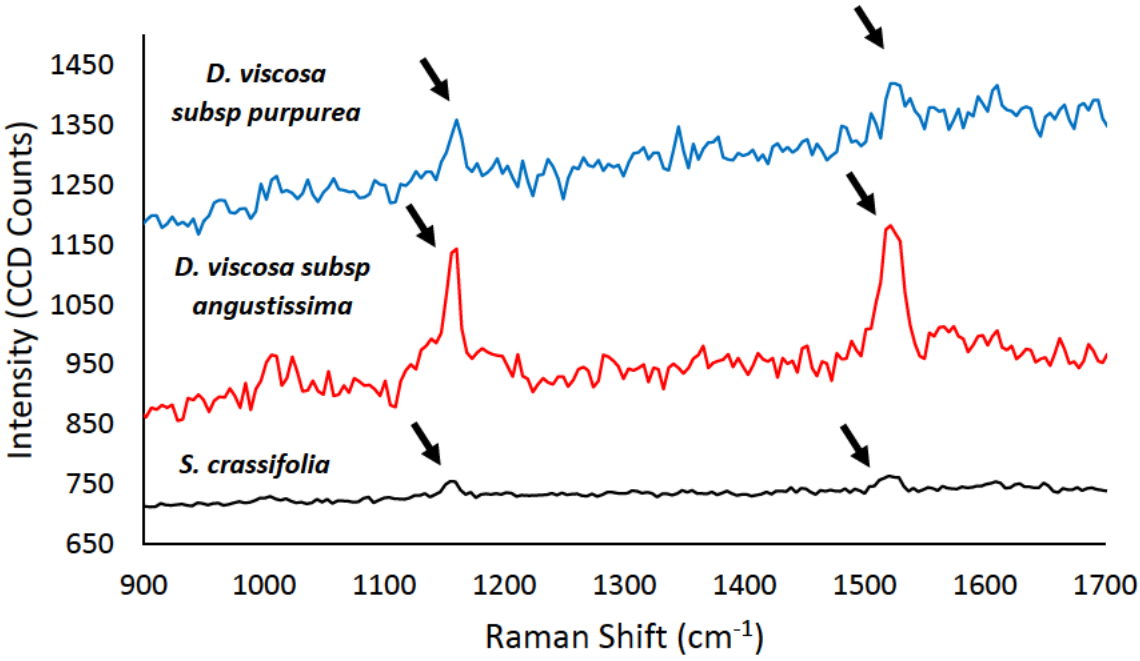

Figure 3.7. *Representative Raman spectra of* S. crassifolia, D. viscosa *subsp* angustissima *and* D. viscosa *subsp* pupurea *leaf surfaces. Black arrows indicate key peaks.*

Unfortunately, due to autofluorescence and strong carotenoid signals, natural products could not directly be imaged on the surface of plant leaves. However, an alternate method for the specific detection of caryophyllenes in the surface leaf resin of *S. crassifolia* was developed; this method was to specifically image caryophllenes in thin sections of leaf tissue, where the outside resin layer has been preserved. This is described in Section 3.5.

3.5 Raman spectroscoping imaging of caryophyllenes

Efforts to map the distribution of caryophyllenes through direct imaging of the leaf surface of *S. crassifolia* were explored. However, the key issue is the presence of chlorophyll within the plant cells, which contributed to the bulk of the autofluorescence. Spectroscopic mapping of a leaf section where the leaf resin had remained intact would allow for spectroscopic mapping without background autofluorescence from chlorophyll. Sectioning of plant leaves without disturbing the surface leaf resin is difficult however, as embedding the leaf tissue is not possible.

Manual sectioning of *S. crassifolia* leaves using a razor blade was attempted, but the leaf sections produced were unfortunately too thick for imaging purposes. The primary issue

with sectioning of plant leaves without an embedding medium was the flexibility of the fresh leaves made sectioning difficult. Frozen tissue, however, was significantly more rigid, so another viable method was available. Flash freezing of biological tissues is a well-established technique for preserving biological tissues for sectioning and fixation.[95] The top of the *S. crassifolia* leaf was removed and the remaining section of leaf and stem was flash frozen in liquid nitrogen. The flash frozen leaf was then embedded in OCT with the stem. Sections of 10 µm thickness were prepared to allow for spectroscopic mapping on the surface leaf resin.

Sectioning of the frozen leaf tissue was still difficult, because the sections had a tendency to crumble and disintegrate when cut at 10 µm thickness. However, several sections of the leaf tissue with intact leaf resin were successfully prepared. The resin of the leaf section could now be spectroscopically mapped using the green 532 nm Raman laser. Analysis of the leaf resin displayed the characteristic Raman scattering peaks attributed to the strained endocyclic alkenes and exocyclic alkenes of caryophyllenes, at 1670 and 1630 cm^{-1} respectively.[70] The presence of the caryophyllenes was confirmed through a comparison with Raman spectra of compounds isolated from the surface leaf resin (Figure 3.8).

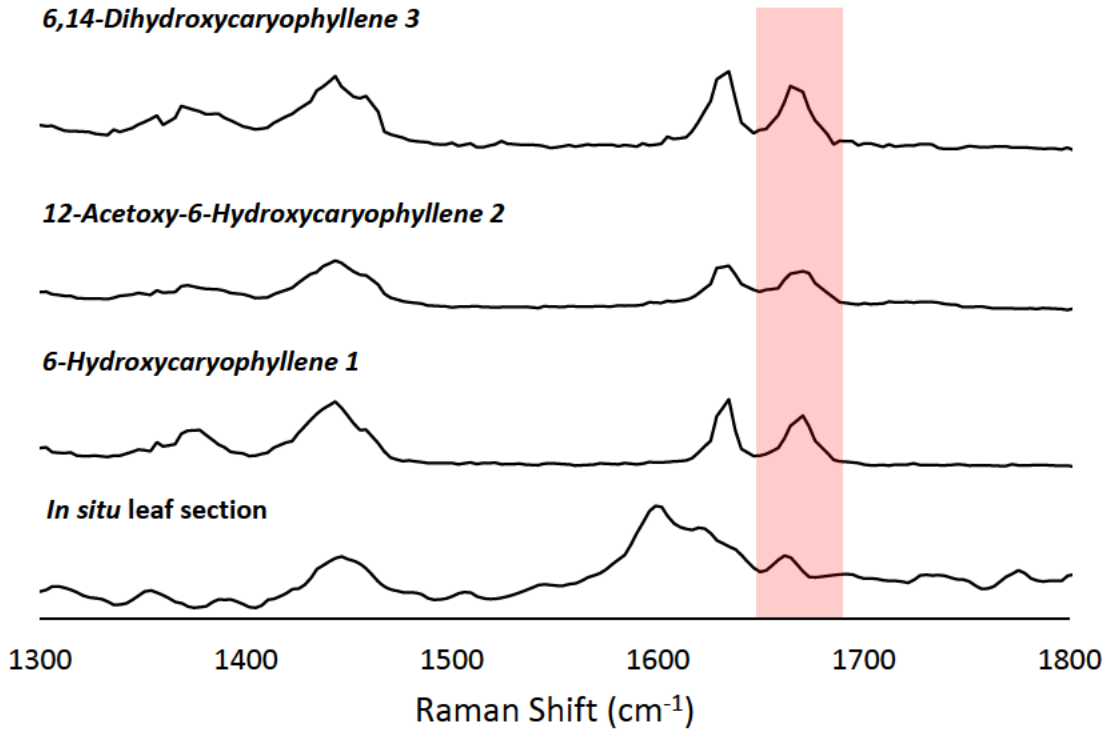

Figure 3.8. *Representative Raman spectra of 6-hydroxycaryophyllene* ***1****, 12-acetoxy-6-hydroxycaryophyllene* ***2****, 6,12-dihydroxycaryophyllene* ***3*** *and an* in situ S. crassifolia *leaf section [Red region highlights the Raman scattering band at 1670 cm^{-1} attributed to the strained alkene].*

The spatial distribution of the caryophyllenes was successively mapped using the Raman peak centred at 1667 cm^{-1}, corresponding to the strained endocyclic alkene. The autofluorescence of phenolic compounds in the resin and the C=C stretches of lignin dominated the Raman spectra and unfortunately prevented the use of the peak at 1630 cm^{-1}, corresponding to the exocyclic alkene. Integration of the area under the curve of the peak centred at 1667 cm^{-1}, unexpectedly revealed that the caryophyllenes were not evenly distributed throughout the resin (Figure 3.9). The distinct regions in which the caryophyllenes were mapped potentially indicated that the secretion of the caryophyllene compounds is biologically separate to the secretion of the phenolic compounds. Specifically, the concentrated regions of caryophyllenes were located closer to the surface of the resin than the phenolic compounds. The absence of characteristic caryophyllene signals in other regions of the resin may not be indicative of a lack of the compounds, but rather that the signal may be masked by the phenolic autofluorescence. However, the successful spectroscopic mapping of the caryophyllene distribution definitively shows that caryophyllenes are highly localised on the surface resin of *S. crassifolia* leaves.

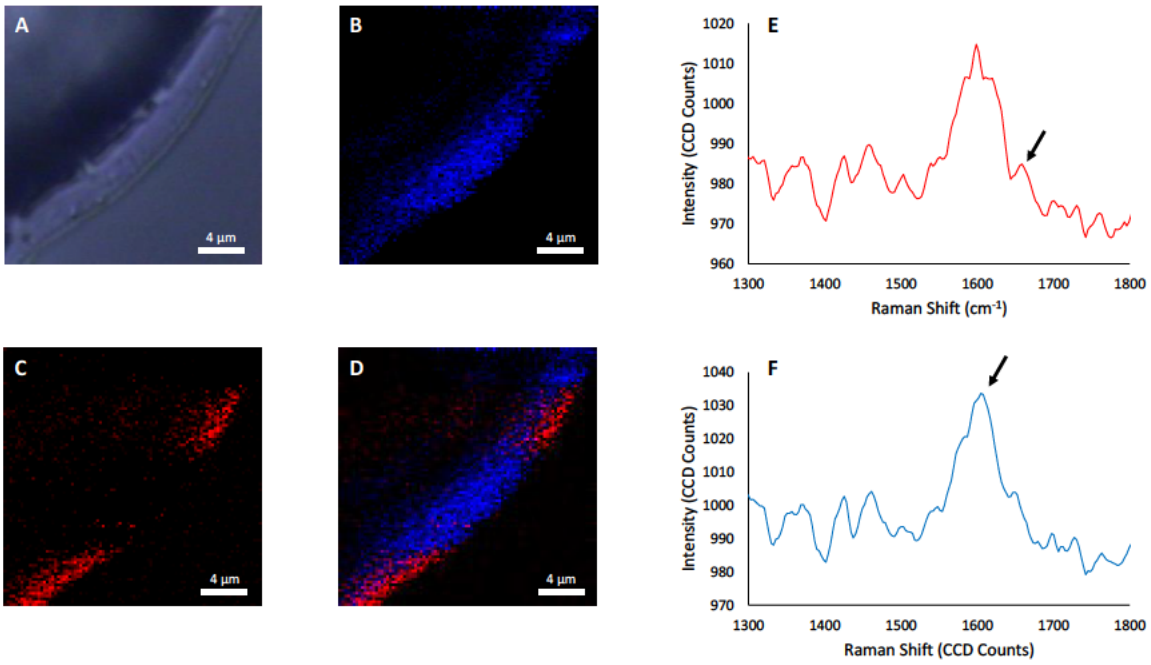

Figure 3.9. *Raman spectroscopic imaging (A-F) of* S. crassifolia *leaf resin. (A) Bright field image of a* S. crassifolia *plant cell, and the surface leaf resin (B) Raman spectroscopic map of the phenol distribution (area under the curve aromatic C = C stretching bands, centred at 1600 cm^{-1}), (C) Raman spectroscopic map of the caryophyllene distribution (area under the curve strained C = C stretching band centred at 1667 cm^{-1}), (D) Composite Raman spectroscopic map of caryophyllene and phenol distribution, (E) representative Raman spectrum of caryophyllene distribution, (F) representative Raman spectrum of phenolic distribution. Black arrows indicate key peaks. Scale bars are 4 µm. To improve S/N in individual Raman spectra (panel E and F) have been smoothed with a 13 point Savitzky-Golay smoothing function.*

3.6 Analysis of additional biospectroscopic markers in plant leaf tissue using Raman microscopy

The autofluorescence due to the presence of fluorescent natural products, such as flavonoids, was largely masking the presence of other natural products on the surface of the plant leaves. As a result, the spectroscopic mapping of different metabolic biospectroscopic markers in plant cells in leaf tissue sections was also investigated. The quantities of natural products inside the plant leaf tissue are significantly lower than that on the leaf surface. However, localised regions of target natural products within the plant cell may be detectable with less interference from other fluorescent natural products.

Plant leaves contain a variety of different types of tissues and cells, including dermal tissue, ground tissue, and vascular tissue.[96] Dermal tissue includes the cuticle and epidermal cells, which protect the plant from external threats. Ground tissue includes palisade parenchyma, bundle sheath parenchyma and spongy mesophyll cells. Finally, vascular tissue includes the xylem and phloem, which transport water and nutrients throughout the plant. Spectroscopic mapping of xylem and phloem using Raman microscopy has been extensively reported, which provided a convenient means to optimise the experimental set up for analysis of the plant leaf sections. Analysis of a section of the xylem and phloem cell wall in a 50 µm thick *S. crassifolia* leaf section showed C-H stretching bands (2850-3000 cm^{-1}) attributed to the composite of cellulose and hemicellulose (Figure 3.10). The C-H stretching bands observed were consistent with the values reported by Dinant *et al*. for the xylem of wild-type *Arabidopsis* floral stem.[97]

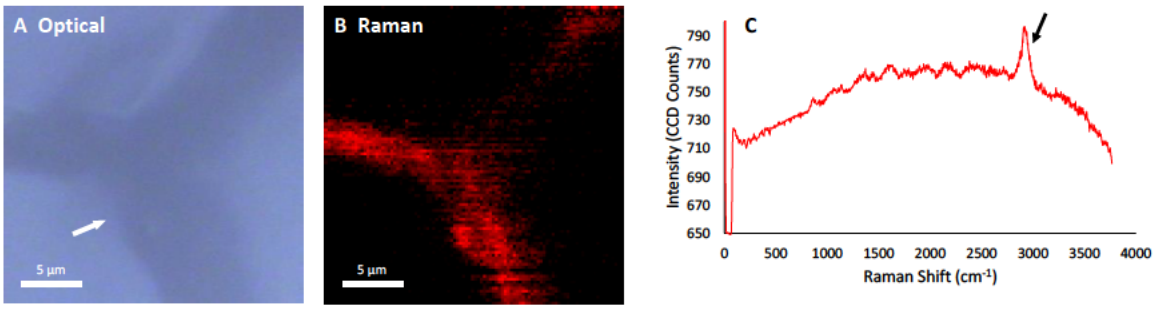

Figure 3.10. *Raman spectroscopic imaging (A-B) of* S. crassifolia *xylem cell wall. Tissue is unstained, so low contrast is visible in the image. (A) Bright field image of xylem cell wall with white arrow showing location of cell wall, (B) Raman spectroscopic map of the cellulose and hemicellulose distribution (area under the curve skeletal C-H stretching band centred at 2923 cm^{-1}), (C) Representative Raman spectrum of composite cellulose and hemicellulose in xylem cell walls. Black arrow indicates key peaks. Scale bars are 5 µm.*

The successful imaging of the xylem cell wall was promising, so the epidermal cells of *S. crassifolia* were analysed next. Epidermal cells are responsible for protecting the plant leaf from external threats, and consequently have thicker cells walls than plants cells found in ground tissue. The thicker cell walls result in a greater proportion of epidermal cells remaining undamaged during tissue sectioning. Spectroscopic mapping of *S. crassifolia* epidermal cells, similar to the leaf surface, did not exhibit the expected caryophyllene C=C stretching band at 1670 cm^{-1}. However, strong signals at 1000 cm^{-1} were visible, which was attributed to the C_1-C_2-C_3 angular bending of phenylalanine (Figure 3.11). Phenylalanine is abundant in many plants and fungi as it is a key component of many proteins and is a precursor for many natural products, such as flavonoids. The phenylalanine was localised in close proximity to the cell walls, suggesting that the phenylalanine was likely in the form of a protein. Many proteins are found in or on the cell wall to aid in functions such as transport, signalling and storage.[98] The spatial distribution of phenylalanine in plant cells using vibrational spectroscopy has not been previously reported. Another band was visible at 1087 cm^{-1}, which can be attributed to the C-C stretch of fatty acids/lipids. The fatty acids/lipids appear to create an envelope around the phenylalanine concentrated in the middle of the cell, suggesting that the high protein concentration in the region may be attributed to an organelle with a lipid membrane (Figure 3.11).

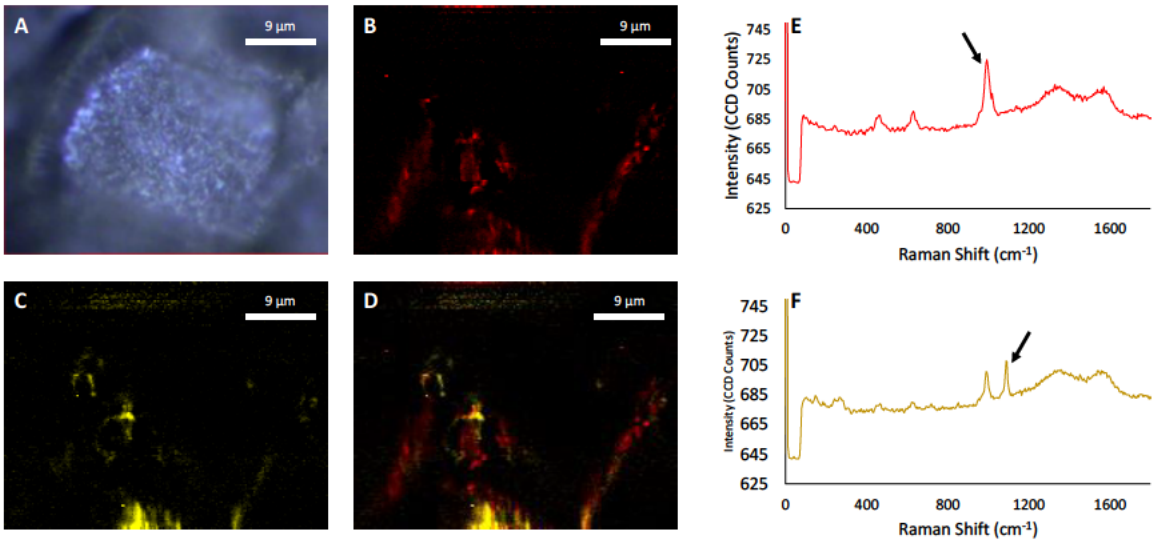

Figure 3.11. *Raman spectroscopic imaging (A-D) of 20 µm thick* S. crassifolia *epidermal plant cell (A) Bright field image of epidermal plant cell, (B) Raman spectroscopic map of the phenylalanine distribution (area under the curve skeletal C_1-C_2-C_3 angular bending band centred at 987 cm^{-1}), (C) Raman spectroscopic map of the fatty acid/lipid distribution (area under the curve skeletal C-C stretching band centred at 1093 cm^{-1}), (D) Composite Raman spectroscopic map of phenylalanine (red) and fatty acid/lipid (yellow) distribution, (E) Representative Raman spectrum of phenylalanine distribution, (F) Representative Raman spectrum of fatty acid/lipid distribution. Black arrows indicate key peaks. Scale bars are 9 µm.*

Although, the caryophyllene strained alkene was not observed *in situ* within internal plant cells due to autofluorescence, the successful spectroscopic mapping of phenylalanine and fatty acid/lipids in the plant tissue was promising. Plant cells in the ground tissue of *S. crassifolia* leaves were similarly analysed. The C_1-C_2-C_3 angular bending band of phenylalanine and the C-C stretching band of fatty acids/lipids were observed at 1008 cm^{-1} and 1113 cm^{-1}, respectively (Figure 3.12). The phenylalanine and fatty acids/lipids were distributed around the perimeter of the cell, similar to what was observed in the epidermal cell. The fatty acids/lipids appeared to be co-localised with the phenylalanine near the cell wall. The distribution of phenylalanine and fatty acids/lipids in the cell interior were not visualised, which can be attributed to the internal cell contents being more sensitive and susceptible to burning under the laser compared to the cell wall.

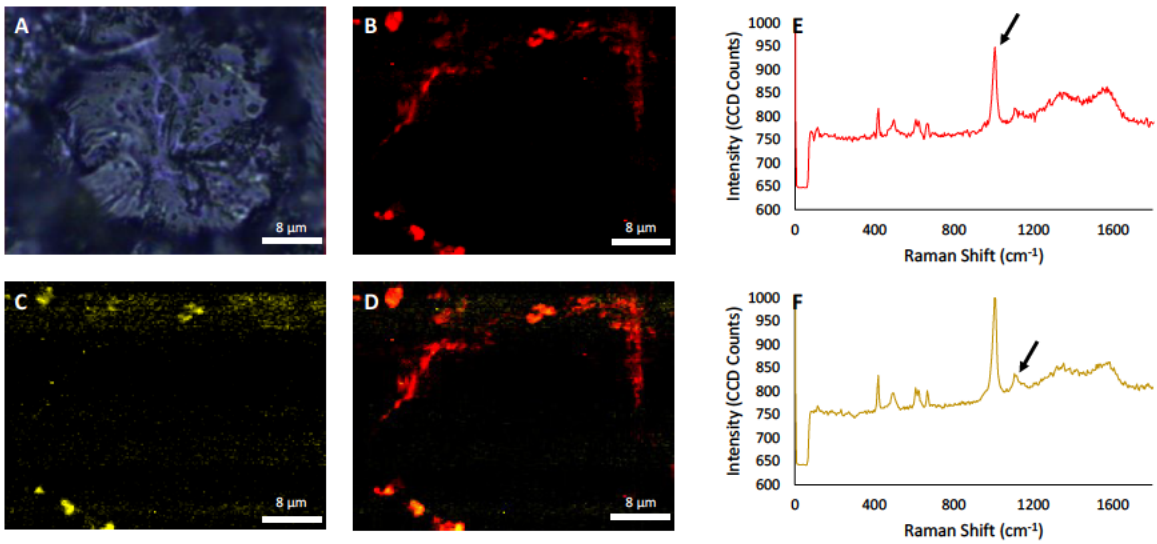

Figure 3.12. *Raman spectroscopic imaging (A-D) of 30 µm thick* S. crassifolia *ground tissue plant cell (A) Bright field image of ground tissue plant cell, (B) Raman spectroscopic map of the phenylalanine distribution (area under the curve skeletal C_1-C_2-C_3 stretching band centred at 1008 cm^{-1}), (C) Raman spectroscopic map of the fatty acid/lipid distribution (area under the curve skeletal C-C stretching band centred at 1113 cm^{-1}), (D) Composite Raman spectroscopic map of phenylalanine (red) and fatty acid/lipid (yellow) distribution, (E) Representative Raman spectrum of phenylalanine distribution, (F) Representative Raman spectrum of fatty acid/lipid distribution. Black arrows indicate key peaks. Scale bars are 8 µm.*

The distribution of phenylalanine and fatty acids had been successfully imaged in *S. crassifolia*, but detection of caryophyllenes remained elusive. The furans of natural products found in *Dodonaea* species provided an alternative spectroscopic biomarker that may be visible in the Raman spectrum. For example, Simpson *et al.* isolated furan-containing labdane **129** from *D. polyandra* (Figure 3.13).[99] The same labdane has been isolated by Atkinson *et al.* from *D. viscosa* "Mr Green Sheen", and as a result the leaves of *D. viscosa* "Mr Green Sheen" warranted spectroscopic analysis.[100]

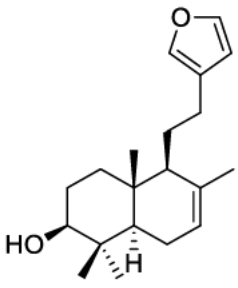

129

Figure 3.13. *Structure of labdane* ***129*** *isolated from* D. viscosa *"Mr Green Sheen".*

Raman mapping of a 30 µm thick *D. viscosa* "Mr Green Sheen" epidermal cell showed a prominent signal at 949 cm^{-1}, which was tentatively attributed to the skeletal C-O-C stretching band of a polysaccharide (Figure 3.14). The presence of the polysaccharide within the main cell bulk as opposed to the cell suggested that the polysaccharide was not a structural polysaccharide like cellulose. The signal possibly corresponded to amylose, which is a key component of a starch.[70] Signals corresponding to furans, phenylalanine or fatty acids/lipids were absent in the Raman spectra.

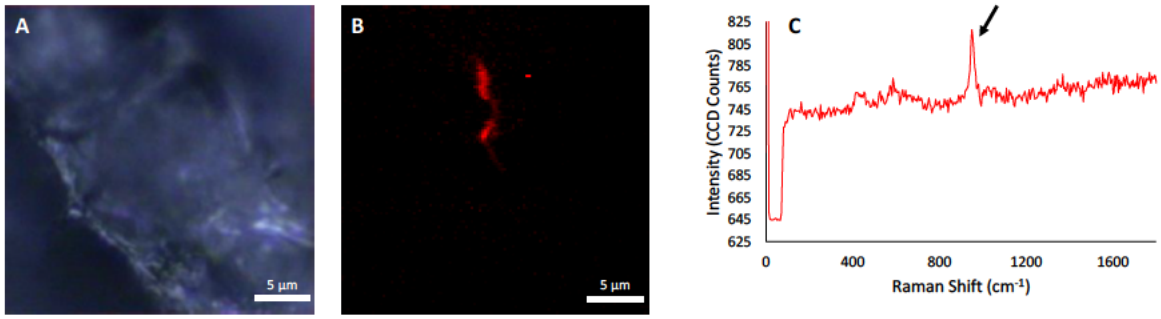

Figure 3.14. *Raman spectroscopic imaging (A-B) of 30 µm thick* D. viscosa *"Mr Green Sheen" epidermal plant cell (A) Bright field image of epidermal plant cell, (B) Raman spectroscopic map of the polysaccharide distribution (area under the curve skeletal C-O-C stretching band centred at 949 cm^{-1}, (C) Representative Raman spectrum of polysaccharide distribution. Black arrow indicates key peaks. Scale bars are 5 µm.*

The absence of any furan, phenylalanine or fatty acid/lipid responses was unexpected, so further analysis was conducted on the ground tissue of *D. viscosa* "Mr Green Sheen". Spectroscopic mapping of a ground tissue cell exhibited similar signals to the epidermal cell. A signal at 965 cm^{-1} was visible that was present through the cell body, which was also attributed to the skeletal C-O-C stretching band of starch. Another signal was visible at 1073 cm^{-1} that was visible in discrete regions, which was attributed to the C-C stretching of fatty acids/lipids (Figure 3.15). The fatty acids/lipids appeared to be localised in both the cell wall and within the cell body, but in significantly lower quantities than starch. The co-localisation of the fatty acids and the polysaccharides in some regions suggests that fatty acids may have involvement with starch production and/or storage. However, sectioning of the *D. viscosa* "Mr Green Sheen" leaves was unwieldy due to the low thickness of the leaves, so co-localisation of the fatty acids/lipids and the polysaccharides may also be due to artefacts from sectioning of the leaves.

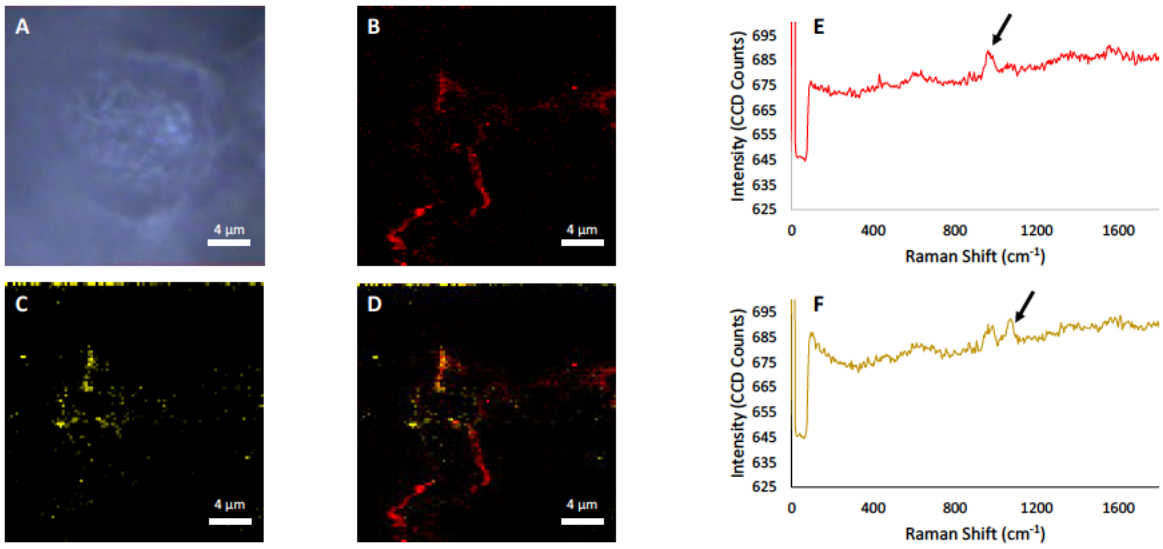

Figure 3.15. *Raman spectroscopic imaging (A-D) of 30 µm thick* D. viscosa *"Mr Green Sheen" ground tissue plant cell (A) Bright field image of ground tissue plant cell, (B) Raman spectroscopic map of polysaccharide distribution (area under the curve skeletal stretching band centred at 965 cm^{-1}), (C) Raman spectroscopic map of the fatty acid/lipid distribution (area under the curve skeletal C-C stretching band centred at 1073 cm^{-1}), (D) Composite Raman spectroscopic map of polysaccharide (red) and fatty acid/lipid (yellow) distribution, (E) Representative Raman spectrum of polysaccharide distribution, (F) Representative Raman spectrum of fatty acid/lipid distribution. Black arrows indicate key peaks. Scale bars are 4 µm.*

The ground tissue of a 50 µm leaf section from *G. varia* was similarly analysed using confocal Raman microscopy, to determine whether phenylalanine, fatty acids/lipids or polysaccharides were visible. A prominent peak at 1088 cm^{-1} was apparent, which was attributed to the C-C stretching band of fatty acids/lipids and was consistent with the fatty acid/lipid bands visible in the Raman spectra for *S. crassifolia* and *D. viscosa* "Mr Green Sheen" (Figure 3.16). The fatty acids/lipids appeared to be distributed near the cell wall and within the body of the cell, which was also consistent with *S. crassifolia* and *D. viscosa* "Mr Green Sheen".

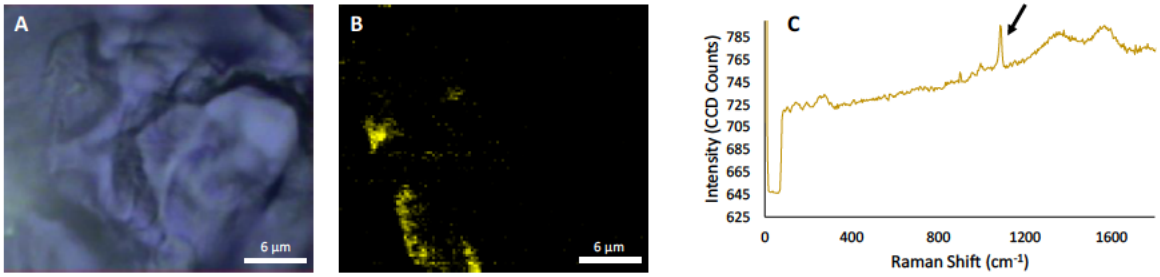

Figure 3.16. *Raman spectroscopic imaging (A-B) of 50 µm thick* G. varia *ground tissue plant cell (A) Bright field image of ground tissue plant cell, (B) Raman spectroscopic map of the fatty acid/lipid distribution (area under the curve skeletal C-C stretching band centred at 1088 cm^{-1}, (C) Representative Raman spectrum of fatty acid/lipid distribution. Black arrow indicates key peaks. Scale bars are 6 µm.*

Confocal Raman spectroscopic mapping of plant cells in *S. crassifolia*, *D. viscosa* "Mr Green Sheen" and *G. varia* demonstrated that imaging of natural products was not viable using the 532 nm green laser for excitation. However, mapping of the spatial distribution of proteins, fatty acids/lipids and biopolymers, like cellulose, could still be achieved despite the strong background autofluorescence from endogenous fluorophores.

3.7 Investigation of autofluorescence mitigation methods

Autofluorescence can be mitigated using a number of methods, including changing the excitation wavelength and modification of the Raman spectrum acquisition time. Raman scattering strength increases as a function of the fourth power of laser frequency. Consequently, an increase in the laser wavelength produces a proportionate decrease in the Raman scattering strength, leading to longer acquisition times being required. A 633 nm red excitation wavelength was used for spectroscopic mapping to potentially shift the excitation wavelength outside the excitation region of endogenous fluorophores.

The epidermal cell of a 50 µm *S. crassifolia* leaf section was spectroscopically mapped using the 633 nm red laser. A peak at 1011 cm^{-1} was apparent that corresponded to the C_1-C_2-C_3 angular bending of phenylalanine, which was consistent with the signals observed in *S. crassifolia* using the 532 nm green laser (Figure 3.17). However, the signal-to-noise ratio was noticeably lower, and the other signals associated with phenylalanine and the proteins are not visible in the Raman spectrum. Significant autofluorescence was also apparent, indicating that excitation of endogenous fluorophores was still occurring. The significant autofluorescence using the red region light can be attributed to the presence of chlorophyll

in plant leaves, which has a region of maximal absorption at 642 nm, which is very close to the 633 nm excitation wavelength.

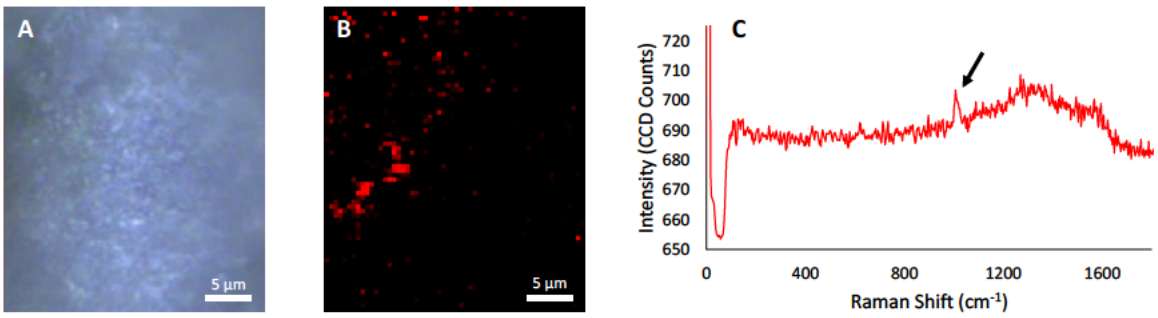

Figure 3.17. *Raman spectroscopic imaging (A-B) of 50 µm thick* S. crassifolia *epidermal plant cell (A) Bright field image of epidermal plant cell, (B) Raman spectroscopic map of the phenylalanine distribution (area under the curve C_1-C_2-C_3 angular bending band centred at 1011 cm^{-1}, (C) Representative Raman spectrum of phenylalanine distribution. Black arrow indicates key peaks. Scale bars are 5 µm.*

The efficacy of the longer wavelength 633 nm red laser was further investigated by analysing a ground tissue plant cell of a 50 µm leaf section of *S. crassiolia* Labill. As previously observed in the epidermal cell, the C_1-C_2-C_3 angular bending of phenylalanine was observed at 1116 cm^{-1} (Figure 3.18). Significant background autofluorescence was still present, however, so use of a 633 nm excitation source was deemed ineffective for plant tissue. A near infrared excitation source such as a 785 or 1064 nm laser may have been able to successfully image the distribution of compounds in plant tissue without the occurrence of significant autofluorescence, however this was not accessible in the available facilities.

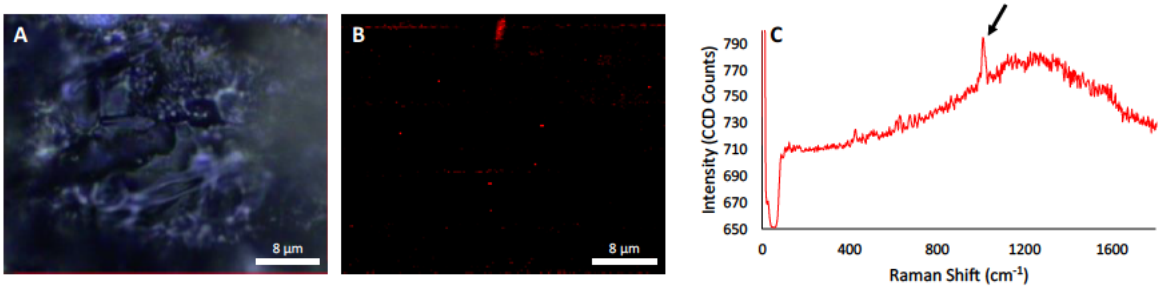

Figure 3.18. *Raman spectroscopic imaging (A-B) of 50 µm thick* S. crassifolia *ground tissue plant cell (A) Bright field image of ground tissue plant cell, (B) Raman spectroscopic map of the phenylalanine distribution (area under the curve C_1-C_2-C_3 angular bending band centred at 1016 cm^{-1}, (C) Representative Raman spectrum of phenylalanine distribution. Black arrow indicates key peaks. Scale bars are 8 µm.*

3.8 Exploration of 3D confocal Raman imaging of plant leaf tissue

Spectroscopic mapping of the surface of a biological sample using FTIR and Raman microscopy can provide a wealth of chemical information, including the spatial distribution of biomolecules. However, the spectra that are acquired using a standard area scan are only two dimensional. Many biological samples possess complex three-dimensional structures, so a two-dimensional spectroscopic map of a sample only provides chemical information about the region of the sample that is within the focal point of the light source, which is especially apparent with confocal Raman microscopy. However, confocal Raman microscopy allows for the three-dimensional imaging of samples by imaging a sample in "virtual-slices", with each slice corresponding to a different focal point. Three dimensional (3D) Raman imaging has increased in popularity over the last two decades and is being used in areas such as materials science and biomedical research. Kalleptis *et al*. used 3D Raman imaging to visualise the cell shape, cytoplasm, nucleus, protein rich clusters and other regions of interest in pluripotent stem cells and monocytes/macrophages in conventional culture systems.[101] Similarly, Majzner *et al*. used 3D Raman imaging to study the biochemical and structural components of isolated endothelial cells and endothelial cells in vascular tissue.[102] However, despite the wealth of information provided by 3D Raman imaging, limited work has been conducted on plant tissue and has primarily involved analysis of biopolymers like lignin. In particular, Chu *et al*. reported the use of 3D Raman imaging to monitor the structural and chemical changes to *Miscanthus x giganteus* upon treatment with sodium hydroxide.[103]

The lack of existing literature indicated that the potential of 3D Raman imaging of plant tissues had yet to be fully explored, and further method development could be conducted. The technique also had the potential to detect localised areas of natural products or biomolecules that may have been missed with 2D spectral imaging or altered/removed during physical sectioning of the tissues. Preliminary imaging experiments were conducted on the cell walls of a 50 μm section of *S. crassifolia* tissue, because ligno-cellulose materials are well characterised and in high abundance in plant cells. The prominent C-H stretching band at 2930 cm^{-1} was a useful biomarker for cellulose and allowed for the successful 3D imaging of a cell wall junction between cells, by excitation with the 532 nm green laser (Figure 3.19). The visualisation of the C-H stretching band showed that the cell wall junction possessed a hollow cavity in the centre with bottom consisting of ligno-cellulose. Visualising the hollow cavity structure highlighted the potential of 3D Raman

microscopy. A standard 2D area scan would only visualise the surface of the cell wall junction while missing other structural aspects that could be picked up with 3D Raman microscopy.

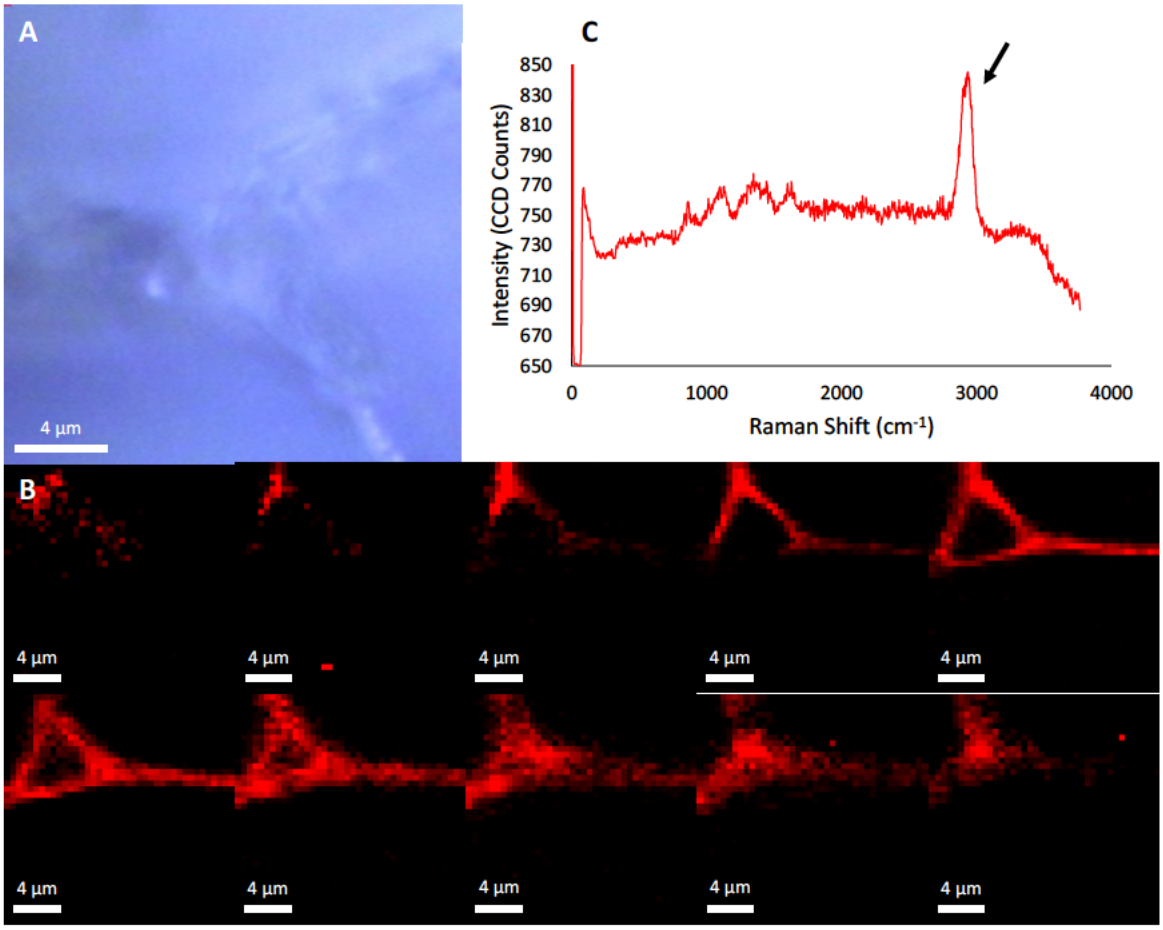

Figure 3.19. *3D Raman spectroscopic imaging (A-B) of 50 µm thick* S. crassifolia *xylem and phloem cell wall junction (A) Bright field image of xylem and phloem cell wall junction, (B) Montage of Raman spectroscopic maps of the ligno-cellulose distribution (area under the curve C-H stretching band centred at 2930 cm^{-1}) with 1 µm step between each map, (C) Representative Raman spectrum of ligno-cellulose (indicated by black arrow). Scale bars are 4 µm.*

The successful imaging of the ligno-cellulose distribution in the cell wall junction was encouraging, so similar 3D Raman imaging on a *S. crassifolia* ground tissue cell wall junction was conducted. Interestingly, the C-H stretching bands between 2850 and 3000 cm^{-1}, characteristic of ligno-cellulose, were not observed. Instead, prominent signals at 1000 and 1090 cm^{-1} were observed, corresponding to the C_1-C_2-C_3 angular bending of phenylalanine and the skeletal C-C stretching band of fatty acids/lipids. The high quantity of fatty acids/lipids found towards the centre of the junction suggested that a vacuole or organelle could be present in the cell wall junction. However, it is also possible that the

high fatty acids/lipid concentration was an artefact of the sample preparation process. The 3D Raman image also revealed that the distribution of the fatty acids/lipids was not of a uniform thickness and varied across the surface of the cell wall junction. The distribution of phenylalanine was predominantly found towards the edges of the cell wall in the darker regions present in the brightfield image (Figure 3.20). The localisation of phenylalanine on the outside of the cell wall was consist with previous observations by 2D Raman mapping. Unfortunately, key C=C stretching signals associated with the caryophyllene endocyclic alkene were not observed in the Raman spectra, indicating that autofluorescence was still a major inhibitor for the spectroscopic mapping of natural products. The successful 3D Raman mapping of the phenylalanine and fatty acid/lipid distribution has provided unique insight into the three-dimensional distribution of these biomolecules in plant cell wall junctions. However, there is still significant untapped potential for the use of 3D Raman spectroscopy in plant sciences.

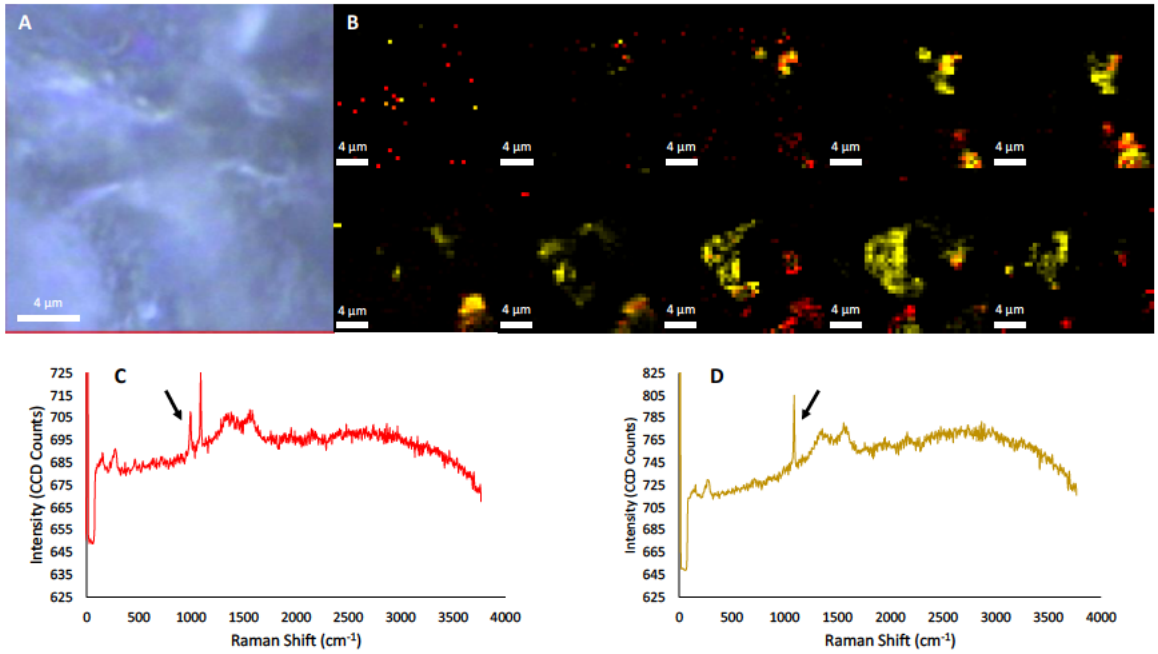

Figure 3.20. *3D Raman spectroscopic imaging (A-B) of 50 µm thick* S. crassifolia *ground tissue cell (A) Bright field image of ground tissue cell, (B) Montage of Raman spectroscopic maps of the phenylalanine (area under the curve C_1-C_2-C_3 angular bending band centred at 1000 cm^{-1}) and fatty acid/lipid distribution (area under the curve C-H stretching band centred at 1090 cm^{-1}) with 1 µm step between each map, (C) Representative Raman spectrum of phenylalanine distribution (indicated by black arrow), (D) Representative Raman spectrum of fatty acid/lipid distribution (indicated by black arrow). Scale bars are 4 µm.*

3.9 Investigation of synchrotron FTIR microspectroscopy for the biochemical mapping of plant leaf tissue

Analysis of plant leaf tissue using Raman microscopy had demonstrated that inherent difficulties in overcoming autofluorescence from endogenous fluorophores and fluorescent natural products. FTIR spectroscopy, however, does not generate autofluorescence due to the low energy of infrared light being insufficient for electronic excitation of molecules. FTIR spectra of the leaf surface of plants with known natural product compositions were collected to determine whether viable spectroscopic markers were visible on the surface, where high concentrations of natural products were available.

S. crassifolia is known to possess large quantities of flavanones and caryophyllenes in the surface leaf resin. The strained endocyclic alkene of caryophyllenes are known to have a higher C=C absorbance at 1670 cm^{-1}, attributed to the strain caused by the *E* conformation. Analysis of the leaf surface of *S. crassifolia* by ATR-FTIR showed strong absorbance at 1600 and 1630 cm^{-1}, which were characteristic of the C=C stretches for alkenes in α,β-unsaturated systems and substituted alkene systems, respectively. However, a clearly resolved absorbance band at 1670 cm^{-1} was not visible. FTIR spectra can be derived to provide the second derivative spectrum, as an approach to spectral deconvolution. The second derivative spectrum provides an apparent increase in spectral resolution, at the expense of increased noise. In the second derivative FTIR spectrum, a small peak at 1674 cm^{-1} was visible, which had not previously been visible due to spectral overlap with the large absorbance band at 1630 cm^{-1} (Figure 3.4). Therefore, the caryophyllene strained alkene was visible in FTIR spectra, but required processing using the second derivative for analysis.

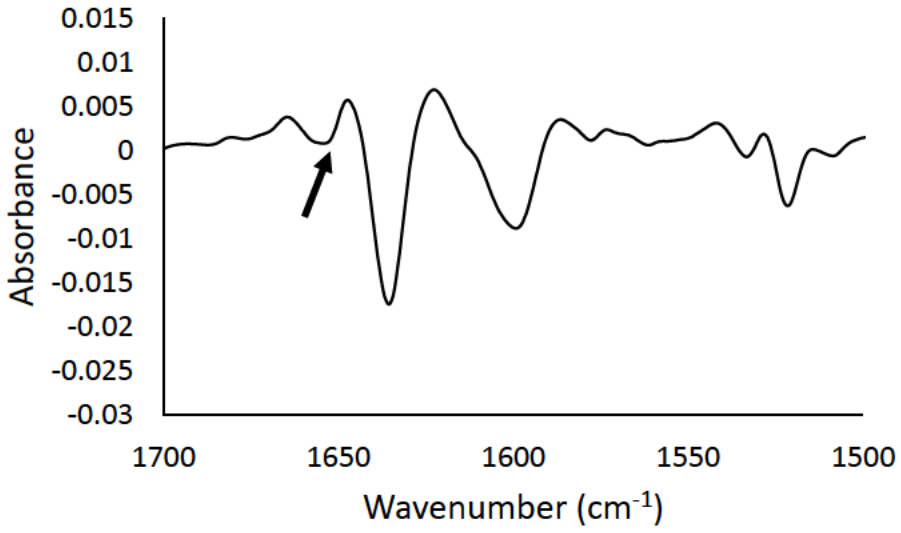

Figure 3.21. *Representative second derivative FTIR spectrum of a* S. crassifolia *leaf surface. Black arrow indicates presence of caryophyllene strained C=C stretching band at 1674 cm^{-1}.*

Furans are a unique moiety that appear in a variety of natural products, such as pallescensin A **130** and bhimamycin B **131** (Figure 3.22).[104] However, natural products containing furan moieties are still uncommon relative to other functional groups, making them ideal for use as spectroscopic markers.

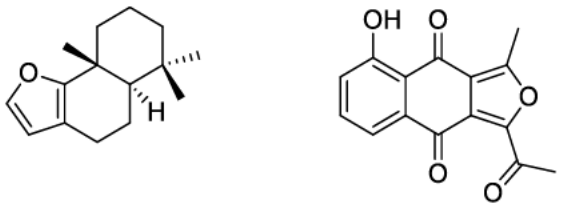

130 **131**

Figure 3.22. *Structures of pallescensin A **130** and bhimamcycin B **131**.*

Plants in the *Dodonaea* genus are known to possess furan-containing natural products, including labdanes and clerodanes.[105] Furans exhibit several key absorbances in FTIR spectra, including the C=C stretch at approximately 1500 cm^{-1}, the C-O-C stretch at approximately 1180 cm^{-1} and C-H bending at 873 cm^{-1}.[106] Leaves from *D. viscosa* subsp *angustissima*, *D. viscosa* subsp *purpurea*, *D. viscosa* "Mr Green Sheen" and *D. ceratocarpa* were analysed by ATR-FTIR. Distinct absorbance bands at 1517 and 1171 cm^{-1} were visible, indicative of the C=C and C-O-C stretches of the furan. An absorbance band at 873 cm^{-1} was also visible in all the *Dodonaea* species, which could also act as a valuable

spectroscopic marker for furans (Figure 3.23). The intensity of the signals varied depending on the quantity of furan containing natural products found in the plant.

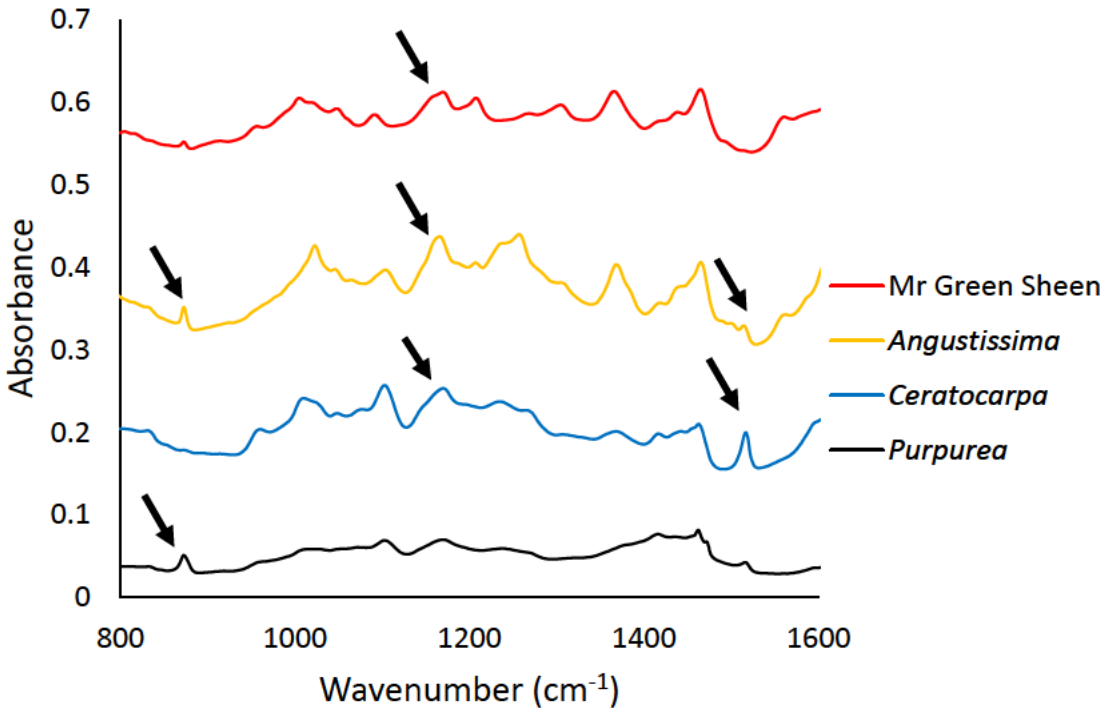

Figure 3.23. *Representative FTIR spectra of* D. viscosa *subsp* angustissima, purpurea, *"Mr Green Sheen" and* D. ceratocarpa *leaf surfaces. Black arrows show the location of furan C=C (1517 cm^{-1}), C-O-C stretching (1171 cm^{-1}) and C-H bending (873 cm^{-1}) bands.*

Analysis using ATR-FTIR allowed for viable FTIR spectroscopic markers of natural products to be determined. However, spectroscopic mapping of the distribution of the natural products using a benchtop FTIR microscope was not viable due to the relatively poor spatial resolution of the instrument (25 µm, linear array detector). A spatial resolution of 25 µm would not allow for imaging of plant cells and was unsuitable for the determination of natural products distribution.

Confocal Raman imaging had demonstrated that successful imaging of the distribution of a variety of biomolecules could be achieved at a sub-micrometre resolution. Synchrotron FTIR allows for subcellular imaging to provide complementary chemical information to Raman imaging. FTIR imaging of 50 µm sections of *S. crassifolia* ground tissue plant cell showed that, unfortunately, the distribution of caryophyllenes was unable to be mapped in the cell due to the overlap in the 1670 cm^{-1} strained C=C stretch with the amide I band (amide C=O stretching) between 1620 and 1680 cm^{-1}. However, FTIR imaging of the

distribution of a broad variety of other biomolecules was possible. Spectroscopic mapping of the plant cell revealed a broad distribution of lipids (C-H stretching, 2800-3000 cm^{-1}) throughout the plant cell (Figure 3.24).

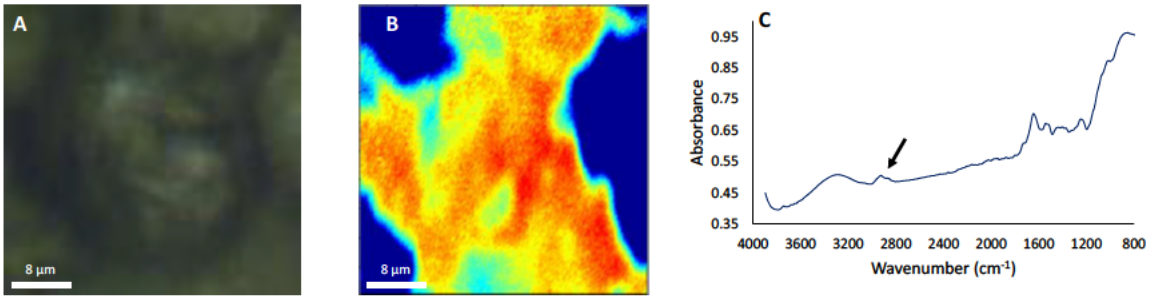

Figure 3.24. *Synchrotron FTIR spectroscopic imaging (A-B) of 50 µm thick* S. crassifolia *ground tissue plant cell (A) Bright field image of ground tissue plant cell, (B) FTIR spectroscopic map of the lipid/fatty acid distribution (area under the curve C-H stretching band centred at 2800-3000 cm^{-1}), (C) Representative FTIR spectrum of lipid/fatty acid distribution. Black arrow indicates key absorbances. Scale bars are 8 µm.*

The carbonyl region (C=O, 1710-1760 cm^{-1}) encompassing functional groups including aldehydes, ketones and esters, exhibited more distinct localisation within the leaf tissue (Figure 3.25). Unsurprisingly, overlap was observed between the lipid C-H stretching regions and the C=O stretching regions, likely due to the presence of fatty acid/lipid esters in the tissue.

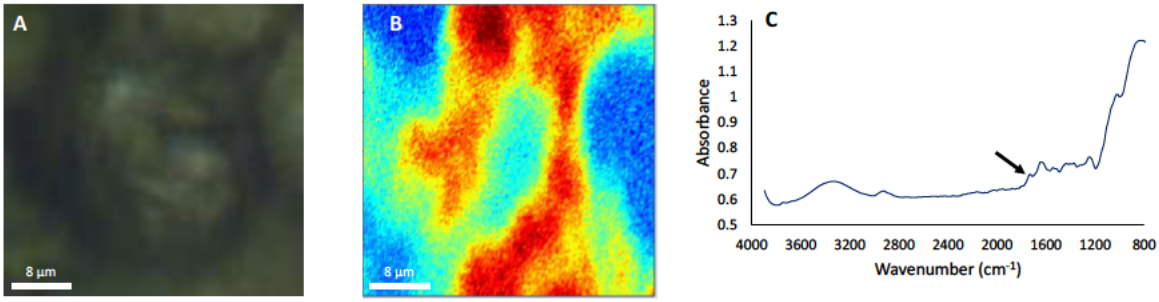

Figure 3.25. *Synchrotron FTIR spectroscopic imaging (A-B) of 50 µm thick* S. crassifolia *ground tissue plant cell (A) Bright field image of ground tissue plant cell, (B) FTIR spectroscopic map of the carbonyl distribution (area under the curve C=O stretching band centred at 1710-1760 cm^{-1}), (C) Representative FTIR spectrum of carbonyl distribution. Black arrow indicates key absorbances. Scale bars are 8 µm.*

A broad distribution of amides (Amide I C=O, 1620-1680 cm^{-1}) was similarly observed in the leaf tissue sections, but overlap between the lipid and amide distributions was limited (Figure 3.26). The amide peaks generally indicative of the presence of proteins with cells.

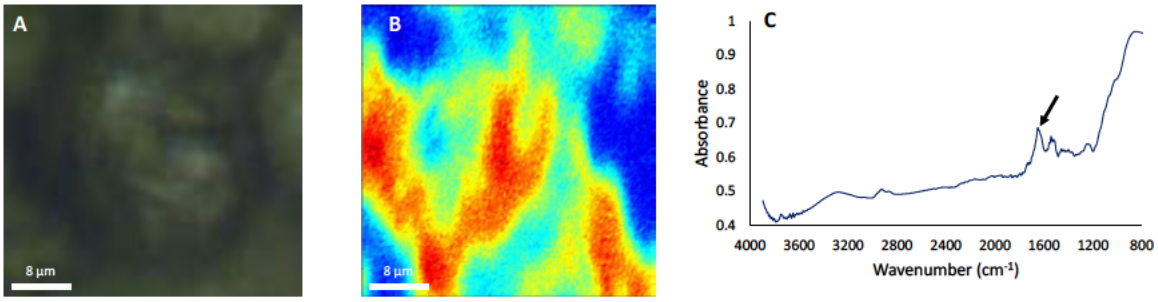

Figure 3.26. *Synchrotron FTIR spectroscopic imaging (A-B) of 50 µm thick* S. crassifolia *ground tissue plant cell (A) Bright field image of ground tissue plant cell, (B) FTIR spectroscopic map of the amide distribution (area under the curve C=O stretching band centred at 1620-1680 cm^{-1}), (C) Representative FTIR spectrum of amide distribution. Black arrow indicates key absorbances. Scale bars are 8 µm.*

Imaging of the aromatic stretching region (C=C, 1500-1550 cm^{-1}) showed significant overlap with the amide II stretching region (Figure 3.27). The aromatic stretching can likely be attributed to the presence of phenylalanine in the leaf tissue. The phenylalanine is most likely present as amino acid residues in a protein or peptide, so the overlap with the amide carbonyl stretching regions is logical due to the amide bonds present in proteins and peptides.

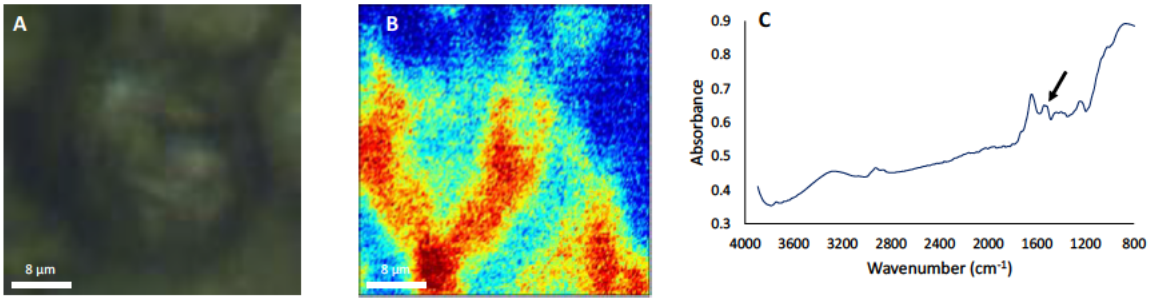

Figure 3.27. *Synchrotron FTIR spectroscopic imaging (A-B) of 50 µm thick* S. crassifolia *ground tissue plant cell (A) Bright field image of ground tissue plant cell, (B) FTIR spectroscopic map of the aromatic distribution (area under the curve C=C stretching band centred at 1500-1550 cm^{-1}), which is strongly overlapped with the amide II band (C) Representative FTIR spectrum of aromatic distribution. Black arrow indicates key absorbances. Scale bars are 8 µm.*

Imaging of the amine stretching region (3500-3600 cm^{-1}) exhibited highly localised regions of primary amines, characterised by two absorbance bands at 3400 and 3500 cm^{-1} (Figure 3.28).

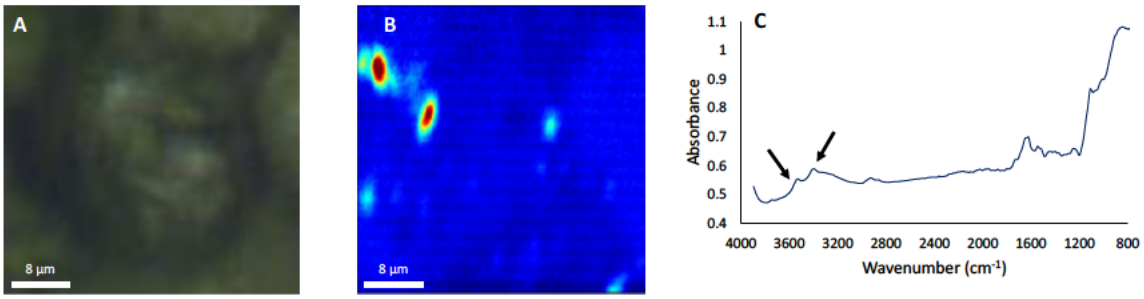

Figure 3.28. *Synchrotron FTIR spectroscopic imaging (A-B) of 50 µm thick* S. crassifolia *ground tissue plant cell (A) Bright field image of ground tissue plant cell, (B) FTIR spectroscopic map of the amine distribution (area under the curve N-H stretching band centred at 3500-3600 cm^{-1}), (C) Representative FTIR spectrum of amines distribution. Black arrows indicate key absorbances. Scale bars are 8 µm.*

Lysine is the only essential α-amino acid with a primary amine sidechain, and arginine, asparagine and glutamine all possess primary amide or guanidinium-containing side chains that include -NH_2 groups (Figure 3.29).

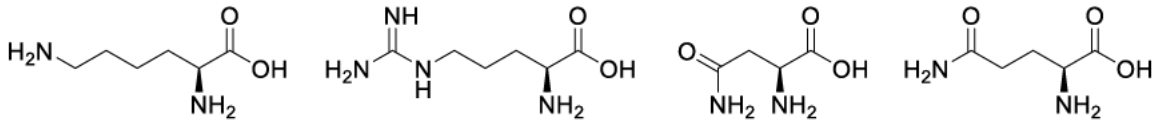

132 **133** **134** **135**

Figure 3.29. *Structures of lysine* ***132****, arginine* ***133****, asparagine* ***134*** *and glutamine* ***135****.*

The highly localised nature of the –NH_2 stretching suggests that a highly organised storage organelle or vacuole was present in the cell. Plant cells possess a number of different types of vacuoles, including lytic and protein storage vacuoles.[107] Lytic vacuoles in plant cells contain hydrolases that serve to degrade of cellular waste. Protein storage vacuoles have been reported to accumulate large quantities of defence and storage proteins.[107] Localisation of protein storage vacuoles has been conducted using a number of techniques, including fluorescence microscopy, synchrotron soft X-ray microscopy and synchrotron FTIR spectromicroscopy. The distribution of protein storage vacuoles has primarily been investigated in plant seeds, but only limited work has looked at the distribution in other plant organs such as the leaves.[108] Park *et al*. mapped the distribution of the protein storage vacuole and the protein targeting the protein storage vacuole in the leaf cells of tobacco (*Nicotiana tabacum*), common bean (*Phaseolus vulgaris*) and *Arabidopsis* using green fluorescent protein (GFP) and fluorescence microscopy.[109] Similarly, vacuoles were imaged in the roots of *Arabidopsis* by Gattolin *et al*. using fluorescent protein tagging.[110]

Withana-Gamage reported the use of synchrotron FTIR microscopy to map the distribution of protein in *Arabidopsis* seed tissues,[108b] but the FTIR spectroscopic mapping of protein storage vacuoles in plant leaf tissue has not been previously reported.

3.10 Conclusions

This chapter has investigated capabilities of confocal Raman microscopy and synchrotron FTIR microspectroscopy for spectroscopic mapping of natural products in plant leaf tissue. An effective method for the preparation of leaf tissue for spectroscopic mapping was developed, using layered OCT and a cryomicrotome. Synchrotron FTIR microspectroscopy was determined unsuitable for mapping of low abundance natural products in plant leaf tissue due to a lack of chemical specificity that results from the overwhelming spectral overlap with other biomolecules. However, the distribution of protein storage vacuoles in plant leaf tissue was mapped using synchrotron FTIR microspectroscopy for the first time. Confocal Raman microscopy, using a 532 nm and 633 nm laser, was ineffective for the detection of low abundance natural products on the plant leaf surface and in plant leaf tissue due to autofluorescence from endogenous fluorophores. A longer wavelength laser, such as a near infrared 785 nm or 1064 nm laser, would potentially show greater success, due to the wavelength being outside the absorbance regions of most molecules. However, a method was successfully developed to allow for spectroscopic mapping of leaf tissue resin and the distribution of caryophyllenes was successfully mapped using confocal Raman microscopy in the leaf resin *S. crassifolia* Confocal Raman imaging using the 532 nm laser allowed for the first reported mapping of the distribution of phenylalanine and fatty acid/lipids in plant leaf tissue. A method for the 3D Raman imaging of plant leaf tissue was successfully developed, allowing for the 3D spectroscopic imaging of ligno-cellulose, phenylalanine and fatty acids/lipids in plant leaf tissue. The FTIR and Raman data, taken together, highlight future potential of these techniques to study proteins in living, intact plant tissues, possibly in 3D, but further exploration was beyond the scope of this thesis. Although this chapter identified that imaging natural products in plant cells *in situ* and in 3D is not likely to be routinely possible using Raman or FTIR spectroscopy; this chapter highlighted that cryosectioning of plant tissues combined with Raman imaging of tissue regions not-enriched in endogenous fluorophores, such as resin surfaces in 2D tissue sections offers scope for natural product imaging. This is believed to be the first demonstration of sub-micron spatial resolution imaging of natural products in plant samples.

Chapter 4
Synthetic and spectroscopic investigation of natural products from *Scaevola crassifolia*

S. crassifolia, commonly known as the thick leafed fanflower, is a shrub native to Western Australia that is found along coastal plains, sand dunes and limestone cliffs.[111] The plant is an erect, viscid shrub that grows between 0.1 and 1.5 m in height. The flowers are blue or white and are in bloom from July to December, and from January to February. The leaves of the plant are covered in a thick, sticky resin. *S. crassifolia* has not been previously investigated as a source of natural products. A preliminary investigation into the natural products composition of this leaf resin was conducted during my Honours year. The plant material was collected from the grounds of Curtin University in Perth, Western Australia. The natural products were separated into the amines, neutrals, carboxylic acids and phenols through acid-base partitioning. Four major compounds were isolated from the neutrals fraction: 6-hydroxycaryophyllene **1**, 12-acetoxy-6-hydroxycaryophyllene **2**, 6,12-dihydroxycaryophyllene **3** and 1,4-dihydroxy-α-bisabolol-2,10-diene **137** (Figure 4.1). A mixture of two flavanones were isolated from phenols fraction: 8-prenylflavanone **138** and 8-prenylflavanone **139** (Figure 4.1).

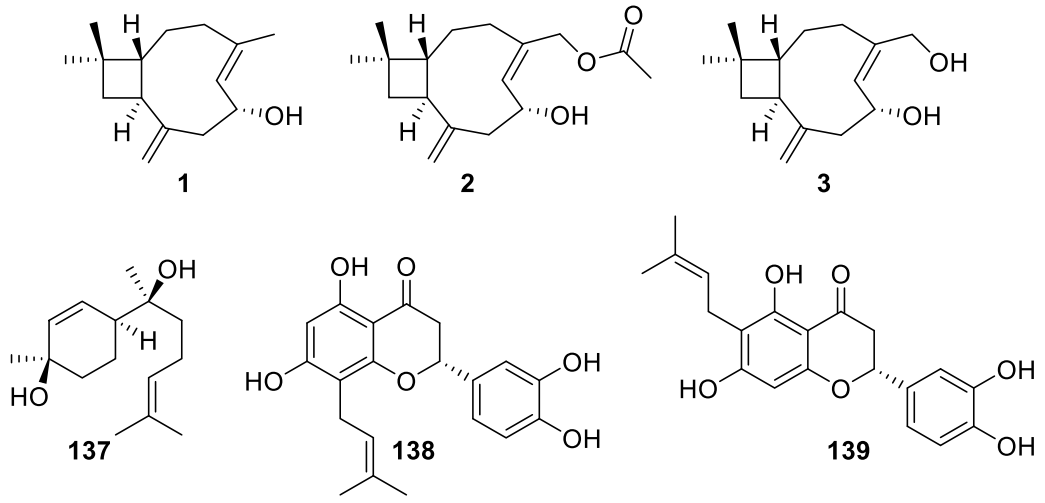

Figure 4.1. *Compounds previously isolated from* S. crassifolia

4.1 Exploring the natural products composition of native *Scaevola crassifolia*

A preliminary investigation into the natural products composition of *S. crassifolia* found at Curtin University had been conducted, but the plants were introduced to the campus externally. The natural products composition of plants are affected by the environment and stressors that they are exposed to, such as soil composition, soil acidity, light quantity and salinity.[112] As a result, the natural products composition of *S. crassifolia* found in its natural coastal environment was explored. Fresh *S. crassifolia* leaves were collected from Port Beach, North Fremantle, Western Australia on the 27th of April 2020. The leaves were steeped in Et_2O and the compounds were partitioned using acid-base chemistry into the amines, carboxylic acids, neutrals and phenols.

The neutrals fraction was purified by column chromatography to afford five compounds. The first compound was isolated as a colourless oil. The FTIR spectrum showed a broad OH absorbance at 3411 cm^{-1} and no carbonyl stretches. The ^{13}C NMR spectrum contained 30 signals, indicating that it was a mixture of compounds. The ^{1}H NMR spectrum similarly looked like a mixture of compounds. Two sets of singlets at 4.77 and 4.94 ppm, and 4.89 and 5.06 ppm that each integrated for 1H were reminiscent of the exocyclic alkenes of caryophyllenes. A doublet and a doublet of doublets at 5.37 and 5.45 ppm, respectively, each integrated for 1H, indicated the presence of the C5 vinylic hydrogen of caryophyllenes (Figure 4.2). Two sets of doublets were present at 3.93 and 4.17 ppm, and 3.69 and 4.12 ppm that each integrated for 1H. The HSQC spectrum indicated that the hydrogens correlated to two carbons between 60 and 80 ppm, indicating the presence of two primary hydroxyl groups. However, the NMR spectra of the mixture of caryophyllenes was too complex to identify the compounds. The presence of hydroxyl groups indicated by the FTIR spectrum meant that the hydroxyl groups could be functionalised to separate the two compounds.

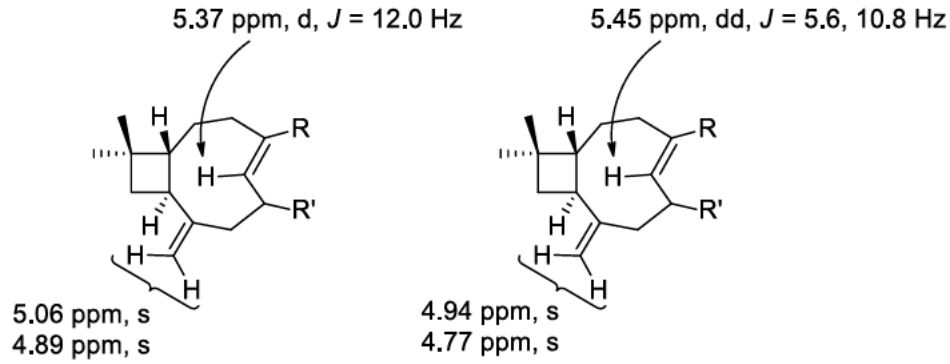

Figure 4.2. *Analysis of mixture of unknown caryophyllenes.*

Esterification of hydroxyl groups is a convenient method to functionalise hydroxyl groups and allow for easier separation of compounds by changing their polarity. The mixture of caryophyllenes was acetylated using Ac_2O, with Et_3N, DMAP in dry CH_2Cl_2. The crude product was purified by column chromatography to give a cloudy white oil. The FTIR spectrum showed no OH absorbance and a prominent carbonyl absorbance at 1733 cm^{-1}, indicating that the acetylation was successful. The ^{13}C NMR spectrum contained 34 signals indicating that a mixture of compounds was still present. Two overlapping signals at 171.3 ppm further supported the successful acetylation of the caryophyllenes. The ^{1}H NMR spectrum similarly showed two sets of signals, however the ratio of peaks had changed. Two sets of singlets were now present at 4.81 and 4.96 ppm, and 4.87 and 4.99 ppm, with integrations of 0.5H and 1H respectively. Similarly, the doublet and doublet of doublets had shifted downfield to 5.53 and 5.59 ppm and had integrations of 0.5H and 1H respectively. Of particular note was the change in chemical shift of the doublets between 3 and 4 ppm, which had shifted downfield to 4.44 and 4.68 ppm, and 4.31 and 4.68 ppm, integrating for 1H and 0.5H respectively. The doublet at 4.68 ppm consisted of two overlapping peaks and integrated for 1.5H. The significant downfield shift indicated that the hydrogens were being deshielded by a strongly electron withdrawing group, such as an ester. Therefore, the primary alcohol had likely been acetylated. The majority presence of one compound over the other based on the integration values allowed for the structure to be further elucidated for the major compound. The HMBC spectrum indicated that the methylene of the acetate was adjacent to the endocyclic alkene, suggesting that it was a C12 acetate. No signals were present that corresponded to the C6 hydroxyl group, indicating that C7 was likely an unfunctionalised methylene. Therefore, based on the FTIR, ^{1}H, ^{13}C and 2D NMR spectra the major compound was assigned as 12-

acetoxycaryophyllene **140**, in 48% yield (Scheme 4.1). 12-Acetoxycaryophyllene **140** has been previously synthesised by Barrero *et al*.[48b]

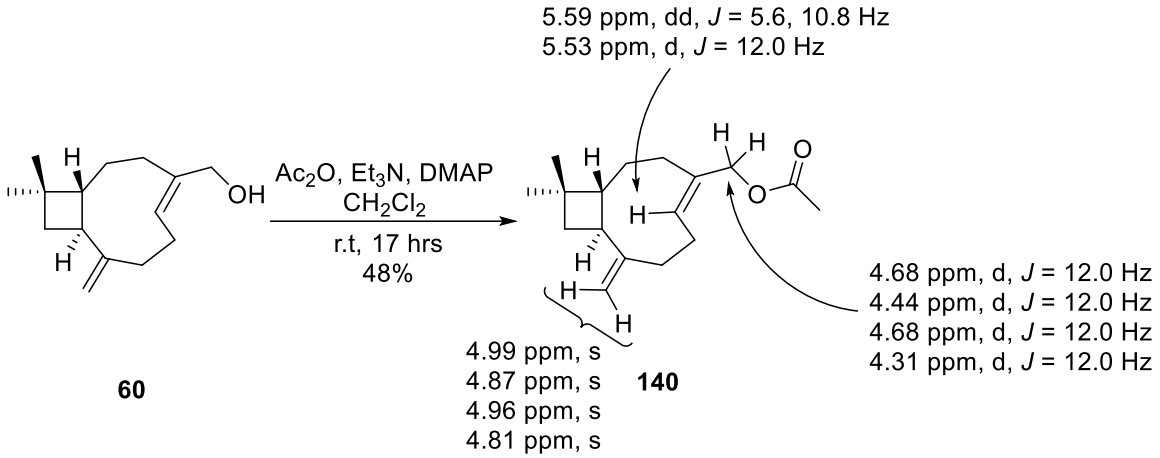

Scheme 4.1. *Acetylation of 12-hydroxycaryophyllene **60**.*

The precursor compound isolated from *S. crassifolia* was therefore 12-hydroxycaryophyllene **60** in 0.02% yield (Figure 4.3).

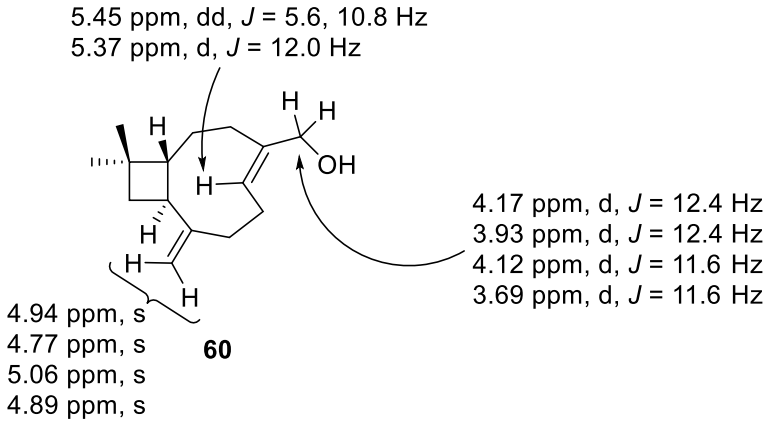

Figure 4.3. *Analysis of 12-hydroxycaryophyllene **60**.*

Interestingly, Barrero *et al*. reported that both 12-hydroxycaryophyllene **60** and 12-acetoxycaryophyllene **140** existed as mixtures of the βα and ββ conformers, which are both visible in the ^{1}H and ^{13}C NMR spectra.[48b] They also reported that the ratio of the βα and ββ changed between the 12-hydroxycaryophyllene **60** and the 12-acetoxycaryophyllene **141**, going from a βα:ββ ratio of 42:58 to 68:32. The isolated 12-hydroxycaryophyllene **60** had a βα:ββ ratio of 42:58 and the 12-acetoxycaryophyllene **140** had a βα:ββ ratio of 33:67, which both closely matched the values reported by Barrero *et al*.[48b]

The other four compounds isolated from the neutrals fraction were identified by ^{1}H NMR spectroscopy as 6-hydroxycaryophyllene **1** in 0.01 % yield, 12-acetoxy-6-hydroxycaryophyllene **2** in 0.16% yield, ursolic acid **110** in 0.02% yield and 6,12-dihydroxycaryophyllene **3** in 0.05% yield.

The phenols fraction was purified by column chromatography giving a mixture of two compounds as a yellow solid and a second mixture of compounds as a yellow solid. The first mixture of compounds was identified by ^{1}H NMR spectrscopy as a mixture of 8-prenylflavanone **138** and 6-prenylflavanone **139** in 0.01% yield. The second mixture of compounds was further purified by column chromatography to afford compound **141** as a yellow solid in 0.01% yield.

The FTIR spectrum showed two prominent OH absorbances at 3490 and 3406 cm^{-1}, indicating the hydroxyl groups are potentially participating in hydrogen bonding. A prominent carbonyl absorbance was visible at 1604 cm^{-1}, indicating that the carbonyl was heavily conjugated. The ^{13}C NMR spectrum contained 20 signals, of which only three were between 10 and 30 ppm, indicating that the compound was highly aromatic. A signal at 183.1 ppm confirmed the presence of a ketone in the compound. The ^{1}H NMR spectrum showed a singlet at 13.30 ppm that integrated for 1H, indicating that the compound contained a hydrogen bonded phenol, which is characteristic of a flavonoid. A triplet at 5.28 ppm that integrated for 1H suggested that an alkene was present in the compound. A doublet at 3.35 ppm integrated for 2H, indicating that a methylene was present and the HMBC spectrum showed that the methylene was adjacent to the alkene. Two doublets at 1.65 ppm and 1.78 ppm each integrated for 3H, indicating that two methyl groups were present in the compound. The two methyl groups correlated with the alkene, indicating they were adjacent to the alkene. The arrangement of the two methyls, alkene and methylene was characteristic of a prenyl group (Figure 4.4).

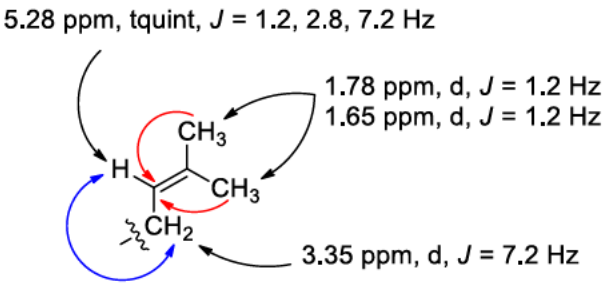

Figure 4.4. *Analysis of prenyl group in unknown flavonoid* ***141****. Red lines show HMBC correlations. Blue lines show COSY correlations.*

A doublet of doublet of doublets and a doublet at 7.46 ppm and 7.49 ppm, respectively, each integrated for 1H. Similarly, a doublet at 7.00 ppm also integrated for 1H. The COSY spectrum indicated that all three hydrogens were coupling to each other, suggesting that they were part of a trisubstituted aromatic ring. The doublet at 7.49 ppm had a coupling constant of 2.4 Hz, suggesting that it was coupling with the doublet of doublet of doublets through long range coupling. In contrast, the doublet at 7.00 ppm had a coupling constant of 8.4 Hz, which was similar to the coupling constant of the doublet of doublet of doublets, indicating that these hydrogens were adjacent.

The doublet at 6.59 ppm integrated for 1H and the HMBC spectrum showed that the hydrogen correlated to four quaternary aromatic signals and the ketone. The correlation to the ketone also suggested that the phenol was hydrogen bonded to the ketone, and was part of the ring. The methylene of the prenyl group correlated to carbons in the same aromatic ring, indicating that the prenyl group was bonded to the aromatic ring. Therefore, the aromatic ring was likely pentasubstituted.

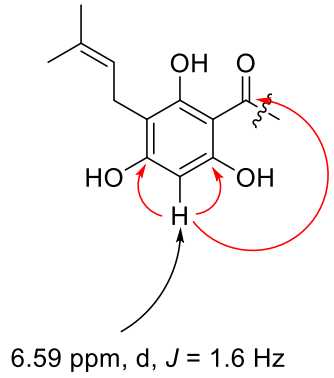

Figure 4.5. *Analysis of fragment of unknown flavonoid* ***141****. Red lines show HMBC correlations.*

The doublet at 6.57 ppm integrated for 1H. The HMBC spectrum showed that it correlated with four quaternary carbons including the ketone, but was not part of the same aromatic ring that the hydrogen at 6.59 ppm was a part of. However, the signal also appeared to be in an isolated spin system according to the COSY spectrum, suggesting that it was not part of the trisubstituted aromatic ring either and had long range coupling with an aromatic hydrogen in one of the rings. The correlation with the quaternary carbons and the ketone therefore indicated that the hydrogen was likely a vinylic hydrogen, such as that found in an α,β-unsaturated carbonyl system. Therefore, based on the FTIR, ^{1}H, ^{13}C and 2D NMR spectra, the compound was assigned as 4',5,7-trihydroxy-6-(3,3- dimethylallyl)-flavone **141**. 4',5,7-Trihydroxy-6-(3,3-dimethylallyl)-flavone **141** has been previously isolated by

Bohlmann *et al*. and the NMR spectral data is consistent.[113] However, the compound was incorrectly assigned by Bohlmann *et al*. as licoflavone C and was corrected by Kajiyana *et al*.[114]

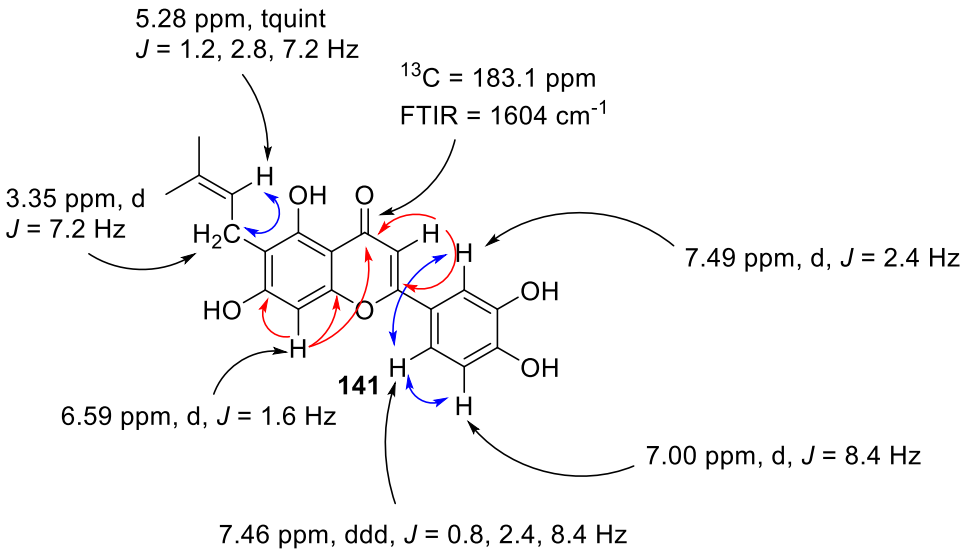

Figure 4.6. *Analysis of fragment of 4', 5,7-trihydroxy-6-(3,3- dimethylallyl)-flavone* ***141****. Red lines show HMBC correlations. Blue lines show COSY correlations.*

The natural products composition of *S. crassifolia* from Port Beach closely resembled that of the plants growing at Curtin University. However, the absence of 1,4-dihydroxy-α-bisabolol-2,10-diene **137** was notable and may have been produced due to environmental stressors.

4.2 Optimisation of natural products isolation from *Scaevola crassifolia*

Many interesting natural products have been isolated from *S. crassifolia*, with a variety of compounds that have potential for interesting chemistry. Extraction of the leaf resin followed by partitioning using acid-base chemistry was used as a standard procedure. However, alternate extraction and partitioning methods exist, including the use of different solvents or solid phase separation methods. For example, Moustafa *et al*. used EtOH for the extraction of the dried aerial components of *C. procera*.[28] Consequently, the effect of solvents, extraction times and extraction methods was investigated for extracting the leaf resin of *S. crassifolia* The extraction efficiency was determined by measuring the mass of extracted material and analysing the ^{1}H NMR spectrum of the extract to determine the chemical composition.

First, different solvents were trialled using a standard 20 min extraction time. Extraction using Et_2O, CH_2Cl_2 and EtOH yielded similar chemical compositions based on the ^1H NMR spectra (Figure 4.7). However, the yields of Et_2O and EtOH were significantly higher than that of CH_2Cl_2 at 2.47% and 2.24% versus 1.83% (Table 4.1). However, the higher yield from the EtOH extraction was attributed to the presence of residual EtOH in the extract.

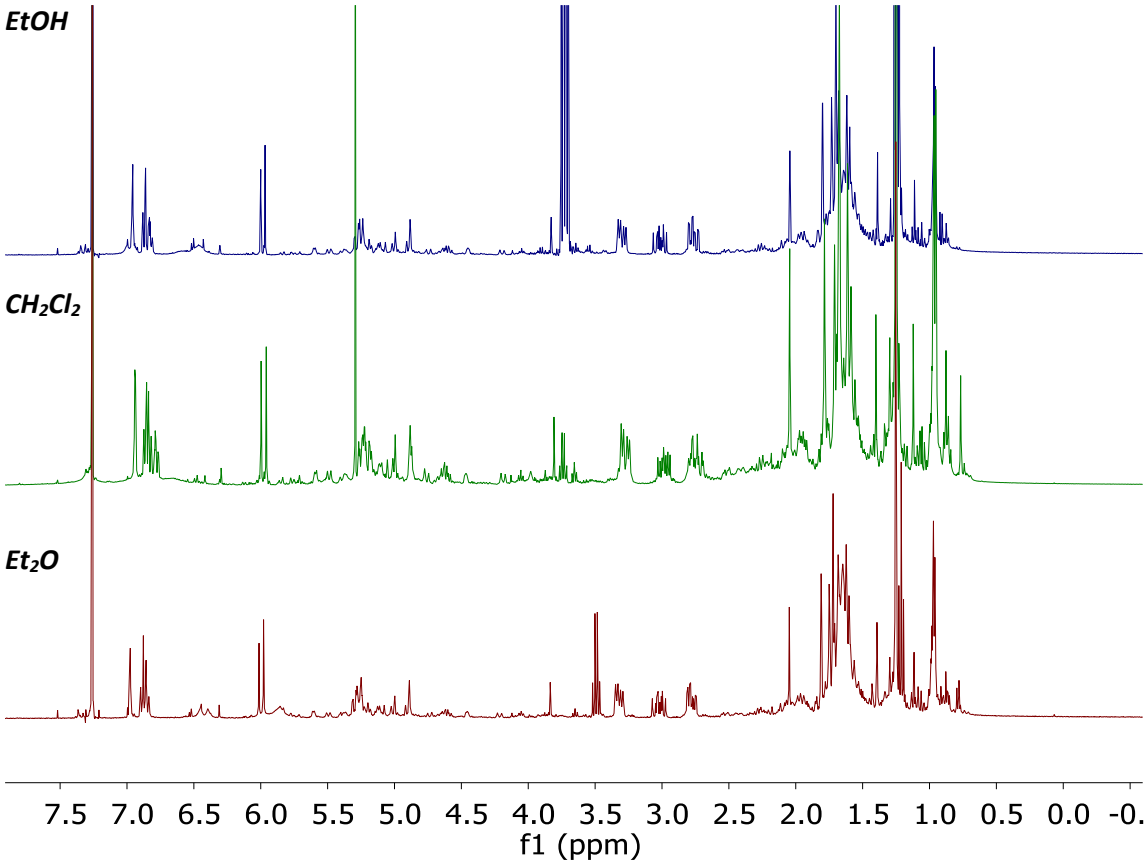

Figure 4.7. *^1H NMR spectra of EtOH (blue), CH_2Cl_2 (green) and Et_2O (maroon) extracts of* S. crassifolia *leaves.*

The PS extract was significantly lower in yield at 0.29% and contained primarily compounds from the neutrals fraction, with trace amounts of phenols visible (Figure 4.8) (Table 4.1). The lower yield and selective extractions of neutrals compounds indicated that the PS was too non-polar for extraction of many of the compounds found in the leaf resin.

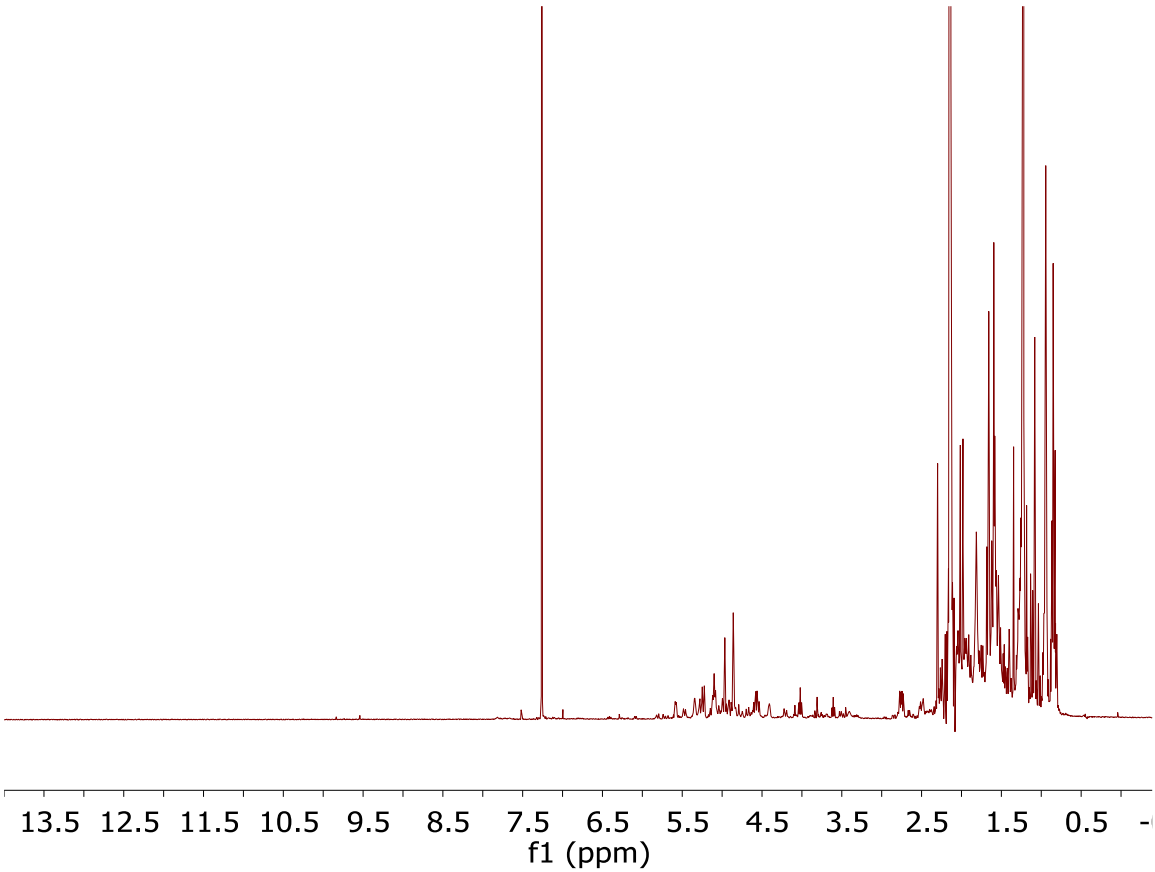

Figure 4.8. *^{1}H NMR spectrum of PS extract of* S. crassifolia *leaves.*

Extraction using deionised water for 20 mins was similarly low yielding, but interestingly the ^{1}H NMR spectrum showed that the dihydroxycaryophyllene **3** was almost exclusively extracted from the leaves (Figure 4.9). To determine if the yield could be improved, the deionised water extraction was repeated except the extraction time was increased to 24 hours. The yield increased significantly from 0.03% to 0.43% (Table 4.1). The ^{1}H NMR spectrum indicated that along with the dihydroxycaryophyllene **3**, flavonoids were also being extracted through the increased extraction time, based on the presence of hydrogen bonded phenol signals between 12 and 14 ppm (Figure 4.9). The presence of phenols in the aqueous extract suggested that rain has the potential to leach phenols from the leaf resin.

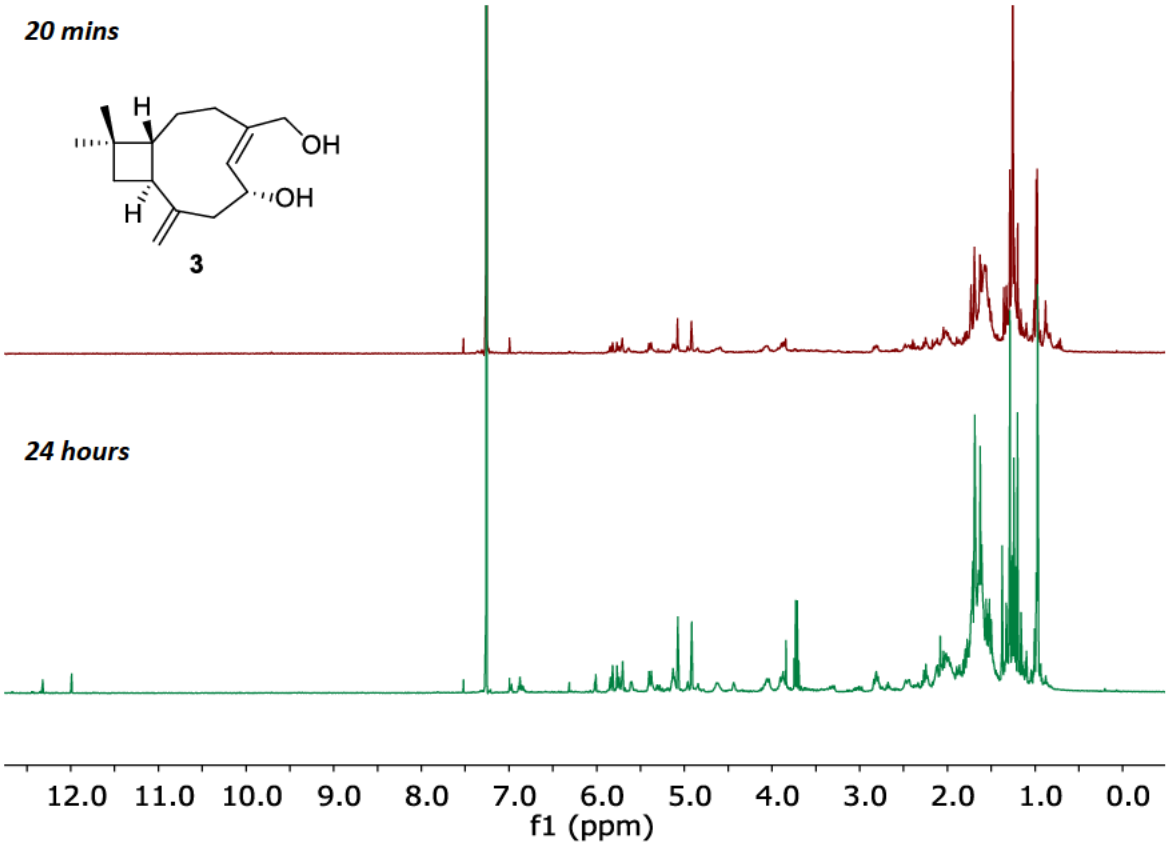

Figure 4.9. *^{1}H NMR spectra of deionised water extracts of* S. crassifolia *leaves with extraction times of 20 mins and 24 hours.*

Table 4.1. *Leaf masses, extraction solvents and volumes and extract masses from* S. crassifolia

Mass of leaves (g)	Solvent	Solvent Volume (mL)	Extraction time	Extract mass (g)	Percentage mass (%)
55.74	PS	200	20 mins	0.162	0.29
55.59	EtOH	200	20 mins	1.245	2.24
58.12	CH_2Cl_2	200	20 mins	1.062	1.83
63.35	Deionised water	300	20 mins	0.016	0.03
64.53	Deionised water	300	24 hours	0.277	0.43
54.92	Et_2O	200	20 mins	1.356	2.47

The neutrals fraction of the leaf extract contains the caryophyllenes, which were both of synthetic and spectroscopic interest. Consequently, a method to remove the unwanted components of the plant extracts, such as the phenols fraction, would reduce the labour involved in the isolation of the neutrals. Activated carbon is commonly used for the removal of contaminants including organic pollutants and metals.[115] Activated carbon is particularly effective at the removal of polar organic compounds. The removal of phenols from the resin extract using activated carbon was therefore investigated as a less labour intensive method for the isolation of the neutrals fraction. Fresh *S. crassifolia* leaves were steeped in Et_2O and the Et_2O extract was stirred with activated carbon twice. The ^1H NMR spectra before and after the addition of activated carbon showed that the compounds characteristic of the neutrals fraction remained in the extract while the phenols were mainly absent, showing that activated carbon was an effective method for the removal of phenols from the leaf resin extract (Figure 4.10). However, significant product loss is incurred through the use of activated carbon, with 1.356 g of extract prior to the addition of activated charcoal and 0.331 g after the second purification using activated carbon. Therefore, only a single purification step using activated carbon is recommended.

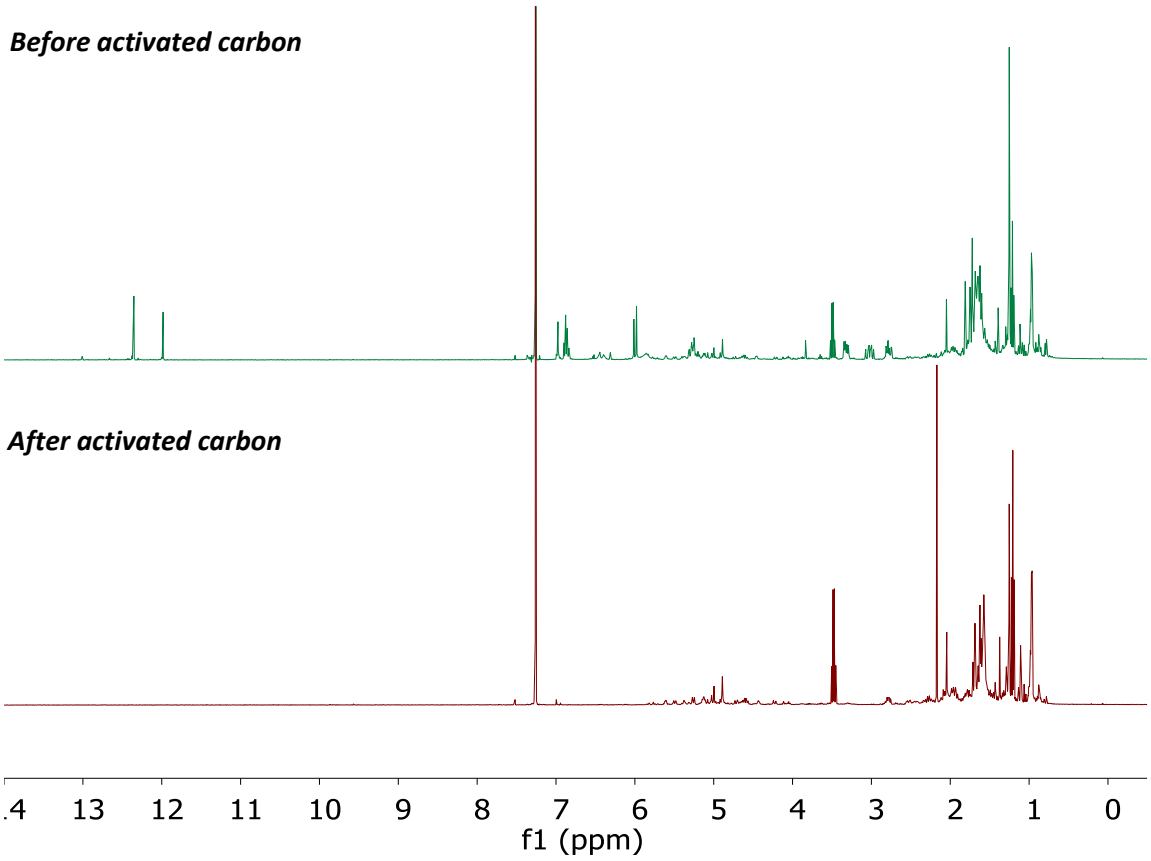

Figure 4.10. *^{1}H NMR spectra of Et_2O extract of* S. crassifolia *leaves pre- and post-purification using activated carbon.*

Interestingly, all the leaves after extractions using solvents apart from deionised water, had dried out after 24 hours, including the PS extracted leaves (Figure 4.11). The quick loss of water and degradation of the leaves indicates that the leaf resin played a crucial role in minimising water loss.

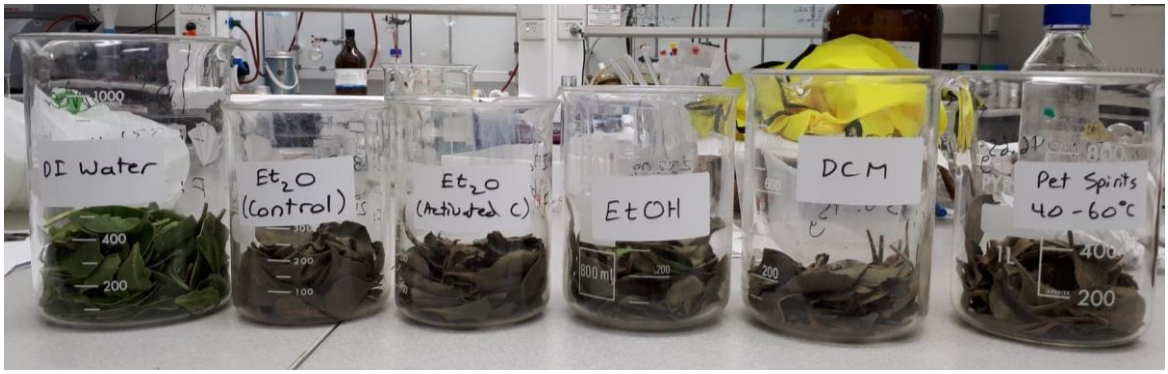

Figure 4.11. S. crassifolia *leaves after extraction with various solvents.*

Therefore, based on the experimental evidence extraction using Et_2O is still the most effective method for the extraction of the *S. crassifolia* leaf resin, and activated charcoal can be used for purification if only the neutrals fraction is required.

4.3 Biosynthetic investigation of birkenal 142, caryolan-1,3,4-triol 152 and diene 154

A preliminary investigation of the chemistry of 6-hydroxycaryophyllenes isolated from *S. crassifolia* was conducted as part of my Honours research. 6-Hydroxycaryophyllenes have a variety of interesting functional groups that would facilitate a variety of reactions. The endocyclic alkene is in a strained *E* configuration, resulting in it being significantly more reactive than the exocyclic alkene. The C6 allylic hydroxyl group is also perfectly positioned to undergo an allylic oxidation and generate an α,β-unsaturated ketone. Consequently, an allylic oxidation of the C6 hydroxyl group of 6-hydroxycaryophyllene **1** was attempted using activated MnO_2. Activated MnO_2 was added to a solution of 6-hydroxycaryophyllene **1** in dry CH_2Cl_2 and stirred at room temperature. After 4 hours, the reaction was worked up to give a colourless oil. The ^{1}H NMR spectrum showed that an aldehyde had been formed as the primary product, but the compound could not be isolated in sufficient purity to accurately confirm the identity of the compound. The procedure was optimised during this PhD study, whereby the colourless oil was isolated using a weak vacuum and the oil was purified by column chromatography to afford compound **142** as a colourless oil.

The FTIR spectrum showed no OH absorbance and a prominent carbonyl stretch at 1725 cm^{-1}. The ^{13}C NMR spectrum contained 14 signals and only two vinylic signals at 107.4 and 150.6 ppm. The ^{1}H NMR spectrum showed that the exocyclic alkene signals had shifted upfield from 4.97 and 4.86 ppm to 4.77 and 4.57 ppm respectively. The vinylic signal at 5.25 ppm was absent indicating that the endocyclic alkene was no longer present. The allylic hydrogen signal at 4.56 ppm was also absent, suggesting that the allylic hydroxyl group was similarly absent. A prominent singlet at 9.57 ppm, indicated the presence of an aldehyde in an isolated spin system. A doublet of quartets and a doublet at 2.46 and 2.60 ppm respectively that each integrated for 1H with an AB splitting pattern was also present that corresponded to a methylene. The HMBC spectrum indicated that the methylene hydrogens correlated with both the exocyclic alkene and the aldehyde, suggesting that the methylene was adjacent to or in close proximity to both groups. A

singlet at 1.04 ppm that integrated for 3H indicated the presence of a methyl and the HMBC spectrum showed that it strongly correlated to the aldehyde and the methylene. Therefore, based on the FTIR, ^{1}H, ^{13}C and 2D NMR spectra, the compound was assigned as the norsequiterpene birkenal **142** (Scheme 4.2) in 19% yield. Birkenal **142** was first isolated from the buds of the birch tree (*Betula pubescens*) by Klika *et al*. in 2004 and was synthesised by total synthesis by Hirokawa *et al*. in 2013.[116]

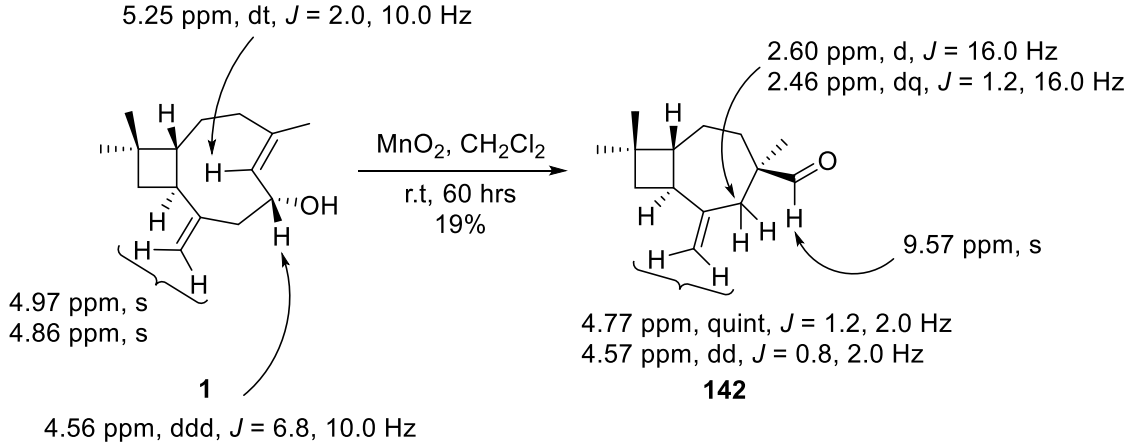

Scheme 4.2. *Oxidation of 6-hydroxycaryophyllene **1** using activated MnO_2.*

Trace quantities of the norsesquiterpene birkenal **142** have been detected in the leaf resin extract of *S. crassifolia*. The serendipitous reaction was unexpected and solicited further investigation. After scouring the literature, it was apparent that 6-hydroxycaryophyllene **1** and birkenal **142** had typically been found together, suggesting that there was a viable biosynthetic link between the two compounds.[117] The formation of birkenal **142** as a single diastereomer in the MnO_2 reaction suggested that the synthesis in plants may be an abiotic process, rather than an enzymatic process.

A biosynthetic mechanism for the formation of birkenal **142** has been previously postulated by Vedernikov *et al*.[118] Birkenal **142** is postulated to form through the oxidation of hydrocarbon **143**, which is biosynthesised through a reaction between geranyl pyrophosphate and isopenthenyl pyrophosphate (Scheme 4.3).

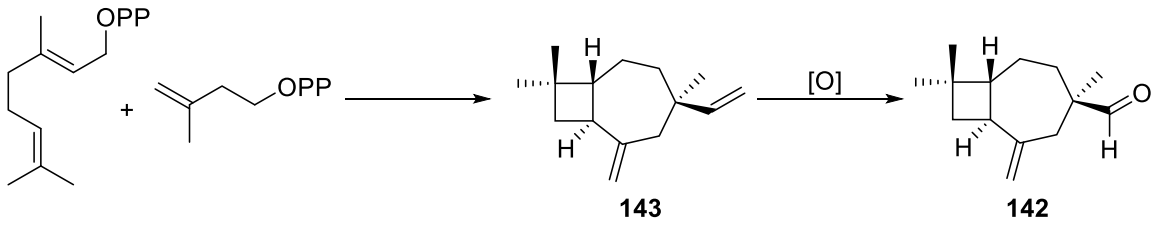

Scheme 4.3. *Proposed formation of birkenal **142** from hydrocarbon **143**.*

The formation of hydrocarbon **143** has been reported by Ohloff *et al*. through a Cope rearrangement of β-caryophyllene **58**. The primary product formed was isocaryophyllene **75** in 82% yield and hydrocarbon **143** in a 10% yield along with the C4 epimer **144** in an 8% yield (Scheme 4.4).

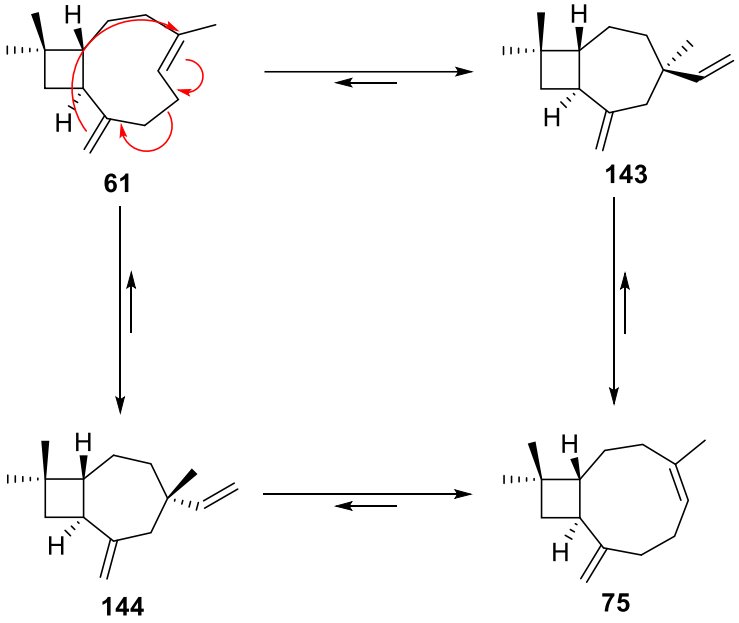

Scheme 4.4. *Proposed formation of hydrocarbon **143** from β-caryophyllene **58**.*

However, other than birkenal **142**, only one other oxidised derivative of hydrocarbon **143** has been tentatively reported, the diacid **145**, to date by Lutz *et al* (Figure 4.15).[119]

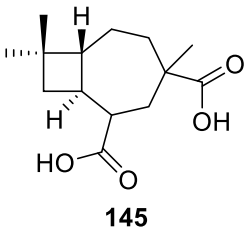

Figure 4.12. *Compound **145** synthesised by Lutz and Reid.*[119]

The lack of direct synthesis of birkenal **142** from β-caryophyllene **58** or hydrocarbon **143** and the observed formation of birkenal **142** from 6-hydroxycaryophyllene **1**, suggested that an alternate synthetic pathway was occurring. The formation of an intermediate was observed during the formation of birkenal **142** through careful monitoring of the reaction using TLC and ^{1}H NMR spectroscopy. Isolation of the intermediate would provide valuable insights into the synthetic mechanism for the formation of birkenal **142**. Activated MnO_2 was added to a solution of 6-hydroxycaryophyllene **1** in dry CH_2Cl_2 and stirred at room temperature for 1 hour. The reaction was worked up to afford a yellow oil, and the oil was purified by column chromatography to afford a colourless oil.

The FTIR spectrum of the compound showed a broad OH absorbance at 3405 cm^{-1} and no carbonyl absorbance. The ^{13}C NMR spectrum contained 15 signals, including two signals in the vinylic region at 114.4 and 147.7 ppm. The ^{1}H NMR spectrum showed that the C5 vinylic signal of 6-hydroxycaryophyllene at 5.25 ppm was absent, indicating that the endocylic alkene was no longer present. The triplet of doublets at 4.56 ppm had shifted upfield to 3.58 ppm, indicating that it was significantly more shielded. A new doublet was present at 2.99 ppm that integrated for 1H. The COSY and HMBC spectra showed that the doublet and the triplet of doublets were coupling to each other and were likely adjacent to one another. The allylic methyl of 6-hydroxycaryophyllene **1** had shifted upfield from 1.60 ppm to 1.29 ppm, indicating that it was no longer allylic, but still deshielded relative to the C14 and C15 methyl groups. The HMBC spectrum indicated that the C12 methyl was adjacent carbon that had a 3º alcohol. Therefore, based on the FTIR, ^{1}H, ^{13}C and 2D NMR spectra the compound was assigned as 4,5,6-trihydroxycaryophyllene **146** in 10% yield (Scheme 4.5).

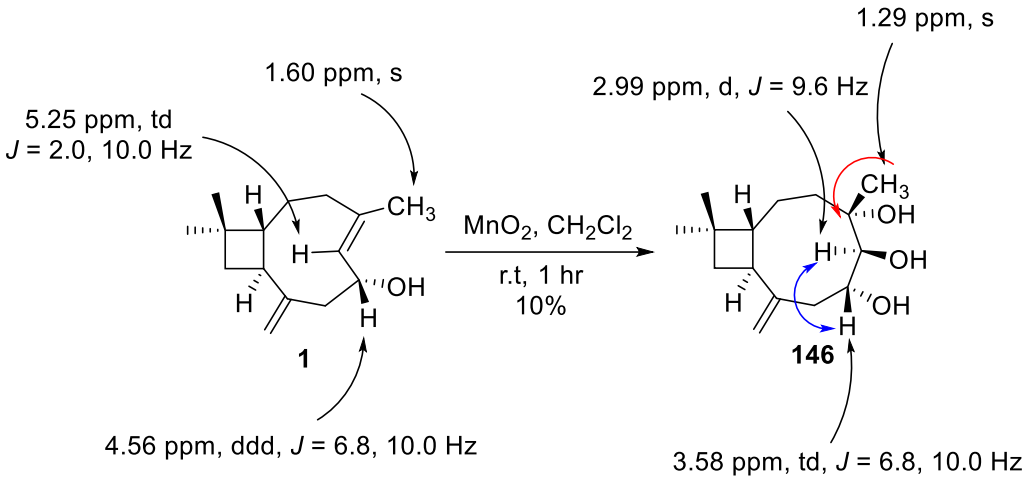

Scheme 4.5. *Synthesis of methyl triol caryophyllene* ***146*** *from 6-hydroxycaryophyllene* ***1****. Red lines show HMBC correlations. Blue lines show COSY correlations.*

The stereochemistry of methyl triol caryophyllene **146** was determined through NOESY correlations. The NOESY spectrum showed correlations between H3β-H5, H5β-H9 and H9-H3β, and between H2α-H15 and H15-H6 (Figure 4.15). The correlations showed the triol to be a product of a *syn*-dihydroxylation of the exposed face of the endocyclic alkene in the ββ-conformation.

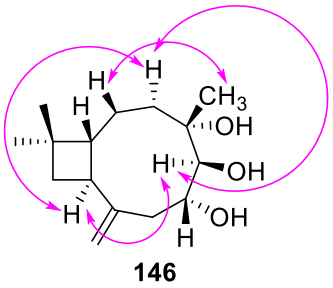

Figure 4.13. *NOESY correlations for 4,5,6-trihydroxycaryophyllene* ***146****.*

The dihydroxylation of alkenes using activated MnO_2 is rare, and can likely be attributed to the unique reactivity of the strained endocyclic alkene. Similar reactivity was observed during my Honours research, where reaction of β-caryophyllene **58** with activated MnO_2 afforded caryophyllene oxide **81** in 54% yield (Scheme 4.6). The formation of the epoxide suggested that the dihydroxylation potentially proceeded via a formation of the epoxide followed by hydrolysis of the epoxide to afford the diol.

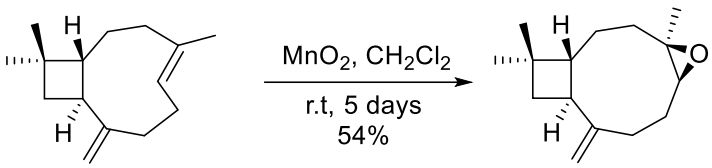

58 81

Scheme 4.6. *Synthesis of caryophyllene oxide* ***81*** *from β-caryophyllene* ***58****.*

6-Hydroxycaryophyllene oxide **147** has been previously isolated by Vedernikov *et al*. from the buds of *Betula pendula* Roth.[120] Epoxidation of β-caryophyllene to generate caryophyllene oxide indicated that selective epoxidation of the endocylic alkene was indeed possible. The auto-oxidation of β-caryophyllene through exposure to atmospheric oxygen has been previously reported Sköld *et al*.[121] They reported that after five weeks of exposure, almost 50% of the β-caryophyllene had been oxidised and after 48 weeks 99% of the β-caryophyllene had been oxidised.[121] β-Caryophyllene oxide had been formed along with a number of other oxidation products. It was therefore possible that 6-hydroxycaryophyllene oxide **147** could be similarly generated through auto-oxidation of 6-hydroxycaryophyllene **1**. A sample of crude neutrals fraction containing 6-hydroxycaryophyllene **1** was adsorbed to silica gel and left to stand for 2 weeks. The adsorbed material was then purified by column chromatography to afford compound **147** as a colourless oil.

The FTIR spectrum for compound **147** showed a broad OH absorbance at 3449 cm^{-1}. The ^{13}C NMR spectrum contained 15 signals, with two signals in the vinylic region at 114.1 and 147.8 ppm. Three signals were between 60 and 80 ppm, indicating the presence of three oxyegnated carbons. The ^{1}H NMR spectrum did not match that of methyl triol caryophyllene **146**. The ^{1}H NMR spectrum showed that vinylic H6 at 5.25 ppm was absent, indicating that the endocyclic alkene was absent. A doublet and singlet at 5.04 and 5.17 ppm that each integrated for 1H corresponded to the exocyclic alkene, indicating that the exocyclic alkene was still present. A new multiplet at 4.32 ppm that integrated for 1H was visible. The downfield shift indicated that hydrogen was signficantly deshielded and the HMBC spectrum showed a correlation to a quaternary carbon at 60.6 ppm, indicating the deshielded carbon was in close proximity. An overlapping doublet of doublets and a doublet were present at 2.90 ppm, that integrated for 2H, indicating the each signal likely integrated for 1H. The HSQC spectrum showed that the doublet correlated to a deshielded carbon at 64.4 ppm and the HMBC spectrum indicated showed that the doublet was in close

proximity to the hydrogen at 4.32 ppm. The doublet of doublets at 2.90 ppm and the triplet of doublets at 1.96 ppm, were both part of the same methylene and correlated to the exocyclic alkene and the multiplet at 4.32 ppm, indicating that it was likely the C7 methylene. The multiplet at 4.32 ppm was therefore most likely the C6 hydrogen, but was no longer allylic. Therefore based on the FTIR, ^{1}H, ^{13}C and 2D NMR spectra the compound was tentatively assigned as 6-hydroxycaryophyllene oxide **147** (Scheme 4.7) in 0.5% yield. The structure was confirmed by HRMS, which provided an exact mass of 237.1846 *m/z* for the $[M+H]^{+}$ molecular ion, that corresponded to a molecular formula of $C_{15}H_{24}O_2$.

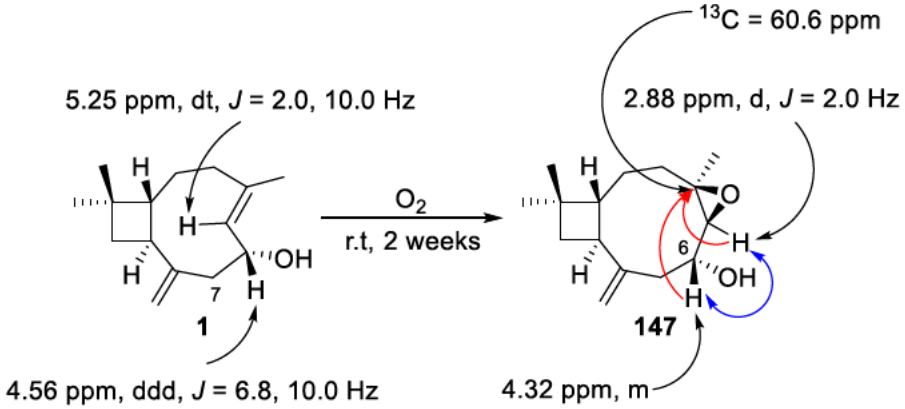

Scheme 4.7. *Synthesis and analysis of 6-hydroxycaryophyllene oxide **147** from 6-hydroxycaryophyllene **1**. Red lines show HMBC correlations. Blue lines show COSY correlations.*

The formation of 6-hydroxycaryophyllene oxide **147** from 6-hydroxycaryophyllene **1**, indicated that the 6-hydroxycaryophyllene oxide **147** may be an artifact of aerial oxidation rather than enzymatic biosynthesis. The low yield also suggested that the process was quite slow under ambient conditions, which can be supported by the low number of reports of this compound being isolated, even though 6-hydroxycaryophyllenes have been identified in several different plants.

The dihydroxylation of the endocyclic alkene was further explored through a reaction of the caryophyllene acetate **2** with activated MnO_2. Activated MnO_2 was added to a solution of caryophyllene acetate **2** in dry CH_2Cl_2 and stirred at room temperature. After 4 hours, the reaction was worked up to afford a white solid, which was purified by column chromatography to give compound **148** as a colourless oil.

The FTIR spectrum showed a broad OH absorbance at 3426 cm^{-1} and a prominent carbonyl absorbance at 1738 cm^{-1}. The ^{13}C NMR spectrum contained 17 signals, but only two in the vinylic region at 147.9 and 114.7 ppm. The ^{1}H NMR spectrum closely resembled that of

methyl triol caryophyllene **146** (Figure 4.16). Two doublets corresponding to the C12 methylene had shifted upfield from 4.17 and 4.69 ppm to 3.79 and 4.32 ppm respectively, indicating that they were more shielded. The doublet at 5.46 ppm corresponding to H5 was also absent, indicating that the endocyclic alkene was no longer present. The triplet of doublets corresponding to H6 had also shifted upfield from 4.58 ppm to 3.64 ppm, which was characteristic of the methyl triol caryophyllene **146**. A doublet that integrated for 1H was visible at 3.12 ppm that coupled with the triplet of doublets at 3.64 ppm according to the COSY spectrum. Therefore, based on the FTIR, ^{1}H, ^{13}C and 2D NMR spectra the compound was tentatively assigned as 12-acetoxy-4,5,6-trihydroxycaryophyllene **148** in 63% yield (Scheme 4.8). The structure was confirmed by HRMS, which gave an exact mass of 313.2004 *m/z* for the $[M+H]^{+}$ molecular ion, corresponding to a molecular formula of $C_{17}H_{28}O_5$.

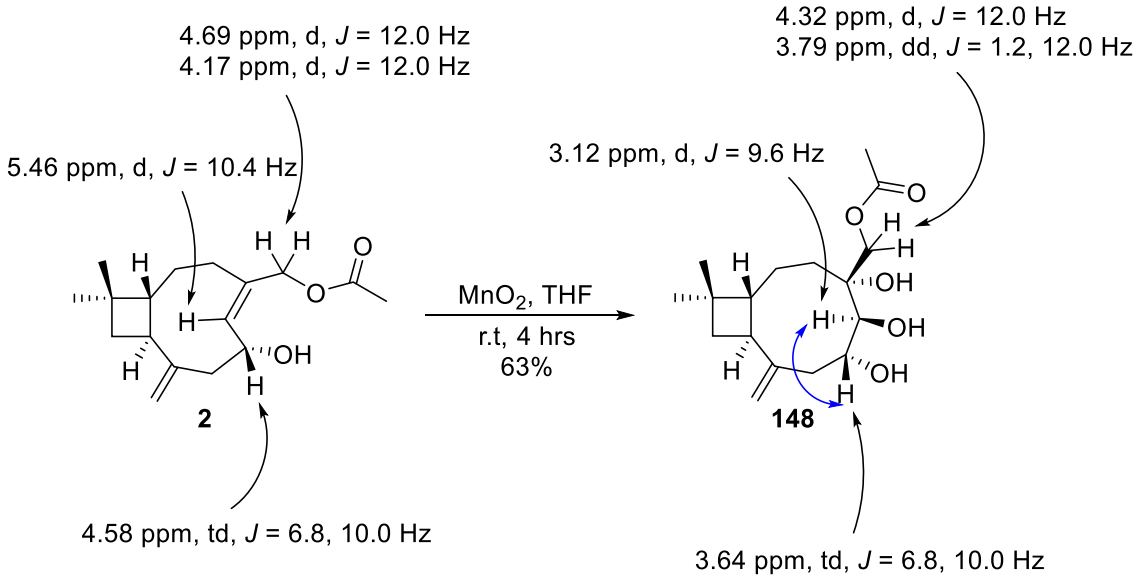

Scheme 4.8. *Synthesis of acetate triol caryophyllene **148** from 12-acetoxy-6-hydroxycaryophyllene **2**. Blue lines show COSY correlations.*

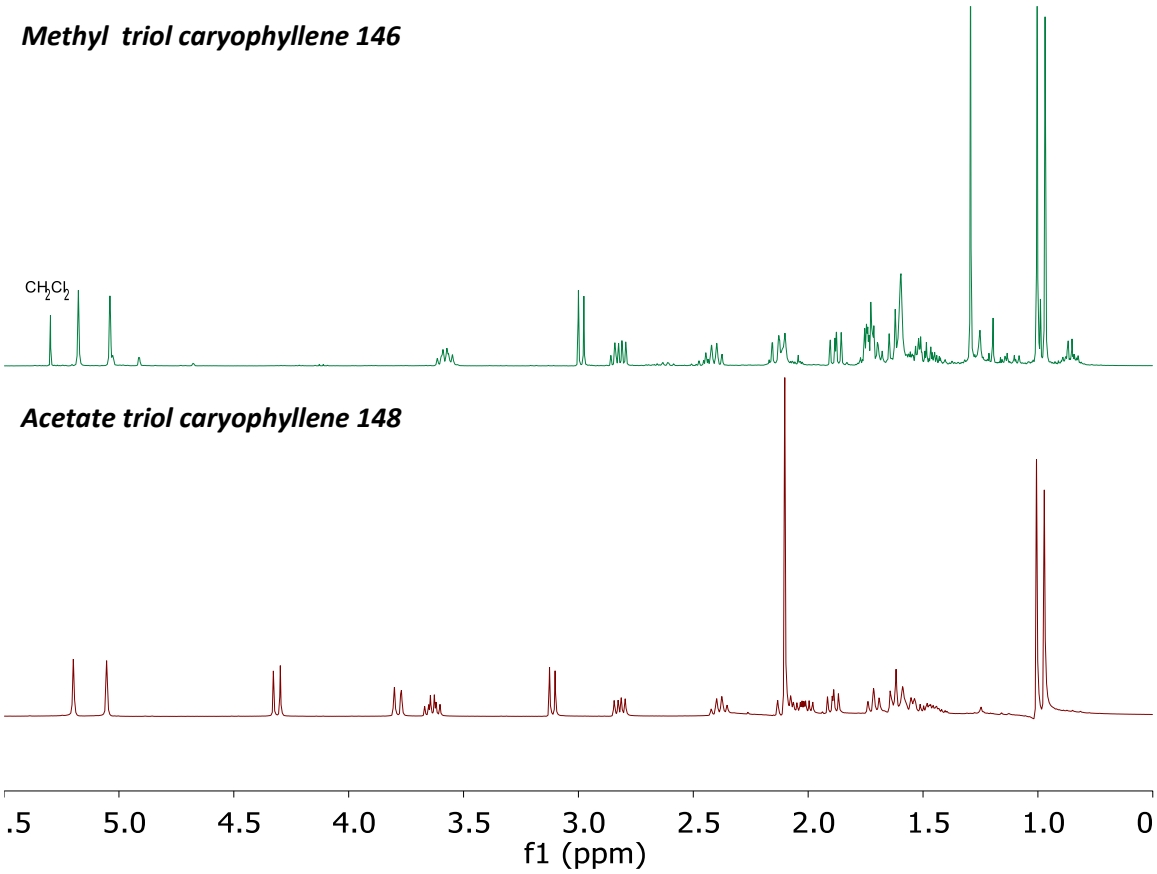

Figure 4.14. *^{1}H NMR spectra of methyl triol caryophyllene **146** and acetate triol caryophyllene **148**.*

Similar to methyl triol caryophyllene **146**, the stereochemistry of acetate triol caryophyllene **148** was assigned using NOESY. The NOESY spectrum showed correlations between H5-H9, H9-H3β and H3β-H5, and between H1-H14 (Figure 4.17). The NOESY correlations confirmed that the stereochemistry of methyl triol caryophyllene **146** supporting the proposed formation through a *syn*-dihydroxylation of the endocyclic alkene.

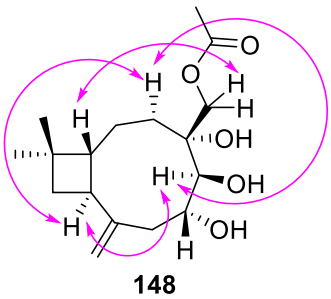

148

Figure 4.15. *NOESY correlations for acetate triol caryophyllene **148**.*

The acetate triol caryophyllene **148** was then further reacted with activated MnO_2 at reflux, as no further reaction had been observed at room temperature. Activated MnO_2 was added to a solution of acetate triol caryophyllene **148** in dry CH_2Cl_2 and the reaction was heated at reflux. After 16 hours, the reaction was worked up to give a yellow oil, which was purified by column chromatography to afford compound **149** and a colourless oil.

The FTIR spectrum for the compound showed no OH absorbances and a prominent carbonyl absorbance at 1743 cm^{-1}. The ^{13}C NMR spectrum contained 16 signals. Two carbonyl signals were visible at 204.4 and 170.8 ppm, which were characteristic of an aldehyde or ketone, or an ester. Two vinylic signals were also observed at 108.5 and 149.1 ppm. The ^{1}H NMR spectrum closely resembled that of birkenal **142** (Figure 4.18). A singlet at 9.62 ppm that integrated for 1H indicated the presence of an aldehyde in an isolated spin system. Two signals at 4.62 and 4.83 ppm that each integrated for 1H were characteristic of an exocyclic alkene. The triplet of doublets and doublet at 3.64 and 3.12 ppm, of **148**, were absent, reinforcing the absence of hydroxyl groups in the compound. A singlet was observed at 4.03 ppm that integrated for 2H. The HSQC and HMBC spectra indicated that the singlet corresponded to the methylene of the acetate. The singlet at 2.04 ppm that integrated for 3H confirmed the presence of the acetate in the compound. A doublet of doublets and a doublet at 2.47 and 2.69 ppm, respectively, was reminiscent of similar signal observed in the ^{1}H NMR spectrum for birkenal **142** that correpsonded to the C7 methylene. The HMBC spectrum showed that the methylene of the acetate correlated with the carbonyl of the aldehyde, indicating that they were in close proximity. Therefore based on the FTIR, ^{1}H, ^{13}C and 2D NMR spectra the compound was assigned as 12-acetoxybirkenal **149** in 12% yield (Scheme 4.9). The structure was confirmed by HRMS, which gave an exact mass of 265.1795 *m/z* for the $[M+H]^+$ molecular ion, corresponding to a molecular formula of $C_{16}H_{24}O_3$.

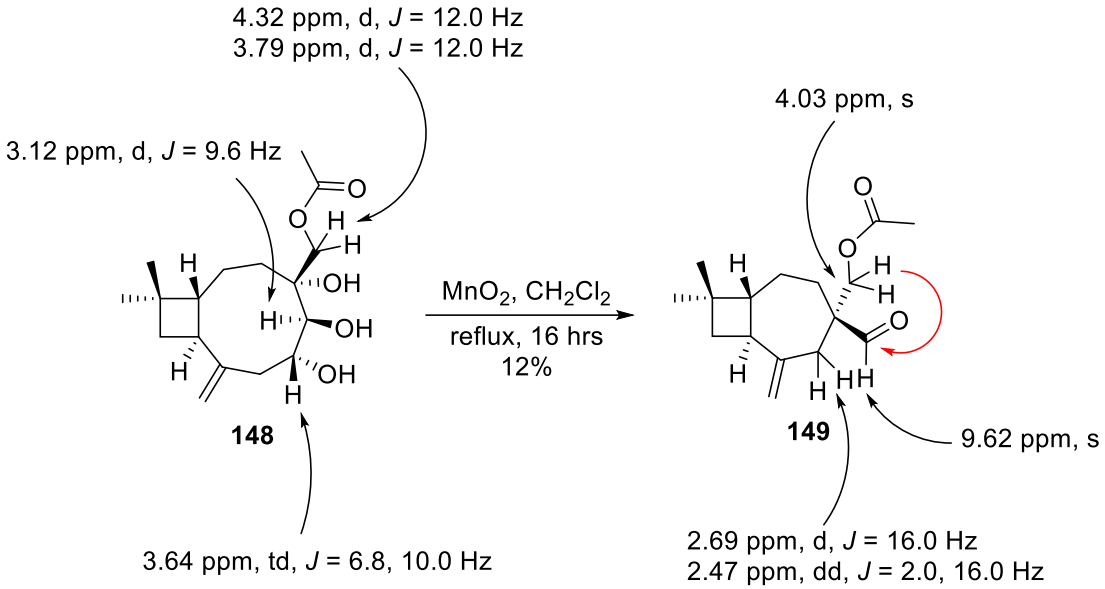

Scheme 4.9. *Synthesis of 12-acetoxybirkenal* ***149*** *from acetate triol caryophyllene* ***148****. Red lines show HMBC correlations.*

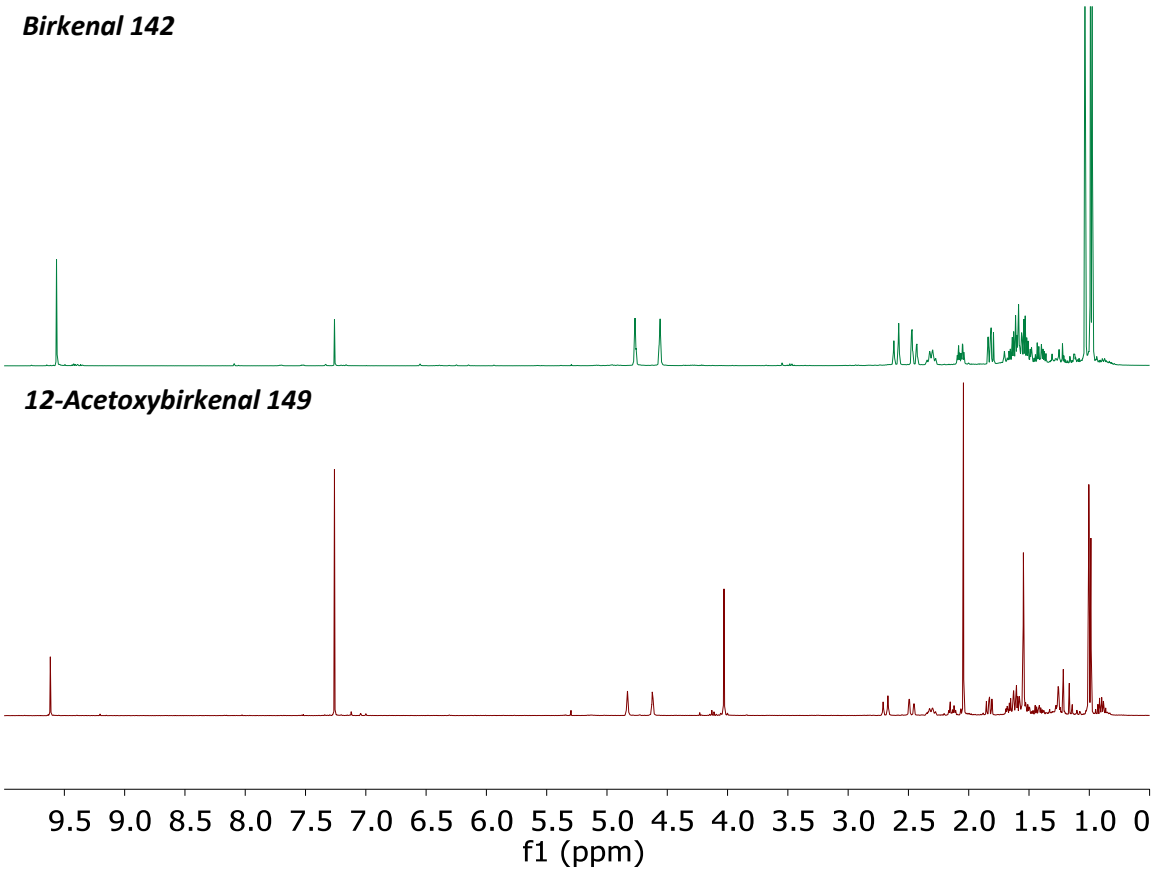

Figure 4.16. *^{1}H NMR spectra of birkenal* ***142*** *and 12-acetoxybirkenal* ***149****.*

The formation of 12-acetoxybirkenal **149** provided strong evidence that triol **146** was the intermediate in the formation of birkenal **142**. The *syn*-dihydroxylation of the 6-

hydroxycaryophyllene appeared to be the first step in the synthetic cascade to form birkenal **142** and its analogues, but gaps in the mechanism form birkenal from triol **142** were still apparent. The chemistry of acetate triol caryophyllene **148** was further explored to fill this gap, as it was more stable than methyl triol caryophyllene **146**. To further explore the reactivity of the exocyclic alkene, the acetate triol caryophyllene was protected via acetylation. Catalytic DMAP, Et_3N and Ac_2O were added to a solution of acetate triol caryophyllene **148** in dry CH_2Cl_2 and stirred at room temperature. After 16 hours the reaction was worked up to afford a yellow oil, and the oil was purified by column chromatography, giving compound **150** as a yellow oil.

The FTIR spectrum for compound **150** showed no OH absorbances and a prominent carbonyl absorbance at 1741 cm^{-1}, indicating that the acetylation was successful. The ^{13}C NMR spectrum contained 19 signals. However, only two carbonyl signals were observed at 170.3 and 170.9 ppm, indicating that only two acetates were present in the compound. The ^{1}H NMR spectrum showed two singlets at 2.07 and 2.10 ppm that each integrated for 3H, confirming the presence of only two acetates in the molecule. Two singlets at 5.15 and 5.25 ppm that each integrated for 1H indicated that the exocyclic alkene was still present. The triplet of doublets that corresponded to H6 had shifted downfield from 3.12 ppm to 4.80 ppm, indicating that it had become significantly deshielded. The C6 hydroxyl group had therefore likely been acetylated. A doublet of doublets and a doublet at 3.81 ppm and 4.42 ppm, respectively, each integrated for 1H and corresponded to the C12 methylene according to the HSQC spectrum. The high chemical shift suggested that the methylene hydrogens were also significantly deshielded by an electron withdrawing group, such as an ester, so the C12 acetate was also likely still present. A doublet was observed at 3.23 ppm that integrated for 1H, which closely matched the doublet found the in the ^{1}H NMR spectrum for acetate triol caryophyllene **148**, corresponding to H5. The HMBC spectrum showed that H5, H6 and H14 all correlated to a deshielded quarternary carbon at 61.2 ppm. The lack of hydroxyl groups and the presence of deshielded hydrogens and carbons in the compound indicated that epoxide had formed between C4 and C5. The structure of compound **150** was therefore tentatively assigned as 6,12-diacetoxycaryophyllene oxide **150** based on the FTIR, ^{1}H, ^{13}C and 2D NMR spectra in 36% yield (Scheme 4.10). The structure was confirmed by HRMS, which gave an exact mass of 359.1822 *m/z* for the $[M+H]^+$ molecular ion, corresponding to a molecular formula of $C_{19}H_{28}O_5$.

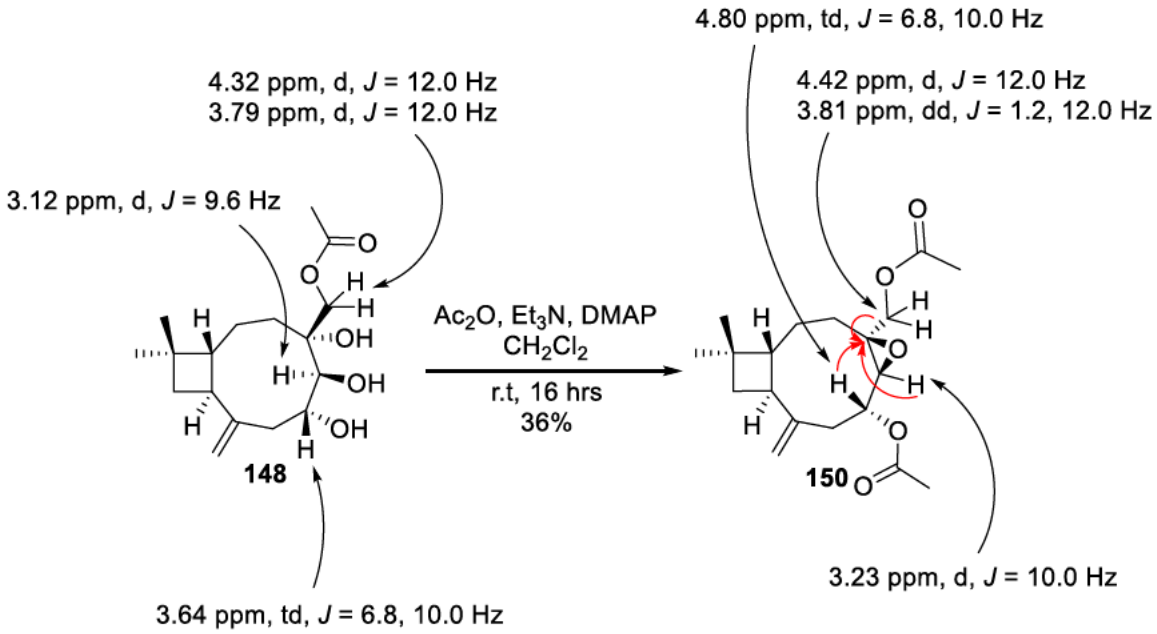

Scheme 4.10. *Synthesis of 6,12-diacetoxycaryophyllene oxide* ***150*** *from acetate triol caryophyllene* ***148****. Red lines show HMBC correlations.*

The formation of the epoxide was unexpected, but could be explained through the acetylation of the C4 hydroxyl group. Acetates can be leaving groups due to resonance stabilisation of the negative charge across the carboxylate. Loss of the acetate would generate a 3° carbocation, which then partipates in an addition reaction with the C5 hydroxyl group to generate the epoxide (Scheme 4.11). The formation of a single diastereomer can potentially be attributed to the natural stereoselectivity present within caryophyllenes, where one face of the molecule is less sterically hindered than the other.

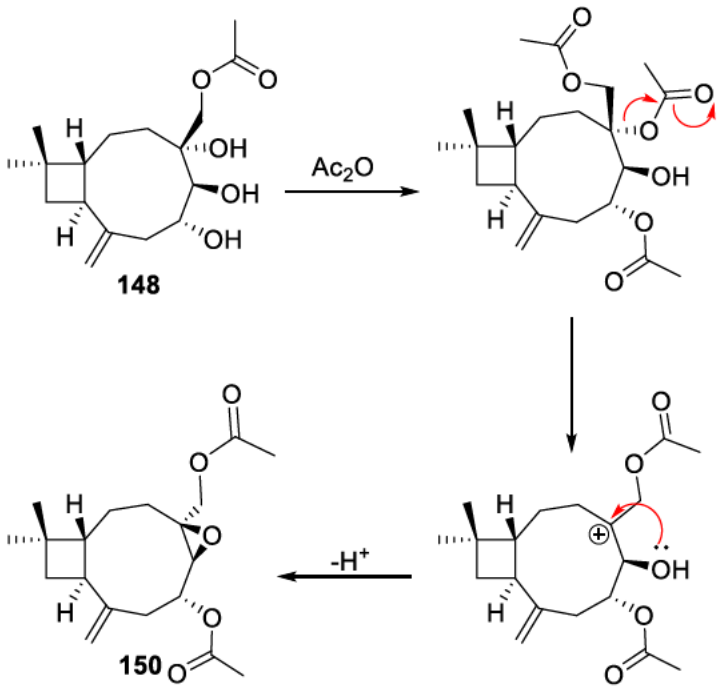

Scheme 4.11. *Proposed mechanism for the formation of 6,12-diacetoxycaryophyllene oxide* ***150*** *from acetate triol caryophyllene* ***148****.*

The formation of the epoxide highlighted the ease with which a carbocation was generated in the C4 position and warranted further investigation. Epoxides can be activated using a Lewis acid and can then be ring opened through the addition of a nucleophile. Surendra *et al*. reported the use of $MeAlCl_2$ to generate pentacyclic triterpenes through cationic cyclisation (Scheme 4.12).[122]

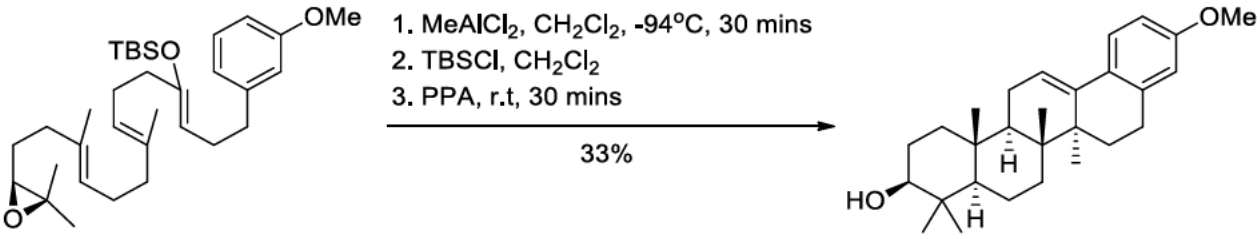

Scheme 4.12. *Cationic cyclisation facilitated by $MeAlCl_2$ used by Surendra et al. towards the synthesis of germanicol.*[122]

Cationic cylisation facilitated by $MeAlCl_2$ was attempted on epoxide **150** following a similar procedure to Surendra *et al*. A solution of $MeAlCl_2$ in hexane was added in portions to a solution of epoxide **150** in dry CH_2Cl_2. After 200 mins, the reaction was worked up to afford compound **151** as a colourless oil.

The FTIR spectrum showed a broad OH absorbance at 3484 cm^{-1} and a prominent carbonyl absorbance at 1742 cm^{-1}. Analysis was conducted in both $CDCl_3$ and acetone-d_6 due to overlap in peaks in the ^{13}C NMR spectra. The ^{13}C NMR spectrum ($CDCl_3$) contained 19 signals, with two visible signals in the carbonyl region but no vinylic signals present. Four signals were observed between 60 and 80 ppm, with two overlapping signals at 69.6 ppm. The ^{1}H NMR spectrum in $CDCl_3$ showed that the two signals at 5.15 and 5.25 ppm that were characteristic of the exocyclic alkene were absent, indicating the exocyclic alkene was no longer present in the molecule. The signals corresponding to the C14 methylene at 3.81 and 4.42 ppm had shifted closer together to 3.96 ppm and 4.06 ppm. The doublet corresponding to H5 had also shifted further downfield to 3.83 ppm. The triplet of doublets correpsonding to H6 had shifted downfield to 5.30 ppm from 4.80 ppm.

In the acetone-d_6 ^{13}C NMR spectrum four peaks between 60 and 80 ppm were visible, indicating the presence of four oxygenated carbons, including one 3º hydroxyl group. In the acetone-d_6 ^{1}H NMR spectrum a doublet and multiplet at 2.19 and 2.10-2.00 (containing two overlapping signals) that integrated for 1H and 2H, respectively, both corresponded to the same methylene. The hydrogens of the methylene correlated to the 3º hydroxyl in the HMBC spectrum, indicating that it was likely the methylene bridge that formed from the addition of the exocyclic alkene to the epoxide. The hydrogens of the C13 methylene and the suspected methylene bridge both correlated to a quaternary carbon in the HMBC spectrum, which was likely C4, further suggesting that the cationic cyclisation was successful. Therefore based on the FTIR, ^{1}H, ^{13}C and 2D NMR spectra, the compound was assigned as 3,12-diacetoxycaryolan-1,4-diol **151** in 12% yield (Scheme 4.13). 3,12-Diacetoxycaryolan-1,4-diol **151** is an analogue of caryolan-1,3,4-triol **152** which was isolated by Vedernikov *et al*. in 2012 from the buds of *Betula pendula* Roth (Figure 4.19).[123]

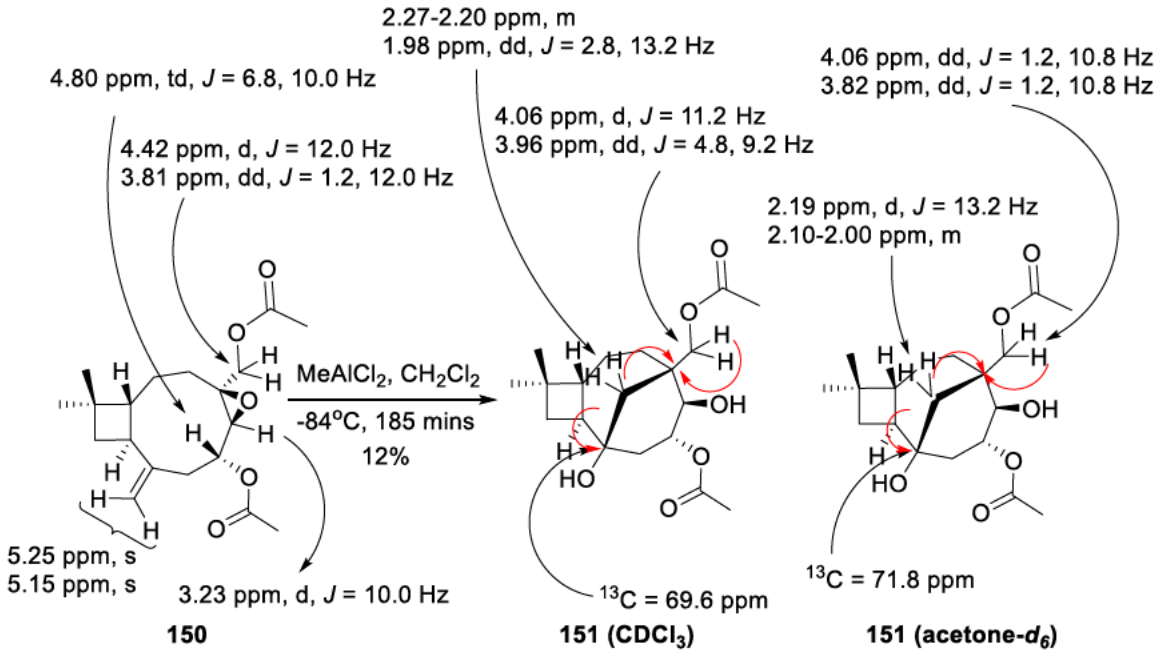

Scheme 4.13. *Synthesis of 3,12-diacetoxycaryolan-1,4-diol* ***151*** *from 6,12-diacetoxycaryophyllene oxide* ***150****. Red lines show HMBC correlations.*

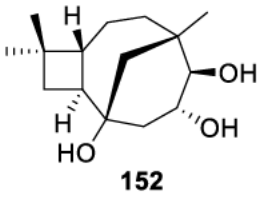

Figure 4.17. *Structure of caryolan-1,3,4-triol* ***152****.*

The Lewis acid catalysed cationic rearrangement of the caryophyllene epoxide derivative supported the hypothesis that a cation was easily formed in the C4 position and could be cyclised. However, if the formation of caryolan-1,3,4-triol **152** were to occur via an abiotic mechanism, then the presence of a coordinating Lewis acid would be unlikely. The formation of the 3° carbocation should be equally likely to occur using a Brønsted-Lowry acid. Therefore, the formation of similar ring systems should theoretically be possible using a triol compound rather than the protected epoxide (Scheme 4.14).

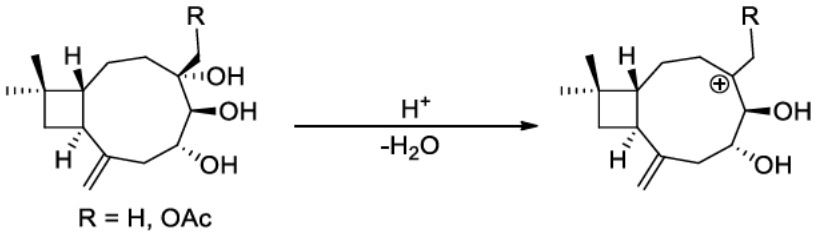

Scheme 4.14. *Formation of 3° carbocations in caryophyllene triols.*

The cyclisation of acetate triol caryophyllene **148** was investigated using glacial AcOH. The acid was added to a solution of acetate triol caryophyllene **148** in dry CH_2Cl_2 and the reaction mixture was heated at reflux (Scheme 4.15). After 72 hours, no visible reaction had occurred by NMR spectroscopy. It was apparent that the more mild conditions used for this reaction were insufficient to induce a skeletal rearrangement.

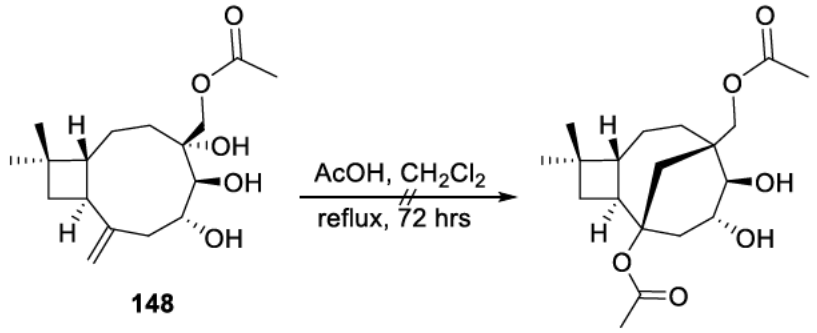

Scheme 4.15. *Glacial AcOH catalysed rearrangement of acetate triol caryophyllene **148**.*

Glacial AcOH is a weak acid and may not have been sufficiently acidic to catalyse the rearrangement at a lower temperature. The reaction was therefore repeated using a stronger acid, such as trifluoroacetic acid (TFA), which has a lower pKa (0.52) than glacial AcOH (4.76). TFA was added dropwise to a solution of acetate triol caryophyllene **148** in dry CH_2Cl_2 and the reaction mixture was stirred at room temperature. After 24 hours, the reaction was worked up, and the crude product was purified by column chromatography to afford compound **153** as a colourless oil.

The FTIR spectrum for compound **153** contained a broad OH absorbance at 3450 cm^{-1} and two carbonyl absorbances at 1738 and 1718 cm^{-1}, that may correspond to symmetric and asymmetric stretches of an ester. The ^1H NMR spectrum showed that the two singlets at 5.06 and 5.20 ppm were absent indicating that the exocylic alkene was no longer present. A singlet that integrated for 3H at 2.08 ppm was present, confirming the presence of the acetate in the compound. A new doublet of doublets was present at 4.24 ppm that integrated

for 1H. The HSQC and COSY spectra indicated that it corresponded to the C6 hydrogen. The ^{13}C NMR spectrum showed that four signals were present between 60 and 80 ppm, which indicated that oxygenated carbons were in the compound, one of which was a quaternary carbon. Two 2º alcohols, a 3º alcohol and a 2º acetate was consistent with the formation of the tricyclic product. Two hydrogens at 2.09-2.04 and 1.48-1.20 ppm corresponded to a methylene group. The methylene hydrogens correlated to the 3º alcohol and the methylene of the acetate, indicating that it was likely the methylene bridge formed from the addition of the exocyclic alkene to the 3º carbocation. Therefore, based on FTIR, ^{1}H, ^{13}C and 2D NMR spectra the compound **153** was assigned as 12-acetoxy-caryolan-1,3,4-triol **153** in 14% yield (Scheme 4.16).

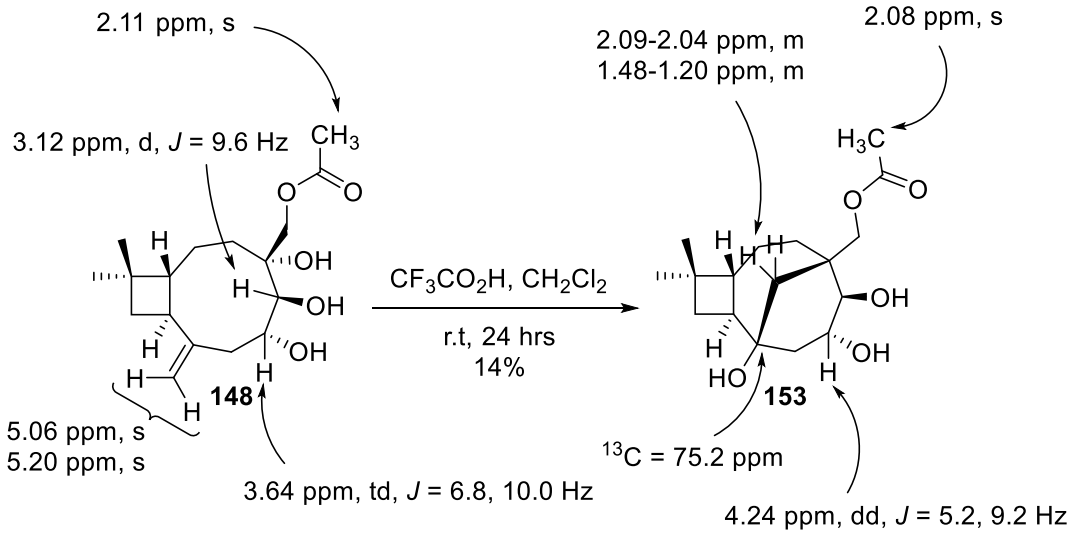

Scheme 4.16. *TFA catalysed cyclisation of acetate triol caryophyllene **148**.*

Based on the acid-catalysed rearrangement of acetate triol caryophyllene **148** to form 12-acetoxy-dihydroxycaryolan-1,3,4-triol **153**, it can therefore be postulated that caryolan-1,3,4-triol **152** can be synthesised from methyl triol caryophyllene **146** under acidic conditions. Glacial AcOH was added to a solution of freshly prepared methyl triol caryophyllene **146** in dry CH_2Cl_2 and the reaction mixture was stirred at room temperature. After 8 days, the reaction was worked up and the crude product was purified by column chromatography to afford compound **154** as a colourless oil.

The FTIR spectrum for compound **154** showed a broad OH absorbance at 3404 cm^{-1} and a prominent C=C stretch was visible at 1631 cm^{-1}. The ^{13}C NMR spectrum showed 15 signals, with four signals between 110 and 150 ppm, indicating that two alkenes were present in the molecule. Two signals were also visible at 71.2 and 74.2 ppm, which both

corresponded to a 2º alcohol. The ^{1}H NMR spectrum contained three peaks in the vinylic region of 4.5 to 6.0 ppm, at 4.82, 4.92 and 5.57 ppm. The peaks at 4.82 and 4.92 ppm correlated to the same carbon in the HSQC spectrum and correlated to the quaternary carbon of an alkene in the HMBC spectrum, indicating that they belonged to the exocyclic alkene. The new triplet at 5.57 ppm that integrated for 1H and correlated to a trisubstituted alkene. A singlet at 1.70 ppm integrated for 3H, indicating that it was a methyl and the higher chemical shift suggested it was an allylic methyl. A doublet at 4.33 ppm that integrated for 1H corresponded to the C5 hydrogen. The HMBC spectrum showed that the hydrogen correlated with the alkene, indicating that the alkene was located across C3 and C4. Therefore, based on the FTIR, ^{1}H, ^{13}C and 2D NMR spectra, compound **154** was assigned as 5,6-dihydroxycaryophyll-3,8-diene **154** in 10% yield (Scheme 4.17). The compound was previously isolated from birch buds by Vedernikov *et al*. and the spectral data was consistent.[123]

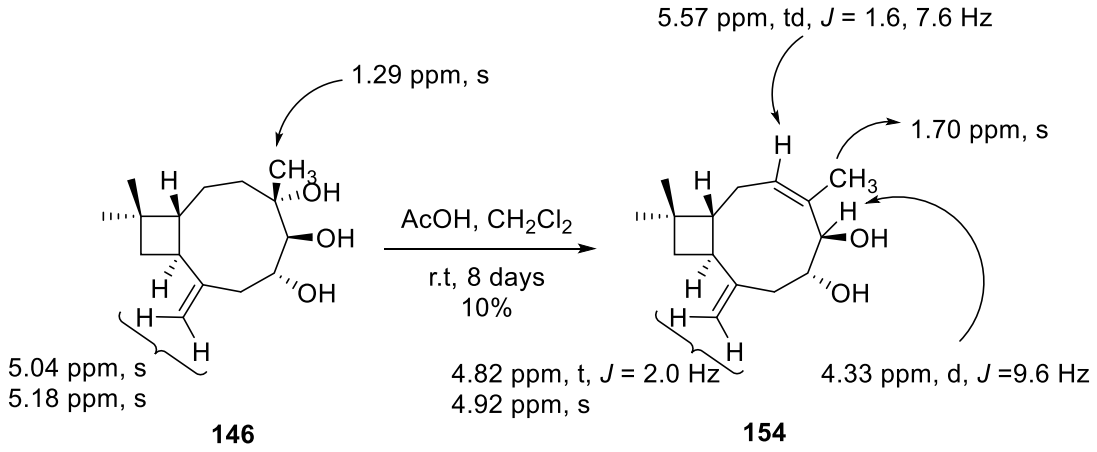

Scheme 4.17. *Glacial AcOH catalysed elimination of methyl triol caryophyllene **146**.*

The formation of the diene **154** over the tricyclic product indicated that the C12 acetate of acetate triol caryophyllene **148** significantly influences the reactivity of the compound. The acetate potentially sterically hinders the molecule making it unfavourable for an elimination reaction to occur, or distorts the molecular conformation to a similar end.

Vedernikov *et al*. proposed a biosynthetic mechanism for the formation of caryolan-1,3,4-triol **152** along with other rearranged products, starting from 6-hydroxycaryophyllene oxide **147**.[123] The epoxide is cleaved under acidic conditions to generate a 3º carbocation. An elimination reaction can then occur to generate diene **154** or a nucleophilic addition can occur through addition of the exocyclic alkene to the carbocation. The addition generates a

new 3° carbocation at the former C8 position, which is hydroxylated through a hydroxyl source such as water, to produce caryolan-1,3,4-triol **152** (Scheme 4.18).

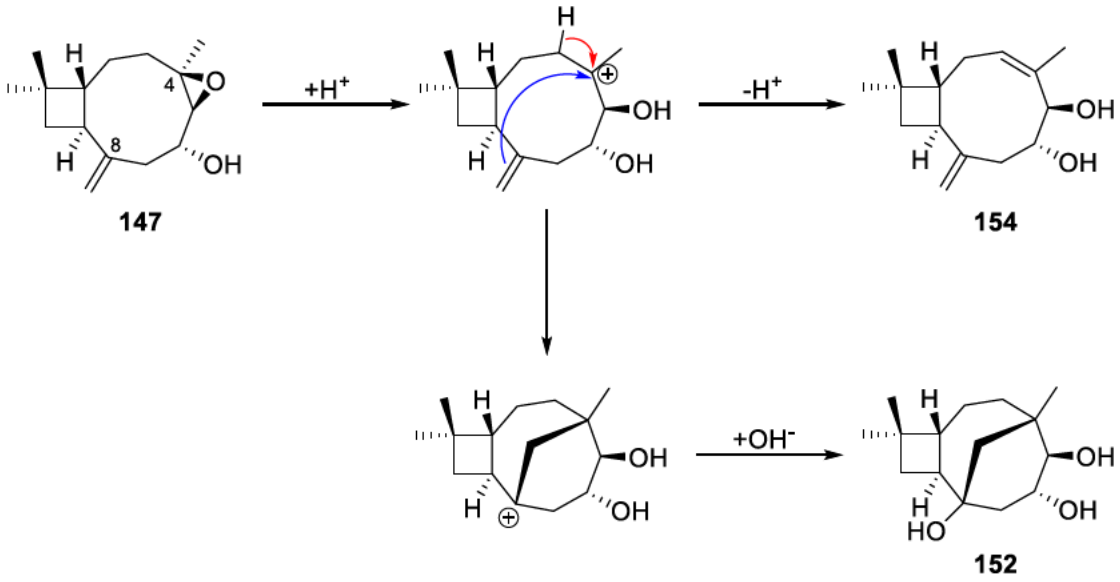

Scheme 4.18. *Proposed biosynthetic pathway for the formation of diene* ***154*** *and caryolan-1,3,4-triol* ***147*** *by Vedernikov et al.*[123]

The synthesis of 12-acetoxycaryolan-1,3,4-triol **153** and 3,12-diacetoxycaryolan-1,4-diol **151** from acetate triol caryophyllene **148** suggested that the formation of caryolan-1,3,4-triol **152** may be a competing biosynthetic pathway to that of the formation of birkenal **143**. The formation of 3,12-diacetoxycaryolan-1,4-diol **151** therefore validated the proposed mechanism for the formation of caryolan-1,3,4-triol **152** isolated from the silver birch tree (*Betula pendula* Roth) by Vedernikov *et al.*[123] Similarly, the formation of 5,6-dihydroxycaryophyllen-3,8-diene **154** from methyl triol caryophyllene **146** indicated that the formation of diene **154** was also a competing biosynthetic pathway to that of the formation of birkenal **142**. The formation of 5,6-dihydroxycaryophyllen-3,8-diene **154** under acidic conditions similarly validated the proposed mechanism for the formation of diene **154** from Vedrenikov *et al.*[123]

With methyl triol caryophyllene **146** and acetate triol caryophyllene **148** established as intermediates for the formation of birkenal **142** and 12-acetoxybirkenal **149**, a mechanism for the formation of birkenal **142** and its derivatives from the reaction of 6-hydroxycaryophyllene **1** and activated MnO_2 could be proposed (Scheme 4.19). The 6-hydroxycaryophyllene **1** first undergoes a *syn*-dihydroxylation to form methyl caryophyllene triol **146**. Protonation of the C4 hydroxyl group results in the generation of

a 3° carbocation through the loss of H_2O. The exocyclic alkene then adds to the newly formed carbocation to form the new seven membered ring of birkenal **142**. Addition of water to the newly formed 3° carbocation will then generate caryolan-1,3,4-triol **152**. However, a retro-Prins reaction can also occur to regenerate the exocyclic alkene and create a hydroxyaldehyde. Activated MnO_2 has been known to oxidatively cleave 1,2-diols.[124] The hydroxyaldehyde **155** therefore undergoes an oxidative cleavage of the aldehyde to generate formic acid and the norsequiterpenoid birkenal **142**. The biosynthesis of birkenal would follow a similar mechanism, but the initial oxidation step for the formation of methyl triol caryophyllene **146** or 6-hydroxycaryophyllene oxide **147** would be either aerial or enzymatic.

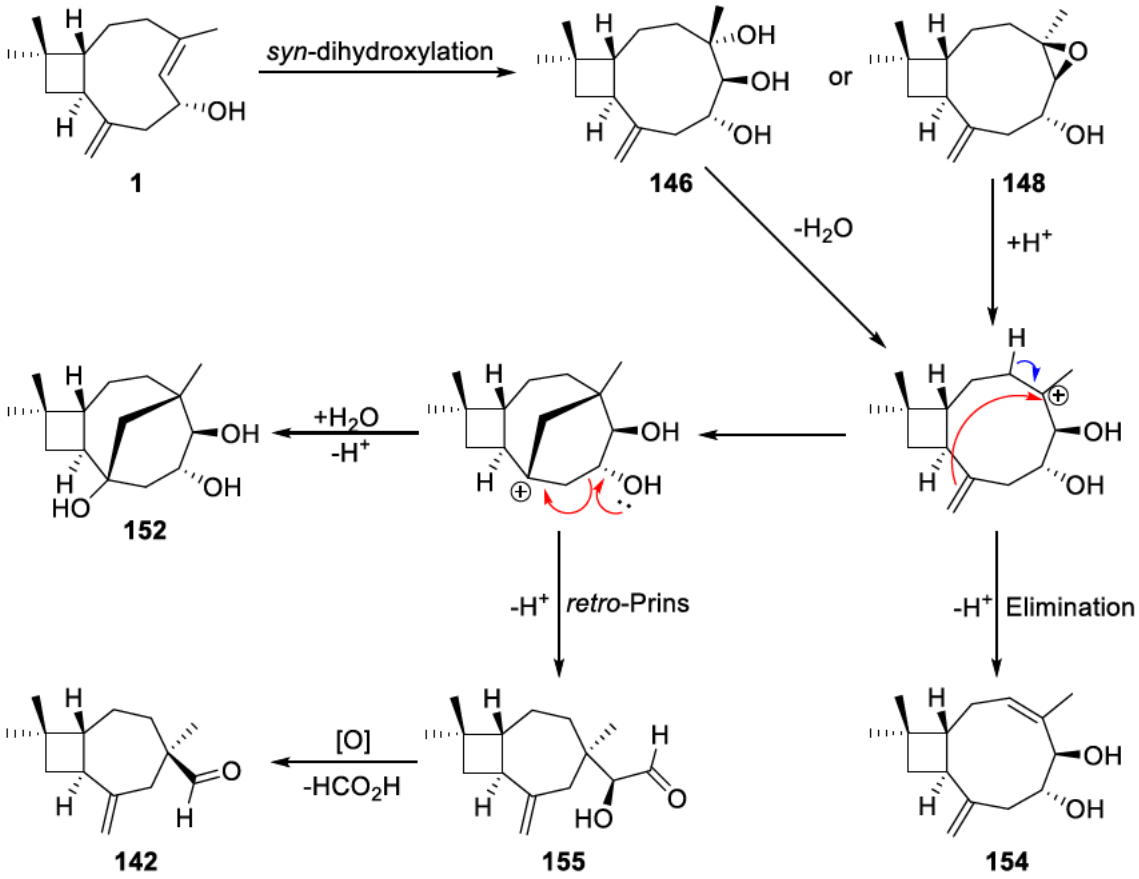

Scheme 4.19. *Proposed biosynthetic pathway for the formation of birkenal* ***142****.*

4.4 NMR spectroscopic investigation of auto-oxidation of 6-hydroxycaryophyllenes

A proposed mechanism had been developed for the formation of birkenal **142** from 6-hydroxycaryophyllene **1**. However, aside from the *syn*-dihydroxylation of 6-hydroxycaryophyllene **1** to form methyl triol caryophyllene **146**, all other steps in the proposed synthesis are acid-catalysed and should therefore potentially be able to be replicated *in vitro*. The formation of 6-hydroxycaryophyllene oxide **147** through exposure to air also suggested that the initial oxidation of 6-hydroxycaryophyllene **1** should be able to occur *in vitro*. Therefore, the conversion of 6-hydroxycaryophyllene **1** into birkenal **142** should theoretically occur in the presence of O_2 under acidic conditions, and the progress of the reaction could be monitored spectroscopically.

A time course study monitoring the gradual reaction of 6-hydroxycaryophyllene **1** was conducted. Three solutions of 6-hydroxycaryophyllene **1** were prepared in untreated $CDCl_3$, $CDCl_3$ treated with anhydrous K_2CO_3 and CD_3CN and the solutions were analysed by ^1H NMR spectroscopy at regular intervals. $CHCl_3$ is known to oxidise in air to form phosgene ($COCl_2$) and HCl, consequently resulting in the acidification of the $CHCl_3$ (Scheme 4.16). The basified $CDCl_3$ is used as a direct point of comparison with the standard $CDCl_3$, and the CD_3CN is used as a control that has a negligible possibility of acidification due to degradation at room temperature.

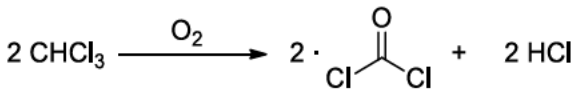

Scheme 4.16. *Generation of H_2CO_3 and HCl from degradation of $CHCl_3$.*

The 6-hydroxycaryophyllene **1** seemed to contain trace quantities of birkenal **142** initially, as indicated by the peak at 9.58 ppm. However in the standard $CDCl_3$, the 6-hydroxycaryophyllene **1** rapidly oxidised to form a new aldehyde within three days, and then continued to oxidise and rearrange to form a variety of new aldehyde containing compound (Figure 4.20). The birkenal **142** aldehyde signal also grew in intensity, but was still a minor product relative to other aldehyde products that were formed. After day 42 however, the newly formed aldehydes, such as the one at 9.84 ppm started to decompose and a new signal at 9.86 ppm was prominent. The new aldehyde remained stable in solution after day 109. Trace quantities of birkenal **142** remained, with the aldehyde signals at

9.58 ppm increasing slightly in intensity suggesting that trace quantities of birkenal **142** may indeed be formed through oxidation followed by acid catalysed rearrangements.

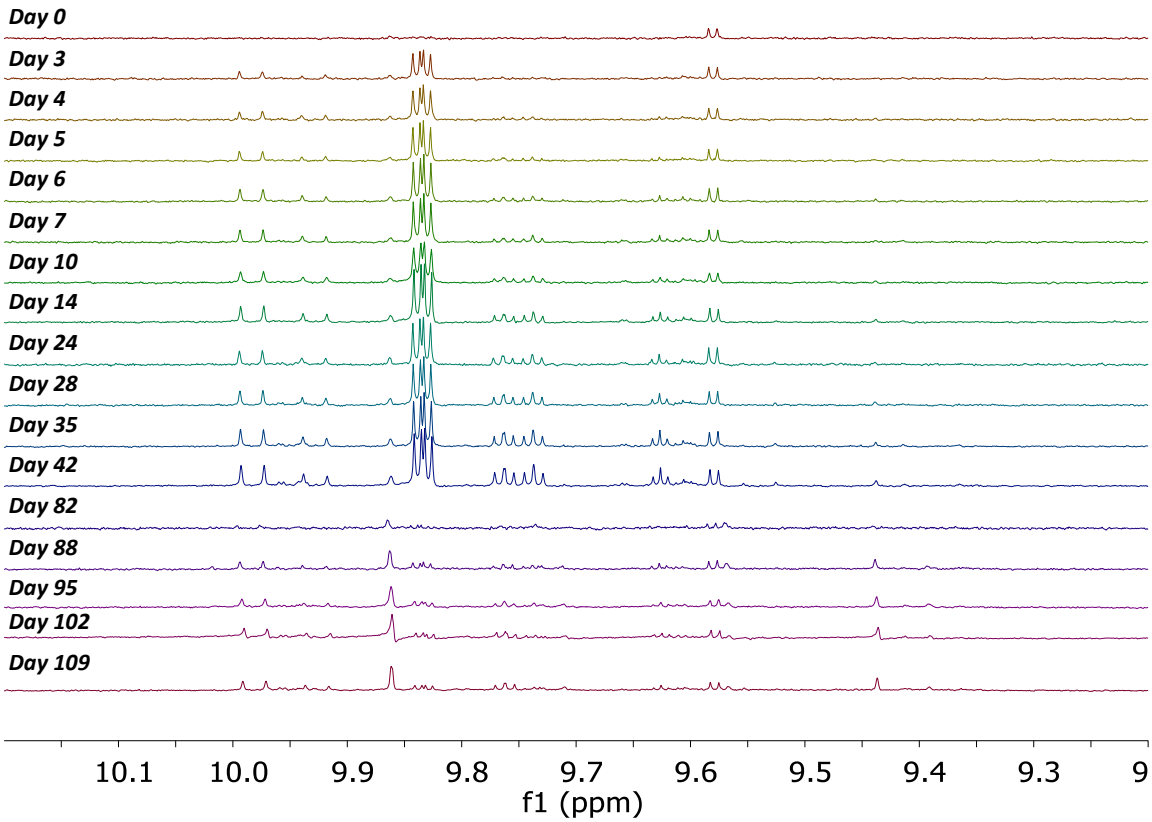

Figure 4.18. *Auto-oxidation of 6-hydroxycaryophyllene **1** in $CDCl_3$.*

In contrast, the auto-oxidation of the 6-hydroxycaryophyllene **1** in basified $CDCl_3$ was quite slow, indicating that the presence of acid greatly increases the rate of reaction. In an exciting observation, the 6-hydroxycaryophyllene **1** auto-oxidised to form the methyl triol caryophyllene **146** between day 30 and day 76, as indicated by the formation of singlets at 5.04 and 5.18 ppm and the doublet at 2.99 ppm (Figure 4.21). However, over time the intensity of the methyl triol caryophyllene **146** signals started to decrease and a new set of peaks at 4.80 and 4.90 ppm started to form, along with a doublet at 4.33 ppm (Figure 4.21). The newly formed peaks matched that of 5,6-dihydroxycaryophyllen-3,8-diene **154**, indicating that methyl triol caryophyllene **146** predominantly formed 5,6-dihydroxycaryophyllen-3,8-diene **154** under ambient conditions. The formation of diene **154** from 6-hydroxycaryophyllene **1** through exposure to O_2 and an acidic environment indicated that the reaction was likely abiotic and the occurrence of diene **154** was an artefact rather than a biosynthesised natural product. The formation of birkenal **142** was not detected in the ^{1}H NMR spectra.

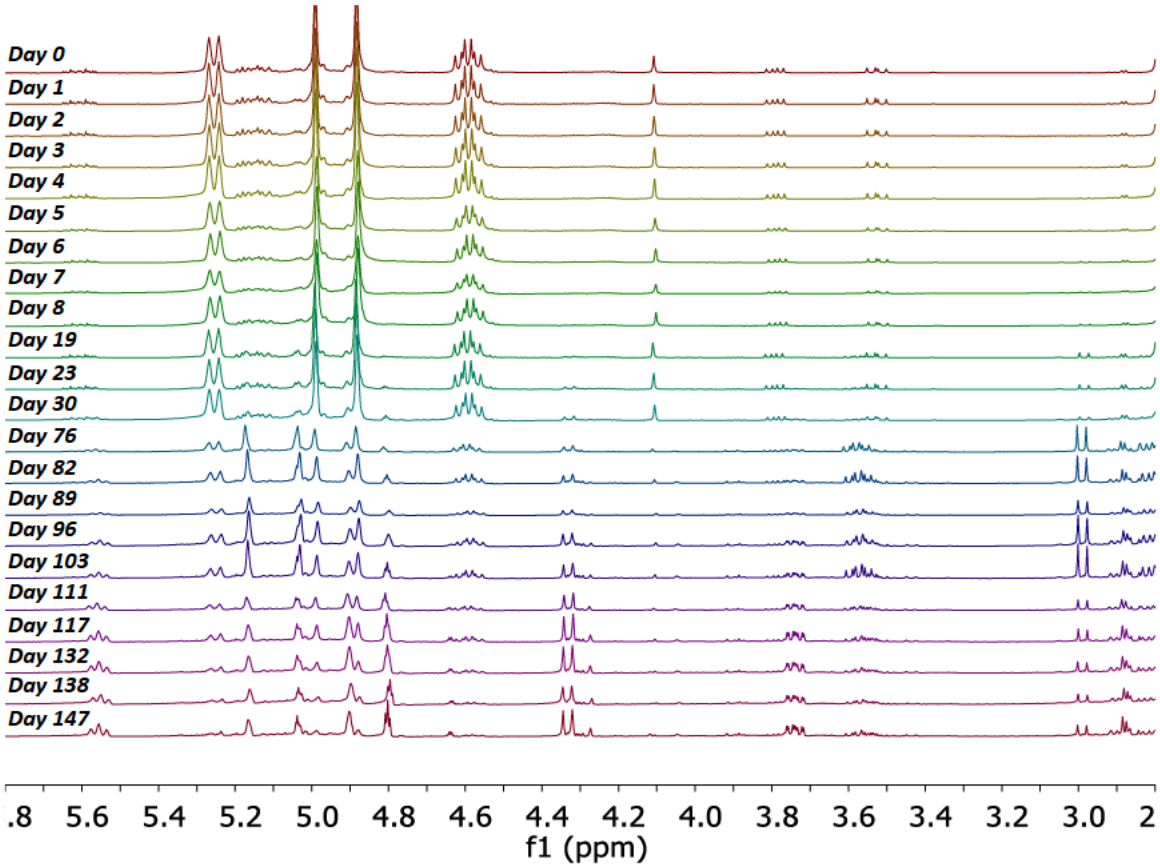

Figure 4.19. *Auto-oxidation of 6-hydroxycaryophyllene* ***1*** *in basified* $CDCl_3$.

The time course experiment in CD_3CN displayed no significant auto-oxidation, indicating that acid catalysis was a key factor in the formation of methyl triol caryophyllene **146** and the subsequent products. However, a change in the multiplicity of H6 at 4.48 ppm was observed. The signal changed from a doublet of doublet of doublet of doublets to a triplet of doublets, which can be attributed to a gradual deuterium exchange between the C6 hydroxyl group and deuterated water in the CD_3CN (Figure 4.22). In $CDCl_3$, H6 is typically observed as a triplet of doublets due to deuterium exchange between the $CDCl_3$ and the C6 hydroxyl group occurring, which prevents splitting with the hydroxyl hydrogen and H6. However, CD_3CN is an aprotic solvent, so deuterium exchange does not occur readily. Consequently, splitting between the C6 hydroxyl group hydrogen and H6 can be observed, resulting in the changed multiplicity. Deuterium exchange then slowly occurs between the C6 hydroxyl group and HOD, resulting in the slow observable change in multiplicity of H6.

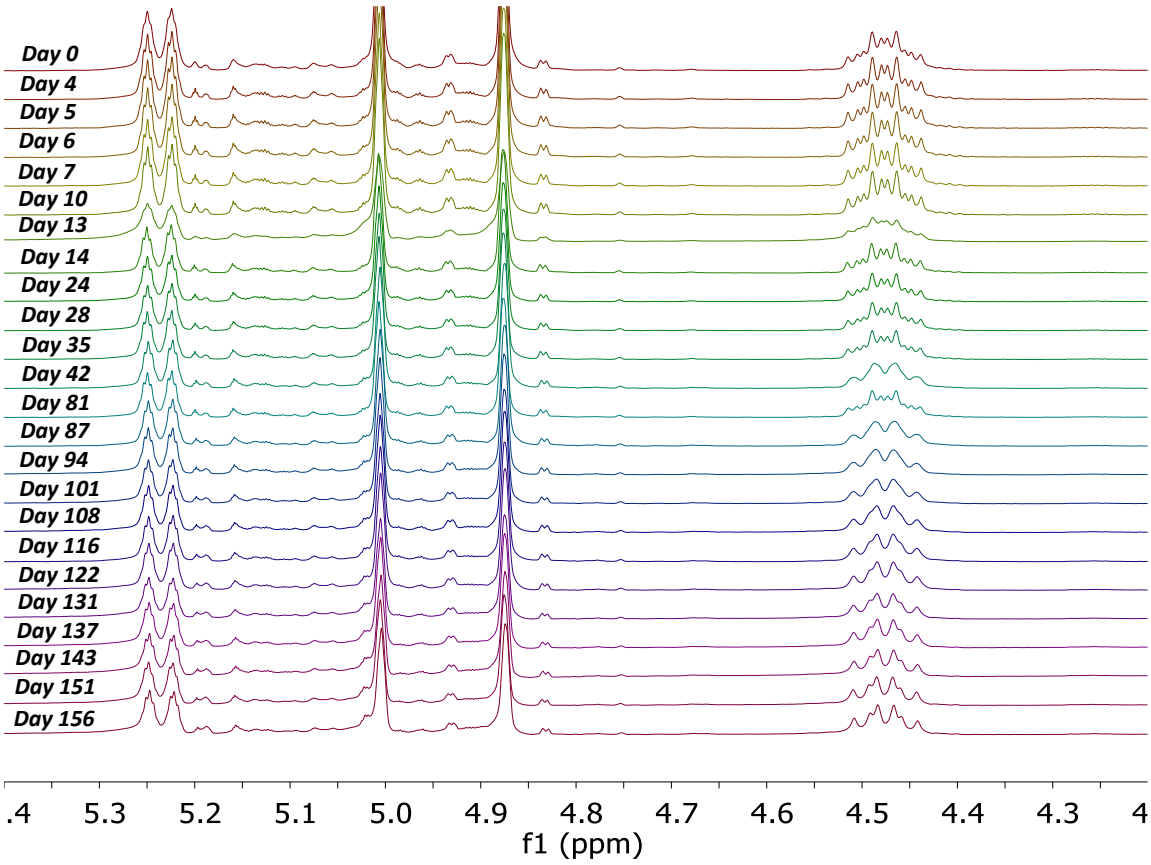

Figure 4.20. *Deuterium exchange of 6-hydroxycaryophyllene **1** in CD_3CN.*

Therefore based on the ^{1}H NMR experiments, it was apparent that oxidation of 6-hydroxycaryophyllene **1** was catalysed by the presence of acid. An acidic environment was also required for full conversion of 6-hydroxycaryophyllene **1** into aldehyde species. The trace quantities of birkenal **142** formed can be attributed to the numerous reaction pathways that can occur, resulting in only minor conversion of 6-hydroxycaryophyllene **1** into birkenal **142**.

4.5 Exploring the impact of antioxidants on the auto-oxidation of natural products from *Scaevola crassifolia*

The formation of a number of aldehydes, along with trace quantities of birkenal **137** through acid-catalysed auto-oxidation of 6-hydroxycaryophyllene **1** indicated that chemical transformation of 6-hydroxycaryphyllene **1** occurred readily. Over time, one would expect a significant quantity of aldehydes and related compounds to be present on the leaf surface of *S. crassifolia*. However, the presence of 6-hydroxycaryophyllenes is still predominant compared to the trace quantities of aldehydes detectable by NMR spectroscopy. Significant quantities of polyphenolic compounds such as flavanones were also present in the leaf resin

of *S. crassifolia*. Flavonoids have been reported to possess antioxidant properties.[125] Therefore, the antioxidant effect of flavonoids found within the surface leaf resin were potentially inhibiting the oxidation of other compounds found within the leaf resin and the antioxidant effect of the flavonoids warranted further investigation.

Samples of *S. crassifolia* neutrals fraction were prepared in a solution of Et_2O and dispensed into glass sample vials, after which the Et_2O was allowed to evaporate to dryness at room temperature. The impact of auto-oxidation on 2-3 samples of neutrals fraction was monitored using FTIR spectroscopy. The sampled was analysed by dissolution of the sample in the sample vial with a known volume of Et_2O and dispensing an aliquot of the solution on to the ATR crystal, after which the solvent was allowed to evaporate. The sample was analysed once a day and two key spectroscopic regions were monitored using the second derivative FTIR spectra: 2950-2830 cm^{-1} (aliphatic CH stretching) and 1700-1610 cm^{-1} (alkene C=C stretching). In the 2950-2830 cm^{-1} region, a significant change was observed after day 1. On day 1, CH stretching intensity in the asymmetric methylene region (2940 – 2900 cm^{-1}) rapidly decreased at 2925 cm^{-1}, while intensity at 2915 cm^{-1} rapidly increased, before stabilising over 2 days, with a gradual increase in the absorbance still being observed over the next 18 days (Figure 4.23). A similar trend was observed in the symmetric methylene C-H stretching region (2870 – 2830 cm^{-1}), specifically a drastic decrease in intensity was observed at 2855 cm^{-1}, with a drastic increase at 2848 cm^{-1}). The local second derivative intensity minima for each specific stretching region, could be measured and plotted in a scatterplot and then fitted using linear regression. The gradient of the trendlines could then provide an approximate measure of the rate of oxidation. Although not known with certainty, the spectroscopic changes observed in the C-H stretching region support a change in the intermolecular bonding environment of methylene ($-CH_2-$ functional groups), which is consistent with sample oxidation. The rapid changes across the 2950-2830 cm^{-1} range may indicate that the neutrals fraction is rapidly oxidised and then appears to oxidise more slowly after the initial reaction.

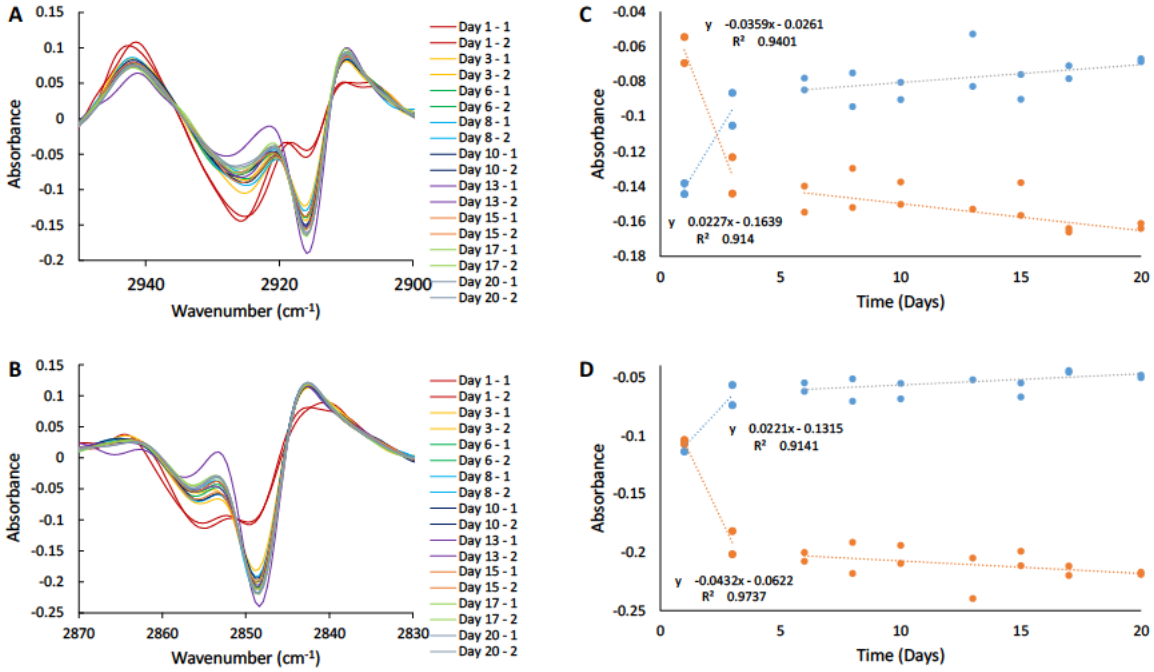

Figure 4.21. *Analysis of auto-oxidation of* S. crassifolia *neutrals. (A) Compiled second derivative FTIR spectra of neutrals fraction in the 2950-2900 cm^{-1} range (asymmetric methylene C-H stretching), (B) compiled second derivative FTIR spectra of neutrals fraction in the 2870-2830 cm^{-1} range (symmetric methylene C-H stretching), (C) scatter plot and linear trends of local minima in the 2940-2920 cm^{-1} region (blue), and in the 2920-2910 cm^{-1} region (orange), and (D) scatter plot and linear trends of local minima in the 2860-2853 cm^{-1} region (blue), and in the 2852-2840 cm^{-1} region (orange).*

Although the changes in the C-H stretching region may reflect sample oxidation, negligible change was observed in the alkene C=C stretching regions between 1700 and 1620 cm^{-1} (Figure 4.24). The lack of visible change suggested that oxidation of the alkenes of 6-hydroxycaryophyllenes may not be occurring and it could be other parts of the molecule, such as allylic positions, or other compounds in the neutrals fractions that were primarily oxidising.

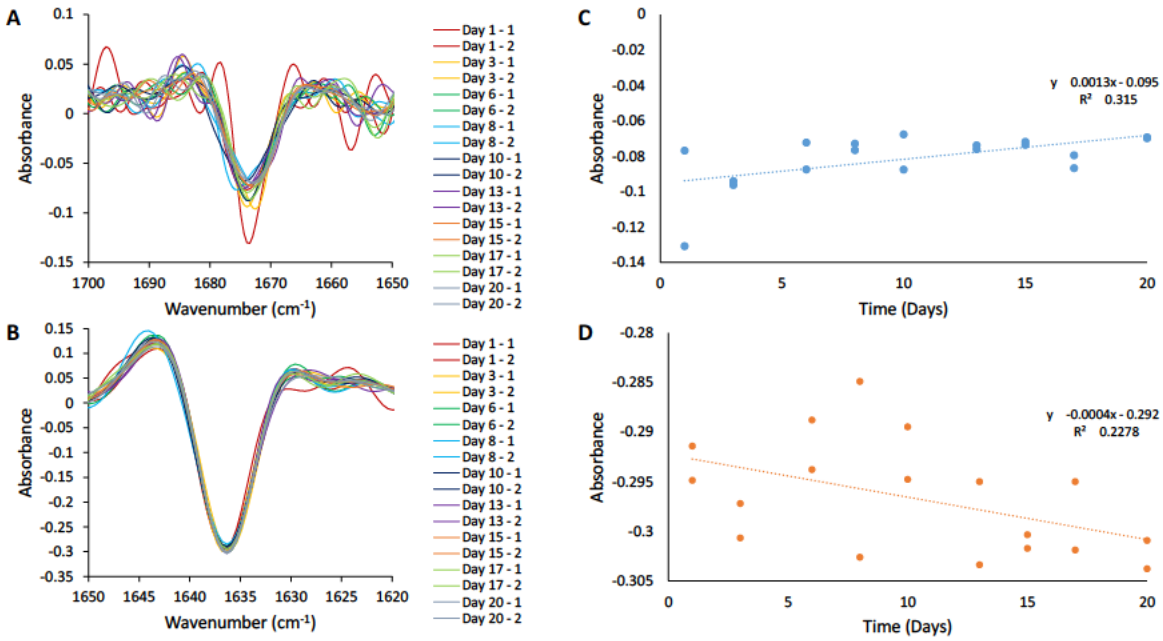

Figure 4.22. *Analysis of auto-oxidation of* S. crassifolia *neutrals. (A) Compiled second derivative FTIR spectra of neutrals fraction in the 1700-1650 cm^{-1} range (strained alkene C=C stretching), (B) compiled second derivative FTIR spectra of neutrals fraction in the 1650-1620 cm^{-1} range (alkene C=C stretching), (C) scatter plot and linear trends of local minima in the 1680-1660 cm^{-1} region (blue), and (D) scatter plot and linear trends of local minima in the 1640-1630 cm^{-1} region (orange).*

Although definitive proof of sample oxidation was not obtained, it is a likely explanation of the spectroscopic changes, so further studies were undertaken to see if the addition of anti-oxidants could inhibit the spectroscopic changes. The impact of phenols on the auto-oxidation of the neutrals was then monitored through measuring the changes in the aliphatic CH stretching after doping with 10%, 30%, 50% and 100% w/w phenols fraction from *S. crassifolia* over the course of 20 days. If a significant antioxidant effect is observed then the change in peak intensity between the 2925 cm^{-1} (unoxidised) to 2915 cm^{-1} (oxidised) and 2855 cm^{-1} (unoxidised) to 2847 cm^{-1} (oxidised) should be significantly slowed or halted entirely. A control using pure phenols fraction was also measured for comparison and showed no significant changes over the 20 day experimental period. The key CH stretch observed for the phenols is also present at 2976 cm^{-1}, which does not overlap with the key spectroscopic markers for the neutrals fraction. Weaker C-H stretches are present that have some spectral overlap with the C-H stretches at 2925 and 2855 cm^{-1}, but changes in the peak absorbance intensities should still be noticeable. However, the minimum absorbance

of the peaks at 2925 and 2855 cm^{-1} will likely increase as the phenols content within the samples is increased.

The neutrals fraction with 10% phenols (i.e. 10:1 neutrals/phenols by mass) exhibited similar rates of auto-oxidation based the trendline gradients from the scatter plots, with ratios of ~1.2:1 between the control and 10% phenols gradients (Figure 4.25). A ratio of ~4:1 was observed for the trendline gradient corresponding to an increase in intensity of the C-H stretching peak at 2915 cm^{-1}, but that may be due to outlier measurements distorting the data. The low change in the rate of oxidation suggested that a 10% phenol content was too low to significantly inhibit the oxidative effect of atmospheric oxygen.

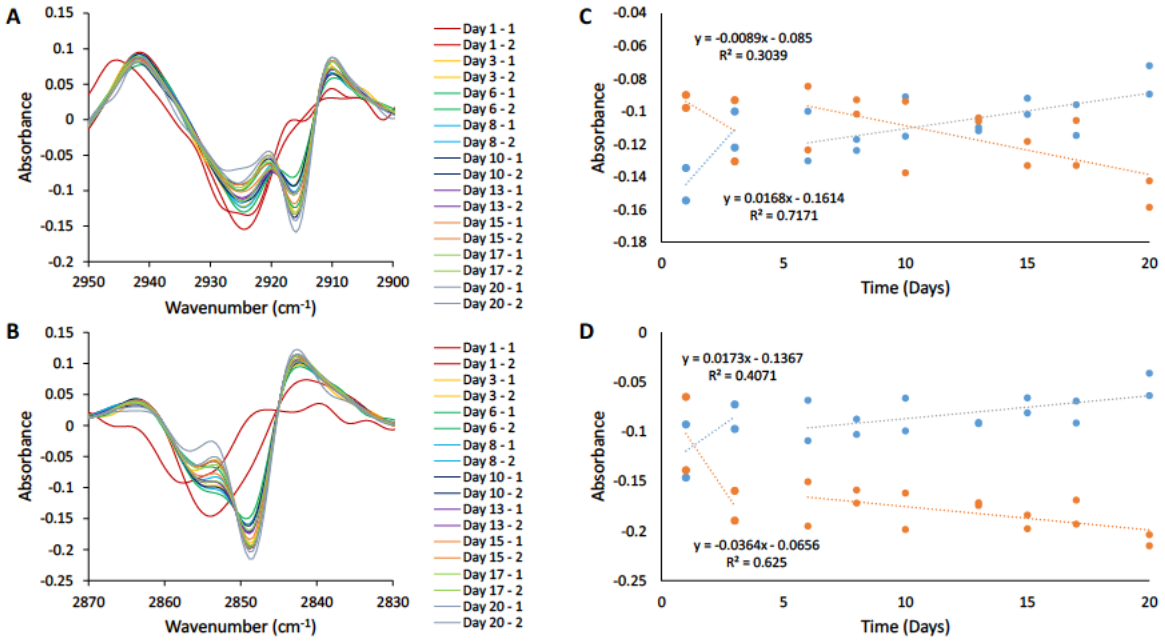

Figure 4.23. *Analysis of auto-oxidation of* S. crassifolia *neutrals with 10% phenols. (A) Compiled second derivative FTIR spectra of neutrals fraction in the 2950-2900 cm^{-1} range (asymmetric methylene C-H stretching), (B) compiled second derivative FTIR spectra of neutrals fraction in the 2870-2830 cm^{-1} range (symmetric methylene C-H stretching), (C) scatter plot and linear trends of local minima in the 2940-2920 cm^{-1} region (blue), and in the 2920-2910 cm^{-1} region (orange), and (D) scatter plot and linear trends of local minima in the 2860-2853 cm^{-1} region (blue), and in the 2852-2840 cm^{-1} region (orange).*

The neutrals fraction with 30% phenols showed a significant antioxidant effect had occurred. The peak intensity of the signals at 2916 and 2847 cm^{-1} had still increased over the 20 days, but the rate of change had been significantly decreased (Figure 4.26). The trendline gradients had decreased by a factor of 17-22, indicating that the rate of oxidation had slowly significantly.

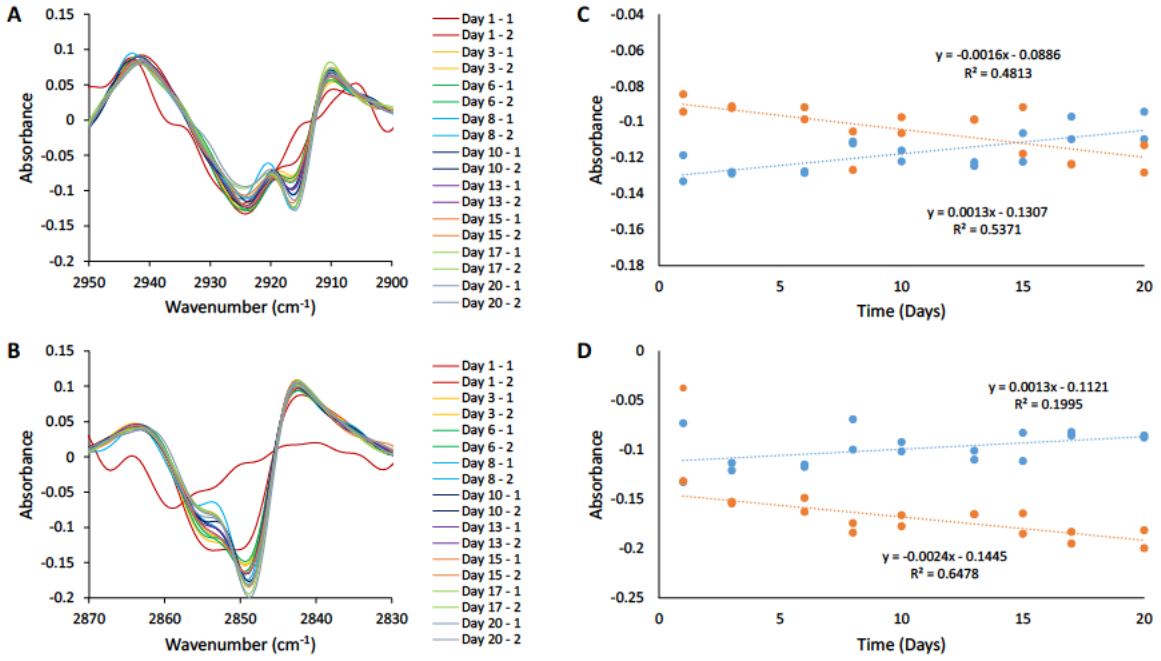

Figure 4.24. *Analysis of auto-oxidation of* S. crassifolia *neutrals with 30% phenols. (A) Compiled second derivative FTIR spectra of neutrals fraction in the 2950-2900 cm^{-1} range (asymmetric methylene C-H stretching), (B) compiled second derivative FTIR spectra of neutrals fraction in the 2870-2830 cm^{-1} range (symmetric methylene C-H stretching), (C) scatter plot and linear trends of local minima in the 2940-2920 cm^{-1} region (blue), and in the 2920-2910 cm^{-1} region (orange), and (D) scatter plot and linear trends of local minima in the 2860-2853 cm^{-1} region (blue), and in the 2852-2840 cm^{-1} region (orange).*

The neutrals fraction with 50% phenols exhibited a similar rate of oxidation to that of the neutrals fractions with 30% phenols based on the trendline gradients, indicating that a 20% increase in phenols content did not result in a significant change in the antioxidant effect (Figure 4.27). However, significant variability was observed with the early measurements, and the change in the spectrum for Sample 1 (Day 1-1), indicated that rapid oxidation had still occurred.

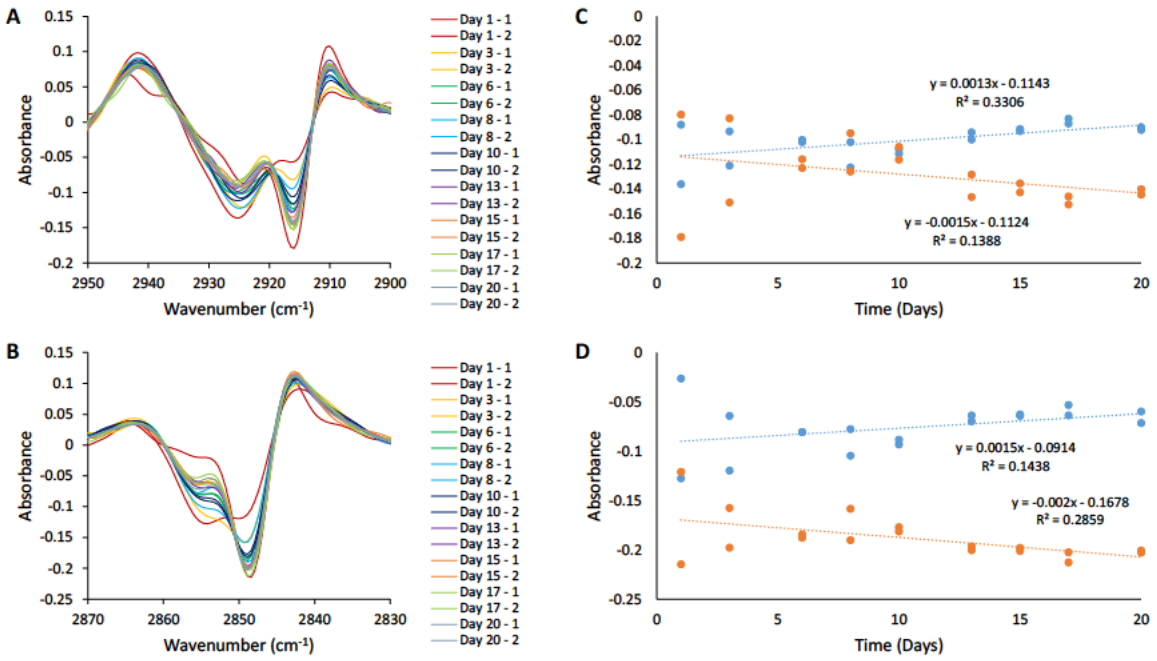

Figure 4.25. *Analysis of auto-oxidation of* S. crassifolia *neutrals with 50% phenols. (A) Compiled second derivative FTIR spectra of neutrals fraction in the 2950-2900 cm^{-1} range (asymmetric methylene C-H stretching), (B) compiled second derivative FTIR spectra of neutrals fraction in the 2870-2830 cm^{-1} range (symmetric methylene C-H stretching), (C) scatter plot and linear trends of local minima in the 2940-2920 cm^{-1} region (blue), and in the 2920-2910 cm^{-1} region (orange), and (D) scatter plot and linear trends of local minima in the 2860-2853 cm^{-1} region (blue), and in the 2852-2840 cm^{-1} region (orange).*

The neutrals fraction with 80% phenols exhibited a significant antioxidant effect based on the trendline gradients. The 80% phenol doped samples showed a 44-227 fold decrease in the gradient, indicating that a significant decrease in the rate of oxidation had occurred (Figure 4.28). A critical threshold for the antioxidant activity of the phenols to have a significant effect had potentially been passed with 80% doping of the neutrals sample.

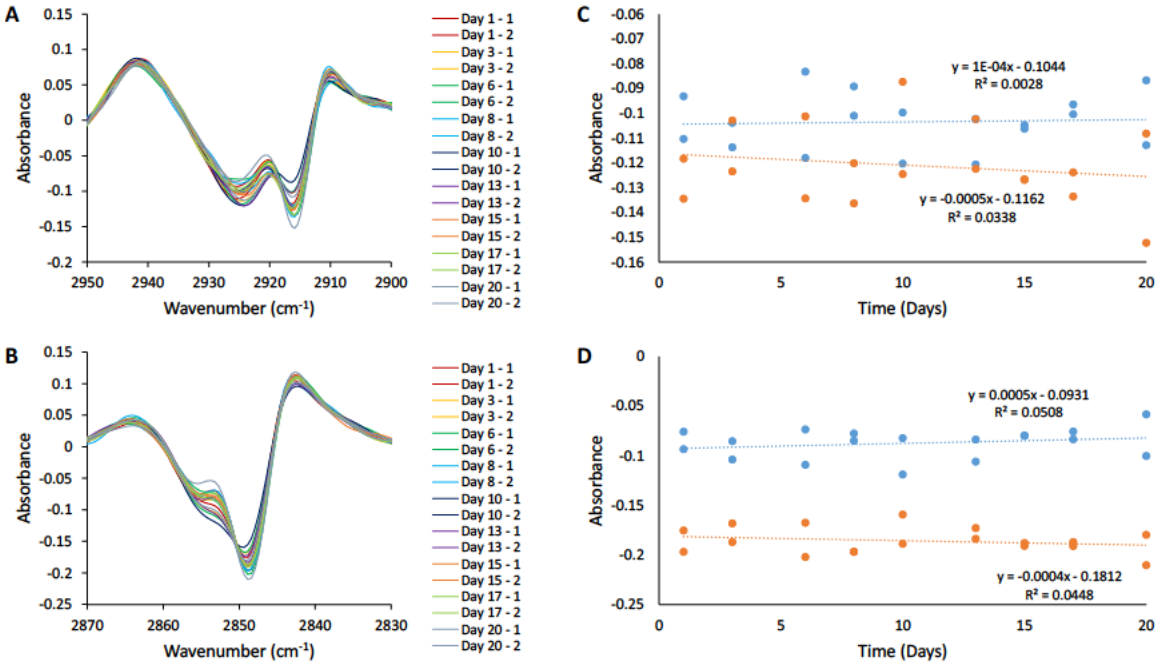

Figure 4.26. *Analysis of auto-oxidation of* S. crassifolia *neutrals with 80% phenols. (A) Compiled second derivative FTIR spectra of neutrals fraction in the 2950-2900 cm^{-1} range (asymmetric methylene C-H stretching), (B) compiled second derivative FTIR spectra of neutrals fraction in the 2870-2830 cm^{-1} range (symmetric methylene C-H stretching), (C) scatter plot and linear trends of local minima in the 2940-2920 cm^{-1} region (blue), and in the 2920-2910 cm^{-1} region (orange), and (D) scatter plot and linear trends of local minima in the 2860-2853 cm^{-1} region (blue), and in the 2852-2840 cm^{-1} region (orange).*

Finally, the neutrals fraction with 100% phenols similarly exhibited a substantial antioxidant effect based on the trendline gradients (Figure 4.30). The 100% phenol doped samples showed a 55-284 fold decrease in the gradient, exceeding that of the 80% phenol doped samples. The 1:1 ratio of neutrals to phenols closely matches that which is naturally found in the surface leaf resin of *S. crassifolia*. The significant decrease in the rate of oxidation observed with 100% phenols, therefore, supports the observation that 6-hydroxycaryophyllenes are readily present in the surface leaf resin even though they are readily oxidised, due to the antioxidant effects of endogenous phenols in same leaf resin.

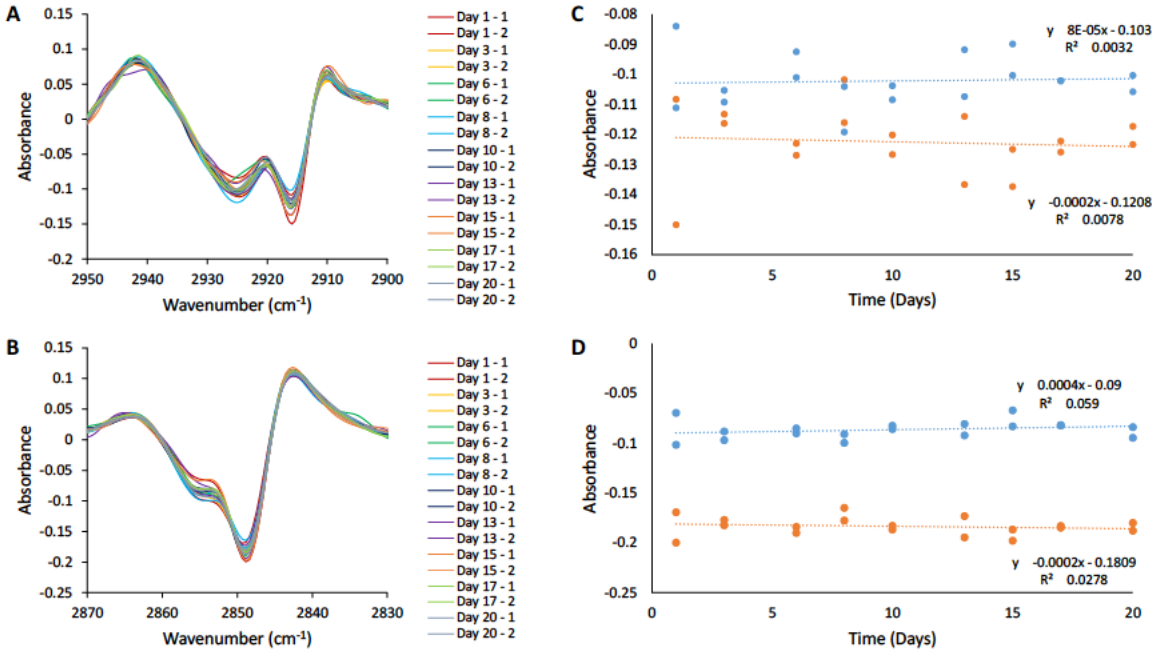

Figure 4.27. *Analysis of auto-oxidation of* S. crassifolia *neutrals with 100% phenols. (A) Compiled second derivative FTIR spectra of neutrals fraction in the 2950-2900 cm^{-1} range (asymmetric methylene C-H stretching), (B) compiled second derivative FTIR spectra of neutrals fraction in the 2870-2830 cm^{-1} range (symmetric methylene C-H stretching), (C) scatter plot and linear trends of local minima in the 2940-2920 cm^{-1} region (blue), and in the 2920-2910 cm^{-1} region (orange), and (D) scatter plot and linear trends of local minima in the 2860-2853 cm^{-1} region (blue), and in the 2852-2840 cm^{-1} region (orange).*

A variety of antioxidants with known mechanisms are widely used, such as BHT **156** (Figure 4.30). BHT **156** is known to act as an antioxidant by acting as a radical scavenger and trapping radicals on the oxygen atom of the phenol.[126] The phenolic radical is resonance stabilised and is not accessible to other reactive species due to the bulky *t*-butyl groups in *ortho* positions.

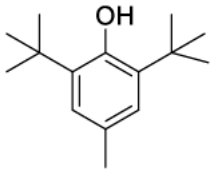

156

Figure 4.28. *Structure of 2,6-di-tert-butyl-4-methylphenol (BHT)* ***156****.*

The antioxidant properties of BHT **156** have been well established, which made it a suitable point of comparison to the naturally occurring phenols from *S. crassifolia*. A time course study in a similar vein to that of the phenols with the neutrals fractions was conducted using

BHT instead, using 10%, 50% and 100% BHT **156** doped neutrals fractions. The neutrals fraction control appeared to be partially oxidised prior to use, but still exhibited oxidation over time based on the trendline gradients (Figure 4.31).

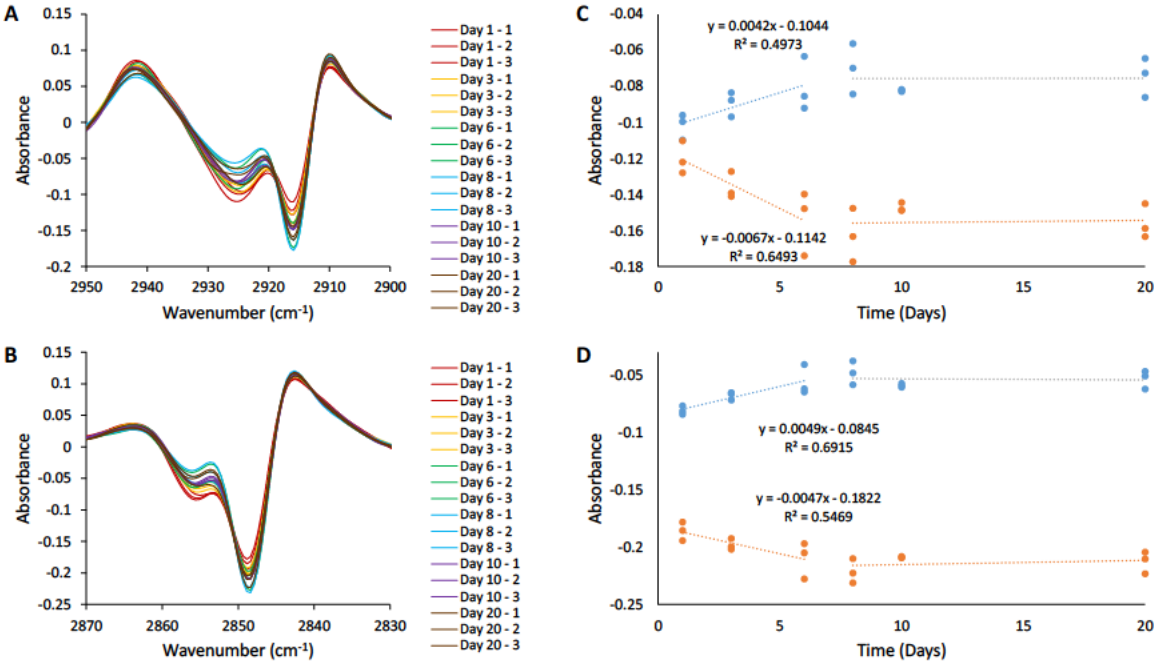

Figure 4.29. *Analysis of auto-oxidation of* S. crassifolia *neutrals. (A) Compiled second derivative FTIR spectra of neutrals fraction in the 2950-2900 cm^{-1} range (asymmetric methylene C-H stretching), (B) compiled second derivative FTIR spectra of neutrals fraction in the 2870-2830 cm^{-1} range (symmetric methylene C-H stretching), (C) scatter plot and linear trends of local minima in the 2940-2920 cm^{-1} region (blue), and in the 2920-2910 cm^{-1} region (orange), and (D) scatter plot and linear trends of local minima in the 2860-2853 cm^{-1} region (blue), and in the 2852-2840 cm^{-1} region (orange).*

The neutrals fraction with 10% BHT **156** showed similar rates of oxidation to that of the control, suggesting that 10% BHT **156** was too low for any significant antioxidant effect to be observed (Figure 4.32).

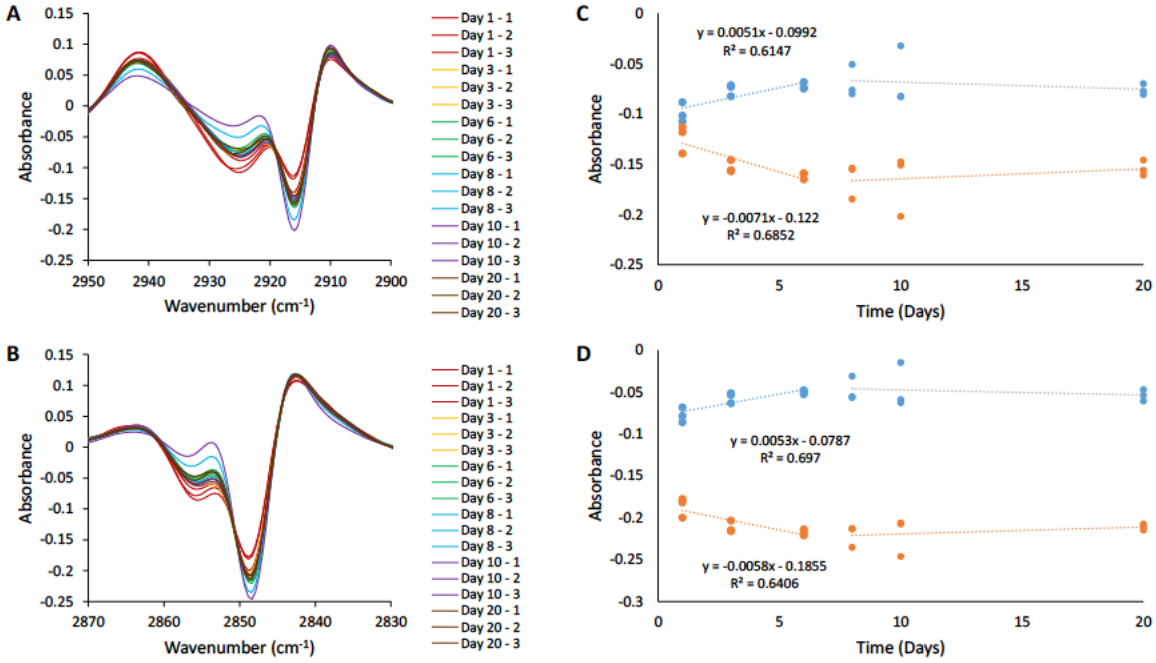

Figure 4.30. *Analysis of auto-oxidation of* S. crassifolia *neutrals with 10% BHT* ***156****. (A) Compiled second derivative FTIR spectra of neutrals fraction in the 2950-2900 cm^{-1} range (asymmetric methylene C-H stretching), (B) compiled second derivative FTIR spectra of neutrals fraction in the 2870-2830 cm^{-1} range (symmetric methylene C-H stretching), (C) scatter plot and linear trends of local minima in the 2940-2920 cm^{-1} region (blue), and in the 2920-2910 cm^{-1} region (orange), and (D) scatter plot and linear trends of local minima in the 2860-2853 cm^{-1} region (blue), and in the 2852-2840 cm^{-1} region (orange).*

The neutrals fraction with 50% BHT **156** also exhibited similar rates of oxidation, which was in contrast to the significantly decreased rates of oxidation observed when using the phenols fraction as an antioxidant (Figure 4.33).

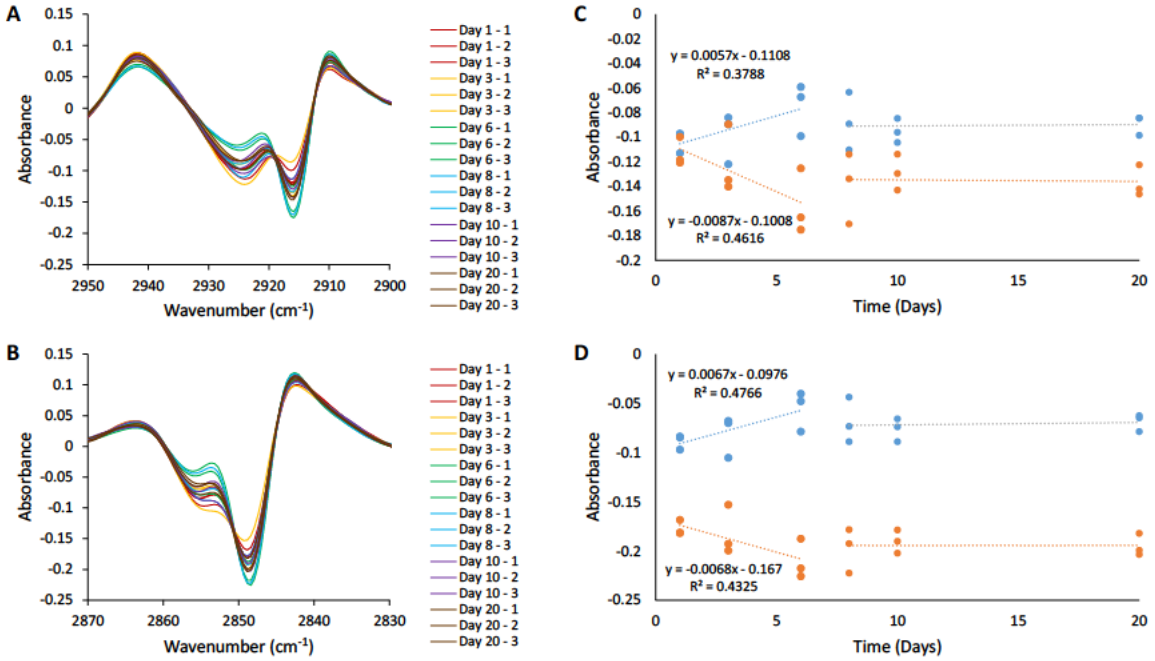

Figure 4.31. *Analysis of auto-oxidation of* S. crassifolia *neutrals with 50% BHT* ***156****. (A) Compiled second derivative FTIR spectra of neutrals fraction in the 2950-2900 cm^{-1} range (asymmetric methylene C-H stretching), (B) compiled second derivative FTIR spectra of neutrals fraction in the 2870-2830 cm^{-1} range (symmetric methylene C-H stretching), (C) scatter plot and linear trends of local minima in the 2940-2920 cm^{-1} region (blue), and in the 2920-2910 cm^{-1} region (orange), and (D) scatter plot and linear trends of local minima in the 2860-2853 cm^{-1} region (blue), and in the 2852-2840 cm^{-1} region (orange).*

Finally, the neutrals fraction with 100% BHT **156** also exhibited similar rates of oxidation to that of the neutrals fraction controls (Figure 4.34). The similar rates of oxidation may be attributed to a number of factors. The partial oxidation of the starting neutrals fraction may have been the only oxidative step, and any other observed changes in the aliphatic C-H stretching may be attributed to other subsequent chemical changes. The BHT **156** was also observed to precipitate out of the neutrals fraction, so the antioxidant effect of BHT **156** was likely limited by solubility due to limited contact between the BHT **156** and the neutrals fraction.

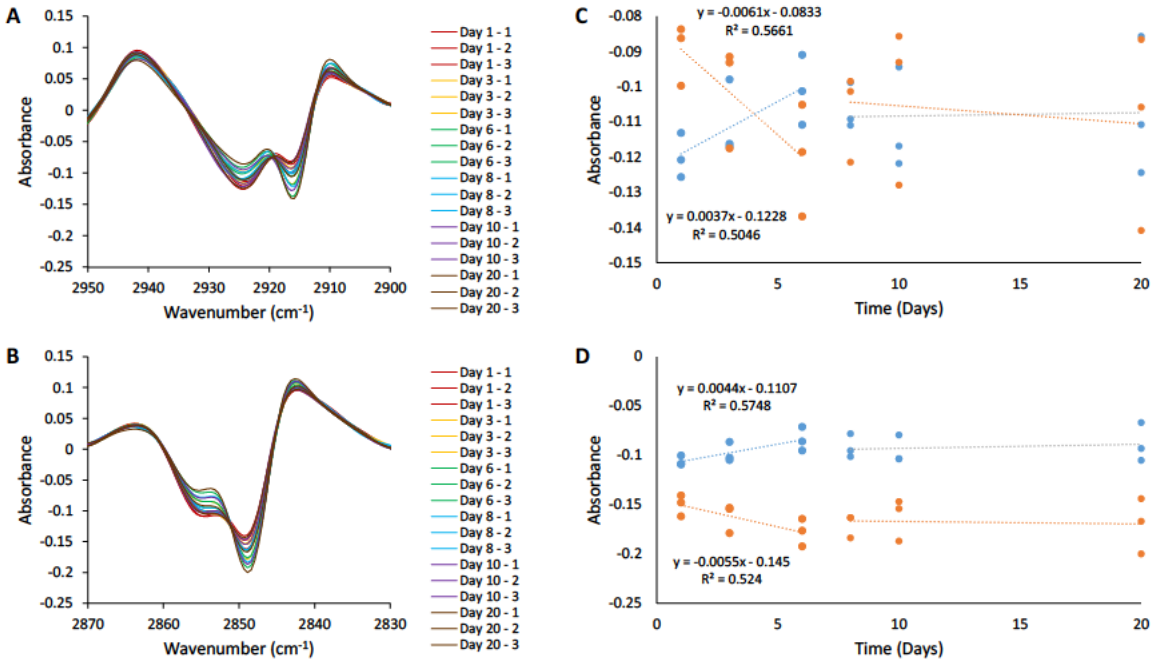

Figure 4.32. *Analysis of auto-oxidation of* S. crassifolia *neutrals with 100% BHT* ***156****. (A) Compiled second derivative FTIR spectra of neutrals fraction in the 2950-2900 cm^{-1} range (asymmetric methylene C-H stretching), (B) compiled second derivative FTIR spectra of neutrals fraction in the 2870-2830 cm^{-1} range (symmetric methylene C-H stretching), (C) scatter plot and linear trends of local minima in the 2940-2920 cm^{-1} region (blue), and in the 2920-2910 cm^{-1} region (orange), and (D) scatter plot and linear trends of local minima in the 2860-2853 cm^{-1} region (blue), and in the 2852-2840 cm^{-1} region (orange).*

Therefore, based on the FTIR spectroscopic data from the time course studies, the phenols present in the leaf resin of *S. crassifolia* exhibits a significant antioxidant effect that reduces the rate of auto-oxidation of other compounds in the leaf resin including 6-hydroxycaryophyllenes.

4.6 Conclusions

This chapter further investigated the composition of natural products found in *S. crassifolia* and the biosynthesis of selected natural products using organic synthesis and vibrational spectroscopy. The natural product composition of *S. crassifolia* found in its natural environment (Port Beach, North Fremantle, Perth, Western Australia) was investigated and 12-hydroxycaryophyllene **60** and flavone **141** were isolated, in addition to the compounds isolated from the plant at the Curtin University campus. The extraction efficiency of different solvents for the isolation of the *S. crassifolia* leaf resin was investigated. Similar extraction efficiencies were observed for Et_2O, EtOH and CH_2Cl_2, while PS showed extracted a significantly lower quantity of resin. Deionised water extracted 6,12-dihydroxycaryophyllene **3** and phenols but required an extended time. It was also determined that activated carbon could be used as a simple means of removing phenols from the resin extract, although this purification should only be conducted once to minimise product loss. A new synthetic mechanism for the formation of birkenal **142** was proposed and the relationship between the biosynthesis of birkenal **142** and the formation of caryolan-1,3,4-triol **152** and diene **154** was explored synthetically. The formation of birkenal **142** was explored through an NMR spectroscopy time course study, showing the necessity of both oxygen and an acidic environment to catalyse the formation of an aldehyde from 6-hydroxycaryophyllene **1**. Finally, the antioxidant effects of phenolic natural products in the leaf resin of *S. crassifolia* was investigated. The experimental data revealed that the phenols had a significant antioxidant effect that greatly reduced the rate of oxidation of other natural products present in the surface leaf resin. Overall, this chapter highlighted how synthetic chemistry and spectroscopy could be used in conjunction to improve our understanding of natural products composition and biosynthesis.

Chapter 5
The chemistry of flavanones from *Scaevola crassifolia*

Flavonoids are an abundant class of polyphenolic natural products found in over 6500 plant species and have also been isolated from the leaf resin of *S. crassifolia*.[127] Flavonoids are biosynthesised through the phenylpropanoid biosynthetic pathway, starting from L-phenylalanine (Scheme 5.1). L-Phenylalanine is first converted to cinnamic acid through a deamination with phenylalanine ammonia lyase (PAL). Cinnamic acid is hydroxylated by 4-cinnamic acid hydroxylase (C4H) to form *p*-coumaric acid. *p*-Coumaric acid undergoes a condensation reaction with coenzyme-A facilitated by 4-coumerate-CoA ligase (4CL1) to afford the thioester coumaroyl-CoA. Coumaroyl-CoA then reacts with three molar equivalents of malonyl-CoA in the presence of chalcone synthase (CHS) to produce the chalcone intermediate. The chalcone can then undergo a variety of transformations to afford different flavonoid species. In particular, the chalcone can cyclise via a Michael addition facilitated by chalcone isomerase (CHI) to afford a flavanone.[128]

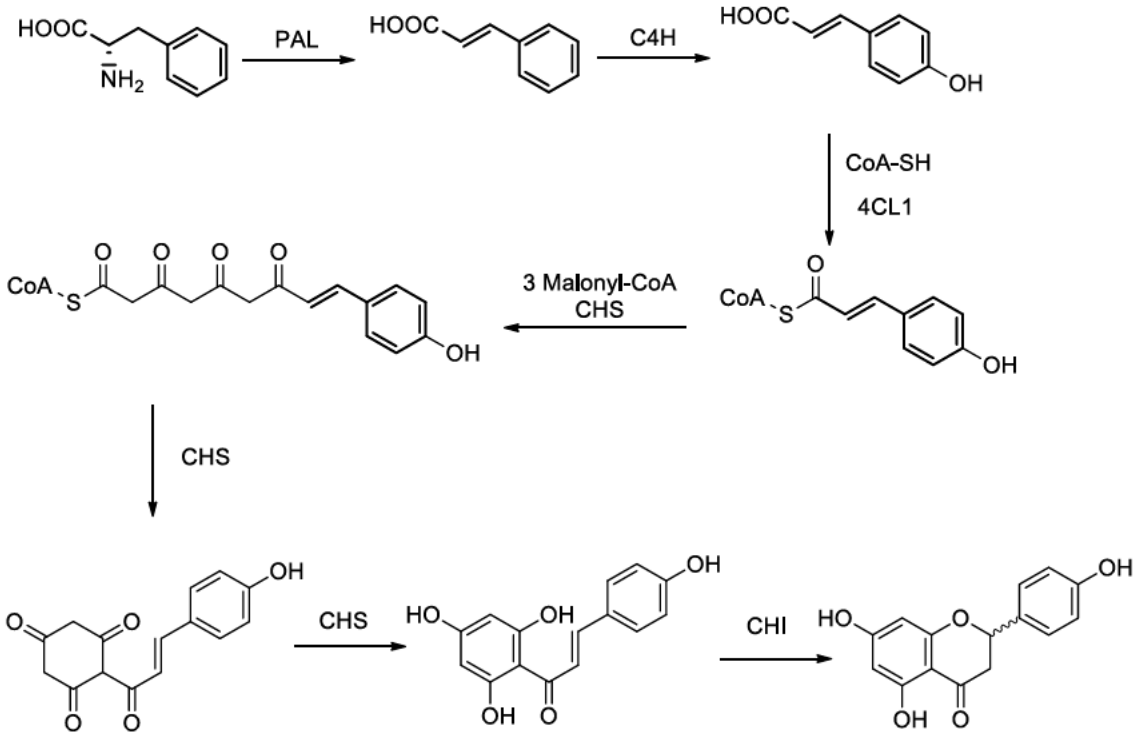

Scheme 5.1. *Biosynthetic pathway for the synthesis of flavanones.*

Two flavanones and the precursor chalcone were isolated from the leaf resin of *S. crassifolia*, providing a unique opportunity to investigate the synthesis of the flavanones through biomimetic synthesis using the precursor chalcone.

5.1 Isolation and structure elucidation of flavanones 138 and 139, and chalcone 157

The natural product composition of the leaf resin of *S. crassifolia* has been previously investigated in earlier work conducted as part of this research. The resin was extracted by soaking the leaves of the plant (1.16 kg) in Et_2O for 20 mins, followed by filtration of the ether extract. The filtration step ensured the removal of detritus from the extraction. The filtrate was concentrated *in vacuo* to afford the resin as a sticky, yellow oil (33.7 g). The resin was dissolved in Et_2O and the solution was partitioned using acid-base chemistry to separate the major components of the leaf resin into amines (0.169 g), carboxylic acids (0.190 g), phenols (9.680 g) and neutrals (9.578 g). A portion of the phenols fraction (451 mg) was purified by flash chromatography to afford two primary fractions.

The first fraction afforded a yellow powder (163 mg) and the ^{1}H NMR spectrum indicated a mixture of two products in a 1:3 ratio. The signals observed in the ^{1}H NMR spectrum was consistent with the mixture of flavanones that had been previously reported by Fukai *et al*.[129] Trituration of the yellow solid using dry MeCN afforded a pure off-white solid (14 mg). The ^{1}H NMR and ^{13}C NMR spectra were consistent with 5,7,3',4'-tetrahydroxy-8-[3,3'-dimethylallyl]-flavanone **138** (Figure 5.1) (Table 5.1). The structure was confirmed by a comparison of the ^{1}H and ^{13}C NMR data with that of the same flavanone synthesised and characterised by Fukai *et al*.[129] The other product could not be isolated, but the signals in the impure ^{1}H and ^{13}C NMR data were consistent with that of 5,7,3',4'-tetrahydroxy-6-[3,3'-dimethylallyl]-flavanone **139**.[129]

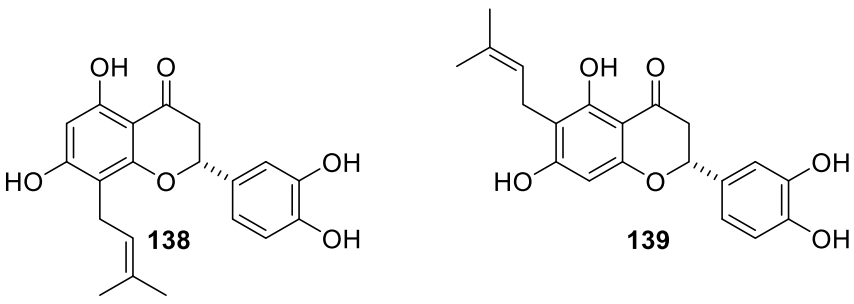

Figure 5.1. *Structures of 5,7,3',4'-tetrahydroxy-8-[3,3'-dimethylallyl]-flavanone* ***138*** *and 5,7,3',4'-tetrahydroxy-6-[3,3'-dimethylallyl]-flavanone* ***139****.*

Table 5.1. *^{13}C NMR data for flavanones* ***138*** *and* ***139***

Carbon	Literature (ppm)	Flavanone 138 (ppm)	Literature (ppm)	Flavanone 139 (ppm)
2	79.75	79.70	79.89	79.85
3	43.52	43.49	43.74	43.65
4	197.55	197.50	197.14	197.25
4a	103.29	103.25	103.04	103.07
5	162.95	162.89	162.28	162,20
6	96.33	96.33	109.06	108.96
7	164.56	164.77	165.19	164.92
8	108.30	108.27	95.42	95.28
8a	161.04	160.98	161.98	161.90
1'	131.22	131.19	131.11	131.19
2'	114.62	114.57	114.70	114.65
3'	146.26	146.19	146.42	146.31
4'	146.05	146.97	146.07	146.97
5'	115.99	115.99	116.03	115.97
6'	119.01	118.99	119.14	119.18
1''	22.26	22.25	21.66	21.61
2''	123.67	123.57	123.71	123.63
3''	131.88	131.83	131.74	131.66
4''	17.87	17.87	17.84	17.84
5''	25.90	25.90	25.85	25.86

The second fraction was isolated as an orange solid (72 mg). The ^{13}C NMR spectrum contained 20 signals, with 14 signals between 100 and 170 ppm, indicating the presence of at least two aromatic rings. A signal at 193.3 ppm was characteristic of a ketone. The FTIR spectrum contained a carbonyl stretch at 1600 cm^{-1}, suggesting that the ketone was heavily conjugated due to the lower stretching frequency. The molecular formula was confirmed by HRMS as the $[M+H]^+$ molecular ion having an exact mass of 357.1325 *m/z* which was consistent with the formula of $C_{20}H_{20}O_6$. The ^1H NMR spectrum showed a sharp singlet at 14.45 ppm, which was indicative of a hydrogen bonded phenol. Four aromatic signals at 6.09, 6.88, 7.08 and 7.19 ppm showed similar multiplicities and chemical shifts to the

aromatic ^{1}H signals from flavanone **139**, indicating a similar aromatic substitution pattern. The presence of a prenyl group was suggested by the presence of a vinylic hydrogen at 5.24 ppm, an allylic methylene at 3.36 ppm and two allylic methyl signals at 1.63 and 1.65 ppm. Two doublets were present at 7.69 and 8.07 ppm that integrated for 1H each, with a coupling constant of 15.2 Hz, consistent with a *trans* alkene. Based on analysis of the ^{1}H NMR, ^{13}C NMR, 2D NMR, HRMS and FTIR spectra, the compound was assigned as 5,7,9,3',4'-pentahydroxy-8-[3,3'-dimethylallyl]-chalcone **157** (Figure 5.2). Chalcone **157** has not been previously identified outside of computational studies.[130]

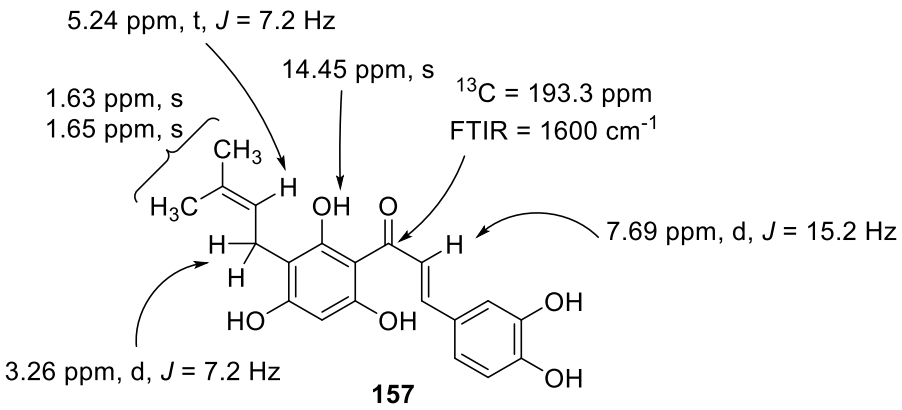

Figure 5.2. *Structure of 5,7,9,3',4'-tetrahydroxy-8-[3,3'-dimethylallyl]-chalcone **157**.*

Isolation of the precursor chalcone **157** alongside the corresponding flavanones from the surface resin was unexpected and warranted further investigation. Flavanones can undergo a retro-Michael addition under acidic conditions to afford the precursor chalcone, and concentrated HCl was used to separate the major components of the leaf resin. Partitioning of the major components of the resin using acid-base chemistry was repeated, but the pH of the phenols fraction was closely monitored to ensure that it was close to pH 7 after acidification. Analysis of the ^{1}H NMR spectrum indicated that the 8-prenyl and 6-prenyl flavanones **138** and **139** were found in a 4:5 ratio, with no chalcone **157** present in the spectrum. Over acidification, therefore, did result in a retro-Michael addition occurring to afford the precursor chalcone. Interestingly, the 6-prenyl flavanone **139** is preferentially hydrolysed, likely due to the lower steric hinderance around the C5 ether compared to the 8-prenyl flavanone **138**.

5.2 Previous syntheses of flavanones

The cyclisation of chalcones to the corresponding flavanones occurs via a Michael addition of the C9 hydroxyl group to the enone. The synthesis of flavanones can occur via a number of different pathways. In biological systems, the biosynthesis of flavavones from chalcones is typically facilitated enzymatically by CHI. A crystal structure of (2*S*)-naringenin complexed with CHI was reported by Jez *et al*., and showed that two hydrogen bonding networks facilitated the cyclisation of chalcones into flavanones.[131] A hydrogen bonding network that involved two water molecules and several amino acids (Thr^{48}, Ala^{49}, Lys^{97}, Tyr^{106}, Tyr^{152}) was responsible for one set of interactions that centres on one water molecule in contact with the C-ring ketone. The second set of hydrogen bonds comes from Asn^{113} and Thr^{190}, and bonds to the 4'-hydroxyl group of the chalcone. Jez *et al*. proposed a mechanism for the cyclisation of the chalcone to the flavanone, based on the binding exhibited in the crystal structure (Scheme 5.2).

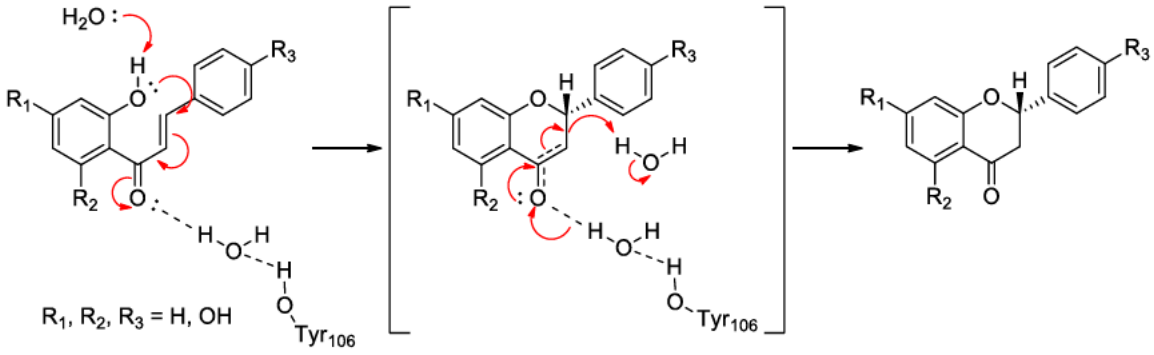

Scheme 5.2. *Proposed mechanism for cyclisation of chalcones via CHI. Adapted from work by Jez et al.*[131]

A number of synthetic methods for the preparation of flavanones have been reported in literature, including total syntheses and semisyntheses. One such total synthesis was reported in 2010, when Jung *et al*. reported the first total synthesis of a number of geranylated flavanones including (±)-prostatol F **158**.[132] The synthesis followed the classical route of first preparing the substituted acetophenone and benzaldehyde precursors and reacting them to form the key chalcone intermediate via an aldol condensation. The chalcone is then cyclised under basic conditions via a Michael addition to form the target flavanone (Scheme 5.3).

In the synthesis of (±)-prostatol F **159**, 2,4-dihydroxyacetophenone was reacted with geranyl bromide under basic conditions to afford the geranylated product. The C4 hydroxyl group was then selectively protected with a MOM ether group using 1.0 equivalents of

MOMCl and *i*-Pr_2EtN. The protected acetophenone underwent an aldol condensation with the protected 4-hydroxybenzaldehyde to afford chalcones **159** and **160**. The chalcones are then cyclised via a Michael addition of the C2 hydroxyl group to the enone in the presence of NaOAc to afford the protected flavanones **161** and **162**. The flavanones were deprotected using HCl in MeOH to afford (±)-prostatol F **158**, and (±)-8-geranyl-3',4',7-trihydroxyflavanone **163** in 72% and 74% yields respectively (Scheme 5.3).

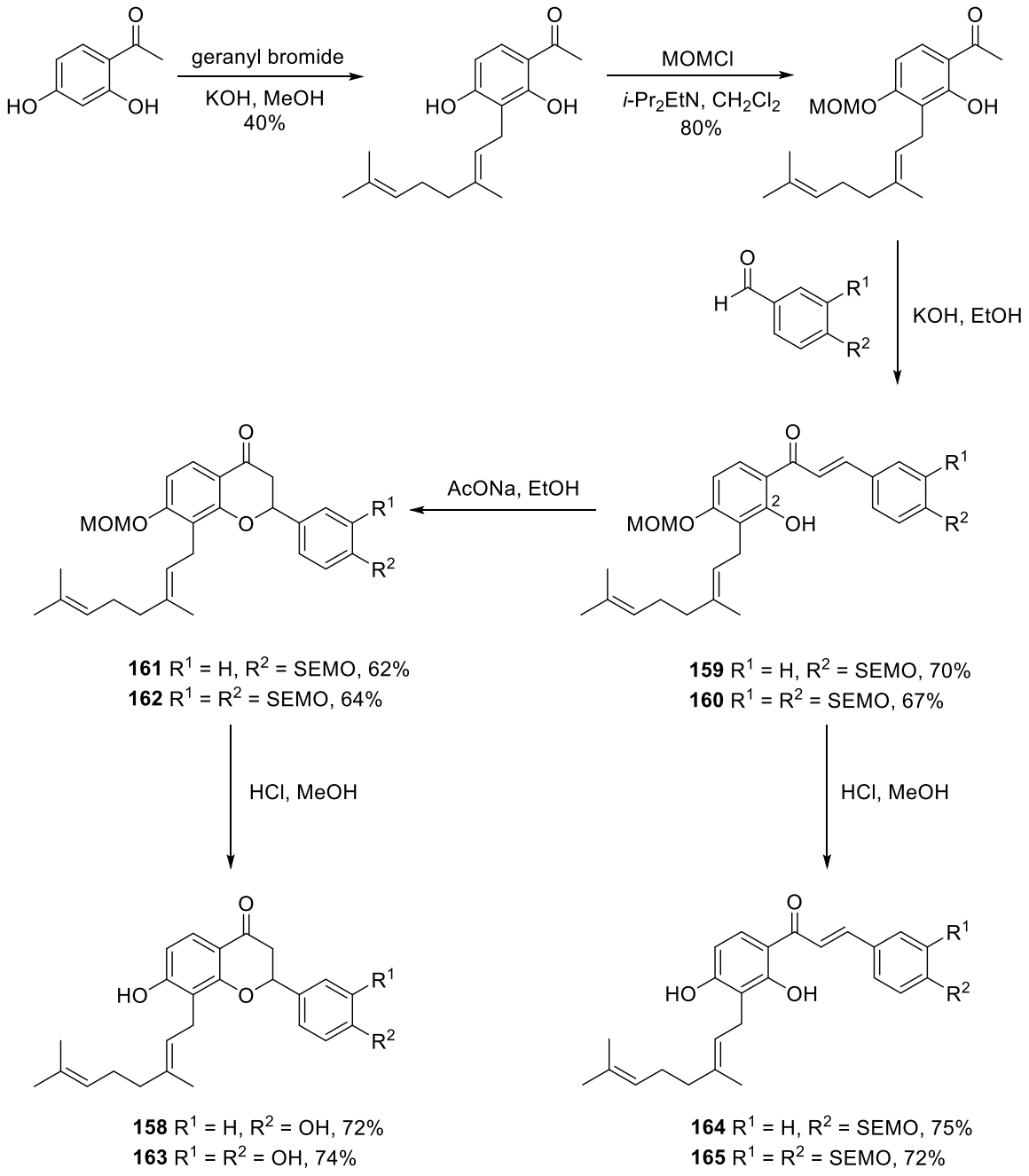

Scheme 5.3. *Synthesis of (±)-prostatol F **158**, (±)-8-geranyl-3',4',7-trihydroxyflavanone **163**, and natural geranylated chalcones **164** and **165**.*

Interestingly, when Jung *et al*. synthesised (±)-6-geranyl-5,7-dihydroxy-3',4'-dimethoxy flavanone **166** using a similar method, the product was afforded as a mixture of (±)-6-geranyl-5,7-dihydroxy-3',4'-dimethoxy flavanone **166** and (±)-8-geranyl-5,7-dihydroxy-3',4'-dimethoxy flavanone **167** in 51% and 7% yields respectively (Scheme 5.4). The formation of the 6-geranylflavanone as the major product indicates that substitution at the C6 position is more favourable than at the C8 position.

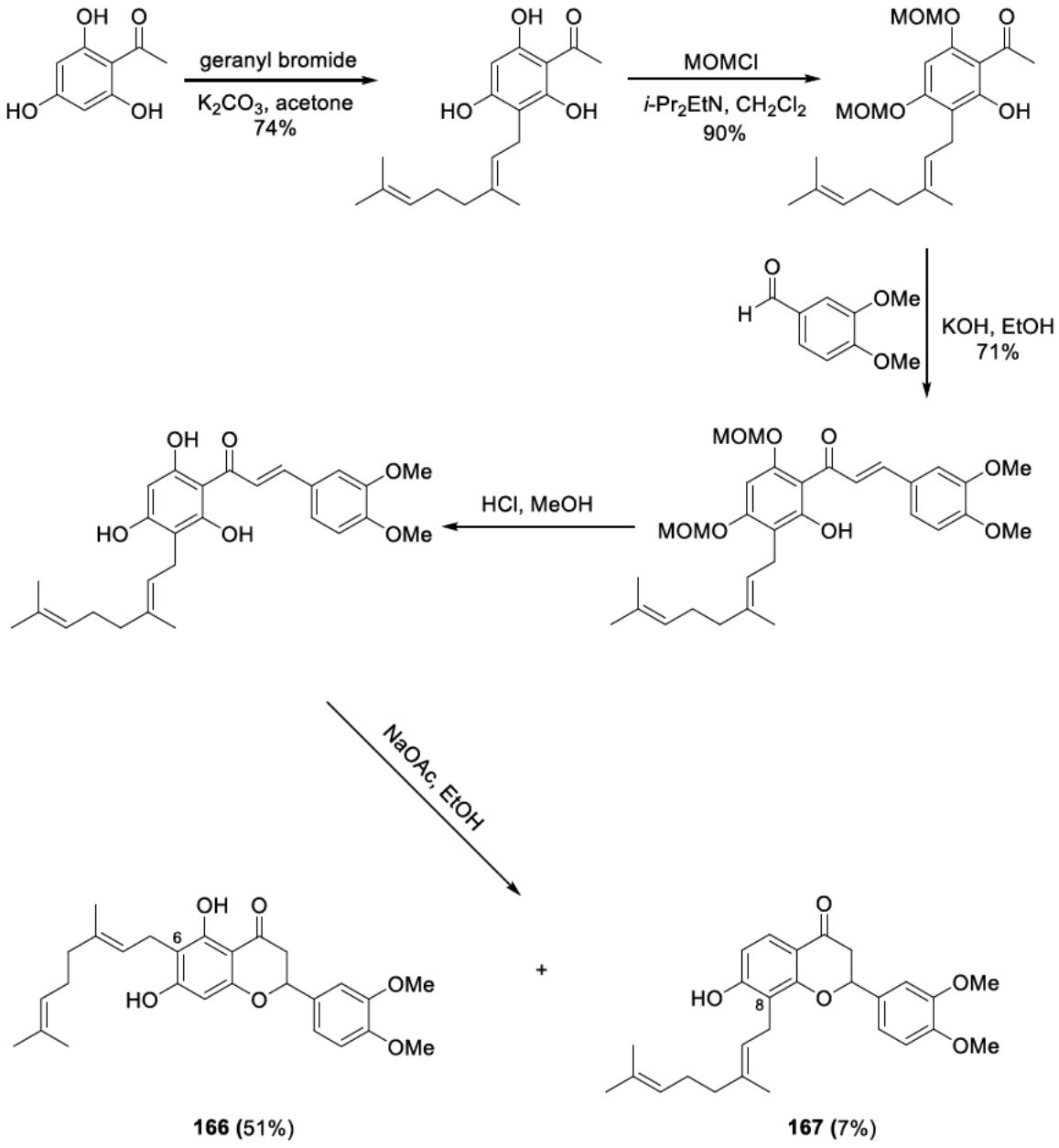

Scheme 5.4. *Synthesis of (±)-6-geranyl-5,7-dihydroxy-3',4'-dimethoxyflavanone* ***166*** *and (±)-8-geranyl-5,7-dihydroxy-3',4'-dimethoxyflavanone* ***167****.*

5.3 Investigation of flavanone synthesis from chalcones

The 8-prenyl- and 6-prenylflavanones **138** and **139** are found in a 4:5 ratio in the phenols fraction of the leaf resin extract from *S. crassifolia*. Isolation of the precursor chalcone **157** due to excess acidification of the phenols extract, suggested that the flavanones were synthesised directly from the chalcone **157**. The cyclisation of a chalcone is typically facilitated by the CHI in biological systems, and enzymatic systems are known to react with high levels of stereo- and regioselectivity. Computational and experimental studies have been conducted on CHI to investigate the stereo- and regioselectivity of the enzyme when facilitating the formation of flavanones from chalcones.[131, 133] CHI has been shown to exhibit high, but not complete regioselectivity, which is unusual for enzymes. For example, Li *et al*. observed that GuCHI did not exhibit complete regioselectivity when using GuCHI, a stereospecific CHI, to cyclise a prenylated naringenin chalcone **168** into prenylated naringenin **169** and **170**, affording a 17:3 ratio of the 8-prenyl to the 6-prenyl product (Scheme 5.5).[133b]

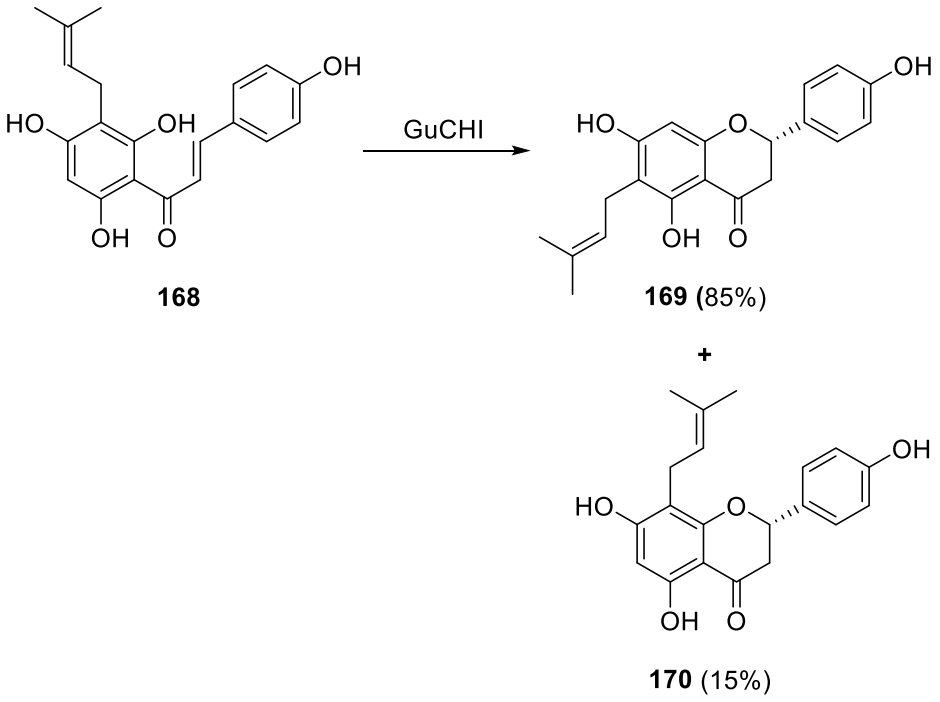

168 **169** (85%) + **170** (15%)

Scheme 5.5. *Synthesis of 6-prenylnaringenin **169** and 8-prenylnaringenin **170**.*

Abiotic factors influencing the regioselectivity of the cyclisation of substituted chalcones into flavanones warranted further research. A number of non-enzymatic synthetic pathways for the formation of flavanones are possible, including acid or base catalysed Michael additions and photochemical cyclisations.

The synthesis of the flavanones **138** and **139**, starting from the chalcone **157** was investigated. Based on a procedure by Fukai *et al.*, chalcone **157** was cyclised by heating in MeOH at 50ºC overnight in the presence of NaOAc (Scheme 5.6). The crude product was afforded as a yellow solid in 66% yield. The ^{1}H NMR spectrum of the crude product showed two new singlets at 12.46 and 12.13 ppm, characteristic of the hydrogen bonded phenols found in flavanones **138** and **139**.[129] The ratio of the integrals of the phenol signals for the 6-prenyl- to the 8-prenylflavanone was 3:1, which had a significantly higher bias towards the 6-prenylflavanone **138** than the 5:4 ratio present in the plant extract. The ratio of 6- to 8- prenylated products was similar to that of the geranylated flavanones synthesised by Jung *et al.*, where the 6- and 8-geranylated products were afforded in 51% and 7% yields respectively.[132] The preferential formation of the 6-prenylflavanone **139** was likely due to the steric bulk of the prenyl group reducing access to the C5 hydroxyl group, and favouring reaction of the less hindered C9 hydroxyl group. The significant difference between the experimental and isolated flavanone ratios prompted further investigation into the reaction, and a variety of reaction conditions were trialled, which are summarised in Table 5.2.

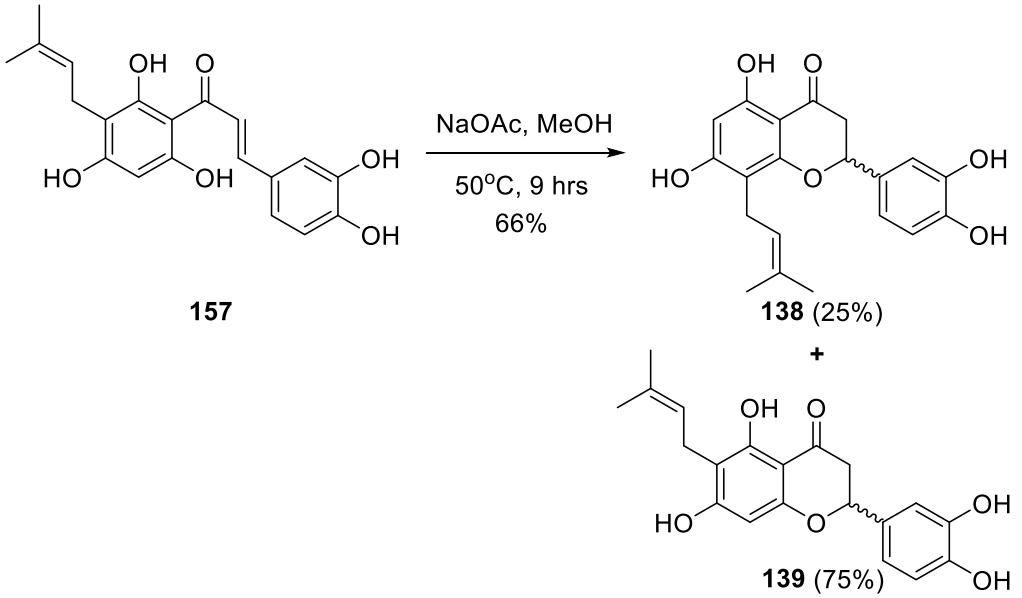

Scheme 5.6. *Synthesis of 8-prenylflavanone **138** and 6-prenylflavanone **139** using NaOAc.*

The effect of steric bulk was further examined by using Et_3N as a sterically bulky base in THF at reflux (Scheme 5.7). Interestingly, the 6-prenylflavanone **139** was afforded almost exclusively, with only trace quantities of the 8-prenylflavanone **138** visible in the ^{1}H NMR spectrum. The high regioselectivity was likely because the C5 hydroxyl, adjacent to the prenyl group, is significantly more sterically hindered than the C9 hydroxyl group, resulting in the exclusive formation of the 6-prenylflavanone **139**. Another product was visible in

the ^{1}H NMR spectrum in a 3:2 ratio to the 6-prenylflavanone **139**. The compound contained a prenyl group, indicated by a vinylic triplet at 5.15 ppm that integrated for 1H and two methyl singlets that integrated for 3H each at 1.83 and 1.86 ppm respectively. The compound was not successfully isolated.

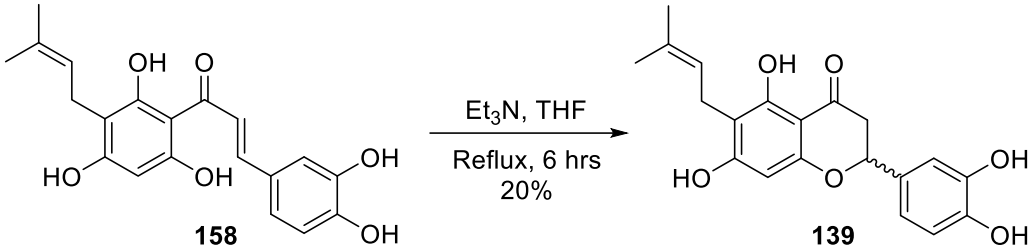

Scheme 5.7. *Synthesis of 6-prenylflavanone **139** using Et_3N.*

The reactions were repeated with NaOAc/LiCl and $Zn(OAc)_2$ respectively, to determine if the size of the cation affected the regioselectivity of the reaction (Scheme 5.8). The coordination chemistry of Li^+ is well established and Li^+ is known to coordinate more effectively than Na^+ to hard bases such as hydroxyl groups.[134] LiCl would undergo cation exchange with NaOAc to form LiOAc, thus incorporating a smaller cation into the reaction. However, no change in ratio of products formed was observed in the ^{1}H NMR spectrum of the crude product, indicating that a smaller cation did not influence the regioselectivity.

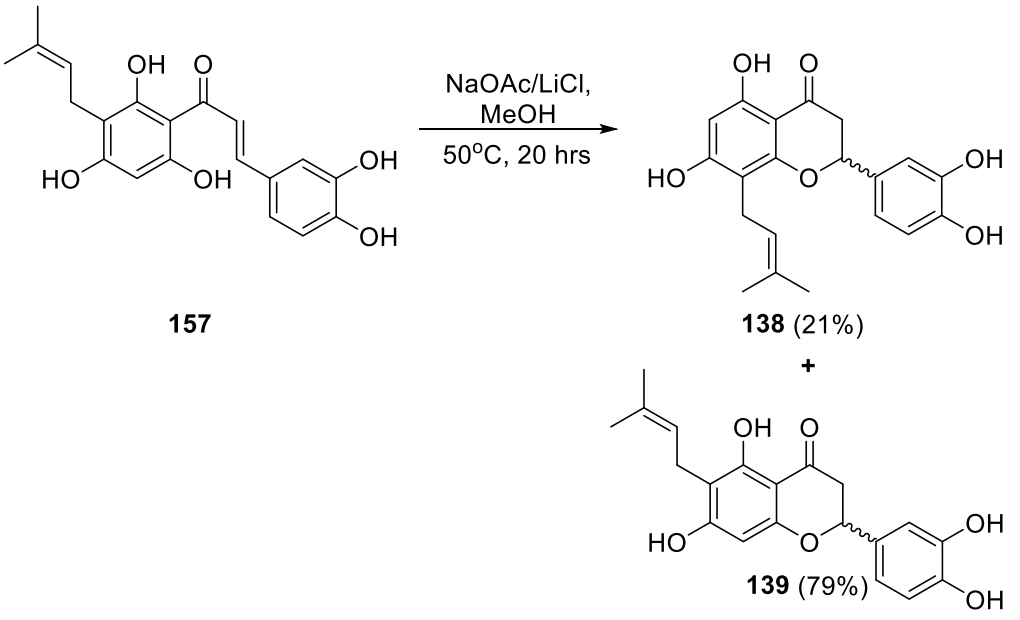

Scheme 5.8. *Synthesis of 8-prenylflavanone **138** and 6-prenylflavanone **139** using NaOAc and LiCl in a 4:1 ratio.*

The reaction was repeated, but using $Zn(OAc)_2$ as a source of a larger cation (Scheme 5.9). The use of $Zn(OAc)_2$ resulted in the formation of a complex mixture that did not contain the target flavanones. An aldehyde signal at 9.78 ppm and several aromatic signals suggested that a retro-Aldol condensation may have occurred, to afford the benzaldehyde derivative along with a mixture of other products. The formation of several by-products was likely due to the $Zn(OAc)_2$ acting as a Lewis acid, resulting in a number of side reactions occurring.

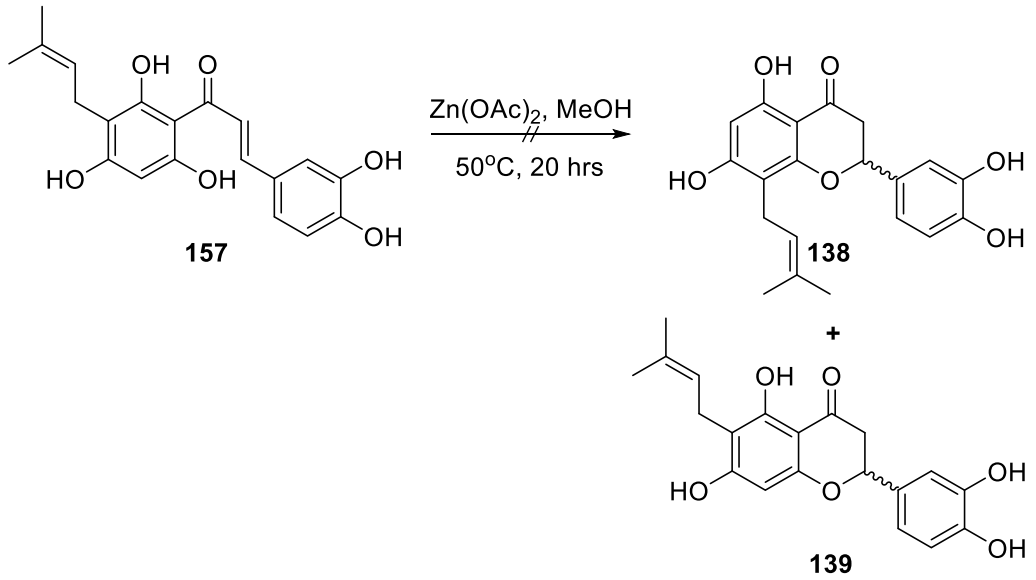

Scheme 5.9. *Attempted synthesis of 8-prenylflavanone* ***138*** *and 6-prenylflavanone* ***139*** *using* $Zn(OAc)_2$.

The effect of altering the catalyst from a base to a Brønsted-Lowry acid was also explored. The use glacial acetic acid resulted in no visible reaction after heating in THF at reflux. The reaction was repeated using CSA in THF at reflux, which had a lower pKa (1.2) (Scheme 5.10). The ^{1}H NMR spectrum indicated that a complex mixture had formed due to the high acidity of CSA.

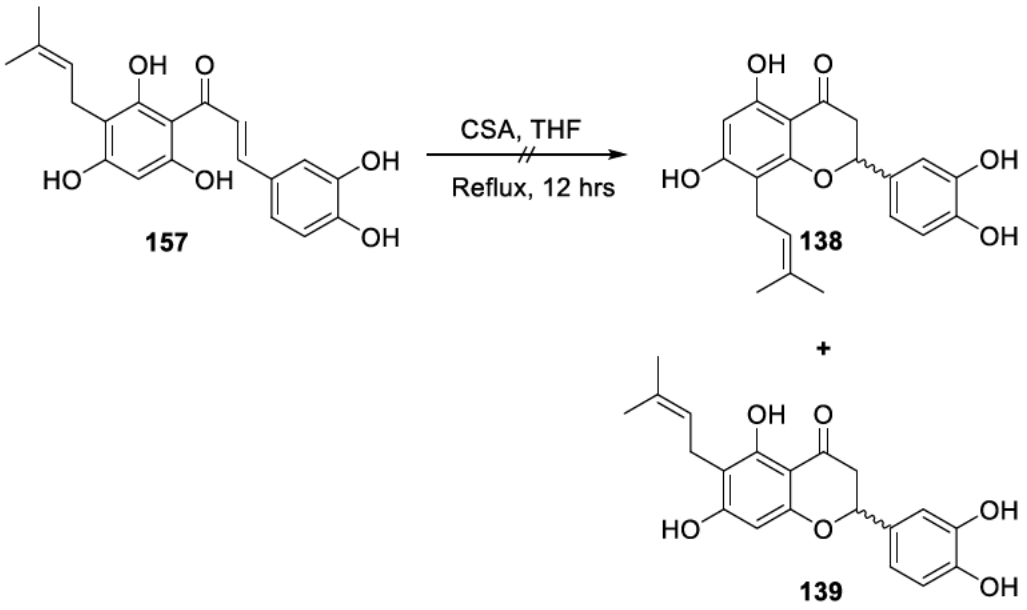

Scheme 5.10. *Attempted synthesis of 6-prenylflavanone* ***138*** *and 8-prenylflavanone* ***139*** *using CSA.*

Table 5.2. *Summary of reaction conditions and product ratios for synthesis of flavanones* ***138*** *and* ***139****.*

Catalyst	Solvent	Temperature (°C)	8-Prenyl 138	6-Prenyl 139
NaOAc	MeOH	50	1	3
NaOAc/LiCl	MeOH	50	1	4
$Zn(OAc)_2$	MeOH	50	Complex mixture	
Et_3N	THF	Reflux	0	1
AcOH	THF	Reflux	No reaction	
CSA	THF	Reflux	Complex mixture	

Michael additions have been reported to occur through radical initiated mechanisms, including photocatalysed reactions through use of photoredoxcatalysts.[135] A photocatalysed Michael addition of the chalcone **157** to form flavanones **138** and **139** was therefore a possibility through exposure to UV light from sunlight, if the chalcone **157** was excreted on the surface of the *S. crassifolia* leaves. The effect of exposure to UV light was explored through exposure of a solution of the chalcone **157** in CD_3CN to a UV light source (Repti Glo 5.0 Compact, 26W) (Scheme 5.11). The reaction was monitored by ^{1}H NMR spectroscopy. Initially, few changes to the chalcone **157** were observed in the ^{1}H NMR spectra, but after four days, the aromatic and vinylic signals between 6.00 and 8.00 ppm

were primarily absent in the ^{1}H NMR spectra (Figure 5.3). The changes in the ^{1}H NMR spectra indicated that the chalcone **157** had polymerised.

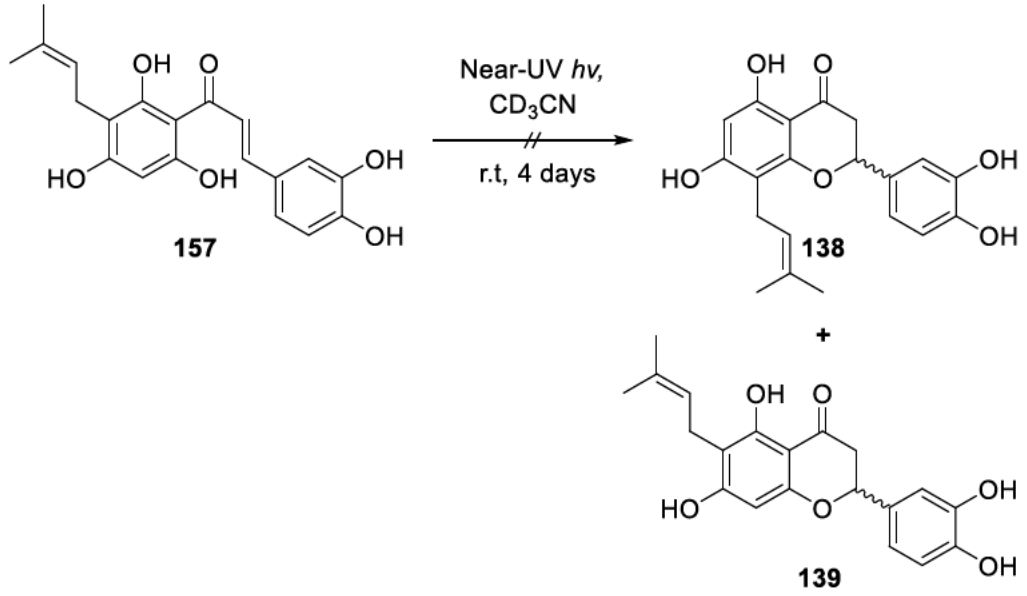

Scheme 5.11. *Attempted synthesis of 8-prenylflavanone* ***138*** *and 6-prenylflavanone* ***139*** *using a near-UV light source.*

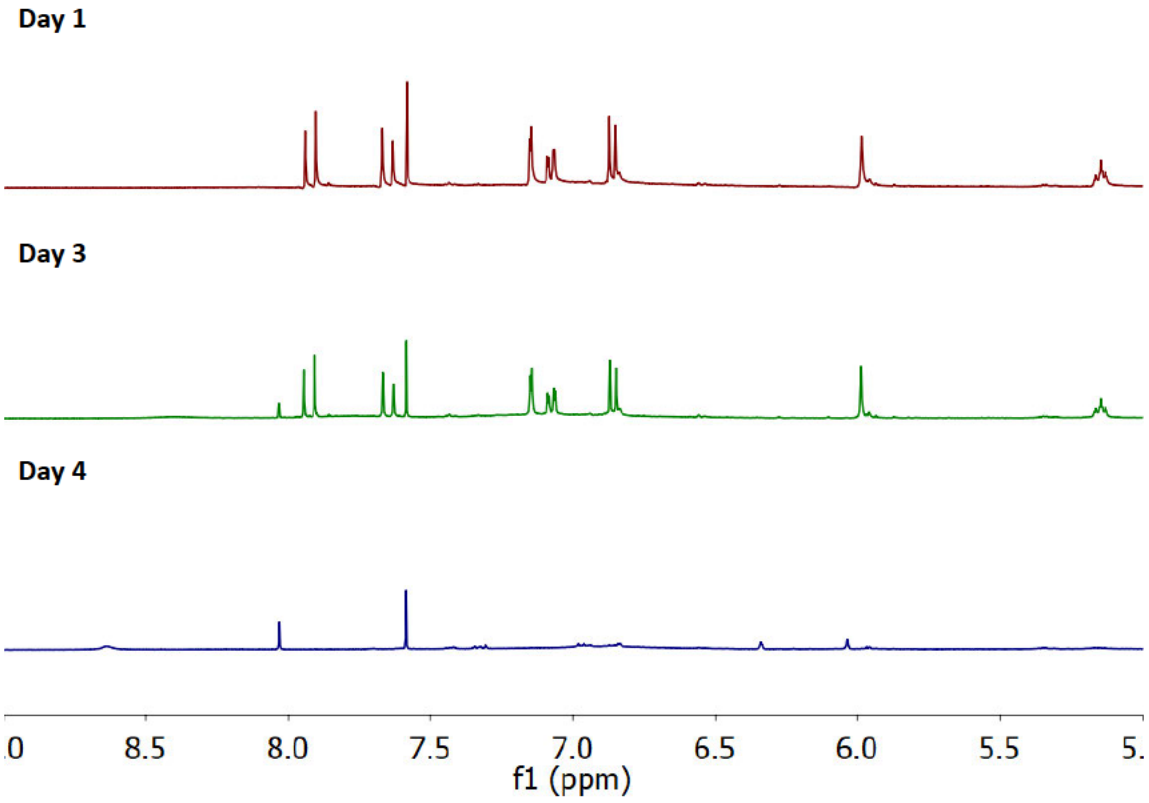

Figure 5.3. *^{1}H NMR spectra of chalcone* ***157*** *in CD_3CN after exposure to UV light.*

The reaction was repeated using direct sunlight as the light source and was similarly monitored by ^{1}H NMR spectroscopy (Scheme 5.12). Similar changes in the ^{1}H NMR spectra were observed to that of the near-UV light experiment. Intermediate products formed suggested that the chalcone **157** may undergo a retro-Aldol condensation to form acetophenone and benzaldehyde derivatives (Figure 5.4). The polymerisation of the chalcone was a significantly slower process in sunlight, taking up to 45 days for the reaction to complete. The polymerisation of chalcones, also known as resinification, has been reported previously and has been used in materials science, such as in the development of new sealants and adhesives as part of a polymer blend.[136]

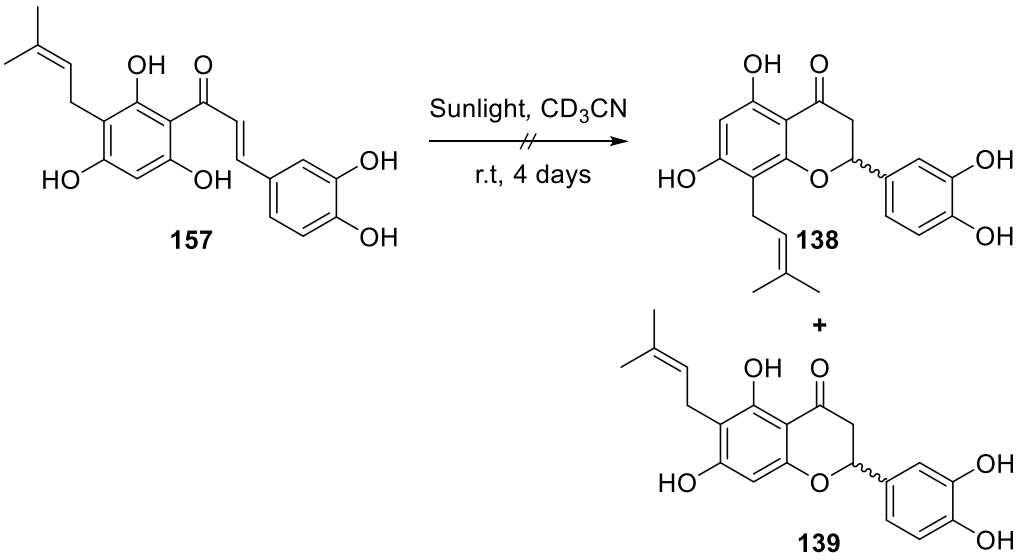

Scheme 5.12. *Attempted synthesis of 8-prenylflavanone* ***138*** *and 6-prenylflavanone* ***139*** *using sunlight.*

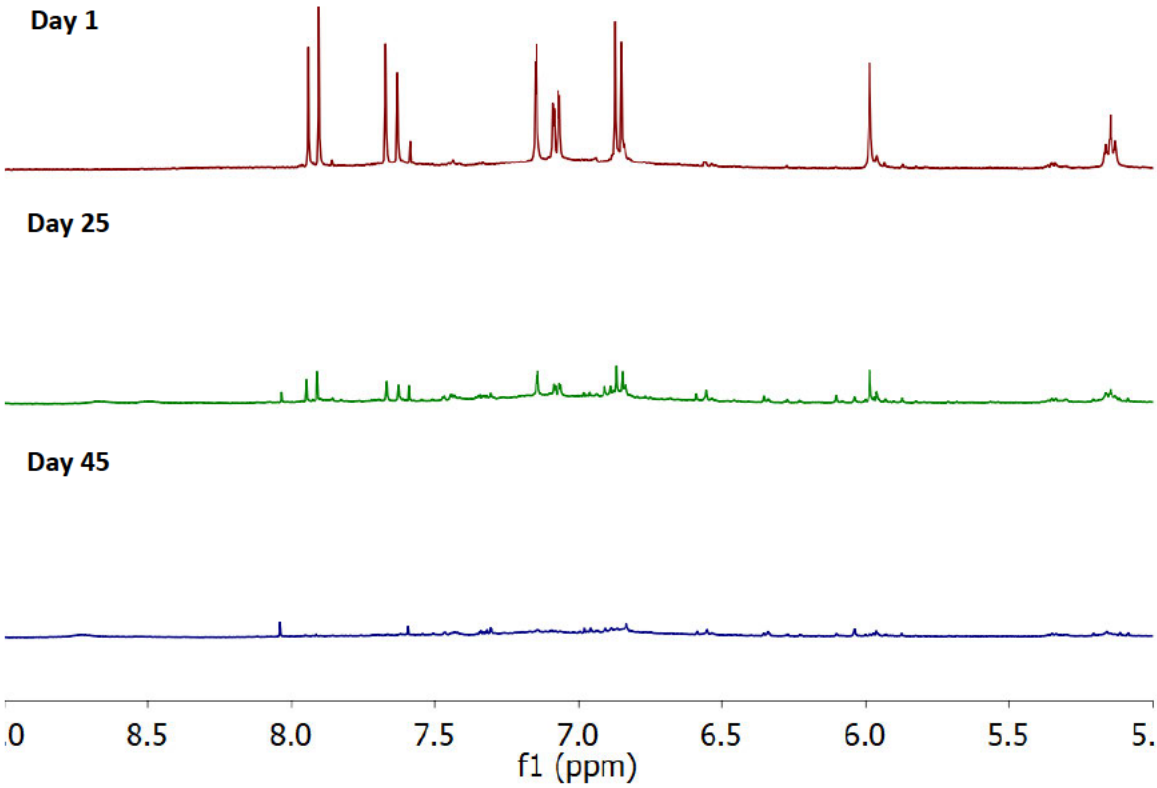

***Figure 5.4**. ^{1}H NMR spectra of chalcone **157** in CD_3CN after exposure to sunlight.*

5.4 Conclusions

The phenolic compounds **138**, **139** and **157** were isolated from *S. crassifolia* but chalcone **157** was determined to be an artefact of isolation. The synthesis of 8-prenyl- and 6-prenylflavanones **138** and **139** from chalcone **157** was conducted under a variety of conditions to replicate the naturally occurring ratio of 5:4. Cyclisation using a basic salt afforded 8-prenyl- and 6-prenylflavanones **138** and **139** in a 1:3 ratio, and use of a bulky based exclusively afforded the 6-prenylflavanone **138**. Cyclisation using Lewis and Brønsted-Lowry acids, resulted in no visible reaction occurring or degradation of the starting material. Photocatalysis using a near-UV light source or sunlight resulted in polymerisation of the chalcone **157**, which is a known phenomenon. In conclusion, the 4:5 ratio of flavanones **138** and **139** naturally occurring in *S. crassifolia* is likely due to a natural bias in the enzymatic reaction as opposed to an abiotic chemical reaction.

Chapter 6

Chemistry of 6-hydroxycaryophyllenes

The chemistry of β-caryophyllene **58** has been extensively investigated, but only limited work has been conducted on 6-hydroxycaryophyllenes. 6-Hydroxycaryophyllenes possess similar characteristics to β-caryophyllene **58** such as the strained endocyclic alkene, which is more reactive than the exocyclic alkene. The hydroxyl group in the C6 position also results in the compounds existing as a single conformer, which simplifies characterisation of compounds derived from 6-hydroxycaryophyllenes. In contrast β-caryophyllene **58** exists as a mixture of four conformers (αα, αβ, βα, ββ) while the structural isomer 12-hydroxycaryophyllene exists as a mixture of two conformers (βα, ββ). 6-Hydroxycaryophyllenes are well positioned to undergo a variety of chemical reactions. The endocyclic alkene can be used as a dienophile for Diels-Alder reactions. The exocylic alkene can be used as a nucleophile for cyclisation reactions if the endocyclic alkene is functionalised, allowing for the creation of tricylic compounds. The C6 hydroxyl group can be activated or functionalised to undergo a variety of transformations including alkylation, esterification and S_N2' reactions. The C6 hydroxyl group can also be oxidised to create an α,β-unsaturated ketone, which can act as a Michael acceptor. Analogues of 6-hydroxycaryophyllene **1** such as 12-acetoxy-6-hydroxycaryophyllene **2** and 6,12-dihydroxy caryophyllene **3** can also be functionalised in the C12 position.

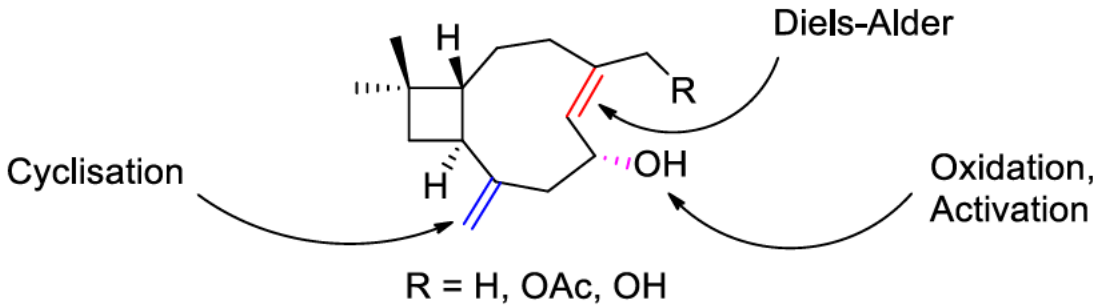

Figure 6.1. *General structure of 6-hydroxycaryophyllenes and possible functionalisation opportunities.*

6.1 Synthesis of caryophyllene hexol 168 and its analogues

Amphipathic compounds, compounds that contain both hydrophilic and hydrophobic functional groups, have attracted interest in medicinal chemistry due to their ability to be soluble in both hydrophilic and hydrophobic environments. This allows for amphipathic compounds to interact and bind within the lipid bilayer membrane of cells. For example, amphotericin B **171** is an amphipathic drug used for the treatment of serious fungal infections and leishmaniasis.

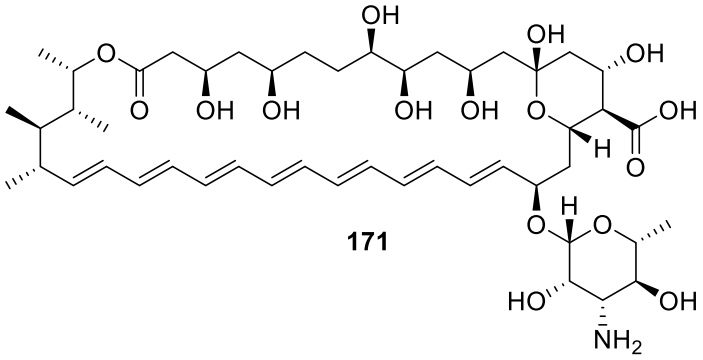

171

Figure 6.2. *Structure of amphotericin B **171**.*

12-Acetoxy-6-hydroxycaryophyllene **2** and 6,12-dihydroxycaryophyllene **3** are ideal candidates for preparation of an amphipathic compound that may possess interesting biological activity. In particular, 12-acetoxy-6-hydroxycaryophyllene **2** was the more suitable starting material, because the primary C12 hydroxyl group was already protected with an acetate. The C6 hydroxyl group and the masked C12 hydroxyl group provided easy access to a diol compound. Each of the alkenes in the molecule could also be dihydroxylated to each form a diol. Therefore, a viable synthetic pathway to prepare an amphipathic hexol caryophyllene was the dihydroxylation of the endocyclic and exocyclic alkene followed by deprotection of the C12 acetate (Scheme 6.1).

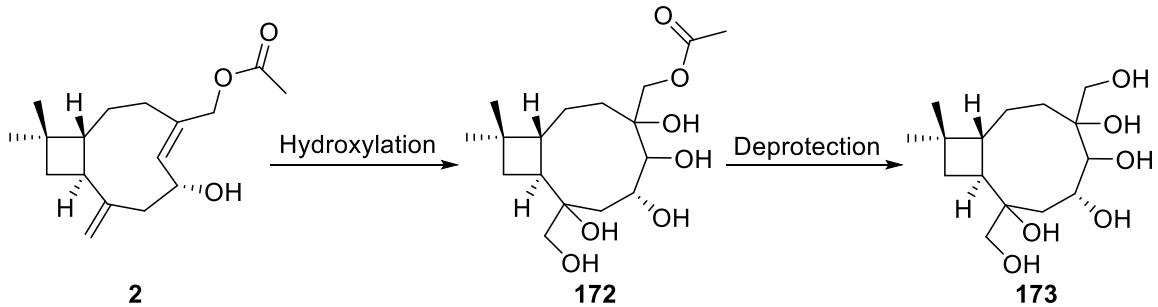

2 **172** **173**

Scheme 6.1 *Proposed synthesis of caryophyllene hexol **173**.*

Several methods are available for the dihydroxylation of alkenes, including the use of $KMnO_4$, OsO_4 and Prévost dihydroxylation. $KMnO_4$ is a traditional dihydroxylation method, whereby MnO_4^- facilitates a *syn*-dihydroxylation of the alkene to form a vicinal diol, and forms MnO_2 as a byproduct (Scheme 6.2). However, dihydroxylation using $KMnO_4$ typically results in poor yields due to over oxidation and oxidative cleavage of the newly formed 1,2-diol systems.

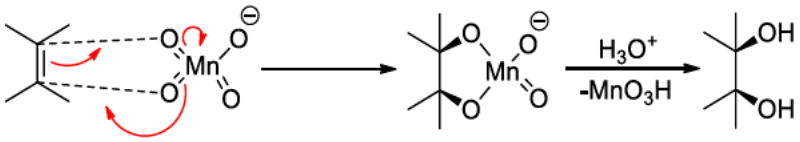

Scheme 6.2. *Mechanism for dihydroxylation of alkenes by MnO_4^-.*

Perhydroxylation of 12-acetoxy-6-hydroxycaryophyllene **2** was attempted using $KMnO_4$ in an EtOH/H_2O mixture at 0ºC, adapted from a procedure by Shih *et al.*[137] However, a complex mixture of products was afforded, indicating that a multiple reactions had occurred, likely including oxidative cleavages.

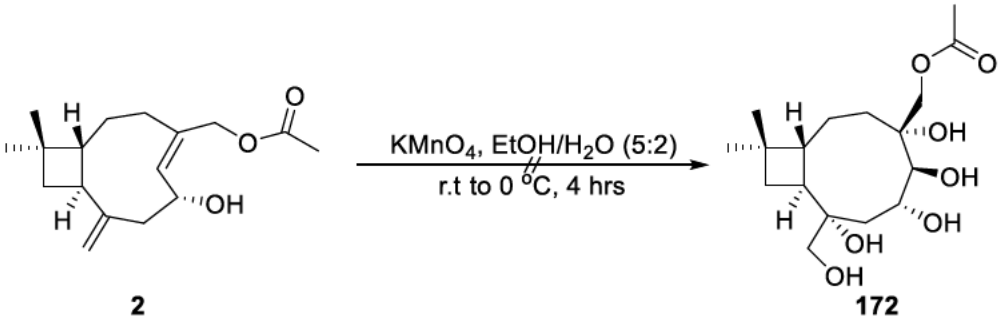

2 **172**

Scheme 6.3. *Attempted perhydroxylation of 12-acetoxy-6-hydroxycaryophyllene **2** using $KMnO_4$*

Consequently, individual dihydroxylation of each alkene was considered to be a more viable synthetic route, by reducing the number of side reactions that could occur. The endocyclic *E*-alkene of caryophyllenes are strained and therefore are more reactive than the exocyclic alkene. As a result, the endocyclic alkene can be specifically dihydroxylated using activated MnO_2. Dihydroxylation reactions using activated MnO_2 have not been previously reported, but it is postulated that the mechanism would be similar to that of $KMnO_4$, affording $Mn(OH)_2$ as the byproduct (Scheme 6.3).

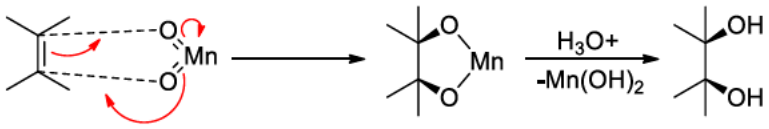

Scheme 6.4. *Proposed mechanism for dihydroxylation of alkenes by activated MnO_2.*

The selective dihydroxylation of the endocyclic alkene of 12-acetoxy-6-hydroxycaryophyllene **2** using activated MnO_2 was previously observed (Chapter 4). Acetate triol caryophyllene **148** was successfully prepared by reaction with activated MnO_2 in dry CH_2Cl_2 at room temperature over 4 hours. Purification of the crude product by column chromatography afforded the pure acetate triol caryophyllene **148** as a colourless oil in 63% yield.

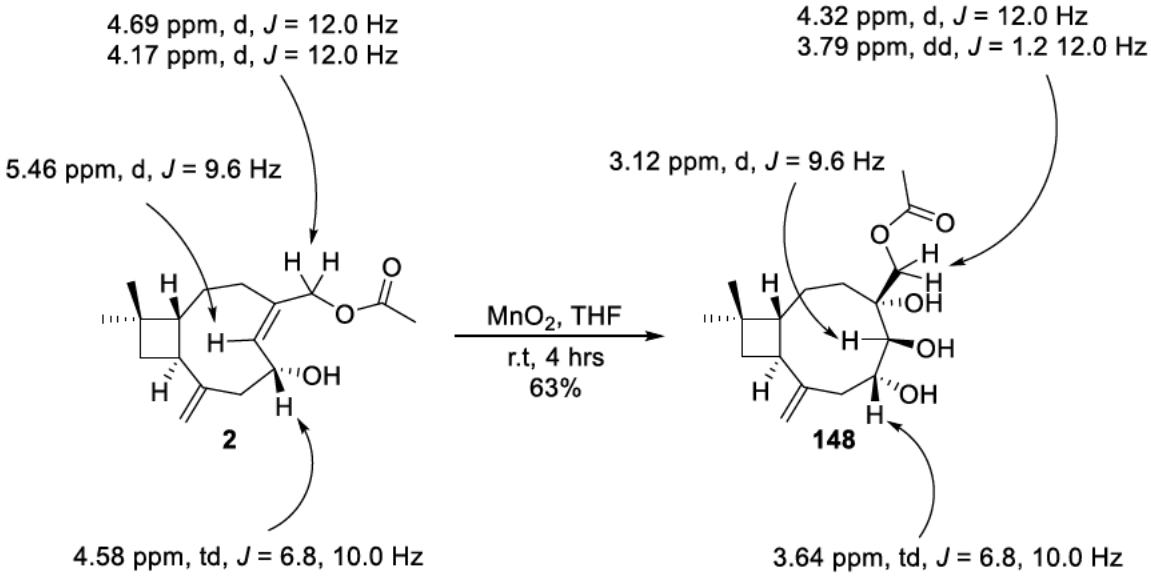

Scheme 6.5. *Dihydroxylation of 12-acetoxy-6-hydroxycaryophyllene **2** using activated MnO_2.*

Dihydroxylation of the endocyclic alkene provided access to a simpler amphipathic molecule, via the hydrolysis of the C12 acetate to afford tetrol **174**. Multiple hydrolysis methods are available including traditional methods such NaOH in MeOH, and NH_3 in MeOH. The acetate was hydrolysed using NH_3 in MeOH, because the tetrol **174** was likely to be water soluble and no water is involved in the work-up. A solution of aqueous NH_3 (30%) was added to a solution of acetate triol caryophyllene **148** in MeOH at room temperature for 48 hours (Scheme 6.6). After work-up, the crude product was purified by column chromatography to afford a colourless oil. The FTIR spectrum did not contain a carbonyl peak at 1700 cm^{-1} and the ^1H NMR spectrum showed that a singlet at ~2 ppm was absent, which was characteristic of an acetate, indicating that the acetate was absent in the

compound. Two singlets at 5.30 and 5.10 ppm were present, indicating that the exocylic double bond as still present. Based on the FTIR, ^{1}H, ^{13}C and 2D NMR spectra, the compound was assigned as tetrol **174**.

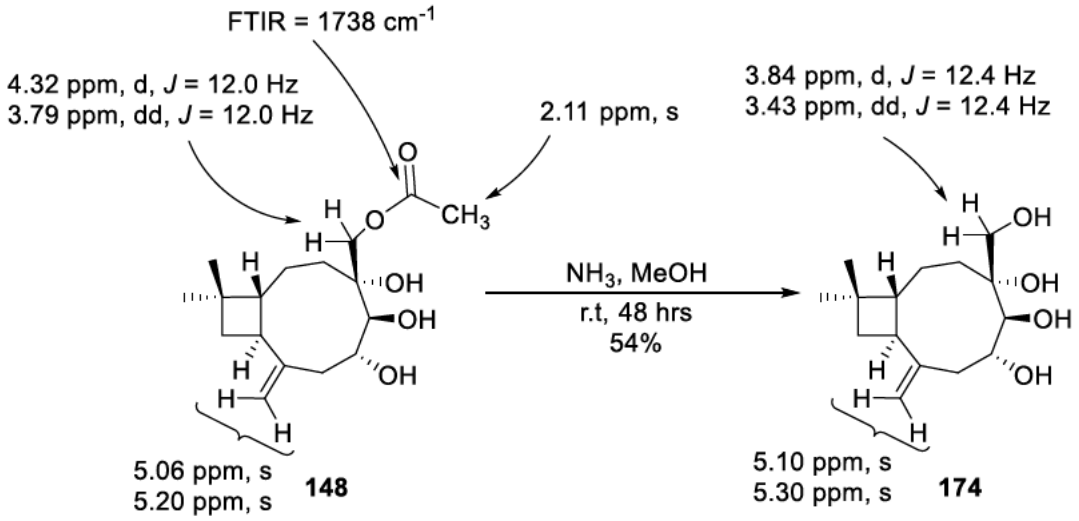

Scheme 6.6. *Hydrolysis of acetate triol caryophyllene* ***148****.*

With the successful dihydroxylation of the endocyclic alkene, the next step was to dihydroxylate the exocyclic alkene. Alternative dihydroxylation methods to $KMnO_4$ were considered due to the risk of over oxidation and unprotected alcohols present in the compound. OsO_4 is commonly used instead of $KMnO_4$ for *syn*-dihydroxylation reactions due to the lower risk of over oxidation. The dihydroxylation mechanism of OsO_4 is similar to that of $KMnO_4$ and forms OsH_2O_4 as a by-product.

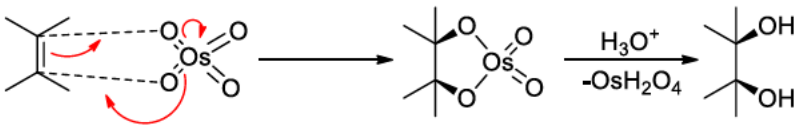

Scheme 6.7. *Mechanism for dihydroxylation of alkenes by* OsO_4*.*

However, OsO_4 poses significant health risks, including carcinogenicity and blindness, so use of OsO_4 by itself is not recommended. Kolb *et al.* developed the Sharpless asymmetric dihydroxylation, which uses OsO_4 in the presence of a chiral ancillary ligand and $K_3Fe(CN)_6$ to asymmetrically dihydroxylate alkenes.[138] The reaction also only requires a catalytic amount of OsO_4, because the OsO_4 is regenerated by the $K_3Fe(CN)_6$, making it significantly safer to handle. Chiral ancillary ligands used include dihydroquinidine (DHQD) **175** and dihydroquinine (DHQ) **176** (Figure 6.3).

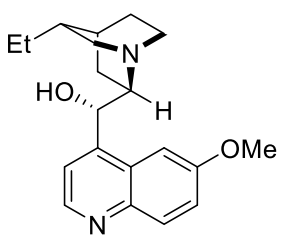

175

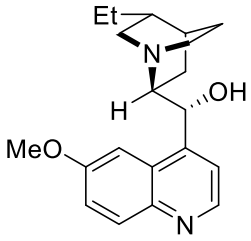

176

Figure 6.3. *Structures of DHQD* ***175*** *and DHQ* ***176****.*

Asymmetric dihydroxylation (AD) mixes are commercially available reagents used for Sharpless dihydroxylations, and come as AD-mix-α and AD-mix-β. Both AD mixes contain $K_2[OsO_2(OH)_4]$, $K_2Fe(CN)_6$m K_2CO_3 and one of two chiral phthalazine ligands. AD-mix-α contains dihydroquinine-phthalazine ($(DHQ)_2PHAL$) **177**, and AD-mix-β contains dihydroquinidine-phthalazine ($(DHQD)_2PHAL$) **178** (Figure 6.4).

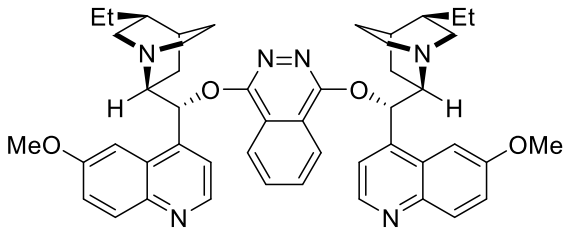

177

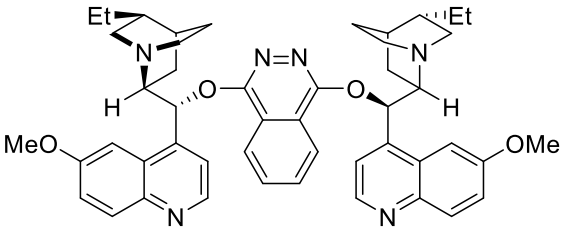

178

Figure 6.4. *Structures of* $(DHQ)_2PHAL$ ***177*** *and* $(DHQD)_2PHAL$ ***178****.*

AD-mix-α typically gives the α-diol and AD-mix-β typically gives the β-diol. Dihydroxylation using both AD-mix-α and AD-mix-β using a procedure adapted by Kolb *et al.* was attempted using acetate triol caryophyllene **148**.[138] A solution of AD-mix α/β in a 1:1 mixture of *t*-BuOH and H_2O was added to acetate triol caryophyllene **148** at 0ºC and then allowed to warm to room temperature. Unfortunately, no reaction was observed by NMR spectroscopy using both AD-mixes. The lack of reaction was potentially due to incompatibility between the chiral ancillary ligands and the alkenes in the caryophyllenes due to the molecular conformation of the caryophyllene scaffold.

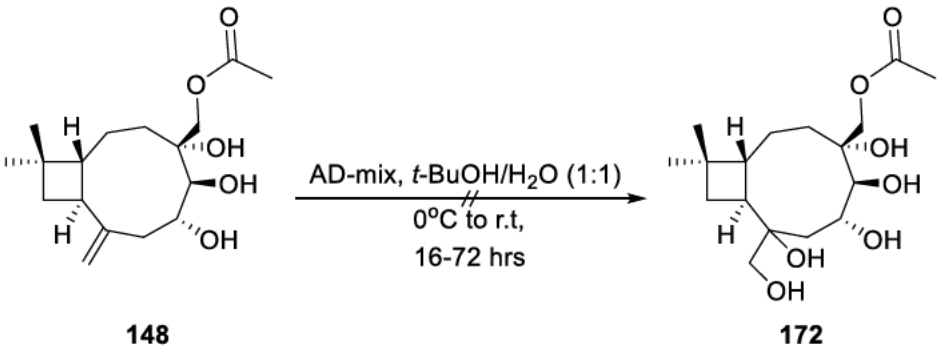

Scheme 6.8. *Attempted dihydroxylation of acetate triol caryophyllene* ***148*** *using AD-mix-α/β.*

Direct dihydroxylation of the exocyclic double bond was proving difficult, so alternative approaches were considered. The hydrolysis of epoxides to form diols is well established, and multiple methods are available for the epoxidation of alkenes. A new synthetic approach was proposed, whereby 12-acetoxy-6-hydroxycaryophyllene **2** is dihydroxylated first using activated MnO_2, then the exocyclic alkene of acetate triol caryophyllene **148** is epoxidised. Then epoxide and acetate can then be hydrolysed to afford the target hexol **173**.

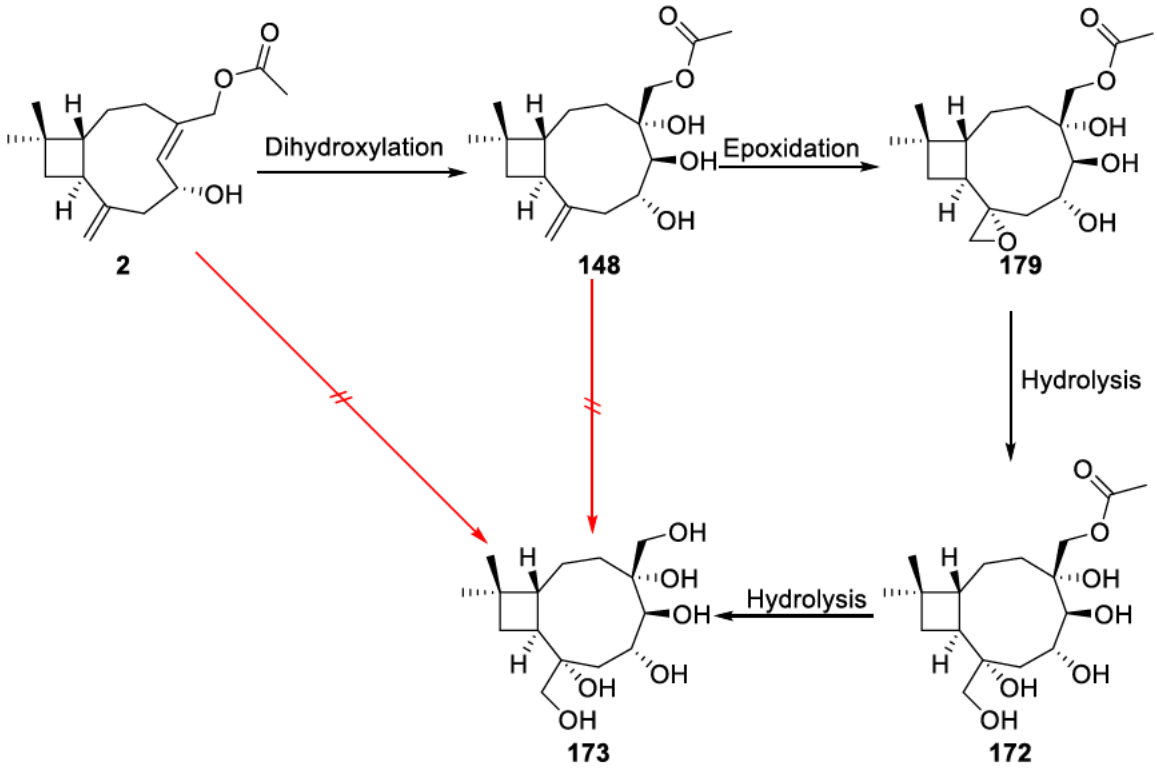

Scheme 6.8. *Proposed synthesis of hexol* ***173*** *via epoxidation of the exocyclic alkene.*

Many methods exist for the epoxidation of alkenes, but one of the most common is the use of *m*-CPBA. The reagent *m*-CPBA epoxidises alkenes under mild conditions and affords 3-chlorobenzoic acid as a by-product, which can be easily removed during the reaction work-up.

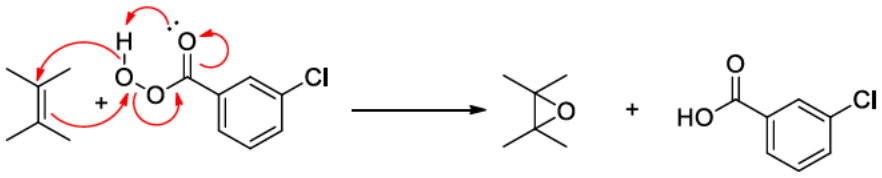

Scheme 6.9. *Mechanism for epoxidation of alkenes using m-CPBA.*

Acetate triol caryophyllene **148** was epoxidised through addition of *m*-CPBA in CH_2Cl_2 to a solution of acetate triol caryophyllene **148** in CH_2Cl_2 at 0°C, and allowing the reaction mixture to stir at room temperature for 32 hours. The two singlets at 5.06 and 5.20 ppm were absent in ^{1}H NMR spectrum of the epoxide **179**, indicating that the exocyclic alkene was absent. A doublet of doublets and a doublet at 2.77 and 2.69 ppm respectively both had a coupling constant of 4.4 Hz, indicating that they were coupling to each other. The HRMS $[M+H]^+$ molecular ion had an exact mass of 311.1851 *m/z* corresponding to a molecular formula of $C_{17}H_{27}O_5$, which is consistent with the molecular formula of $C_{17}H_{28}O_6$ after the loss of a hydroxyl group as water during HRMS analysis. Therefore, based on ^{1}H NMR and ^{13}C NMR spectroscopy, and HRMS, the compound was assigned as caryophyllene epoxide **179**. The stereochemistry of the epoxide could be postulated mechanistically based on the ββ conformation of 6-hydroxycaryophyllenes, where the bottom face of the exocyclic alkene is more accessible than the top face.

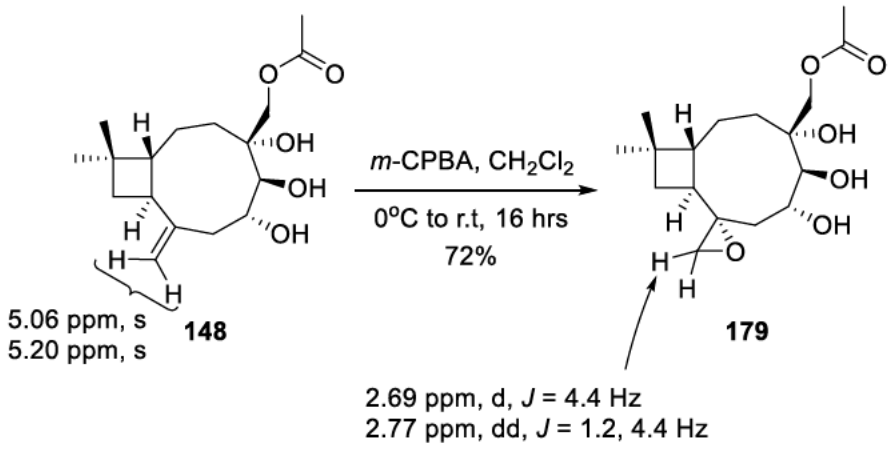

Scheme 6.10. *Epoxidation of acetate triol caryophyllene **148** using* m-*CPBA.*

With the successful synthesis of the epoxide, the next step was to hydrolyse the epoxide to afford the pentol acetate **172**. Epoxides can be easily cleaved using dilute HCl in water e.g. 0.1M to afford a vicinal diol. Aqueous HCl solution (0.1 M) was added to neat epoxide **179** and left to stir at room temperature overnight. After work-up, the epoxide had degraded, likely due to the reaction between the unprotected hydroxyl group and the HCl resulting in the formation of a carbocation, causing side reactions.

An alternate approach reported by Harayama *et al.* was the one pot epoxidation and hydrolysis of alkenes using TFAA and molecular O_2 in anhydrous pyridine.[139] Reaction with the epoxide **179** would afford the pentatrifluoroacetoxy caryophyllene monoacetate, which could then be hydrolysed to afford the hexol product. Reaction of acetate triol caryophyllene oxide **179** with TFAA and dry O_2 in anhydrous pyridine over 72 hours afforded a colourless oil after purification with column chromatography (Scheme 6.11). The ^{1}H NMR spectrum showed the absence of the two signals at 2.77 and 2.69 ppm, indicating that the epoxide had changed. Instead, a doublet of doublets at 2.73 ppm was present that integrated for 1H. A singlet at 9.88 ppm that integrated for 1H indicated that an aldehyde was present in the compound, and was likely formed through the ring opening and oxidation of the epoxide on C13. The doublet at 3.16 ppm that corresponded to H5 had shifted to downfield to 4.33 ppm, indicating that it was bonded to a strongly deshielding group, such as a trifluoroacetate. Similarly, the signal at 3.71 ppm in the epoxide corresponding to H6 had shifted downfield to 4.23 ppm, indicating that it was also bonded to a strongly electron withdrawing group like a trifluoroacetate. Therefore based on the ^{1}H NMR and COSY spectra, the compound was tentatively assigned as aldehyde **180** with a 4% yield.

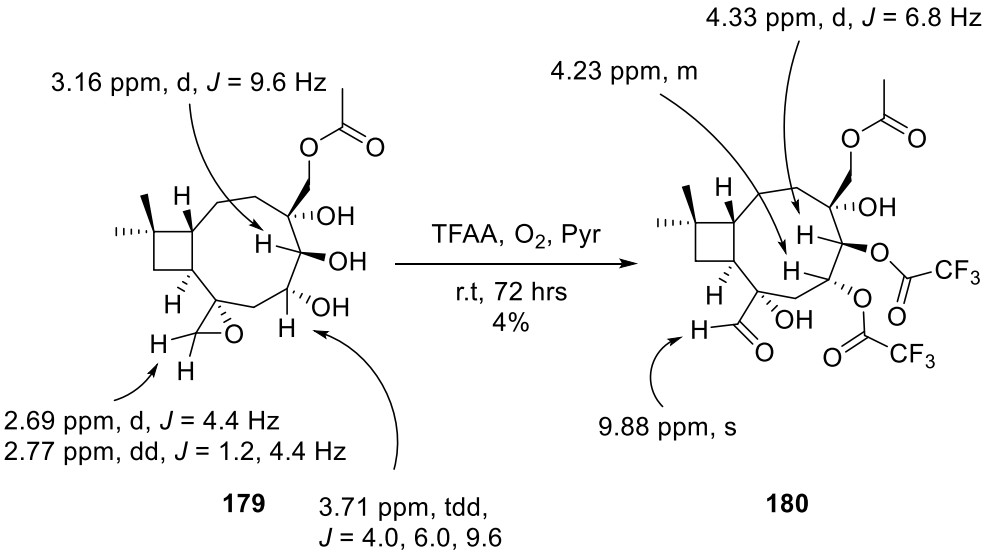

Scheme 6.11. *Epoxide ring opening and trifluoroacetylation of epoxide* ***179****.*

The method proposed by Harayama *et al.* did open the epoxide, but the yields were too low to be viable and it generated an aldehyde rather than the desired trifluoroacetate.[139] Amphipathic compounds do not exclusively require oxygen-containing functional groups. Nitrogen-containing functional groups also improve the aqueous solubility of compounds while also potentially increasing the bioactivity of the compound. Amines can be generated from the reduction of an azide. Sabitha *et al.* reported the a method for the $CeCl_3$ promoted ring opening of epoxides and aziridines using NaN_3 in MeCN.[140] The reaction was attempted using epoxide **179**, but unfortunately the reaction proceeded incredibly slowly in a 11:1 MeCN/H_2O mixture even when heated under reflux (Scheme 6.12). ^{1}H NMR spectroscopy showed that most starting material remained unreacted after 4 days, with only a small quantity of the product forming.

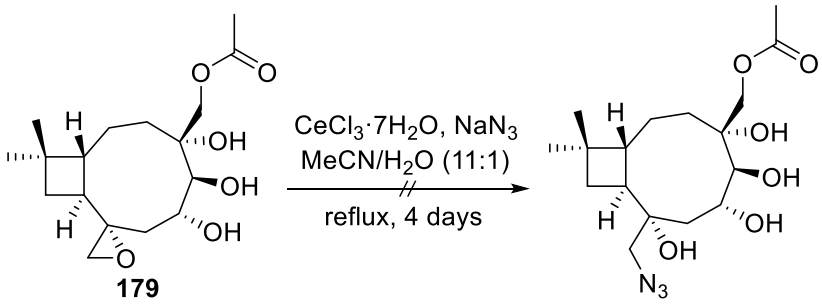

Scheme 6.12. *Attempted ring opening of epoxide* ***179*** *using* $CeCl_3 \cdot 7H_2O$ *and* NaN_3*.*

Difficulties were similarly being encountered for ring opening of the epoxide, so a reduction approach was considered. Epoxides could be reduced using a reducing agent such

as $LiAlH_4$ to afford a single hydroxyl group. Hydride addition typically occurs at the less substituted position. Reduction of epoxide **179** would have the added advantage of reducing the C12 acetate to the primary alcohol, reducing the number of synthetic steps to produce the pentol caryophyllene derivative (Scheme 6.13). Reduction of epoxide **179** with $LiAlH_4$ unfortunately afforded a complex mixture after repeated attempts, indicating that other rearrangements or reactions may be occurring.

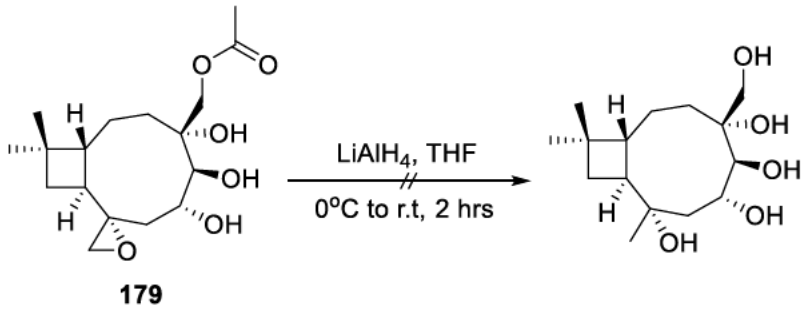

Scheme 6.13. *Attempted reduction of epoxide **179** using $LiAlH_4$.*

The epoxide synthetic route was no longer proving to be viable for synthesis of the hexol, and the free hydroxyl groups in both the acetate triol caryophyllene **148** and epoxide **179** were problematic for dihydroxylation of the exocyclic double bond. A new synthetic route was therefore considered, whereby the free hydroxyl groups of acetate triol caryophyllene **148** would be protected, allowing for selection dihydroxylation of the exocyclic alkene. The acetylation of acetate triol caryophyllene **148** using Ac_2O, Et_3N and catalytic DMAP to afford diacetoxycaryophyllene oxide **150** was previously established in Chapter 4 and provided a protected form of the compound (Scheme 6.14).

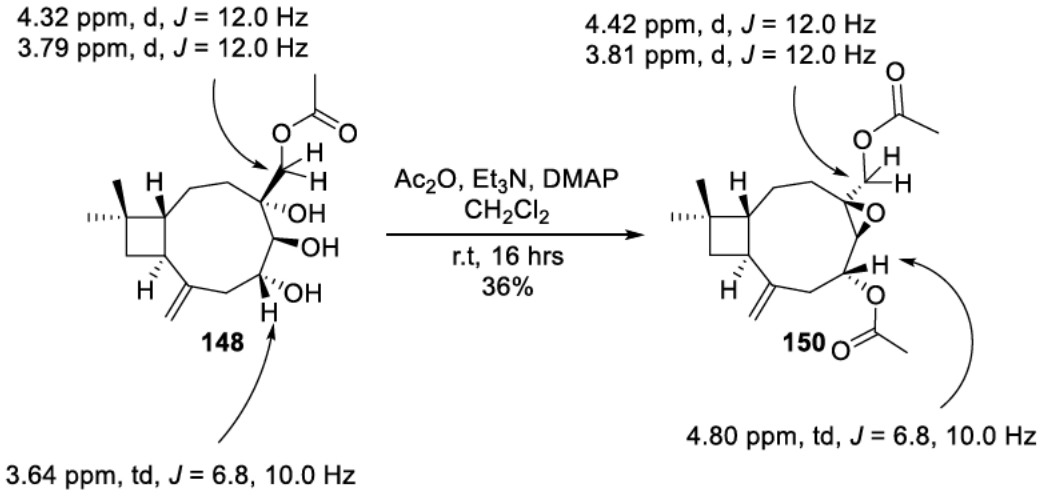

Scheme 6.14. *Acetylation of acetate triol caryophyllene **148**.*

A classic dihydroxylation method is the Prévost reaction, developed by Prévost in 1933.[141] The Prévost reaction uses I_2 and $PhCO_2Ag$ to generate the *anti*-vicinal diol from the alkene as the di-benzoate, which can then be hydrolysed to afford the vicinal diol.

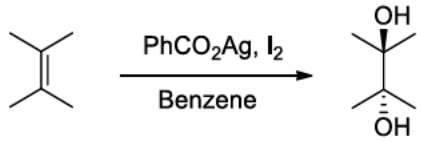

Scheme 6.15. *Dihydroxylation via a Prévost reaction.*

Sudalai *et al.* reported a modified Woodward-Prévost dihydroxylation using catalytic $NaIO_4$ to afford the *syn*-diol and catalytic $PhI(Oac)_2$ to afford the *anti*-diol.[142] Dihydroxylation of the exocyclic alkene of diacetoxycaryophyllene oxide **150** was conducted using $NaIO_4$ in an attempt to synthesise the *syn*-diol. A solution of diacetoxycaryophyllene oxide **150**, $NaIO_4$ and NaBr in glacial AcOH was heated at 95°C for 18 hours. The crude product was afforded after the work-up and purified by column chromatography to afford a yellow-orange oil. The ^{1}H NMR spectrum showed that the two singlets at 5.15 and 5.25 ppm corresponding to the exocyclic alkene were absent, indicating that the alkene was no longer present in the compound. Three singlet peaks that each integrated for 3H were present at 1.99, 2.09 and 2.13 ppm, which indicated that three acetate esters were present in compound, which was one more than in the starting material. The ^{1}H NMR spectrum closely resembled that of 3,12-diacetoxycaryolan-1,4-diol **151** apart from the additional acetate signal, indicating that the product was likely 1,3,12-triacetoxycaryolan-4-ol **182** (Scheme 6.16). The HRMS showed that the $[M+H]^+$ molecular ion had an exact mass of 410.2031 *m/z*, corresponding to a molecular formula of $C_{21}H_{32}O_7$ which confirmed the molecular formula corresponding to the proposed structure. The glacial AcOH likely catalysed the cyclisation through protonation of epoxidation, followed by a nucleophilic addition to C4 by the exocyclic alkene and an addition of an acetate to the newly formed 3° carbocation (Scheme 6.17). The proposed mechanism is similar to that of the formation of caryolan-1-ol **62**. Carolan-1-ol is formed through treatment of β-caryophyllene **58** with acid, resulting in proton of endocyclic alkene and the formation of a 3° carbocation on C4. The exocyclic alkene then adds from the top face to the carbocation to cyclise the molecule and form a new carbocation on C8. The addition of water to the carbocation generates the new alcohol and regenerates the acid catalyst, yielding caryolan-1-ol **62**. Therefore based on the formation of mechanism of formation of caryolan-1-ol **62**, the stereochemistry of caryolanol **182** could be postulated.

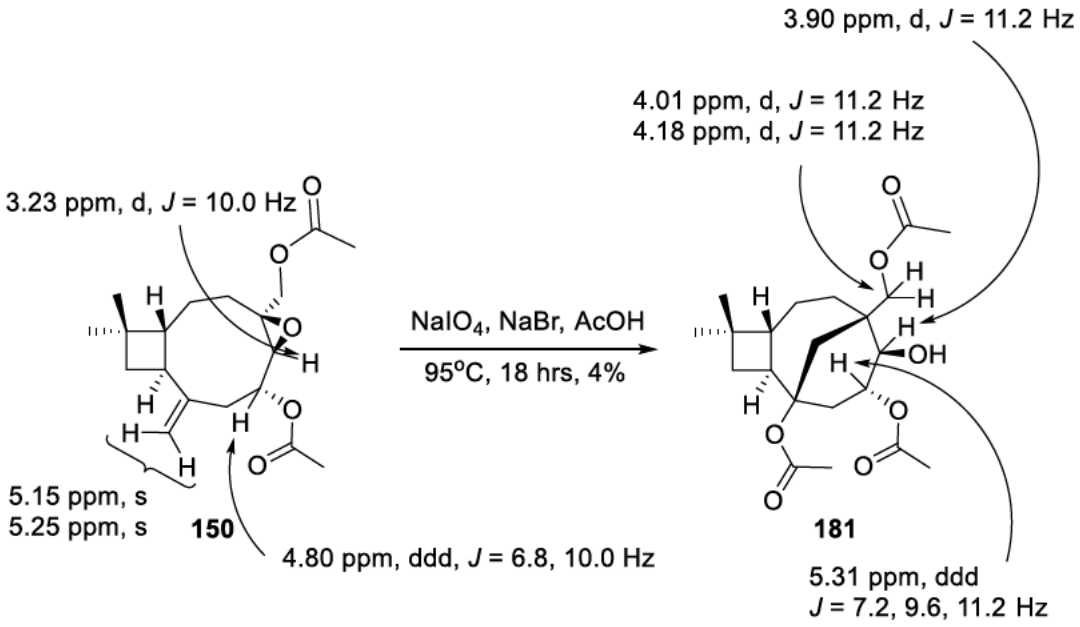

Scheme 6.16. *Synthesis of 1,3,12-triacetoxycaryolan-4-ol* ***181****.*

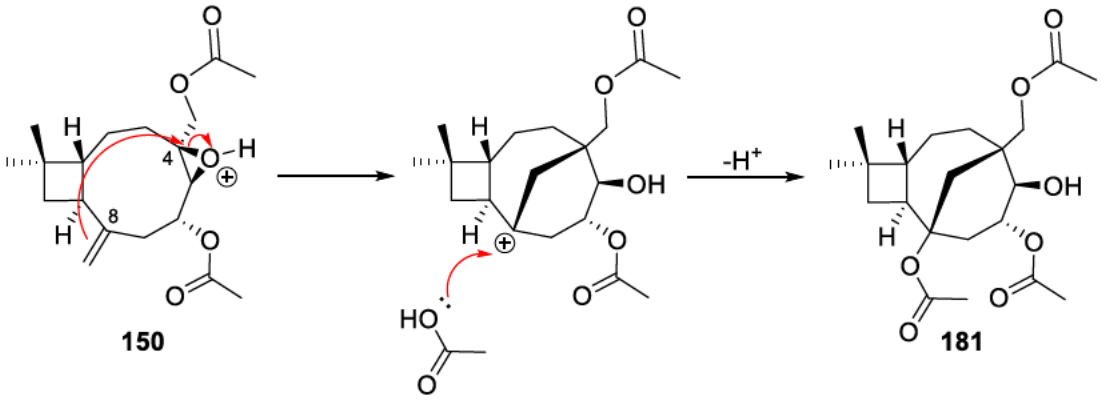

Scheme 6.17. *Proposed mechanism for synthesis of 1,3,12-triacetoxycaryolan-4-ol* ***181****.*

The product of the modified Woodward-Prévost dihydroxylation was intriguing, but unfortunately not the target diol. A less subtle approach seemed to be required so dihydroxylation using $KMnO_4$ was once again attempted, except now the whole compound was protected apart from the exocyclic alkene. The procedure from Shenvi *et al.* was similarly adapted.[143] An aqueous solution of $KMnO_4$ was added dropwise to a stirred solution of 6,12-diacetoxycaryophyllene oxide **150** at 0ºC. The FTIR spectrum of the product showed a broad absorbance at 3467 cm^{-1}, which was indicative of the OH stretch of an alcohol. The ^1H NMR spectrum showed that the singlets at 5.15 and 5.25 ppm that corresponded to the vinylic hydrogens of the exocyclic alkene were absent, indicating the alkene was no longer present. Two new doublets at 3.51 and 3.66 ppm that both had a coupling constant of 11.2 Hz and integrated for 1H each was also visible in the spectrum.

The HSQC spectrum indicated that those hydrogens were on the same carbon at 64.5 ppm, which corresponded to a methylene, indicating that the methylene was part of a 1º alcohol. The two doublets correlated to a quarternary carbon at 74.1 ppm that corresponded to a 3º alcohol, suggesting that the primary alcohol was adjacent to the 3º alcohol. Therefore, based on the FTIR, ^{1}H NMR, ^{13}C NMR and 2D NMR spectra, the compound was tentatively assigned as 6,12-diacetoxy-8,13-dihydroxycaryophyllene oxide **182**. The HRMS gave the $[M+Na]^+$ molecular ion an exact mass of 393.1873 *m/z*, which corresponded to a molecular formula of $C_{19}H_{30}O_7$, and thus confirmed the proposed structure with a 23% yield. The stereochemistry could be postulated similar to the epoxide **179**. The ββ conformation of 6-hydroxycaryophyllenes results in the bottom face of the exocyclic alkene being the least sterically hindered. Consequently, dihydroxylation using $KMnO_4$ would most likely occur on the bottom face of the exocyclic alkene.

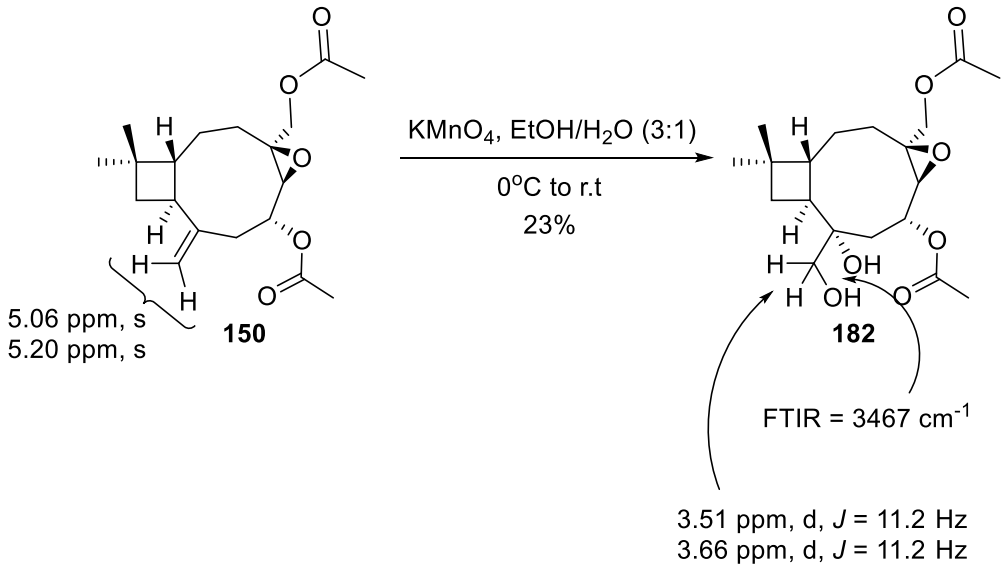

Scheme 6.18. *Synthesis of 6,12-diacetoxy-8,13-dihydroxycaryophyllene oxide **182**.*

The successful synthesis of the diacetoxy diol epoxide **182** was promising, and the next step was to hydrolyse the acetates. A similar hydrolysis method to the synthesis of the tetrol **174** was used, using NH_3 in MeOH to minimise water involved in the work-up. Aqueous NH_3 was added to a solution of 6,12-diacetoxy-8,13-dihydroxycaryophyllene oxide **182** in MeOH at room temperature. After 16 hours, the reaction was worked up to afford the crude product, which was purified by column chromatography using Et_3N treated silica gel, to afford two different compounds as colourless oils (Scheme 6.19).

The FTIR spectrum for the first compound showed a broad OH stretch at 3405 cm^{-1} and two sharp peaks at 3526 and 3501 cm^{-1} that corresponded to residual Et_3NH^+ salts. A prominent peak at 1716 cm^{-1} was also visible that corresponded to an ester carbonyl stretch. The ^1H NMR spectrum showed a singlet at 2.13 ppm that integrated for 3H, indicating that an acetate was still present. A doublet of doublet of doublets at 5.10 ppm indicated that the hydrogen was significantly deshielded and adjacent to a highly electron withdrawing group such as an ester. The multiplicity indicated that it was adjacent to multiple inequivalent hydrogens. Therefore, the acetate was likely located on the C6 hydroxyl group, while the C12 acetate had been hydrolysed. Five doublets between 3 and 4 ppm that each integrated for 1H were also consistent with a partially hydrolysed product, corresponding to the C5, C12 and C13 hydrogens. The chemical shifts of the hydrogens between 3 and 4 ppm were higher than would be expected for an epoxide, with the lowest chemical shift being 3.46 ppm. The high chemical shifts suggested that the epoxide may have ring opened during column chromatography, which can be attributed to the acidity of silica gel in organic solvents. Therefore, based of FTIR, ^1H, ^{13}C and 2D NMR spectra the first compound was tentatively assigned as 6-acetoxy-4,5,8,12,13-pentahydroxycaryophyllene **172** in 11% yield. The partial hydrolysis was likely due to the steric hindrance reducing access to the C6 acetate.

The FTIR spectrum for the second compound showed a broad OH stretch at 3362 cm^{-1} and no carbonyl stretch at 1700 cm^{-1}. The ^1H NMR spectrum showed six signals between 3 and 4 ppm that each integrated for 1H. The doublet of doublet of doublets that was at 5.10 ppm for the pentol acetate **183** had shifted upfield to 3.84 ppm, indicating that it was more shielded and therefore the acetate was no longer present. The six signals between 3 and 4 ppm was consistent with a fully hydrolysed product, corresponding to the C5, C6, C12 and C13 hydrogens. Similar to pentol acetate **183**, it appeared that the epoxide may have been hydrolysed during purification. Therefore, based on the FTIR, ^1H, ^{13}C and 2D NMR spectra the structure was tentatively assigned as 4,5,6,8,12,13-hexahydroxycaryophyllene **173** in 15% yield. Both the pentol acetate **183** and the hexol **173** were highly water-soluble, and insoluble in aprotic organic solvents such as CH_2Cl_2 and $CHCl_3$, similar to sugars. However, the both compounds were still soluble in protic polar organic solvents such as MeOH and EtOH. Analysis of the pentol acetate **183** and the hexol **173** using NMR spectroscopy were conducted in D_2O. The successful synthesis of

hexol **173** demonstrated that complex amphipathic compounds could be synthesised from readily available 6-hydroxycaryophyllene scaffolds (Scheme 6.20).

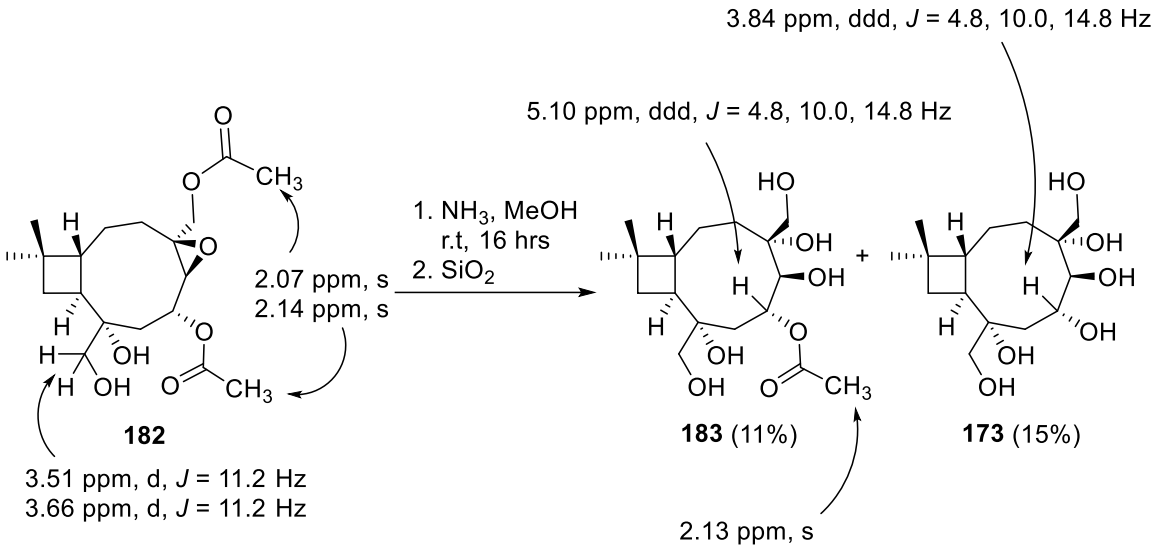

Scheme 6.19. *Synthesis of pentol acetate **183** and hexol **173**.*

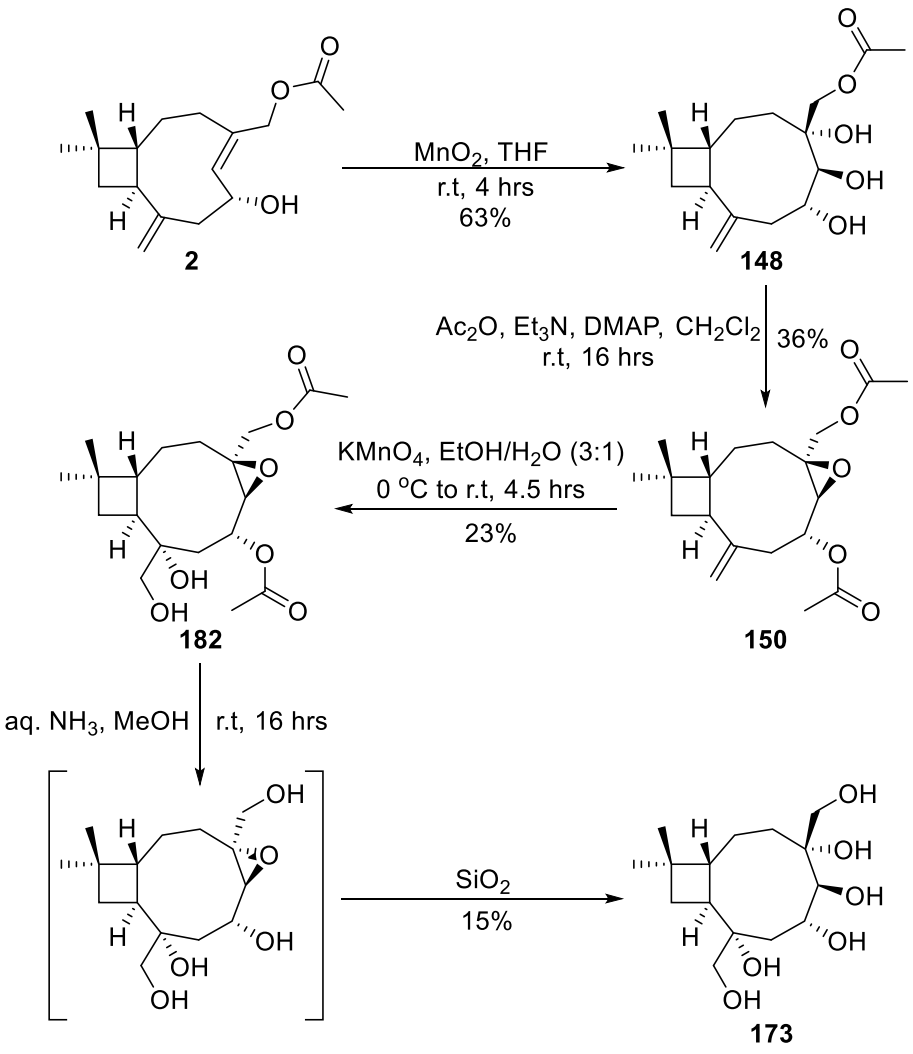

***Scheme 6.20**. Complete synthesis of caryophyllene hexol **173** from caryophyllene acetate **2**.*

6.2 Exploring the chemistry of the C6 hydroxyl group

The allylic hydroxyl group in the 6 position in 6-hydroxycaryophyllenes is a functional group that has the potential to undergo a variety of interesting reactions. At its simplest, the hydroxyl group can be protected with an ester or ether. However, conversion of the hydroxyl group into a good leaving group enables for a variety of interesting skeletal rearrangements to occur, such as S_N2' reactions, whereby a nucleophile adds to the alkene which then rearranges to lose the leaving group (Scheme 6.21).

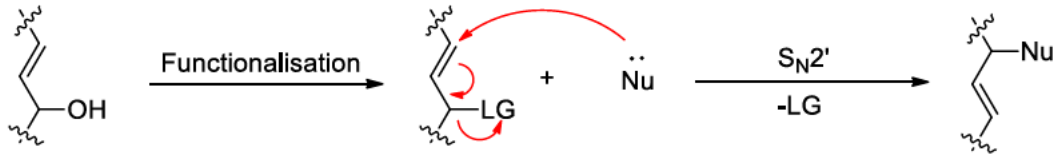

***Scheme 6.21.** Mechanism for an S_N2' reaction.*

The esterification of the C6 hydroxyl group has been reported in literature using a variety of esters including acetates, benzoates and *p*-coumarates.[48a, 117d, 144] The esterification of the C6 hydroxyl group can potentially provide a valuable means of stabilising the product after dihydroxylation of the endocyclic alkene. Clericuzio *et al.* reported the benzoylation of 6-hydroxycaryophyllene **1** to afford 6-hydroxycaryophyllenyl benzoate **109**, and that procedure was followed.[48a] Benzoyl chloride was added to a solution of 6-hydroxycaryophyllene **1** in dry CH_2Cl_2, followed by Et_3N and catalytic DMAP at 0°C. The reaction mixture was allowed to warm to room temperature and then was heated at reflux for 60 hours with the additional CH_2Cl_2 added to maintain a sufficiently high solvent volume. The reaction was worked up and unreacted benzoyl chloride was esterified with MeOH to afford methyl benzoate, and the mixture of esters was purified by column chromatography to afford a compound as a colourless oil.

The FTIR spectrum of the compound showed no OH absorbance, and a prominent carbonyl absorbance at 1716 cm^{-1}, indicating that the hydroxyl group had likely been esterified. The ^1H NMR spectrum showed a three sets of peaks between 7 and 8.5 ppm that integrated for 5H, which was consistent with a monosubstituted phenyl ring. The triplet of doublets that corresponded to H6 had shifted downfield from 4.56 ppm to 5.77 ppm, indicating that the hydrogen was adjacent to a highly deshielding functional group such as an ester. The ^{13}C NMR spectrum contained 20 carbon signals. The signal at 166.1 was characteristic of an

ester carbonyl, and four additional signals between 110 and 150 ppm supported the presence of a monosubstituted aromatic ring. Therefore, based on the FTIR, ^{1}H and ^{13}C NMR spectra, the compound was assigned as 6-hydroxycaryophyllenyl benzoate **109** (Scheme 6.22). The spectral data was consistent with the values reported by Clericuzio *et al.*[48a]

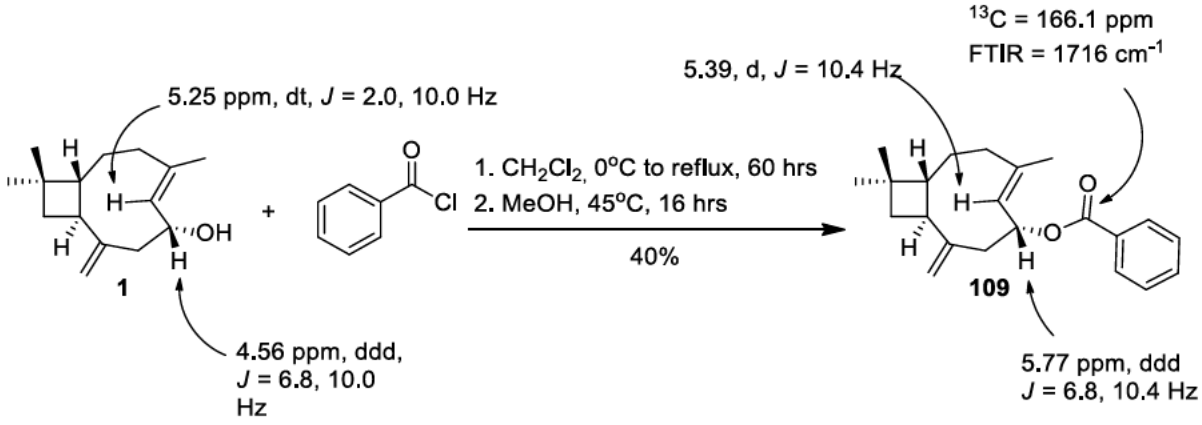

Scheme 6.22. *Benzoylation of 6-hydroxycaryophyllene **1**.*

Reaction of 6-hydroxycaryophyllenyl benzoate **109** with activated MnO_2 in dry CH_2Cl_2 resulted in the slow formation of an unknown product (Scheme 6.23). However, heating the reaction mixture under reflux did not push the reaction to completion. As a result, the reaction was no longer pursued. The limited reactivity can be attributed to the steric bulk of the benzoate ester limiting access of the MnO_2 to the endocyclic alkene.

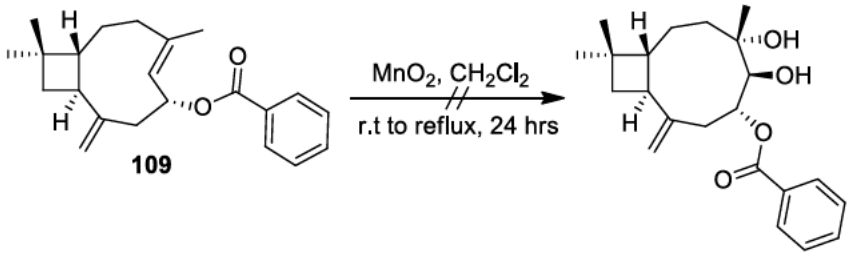

Scheme 6.23. *Dihydroxylation of 6-hydroxycaryophyllenyl benzoate **109** using activated MnO_2.*

The reactivity of the endocyclic alkene can be modified through conversion of the allylic C6 hydroxyl group into a better leaving group. The conversion into a better leaving group would enable S_N2' reactions to occur, which may lead to interesting skeletal rearrangements. Elimination can also allow for the generation of new alkenes or conjugated systems, which can facilitate other possible skeletal rearrangements. Several methods exist for the activation of hydroxyl groups including conversion into halides, such as chlorides and bromides, and functionalisation into tosylates, mesolates or triflates.

A common method for the chlorination of hydroxyl groups is through the use of PCl_5. The proposed mechanism for the chlorination is that PCl_5 reacts with the hydroxyl group and loses a chloride to form the phosphite intermediate (Scheme 6.24). The chloride then acts as a nucleophile and adds to the carbon of the phosphite via an S_N2 reaction to displace the phosphite and introduce the new chlorine. The PCl_3OH compound then eliminates HCl to form $POCl_3$.

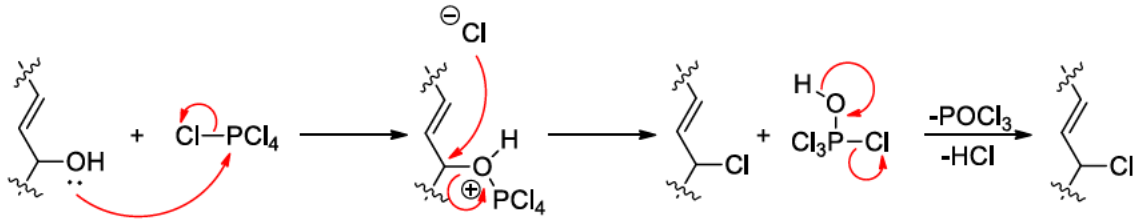

Scheme 6.24. *Proposed mechanism for the chlorination of hydroxyl groups using PCl_5.*

A solution of 6-hydroxycaryophyllene in dry $CHCl_3$ was added to a slurry of PCl_5 and anhydrous Na_2CO_3 in dry $CHCl_3$ at 0ºC and the reaction mixture was allowed to warm to room temperature (Scheme 6.25). After 18 hours, the reaction mixture was worked up to give the compound **179** as a yellow tinged oil.

The FTIR spectrum showed that the compound did not contain an OH absorbance. The ^1H NMR spectrum was similar to that of 6-hydroxycaryophyllene **1**, except the peaks had were slightly shifted. The vinylic doublet at 4.56 ppm in 6-hydroxycaryophyllene **1** had shifted downfield to 4.71 ppm. Similarly, the doublet of doublet of doublets at 5.25 ppm had also shifted downfield to 5.34 ppm. The ^{13}C NMR spectrum contained 15 signals, but no signals were present between 60 and 80 ppm, indicating that no hydroxyl groups were present in the compound. Therefore based on the FTIR, ^1H, ^{13}C and 2D NMR spectra, the compound was assigned as 6-chlorocaryophyllene **179** in 77% yield. The structure was confirmed by HRMS, with the $[M+H]^+$ molecular having an exact mass of 239.1555 *m/z*, corresponding to a molecular formula of $C_{15}H_{23}Cl$.

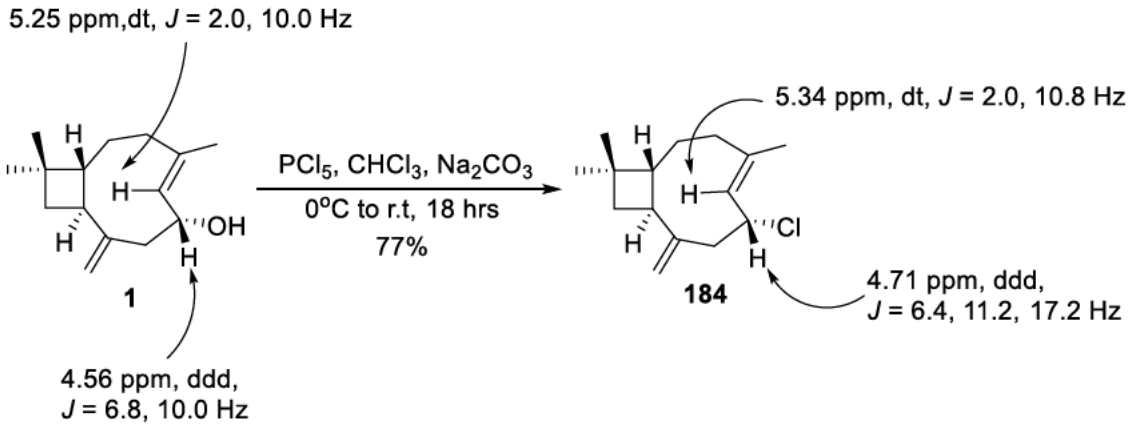

Scheme 6.25. *Chlorination of 6-hydroxycaryophyllene **1** using PCl_5.*

The successful synthesis of 6-chlorocaryophyllene **184** was promising, but synthesis of the compound was unreliable. The lack of consistency was likely due to side reaction occurring or the addition of the chloride to the C4 position via an S_N2' mechanism, resulting in the formation of other by-products.

Silver salts, such as AgOTf and $AgBF_4$, can be used to facilitate structural rearrangements in compounds containing a halide. The Ag^+ cation reacts with halides in molecules to generate the silver halide salt, which typically precipitates out of organic solvents. As a result, a cation is generated due to the loss of the halide, which can then facilitate structural rearrangements or be used as a site for the addition of a new nucleophile. For example, Kanda *et al.* used AgOTf to generate a carbocation from a bromide that was substituted with triethylsilanol (Scheme 6.26).[145]

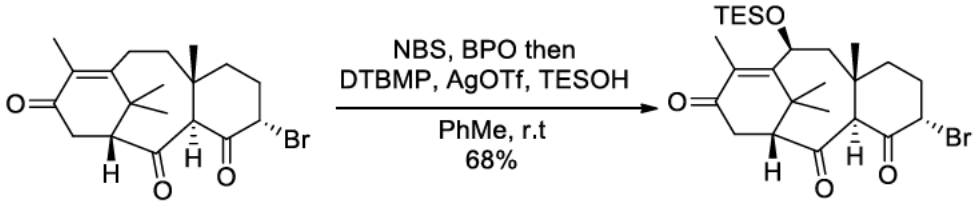

Scheme 6.26. *Substitution of C10 bromide using AgOTf and TESOH by Kanda et al.[145]*

$AgBF_4$ was added to a solution of 6-chlorocaryophyllene **184** in dry THF and stirred at 0ºC. After 2 hours the reaction mixture was quenched with deionised water. The crude oil was purified by column chromatography giving two compounds as colourless oils.

The ^1H NMR spectrum of the first compound showed that the methyl signal that had previously been at 1.63 ppm in the 6-chlorocaryophyllene **184** had shifted upfield to 1.28 ppm, indicating that it was no longer allylic. Four signals were present between 4 and

6 ppm, indicating that there were four vinylic hydrogens in the compound. The two singlets at 4.84 and 4.87 ppm each integrated for 1H and were likely part of the exocylic alkene. The doublet of doublets at 5.39 ppm integrated for 1H and had a coupling constants of 2 and 16.4 Hz. The doublet of doublet of doublets at 5.85 ppm integrated for 1H and had coupling constants of 4.8, 8.4 and 16.4 Hz. The common coupling constant of 16.4 Hz indicated that the two hydrogens were coupling to each other and were likely part of a *trans* alkene. The smaller coupling constants suggested coupling to aliphatic hydrogens such as those in a methylene. Therefore, based on the ^{1}H NMR spectrum, the structure of the compound was tentatively assigned as 4-hydroxycaryophyll-5,8-diene **185** in 19% yield (Scheme 6.27). 4-Hydroxycaryophyll-*trans*-5,8-diene **185** was previously reported by Gollnick *et al*. in 1968, but ^{1}H NMR data was collected using CCl_4.[146]

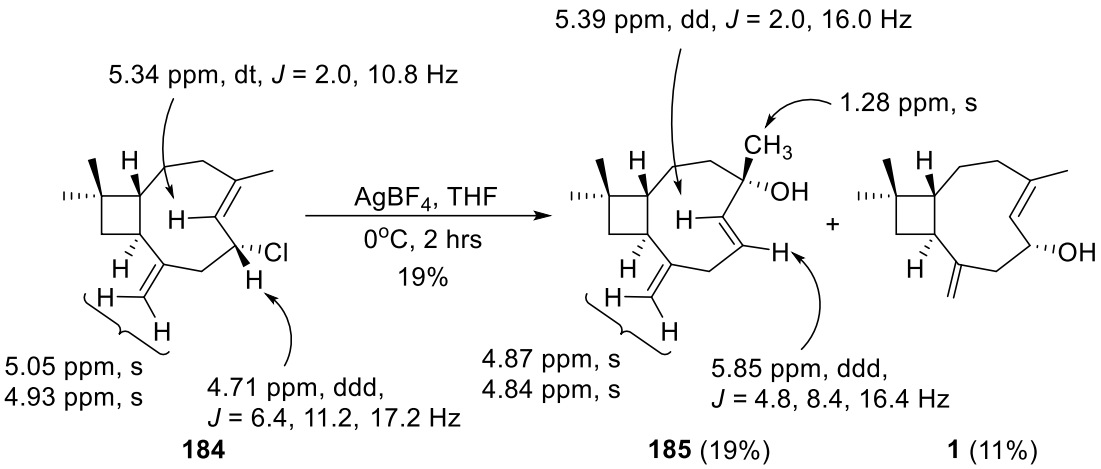

Scheme 6.27. *Cationic rearrangement of 6-chlorocaryophyllene **184** using $AgBF_4$.*

The ^{1}H NMR spectrum of the second compound was consistent with that of 6-hydroxcaryophyllene **1**, which was given in 11% yield. The formation of both diene **185** and 6-hydroxycaryophyllene **1** indicated that the carbocation formed by 6-chlorocaryophyllene **184** after reaction with $AgBF_4$ was resonance stabilised and primarily distributed between the C4 and C6 positions (Scheme 6.28). The formation of a single diastereomer of both the diene **185** and 6-hydroxycaryophyllene **1** was interesting, because it showed that only a single face of the molecule was accessible, even if the resonance stabilised cation was planar, resulting in inherent stereoselectivity. The accessibility of a single face to nucleophilic addition allowed the stereochemistry of caryophyllene **185** to be inferred.

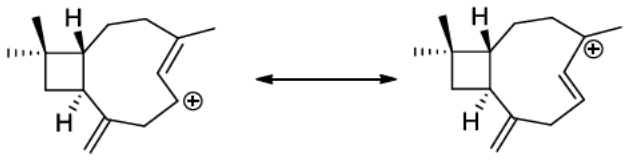

Scheme 6.28. *Resonance forms of the allylic cation of 6-chlorocaryphyllene* ***184****.*

The structural rearrangements exhibited by 6-chlorocaryophyllene **184** upon reaction provided new insights into the chemistry of caryophyllenes, so the chlorination of 12-acetoxy-6-hydroxycaryophyllene **2** was similarly explored. Azides can be introduced into compounds through a variety of methods, including nucleophilic substitutions. Azides provide a convenient means of incorporating amines into molecules, through the reduction of the amine via hydrogenation or a Staudinger reaction using PPh_3. A possible pathway to introduce amines into caryophyllene acetate **2** is shown below in Scheme 6.29.

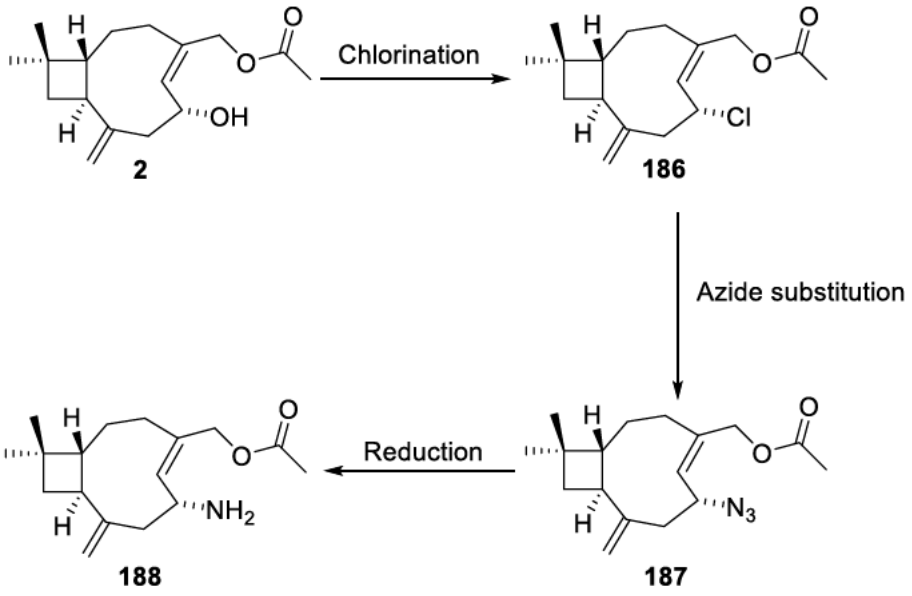

Scheme 6.29. *Proposed synthesis of 12-acetoxy-6-aminocaryophyllene* ***188****.*

A solution of caryophyllene acetate **2** in dry CH_2Cl_2 was added to a slurry of PCl_5 and anhydrous Na_2CO_3 in dry CH_2Cl_2 at 0ºC. After 90 mins, the reaction was worked up to afford the product as a yellow oil (Scheme 6.30). The crude product was insufficiently pure to confirm the presence of the product, so it was used for the subsequent azide substitution with the intention that the azide product can be purified afterwards.

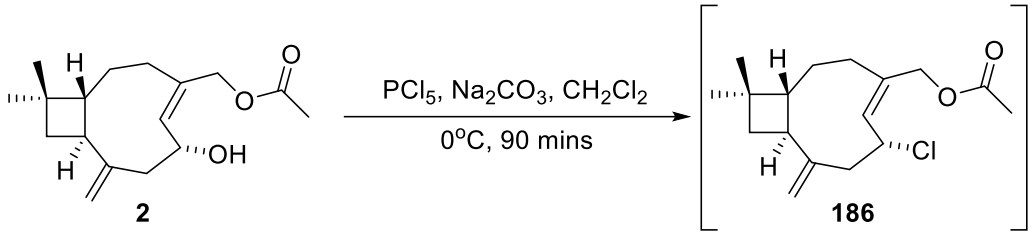

Scheme 6.30. *Chlorination of 12-acetoxy-6-hydroxycaryophyllene **2** using PCl_5.*

NaN_3 was added to a solution of 12-acetoxy-6-chlorocaryophyllene **186** in acetone and the reaction mixture was stirred at room temperature. After four days, the reaction was worked up and the crude product was purified by column chromatography to afford a compound as a colourless oil. The FTIR spectrum of the compound showed a broad OH absorbance at 3393 cm^{-1}, and a prominent carbonyl absorbance at 1738 cm^{-1}. The characteristic azide absorbance at 2100 cm^{-1} was absent, indicating that the azide substitution had not proceeded. The ^1H NMR spectrum looked similar to that of caryophyllene acetate **2** except the peaks had shifted. The exocyclic alkene peaks at 4.86 and 4.97 ppm had shifted downfield to 4.94 and 5.08 ppm. The two doublets exhibiting corresponding the C12 methylene had shifted closer together from 4.17 and 4.69 ppm to 4.36 and 4.56 ppm. The ^{13}C NMR spectrum contained 17 signals, and the C6 signal had shifted from 69.8 ppm to 56.4 ppm. Therefore based on the FTIR, ^1H, ^{13}C and 2D NMR spectra the compound was assigned as 12-acetoxy-6-hydroxy-*Z*-caryophyllene **189** in 70% yield (Scheme 6.31). The isolation of 12-acetoxy-6-hydroxy-*Z*-caryophyllene **189** indicated that the product had likely formed during the chlorination of the 12-acetoxy-6-hydroxy-*E*-caryophyllene **2**.

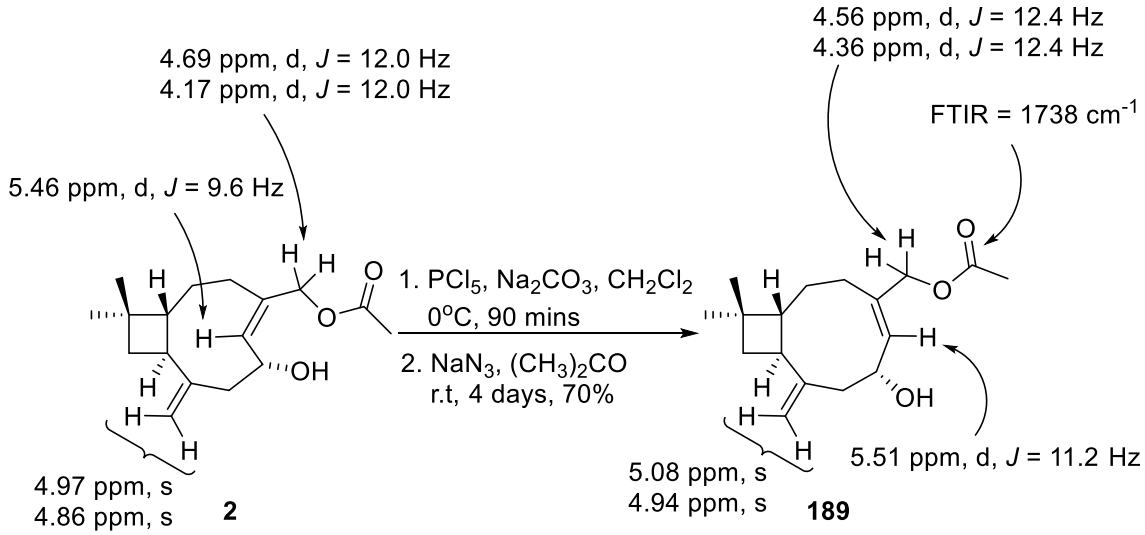

Scheme 6.31. *Synthesis of 12-acetoxy-6-hydroxy-Z-caryophyllene **189**.*

Chlorination of the C6 hydroxyl group had generated interesting structural rearrangements, but the chlorides **184** and **186** was too inconsistent to be reliable. An alternative to halogenation of hydroxyl groups, is conversion of the hydroxyl group into a good leaving using sulfonyl chloride derivatives such as tosyl chloride, mesyl chloride and triflic anhydride. Tosylation of a hydroxyl group generates a tosylated product that can be isolated, while mesolates and triflates cannot. As a result, the tosylation of caryophyllene acetate **2** was pursued with a similar intention of incorporating an amine into the compound.

Catalytic DMAP and Et_3N were added to a stirred solution of the caryophyllene acetate **2** and tosyl chloride in dry CH_2Cl_2. The reaction mixture was stirred at room temperature. After three days, the reaction was worked up and crude product was purified to afford the compound **190** as a colourless oil. The FTIR spectrum for compound **190** showed a narrow OH absorbance at 3476 cm^{-1} and a strong carbonyl absorbance at 1739 cm^{-1}. The ^{13}C NMR spectrum contained 17 signals which was the same as the starting material, so the caryophyllene acetate **2** had likely rearranged. Four signals were present between 100 and 160 ppm, indicating that two alkenes were present in the compound, both of which were disubstituted according to the DEPT135 and HMBC spectra. Two signals were visible between 70 and 80 ppm, indicating that two oxygenated carbons were present in compound, one of which was quaternary and therefore a 3º alcohol was present in the compound. The ^1H NMR spectrum closely resembled that of 4-hydroxycaryophyll-5,8-diene **185**. However, an additional pair of doublets were present at 3.98 and 4.08 ppm that each integrated for 1H, which corresponded to the C14 methylene group. A singlet at 2.08 ppm that integrated for 3H indicated that the acetate was still present in molecule. Therefore, based on the FTIR, ^1H, ^{13}C and 2D NMR spectra the compound was assigned as 12-acetoxy-4-hydroxycaryphyll-*trans*-5,8-diene **190** in 9% yield (Scheme 6.32).

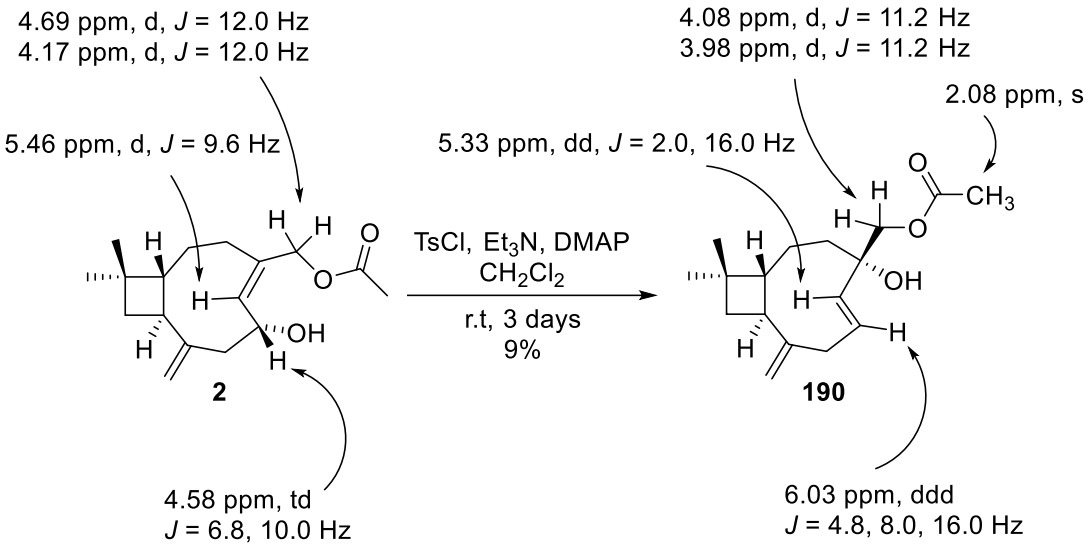

Scheme 6.32. *Tosylation of 12-acetoxy-6-hydroxycaryophyllene* ***2****.*

The isolation of the rearranged product indicated that the tosylation was likely successful. The tosylated product likely rearranged via a S_N2' with water to form 12-acetoxy-4-hydroxycaryphyll-*trans*-5,8-diene **190**.

6.3 Oxidation of 6-hydroxycaryophyllenes

Oxidation of 6-hydropxycaryophyllenes has been established to generate unique compounds due to the interesting reactivity of the strained endocyclic alkene. The prime examples being the dihydroxylation of the endocyclic double bond and subsequent rearrangement of caryophyllene triols into birkenal **142** and its analogues. The oxidative chemistry of 6-hydroycaryophyllenes is still largely unexplored, especially the oxidation of the C6 hydroxyl group to generate enone compounds that could act as Michael acceptors or dienes for hetero Diels-Alder reactions.

The MnO_2 oxidation of 6,12-dihydroxycaryophyllene **3** has not yet been investigated and based on previous experimental evidence from other 6-hydroxycaryophyllenes, has the potential to generate truly unique compounds. Activated MnO_2 was added to a solution of the diol caryophyllene **3** in dry CH_2Cl_2 and the reaction mixture was stirred at room temperature. After 50 mins, the reaction was worked up and the crude product was purified by column chromatography to afford compound **191** as a yellow tinged oil (Scheme 6.33). The FTIR spectrum showed a broad OH absorbance at 3415 cm^{-1} and a prominent carbonyl absorbance at 1722 cm^{-1}. The ^{13}C NMR spectrum contained 15 signals, including a carbonyl signal at 197.7 ppm, which was characteristic of an aldehyde. Only two vinylic carbon signals were visible between 110 and 150 ppm, indicating that an alkene had been lost. Two additional signals were visible between 60 and 80 ppm, indicating that two new oxygenated carbons were present in the compound. The ^1H NMR spectrum showed two vinylic singlets at 4.96 and 5.01 ppm that each integrated for 1H, indicating that the exocyclic alkene was still present. However, the doublet at 5.37 ppm for the diol caryophyllene **3** was absent and a new doublet was present at 3.33 ppm, indicating that the endocyclic alkene was absent. The doublet of doublet of doublets had shifted upfield from 4.59 ppm to 3.86 ppm, suggesting that the hydrogen was no longer allylic. The singlet at 9.18 ppm that integrated for 1H confirmed the presence of an aldehyde in an isolated spin system. The HMBC spectrum showed that the aldehyde correlated with the carbon of a 3º alcohol. Therefore based on the FTIR, ^1H, ^{13}C and 2D NMR spectra the compound was assigned as aldehyde triol caryophyllene **191** in 12% yield.

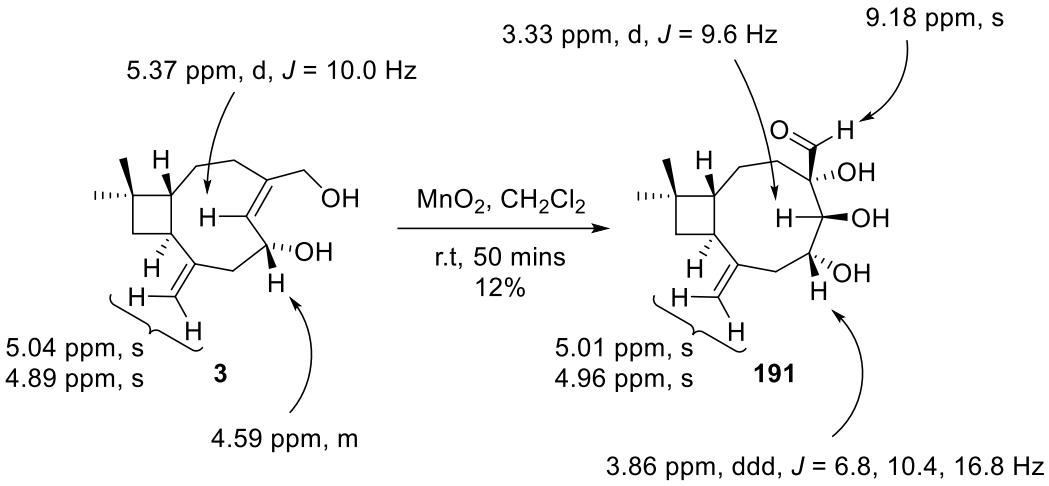

Scheme 6.33. *Oxidation of 6,12-dihydroxycaryophyllene **3** using activated MnO_2.*

The formation of the aldehyde triol caryophyllene **191** was unexpected, but provided new insights into the reactivity of the endocyclic alkene. The allylic oxidation of the C12 hydroxyl group of diol caryophyllene **3** likely occurred first, forming an α,β-unsaturated aldehyde followed by dihydroxylation (Scheme 6.34). Further rearrangements did not proceed likely due to the deactivation of the system by the aldehyde.

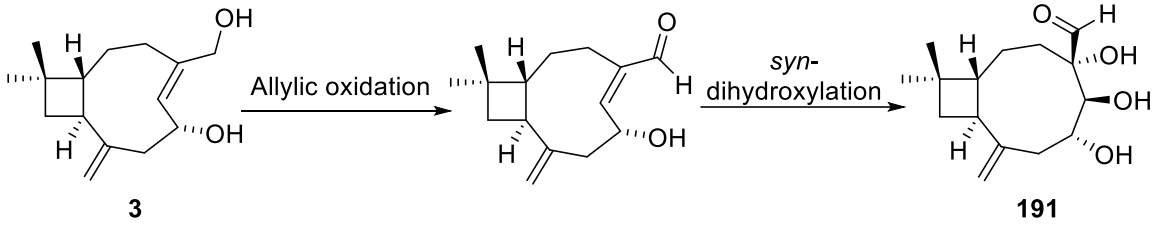

Scheme 6.34. *Proposed formation of aldehyde triol caryophyllene **191** from diol caryophyllene **3**.*

Similar deactivating effects are apparent when comparing the reaction of the 6-hydroxycaryophyllene **1** and caryophyllene acetate **2** with activated MnO_2. The acetate ester of caryophyllene acetate **2** is electron withdrawing and deactivates the endocyclic alkene, resulting in exclusive formation of the acetate triol caryophyllene **148**. However, the methyl group of 6-hydroxycaryophyllene is weakly electron rich and consequently, the methyl triol caryophyllene **146** is quickly formed and consumed to afford birkenal **142** (Scheme 6.35).

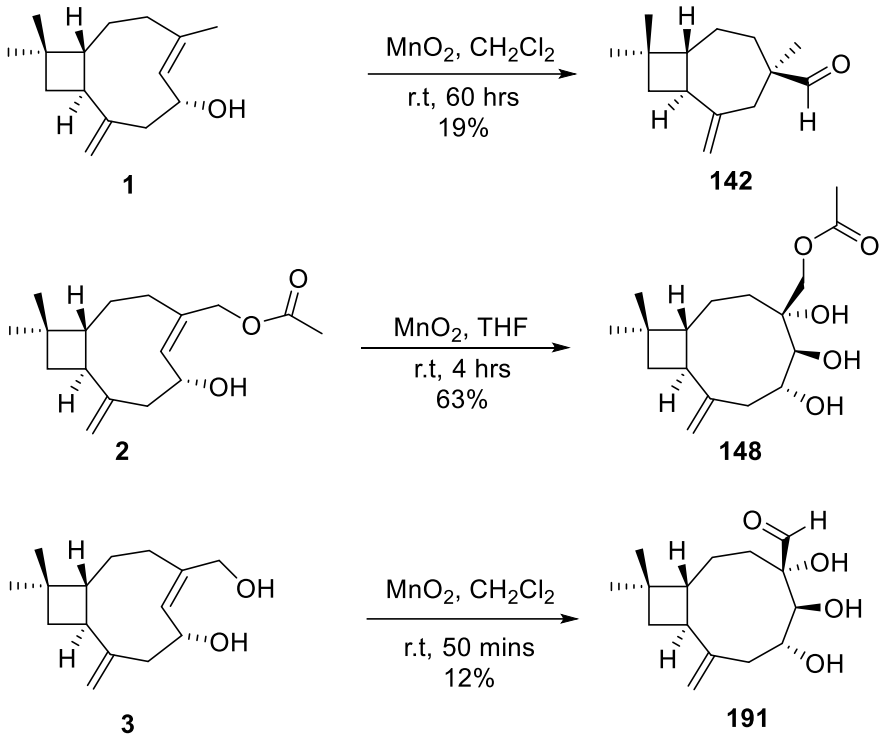

Scheme 6.35. *Reactions of 6-hydroxycaryophyllenes with activated MnO_2 at room temperature.*

The formation of the aldehyde triol caryophyllene **191** at room temperature suggested that harsher reaction conditions are required for further reactions to occur. Activated MnO_2 was added to a solution of aldehyde triol caryophyllene **191** in dry CH_2Cl_2 and the reaction mixture was heated at reflux. After 82 hours, the reaction was worked up and the crude product was purified by column chromatography to give compound **192** as a white solid (Scheme 6.36).

The FTIR spectrum of the compound **192** did not contain OH absorbances and showed a prominent carbonyl peak at 1750 cm^{-1}. The ^{13}C NMR spectrum contained 15 signals. A carbonyl peak was visible at 174.0 ppm along with four vinylic carbon peaks between 110 and 150 ppm, indicating the presence of two alkenes. A peak at 78.4 ppm indicated the presence of secondary oxygenated carbon. The ^{1}H NMR spectrum showed two peaks that each integrated for 1H at 4.96 and 5.14 ppm that corresponded to the exocyclic alkene. A doublet at 5.13 ppm that integrated for 1H corresponded to the secondary oxygenated carbon. The vinylic singlet at 6.86 ppm integrated for 1H and correlated to a quaternary vinylic carbon and the oxygenated carbon carbon at 78.4 ppm, indicating that the alkene was in close proximity to the secondary oxygenated carbon. A methylene signal at 2.19 ppm correlated with the carbonyl group and same alkene that was in close proximity to the secondary oxygenated carbon. The multiplet at 2.79-2.52 ppm correlated to a methylene

and the HMBC spectrum showed that the methylene was adjacent to the exocyclic alkene and the other alkene, and therefore likely correlated to the C7 methylene. Therefore, based on the FTIR, ^{1}H, ^{13}C and 2D NMR spectra the compound was assigned as butenolide **192** in 10% yield. The butenolide **192** has not been previously reported, however Ghalib *et al.* reported a similar compound, aspfalcolide **193**, except with a hydroxyl group on C6 and it has been reported to possess anti-angiogenic activity (Figure 6.6).[147]

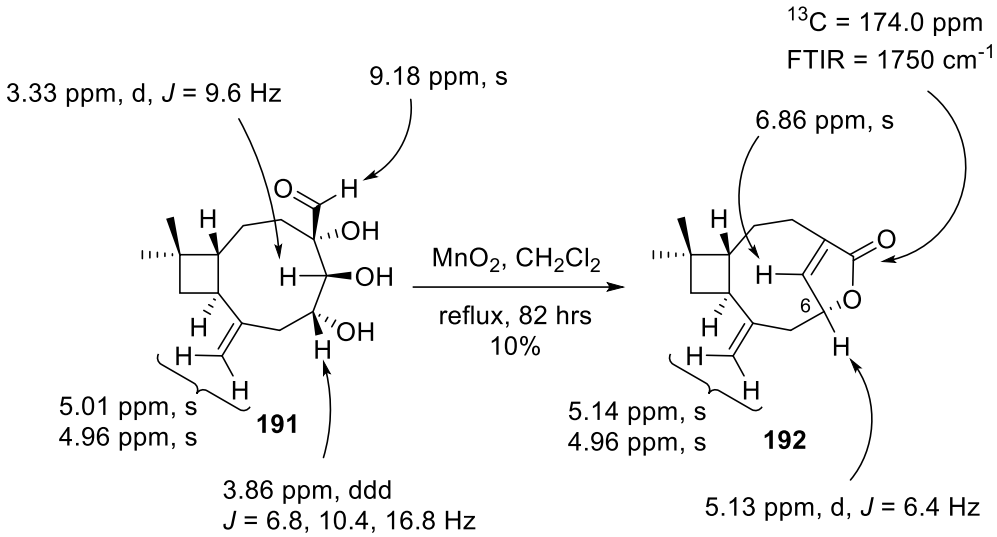

Scheme 6.36. *Oxidation of aldehyde triol caryophyllene* ***192*** *using activated* MnO_2.

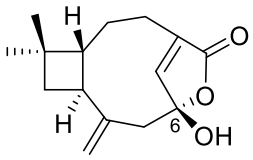

193

Figure 6.6. *Structure of aspfalcolide* ***193****.*

Butenolide **192** is likely formed through a series of acid catalysed rearrangements (Scheme 6.37). First a hemiacetal is formed through the addition of the C6 hydroxyl group to the C12 aldehyde. Acid catalysed elimination of water results in the formation of an enol across C4-C12. The enol then tautomerises to the ketone. The C5 hydroxyl group is then eliminated as water to form the butenolide **192**.

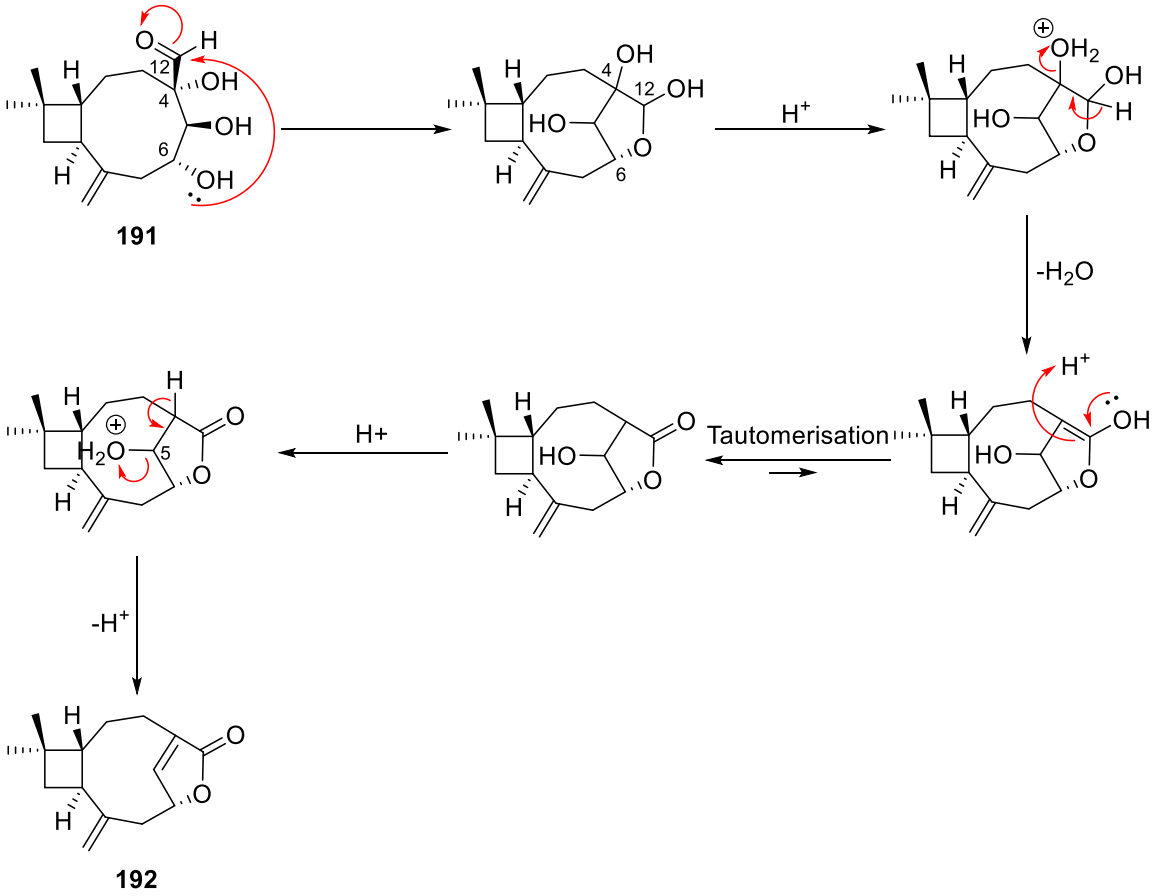

Scheme 6.37. *Proposed mechanism for formation of butenolide* ***192*** *from aldehyde triol caryophyllene* ***191****.*

Butenolide moieties are found in a variety of natural products, including karrikins. Karrikins are most well-known for the ability to trigger seed germination in plants whose reproduction is fire dependent (Figure 6.7).[148] The incorporation of a butenolide moiety into a caryophyllene through a simple oxidation using activated MnO_2 demonstrates the incredible reactions and rearrangements that 6-hydroxycaryophyllenes can undergo.

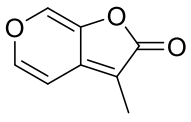

194

Figure 6.7. *Structure of 3-methyl-2*H*-furo[2,3-c]pyran-2-one* ***194****.*

The use of activated MnO_2 with 6-hydroxycaryophyllenes has demonstrated that it is not an effective method of oxidation of the C6 allylic hydroxyl group. Consequently, an alternate oxidation strategy was pursued. Use of the Swern oxidation was first explored using 6-hydroxycaryophyllene **1**. The active species was generated through the addition of

dry DMSO to a solution of $(COCl)_2$ in dry CH_2Cl_2 at -84ºC. After 20 mins, a solution of 6-hydroxycaryophyllene **1** in dry CH_2Cl_2 was added to the reaction mixture and stirred. After 3 hours, the reaction was quenched with Et_3N and worked up to afford the crude product, which was purified by column chromatography to give the compound **195** as a yellow tinged oil. The FTIR spectrum for compound **195** showed no OH absorbance and a prominent carbonyl stretch at 1716 cm^{-1}. The ^{13}C NMR spectrum showed 15 signals, but many of the signals were poorly resolved due to conformational changes within the NMR timescale. A carbonyl signal at 202.8 ppm was present, which supported the observed absorbance in the FTIR spectrum. The ^{1}H NMR spectrum showed that the doublet 5.25 ppm corresponding to the C5 vinylic hydrogen of 6-hydroxycaryophyllene **1** was absent. Instead, a singlet at 6.17 ppm that integrated for 1H was present, indicating that the vinylic hydrogen was now in an isolated spin system. The doublet of doublet of doublets at 4.56 ppm was also absent, indicated that the allylic C6 hydrogen was absent. A pair of doublets at 2.85 and 3.09 ppm that each integrated for 1H both had a coupling constant of 16.8 Hz, indicating they were coupling to each other. The two hydrogens corresponded to the C7 methylene hydrogens. Therefore, based on the FTIR, ^{1}H, ^{13}C and 2D NMR spectra the compound was assigned as *E*-caryophyllene enone **195** in 37% yield (Scheme 6.38).

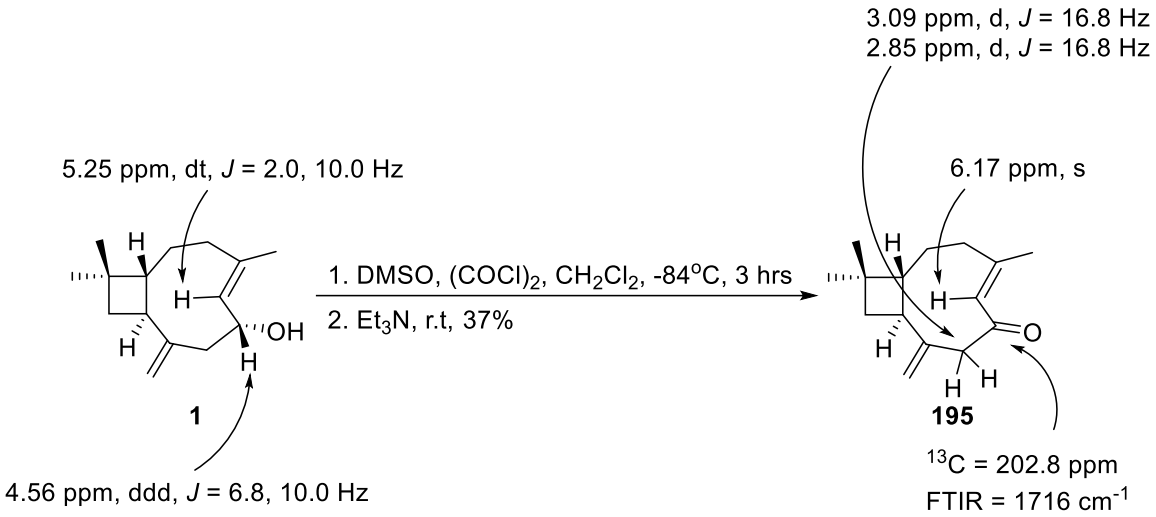

Scheme 6.38. *Swern oxidation of 6-hydroxycaryophyllene **1**.*

The successful synthesis of caryophyllene enone **195** using a Swern oxidation was promising, so the reaction was replicated using the caryophyllene acetate **2**. The FTIR spectrum of the compound obtained showed no OH absorbance and a prominent carbonyl absorbance was visible at 1742 cm^{-1}. The ^{13}C NMR spectrum showed 17 signals, but several of the signals were poorly resolved similar to that of caryophyllene enone **195**. The

^{1}H NMR spectrum closely resembled that of caryophyllene enone **195**. The vinylic doublet of caryophyllene acetate **2** at 5.46 ppm was absent and instead a vinylic singlet that integrated for 1H at 6.20 ppm was visible. The presence of the singlet indicated that the vinylic C5 hydrogen was now in an isolated spin system, characteristic of the formation of the enone. The triplet of doublets at 4.58 ppm corresponding to the C6 allylic hydrogen was absent, further supporting that the allylic alcohol had been oxidised. Similar to caryophyllene enone **195**, two doublets at 2.92 and 3.14 ppm were present, corresponding to the C7 methylene. The two doublets corresponding to the C12 methylene were visible at 4.54 and 4.78-4.61 ppm. However, the doublet at 4.78-4.61 ppm was poorly resolved, indicating that conformational changes were occurring on a NMR timescale, which was consistent with what was observed with caryophyllene enone **195**. Therefore, based on the FTIR, ^{1}H, ^{13}C and 2D NMR spectra, the compound was assigned as caryophyllene acetate enone **196** in 25% yield.

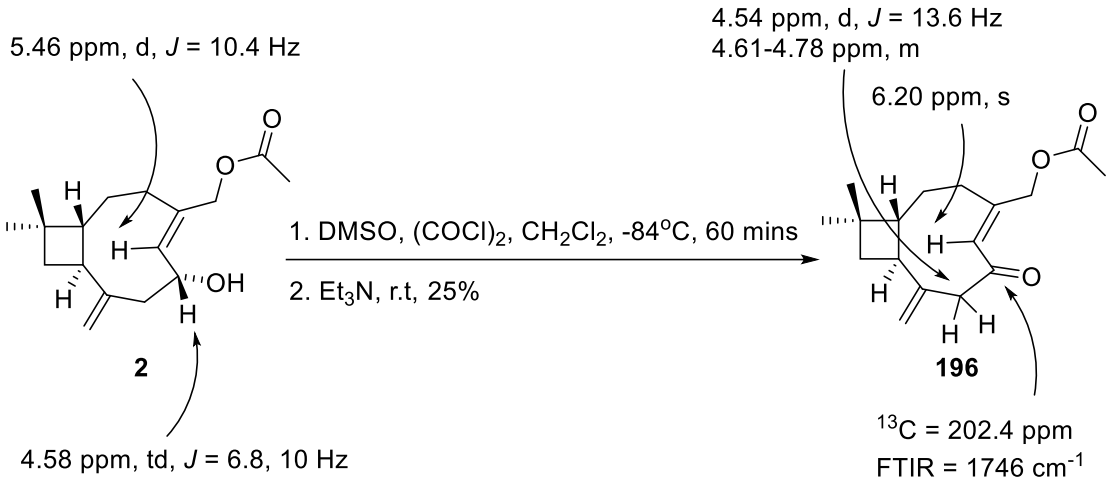

Scheme 6.39. *Swern oxidation of 12-acetoxy-6-hydroxycaryophyllene **2**.*

The Swern oxidation of 6-hydroxycaryophyllene **1** and 12-acetoxy-6-hydroxycaryophyllene **2** had both proceeded as expected to generate enones **195** and **196**. Oxidation of diol caryophyllene **3** gave a different result. When the diol **3** was reacted under Swern conditions a crystalline product **197** was obtained (Scheme 6.40). The FTIR spectrum of compound **197** showed a broad OH absorbance at 3401 cm^{-1} and a prominent carbonyl absorbance at 1677 cm^{-1}. The low wavenumber of the carbonyl stretch suggested that it was part of an α,β-unsaturated system. The ^{13}C NMR spectrum contained 15 signals. A ketone signal was present at 201.8 ppm and another signal was present at 189.3 ppm, which appeared to be a vinylic quaternary carbon. Three other vinylic carbon signals were

present between 110 and 150 ppm, indicating that two alkenes were present in the compound. Two signal were present between 70 and 80 ppm, indicating that two oxygenated carbons were present, where at least one of them was a hydroxyl group. The ^{1}H NMR spectrum contained a doublet of doublets at 5.97 ppm that integrated for 1H. The HSQC and HMBC spectra indicated that the signal was a vinylic hydrogen that was adjacent to a quaternary vinylic carbon and the carbonyl. Therefore, it was likely part of a trisubstituted alkene that was conjugated with the ketone to form an enone. A doublet of doublets was present at 4.82 ppm that integrated for 1H. The HSQC and HMBC spectra indicated that the hydrogen was on the same carbon as an oxygen containing functional group and was in close proximity to the alkene of the enone, but not the carbonyl. The high chemical shift suggested that the hydrogen was heavily deshielded, and may be part of a functional group, such as an acetal or hemiacetal. The presence of two triplets that each integrated for 1H at 5.01 and 5.13 ppm that were on the same carbon, indicated that the exocylic alkene was still present in the molecule. The ^{1}H NMR spectrum showed a doublet at 3.73 ppm that integrated for 1H and was on the same carbon as an oxygen containing functional group. The HMBC spectrum showed that the hydrogen correlated with both alkenes, the ketone and the other oxygenated carbon, suggesting that it was between the enone and the exocyclic alkene. Therefore, based on the FTIR, ^{1}H, ^{13}C and 2D NMR spectra, the compound was tentatively assigned as hemiacetal enone **197**. The HRMS gave an exact mass for the $[M+H]^{+}$ molecular ion of 249.1482 *m/z* corresponding to a formula of $C_{15}H_{20}O_3$, thus confirming the assigned structure.

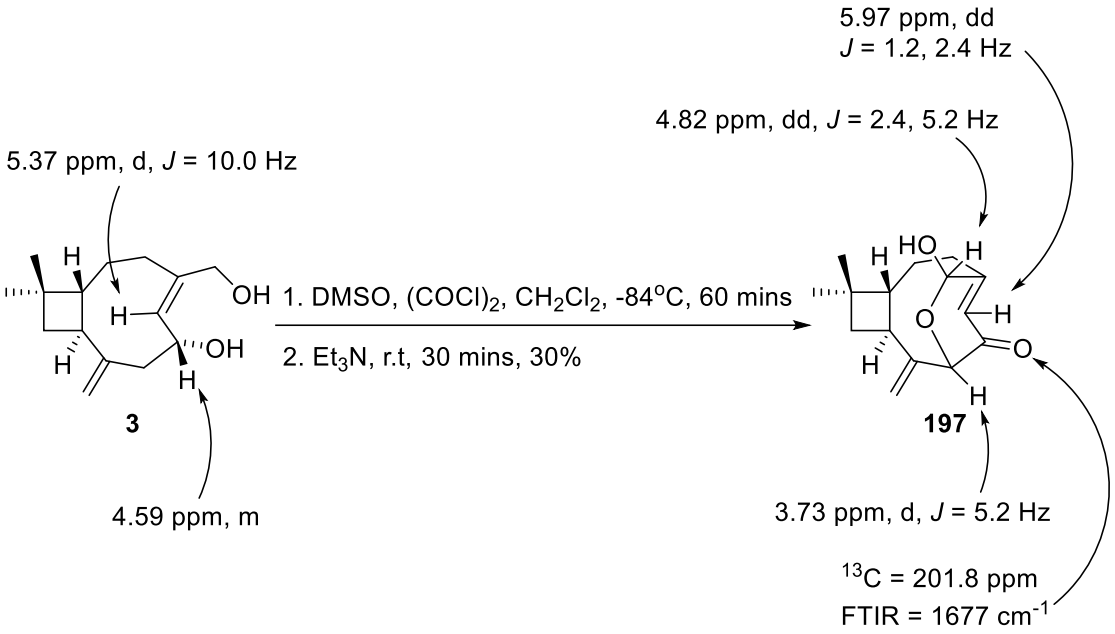

Scheme 6.40. *Swern oxidation 6,12-dihydroxycaryophyllene **3**.*

The formation of hemiacetal enone **197** was unexpected, but exciting, due to the creation of a complex tricylic molecule in one step. A proposed mechanism is shown below in Scheme 6.41. The C6 and C12 hydroxyl groups are first oxidised following the standard Swern oxidation mechanism. The enone then tautomerises to generate an enol. The enol is part of an extended 8 πe^- system, which is perfectly set up to act as a Michael acceptor. The reaction was conducted in excess DMSO, which can act as nucleophile and add to C7 via a Michael addition. The enolate formed with the C12 aldehyde deprotonates C7 to facilitate an elimination reaction, generating a ketone and losing dimethyl sulfide (DMS). The dienol system then tauomerises back to the conjugated aldehyde and enone system. The newly formed C7 hydroxyl group acts as a nucleophile and adds to the aldehyde to form hemiacetal enone **197**.

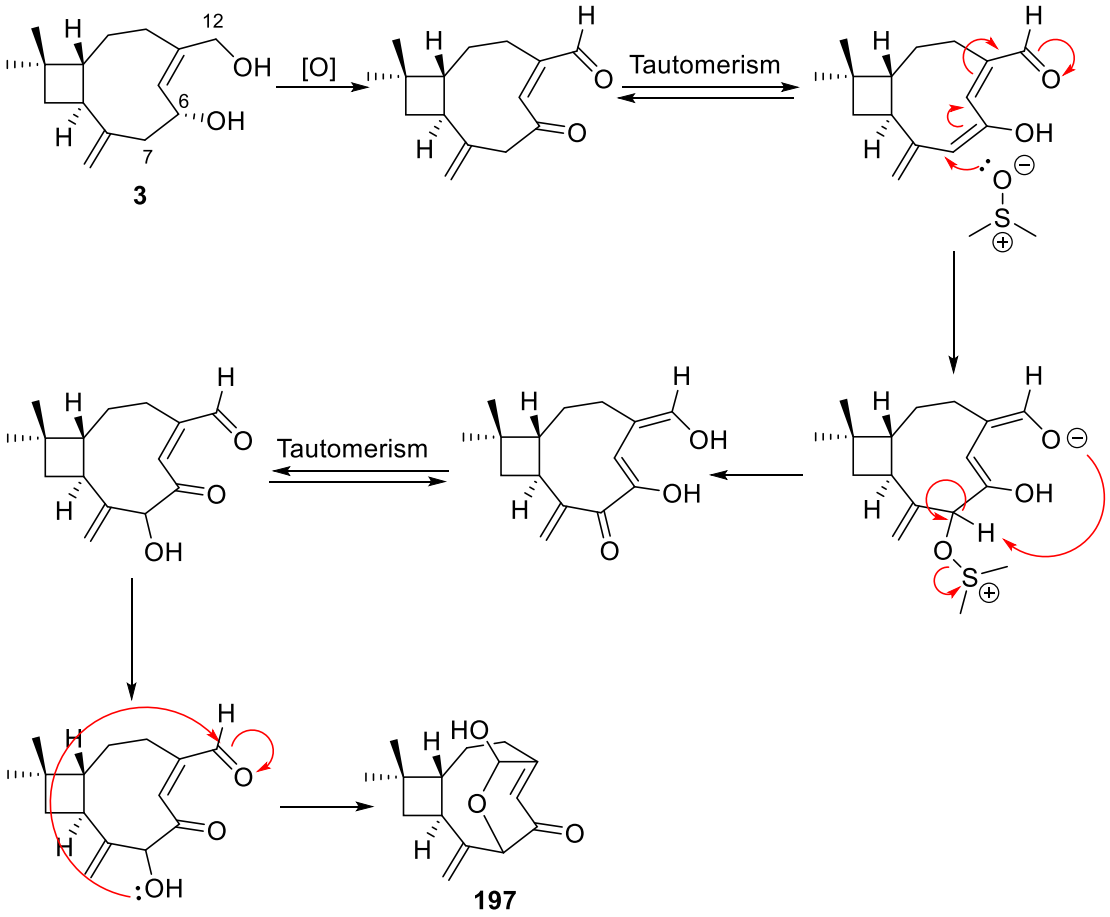

Scheme 6.41. *Proposed mechanism for the formation of hemiacetal enone* ***197****.*

Indoles are commonly used as nucleophiles for 1,4-conjugate additions due to ease of reaction and the ability to increase the structural complexity of a target compound. The C3 position of indoles are good nucleophiles and ideal for use as a nucleophile in 1,4-conjugate additions. 1,4-Conjugate addition reactions using indoles are typically catalysed using a Lewis acid or a protic acid to activate the carbonyl of the α,β-unsaturated carbonyl system. A 1,4-conjugate addition of indole to caryophyllene enone **195** using $BF_3{\cdot}Et_2O$ was explored following a procedure by Swetha *et al.*[149] $BF_3{\cdot}Et_2O$ was added dropwise to a stirred solution of caryophyllene enone **195** and indole in dry CH_2Cl_2. After 90 mins, the reaction was quenched with solid $NaHCO_3$ to give compound **195** as a colourless oil (Scheme 6.42). The ^{13}C NMR spectrum contained 15 signals, indicating that reaction was unsuccessful. A signal at 200.0 ppm suggested the presence of a ketone. Four signals between 110 and 160 ppm indicated that two alkenes were present in the compound. The ^{1}H NMR spectrum for compound **198** resembled that of the starting material, caryophyllene enone **198**. The vinylic singlet at 6.17 ppm appeared to have shifted upfield to 5.90 ppm. The two doublets at 2.85 and 3.09 ppm corresponding to the C7 methylene had shifted

downfield to 3.42 and 3.47 ppm. A doublet and singlet at 4.89 and 5.00 ppm, respectively, each integrated for 1H, and corresponded to the exocyclic alkene based on the HSQC spectrum. HRMS gave an exact mass of 219.1741 *m/z* for the $[M+H]^+$ molecular ion, corresponding to a molecular formula of $C_{15}H_{20}O$. The molecular formula matched that of caryophyllene enone **195**, indicating that the product was a rearranged product. Therefore, based on the HRMS, ^1H, ^{13}C and 2D NMR spectra, compound **198** was assigned as *Z*-caryophyllene enone **198**. *Z*-Caryophyllene enone **198** has been previously reported in a patent by Hiroshi *et al* and the characteriusation data is consistent with the reported values.[150]

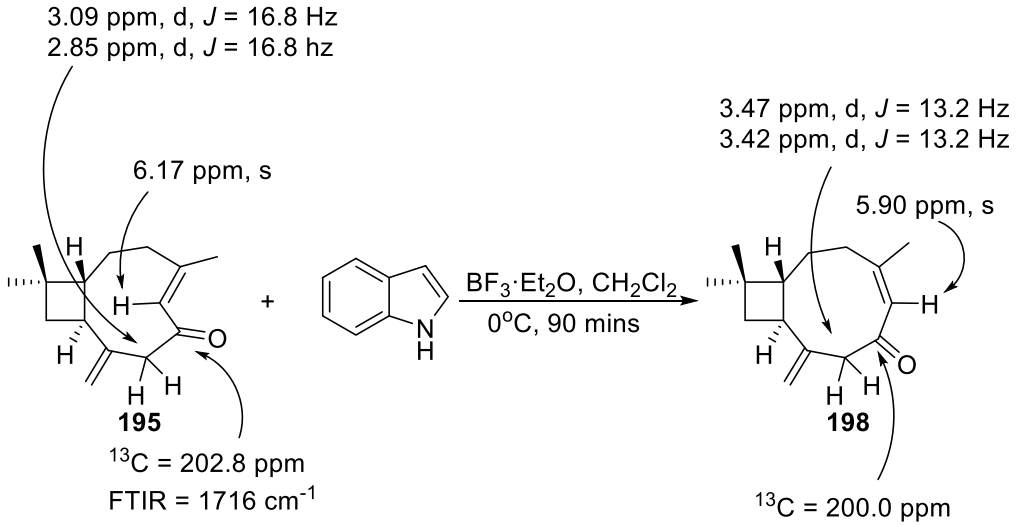

Scheme 6.42. *$BF_3{\cdot}Et_2O$ catalysed 1,4-conjugate addition of indole to E-caryophyllene enone **195**.*

A variety of compounds containing 1,2,4-triazoles have been reported to possess antifungal activity, such as itraconazole **199** (Figure 6.7). The addition of 1*H*-1,2,4-triazole to *E*-caryophyllene enone **195** was therefore attempted using the procedure reported by Hou *et al*.[151] K_3PO_4 was added to a solution of *E*-caryophyllene enone **195** and 1*H*-1,2,4-triazole in dry MeCN and the reaction mixture was heated at reflux. After 24 hours, the reaction gave three compounds as colourless oils (Scheme 6.43).

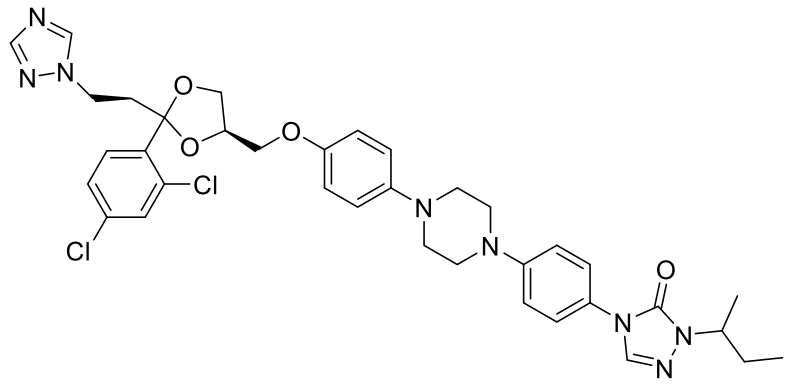

199

Figure 6.7. *Structure of itraconazole* ***199.***

The ^{1}H NMR spectrum of the first compound was consistent with that of *Z*-caryophyllene enone **198** and was afforded in a 7% yield. The ^{1}H NMR spectrum for the second compound **200** showed that the singlets at 5.04 and 5.25 ppm corresponding to the exocyclic alkene were absent, indicating that the exocyclic alkene was absent. A singlet at 5.64 ppm integrated for 1H, indicating that a vinylic hydrogen was highly deshielded, such as in an α,β-unsaturated carbonyl system. Two doublets 3.00 and 3.63 ppm each integrated for 1H and both had a coupling constant of 13.2 Hz, indicating that they were coupling to each other. The two doublets displayed a characteristic AB splitting pattern indicating that they were hydrogens on the same carbon, and were likely part of an isolated methylene. A doublet that integrated for 3H at 1.89 ppm had a coupling constant of 1.2 Hz, indicating that a methyl group in proximity to a strongly deshielding group, such as an enone, was present. A singlet at 1.47 ppm integrated for 3H, indicating that another methyl group was present in the compound. The HRMS gave an exact mass of 219.1743 *m/z* for the $[M+H]^{+}$ molecular ion, which corresponded to the molecular formula of $C_{15}H_{22}O$, which was same molecular formula of caryophyllene enone **195**. Therefore, the compound **200** had likely formed through a base catalysed rearrangement, and was tentatively assigned as dimethyl caryophyllene enone **200** in a 5% yield.

The FTIR spectrum for the third compound **201** showed no OH absorbance and a prominent carbonyl stretch at 1602 cm^{-1}. The significantly lower wavenumber for the carbonyl stretch indicated that the carbonyl was heavily conjugated. The ^{13}C NMR spectrum contained 15 signals. A signal at 193.5 ppm indicated the presence of a ketone in the compound. Four sets of vinylic signals between 120 and 160 ppm suggested that two alkenes were present in the molecule. The ^{1}H NMR spectrum showed two singlets at 6.01 and 6.10 ppm that

each integrated for 1H. The DEPT135 and HSQC spectra indicated that they corresponded to separate carbons, and not the exocyclic alkene as would have been expected. Instead, two trisubstituted alkenes were now present in the compound. The HMBC spectrum showed that the two vinylic hydrogens were in close proximity to each in the molecule. Two doublets at 1.96 and 1.97 ppm each integrated for 3H, indicating that they are methyl groups. The high chemical shift suggested that they were heavily deshielded. The HMBC spectrum indicated that the two methyls correlated with the alkenes, which were likely conjugated with the ketone to make a deshielding dienone system. The HRMS gave an exact mass for the $[M+H]^+$ molecular ion of 219.1743 *m/z*, corresponding to a molecular formula of $C_{15}H_{20}O$, confirming that the compound was a rearranged product of caryophyllene enone **195**. Therefore, based on the FTIR, HRMS, ^{1}H, ^{13}C and 2D NMR spectra, compound **201** was assigned as dienone **201** in 25% yield. Dienone **201** has been previously reported in a patent by Hiroshi *et al* and the characterisation data was consistent with the reported values.[150]

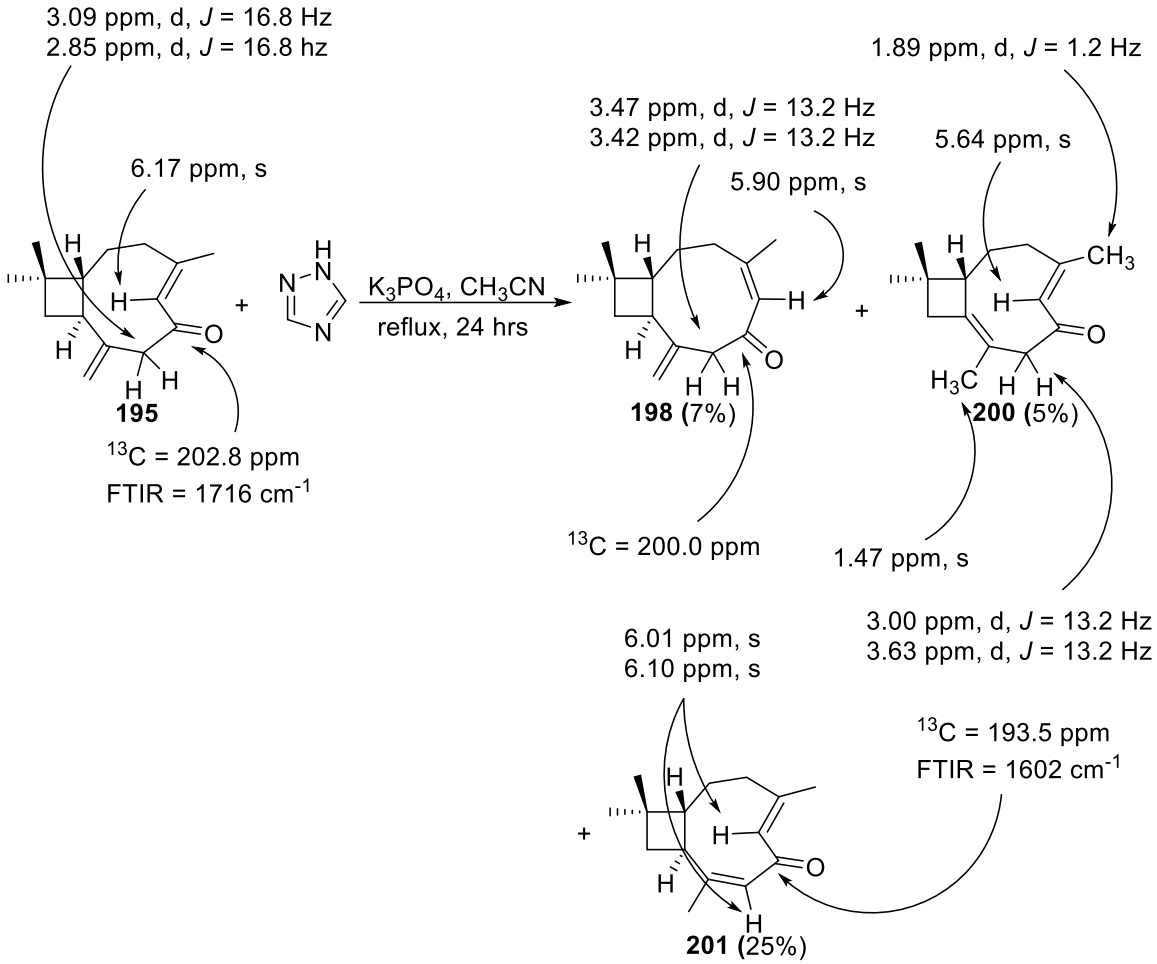

Scheme 6.43. *K_3PO_4 catalysed 1,4-conjugate addition of 1*H*-1,2,4-triazole to caryophyllene enone* ***195****.*

Another method for the incorporation of nitrogen into a compound is through the formation of imines, followed by reduction into amines. In α,β-unsaturated carbonyl systems, amines can act as a nucleophile and undergo a 1,4-conjugate addition or a direct addition to the carbonyl, allowing the potential inclusion of up to two nitrogens in a compound. The condensation of *E*-caryophyllene enone **195** with benzylamine was therefore investigated. Benzylamine was added to a solution of the *E*-caryophyllene enone **195** and anhydrous $MgSO_4$ in dry CH_2Cl_2 (Scheme 6.44). Unfortunately, the ^{1}H NMR spectra indicated that the benzyl imine had not been formed and the *E*-caryophyllene enone **195** had degraded.

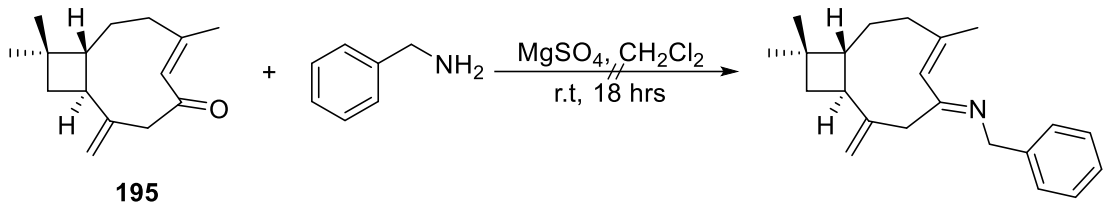

Scheme 6.44. *Attempted imination of* E-*caryophyllene enone* ***195*** *with benzylamine.*

The α,β-imine was potentially unstable and therefore unable to be isolated. An alternative method to isolating the imine and then reducing it to the amine in a separate reaction, is to form the imine and then reduce it in a one-pot reaction, known as a reductive amination. $NaBH_4$ is commonly used as a reducing for the reduction of imines to amines, and a procedure by Abdel-Magid *et al.* was adapted.[152] Benzylamine was added to a solution of *E*-caryophyllene enone **195** and anhydrous $MgSO_4$ in dry CH_2Cl_2 (Scheme 6.45). After 20 hours, $NaBH_4$ was added to the reaction mixture at room temperature. The ^1H NMR spectrum of the crude product indicated that the *E*-caryophyllene enone **195** had likely degraded and the neither amine nor imine had formed.

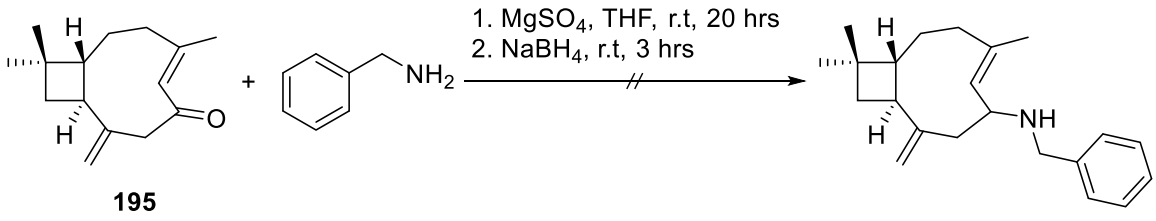

Scheme 6.45. *Attempted reductive amination of* E-*caryophyllene enone* ***195*** *with benzylamine.*

The high reactivity of the α,β-unsaturated ketone of *E*-caryophyllene enone **195** likely made it unsuitable for imination or 1,4-conjugate additions due to high likelihood of side reactions occurring. As a result, further functionalisation of caryophyllene enones was not pursued further.

6.4 Diels-Alder chemistry of 6-hydroxycaryophyllenes

The Diels-Alder reaction is a convenient means of increasing molecular complexity, especially for the generation of new ring structures. A Diels-Alder reaction involves the reaction between a diene and a dienophile through a concerted pericyclic mechanism to form a new six-membered ring (Scheme 6.46).

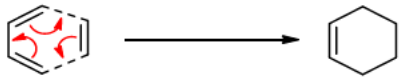

Scheme 6.46. *Mechanism for a Diels-Alder reaction.*

The strained endocyclic alkene of caryophyllenes is a good dienophile for Diels-Alder reactions. Extensive research has been conducted on the Diels-Alder chemistry of β-caryophyllene **58** and a handful caryophyllene derived compounds. For example, Lv *et al.* achieved a biomimetic synthesis of myrtucommulone K, N and O through a Diels-Alder reaction between β-caryophyllene **58** and isobutylidene-syncarpic acid **202** (Scheme 6.47).[153]

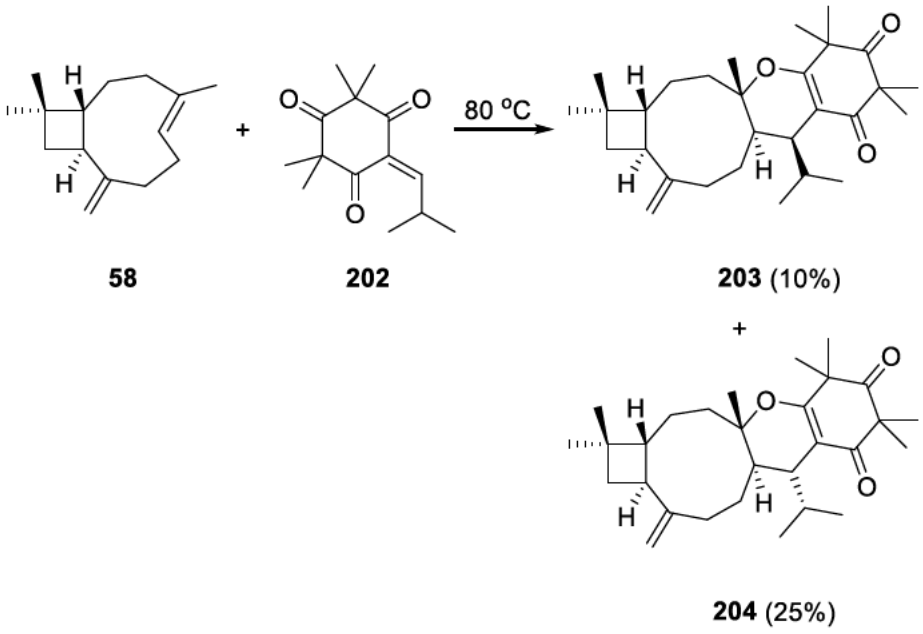

Scheme 6.47. *Preparation of myrtucommulone N* ***203*** *and K* ***204****.*

A limited amount of work has been conducted on using C6 functionalised caryophyllene-type compounds. In particular, Takao *et al.* synthesised (+)-cytosporolide A **205** via a Diels-Alder reaction between (-)-fuscotrol A **206** and isochroman carboxylic acid (+)-CJ-12,373 **207** (Scheme 6.48).[154] However, the Diels-Alder chemistry of C6 functionalised caryophyllenes can be further explored.

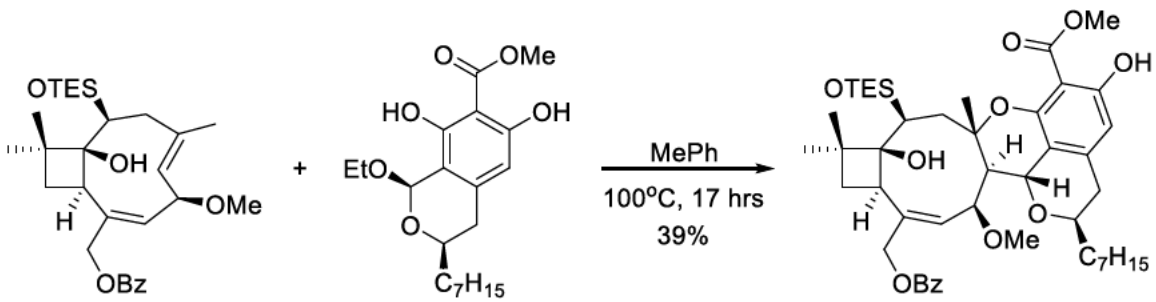

Scheme 6.48. *Synthesis of (+)-cytosporolide A* ***205****.*

Thiophene-1,1,-dioxide compounds are compounds that can act of dienes for Diels-Alder reactions, and are valuable due to the ability to for diene products after a Diels-Alder reaction. The compounds first undergo a standard Diels-Alder reaction, but then undergo a chelotropic elimination through the loss of SO_2, to reform the diene (Scheme 6.49).

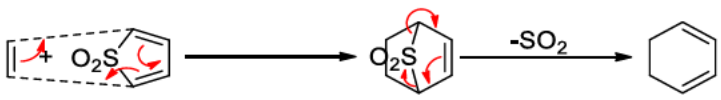

Scheme 6.49. *Mechanism for the Diels-Alder reaction of thiophene-1,1-dioxides.*

The Diels-Alder reaction using 3,4-dichlorothiophene-1,1-dioxide was therefore investigated, exploring the Diels-Alder chemistry of 6-hydroxycaryophyllenes. The reaction was conducted using β-caryophyllene **58**, to act as a point of comparison. 3,4-Dichlorothiophene-1,1-dioxide was added to a solution of β-caryophyllene **58** in $C_2H_4Cl_2$ and the reaction mixture was heated at reflux for 40 hours, to give a new compound **208** as a colourless oil (Scheme 6.50).

The ^{13}C NMR spectrum contained 19 signals. Six signals were between 110 and 160 ppm, indicating that six vinylic carbons were present. The ^{1}H NMR spectrum showed four signals between 4.5 and 6 ppm, indicating the presence of vinylic hydrogens. Three singlets were present at 4.86, 4.95 and 5.53 ppm that each integrated for 1H, which indicated that three of the hydrogens were in isolated spin systems, which was consistent with the expected Diels-Alder adduct. The hydrogens at 4.86 and 4.95 ppm were both on the same carbon according to the HSQC spectrum, indicating that the exocyclic alkene was still present. A doublet was present at 5.56 ppm that integrated for 1H and coupled to a multiplet at 2.60 ppm that integrated for 1H, which was consistent with a vinylic hydrogen that was adjacent to a methine. The methyl singlet at 1.62 ppm for β-caryophyllene **58** had shifted upfield to 0.92 ppm, indicating that it was no longer allylic. Therefore, based on the ^{1}H, ^{13}C

and 2D NMR spectra, compound was assigned as Diels-Alder adduct **208**, obtained in 13% yield. The stereochemistry of this adduct was not determined, but a *trans* ring junction is expected. Based on previous semisyntheses, such as the synthesis of myrtucommulone K, N and O by Lv *et al*, the stereochemistry of the Diels-Alder adduct **208** was inferred.[153]

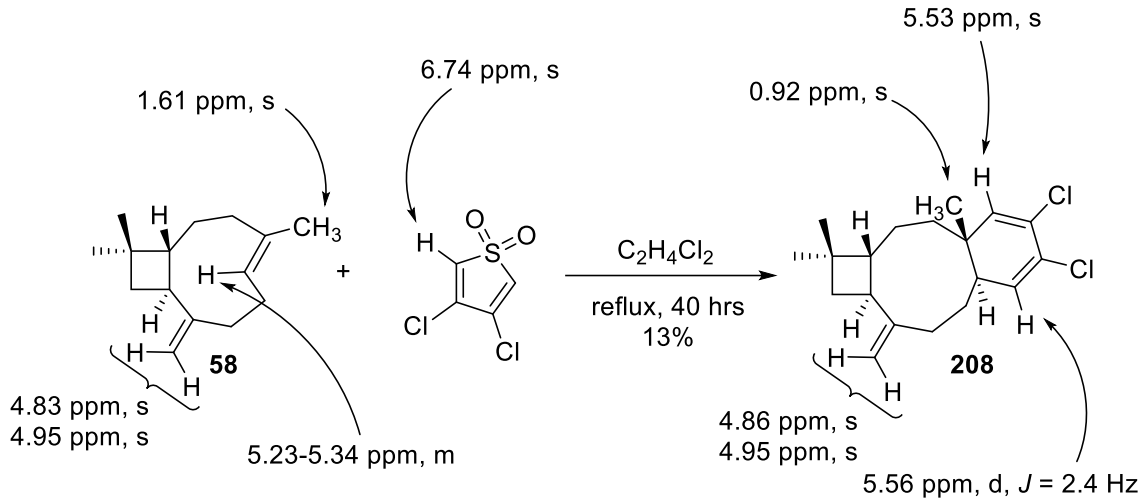

Scheme 6.50. *Diels-Alder reaction between β-caryophyllene **58** and 3,4-dichlorothiophene-1,1-dioxide.*

The successful formation of Diels-Alder adduct **208** was promising, so the same reaction was attempted using 12-acetoxy-6-hydroxycaryophyllene **2**. A solution of caryophyllene acetate **2** and 3,4-dichlorothiophene-1,1-dioxide in $CHCl_3$ was heated at reflux. After 8 hours, no reaction was observed by analysis of the ^1H NMR spectrum. The fixed conformation of 12-acetoxy-6-hydroxycaryophyllene **2** seemed to be unsuitable for a Diels-Alder reaction, indicating that (6*R*)-6-hydroxycaryophyllenes could not undergo Diels-Alder reaction at the endocyclic double bond. It was worth noting that the biomimetic synthesis of (+)-cytosporolide A by Takao *et al.* used the 6*S* isomer of (-)-fuscotrol A **206**, which may have contributed to its success.[154]

However, further evidence was required to support this hypothesis, so the Diels-Alder chemistry of 6-hydroxycaryophyllenes was explored further. In 2010, Lawrence *et al.* reported the biomimetic synthesis of guajadial and psidial A.[155] Guajadial and psdial A were synthesised through a Diels-Alder reaction between β-caryophyllene **58**, benzaldehyde and diformylphloroglucinol **209**. The synthesis of guajadial and psiadial A analogues using 6-hydroxycaryophyllenes was an interesting synthetic target and was attempted using 6-hydroxycaryophyllene **1** and caryophyllene acetate **2**.

The synthesis of diformylphloroglucinol **209** was attempted using a procedure by Bharate and Singh.[156] $POCl_3$ was added to a solution of phloroglucinol and dry DMF in dry EtOAc. After 2.5 hours the reaction was quenched with deionised water and worked up to give the crude product, which was purified by column chromatography to give a compound as an off-white solid (Scheme 6.51). The FTIR spectrum for the compound showed a broad OH absorbance at 3318 cm^{-1} and carbonyl absorbances at 1601 and 1638 cm^{-1}. The ^1H NMR spectrum showed a singlet at 9.92 ppm that integrated for 1H and a singlet at 5.78 ppm that integrated for 2H. Therefore, based on the ^1H NMR spectrum, the compound was assigned as formylphloroglucinol **210** in 6% yield, rather than the desired diformylphloroglucinol **209**. The FTIR and NMR spectral data were consistent with the values reported by Lawrence *et al.*[155]

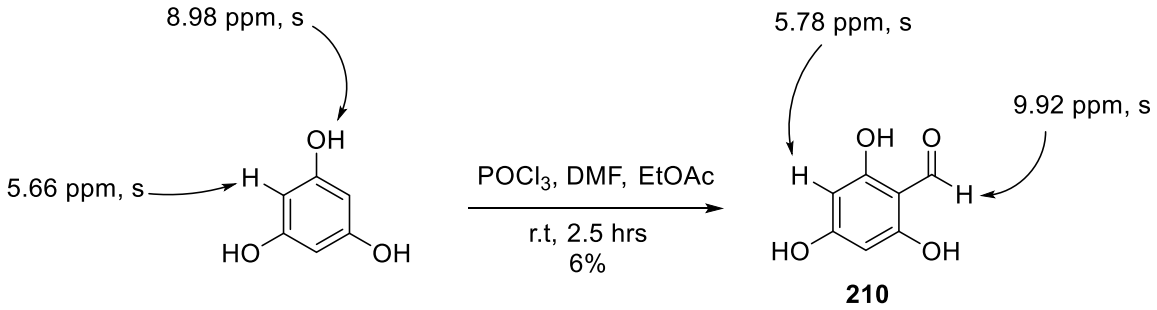

Scheme 6.51. *Formylation of phloroglucinol via a Vilsmeier-Haack reaction.*

Lawrence *et al.* had experienced similar issues with the synthesis of diformylphloroglucinol, and had used a procedure by Dittmer *et al.* instead.[157] The key difference was that anhydrous phloroglucinol and dry dioxane were used in the reaction instead of phloroglucinol hydrate and EtOAc. The Vilsmeier reagent was first prepared through the addition of $POCl_3$ to dry DMF at room temperature. A solution of phloroglucinol in dry dioxane was then added dropwise to the Vilsmeier reagent over 5 minutes. After 18 hours, the reaction was worked up and a compound was isolated as an orange solid. The FTIR spectrum for the compound showed a broad OH absorbance at 3350 cm^{-1} and a prominent carbonyl stretch at 1605 cm^{-1}. The ^1H NMR spectrum showed a singlet at 10.01 ppm that integrated for 2H and another singlet at 5.90 ppm that integrated for 1H. The 2:1 integration ratio indicated that the diformylation had succeeded and the compound was assigned as diformylphloroglucinol **209** in 43% yield (Scheme 6.52). The FTIR and NMR spectral data was consistent with the values reported by Lawrence *et al.*[155]

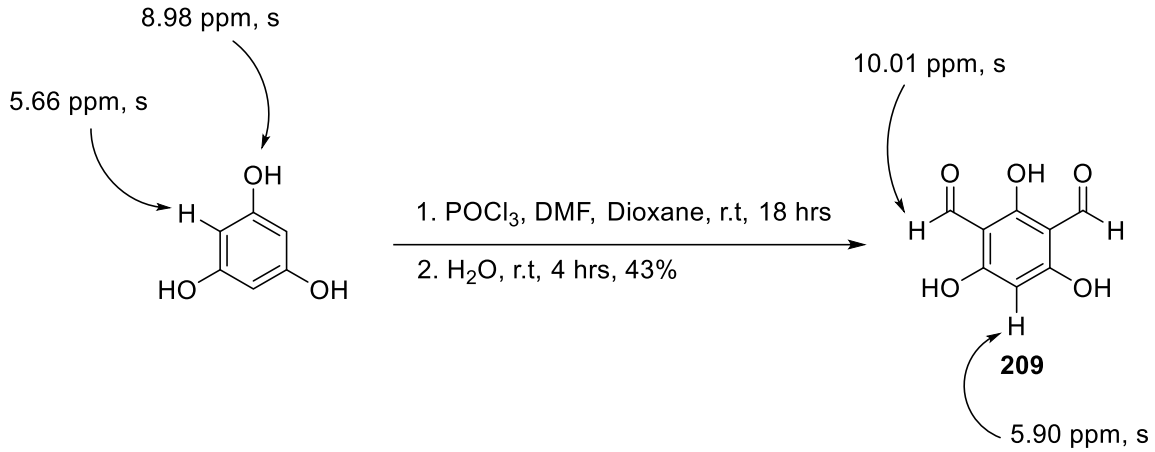

Scheme 6.52. *Diformylation of phloroglucinol via a Vilsmeier-Haack reaction.*

With the successful synthesis of both formylphloroglucinol **210** and diformylphloroglucinol **209**, the synthesis of analogues guajadial and psidial A could be explored using 6-hydroxycaryophyllenes. The reaction was first attempted using 6-hydroxycaryophyllene **1** and diformylphloroglucinol **209** using the procedure by Bharate and Singh.[156] NaOAc was added to a solution of benzaldehyde, diformylphloroglucinol **208** and 6-hydroxycaryophyllene **1** in 0.1M AcOH and the reaction mixture was heated at 80ºC. After 5 days, the reaction was worked up and the crude product was purified by column chromatography to afford compound **211**. The ^{13}C NMR spectrum contained 15 signals and looked similar to that of 6-hydroxycaryophyllene **1**. The ^{1}H NMR spectrum of compound **206** looked similar to that of 6-hydroxycaryophyllene **1**. The vinylic doublet had shifted upfield from 5.25 ppm for 6-hydroxycaryophyllene **1** to 5.19 ppm. The vinylic singlets corresponding to the exocyclic double bond stayed in almost the same positions. The allylic hydrogen doublet of doublet of doublets had shifted from 4.56 ppm in 6-hydroxycaryophyllene **1** to 4.27 ppm, indicating that the allylic hydrogen was more shielded. HRMS gave an exact mass of 423.3621 *m/z* for the $[M+H]^+$ molecular ion, corresponding to the molecular formula of $C_{30}H_{46}O$. The HRMS indicated that the product had likely dimerized, and therefore based on the HRMS, ^{1}H, ^{13}C and 2D NMR spectra the compound was assigned as 6-hydroxycaryophyllene dimer **211** in 2% yield (Scheme 6.53). The rest of the material from the reaction was an unresolved complex mixture.

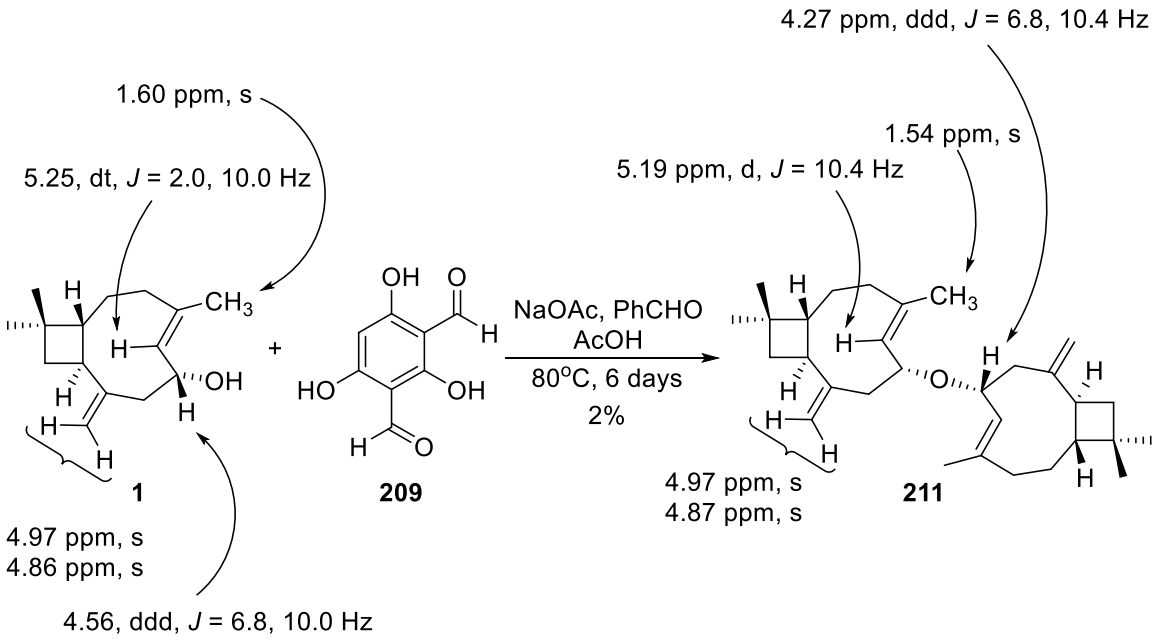

Scheme 6.53. *Synthesis of 6-hydroxycaryophyllene dimer **211**.*

The formation of 6-hydroxycaryophyllene dimer **211** and no detectable quantity of guajadial or psidial A analogues, indicated that the Diels-Alder reaction had not proceeded. This could potentially be attributed to lack of solubility in aqueous AcOH. However, previous lack of reaction between caryophyllene acetate **2** and 3,4-dichlorothiophene-1,1-dioxide suggests that the 6-hydroxycaryophyllene **1** likely had an unsuitable conformation for the Diels-Alder reaction.

The reaction was repeated using caryophyllene acetate **2**. NaOAc was added to a solution of benzaldehyde, diformylphloroglucinol **209** and caryophyllene acetate **2** in 0.1M AcOH and the reaction mixture was heated at 80ºC. After 6 days, the reaction was worked up and the crude product was purified by column chromatography to afford the starting material and diol caryophyllene **3** (Scheme 6.54). The formation of diol caryophyllene **3** indicated that caryophyllene acetate **2** was being hydrolysed under the acidic reaction conditions. No guajadial or psidial A analogues were isolated.

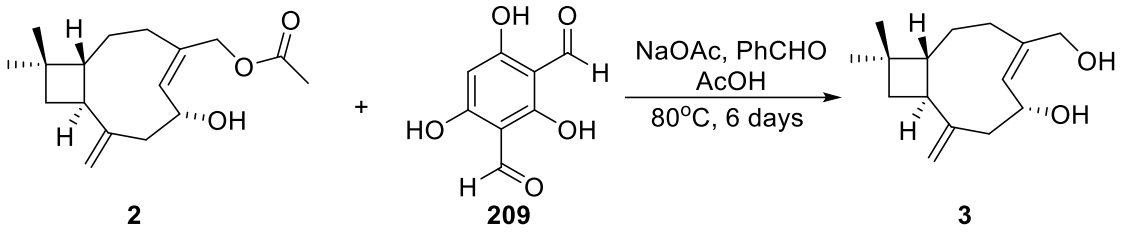

2 **209** **3**

Scheme 6.54. *Attempted synthesis of guajadial and psidial A analogues using caryophyllene acetate **2**.*

The formation of guajadial and psidial A analogues using diformylphloroglucinol and 6-hydroxycaryophyllenes had proven unsuccessful. The reactions were attempted again using formylphloroglucinol **210** to determine if a more electron-rich diene could encourage the Diels-Alder reaction to proceed. The reaction was first attempted using 6-hydroxycaryophyllene **1**. However the reaction afforded an unresolved complex mixture and no identifiable product could be isolated after by purification by column chromatography (Scheme 6.55). The lack of reaction reinforced that the ββ conformer of 6-hydroxycaryophyllenes was unsuitable for Diels-Alder reactions targeting the endocyclic alkene.

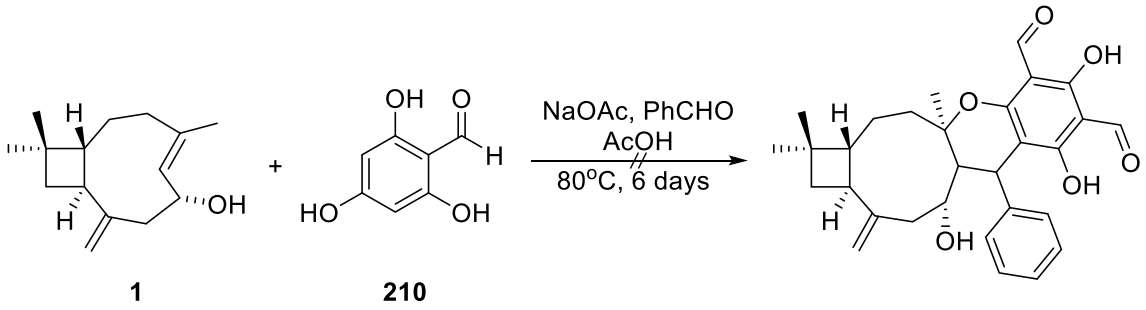

1 **210**

Scheme 6.55. *Attempted synthesis of guajadial and psidial A analogues using 6-hydroxycaryophyllene **1** and formylphloroglucinol **210**.*

The reaction was then repeated using caryophyllene acetate **2** and formylphloroglucinol **210**. NaOAc was added to a solution of benzaldehyde, formylphloroglucinol **210** and 6-hydroxycaryophyllene **1** in 0.1M AcOH and the reaction mixture was heated at 80ºC. After 5 days, the reaction was worked up and the crude product was purified by column chromatography to afford compound **212** as a colourless oil (Scheme 6.56). The ^{13}C NMR spectrum contained 17 signals, including a carbonyl signal at 170.29 ppm and four vinylic signals between 110 and 160 ppm. The ^{1}H NMR spectrum looked very similar to that of caryophyllene acetate **2**, except some key signals had shifted. The doublet of doublet of

doublets at 4.58 ppm corresponding to the C6 allylic hydrogen had shifted downfield to 5.59 ppm, indicating that it was heavily deshielded by an electron withdrawing group, such as an ester. The two doublets at 4.58 and 4.69 ppm that corresponded to the C12 methylene had appeared to have merged into a singlet at 4.05 ppm. The HSQC and HMBC spectra further suggested that the singlet at 4.05 ppm corresponded to the C12 methylene. The acetate singlet was still present at 2.04 ppm, indicating that the acetate was still present in the molecule. The HRMS gave an exact mass of 279.1949 *m/z* for the $[M+H]^+$ molecular ion, corresponding to a molecular formula of $C_{17}H_{26}O_3$. The molecular formula matched that of the starting caryophyllene acetate **2**, indicating that product was a rearranged form of the starting material. Therefore based on the HRMS, ^1H, ^{13}C and 2D NMR spectra, the compound was confirmed to be 6-acetoxy-12-hydroxycaryophyllene **212** in 5% yield. 6-Acetoxy-12-hydroxycaryophyllene **212** has not been previously reported in the literature. The formation of the rearranged 6-acetoxy-12-hydroxycaryophyllene **212** was consistent with an acid catalysed acetate transfer. Unfortunately no guajadial or psidial A could be detected or isolated, indicating that the reaction likely did not proceed.

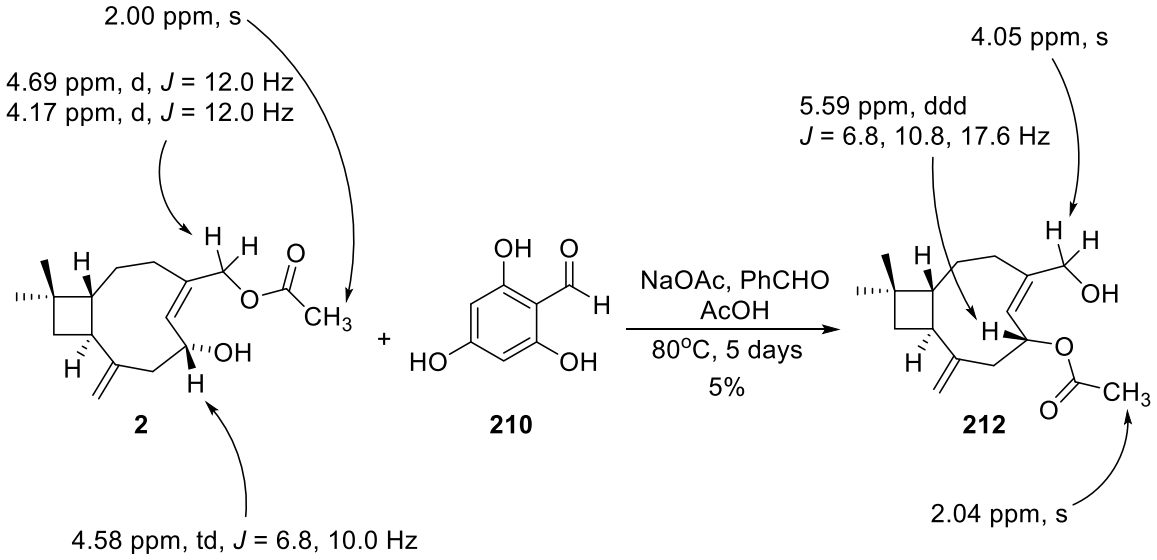

Scheme 6.56. *Synthesis of 6-acetoxy-12-hydroxycaryophyllene* ***212****.*

One final method that was considered was a 1,3-dipolar cycloaddition to either the endocyclic of exocyclic alkenes. A 1,3-dipolar cycloaddition is a percyclic reaction between a dipole and a dipolarophile to form a new ring. One of the most well-known 1,3-dipolar cycloadditions is between an organic azide and an alkyne to form a 1,2,3-triazole (Scheme 6.57). The organic azide is the dipole, while the alkyne is the dipolarophile.

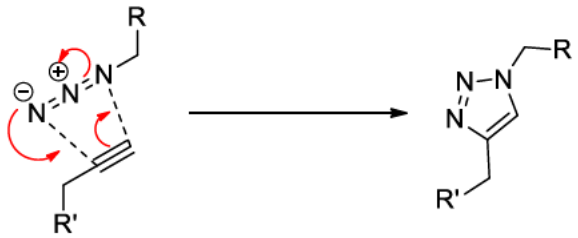

Scheme 6.57. *Mechanism of a 1,3-dipolar cycloaddition between an organic azide and an alkyne.*

Dipoles can be generated from oximidoyl halides through an elimination of the halide with a base (Scheme 6.58). Commonly used oximidoyl halides, include benzimidoyl chloride and bromide. These dipoles can then be used in a 1,3-dipolar cycloaddition with alkenes to generate 4,5-dihydroxoazoles.

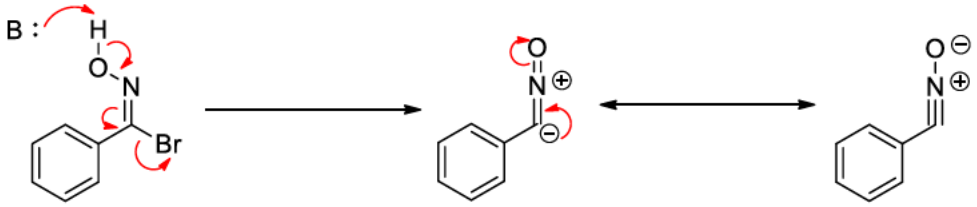

Scheme 6.58. *Mechanism for the generation of a dipole from* N-*hydroxybenzimidoyl bromide* ***213****.*

The synthesis of 4,5-dihydrooxazoles using a benzimidoyl halide with 6-hydroxycaryophyllenes was investigated. The benzimidoyl halide had to first be prepared, and benzimidoyl bromide was selected as the target. The synthesis of benzimidoyl halides has been established and a procedure by King *et al.* was adapted.[158] $NH_2OH{\cdot}HCl$ was added to a stirred solution of benzaldehyde in Et_2O. After 15 mins Et_3N was added to the reaction mixture and after a further 15 mins the reaction mixture was worked up to afford a compound as a yellow-white solid. The ^1H NMR spectrum showed no aldehyde signal between 9 and 10 ppm, and two triplets and a doublet between 7 and 9 ppm that integrated for 5 hydrogens. The HRMS gave an exact mass of 199.9699 *m/z* for the $[M+H]^+$ molecular ion, corresponding to a molecular formula of C_7H_6BrNO. Therefore, based on the FTIR, HRMS, ^1H and ^{13}C NMR data, the compound was assigned as *N*-hydroxybenzimidoyl bromide **213** (Scheme 6.59).

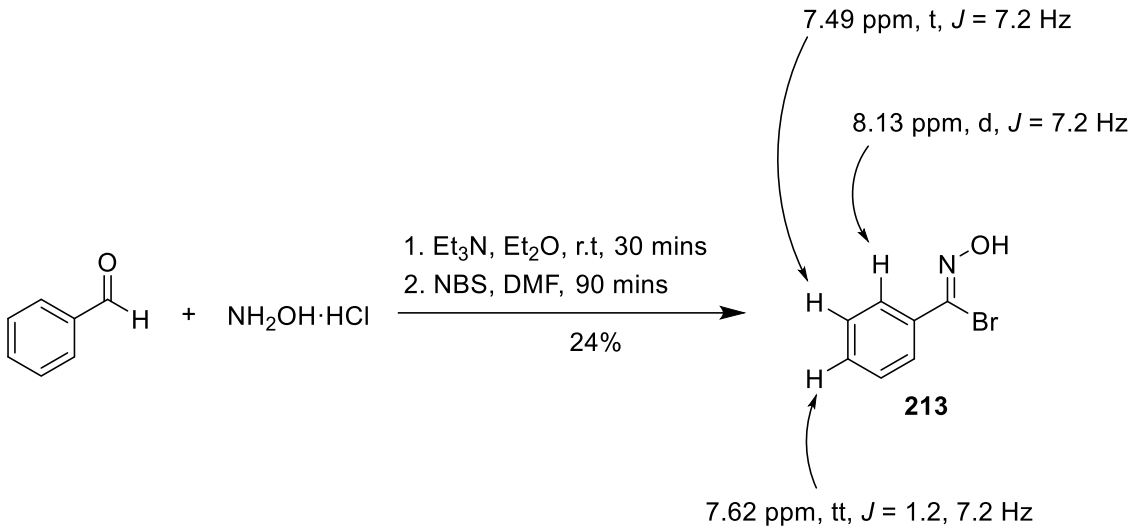

Scheme 6.59. *Preparation of* N*-hydroxybenzimidoyl bromide* ***213****.*

With the successful synthesis of the *N*-hydroxybenzimidoyl bromide **213**, the 1,3-dipolar cycloaddition could be attempted. The reaction was first attempted using β-caryophyllene **58**, as it had been previously shown to undergo cycloaddition reaction. Et_3N was added to a solution of β-caryophyllene **58** and *N*-hydroxybenzimidoyl bromide **213** in $C_2H_4Cl_2$ at room temperature. After 3 days, the reaction mixture was worked up to give the crude product (Scheme 6.60). The ^{1}H NMR spectrum indicated that the starting material was unreacted and the *N*-hydroxybenzimidoyl bromide **213** had degraded to form benzoic acid.

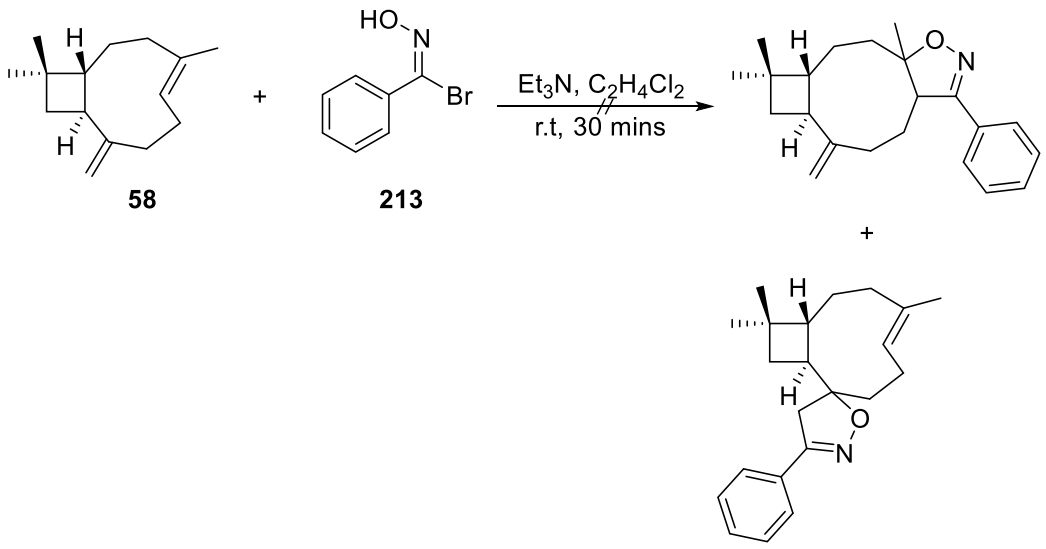

Scheme 6.60. *Attempted preparation of 4,5-dihydrooxazoles from β-caryophyllene* ***58*** *and* N*-hydroxybenzimidoyl bromide* ***213****.*

The lack of reaction was unexpected, so to explore the chemistry further the reaction was repeated using 6-hydroxycaryophyllene **1** instead (Scheme 6.61). However, similar to the reaction with β-caryophyllene **58**, the *N*-hydroxybenzimidoyl chloride appeared to have degraded to benzoic acid. Therefore, consistent with the other attempted reactions, the results indicated that 6-hydroxycaryophyllenes did not have the appropriate conformation for cycloaddition reactions.

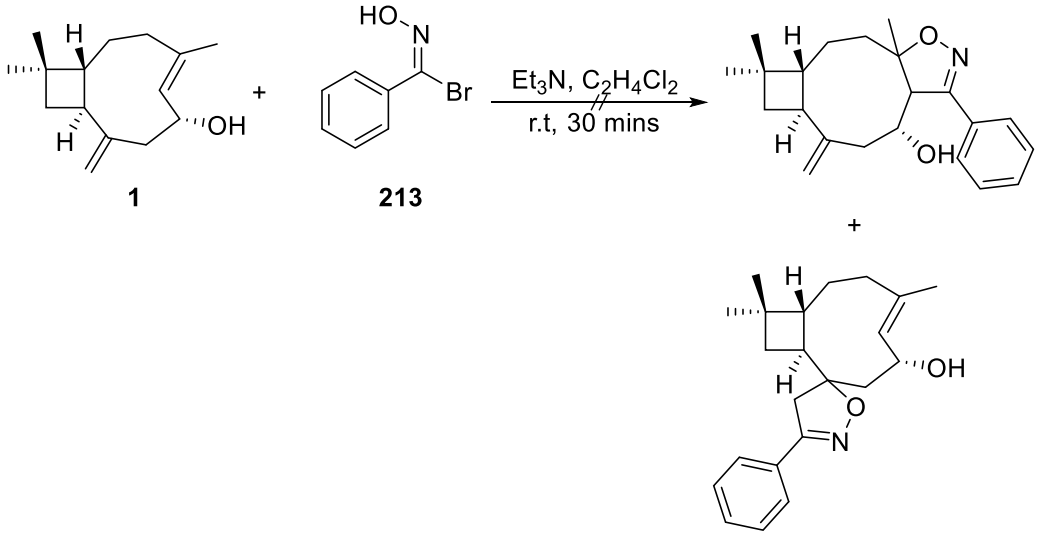

Scheme 6.61. *Attempted preparation of 4,5-dihydrooxazoles from 6-hydroxycaryophyllene* ***1*** *and* N-*hydroxybenzimidoyl bromide* ***213****.*

6.5 Conclusions

The oxidation chemistry of 6-hydroxycaryophyllenes was investigated. Tetrol **174**, pentol **183** and hexol **173** were successfully synthesised, highlighting the ability for 6-hydroxycaryophyllenes to functionalise into amphipathic compounds. A derivative of caryolan-1,3,4-triol **152** was successfully synthesised, 1,3,12-triacetoxycaryolan-4-ol **181**. The C6 hydroxyl group of 6-hydroxycaryophyllenes was functionalised through esterification, chlorination and tosylation to generate several rearranged products, including caryophyllenes **109**, **185** and **190**. Oxidation of diol caryophyllene **3** using activated MnO_2 afforded aldehyde triol **191** and butenolide **192**, while oxidation under Swern conditions gave hemiacetal enone **197**. Caryophyllene enones **195** and **196** were successfully synthesised through Swern oxidations of 6-hydroxycaryophyllene **1** and 12-acetoxy-6-hydroxycaryophyllene **2**. Attempted Michael additions to caryophyllene enone **195** resulted in a variety of structurally rearranged products. Imination and reductive amination of caryophyllene enone **195** was unsuccessful, likely due to the high reactivity of the enone. Diels-Alder adduct **208** was successfully synthesised from a Diels-Alder reaction of β-caryophyllene **58** with 3,4-dichlorothiophene-1,1-dioxide. The conformation of 6-hydroxycaryophyllenes is unsuitable for cycloadditions reactions including Diels-Alder reaction and 1,3-dipolar cycloadditions. Caryophyllene dimer **211** and 6-acetoxy-12-hydroxycaryophyllene **212** were serendipitously synthesised through an attempted synthesis of analogues of guajadial and psidial A using 6-hydroxycaryophyllenes.

Chapter 7
General conclusions

7.1 Isolation and identification of natural products from Western Australian plants

The first aim of the project was to identify natural products that could act as viable chromophores for vibrational spectroscopy. Several species from the Goodeniaceae family were investigated: *S. striata*, *S. caliptera*, *S. nitida*, *S. aemula* (Fairy fan flower, Purple Fanfare, Bondi Blue), *S. albida* and *G. varia*.

Investigation of the leaves of *S. striata* and *S. caliptera* revealed that the dominant natural product was ursolic acid **110**, with minor quantities of oleanolic acid **116** also detected (Figure 7.1). Investigation of the leaves *S. nitida* similarly showed that ursolic acid was the primary product in 0.37% yield. The glycoside of α-bisabolol, α-bisabolol β-D-ribofuranose **111**, was also isolated in 0.07% yield. The presence of ursolic acid **110** and oleanolic acid **116** was detected in all *S. aemula* species along with some unidentified glycosides. The ratio of glycosides to ursolic and oleanolic acids (**110** and **116)** varied depending on the plant leaf morphology of the *S. aemula* cultivar.

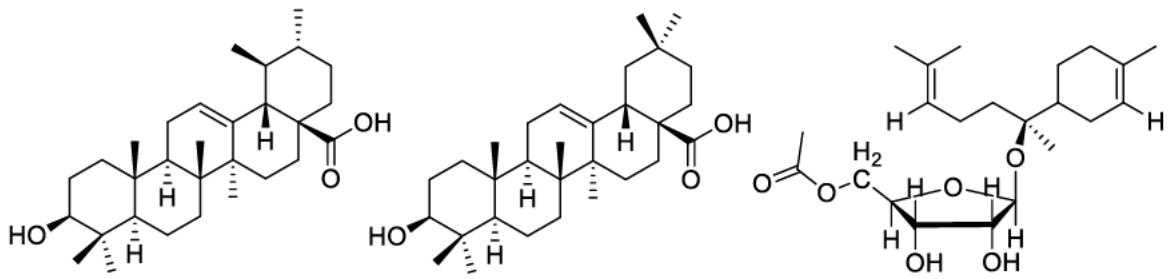

Figure 7.1. *Structures of ursolic acid* ***110****, oleanolic acid* ***116*** *and α-bisabolol β-D-ribofuranose* ***111****.*

The leaf resin of *G. varia* similarly contained ursolic acid **111**, in addition to several beyerene compounds, including beyerenes **117**, **120**, **121**, **122**, **123** and **124** (Figure 7.2). Beyerenes **117**, **120**, and **124** have not been previously identified. Unfortunately, none of the isolated compounds were deemed suitable for biochemical imaging due to the lack of unique spectroscopic markers.

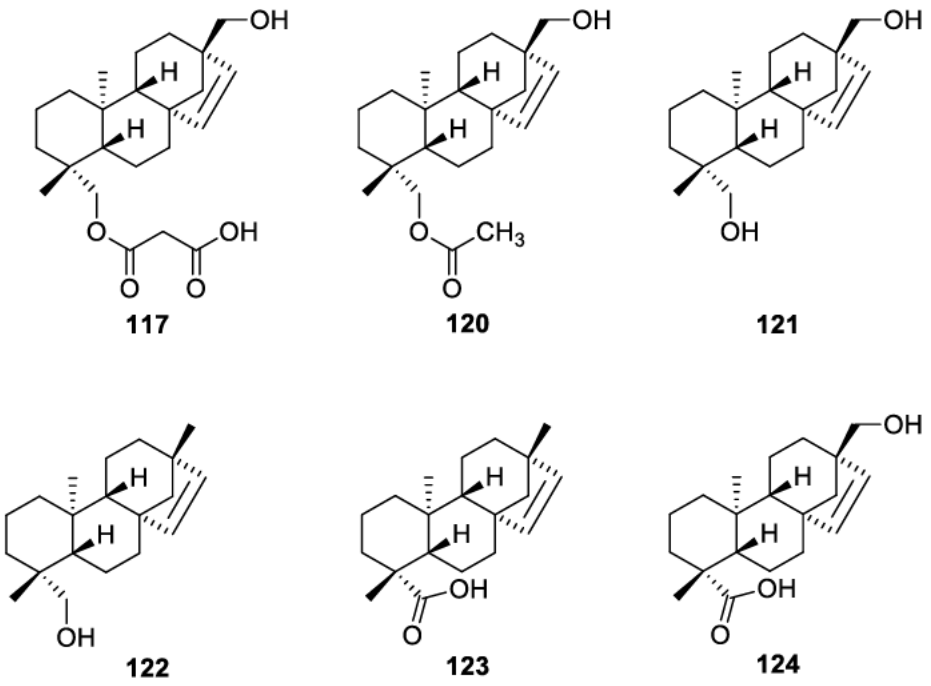

Figure 7.2. *Structures of beyerenes* ***117, 120, 121, 122, 123*** *and* ***124****.*

The natural product composition of *S. crassifolia*. collected from Port Beach, North Fremantle, Western Australia was investigated. The plant is commonly found along coastal environments, and the preliminary investigation of *S. crassifolia* was conducted on plants that were located on the grounds of Curtin University, which was not its native environment. 6-Hydroxycaryophyllene **1**, 12-acetoxy-6-hydroxycaryophyllene **2**, 6,12-dihydroxycaryophyllene **3**, 8-prenylflavanone **138** and 6-prenylflavanone **139** and ursolic acid **110** were all previously isolated from the Curtin University *S. crassifolia* (Figure 7.3). 12-Hydroxycaryophyllene **60** and flavone **141** were newly isolated from the Port Beach plants, and no 1,4-dihydroxy-α-bisabolol-2,10-diene **137** was detected, which had been previously isolated from Curtin University *S. crassifolia* (Figure 7.3).

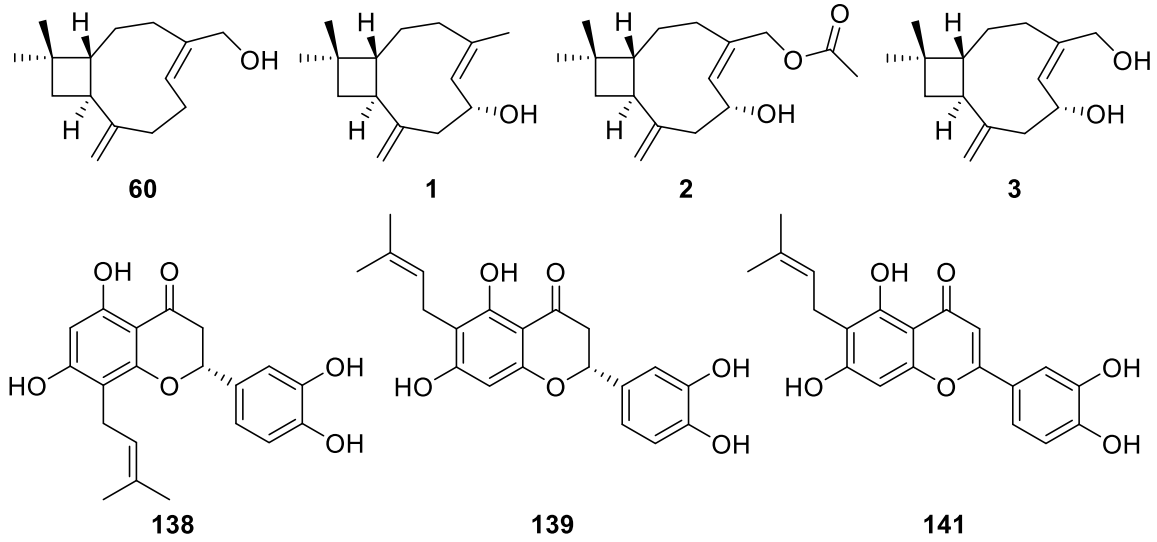

Figure 7.3. *Structures of caryophyllenes **1**, **2**, **3** and **60**, flavanones **138** and **139**, and flavone **141**.*

7.2 Development of protocols for sample preparation and biochemical imaging of Goodeniaceae and Sapindaceae species

A viable methodology for the sectioning of plant leaf tissue for use in biochemical imaging was developed. Conventional embedding techniques such as paraffin embedding, were deemed unsuitable due to potential leeching of compounds from the plant leaf sections from the use of EtOH. Chemical fixation of leaf tissue section was also deemed to unsuitable due to similar leeching concerns and the potential for the formation of chemical artefacts. Room temperature sectioning of plant leaf tissue proved difficult due to the tendency for the tissue sections to curl and the lack of availability of suitable embedding media that would not leech or contaminate the tissue section.

Flash freezing of plant leaf tissue followed by sectioning of the tissue while the base was embedded in OCT proved to be an effective, albeit still difficult method to collect leaf tissue sections with an intact layer of leaf resin. Gradual embedding of leaf tissue in OCT, by repeated layering of OCT over the tissue and letting it set, followed by sectioning of the embedded tissue was effective for the preparation tissue sections for internal cellular imaging.

The strained alkene signal of caryophyllenes could be successfully mapped in the surface leaf resin of *S. crassifolia* using confocal Raman microscopy (Figure 7.4). The distribution of phenylalanine and fatty acids/lipids was successfully mapped in both epidermal and ground tissue of plant leaves using confocal Raman microscopy, which has not been

previously reported (Figure 7.4). A protocol for the use of 3D Raman imaging to map the distribution ligno-cellulose, phenylalanine and fatty acids/lipids in plant leaf tissue was also developed, with few, if any examples of 3D Raman imaging of plant tissue currently available in the literature.

Analyis of *S. crassifolia* leaf tissue sections using the infrared microscopy beamline at the Australian synchrotron highlighted the distribution of highly localised regions of primary amines that could potentially be attributed to the presence of protein vacuoles (Figure 7.4). The presence of protein storage vacuoles could be co-localised using an alternate technique, such as scanning electron microscopy (SEM).

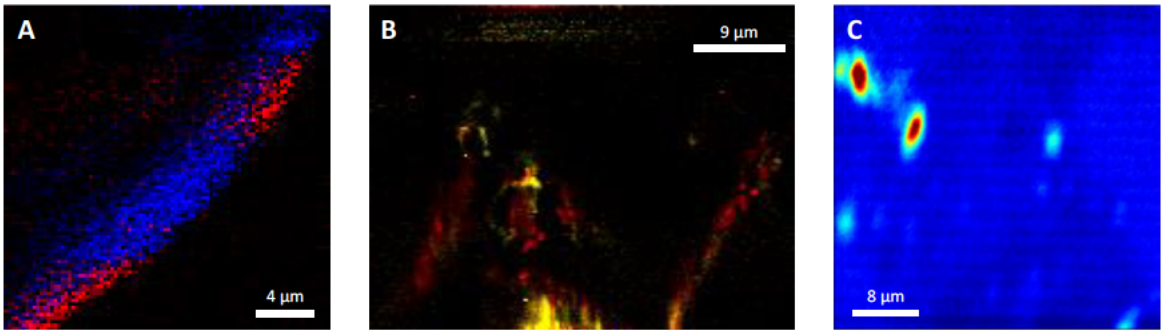

Figure 7.4. *Vibrational spectroscopy images (A-C). (A) Raman image of strained alkenes (red) and phenols (blue) in* S. crassifolia *leaf resin, (B) Raman image of phenylalanine (red) and fatty acids/lipids in* S. crassifolia *leaf cell, and (C) FTIR image of amine N-H stretching (3500-3600 cm^{-1}) in* S. crassifolia *leaf cell.*

The distribution of natural products could be spectroscopically mapped on the surface resin of leaves using confocal Raman microscopy, but alternative methods aside from confocal Raman microscopy or infrared microscopy are required for imaging within plant tissue. A near infrared light source, such as 1064 nm laser would possibly allow for the biochemical imaging of natural products. Time gated Raman microscopy or a multimodal approach using histology would also potentially allow for the localisation of natural products while overcoming the limitations of auto-fluorescence.

7.3 Biosynthetic investigation of natural products using organic synthesis and spectroscopy

The mechanisms for the formation of birkenal **142**, caryolan-1,3,4-triol **152** and 5,6-dihydroxycaryophyll-3,8-diene **154** from 6-hydroxycaryophyllene **1**, and 6- and 8-prenylflavanones **138** and **139** from chalcone **157** were investigated.

The formation of birkenal **142** from the oxidation of 6-hydroxycaryophyllene **1** using activated MnO_2 was observed. Isolation of the intermediate, 4,5,6-trihydroxycaryophyllene **146**, and observation of similar reaction with 12-acetoxy-6-hydroxycaryophyllene **2** allowed for a mechanism for the biosynthesis birkenal **142** to be developed. Further reaction pathways were highlighted through exploration of the chemistry of the triol caryophyllene intermediates. Treatment of acetate triol caryophyllene **148** with TFA afforded the tricylic compound 12-acetoxycaryolan-1,3,4-triol **153**. However, similar treatment of 4,5,6-trihydroxycaryophyllene **146** with glacial AcOH afforded diene caryophyllene **154**, indicating that methyl triol caryophyllene was the reaction intermediate. Therefore the formation of caryolan-1,3,4-triol **152** is likely not fully acid catalysed and may be an enzyme catalysed reaction.

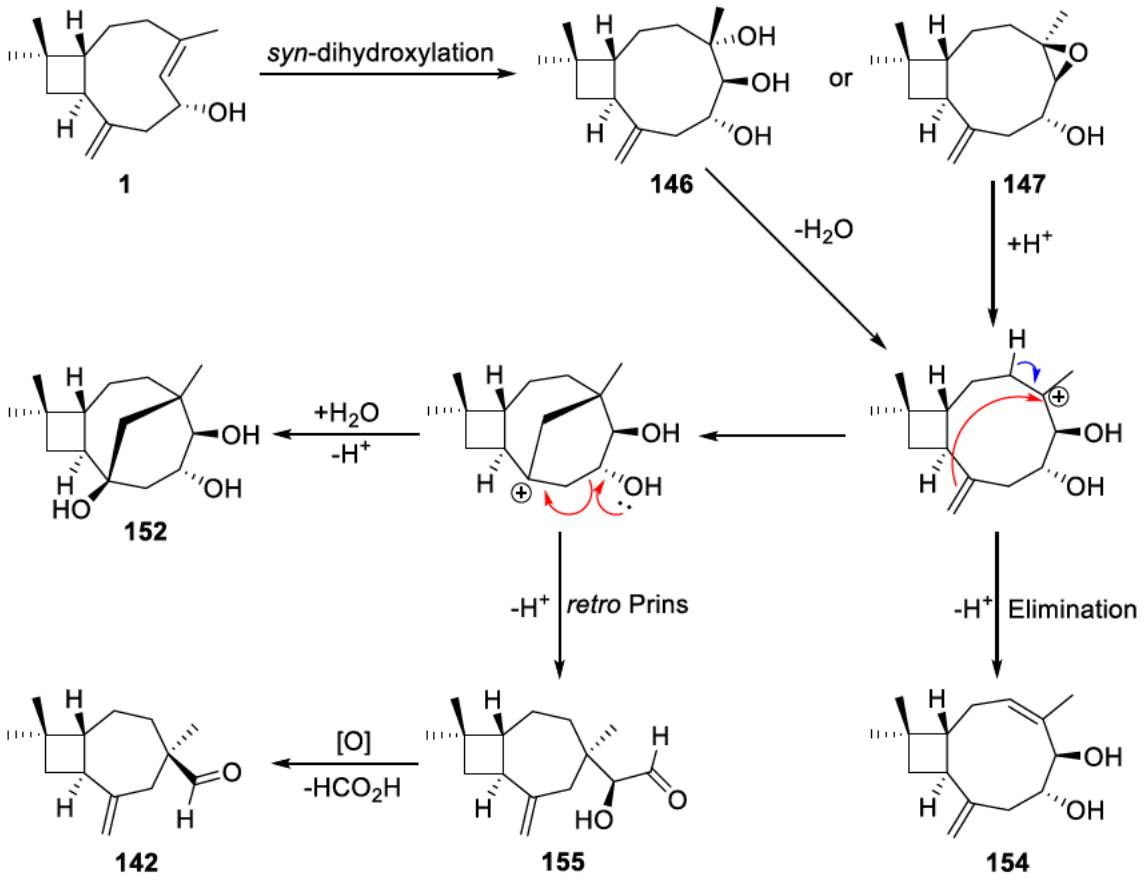

Scheme 7.1. *Proposed biosynthesis of birkenal* ***142****, 5,6-dihydroxycaryophyll-3,8-diene* ***154*** *and caryolan-1,3,4-triol* ***152****.*

Investigation of the acid-catalysed auto-oxidation of 6-hydroxycaryophyllene **1** using NMR spectroscopy was conducted. The spectra showed that an acidic environment catalysed the formation of a variety of aldehydes, including birkenal **142** in trace quantities. A weakly acidic environment resulted in the visible formation of 4,5,6-trihydroxycaryophyllene **146**, followed by elimination to afford diene **154**. No visible reaction, aside form deuterium exchange, was observed in a neutral environment.

A longitudinal study of a mixture of compounds, including caryophyllenes, in the neutrals from from *S. crassifolia* was conducted using ATR-FTIR spectroscopy. The neutrals fraction quickly shown oxidation within 1-3 days, although the change is not attributed to caryophyllenes. The presence of phenols from *S. crassifolia* in quantities of 50-100% w/w inhibits the auto-oxidation of the neutrals fraction. The presence of BHT **156**, a common antioxidant, does not inhibit the auto-oxidation of the neutrals fractions, and is likely due the precipitation of the BHT **156**.

The cyclisation of chalcone **157** to form 8-prenylflavanone **138** and 6-prenylflavanone **139** with a naturally occurring bias of 4:5 8-prenylflavanone **138**/6-prenylflavanone **139** was investigated. Treatment of chalcone **157** using standard inorganic salts such as NaOAc yields a mixture of both the 8- and 6-prenyl products in a 1:3 ratio. The use of a sterically bulky base, such as Et_3N, favours the exclusive formation of 6-prenylflavanone **139**. Exposure of chalcone **157** to UV light or sunlight resulted in polymerisation of the chalcone **157**, with similar examples reported in the literature. Therefore, the formation of the 8-prenylflavanone **138** and 6-prenylflavanone **139** in a 4:5 ratio was likely due to a natural bias in the enzymatic reaction rather than due to an abiotic chemical reaction.

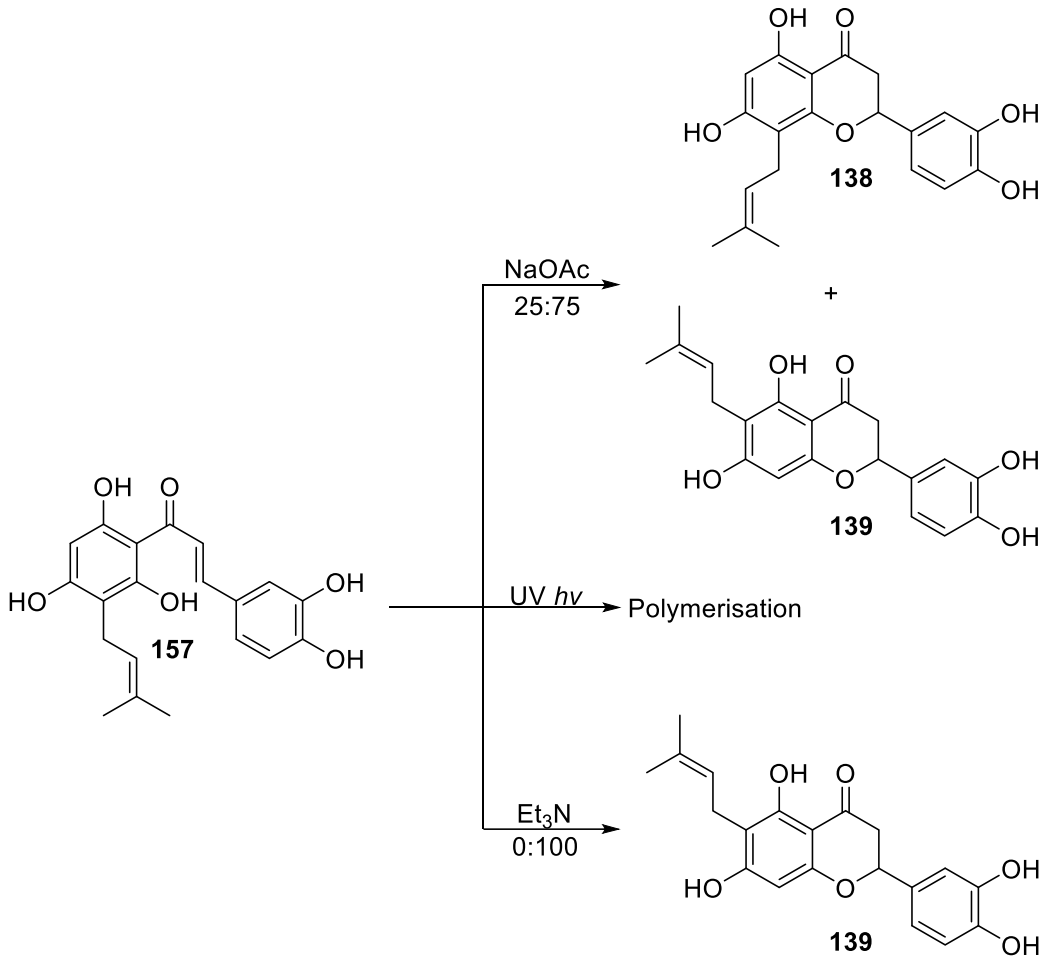

Scheme 7.2. *Impact of reaction conditions on cyclisation of chalcone **157**. Ratios shown are ratio of 8-prenylflavanone **138**:6-prenylflavanone **139**.*

7.4 Exploration of the chemistry of 6-hydroxycaryophyllenes

The chemistry of 6-hydroxycaryophyllenes was explored, with the intention of developing novel scaffolds that could display interesting bioactivity. The first synthetic target was hexol **173**, due to the amphipathic properties of the molecule. The hexol **173** was successfully synthesised from 12-acetoxy-6-hydroxycaryophyllene **2** four synthetic steps (Scheme 7.3).

The chemistry of the C6 allylic hydroxyl group of 6-hydroxycaryophyllenes was also explored. The hydroxyl group was esterified to generate the benzoate ester. Chlorination of the hydroxyl group of 6-hydroxycaryophyllene **1** yielded 6-chlorocaryophyllene **184**. Chlorination of 12-acetoxy-6-hydroxycaryophyllene **2** yielded 12-acetoxy-6-hydroxy-*Z*-caryophyllene **189**. Treatment of 6-chlorocaryophyllene **184** with $AgBF_4$ afforded both 6-hydroxycaryophyllene **1** and 4-hydroxycaryophyll-5,8-diene **185**, demonstrating the resonance stabilisation of the carbocation. Tosylation of the hydroxyl group of 12-acetoxy-

6-hydroxycaryophyllene **2** yielded 12-acetoxy-4-hydroxycaryophyll-5,8-diene **190** (Scheme 7.3).

The oxidation chemistry of the C6 hydroxyl group and the endocyclic alkene was similarly explored. Oxidation of 6,12-dihydroxycaryophyllene **3** using activated MnO_2 at room temperature yielded the aldehyde triol caryophyllene **191**. Treatment of aldehyde triol caryophyllene with activated MnO_2 at reflux in CH_2Cl_2 yielded butenolide **192**. Swern oxidation of the hydroxyl group of 6-hydroxycaryophyllene **1** and 12-acetoxy-6-hydroxycaryophyllene **2** yielded enones **195** and **196**. Swern oxidation of 6,12-dihydroxycaryophyllene **3** yielded hemiacetal enone **197**. Treatment of caryophyllene enone **195** with $BF_3{\cdot}Et_2O$ in the presence of indole isomerised the product to afford *Z*-caryophyllene enone **198**. Treatment of caryophyllene enone **195** with K_3PO_4 in the presence of 1*H*-1,2,4-triazole afforded *Z*-caryophyllene enone **198**, dimethyl caryophyllene enone **200** and dienone **201** (Scheme 7.3).

The cycloaddition chemistry of the endocyclic alkene of 6-hydroxycaryophyllenes was investigated. The Diels-Alder reaction between β-caryophyllene **58** and 3,4-dichlorothiophene-1,1-dioxide afforded Diels-Alder adduct **208** (Scheme 7.3). However, no reaction was observed when attempting the same reaction using 6-hydroxycaryophyllene **1** and 12-acetoxy-6-hydroxycaryophyllene **2**. 6-Hydroxycaryophyllene **1** and 12-acetoxy-6-hydroxycaryophyllene **2** were used replicate the biomimetic synthesis of guajadial and psidial A reported by Bharate and Singh.[156] Reaction of 6-hydroxycaryophyllene **1** in the presence of glacial AcOH and NaOAc yielded 6-hydroxycaryophyllene dimer **211**, whereas reaction of 12-acetoxy-6-hydroxycaryophyllene under the same conditions yielded 6-acetoxy-12-hydroxycaryophyllene **27**. No visible reaction was observed when attempting a [3+2] dipolar cycloaddition to 6-hydroxycaryophyllene **1** and 12-acetoxy-6-hydroxycaryophyllene **2** using *N*-hydroxybenzimidoyl bromide **213**.

The chemistry of 6-hydroxycaryophyllenes has been briefly explored, but there is still significant room for further investigation. The chemistry of 6-hydroxycaryophyllene oxides have yet to be explored in detail and similarly the potential for caryophyllene enones to act as hetero-Diels Alder dienes.

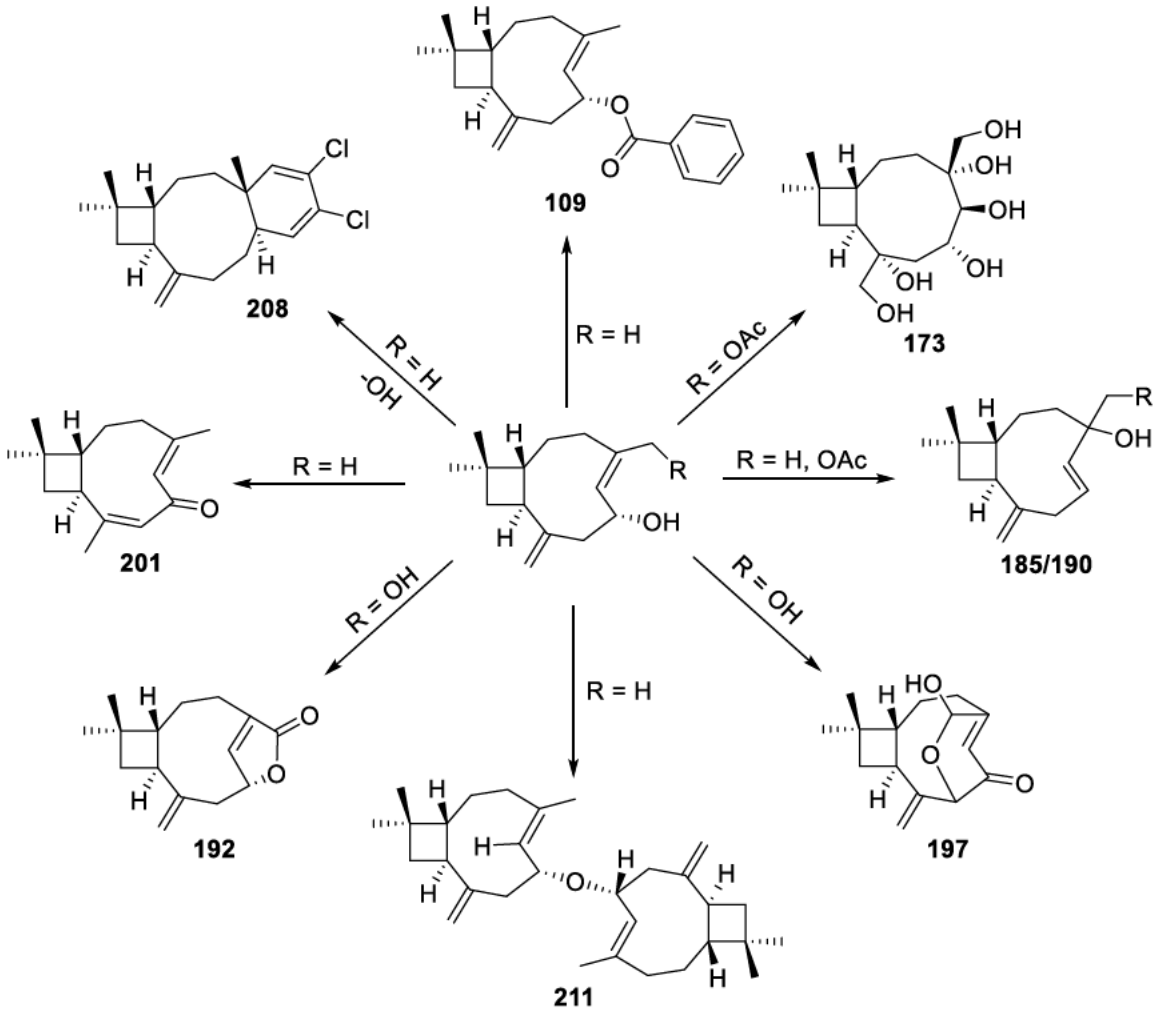

Scheme 7.3. *Examples of transformations using either β-caryophyllene* ***58*** *or a 6-hydroxycaryophyllene compound as the starting material.*

Chapter 8
Experimental Section

8.1 General experimental

All reactions involving moisture or air-sensitive reagents were performed under a positive pressure of nitrogen. Glassware was dried in an oven set at 120ºC for at least 30 minutes. Materials were obtained from commercial sources and used without further purification unless otherwise stated. NMR experiments were performed on a Bruker Ultrashield Avance III 400 spectrometer (^{1}H, 400.1 MHz; ^{13}C, 100.6 MHz). Chemical shifts (δ) are expressed in ppm with reference to the solvents resonances of $CDCl_3$ (^{1}H, 7.26 ppm; ^{13}C, 77.16 ppm), $(CD_3)_2CO$ (^{1}H, 2.05 ppm; ^{13}C, 29.84 ppm), $(CD_3)_2SO$ (^{1}H, 2.50 ppm; ^{13}C, 29.52 ppm), CD_3CN (^{1}H, 1.94 ppm; ^{13}C, 1.32 ppm), pyridine-d_5 (^{1}H, 8.71 ppm; ^{13}C, 149.5 ppm) and D_2O (^{1}H, 4.79 ppm). HRMS spectra were rcorded at the School of Science, Edith Cowan University, Joondalup WA using a Q Exactive™ Focus Hybrid Quadrapole-Orbitrap™ Mass Spectrometer (Thermo Fisher Scientific Corporation, US). Analytes ionisation was achieved using heated electrospray ionisation source (HESI) operated in negative (-eV) mod. Samples were introduced into the HESI using a syringe pump operated at a flow rate of 5 μL min^{-1}. The Q Exactive mass spectrometer was operated in full-scan mode from 70-1000 *m/z* followed by isolation and full MS2 fragmentation of the parent compound in the HDC cell at variable collision energy. Infrared spectra were recorded on a Thermo Fisher Nicolet iS50 Fourier Transform-IR spectrometer equipped with a ZnSe-diamond crystal ATR accessory; spectra were acquired between 4000-400 cm^{-1}. Optical rotations (α) were obtained from a Rudolph Scientific Analytical Autopol I polarimeter. Melting points were determined on a Crown Scientific Barnstead Electrothermal 9100 apparatus. Column/flash chromatography was achieved using the Reveleris X2 flash chromatography system with Buchi 40 μm silica cartridges or SiliaFlash® P60 silica gel (230-400 mesh, SiliaCycle, Canada) with the solvents stated. Radial chromatography was performed on a Harrison Research Chromatotron, model 7924T using chromatotron plates (1 mm and 2 mm) made with Merck silica gel 60 PF_{254} containing gypsum. TLC was completed on Merck aluminium backed silica gel 60 F_{254} sheets and visualised by using short-wave UV light (λ = 254 nm) for conjugates systems, potassium permanganate and vanillin solutions. The solvents tetrahydrofuran, dichloromethane, diethyl ether and acetonitrile are saturated with

nitrogen and dried over activated alumina columns, *N*,*N*-dimethylformamide is saturated with nitrogen and dried over (5Å) molecular sieve columns (Innovative Technology PS-MD-5). Petroleum Spirits 40-60 refers to the fraction of alkanes that boil between 40-60ºC. The reaction conditions of 0ºC and -84ºC refer to an ice, and a liquid nitrogen-EtOAc bath respectively.

8.2 Chapter 2

8.2.1 Scaevola nitida *"Aussie Spirit"*

Fresh *S. nitida* "Aussie Spirit" leaves (9.99 g) were steeped in diethyl ether (200 mL). After 20 mins, the extract was decanted and filtered to remove detritus. The filtrate was concentrated under reduced pressure to afford a yellow powder (64 mg, 0.64%).

A portion of the extract (38 mg) was triturated with MeOH. The insoluble solid was and dried to afford ursolic acid **110** as an off-white solid (22 mg, 0.05 mmol, 0.37%). Selected signals shown for in NMR data.

The MeOH soluble filtrate was concentrated under reduced pressure to afford a yellow-white oil (16 mg, 0.27%). The oil was purified by column chromatography (10:90-100:0 EtOAc/PS, silica gel). Ursolic acid **110** was isolated as a white solid (10 mg, 0.02 mmol, 0.17%) and α-bisabolol β-D-ribofuranose **111** was afforded as a yellow oil (4 mg, 0.01 mmol, 0.07%).

Ursolic Acid 110:

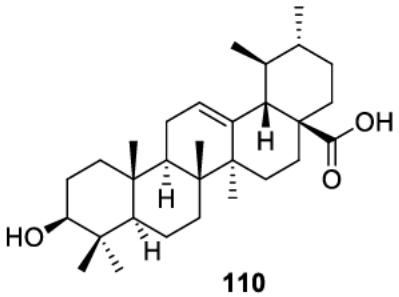

110

^{1}H NMR (400 MHz, d$_5$-pyridine): δ 5.52 (app t, *J* = 5.2 Hz, 1H), 3.49 (m, 1H), 2.67 (d, *J* = 11.6 Hz, 1H), 2.36 (td, *J* = 5.2, 13.6 Hz, 1H), 2.15 (td, *J* = 4.4, 13.2 Hz, 1H), 2.07-1.28 (m, 20H) 1.27 (s, 3H), 1.26 (s, 3H), 1.09 (s, 3H), 1.05 (s, 3H), 1.03 (d, 3H), 0.98 (d, 3H), 0.92 (s, 3H) ppm.

^{1}H NMR (400 MHz, CDCl$_3$): δ 5.26 (app t, *J* = 3.6 Hz, 1H), 3.21 (dd, *J* = 4.8, 10.8 Hz, 1H), 2.19 (d, *J* = 11.2 Hz, 1H), 2.01 (dd, *J* = 4.4, 13.6 Hz, 1H), 1.92 (dd, *J* = 4.0, 8.8 Hz, 1H), 1.97-1.10 (m, 20H), 1.09 (s, 3H), 0.99 (s, 3H), 0.95 (d, *J* = 6.4 Hz, 3H) 0.93 (s, 3H), 0.87 (d, *J* = 6.4 Hz, 3H), 0.80 (s, 3H), 0.78 (s, 3H) ppm.

^{1}H NMR (400 MHz, d$_6$-DMSO): δ 5.13 (app t, 1H), 4.28 (s, 1H, OH), 3.00 (s br, 1H), 2.10 (d, *J* = 11.2 Hz, 1H), 2.00-1.25 (m, 22H), 1.23 (s, 3H), 1.04 (s, 3H), 0.91 (d, 3H), 0.89 (s, 3H) 0.81 (d, *J* = 6.4 Hz, 3H), 0.75 (s, 3H), 0.68 (s, 3H) ppm.

^{13}C NMR (101 MHz, d_5-pyridine): δ 180.5 (CO_2H), 139.8 (C=C), 126.2 (C=C), 78.7 (CHOH), 56.3 (CH_2), 54.1 (CH), 48.6 (C), 48.6 (CH), 43.0 (C), 40.5 (C), 40.0 (CH), 39.9 (C), 39.9 (CH_2), 39.6 (CH), 39.6 (CH_2), 38.0 (C), 37.8 (CH_2), 34.1 (CH_2), 31.6 (CH_2), 29.3 (CH_3), 29.2 (CH_2), 28.6 (CH_2), 25.4 (CH_2), 24.4 (CH_3), 23.5 (CH_2), 21.9 (CH_3), 19.3 (CH_2), 18.0 (CH_3), 18.0 (CH_3), 17.1 (CH_3), 16.2 (CH_3) ppm.

ATR-FTIR: 3424 (OH, s), 2964 (C-H), 2922 (C-H), 2850 (C-H), 1687 (C=O) cm^{-1}.

α-bisabolol β-D-ribofuranose 111:

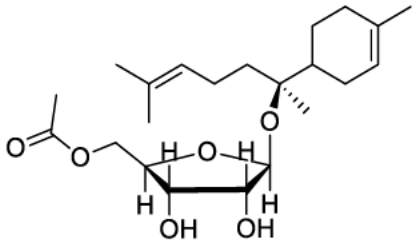

111

^{1}H NMR (400 MHz,$CDCl_3$): δ 5.35 (s, 1H), 5.06 (t, $J_{10\text{-}9}$ = 7.2 Hz, 1H), 4.73 (app s, 1H), 4.72 (app q, $J_{1'\text{-}2'}$ = <1 Hz, $J_{2'\text{-}3'}$ = 5.6 Hz, J = 12.4 Hz, 1H), 4.09 (dd, $J_{5'\alpha\text{-}4'}$ = 4.4 Hz, $J_{5'\alpha\text{-}5'\beta}$ = 12.0 Hz, 1H), 3.70 (app dd, $J_{4'\text{-}5'}$ = 6.8 Hz, $J_{4'\text{-}3'}$ = 4.0 Hz, 1H), 3.62 (app t, $J_{3'\text{-}2'}$ = 6.8 Hz, 1H), 3.35 (dd, J = $J_{5\beta'\text{-}4'}$ = 7.2 Hz, $J_{5'\beta\text{-}5'\alpha}$ = 12.0 Hz, 1H), 2.12 (s, 3H), 2.02-1.89 (m, 6H), 1.87-1.72 (m, 1H), 1.67 (s, 3H), 1.63 (s, 3H), 1.60 (s, 3H), 1.56-1.46 (m, 2H), 1.34-1.19 (m, 2H), 1.15 (s, 3H) ppm.

^{13}C NMR (101 MHz, $CDCl_3$): δ 170.7 (C=O), 134.4 (C), 131.7 (C), 124.5 (CH), 120.4 (CH), 94.4 (CH), 82.6 (C), 73.6 (CH), 73.3 (CH), 70.2 (CH), 63.6 (CH_2), 40.8 (CH), 38.0 (CH_2), 31.1 (CH_2), 29.8 (CH_2), 26.6 (CH_2), 25.9 (CH_3), 23.5 (CH_3), 22.1 (CH_2), 21.1 (CH_3), 20.2 (CH_3), 17.8 (CH_3) ppm.

ATR-FTIR: 3401 (OH), 2962 (C-H), 2921 (C-H), 2854 (C-H), 1732 (C=O), 1637 (vinylic C-H), 1236 (C-O) cm^{-1}.

***R_f* =** 0.22 (50:50 EtOAc/PS, silica gel), Vanillin stain (blue).

8.2.2 Scaevola striata

Fresh *S. striata* leaves (15.76 g) were steeped in diethyl ether (300 mL). After 20 mins, the extract was decanted and filtered to remove detritus. The filtrate was concentrated under reduced pressure to afford a white waxy oil (24 mg, 0.15%).

The oil was purified by column chromatography (15:85 EtOAc/petroleum spirits, silica gel). Ursolic acid **110** was isolated as a white, waxy oil (2 mg, 4 μmol, 0.01%).

8.2.3 Scaevola caliptera

Fresh *S. caliptera* leaves (12.20 g) were steeped in diethyl ether (200 mL). After 20 mins, the extract was decanted and filtered to remove detritus. The filtrate was concentrated under reduced pressure to afford a white waxy oil (31 mg, 0.25%).

8.2.4 Scaevola albida *White Carpet*

Fresh *S. albida* "White Carpet" leaves (10.09 g) were steeped in diethyl ether (200 mL). After 20 mins, the extract was decanted and filtered to remove detritus. The filtrate was concentrated under reduced pressure to afford a white waxy oil (26 mg, 0.26%).

The oil was purified by column chromatography (1:99 MeOH/CH_2Cl_2, silica gel) to afford ursolic acid **110** as a white solid (1 mg, 2 μmol, 0.01%).

8.2.5 Scaevola aemula

Fresh *S. aemula* leaves (21.31 g) were steeped in diethyl ether (100 mL). After 20 mins, the extract was filtered to remove detritus. The filtrate was concentrated under reduced pressure to afford am off-white waxy oil (57 mg, 0.27%). Another batch of fresh *S. aemula* leaves (32.61 g) were steeped in diethyl ether (150 mL). After 20 mins, the extract was filtered to remove detritus. The filtrate was concentrated under reduced pressure to afford a yellow-white solid (68 mg, 0.21%). The two extracts were combined.

The *S. aemula* extract was triturated using MeOH and the filtrate was concentrated under reduced pressure to afford a yellow-white waxy oil (127 mg). The oil was dissolved in Et_2O (50 mL) and washed with $NaHCO_3$ solution (5%, 2 x 50 mL) and NaOH solution (5%, 2 x 50 mL). Upon addition of the $NaHCO_3$ and NaOH solutions, both the organic and aqueous layers turned green. Upon addition of the NaOH solution, a yellow-white precipitate was formed. The organic layer was vacuum filtered, but the precipitate could not be isolated

due to the small mass produced. The filtrate was dried over anhydrous $MgSO_4$ and concentrated under reduced pressure to afford an off-white oil (12 mg, 0.06% w/w).

The $NaHCO_3$ aqueous washes (100 mL) were acidified using concentrated HCl solution (32%) until the solution changed colour from green to colourless. The colourless solution was extracted using EtOAc (2 x 100 mL). The combined organic extracts were dried over anhydrous $MgSO_4$ and concentrated under reduced pressure to afford the carboxylic acids fraction as a yellow oil (21 mg). The higher mass was attributed to residual EtOAc.

The NaOH washes (100 mL) were acidified using concentrated HCl solution (32%) until the green solution turned colourless. After 5 mins, a white solid precipitated out of the solution. The acidified solution was extracted with EtOAc (2 x 100 mL). The combined organic extracts were dried over anhydrous $MgSO_4$ and concentrated under reduced pressure to afford the phenols fraction as a yellow oil (54 mg). The phenols extract was purified by column chromatography (3:97-5:95 MeOH/CH_2Cl_2, silica gel) to afford a mixture of ursolic acid **110** and oleanolic acid **116** as a white solid (5 mg, 0.01% w/w).

8.2.6 Scaevola aemula "*Purple Fandancer"*

Fresh *S. aemula* "Purple Fandancer" leaves (6.16 g) were steeped in Et_2O (150 mL). After 20 mins the extract was decanted and filtered to remove detritus. The filtrate was concentrated under reduced pressure to afford a white, waxy oil (6 mg, 0.10% w/w).

8.2.7 Scaevola aemula *"Bondi Blue"*

Fresh *S. aemula* "Bondi Blue" leaves (3.84 g) were steeped in Et_2O (150 mL). After 20 mins the extract was decanted and filtered to remove detritus. The filtrate was concentrated under reduced pressure to afford a white, waxy oil (3 mg, 0.09% w/w).

8.2.8 Goodenia varia

Fresh *G. varia* leaves (28.11 g) were steeped in Et_2O (150 mL). After 20 mins, the extract was filtered to remove detritus. The filtrate was concentrated under reduced pressure to afford a white solid (430 mg, 1.53% w/w). The extract was triturated with EtOAc (50 mL) and the residue was isolated as an off-white solid (37 mg, 0.08 mmol, 0.13% w/w), which was confirmed to be ursolic acid **110**.

The EtOAc solution was washed with $NaHCO_3$ solution (5%, 2 x 50 mL) and NaOH solution (5%, 2 x 50 mL). The NaOH solution turned bright yellow upon mixing with the

EtOAc solution. The $NaHCO_3$ and NaOH solution washes were set aside. The organic layer was dried over anhydrous $MgSO_4$ and concentrated under reduced pressure to afford the neutrals fraction as an off-white solid (206 mg). The solid was purified by flash chromatography (5:95-50:50 EtOAc/PS, silica gel) to give the beyerene **120** as a colourless oil (29 mg, 0.08 mmol, 0.10%), the beyerene **121** as a white solid (14 mg, 0.05 mmol, 0.05%), ursolic acid **110** as a white solid (41 mg, 0.09 mmol, 0.15% w/w) and a mixture of beyerenes **123** and **122**. Beyerenes **123** and **122** were further purified by column chromatography (5:95-10:90 EtOAc/PS, silica gel) to afford beyerene **123** as a colourless oil (2 mg, 0.01 mmol 0.01% w/w) and beyerene **122** as a colourless oil (< 1 mg).

The combined $NaHCO_3$ washes were acidified using HCl (36%) until the solution turned cloudy white and effervescence ceased. The acidified solution was extracted with CH_2Cl_2 (2 x 100 mL). The combined organic extracts were dried over anhydrous $MgSO_4$ and concentrated under reduced pressure to afford beyerene **117** as a pale white oil (16 mg, 0.06% w/w).

The combined NaOH washes were acidified using HCl (36%) until the solution turned a dull yellow colour and a yellow solid precipitated. The acidified solution was extracted with CH_2Cl_2 (2 x 100 mL). The combined organic extracts were dried over anhydrous $MgSO_4$ to afford a transparent yellow solution. The solution was suspected to contain residual HCl and was diluted further with EtOH (100 mL) to form an azeotrope with water. The solution was concentrated under reduced pressure to afford the phenols fraction as a yellow oil (91 mg). The oil was purified by flash chromatography (20:80-50:50 EtOAc/PS, silica gel) to afford beyerene **124** as a colourless oil (10 mg, 0.04% w/w).

Malonic acid ester beyerene 117:

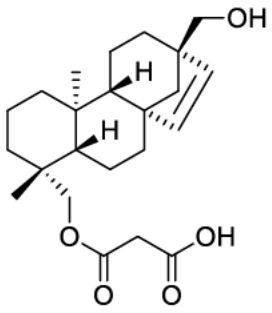

117

^{1}H NMR (400 MHz, $CDCl_3$): δ 5.78 (d, *J* = 5.6 Hz, 1H), 5.58 (d, *J* = 5.6 Hz, 1H), 4.37 (d, *J* = 10.8 Hz, 1H), 3.99 (d, *J* = 10.8 Hz, 1H), 3.55 (d, *J* = 10.8 Hz, 1H), 3.46 (d, *J* = 10.8 Hz, 1H), 3.42 (s, 2H), 1.74-1.57 (m, 6H), 1.51-1.44 (dt, *J* = 3.6, 13.6 Hz, 1H), 1.44-1.34 (m, 4H), 1.30-1.21 (m, 2H), 1.09-0.98 (m, 5H), 0.96 (s, 3H), 0.90-0.82 (m, 2H), 0.75 (s, 3H) ppm.

^{13}C NMR (101 MHz, $CDCl_3$): δ 170.5 (C=O), 168.6 (C=O), 137.1 (CH), 132.2 (CH), 69.0 (CH_2), 68.7 (CH_2), 56.8 (CH), 55.6 (CH_2), 53.4 (CH), 50.1 (C), 48.7 (C), 41.7 (CH_2), 39.0 (CH_2), 37.4 (C), 37.4 (C), 37.2 (CH_2), 36.3 (CH_2), 27.8 (CH_2), 27.5 (CH_3), 20.2 (CH_2), 19.9 (CH_2), 18.2 (CH_2), 15.8 (CH_3) ppm.

ATR-FTIR: 3460 (OH, s, br), 3460 – 2400 (COOH, s, br), 3046 (vinylic CH, w), 2924 (aliphatic CH, s), 2851 (aliphatic CH, s), 1717 (C=O, s), 1155 (C-O, m) cm^{-1}.

***R*$_f$ =** 0.20 (10:90 MeOH/CH_2Cl_2, silica gel), Vanillin stain (purple).

Acetate beyerene 120:

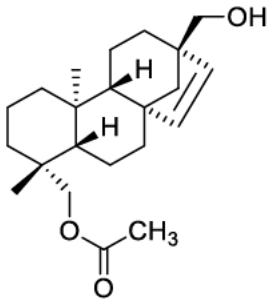

120

^{1}H NMR (400 MHz, $CDCl_3$): δ 5.77 (d, *J* = 5.6 Hz, 1H), 5.57 (d, *J* = 5.6 Hz, 1H), 4.23 (d, *J* = 11.2 Hz, 1H), 3.87 (dd, *J* = 1.6, 11.2 Hz, 1H), 3.53 (d, *J* = 10.8 Hz, 1H), 3.44 (d, *J* = 10.8 Hz, 1H), 2.03 (s, 3H), 1.73-1.52 (m, 6H), 1.47 (dt, *J* = 15.2 Hz, 1H), 1.44-1.33 (m, 4H), 1.29-1.22 (m, 2H), 1.07-0.92 (m, 4H), 0.94 (s, 3H), 0.89 (m, 1H), 0.74 (s, 3H) ppm.

^{13}C NMR (101 MHz, $CDCl_3$): δ 171.6 (C=O), 137.1 (CH), 132.1 (CH), 68.7 (CH_2), 67.2 (CH_2), 56.8 (CH), 55.6 (CH_2), 53.5 (CH), 50.1 (C), 48.7 (C) 39.1 (CH_2), 37.5 (C), 37.4 (C), 37.0 (CH_2), 36.3 (CH_2), 27.9 (CH_2), 27.6 (CH_3), 21.1 (CH_3), 20.2 (CH_2), 19.8 (CH_2), 18.3 (CH_2), 15.8 (CH_3) ppm.

ATR-FTIR: 3420 (OH, s br), 3050 (vinylic C-H, w), 2932 (aliphatic C-H, s), 2848 (aliphatic C-H, s), 1737 (C=O, s), 1720 (C=O), 1238 (C-O, s) cm^{-1}.

HRMS (ESI): $C_{22}H_{34}O_3$ $[M+H]^+$ requires 347.2581 *m/z*, found 347.2581 *m/z*.

Diol beyerene 121:

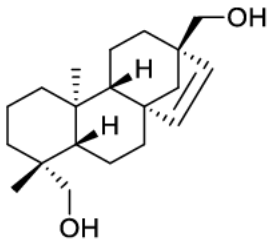

121

^{1}H NMR (400 MHz,$CDCl_3$): δ 5.79 (d, *J* = 6.0 Hz, 1H), 5.57 (d, *J* = 6.0 Hz, 1H), 3.77 (d, *J* = 10.8 Hz, 1H), 3.54 (d, *J* = 10.8 Hz, 1H), 3.45 (d, *J* = 10.8 Hz, 1H), 3.44 (dd, *J* = 1.2, 10.8 Hz, 1H), 1.79 (dddd, *J* = 1.6, 3.2, 13.6 Hz, 1H), 1.71-1.54 (m, 5H), 1.54-1.44 (m, 1H), 1.44-1.30 (m, 4H), 1.30-1.23 (m, 2H), 1.09-0.96 (m, 3H), 0.97 (s, 3H), 0.96-0.84 (m, 2H), 0.73 (s, 3H) ppm.

^{13}C NMR (101 MHz, $CDCl_3$): δ 137.3 (CH), 132.1 (CH), 68.8 (CH_2), 65.7 (CH_2), 56.9 (CH), 55.6 (CH_2), 53.6 (CH), 50.1 (C), 48.8 (C), 39.3 (CH_2), 38.6 (C), 37.6 (C), 37.4 (CH_2), 35.7 (CH_2), 27.9 (CH_2), 27.2 (CH_3), 20.3 (CH_2), 19.9 (CH_2), 18.4 (CH_2), 15.9 (CH_3) ppm.

ATR-FTIR: 3361 (OH, br), 3050 (vinylic CH, w), 2925 (aliphatic CH, s), 2848 (aliphatic CH, s), 1687, 1029 (C-O) cm^{-1}.

HRMS (ESI): $C_{20}H_{32}O_2$ $[M+H]^+$ requires 305.2475 *m/z*, found 305.2471 *m/z*.

$[\alpha]_D^{26}$ = +38.7° (*c*. 0.90, $CHCl_3$).

Erythroxylol A 122:

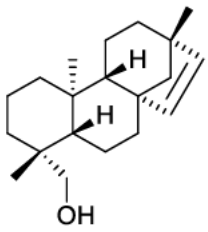

122

^{1}H NMR (400 MHz, $CDCl_3$): δ 5.65 (d, *J* = 5.6 Hz, 1H), 5.45 (d, *J* = 5.6 Hz, 1H), 3.77 (d, *J* = 11.2 Hz, 1H), 3.44 (d, *J* = 11.2 Hz, 1H), 1.78 (ddt, *J* = 1.6, 13.6 Hz, 1H), 1.66-1.59 (m, 3H), 1.53-1.46 (m, 3H), 1.46-1.42 (m, 2H), 1.40-1.32 (m, 2H), 1.32-1.27 (m, 3H), 1.24-1.21 (m, 1H), 0.99 (s, 3H), 0.97 (s, 3H), 0.95-0.82 (m, 3H), 0.72 (s, 3H) ppm.

ATR-FTIR: 3353 (OH, br, s), 3045 (vinylic CH, w), 2922 (aliphatic CH, s), 2846 (aliphatic CH, s), 1024 (C-O, m) cm^{-1}.

HRMS (ESI): $C_{20}H_{32}O$ $[M+H]^+$ requires 289.2526 *m/z*, found 289.2524 *m/z*.

***R*$_f$ =** 0.32 (15:85 EtOAc/PS, silica gel), Vanillin stain (dark blue).

***Ent*-beyere-15-en-19-oic acid 123:**

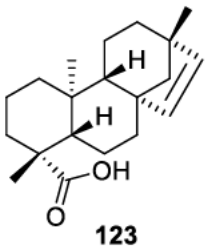

123

^{1}H NMR (400 MHz, $CDCl_3$): δ 5.73 (d, *J* = 5.6 Hz, 1H), 5.46 (d, *J* = 5.6 Hz, 1H), 2.15 (d, *J* = 13.6 Hz, 1H), 1.86-1.76 (m, 3H), 1.72-1.63 (m, 2H), 1.57-1.50 (m, 1H), 1.48-1.37 (m, 2H), 1.33-1.21 (m, 4H), 1.24 (s, 3H), 1.14-1.08 (m, 1H), 1.03-0.92 (m, 3H), 1.00 (s, 3H), 0.89-0.85 (m, 1H) 0.67 (s, 3H) ppm.

ATR-FTIR: 3400-2400 (COOH, br, m), 3042 (vinylic CH, w), 2946 (aliphatic CH, s), 2923 (aliphatic CH, s), 2846 (aliphatic CH, s), 1692 (C=O, s), 1255 (C-O) cm^{-1}.

HRMS (ESI): $C_{20}H_{30}O_2$ $[M+H]^+$ requires 303.2319 *m/z*, found 303.2319 *m/z*.

***R*$_f$ =** 0.41 (15:85 EtOAc/PS, silica gel), Vanillin stain (dark blue).

***Ent*-17-hydroxybeyer-15-en-19-oic acid 124:**

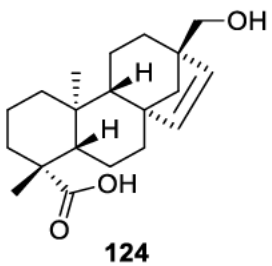

124

^{1}H NMR (400 MHz, $CDCl_3$): δ 5.87 (d, *J* = 5.6 Hz, 1H), 5.58 (d, *J* = 5.6 Hz, 1H), 3.55 (d, *J* = 10.8 Hz, 1H), 3.46 (d, *J* = 10.8 Hz, 1H), 2.15 (d, *J* = 12.4 Hz, 1H), 1.88-1.76 (m, 2H), 1.74-1.66 (m, 2H), 1.66-1.59 (m, 2H), 1.42 (app dt, *J* = 12.8 Hz, 1H), 1.38-1.22 (m, 5H), 1.25 (s, 3H), 1.12 (m, 1H), 1.07-0.96 (m, 3H), 0.90 (m, 1H), 0.68 (s, 3H) ppm.

^{13}C NMR (101 MHz, $CDCl_3$): δ 183.7 (C=O), 137.0 (CH), 132.1 (CH), 68.7 (CH_2), 57.1 (CH), 55.5 (CH_2), 52.9 (CH), 50.1 (C), 48.9 (C), 43.9 (C), 39.6 (CH_2), 38.1 (C), 38.0 (CH_2), 37.5 (CH_2), 29.3 (CH_3), 27.8 (CH_2), 21.7 (CH_2), 20.0 (CH_2), 19.3 (CH_2), 13.9 (CH_3) ppm.

ATR-FTIR: 3361 (OH, br, m), 3400-2400 (COOH, br, m), 3047 (vinylic CH, w), 2935 (aliphatic CH, s), 2848 (aliphatic CH, s), 1692 (C=O, s), 1162 (C-O, m) cm^{-1}.

HRMS (ESI): $C_{20}H_{30}O_3$ $[M+H]^+$ requires 319.2268 *m/z*, found 319.2269 *m/z*.

R_f = 0.38 (50:50 EtOAc/PS, silica gel), Vanillin stain (blue/grey).

8.2.9 Preparation of diazomethane in ether

A solution of KOH (400 mg, 7.13 mmol) in deionised water (1 mL) was prepared in a scratch-free conical flask and allowed to cool to room temperature. Et_2O (20 mL) was added to the KOH solution and the mixture was stirred at 0ºC. *N*-Nitroso-*N*-methylurea (420 mg, 4.07 mmol) was added in portions to the stirred mixture. A yellow colour was formed upon addition of the *N*-nitroso-*N*-methylurea.

A separate scratch-free conical flask was prepared with KOH pellets (300 mg, 5.35 mmol). The ether layer of the ethereal diazomethane solution was decanted into the new conical flask. Additional Et_2O (10 mL) was added to the remaining aqueous KOH and the Et_2O layer was decanted again into the new flask and kept at 0ºC until used.

8.2.10 Methyl esterification of **Goodenia varia** *carboxylic acids fraction*

Ethereal diazomethane solution was added dropwise to a stirred solution of beyerene **117** (16 mg, 0.04 mmol) in Et_2O (20 mL) at 0ºC using a flame polished pipette until the yellow colour persisted. After 1 hour, the reaction was quenched with glacial AcOH (0.5 mL). Upon addition of the glacial AcOH, the reaction mixture turned from yellow to colourless. The solution was diluted with Et_2O (20 mL) and washed with $NaHCO_3$ solution (5%, 3 x 40 mL). The organic layer was dried over anhydrous $MgSO_4$ and concentrated under reduced pressure to afford a colourless oil (9 mg). The oil was purified by column chromatography to afford beyerene methyl ester **118** as a colourless oil (3 mg, 7 μmol, 17%).

Malonic methyl ester beyerene 118:

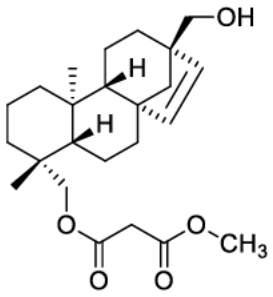

118

^{1}H NMR (400 MHz,$CDCl_3$): δ 5.78 (d, *J* = 5.6 Hz, 1H), 5.58 (d, *J* = 5.6 Hz, 1H), 4.35 (d, *J* = 11.2 Hz, 1H), 3.96 (dd, *J* = 1.2, 11.2 Hz, 1H), 3.75 (s, 3H), 3.54 (d, *J* = 10.8 Hz, 1H), 3.45 (d, *J* = 10.8 Hz, 1H), 3.38 (s, 2H), 1.72-1.53 (m, 6H), 1.49 (dt, *J* = 14.0 Hz, 1H), 1.45-1.34 (m, 4H), 1.34-1.22 (m, 2H), 1.09-0.96 (m, 4H), 0.95 (s, 3H), 0.89 (td, *J* = 4, 13 Hz, 1H) 0.75 (s, 3H) ppm.

^{13}C NMR (101 MHz, $CDCl_3$): δ 161.2 (C=O), 166.8 (C=O), 137.1 (CH), 132.2 (CH), 68.8 (CH_2), 68.5 (CH_2), 56.8 (CH), 55.6 (CH_2), 53.5 (CH), 52.6 (CH_3), 50.1 (C), 48.7 (C), 41.7 (CH_2), 39.0 (CH_2), 37.5 (C), 37.4 (C), 37.2 (CH_2), 36.3 (CH_2), 27.9 (CH_2), 27.5 (CH_3), 20.3 (CH_2), 19.9 (CH_2), 18.3 (CH_2), 15.8 (CH_3) ppm.

ATR-FTIR: 3434 (OH, br, m), 3044 (vinylic CH, w), 2930 (aliphatic CH, s), 2849 (aliphatic CH, s), 1752 (C=O, s), 1734 (C=O, s), 1150 (C-O, m) cm^{-1}.

HRMS (ESI): $C_{24}H_{36}O_5$ $[M+H]^+$ requires 405.2636 *m/z*, found 405.2631 *m/z*.

R_f = 0.19 (30:70 EtOAc/PS, silica gel), Vanillin stain (purple).

8.3 Chapter 3

8.3.1 Sample preparation for Raman spectroscopic analysis of surface resin

The top half of the *S. crassifolia* leaves were removed, because the leaves had greater rigidity closer to the stem (Figure 8.1). The cut leaves were flash-frozen in liquid nitrogen and the stem was embedded in OCT. Serial 10 μm thick sections were cut perpendicular to the stem with a cryo-microtome at -18ºC and placed on regular glass slides.

Figure 8.1. Cut *S. crassifolia* leaf.

8.3.2 Sample preparation for Raman spectroscopic analysis of internal leaf tissue

The top half and bottom portion including the stem of the *S. crassifolia*, *D. viscosa* or *G. varia* leaves were removed. The sides of the leaf section were also removed to create a rectangular leaf section that is approximately 0.5 cm in height and 1 cm in width. The cut leaves were attached to the chuck of the cryomicrotome using OCT perpendicular to the chuck. OCT was then layered on the leaf and allowed to freeze, until the entire leaf was covered. Serial 30-50 μm thick sections were cut perpendicular to the chuck with a cryo-microtome at -18ºC and placed on regular glass slides.

8.3.3 Raman mapping of surface leaf resin

Raman spectroscopic maps were collected with a WITec Alpha 300 SAR instrument. Maps were collected with 532 nm excitation with a 100x objective and a 200 nm laser spot. Raman maps collected with 0.25 μm steps and 80 ms dwell time per pixel. Raman spectroscopic false colour images of the caryophyllene distribution were generated from the area under the curve of strained C = C stretching bands (centred at 1667 cm^{-1}), with linear baseline subtraction (1690-1660 cm^{-1}). False colour images of the phenol distribution were determined from the area under the curve of the aromatic C = C stretching bands, with linear baseline subtraction (1620-1590 cm^{-1}). Project 4 WITec Suite 4.0 software was used for Raman spectral analysis and image generation.

8.3.4 Raman mapping of onion epidermal cells

Maps were collected with 532 nm excitation with a 20x objective and a 200 nm laser spot. Raman maps were collected with 1.00 μm steps and 300 ms dwell time per pixel. Raman spectroscopic false colour images of pectin distribution were generated from the area under the curve of C-O-C skeletal mode centred across 840-880 cm^{-1}, with linear baseline subtraction. Raman spectroscopic false colour images of pectin distribution were generated from the area under the curve of CH_2 bending centred across 1440-1480 cm^{-1}, with linear baseline subtraction. Project 4 WITec Suite 4.0 software was used for Raman spectral analysis and image generation.

8.3.5 Raman mapping of internal leaf tissue

Maps were collected with 532 nm excitation with a 100x objective and a 200 nm laser spot. Raman maps were collected with 0.25 μm steps and 100-300 ms dwell time per pixel. Raman spectroscopic false colour images of polysaccharide distribution were generated from the area under the curve of C-O-C stretching bands centred across 940-980 cm^{-1}, with linear baseline subtraction. Raman spectroscopic false colour images of phenylalanine distribution were generated from the area under the curve of C_1-C_2-C_3 angular bending bands centred across 980-1020 cm^{-1}, with linear baseline subtraction. Raman spectroscopic false colour images of fatty acid/lipid distribution were generated from the area under the curve of skeletal C-C stretching bands centred across 1080-1120 cm^{-1}, with linear baseline subtraction. Project 4 WITec Suite 4.0 software was used for Raman spectral analysis and image generation.

8.3.6 3D Raman mapping of internal leaf tissue

Maps were collected with 532 nm excitation with a 100x objective and a 200 nm laser spot. Raman maps were collected with 0.25-0.5 μm steps, 1 μm layer step and 200-300 ms dwell time per pixel. Raman spectroscopic false colour images of polysaccharide distribution were generated from the area under the curve of C-O-C stretching bands centred across 940-980 cm^{-1}, with linear baseline subtraction. Raman spectroscopic false colour images of phenylalanine distribution were generated from the area under the curve of C_1-C_2-C_3 angular bending bands centred across 980-1020 cm^{-1}, with linear baseline subtraction. Raman spectroscopic false colour images of fatty acid/lipid distribution were generated from the area under the curve of skeletal C-C stretching bands centred at 1080-1120 cm^{-1}, with linear baseline subtraction. Raman spectroscopic false colour images of

cellulose/hemicellulose distribution were generated from the area under the curve of skeletal C-H stretching bands centred across 2900-2950 cm^{-1}, with linear baseline subtraction. Project 4 WITec Suite 4.0 software was used for Raman spectral analysis and image generation.

8.3.7 Synchrotron FTIR mapping

Synchrotron FTIR mapping of biomolecule distribution in 50 μm thick *S. crassifolia* tissue sections was completed at the Australian Synchrotron infrared microspectroscopy beamline. Data were collected in transmission mode with a Bruker Vertex 80v FTIR spectrometer, with a 36x objective and a liquid nitrogen-cooled mercury cadmium telluride detector. Maps were collected with an aperture beam of spot of ~6 μm and a step size of 3 μm.

FTIR spectra were analysed with Cytospec version 2.00.03 and OPUS version 7.0. FTIR false colour images of lipid distribution were generated from the area under the curve of the C-H stretching band (2800-3000 cm^{-1}). FTIR false colour images of the distribution of carbonyl containing compounds including aldehydes, ketones and esters were generated from the area under the curve of C=O stretching bands (1710-1760 cm^{-1}). FTIR false colour images of the distribution of proteins were generated from the area under the curve of amide C=O stretching bands (1620-1680 cm^{-1}). FTIR false colour images of the distribution of phenylalanine were generated from the area under the curve of aromatic C=C stretching bands (1500-1550 cm^{-1}). FTIR false colour images of the distribution of protein storage vacuoles were generated from the area under the curve of amine N-H stretching bands (3500-3600 cm^{-1}).

8.4 Chapter 4

8.4.1 Extraction and isolation of compounds from Port Beach Scaevola crassifolia

Fresh *S. crassifolia* leaves (436.9 g) were collected from Port Beach, North Fremantle, Western Australia on the 27th of April 2020. The fresh leaves were steeped in Et_2O (1 L). After 20 mins, the ether extract was decanted and filtered to remove detritus. The filtrate was concentrated under reduced pressure to afford the resin as a yellow oil (9.039 g, 2.1% w/w).

The resin was dissolved in EtOAc (300 mL) and washed with HCl (1M, 2 x 300 mL). The green aqueous washes were combined and set aside. The organic layer was washed with $NaHCO_3$ solution (5%, 2 x 300 mL). The orange aqueous washes were then set aside. The organic layer was washed with NaOH solution (5%, 2 x 300 mL). Upon addition of the NaOH solution, both organic and aqueous layers turned dark red in colour. The dark red aqueous washes were combined and set aside. The organic layer was dried over anhydrous $MgSO_4$ and concentrated under reduced pressure to afford the neutrals fraction as a yellow oil (2.778 g, 0.64% w/w).

The neutrals fraction was purified using automated column chromatography (1:99-100:0 EtOAc/PS, silica gel). 12-Hydroxycaryophyllene **60** eluted with 6:94 EtOAc/PS and was afforded as a white oil (106 mg, 0.48 mmol, 0.02% w/w). 6-Hydroxycaryophyllene **1** eluted with 6:94 EtOAc/PS and was afforded as a yellow tinged oil (422 mg, 1.92 mmol, 0.10% w/w). 12-Acetoxy-6-hydroxycaryophyllene **2** eluted with 10:90 EtOAc/PS and was afforded as a cloudy yellow oil (689 mg, 2.48 mmol, 0.16% w/w). Ursolic acid **110** eluted with 20:80 EtOAc/PS and was afforded as a yellow solid (94 mg, 0.21 mmol, 0.02% w/w). 6,12-Dihydroxycaryophyllene **3** eluted with 30:70 EtOAc/PS and was afforded as a yellow oil that started to crystallise into white crystals (218 mg, 0.92 mmol, 0.05% w/w).

The aqueous HCl extracts were basified using solid NaOH pellets until the solution turned amber in colour. The amber solution was extracted with EtOAc (2 x 300 mL). The combined organic extracts were dried over anhydrous $MgSO_4$ and concentrated under reduced pressure to afford the amines fraction as a yellow oil (29 mg, 0.01% w/w).

The combined aqueous $NaHCO_3$ solution washes were acidified using concentrated HCl (32%) until the solution turned light yellow-green in colour. The acidified solution was extracted with EtOAc (2 x 300 mL). The combined organic extracts were dried over

anhydrous $MgSO_4$ and concentrated under reduced pressure to the carboxylic acids fraction afford a yellow oil (954 mg, 0.22% w/w).

The combined aqueous NaOH washes were acidified using concentrated HCl (32%) until the solution turned cloudy orange in colour. The acidified mixture was extracted using EtOAc (2 x 300 mL). The combined organic extracts were dried over anhydrous $MgSO_4$ and concentrated under reduced pressure to afford the phenols fraction as a red oil (4.524 g, 1.04% w/w).

The phenols fraction was purified by column chromatography (1:99-10:90 MeOH/CH_2Cl_2, silica gel) giving a mixture of flavanones **138** and **139** as a yellow solid (62 mg, 0.17 mmol, 0.01% w/w) and a mixture of flavone **141** with other compounds as a yellow solid (568 mg). Flavone **141** was further purified by column chromatography (1:99-5:95 MeOH/CH_2Cl_2, silica gel) giving flavone **141** as a yellow solid (51 mg, 0.14 mmol, 0.01% w/w).

Flavanone 139

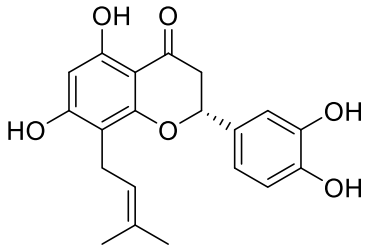

139

Spectroscopic data matched that of Fukai *et al*.[129]

^{1}H NMR (400 MHz, Acetone-d_6): δ 12.14 (s, 1H), 7.06 (d, *J* = 2.0 Hz, 1H), 6.88 (dd, *J* = 1.6 Hz, 1H) 6.87 (s, 1H), 6.02 (s, 1H), 5.39 (dd, *J* = 3.2, 12.4 Hz, 1H), 5.19 (t, *J* = 7.2 Hz, 1H), 3.22 (d, *J* = 7.2 Hz, 2H), 3.09 (dd, *J* = 12.4, 13.2 Hz, 1H), 2.75 (dd, *J* = 3.2, 17.2 Hz, 1H), 1.61 (s, 6H) ppm.

^{13}C NMR (101 MHz, Acetone-d_6): δ 197.5 (C=O), 164.9 (C), 162.9 (C), 161.0 (C), 146.2 (C), 146.0 (C), 131.9 (C), 131.2 (C), 123.6 (CH), 119.0 (CH), 116.0 (CH), 114.6 (CH), 108.3 (C), 103.3 (C), 96.3 (CH), 79.7 (CH), 43.5 (CH_2), 25.9 (CH_3), 22.3 (CH_2), 17.9 (CH_3) ppm.

ATR-FTIR: 3424 (OH), 3267 (OH), 3066 (aromatic CH), 3048 (aromatic CH), 3032 (aromatic CH), 1985 (aliphatic CH), 2963 (aliphatic CH), 2926 (aliphatic CH), 2853 (aliphatic CH), 1598 (C=O) cm^{-1}.

***R*f =** 0.50 (10:90 MeOH/CH_2Cl_2, silica gel), Vanillin stain (pink/red).

Flavone 141

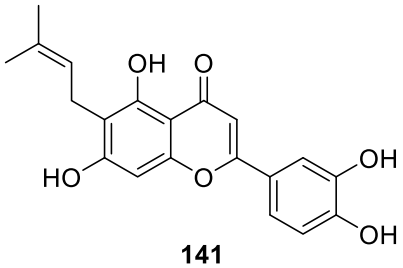

141

Spectroscopic data matched that of Kajiyana *et al*.[114]

^{1}H NMR (400 MHz, Acetone-*d*$_6$): δ 13.30 (s, 1H), 7.49 (d, *J* = 2.4 Hz, 1H), 7.46 (ddd, *J* = 0.8, 2.4, 8.4 Hz, 1H), 7.00 (d, *J* = 8.4 Hz, 1H), 6.59 (d, *J* = 1.6 Hz, 1H), 6.57 (d, *J* = 1.6 Hz, 1H), 5.28 (app tquint, *J* = 1.2, 2.8, 7.2 Hz, 1H), 3.35 (d, *J* = 7.2 Hz, 1H), 1.78 (d, *J* = 1.2 Hz, 3H), 1.65 (d, *J* = 1.2 Hz, 3H) ppm.

^{13}C NMR (101 MHz, Acetone-*d*$_6$): δ 183.1 (C=O), 164.8 (C), 162.4 (C), 160.1 (C), 156.5 (C), 149.9 (C), 146.4 (C), 131.6 (C), 123.9 (C), 123.2 (CH), 120.1 (CH), 116.6 (CH), 114.0 (CH), 112.3 (C), 105.2 (C), 104.1 (CH), 94.0 (CH), 25.9 (CH_3), 22.0 (CH_2), 17.9 (CH_3) ppm.

ATR-FTIR: 3490 (OH), 3406 (OH), 2958 (aliphatic CH), 2923 (aliphatic CH), 2855 (aliphatic CH), 1604 (C=O), 1260 (C-O) cm^{-1}.

12-Hydroxycaryophyllene 60

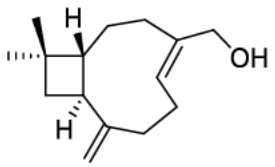

60

Spectroscopic data matched that of Barrero *et al.*[48b]

βα ^{1}H NMR (400 MHz, $CDCl_3$): δ 5.45 (dd, *J* = 5.6, 10.8 Hz, 1H), 4.94 (s, 1H), 4.77 (s, 4.77), 4.17 (d, *J* = 12.4 Hz, 1H), 3.93 (d, *J* = 12.4 Hz, 1H), 2.52-2.25 (m, 4H), 2.25-2.09 (m, 3H), 2.09-1.96 (m, 3H), 1.88-1.72 (m, 3H), 1.71-1.38 (m, 7H), 0.99/0.98 (s, 3H), 0.97 (s, 3H) ppm.

ββ ^{1}H NMR (400 MHz, $CDCl_3$): δ 5.37 (d, *J* = 12.0 Hz, 1H), 5.06 (s, 1H), 4.89 (s, 1H), 4.12 (d, *J* = 11.6 Hz, 1H), 3.69 (d, *J* = 11.6 Hz, 1H), 2.52-2.25 (m, 4H), 2.25-2.09 (m, 3H), 2.09-1.96 (m, 3H), 1.88-1.72 (m, 3H), 1.71-1.38 (m, 7H), 0.99/0.98 (s, 3H), 0.96 (s, 3H) ppm.

βα ^{13}C NMR (101 MHz, $CDCl_3$): δ 154.0 (C), 138.0 (C), 128.9 (CH), 113.2 (CH_2), 60.3 (CH_2), 50.4 (CH), 49.8 (CH), 40.7 (CH_2), 35.0 (CH_2), 33.9 (CH_2), 33.0 (C), 30.2 (CH_3), 30.1 (CH_2), 29.3 (CH_2), 22.2 (CH_3) ppm.

ββ ^{13}C NMR (101 MHz, $CDCl_3$): δ 159.0 (C), 137.8 (C), 129.6 (CH), 110.2 (CH_2), 62.1 (CH_2), 57.0 (CH), 49.2 (CH), 42.7 (CH_2), 40.4 (CH_2), 33.0 (C), 30.7 (CH_2), 30.6 (CH_2), 29.8 (CH_3), 29.3 (CH_2), 22.0 (CH_3) ppm.

ATR-FTIR: 3411 (OH), 3055 (vinylic CH), 2928 (aliphatic CH), 2855 (aliphatic CH), 1631 (exocyclic C=C), 1265 (C-O) cm^{-1}.

6-Hydroxycaryophyllene 1

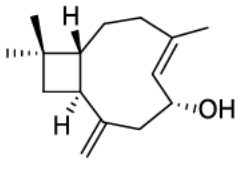

1

Spectroscopic data matched that of Clericuzio *et al.*[48a]

^{1}H NMR (400 MHz, $CDCl_3$): δ 5.25 (dt, *J* = 2.0, 10.0 Hz, 1H), 4.97 (s, 1H), 4.86 (s, 1H), 4.56 (ddd, *J* = 6.8, 10.0 Hz, 1H), 2.75 (dd, *J* = 6.4, 11.6, 1H), 2.51 (br dd, *J* = 6.8, 14.4 Hz,

1H), 2.30 (app q, *J* = 9.2 Hz, 1H), 1.94 (app t, *J* = 10.4 Hz, 1H), 1.76 (dd, *J* = 8.4, 10.8 Hz, 1H), 1.64 (m, 1H), 1.60 (s, 3H), 1.58 (m, 2H), 1.55 (m, 1H), 1.42 (app t, *J* = 9.2 Hz, 1H), 0.95 (s, 3H), 0.94 (s, 3H) ppm.

^{13}C NMR (101 MHz, $CDCl_3$): δ 150.2 (C), 137.0 (C), 128.0 (CH), 112.5 (CH_2), 70.8 (CH), 55.6 (CH), 49.3 (CH_2), 49.0 (CH_2), 42.3 (CH_2), 34.9 (CH_2), 32.9 (C), 31.3 (CH_2), 30.0 (CH_3), 23.1 (CH_3), 22.0 (CH_3) ppm.

ATR-FTIR: 3326 (OH), 3068 (vinylic CH), 2952 (aliphatic CH), 2927 (aliphatic CH), 1856 (aliphatic CH), 1672 (endocylic C=C), 1636 (C=C), 1025 (C-O) cm^{-1}.

R_f = 0.20 (10:90 EtOAc/PS, silica gel), Vanillin stain (blue).

$[\alpha]_D^{23}$ = -43.0 (c 1.00, $CDCl_3$).

12-Acetoxy-6-hydroxycaryophyllene 2

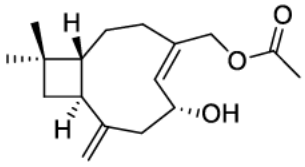

2

^{1}H NMR (400 MHz, $CDCl_3$): δ 5.46 (d, *J* = 10.4 Hz, 1H), 4.98 (s, 1H), 4.85 (s, 1H), 4.69 (d, *J* = 12.0 Hz, 1H), 4.58 (td, *J* = 6.8, 10.0 Hz, 1H), 4.17 (d, *J* = 12.4 Hz, 1H), 2.75 (dd, *J* = 6.8, 11.6 Hz, 1H), 2.38 (m, 1H), 2.18 (app q, *J* = 9.2 Hz, 1H), 2.00 (s, 3H), 1.92 (app t, *J* = 10.4 Hz, 1H), 1.79 (m, 2H), 1.69 – 1.49 (m, 3H), 1.42 (m, 1H), 0.94 (s, 3H), 0.93 (s, 3H) ppm.

^{13}C NMR (101 MHz, $CDCl_3$): δ 171.2 (C=O), 150.6 (C), 133.9 (C), 133.7 (CH), 112.8 (CH_2), 69.8 (CH), 65.4 (CH_2), 55.6 (CH), 48.8 (CH), 48.8 (CH_2), 42.3 (CH_2), 32.9 (C), 31.2 (CH_2), 29.9 (CH_3), 29.8 (CH_2), 21.8 (CH_3), 21.0 (CH_3) ppm.

ATR-FTIR: 3442 (OH), 3070 (vinylic CH), 2951 (aliphatic CH), 2930 (aliphatic CH), 2860 (aliphatic CH), 1737 (C=O), 1637 (C=C), 1233 (C-O) cm^{-1}.

HRMS (ESI): $C_{17}H_{27}O_3$ $[M+H]^+$ requires 279.1955 *m/z*, found 279.1949 *m/z*.

R_f = 0.28 (20:80 EtOAc/PS, silica gel).

$[\alpha]_D^{23}$ = +46.0 (c 1.00, MeOH).

6,12-Dihydroxycaryophyllene 3

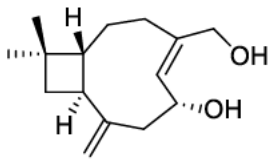

3

^{1}H NMR (400 MHz, $CDCl_3$): δ 5.37 (d, *J* = 10.0 Hz, 1H), 5.04 (s, 1H), 4.89 (s, 1H), 4.59 (m, 1H), 4.02 – 3.89 (m, 2H), 2.77 (dd, *J* = 6.4, 11.6 Hz, 1H), 2.67 (s, 2H), 2.46 (m, 1H), 2.23 (app q, *J* = 8.8 Hz, 1H), 2.01 – 1.89 (m, 2H), 1.78 (dd, *J* = 8.0, 10.8 Hz, 1H), 1.65 – 1.54 (m, 3H), 1.46 (m, 1H), 0.97 (s, 3H), 0.96 (s, 3H) ppm.

^{13}C NMR (101 MHz, $CDCl_3$): δ 153.4 (C), 138.8 (C), 131.7 (CH), 112.1 (CH_2), 70.3 (CH), 63.1 (CH_2), 56.3 (CH), 49.5 (CH_2), 48.8 (CH), 42.3 (CH_2), 33.0 (C), 30.8 (CH_2), 30.3 (CH_2), 29.9 (CH_3), 21.9 (CH_3) ppm.

ATR-FTIR: 3326 (OH), 3070 (vinylic CH), 2951 (aliphatic CH), 2928 (aliphatic CH), 2859 (aliphatic CH), 1669 (endocylic C=C), 1636 (C=C), 1023 (C-O), 1006 (C-O) cm^{-1}.

HRMS (ESI): $C_{15}H_{25}O_2$ $[M+H]^+$ requires 237.3573 *m/z*, found 237.1845 *m/z*.

R_f = 0.14 (50:50 EtOAc/PS, silica gel).

$[\alpha]_D^{23}$ = -22.5 (c 1.03, MeOH).

8.4.2 Preparation of 12-acetoxycaryophyllene 140

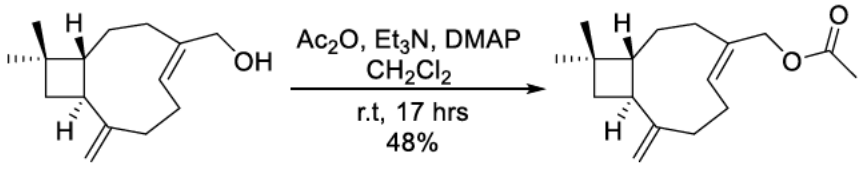

60 **140**

Ac_2O (200 µL, 2.12 mmol) was added to a solution of 12-hydroxycaryophyllene **60** (49 mg, 0.22 mmol) in dry CH_2Cl_2 (10 mL). Et_3N (300 µL, 2.15 mmol), and DMAP (~1 mg) were added and the reaction mixture was stirred at room temperature. After 17 hours, the reaction mixture was diluted with CH_2Cl_2 (20 mL). The organic solution was washed with HCl solution (1M, 2 x 50 mL), followed by $NaHCO_3$ solution (5%, 2 x 50 mL). The organic layer was dried over anhydrous $MgSO_4$ and was concentrated under reduced pressure to give a cloudy white oil (37 mg). The oil was purified by column chromatography (1:99

EtOAc/PS, silica gel) to afford 12-acetoxycaryophyllene **140** as a colourless oil (28 mg, 0.11 mmol, 49%). Spectroscopic data matched that of Barrero *et al*.[48b]

βα ^{1}H NMR (400 MHz, $CDCl_3$) δ 5.59 (dd, *J* = 5.6, 10.8 Hz, 1H), 4.96 (s, 1H), 4.81 (s, 1H), 4.68 (d, *J* = 12.0 Hz, 1H), 4.44 (d, *J* = 12.0 Hz, 1H), 2.50-2.30 (m, 5H), 2.28-2.11 (m, 4H), 2.04 (s, 3H), 2.09-1.99 (m, 2H), 1.90-1.74 (m, 4H), 1.70 (t, *J* = 10.0 Hz, 1H), 1.67-1.49 (m, 6H), 0.99 (s, 3H), 0.98 (s, 6H) ppm.

ββ ^{1}H NMR (400 MHz, $CDCl_3$) δ 5.53 (d, *J* = 12.0 Hz, 1H), 4.99 (s, 1H), 4.87 (s, 1H), 4.68 (d, *J* = 12.0 Hz, 1H), 4.31 (d, *J* = 12.0 Hz, 1H), 2.50-2.30 (m, 5H), 2.28-2.11 (m, 4H), 2.05 (s, 3H), 2.09-1.99 (m, 2H), 1.96-1.90 (m, 1H), 1.90-1.74 (m, 4H), 1.67-1.49 (m, 6H), 0.98 (s, 6H), 0.96 (s, 3H) ppm.

βα ^{13}C NMR (101 MHz, $CDCl_3$) δ 171.3 (C=O), 153.1 (C), 133.5 (C), 131.3 (CH), 113.6 (CH_2), 61.5 (CH_2). 51.4 (CH), 49.4 (CH), 40.4 (CH_2), 35.0 (CH_2), 34.2 (CH_2), 32.9 (C), 30.2 (CH_3), 29.4 (CH_2), 29.0 (CH_2), 22.4 (CH_3), 21.2 (CH_3) ppm.
ββ ^{13}C NMR (101 MHz, $CDCl_3$) δ 171.3 (C=O), 154.9 (C), 133.5 (C), 131.3 (CH), 111.6 (CH_2), 65.5 (CH_2), 56.0 (CH), 49.2 (CH), 42.7 (CH_2), 40.1 (CH_2), 32.9 (C), 30.5 (CH_2), 30.0 (CH_3), 29.7 (CH_2), 29.4 (CH_2), 22.0 (CH_3), 21.2 (CH_3) ppm.
ATR-FTIR: 3062 (vinylic CH), 2925 (aliphatic CH), 2854 (aliphatic CH), 1733 (C=O), 1631 (exocylic C=C), 1237 (C-O) cm^{-1}.

8.4.3 Optimisation of **Scaevola crassifolia** *solvent extraction*

Fresh *S. crassifolia* leaves (344.03 g) were collected in July 2020 from the grounds of Curtin University and divided into 6 portions. Each portion of the leaves was steeped in the extraction solvent for 20 mins or 24 hours. The extract was decanted and filtered to remove detritus. The filtrate was dried over anhydrous $MgSO_4$ and concentrated under reduced pressure to afford the extract. Details are provided in Table 7.1.

Table 7.1. *Leaf masses, extraction solvents and volumes and extract masses from* S. crassifolia

Mass of leaves (g)	Solvent	Solvent volume (mL)	Extraction time	Extract mass (g)	Percentage (%) Mass
55.74	PS	200	20 mins	0.162	0.29
55.59	EtOH	200	20 mins	1.245	2.24
58.12	CH_2Cl_2	200	20 mins	1.062	1.83
63.35	Deionised water	300	20 mins	0.016	0.03
64.53	Deionised water	300	24 hours	0.277	0.43
54.92	Et_2O	200	20 mins	1.356	2.47

8.4.4 Activated charcoal purification of Scaevola crassifolia *extract*

Fresh *S. crassifolia* leaves (55.56 g) were steeped in Et_2O (200 mL). The extract was decanted and filtered to remove detritus. The filtrate was concentrated under reduced pressure to afford a yellow oil (1.356 g). The oil was dissolved in Et_2O (150 mL) and activated charcoal (10.11 g) was added to the organic solution. The mixture was stirred at room temperature. After 60 mins the mixture was filtered through celite and the celite was washed with Et_2O. The combined filtrate and washes were concentrated under reduced pressure to afford a pink oil (631 mg).

The oil was dissolved in Et_2O (100 mL) and activated charcoal (5.23 g) was added to the organic solution. The mixture was stirred at room temperature. After 2 hours, the mixture was filtered through celite and the celite was washed with Et_2O. The combined filtrate and washes were dried over anhydrous $MgSO_4$ and concentrated under reduced pressure to afford a yellow oil (331 mg). The ^1H NMR showed that the yellow oil that no longer contained any phenolic compounds.

8.4.5 Preparation of birkenal 142

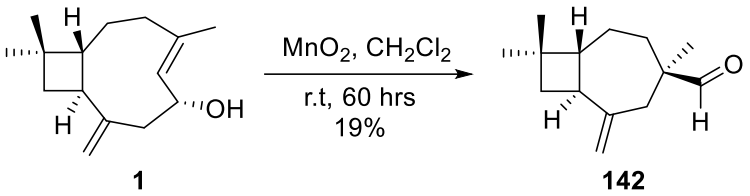

1 **142**

Activated MnO_2 (Merck, >90% activity, Batch# 8.05958.1000) (1.512 g, 17.39 mmol) was added to a solution of the 6-hydroxycaryophyllene **1** (34 mg, 0.15 mmol) in dry CH_2Cl_2 (12 mL) and the mixture was stirred at room temperature. After 60 hours, the MnO_2 was removed by filtration through celite and the celite was washed with CH_2Cl_2 (5 mL) and EtOAc (5 mL). The filtrate and washes were combined and carefully concentrated under reduced pressure without heating to afford a yellow oil (10 mg). The oil was purified by column chromatography (3:97 EtOAc/PS, silica gel) to give birkenal **142** as a colourless oil (6 mg, 0.03 mmol, 19%). Spectroscopic data matched that of Klika *et al*. and Hirokawa *et al*.[116]

^{1}H NMR (400 MHz, $CDCl_3$): δ 9.57 (s, 1H), 4.77 (br app quint, *J* = 1.2, 2.0 Hz, 1H), 4.57 (br app dd, *J* = 0.8, 2.4 Hz, 1H), 2.60 (d, *J* = 16.0 Hz, 1H), 2.46 (dq, *J* = 1.2, 16.0 Hz, 1H), 2.31 (m, 1H), 2.07 (dtd, *J* = 1.2, 4.4, 13.6 Hz, 1H), 1.82 (dd, *J* = 7.6, 10.4 Hz, 1H), 1.68 – 1.61 (m, 1H),1.60 – 1.59 (m, 1H), 1.58 – 1.54 (br m, 1H), 1.53 – 1.47 (m, 1H), 1.46 – 1.36 (m, 1H), 1.04 (s, 3H), 0.99 (s, 3H), 0.98 (s, 3H) ppm.

^{13}C NMR (101 MHz, $CDCl_3$): δ 206.4 (CHO), 150.6 (C), 107.4 (CH_2), 50.6 (CH), 48.9 (C), 44.6 (CH_2), 40.9 (CH), 38.6 (CH_2), 36.3 (CH_2), 34.7 (C), 30.4 (CH_3), 25.6 (CH_3), 25.0 (CH_2), 22.0 (CH_3) ppm.

ATR-FTIR: 3073 (vinylic CH), 2953 (aliphatic CH), 2927 (aliphatic CH), 2862 (aliphatic CH), 1725 (C=O), 1638 (C=C) cm^{-1}.

R_f = 0.58 (3:97 EtOAc/PS, silica gel).

$[\alpha]_D^{27}$ = +36.27° (*c*. 1.00, $CHCl_3$), lit. +25 (*c* = 0.004, EtOH)[116a], +39.6 (*c* = 1.00, EtOH)[116b].

8.4.6 Preparation of 4,5,6-trihydroxycaryophyllene 146

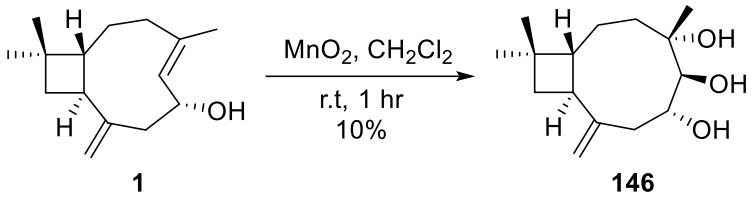

Activated MnO_2 (Merck, >90% activity, Batch# 8.05958.1000) (0.531 g, 6.11 mmol) was added to a solution of 6-hydroxycaryophyllene **1** (34 mg, 0.15 mmol) in dry CH_2Cl_2 (5 mL) and the mixture was stirred at room temperature. After 1 hour, the MnO_2 was removed by filtration through celite and the celite was washed with CH_2Cl_2 (5 mL) and EtOAc (5 mL). The filtrate and washes were combined and concentrated under reduced pressure to afford a yellow oil (31 mg). The oil was purified by column chromatography (10:90 EtOAc/PS, silica gel) to give caryophyllene triol **146** as a colourless oil (4 mg, 0.02 mmol, 10%).

^{1}H NMR (400 MHz, $CDCl_3$): δ 5.18 (s, 1H), 5.04 (s, 1H), 3.58 (td, *J* = 6.8, 10.0 Hz, 1H), 2.99 (d, *J* = 9.6 Hz, 1H), 2.82 (dd, *J* = 6.8, 12.4 Hz, 1H), 2.41 (app q, *J* = 9.6 Hz, 1H), 2.13 (m, 1H), 1.88 (dd, *J* = 8.0, 10.8 Hz, 1H), 1.77 – 1.71 (br m, 2H), 1.66 – 1.58 (br m, 1H), 1.54 – 1.44 (br m, 3H), 1.29 (s, 3H), 1.00 (s, 3H), 0.97 (s, 3H) ppm.

^{13}C NMR (101 MHz, $CDCl_3$): δ 147.7 (C), 114.4 (CH_2), 71.8 (CH), 64.6 (CH), 61.9 (C), 53.8 (CH), 47.2 (CH), 45.3 (CH_2), 42.3 (CH_2), 36.3 (CH_2), 33.2 (C), 30.0 (CH_3), 27.8 (CH_2), 23.7 (CH_3), 21.7 (CH_3) ppm.

ATR-FTIR: 3405 (OH), 3069 (vinylic CH), 2950 (aliphatic CH), 2926 (aliphatic CH), 2858 (aliphatic CH), 1637 (C=C), 1039 (C-O) cm^{-1}.

***R*$_f$ =** 0.11 (20:80 EtOAc/PS, silica gel), Vanillin stain (dark blue).

8.4.7 Preparation of 6-hydroxycaryophyllene oxide 147

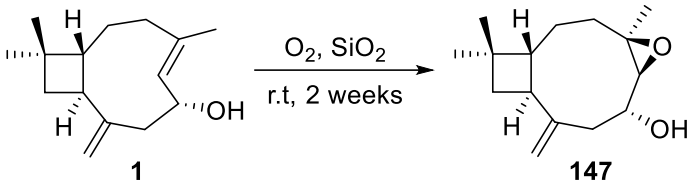

Silica gel was added to a solution of neutrals fraction (3.12 g) in 9:1 EtOAc/MeOH (200 mL). The mixture was concentrated under reduced pressure to afford a yellow solid, which was left to stand at room temperature. After two weeks, the silica adsorbed material was purified by column chromatography to afford a mixture of 6-hydroxycaryophyllene **1** and 6-hydroxycaryophyllene oxide **147** (5:95 EtOAc/PS, silica gel) as a colourless oil. The oil was further purified by column chromatography (12:88 EtOAc/PS, silica gel) to give 6-hydroxycaryophyllene oxide **147** as a colourless oil (16 mg, 0.5%).

^{1}H NMR (400 MHz, $CDCl_3$): 5.17 (s, 1H), 5.04 (d, *J* = 1.6 Hz, 1H), 4.32 (m, 1H), 2.90 (dd, *J* = 6.8, 12.8 Hz, 1H), 2.88 (d, *J* = 2.0 Hz, 1H), 2.52 (app q, *J* = 8.8 Hz, 1H), 2.05-2.03 (m, 1H), 1.96 (dd, *J* = 9.6, 11.6 Hz, 1H), 1.78 (s, 1H), 1.76 (s, 1H), 1.66-1.56 (m, 3H), 1.53 (s, 3H), 1.03-0.96 (m, 1H) 1.01 (s, 3H), 1.00 (s, 3H) ppm.

^{13}C NMR (101 MHz, $CDCl_3$): δ 147.8 (C), 114.1 (CH_2), 67.7 (CH), 64.4 (CH), 60.6 (C), 55.5 (CH), 47.1 (CH), 41.5 (CH_2), 40.4 (CH_2), 39.5 (CH_2), 33.1 (C), 30.1 (CH_3), 27.8 (CH_2), 22.6 (CH_3), 17.0 (CH_3) ppm.

ATR-FTIR: 3449 (OH), 2927 (aliphatic CH), 2858 (aliphatic CH), 1632 (C=C) cm^{-1}.

HRMS (ESI): $C_{15}H_{24}O_2$ $[M+H]^+$ requires 237.1849 *m/z*, found 237.1846 *m/z*.

8.4.8 Preparation of 12-acetoxy-4,5,6-trihydroxycaryophyllene 148

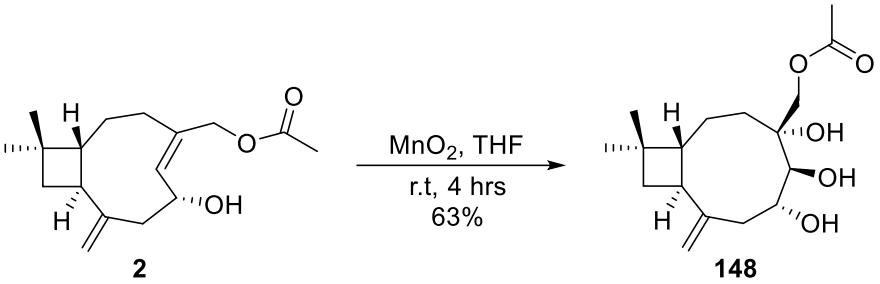

2 **148**

Activated MnO_2 (Merck, >90% activity, Batch# 8.05958.1000) (0.609 g, 7.00 mmol) was added to a solution of the caryophyllene acetate **2** (27 mg, 0.097 mmol) in dry THF (10 mL) and stirred. After 4 hours, the MnO_2 was removed by filtration through celite and the celite was washed with EtOAc (5 mL) and MeOH (5 mL). The filtrate and washes were combined and concentrated under reduced pressure to afford a white solid (21 mg). The solid was purified by flash chromatography (30:70 EtOAc/PS, silica gel) to give 12-acetoxy-4,5,6-trihydroxycaryophyllene **148** as a colourless oil (19 mg, 0.06 mmol, 63%).

^{1}H NMR (400 MHz, $CDCl_3$): δ 5.20 (s, 1H), 5.06 (s, 1H), 4.32 (d, *J* = 12.0 Hz, 1H), 3.79 (dd, *J* = 1.2, 12.0 Hz, 1H), 3.64 (td, *J* = 6.8, 10.0 Hz, 1H), 3.12 (d, *J* = 9.6 Hz, 1H), 2.83 (dd, *J* = 6.8, 12.4 Hz, 1H), 2.39 (app q, *J* = 9.2 Hz, 1H), 2.15-2.05 (m, 1H), 2.11 (s, 3H), 2.03 (dd, *J* = 2.8, 6.0 Hz, 1H), 1.90 (dd, *J* = 8.0, 10.8 Hz, 1H), 1.72 (app t, 1H), 1.66-1.58 (m, 2H), 1.57-1.40 (m, 2H), 1.01 (s, 3H), 0.98 (s, 3H) ppm.

^{13}C NMR (101 MHz, $CDCl_3$): δ 171.1 (C=O), 147.9 (C), 114.7 (CH_2), 71.4 (CH), 68.0 (CH), 64.5 (CH_2), 61.9 (C), 54.1 (CH), 47.3 (CH), 45.2 (CH_2), 42.4 (CH_2), 33.4 (C), 30.4 (CH_2), 29.9 (CH_3), 27.5 (CH_2), 21.6 (CH_3), 21.0 (CH_3) ppm.

ATR-FTIR: 3426 (OH), 1738 (C=O) cm^{-1}.

HRMS (ESI): $C_{17}H_{29}O_5$ $[M+H]^+$ requires 313.2010 *m/z*, found 313.2004 *m/z*.

$\boldsymbol{R_f}$ = 0.32 (30:70 EtOAc/PS, silica gel).

$[\boldsymbol{\alpha}]_{\boldsymbol{D}}^{\boldsymbol{23}}$ = +12.9° (*c*. 1.45. MeOH).

8.4.9 Preparation of 12-acetoxybirkenal 149

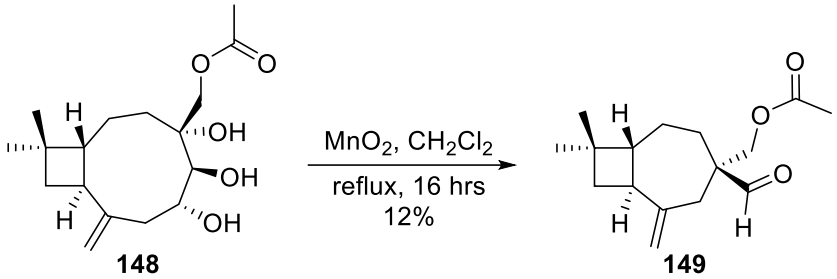

Activated MnO_2 (Merck, >90% activity, Batch# 8.05958.1000) (1.390 g, 15.99 mmol) was added to a solution of acetate triol caryophyllene **148** (50 mg, 0.16 mmol) in dry CH_2Cl_2 (12 mL) and heated at reflux. After 16 hours, the MnO_2 was removed by filtration through celite and the celite was washed with EtOAc (10 mL). The filtrate and washes were combined and concentrated under reduced pressure without heating to afford a yellow oil (6 mg). The oil was purified by column chromatography (5:95 EtOAc/PS, silica gel) to give the 12-acetoxybirkenal **149** as a colourless oil (5 mg, 0.02 mmol, 12%).

^{1}H NMR (400 MHz, $CDCl_3$): δ 9.62 (s, 1H), 4.83 (m, 1H), 4.62 (d, *J* = 2.0 Hz, 1H), 4.03 (s, 2H), 2.69 (d, *J* = 16.0 Hz, 1H), 2.47 (dq, *J* = 2.0, 16.0 Hz, 1H), 2.31 (app q, *J* = 10.4 Hz, 1H), 2.14 (m, 1H), 2.04 (s, 3H), 1.83 (dd, *J* = 10.4, 7.6 Hz, 1H), 1.70 - 1.56 (m, 4H), 1.48 – 1.37 (m, 1H), 1.00 (s, 3H), 0.99 (s, 3H) ppm.

^{13}C NMR (101 MHz, $CDCl_3$): δ 204.4 (CHO), 170.8 (C=O), 149.1 (C), 108.5 (CH_2), 68.7 (CH_2), 52.1 (C), 50.7 (CH), 40.8 (CH), 40.2 (CH_2), 38.4 (CH_2), 34.7 (C), 32.0 (CH_2), 30.4 (CH_3), 24.3 (CH_2), 22.0 (CH_3), 20.9 (CH_3) ppm.

ATR-FTIR: 1743 (C=O, slight shoulder on right side of peak indicating overlapping carbonyl stretches), 1229 (C-O) cm^{-1}.

HRMS (ESI): $C_{16}H_{25}O_3$ $[M+H]^+$ requires 265.1798 *m/z*, found 265.1795 *m/z*.

***R*$_f$ =** 0.43 (10:90 EtOAc/PS, silica gel).

8.4.10 Preparation of 6,12-diacetoxycaryophyllene oxide 150

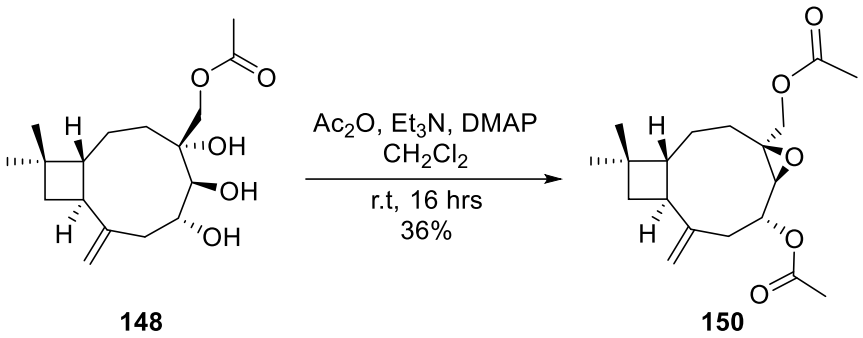

DMAP (~1 mg), Et_3N (110 µL, 0.789 mmol) and acetic anhydride (100 µL, 1.06 mmol) were added to a solution of the acetate triol caryophyllene **148** (37 mg, 0.118 mmol) in dry CH_2Cl_2 and stirred at room temperature. After 16 hours, the reaction mixture was diluted with CH_2Cl_2 (50 mL) and washed with HCl solution (1M, 2 x 50 mL) and $NaHCO_3$ solution (5%, 2 x 50 mL). The organic phase was dried over anhydrous $MgSO_4$ and concentrated under reduced pressure to a yellow oil (32 mg). The oil was purified by flash chromatography (10:90 EtOAc/PS, silica gel) to give epoxide **150** as a yellow oil (14 mg, 0.043 mmol, 36%).

^{1}H NMR (400 MHz, $CDCl_3$): δ 5.25 (s, 1H), 5.15 (s, 1H), 4.80 (td, *J* = 6.8, 10.0 Hz, 1H), 4.42 (d, *J* = 12.0 Hz, 1H), 3.81 (dd, *J* = 1.2, 12.0 Hz, 1H), 3.23 (d, *J* = 10.0 Hz, 1H), 2.94 (dd, *J* = 6.8, 12.4 Hz, 1H), 2.37 (app q, *J* = 8.8 Hz, 1H), 2.12-2.03 (m, 1H), 2.10 (s, 3H), 2.07 (s, 3H), 1.97 (ddd, *J* = 6.0, 12.4, 15.2 Hz, 1H), 1.89 (dd, *J* = 8.4, 10.8 Hz, 1H), 1.72 (app t, *J* = 9.6 Hz, 1H), 1.67 – 1.59 (m, 2H), 1.61 – 1.53 (m, 1H), 1.51 – 1.37 (m, 1H), 1.01 (s, 3H), 0.98 (s, 3H) ppm.

^{13}C NMR (101 MHz, $CDCl_3$): δ 170.9 (C), 170.3 (C), 146.9 (C), 115.6 (CH_2), 73.0 (CH), 67.4 (CH_2), 61.2 (C), 61.0 (CH), 54.1 (CH), 47.3 (CH), 42.8 (CH_2), 42.5 (CH_2), 33.4 (C), 30.8 (CH_2), 29.9 (CH_3), 27.4 (CH_2), 21.6 (CH_3), 21.2 (CH_3), 21.0 (CH_3) ppm.

ATR-FTIR: 1741 (C=O), 1229 (C-O) cm^{-1}.

HRMS (ESI): $C_{19}H_{28}O_5$ $[M+H]^+$ requires 359.1829 *m/z*, found 359.1822 *m/z*.

***R*$_f$** = 0.49 (20:80 EtOAc/PS, silica gel).

8.4.11 Preparation of 3,12-diacetoxycaryolan-1,4-diol 151

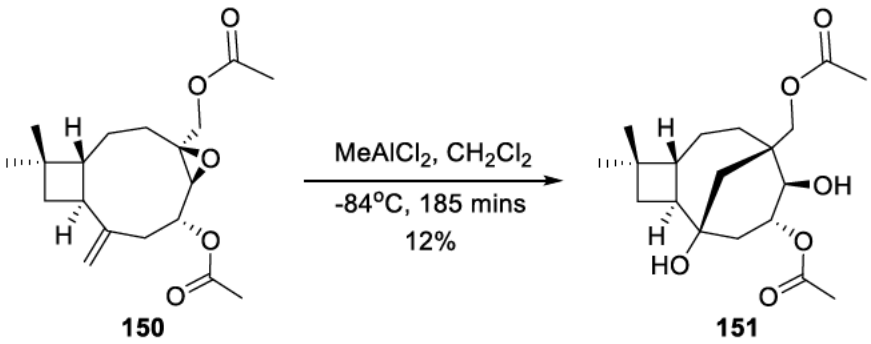

150 151

A solution of $MeAlCl_2$ in hexanes (1M, 700 µL, 0.70 mmol) was added in portions to a solution of epoxide **150** (35 mg, 0.10 mmol) in dry CH_2Cl_2 (9 mL) at -84°C over 185 mins until the consumption of starting material indicated by TLC analysis. After an additional 15 mins, Et_3N (800 µL, 5.74 mmol) was added to the reaction mixture resulting in the evolution of white fumes and a change in colour to dark pink. Rochelle's salt (3 mL) was added to the reaction mixture with stirring. After 5 mins, the mixture was concentrated under reduced pressure to afford a cloudy white mixture. The mixture was diluted with deionised water (40 mL) and was extracted with EtOAc (3 x 40 mL). The combined organic extracts were dried over anhydrous $MgSO_4$ and concentrated under reduced pressure to afford a yellow oil (29.3 mg). The oil (29.3 mg) was purified by column chromatography (30:70 EtOAc/PS, silica gel) to afford 3,12-diacetoxycaryolan-1,4-diol **151** as a colourless oil (5 mg, 0.013 mmol, 12%).

^{1}H NMR (400 MHz, $CDCl_3$): δ 5.30 (td, *J* = 5.6, 9.2 Hz, 1H), 4.06 (d, *J* = 11.2 Hz, 1H), 3.96 (dd, *J* = 4.8, 9.2 Hz, 1H), 3.83 (d, *J* = 11.2 Hz, 1H), 2.73 (dd, *J* = 9.2, 14.4 Hz, 1H), 2.30 (app q, *J* = 9.2 Hz, 1H), 2.27 – 2.20 (m, 1H), 2.13 (s, 3H), 2.11 (s, 3H), 2.05 (ddd, *J* = 2.8, 5.2, 14.0 Hz, 1H), 1.98 (dd, *J* = 2.8, 13.2 Hz, 1H), 1.89 – 1.81 (m, 3H), 1.77 (dt, *J* = 4.8, 14.0 Hz, 1H), 1.67 – 1.54 (m, 1H), 1.54 – 1.41 (m, 1H), 1.28 – 1.19 (m, 1H), 1.03 (s, 3H), 1.01 (s, 3H) ppm.

^{13}C NMR (101 MHz, $CDCl_3$): δ 171.3 (C=O), 170.9 (C=O), 73.4 (CH), 69.6 (CH), 69.6 (C), 68.8 (CH_2), 47.4 (CH), 46.2 (CH_2), 45.5 (CH), 44.4 (CH_2), 41.9 (C), 40.1 (CH_2), 33.3 (C), 32.1 (CH_2), 30.3 (CH_3), 23.6 (CH_2), 21.6 (CH_3), 21.4 (CH_3), 21.2 (CH_3) ppm.

^{1}H NMR (400 MHz, Acetone-*d*$_6$): δ 5.23 (td, *J* = 4.0, 8.0 Hz, 1H), 4.39 (dd, *J* = 1.2, 4.8 Hz, 1H), 4.06 (dd, *J* = 1.2, 10.8 Hz, 1H), 3.97 (dd, *J* = 5.2, 8.0 Hz, 1H), 3.82 (dd, *J* = 1.2, 10.8 Hz, 1H), 2.65 – 2.53 (m, 2H), 2.19 (d, *J* = 13.2 Hz, 1H), 2.10 – 2.00 (m, 2H), 2.04 (s,

3H), 2.03 (s, 3H), 1.98 – 1.87 (m, 1H), 1.86 – 1.74 (m, 3H), 1.70 – 1.57 (m, 1H), 1.57 – 1.46 (m, 1H), 1.45 – 1.36 (m, 1H), 1.04 (s, 3H), 1.03 (s, 3H) ppm.

^{13}C NMR (101 MHz, Acetone-*d*$_6$): δ 171.1 (C=O), 170.4 (C=O), 74.1 (CH), 71.8 (C), 69.9 (CH_2), 69.0 (CH), 46.3 (CH), 46.1 (CH_2), 45.9 (CH), 44.5 (CH_2), 42.6 (C), 40.4 (CH_2), 34.0 (C), 31.9 (CH_2), 30.6 (CH_3), 23.4 (CH_2), 21.7 (CH_3), 21.3 (CH_3), 21.0 (CH_3) ppm.

ATR-FTIR: 3484 (OH), 1742 (C=O), 1240 (C–O) cm^{-1}.

***R*$_f$ =** 0.43 (30:70 EtOAc/PS, silica gel).

8.4.12 Preparation of 12-acetoxycaryolan-1,3,4-triol 153

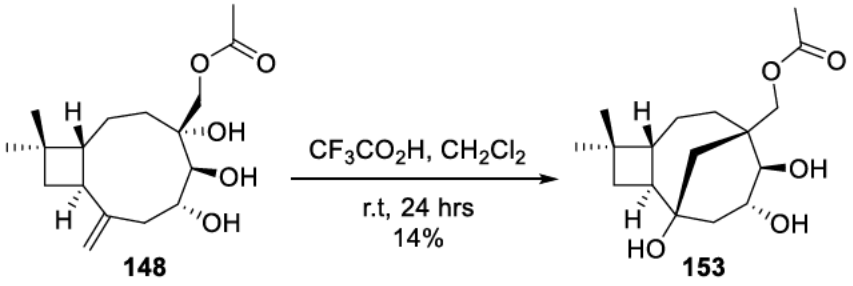

TFA (0.5 mL, 745 mg, 7 μmol) was added dropwise to a solution of acetate triol **148** (23 mg, 0.07 mmol) in dry CH_2Cl_2 (5 mL) at room temperature. The reaction mixture turned bright yellow upon addition and after 2 hours had turned brown in colour. After 24 hours, the reaction mixture was diluted with CH_2Cl_2 (20 mL) and washed with $NaHCO_3$ solution (5%, 3 x 30 mL). The organic layer was dried over anhydrous $MgSO_4$ and concentrated under reduced pressure to afford a yellow oil (31 mg). The product was purified by column chromatography (1:99-30:70 EtOAc/PS, silica gel) to afford 12-acetoxycaryolan-1,3,4-triol **153** as a colourless oil (3 mg, 0.01 mmol, 14%).

^{1}H NMR (400 MHz, $CDCl_3$): δ 4.75 (d, *J* = 11.2 Hz, 1H), 4.24 (dd, *J* = 5.2, 9.2 Hz, 1H), 3.78 (dd, *J* = 1.2, 5.2 Hz, 1H), 3.59 (d, *J* = 11.2 Hz, 1H), 2.33-2.22 (m, 2H), 2.09-2.04 (m, 1H), 2.08 (s, 3H), 2.01 (dt, *J* = 2.4, 8.8 Hz, 1H), 1.86-1.81 (m, 1H), 1.78-1.72 (m, 1H), 1.77 (d, *J* = 12.8 Hz, 1H), 1.68 (dd, *J* = 1.2, 12.8 Hz, 1H), 1.48-1.20 (m, 4H), 1.05 (s, 3H), 1.03 (s, 3H) ppm.

^{13}C NMR (101 MHz, $CDCl_3$): δ 172.4 (C=O), 75.2 (C), 72.6 (CH), 70.4 (CH_2), 68.3 (CH), 50.2 (CH), 45.8 (CH_2), 40.9 (C), 38.9 (CH_2), 35.8 (CH), 33.1 (CH_2), 32.0 (C), 31.8 (CH_2), 31.5 (CH_3), 24.5 (CH_3), 21.3 (CH_3), 20.7 (CH_2) ppm.

ATR-FTIR: 3450 (OH), 2923 (aliphatic CH), 2858 (aliphatic CH), 1738 (C=O), 1248 (C-O) cm^{-1}.

8.4.13 Preparation of 5,6-dihydroxycaryophyll-3,8-diene 154

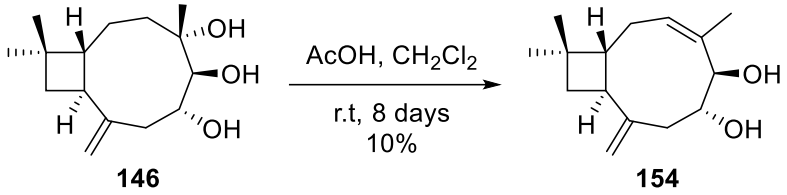

146 **154**

Glacial AcOH (1 mL, 1050 mg, 18 μmol) was added to a solution of freshly prepared methyl triol **146** (23 mg, 0.09 mmol) in dry CH_2Cl_2 (5 mL) until consumption of starting material was indicated by TLC analysis. After 8 days the reaction mixture was diluted with CH_2Cl_2 (20 mL) and the solution was washed with $NaHCO_3$ solution (5%, 3 x 30 mL). The organic layer was dried over anhydrous $MgSO_4$ and concentrated under reduced pressure to afford a colourless oil (16 mg). The oil was purified by column chromatography (0:100-15:85 EtOAc/PS, Et_3N treated silica gel) to afford 5,6-dihydroxycaryophyll-3,8-diene **154** as a colourless oil (2 mg, 8 μmol, 10%).

^{1}H NMR (400 MHz, $CDCl_3$): δ 5.57 (td, *J* = 1.6, 7.6 Hz, 1H), 4.92 (s, 1H), 4.82 (t, *J* = 2.0 Hz, 1H), 4.33 (d, *J* = 9.6 Hz, 1H), 3.74 (m, 1H), 2.70 (app q, *J* = 9.2 Hz, 1H), 2.46-2.32 (m, 2H), 2.15-2.03 (m, 2H), 1.98 (ddd, *J* = 2.0, 8.8, 14.4 Hz, 1H), 1.70 (s, 3H), 1.62 (app t, *J* = 10.0 Hz, 1H), 1.56 (m, 1H), 1.01 (s, 3H), 0.98 (s, 3H) ppm.

^{13}C NMR (101 MHz, $CDCl_3$): δ 148.2 (C), 136.9 (C), 127.2 (CH), 115.6 (CH_2), 74.2 (CH), 71.2 (CH), 49.4 (CH), 43.0 (CH), 40.6 (CH_2), 38.1 (CH_2), 33.3 (C), 30.0 (CH_3), 28.9 (CH_2), 22.6 (CH_3), 17.1 (CH_3) ppm.

ATR-FTIR: 3404 (OH), 3077 (vinylic CH) 2951 (aliphatic CH), 2924 (aliphatic CH), 2856 (aliphatic CH), 1631 (exocyclic C=C), 1040 (C-O) cm^{-1}.

8.4.14 **Scaevola crassifolia** *neutrals auto-oxidation with phenols FTIR timecourse study*

The study was conducted in 20 mL glass sample vials. Seven samples were prepared in duplicate:

- Phenols control
- Neutrals control
- Neutrals + 10% w/w phenols
- Neutrals + 30% w/w phenols
- Neutrals + 50% w/w phenols
- Neutrals + 80% w/w phenols
- Neutrals + 100% w/w phenols

A solution of *S. crassifolia* neutrals fraction in Et_2O was prepared and then distributed evenly into each of the sample vials, apart from the phenols control vials. A stock solution of *S. crassifolia* phenols fraction in Et_2O was prepared and dispensed into each of the neutrals fraction solutions that were doped with phenols. The phenols stock solution was also dispensed into the phenols control sample vials. The Et_2O was evaporated by leaving the solutions to stand at room temperature, allowing for the neutrals, phenols or neutrals and phenols mixtures to be exposed to air.

Analysis of the mixtures using FTIR spectroscopy was achieved by dissolution of each sample in equal volumes of Et_2O and dispensing the solution on to the ATR crystal. After evaporation of the solvent, the spectra were collected.

FTIR spectra were analysed using OPUS version 7.0. The second derivative FTIR spectra were calculated from vector-normalized raw spectra (vector normalized across the asymmetric methylene C-H stretching bands from 2940-2900 cm^{-1} and the symmetric methylene C-H stretching bands from 2870-2830 cm^{-1}) using a nine-point smoothing Savitzky-Golay function.

8.4.14 **Scaevola crassifolia** ***neutrals auto-oxidation with BHT 156 FTIR timecourse study***

The study was conducted in 20 mL glass sample vials. Five samples were prepared in duplicate:

- Phenols control
- Neutrals control
- Neutrals + 10% w/w BHT **156**
- Neutrals + 50% w/w BHT **156**
- Neutrals + 100% w/w BHT **156**

A solution of *S. crassifolia* neutrals fraction in Et_2O was prepared and then distributed evenly into each of the sample vials, apart from the phenols control vials. A stock solution of BHT **156** in Et_2O was prepared and dispensed into each of the of the neutrals fraction solutions that were doped with phenols. The phenols stock solution was also dispensed into the phenols control sample vials. The Et_2O was evaporated by leaving the solutions to stand at room temperature, allowing for the neutrals, BHT **156**, or neutrals and BHT **156** mixtures to be exposed to air.

Analysis of the mixtures using FTIR spectroscopy was achieved by dissolution of each sample in equal volumes of Et_2O and dispensing the solution on to the ATR crystal. After evaporation of the solvent, the spectra were collected.

FTIR spectra were analysed using OPUS version 7.0. The second derivative FTIR spectra were calculated from vector-normalized raw spectra (vector normalized across the asymmetric methylene C-H stretching bands from 2940-2900 cm^{-1} and the symmetric methylene C-H stretching bands from 2870-2830 cm^{-1}) using a nine-point smoothing Savitzky-Golay function.

8.5 Chapter 5

8.5.1 Extraction and isolation of flavanones from Scaevola crassifolia

Fresh *S. crassifolia* leaves (1.16 kg) were steeped in Et_2O. After 20 mins the extract was filtered to removed detritus and the filtrate was concentrated under reduced pressure to afford a dark yellow oil (33.72 g, 2.91% w/w).

The yellow oil (33.72 g) was dissolved in Et_2O (300 mL) and washed with HCl (1M, 2 x 300 mL). The combined HCl washes were set aside. The organic layer was washed with $NaHCO_3$ solution (5%, 2 x 300 mL) and the aqueous washes were set aside. The organic layer was washed with NaOH solution (5%, 2 x 300 mL) and the combined washes were set aside. The organic layer was dried over anhydrous $MgSO_4$ and concentrated under reduced pressure to afford the neutrals fraction as a yellow oil (9.58 g, 0.83% w/w).

The combined HCl washes were basified using NaOH pellets until the solution turned deep red in colour. The basified solution was extracted with CH_2Cl_2 (4 x 150 mL). The combined organic extracts were dried over anhydrous $MgSO_4$ and concentrated under reduced pressure to afford the amines fraction as a green tinged oil (169 mg, 0.01% w/w).

The combined $NaHCO_3$ washes were acidified using concentrated HCl (32%) until the effervescence ceased in solution. The acidified solution was extracted with CH_2Cl_2 (4 x 150 mL) and the combined organic extracts were dried over anhydrous $MgSO_4$. The dried solution was concentrated under reduced pressure to afford the carboxylic acids fraction as a yellow-green oil (190 mg, 0.02% w/w).

The combined NaOH washes were acidified using concentrated HCl (32%) until the solution turned bright yellow with floating dark red components. The mixture was extracted with CH_2Cl_2 (4 x 150 mL). The combined organic extracts were dried over anhydrous $MgSO_4$ and concentrated under reduced pressure to afford the phenols fraction as a red-orange solid (9.68 g, 0.83% w/w).

A fraction of the phenols fraction (451 mg) was purified by column chromatography (0:100-5:95 MeOH/CH_2Cl_2, silica gel) to give a mixture of flavanones **138** and **139** as a yellow solid (163 mg, 0.46 mmol, 0.21%) and chalcone **157** as an orange solid (72 mg, 0.20 mmol, 0.09%). Flavanones **138** and **139** were further purified by trituration using MeCN to afford flavanone **138** as a white solid (24 mg, 0.03 mmol, 0.04%).

Chalcone 157:

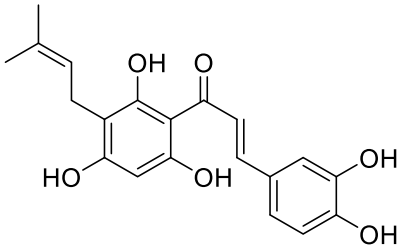

157

^{1}H NMR (400 MHz, Acetone-*d*$_6$): δ 14.45 (s, 1H), 8.08 (d, *J* = 15.2 Hz, 1H), 7.69 (d, *J* = 15.2 Hz, 1H), 7.19 (d, *J* = 2.0 Hz, 1H), 7.08 (dd, *J* = 2.0, 8.4 Hz, 1H), 6.88 (d, *J* = 8.0 Hz, 1H), 6.09 (s, 1H), 5.24 (t, *J* = 7.2 Hz, 1H), 3.26 (d, *J* = 7.2 Hz, 2H), 1.75 (s, 3H), 1.63 (s, 3H) ppm.

^{13}C NMR (101 MHz, Acetone-*d*$_6$): δ 193.3 (C=O), 165.8 (C), 162.7 (C), 160.1 (C), 148.7 (C), 146.3 (C), 143.4 (CH), 130.7 (C), 128.9 (C), 125.6 (CH), 124.2 (CH), 122.9 (CH), 116.4 (CH), 115.3 (CH), 108.0 (C), 105.7 (C), 95.3 (CH), 25.9 (CH_3), 22.0 (CH_2), 17.9 (CH_3) ppm.

ATR-FTIR: 3308 (OH), 2959 (aliphatic CH), 2922 (aliphatic CH), 2854 (aliphatic CH), 1597 (C=O), 1256 (C-O) cm^{-1}.

HRMS (ESI): $C_{20}H_{20}O_6$ $[M+H]^+$ requires 357.1333 *m/z*, found 357.1325 *m/z*.

***R*$_f$ =** 0.27 (10:90 MeOH/CH_2Cl_2, silica gel), Vanillin stain (red).

8.5.2 Base catalysed cyclisation of chalcone 157

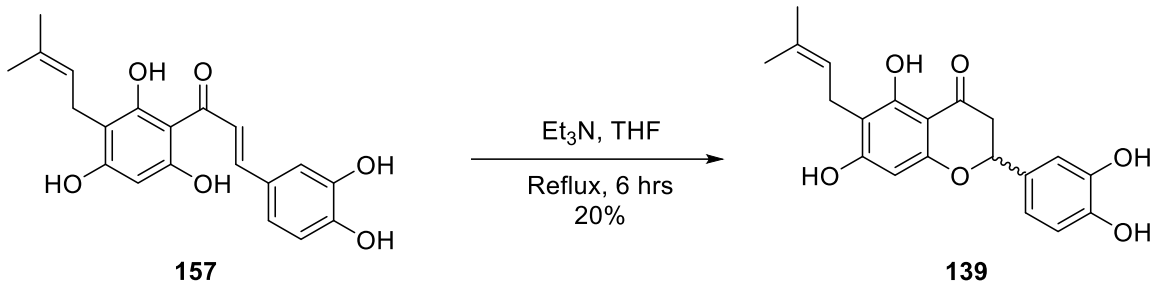

157 **139**

Et_3N (260 µL, 1.87 mmol) was added to a solution of chalcone **157** (10 mg, 0.028 mmol) in dry THF (6 mL) and the reaction mixture was heated at reflux. The reaction mixture turned red upon addition of Et_3N. After 6 hours, the reaction mixture was allowed to cool to room temperature and was concentrated *in vacuo* to afford a sticky orange oil. The oil was diluted with EtOAc (25 mL) and the organic solution was washed with HCl solution (1M, 3 x 25 mL). The organic layer was dried over anhydrous $MgSO_4$ and concentrated *in vacuo* to afford an orange oil (10 mg). The oil was purified by column chromatography (1:99 MeOH/CH_2Cl_2) to afford the flavanone **139** as a yellow oil (2 mg, 20%).

^{1}H NMR (400 MHz, Acetone-*d*$_6$): δ 12.46 (s, 1H), 7.02 (s, 1H), 6.85 (d, *J* = 1.2 Hz, 1H), 6.02 (s, 1H), 5.62 (s, 1H), 5.35 (dd, *J* = 2.8, 12.4 Hz, 1H), 5.23 (tdd, *J* = 1.2, 1.6, 7.2 Hz, 1H), 3.24 (d, *J* = 7.2 Hz, 2H), 3.11 (dd, *J* = 12.8, 17.2 Hz, 1H), 2.70 (dd, *J* = 3.2, 17.2 Hz, 1H), 1.75 (d, *J* = 1.2 Hz, 3H), 1.63 (d, *J* = 1.2 Hz, 3H) ppm.

^{13}C NMR (101 MHz, Acetone-*d*$_6$): δ 197.3 (C=O), 164.8 (C), 162.3 (C), 162.0 (C), 146.4 (C), 146.0 (C), 131.7 (C), 131.2 (C), 123.6 (CH), 119.2 (CH), 116.0 (CH), 114.7 (CH), 109.0 (C), 103.1 (C), 95.3 (CH), 79.9 (CH), 43.7 (CH_2), 25.9 (CH_3), 21.6 (CH_2), 17.8 (CH_3) ppm.

ATR-FTIR: 1634 (C=O, asym), 1603 (C=O, sym) cm^{-1}, 1524 (ar C=C), 1450 (ar C=C), 1158 (C-O) cm^{-1}.

***R*$_f$ =** 0.48 (10:90 MeOH/CH_2Cl_2, silica gel), Vanillin stain (pink/red).

8.6 Chapter 6

8.6.1 Preparation of caryophyllene tetrol 174

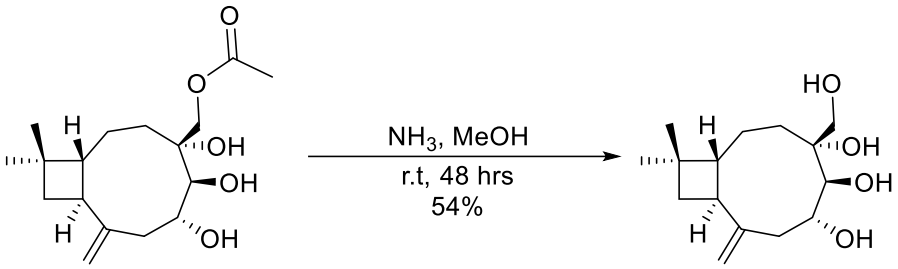

Aqueous NH_3 (30%, 3 mL, 47 mmol) was added to a solution of acetate triol caryophyllene **148** (30 mg, 0.10 mmol) in MeOH (5 mL). The reaction mixture turned green upon addition of the NH_3 solution. The reaction mixture was stirred at room temperature. After 48 hours, the reaction mixture was concentrated under reduced pressure to afford a yellow oil dispersed with yellow solid (28 mg). The mixture was purified by column chromatography (1:99 MeOH/CH_2Cl_2, silica gel) to afford the tetrol **174** as a colourless oil (14 mg, 0.05 mmol, 54%).

^{1}H NMR (400 MHz, D_2O): 5.30 (s, 1H), 5.10 (s, 1H), 3.84 (d, *J* = 12.4 Hz, 1H), 3.73 (ddd, *J* = 7.2, 10.0 Hz, 1H) 3.43 (dd, *J* = 1.2, 12.4 Hz, 1H), 3.30 (d, *J* = 10.0 Hz, 1H), 2.81 (dd, *J* = 6.8, 12.0 Hz, 1H), 2.49 (app q, *J* = 9.2 Hz, 1H), 2.22-2.09 (m, 2H), 1.88 (dd, *J* = 8.0, 10.0 Hz, 1H), 1.78 (app t, *J* = 9.6 Hz, 1H), 1.67-1.46 (m, 4H), 1.01 (s, 3H), 0.99 (s, 3H) ppm.

^{13}C NMR (101 MHz, D_2O): δ 148.2 (C), 114.2 (CH_2), 70.5 (CH), 65.4 (C), 65.2 (CH_2), 64.6 (CH), 53.1 (CH), 46.2 (CH), 44.6 (CH_2), 41.7 (CH_2), 32.5 (C), 29.5 (CH_2), 28.7 (CH_3), 26.5 (CH_2), 20.6 (CH_3) ppm.

ATR-FTIR: 3371 (OH), 3072 (vinylic CH), 2950 (aliphatic CH), 2928 (aliphatic CH), 2859 (aliphatic CH), 1637 (C=C), 1027 (C-O) cm^{-1}.

***R*$_f$** = 0.27 (10:90 MeOH/CH_2Cl_2, silica gel), Vanillin stain (dark blue).

8.6.2 Preparation of acetate triol caryophyllene oxide 179

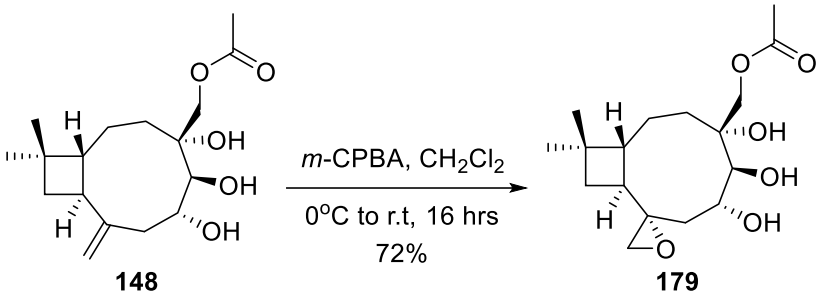

A solution of *m*-CPBA (39 mg, 0.23 mmol) in dry CH_2Cl_2 (6 mL) was added to the acetate triol caryophyllene **148** (21 mg, 0.07 mmol) in portions at 0ºC. The solution was allowed to warm to room temperature and stirred. The solution was allowed to warm to room temperature and stirred. After 16 hours, the solution was diluted with CH_2Cl_2 (40 mL) and washed with NaOH solution (5%, 3 x 40 mL) and deionised water (60 mL). The organic layer was dried over anhydrous $MgSO_4$ and concentrated under reduced pressure to afford a yellow oil (16 mg). The oil was purified by column chromatography (30:70 EtOAc/PS, silica gel) to afford epoxide **179** as a colourless oil (16 mg, 0.05 mmol, 72%).

^{1}H NMR (400 MHz, $CDCl_3$): δ 4.27 (d, *J* = 12.0 Hz, 1H), 4.06 (d, *J* = 12.0, 1H), 3.71 (tdd, *J* = 4.0, 6.0, 9.6 Hz, 1H), 3.16 (d, *J* = 9.6 Hz, 1H), 2.77 (dd, *J* = 1.2, 4.4 Hz, 1H), 2.69 (d, *J* = 4.4 Hz, 1H), 2.36 (app q, *J* = 9.2 Hz, 1H), 2.28 (d, *J* = 3.6 Hz, 1H), 2.21 (ddd, *J* = 1.2, 9.2, 13.6 Hz, 1H), 2.15 (s, 3H), 2.06 – 1.97 (m, 2H), 1.72 – 1.65 (m, 1H), 1.57 (s, 3H), 1.19 (app t, *J* = 10.8 Hz, 1H), 0.96 (s, 3H), 0.93 (s, 3H) ppm.

^{13}C NMR (101 MHz, $CDCl_3$): δ 170.8 (C), 68.0 (CH), 66.7 (CH_2), 64.9 (CH), 62.1 (C), 56.5 (C), 49.8 (CH), 48.5 (CH_2), 46.1 (CH), 43.9 (CH_2), 35.4 (CH_2), 33.7 (C), 30.4 (CH_2), 30.1 (CH_3), 26.6 (CH_2), 21.8 (CH_3), 21.0 (CH_3) ppm.

ATR-FTIR: 3457 (br OH), 1741 (C=O), 1232 (C-O) cm^{-1}.

***R*$_f$** = 0.42 (30:70 EtOAc/PS, silica gel).

8.6.3 Preparation of 12-acetoxy-4,8-dihydroxy-5,6,13-tristrifluoroacetoxycaryophyllene aldehyde 180

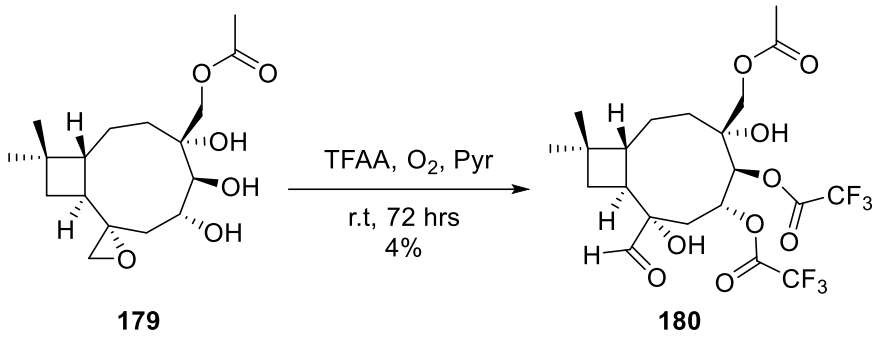

179 **180**

TFAA (0.5 mL, 0.756 g, 3.60 mmol) was added dropwise to a solution of the acetate triol epoxide **179** (23 mg, 0.07 mmol) in dry pyridine (7 mL). The reaction mixture was stirred under an atmosphere of dry air. After 16 hours, the reaction mixture was concentrated under reduced pressure to afford a dark brown oil. The oil was dissolved in water (30 mL) and extracted with Et_2O (3 x 50 mL). The combined organic extracts were dried over anhydrous $MgSO_4$ and concentrated under reduced pressure to afford a dark orange oil (63 mg). The oil was purified by column chromatography (10:90 EtOAc/PS, silica gel) to afford compound **180** as an impure colourless oil (2 mg, 4%). Selected signals shown in the NMR data.

^{1}H NMR (400 MHz, $CDCl_3$): δ 9.88 (s, 1H), 4.33 (d, *J* = 6.8 Hz, 1H), 4.23 (m, 1H), 4.09 (d, *J* = 11.6 Hz, 1H), 3.94 (d, 11.6 Hz, 1H), 2.73 (dd, *J* = 10.4, 14.4 Hz, 1H), 2.02 (s, 3H), 1.89 (td, *J* = 2.8, 11.6 Hz, 1H), 1.71 (dd, *J* = 7.2, 10.0 Hz, 1H), 1.39 (dd, *J* = 4.0, 14.4 Hz, 1H), 1.07 (s, 6H) ppm.

ATR-FTIR: 3430 (OH), 2932 (aliphatic CH), 2864 (aliphatic CH), 1741 (C=O), 1716 (C=O) cm^{-1}.

8.6.4 Preparation of 1,312-triacetoxycaryolan-4-ol 181

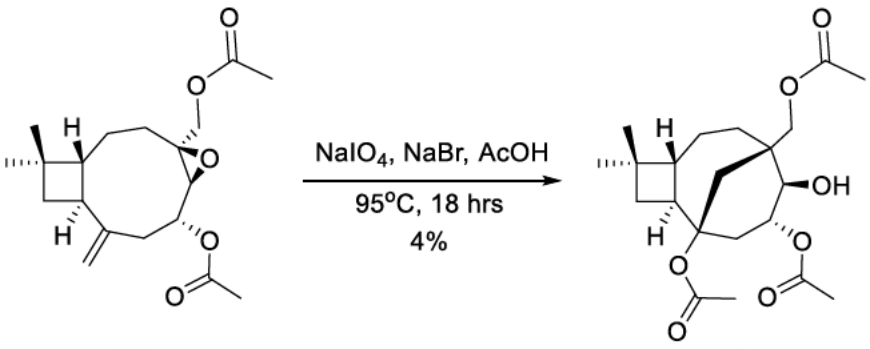

150 **181**

A solution of the epoxide **150** (37 mg, 0.11 mmol), $NaIO_4$ (10 mg, 0.05 mmol), and NaBr (7 mg, 0.07 mmol) in glacial AcOH (5 mL) was heated at 95°C with stirring. After 18 hours, the reaction mixture was allowed to cool to room temperature and was diluted with deionised water (20 mL). The aqueous layer was extracted with EtOAc (3 x 20 mL). The combined organic extracts were washed with $Na_2S_2O_5$ solution (5%, 2 x 100 mL), deionised water (100 mL) and $NaHCO_3$ solution (5%, 2 x 100 mL). The organic layer was dried over anhydrous $MgSO_4$ and concentrated under reduced pressure to afford a brown oil (32 mg). The oil was purified by column chromatography (10:90 - 30:70 EtOAc/PS, silica gel) to afford 1,3,12-triacetoxycaryolan-4-ol **181** as a yellow-orange oil (2 mg, 5 μmol, 4%).

^{1}H NMR (400 MHz, $CDCl_3$): δ 5.31 (ddd, *J* = 7.2, 9.6, 11.2 Hz, 1H), 4.18 (d, *J* = 11.2 Hz, 1H), 4.01 (d, *J* = 11.2 Hz, 1H), 3.90 (d, *J* = 11.2 Hz, 1H), 2.51 (dd, *J* = 9.6, 14.4 Hz, 1H), 2.37 (ddd, *J* = 2.0, 7.2, 14.4 Hz, 1H), 2.25-2.17 (m, 1H), 2.13 (s, 3H), 2.09 (s, 3H), 1.91 (dd, *J* = 2.0, 13.6 Hz, 1H), 1.86-1.77 (m, 4H), 1.52-1.43 (m, 2H), 1.31-1.18 (m, 5H) 0.99 (s, 3H), 0.98 (s, 3H) ppm.

HRMS (ESI): $C_{21}H_{32}O_7$ $[M+H]^+$ requires 419.2040 *m/z*, found 419.2031 *m/z*.

8.6.5 Preparation of diacetate caryophyllene oxide diol 182

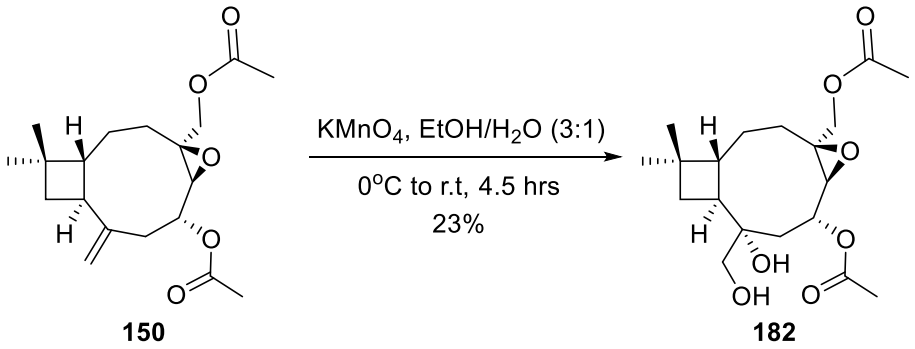

A solution of $KMnO_4$ (40 mg, 0.25 mmol) in deionised water (1.5 mL) was added dropwise to a stirred solution of the diacetate epoxide **150** (38 mg, 0.114 mmol) in EtOH (3 mL) at 0ºC. The $KMnO_4$ solution turned brown upon addition to the epoxide solution. Anhydrous $MgSO_4$ (34 mg, 0.283 mmol) was added to the reaction mixture and the mixture was allowed to warm to room temperature. After 4.5 hours, the reaction mixture was filtered through celite. The celite was washed with EtOAc and the combined filtrate and washes were concentrated under reduced pressure to afford a yellow residue (39 mg). The residue was diluted with deionised water (15 mL) and brine (15 mL). The aqueous solution was set aside and the remaining residue was diluted with EtOAc (30 mL) and set aside. The aqueous solution (30 mL) was extracted with EtOAc (2 x 50 mL) and the organic extracts were combined with the organic residue solution. The organic solution was dried over anhydrous $MgSO_4$ and concentrated under reduced pressure to afford a colourless oil (33 mg). The oil was purified by column chromatography (1:99 MeOH/CH_2Cl_2, silica gel) to afford the diol **182** as a yellow tinged oil (10 mg, 27 μmol, 23%).

^{1}H NMR (400 MHz, $CDCl_3$): δ 5.00 (td, *J* = 4.4, 9.6 Hz, 1H), 4.33 (d, *J* = 12.0 Hz, 1H), 4.22 (d, *J* = 12.0 Hz, 1H), 3.66 (d, *J* = 11.2 Hz, 1H), 3.51 (d, *J* = 11.2 Hz, 1H), 3.31 (d, *J* = 9.6 Hz, 1H), 2.38 – 2.32 (m, 2H), 2.14 (s, 3H), 2.07 (s, 3H), 1.90 (dd, *J* = 9.2, 13.6 Hz, 1H), 1.81 – 1.77 (m, 2H), 1.74 (dd, *J* = 8.4, 10.8 Hz, 1H), 1.67 (app t, *J* = 9.2 Hz, 1H), 1.63 – 1.56 (m, 1H), 1.43 – 1.36 (m, 2H), 0.97, (s, 3H). 0.96 (s, 3H) ppm.

^{13}C NMR (101 MHz, $CDCl_3$): δ 170.7 (C=O), 170.3 (C=O), 74.1 (C), 69.0 (CH), 66.3 (CH_2), 64.5 (CH_2), 62.5 (C), 62.2 (CH), 49.7 (CH), 46.0 (CH), 42.3 (CH_2), 36.1 (CH_2), 33.6 (C), 30.4 (CH_2), 30.2 (CH_3), 27.3 (CH_2), 22.2 (CH_3), 21.2 (CH_3), 20.9 (CH_3) ppm.

ATR-FTIR: 3467 (OH), 1724 (br, C=O) cm^{-1}.

HRMS (ESI): $C_{19}H_{30}O_7$ $[M+Na]^+$ requires 393.1884 *m/z*, found 393.1873 *m/z*.

R_f = 0.32 (5:95 MeOH/CH_2Cl_2, silica gel), Vanillin stain (blue).

8.6.6 Preparation of pentol acetate 172 and hexol 173

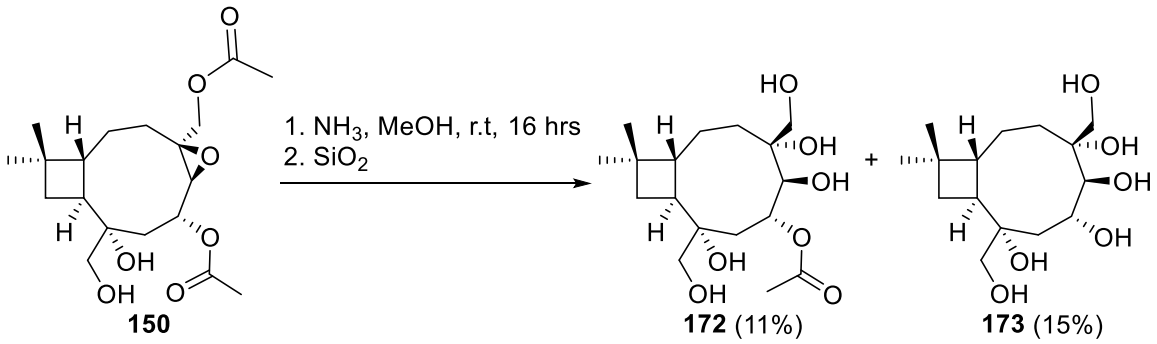

Aqueous NH_3 (30%, 2 mL) was added to a solution of the diacetate caryophyllene epoxide diol **182** (26 mg, 0.07 mmol) in MeOH (5 mL). After 2 hours, the reaction mixture was diluted with EtOH (15 mL) and the solution was concentrated under reduced pressure to a colourless oil (20 mg). The product was purified by column chromatography (3:97 MeOH/CH_2Cl_2, silica gel) to afford the pentol acetate **172** as a colourless oil (3 mg, 8 μmol, 11%) and hexol **173** as a colourless oil (3 mg, 0.01 mmol, 15%).

Pentol acetate 167

^{1}H NMR (400 MHz, D_2O): δ 5.10 (ddd, *J* = 4.8, 10.0, 14.8 Hz, 1H), 3.97 (d, *J* = 12.0 Hz, 1H), 3.80 (d, *J* = 12.4 Hz, 1H), 3.77 (d, *J* = 12.4 Hz, 1H), 3.53 (d, *J* = 12.0 Hz, 1H), 3.46 (d, *J* = 10.0 Hz, 1H), 2.48 (app q, *J* = 9.6 Hz, 1H), 2.43 (dd, *J* = 4.8, 13.6 Hz, 1H), 2.13 (s, 3H), 1.97 (ddd, *J* = 5.6, 12.8, 15.6 Hz, 1H), 1.93 (dd, *J* = 10.8, 13.2 Hz, 1H), 1.75-1.60 (m, 6H), 0.97 (s, 3H), 0.96 (s, 3H) ppm.

ATR-FTIR: 3405 (OH), 2953 (aliphatic CH), 2925 (aliphatic CH), 2856 (aliphatic CH), 1719 (C=O), 1256 (C-O), 1039 (C-O) cm^{-1}.

Hexol 168

^{1}H NMR (400 MHz, D_2O): δ 3.93 (d, *J* = 12.0 Hz, 1H), 3.84 (ddd, *J* = 4.8, 10.0, 14.8 Hz, 1H), 3.80 (d, *J* = 12.0 Hz, 1H), 3.67 (d, *J* = 12.0 Hz, 1H), 3.44 (d, *J* = 12.0 Hz, 1H), 3.26 (d, *J* = 10.0 Hz, 1H), 2.43 (m, *J* = 4.8, 13.2 Hz, 2H), 1.98 (ddd, *J* = 5.6, 13.2, 15.6 Hz, 1H), 1.78 (dd, *J* = 10.8, 12.8 Hz, 1H), 1.74-1.60 (m, 5H), 1.54-1.42 (m 1H), 0.96 (s, 3H), 0.95 (s, 3H) ppm.

^{13}C NMR (101 MHz, D_2O): δ 74.3 (C), 66.1 (C), 65.5 (CH), 64.7 (CH_2), 64.4 (CH), 62.8 (CH_2), 42.3 (CH), 45.8 (CH_2), 45.2 (CH), 36.0 (CH_2), 32.2 (C), 29.5 (CH_2), 28.8 (CH_3), 26.8 (CH_2), 21.2 (CH_3) ppm.

ATR-FTIR: 3362 (OH), 2947 (aliphatic CH), 2921 (aliphatic CH), 2858 (aliphatic CH), 1036 (C-O) cm^{-1}.

8.6.7 Preparation of caryophyllene benzoate 109

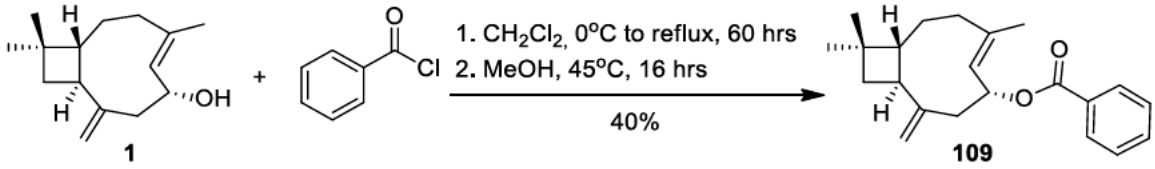

Benzoyl chloride (60 µL, 0.516 mmol) was added to a solution of caryophyllene **1** (46 mg, 0.209 mmol) in dry CH_2Cl_2 (6 mL). Et_3N (70 µL, 0.502 mmol) and DMAP (~1 mg) were added to the solution at 0°C. and after 10 mins the reaction was heated at reflux. After 60 hours the reaction mixture was allowed to cool to room temperature and was concentrated under reduced pressure to afford a green solid (190 mg). A suspension of the green solid in Et_2O (50 mL) was washed with HCl solution (1M, 2 x 75 mL). Upon washing with HCl solution, the green solid dissolved to produce a transparent green solution. The organic layer was washed with saturated $NaHCO_3$ solution (2 x 50 mL) and brine (50 mL). The organic layer was dried over anhydrous $MgSO_4$ and concentrated under reduced pressure to afford a yellow tinged oil (66 mg).

Et_3N (60 µL, 0.430 mmol) and catalytic DMAP (~1 mg) were added to a solution of the oil (66 mg) in MeOH (5 mL) at 0°C and the reaction mixture was heated at 45°C to esterify unreacted benzoyl chloride. After 16 hours, the reaction mixture was allowed to cool to room temperature and was concentrated under reduced pressure to afford a colourless oil. A solution of the colourless oil in Et_2O (50 mL) was washed with HCl solution (1M, 2 x 50 mL), followed by saturated $NaHCO_3$ solution (2 x 50 mL) and brine (50 mL). The organic layer was dried over anhydrous $MgSO_4$ and concentrated under reduced pressure to afford a colourless oil (47 mg). The oil (40 mg) was purified by column chromatography (5:95 EtOAc/PS, silica gel) to afford benzoate **109** as a colourless oil (27 mg, 83 µmol, 40%). NMR and FTIR spectral data matched that reported by Clericuzio *et al.*[48a]

^{1}H NMR (400 MHz, $CDCl_3$): δ 8.04 (d, J = 8.0 Hz, 2H), 7.54 (t, J = 7.6 Hz, 1H), 7.43 (t, J = 8.0 Hz, 2H), 5.77 (td, J = 6.8, 10.4 Hz, 1H), 5.39 (d, J = 10.4 Hz, 1H), 5.10 (s, 1H),

5.04 (s, 1H), 2.94 (dd, *J* = 6.4, 11.6 Hz, 1H), 2.59 (m, 1H), 2.35 (app q, *J* = 9.2 Hz, 1H), 2.17 (app t, *J* = 10.8 Hz, 1H), 1.83 (dd, *J* = 8.4, 10.8 Hz, 1H), 1.77 (s, 3H), 1.73 – 1.65 (m, 1H), 1.61 (m, 3H), 1.48 (app t, *J* = 9.6 Hz, 1H), 1.00 (s, 3H), 0.99 (s, 3H) ppm.

^{13}C NMR (101 MHz, $CDCl_3$): δ 166.3 (C), 149.4 (C), 139.1 (C), 132.8 (CH), 130.9 (C), 129.7 (CH), 128.4 (CH), 124.2 (CH), 113.6 (CH_2), 73.5 (CH), 55.9 (CH), 49.1 (CH), 45.6 (CH_2), 42.4 (CH_2), 35.0 (CH_2), 32.9 (C), 31.2 (CH_2), 30.0 (CH_3), 23.0 (CH_3), 22.0 (CH_3) ppm.

ATR-FTIR: 3071 (vinylic CH), 2928 (aliphatic CH), 2858 (aliphatic CH), 1716 (C=O), 1638 (C=C), 1267 (C-O) cm^{-1}.

***R*$_f$** = 0.68 (5:95 EtOAc/PS, silica gel).

8.6.8 Preparation of 6-chlorocaryophyllene 184

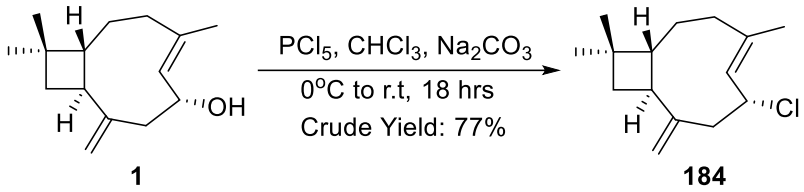

1 **184**

A solution of 6-hydroxycaryophyllene **1** (60 mg, 0.27 mmol) in dry $CHCl_3$ (4 mL) was added to a slurry of PCl_5 (202 mg, 0.97 mmol) and anhydrous Na_2CO_3 (85 mg, 0.80 mmol) in dry $CHCl_3$ (3 mL) at 0ºC with stirring under N_2. The reaction mixture was allowed to warm to room temperature. After 18 hours, the reaction mixture was a filtered and the filtrate was concentrated under reduced pressure to afford a yellow oil (63 mg). The oil was dissolved in EtOAc (50 mL) and the solution was washed with saturated Na_2CO_3 (3 x 50 mL). The organic layer was dried over anhydrous $MgSO_4$ and concentrated under reduced pressure to afford the 6-chlorocaryophyllene **184** (51 mg, 0.21 mmol, 77%).

^{1}H NMR (400 MHz, $CDCl_3$): δ 5.34 (dt, *J* = 2.0, 10.8 Hz, 1H), 5.05 (s, 1H), 4.93 (s, 1H), 4.71 (ddd, *J* = 6.4, 11.2, 17.2 Hz, 1H), 2.92 (dd, *J* = 6.0, 12.0 Hz, 1H), 2.57 (dd, *J* = 6.4, 14.0 Hz, 1H), 2.33-2.22 (m, 2H), 1.78 (dd, *J* = 8.4, 10.8 Hz, 1H), 1.72-1.66 (m 1H), 1.63 (s, 3H), 1.62-1.53 (m, 3H), 1.40 (app q, *J* = 10.0 Hz, 1H), 0.97 (s, 3H), 0.96 (s, 3H) ppm.

^{13}C NMR (101 MHz, $CDCl_3$): δ 151.0 (C), 138.3 (C), 127.0 (CH), 113.5 (CH_2), 58.1 (CH), 56.0 (CH), 51.3 (CH_2), 48.8 (CH), 42.1 (CH_2), 34.8 (CH_2), 32.9 (C), 31.1 (CH_2), 29.9 (CH_3), 22.6 (CH_3) 21.9 (CH_3) ppm.

ATR-FTIR: 3071 (vinylic CH), 2951 (aliphatic CH), 2927 (aliphatic CH), 2858 (aliphatic CH), 1668 (endocyclic C=C), 1634 (exocylic C=C), 757 (C-Cl) cm^{-1}.

HRMS (ESI): $C_{15}H_{23}Cl$ $[M+H]^+$ requires 239.1561 *m/z*, found 239.1555 *m/z*.

8.6.9 Preparation of 4-hydroxycaryophyll-5,8-diene 185

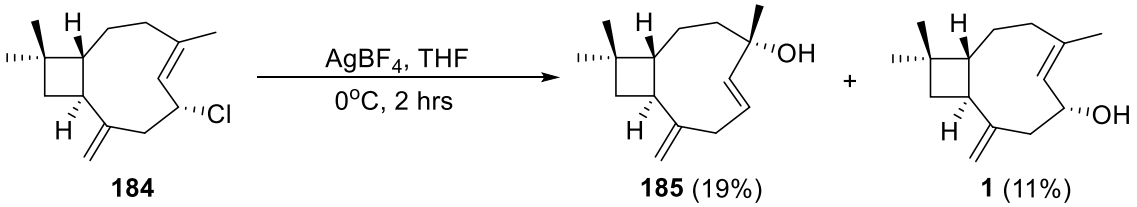

184 **185** (19%) **1** (11%)

$AgBF_4$ (114 mg, 0.58 mmol) was added to a solution of 6-chlorocaryophyllene **184** (25 mg, 0.10 mmol) in dry THF (3 mL) at 0ºC. The reacion mixture was stirred at 0ºC under N_2 and protected from light. After 2 hours, deionised water (3 mL) was added to the reaction mixture and stirred. After 16 hours the mixture was diluted with deionised water (10 mL) and extracted with Et_2O (3 x 15 mL). The combined organic extracts were dried over anhydrous $MgSO_4$ and concentrated under reduced pressure to afford a colourless oil (62 mg). The oil was purified by column chromatography (0:100-50:50 EtOAc/PS, silica gel) to afford 4-hydroxycaryophyll-5,8-diene **185** (4 mg, 19%) and 6-hydroxycaryophyllene **1** (3 mg, 11%) as colourless oils. NMR spectrum of **185** was impure, and selected signals are shown in the NMR data.

^{1}H NMR (400 MHz, $CDCl_3$): δ 5.85 (ddd, *J* = 4.8, 8.4, 16.4 Hz, 1H), 5.39 (dd, *J* = 2.0, 16.0 Hz, 1H), 4.87 (m, 1H), 4.84 (m, 1H), 2.98 (m, 1H), 2.73 (ddt, *J* = 1.6, 8.4, 15.6 Hz, 1H), 2.23 (app q, *J* = 8.0 Hz 1H), 1.87-1.80 (m, 1H), 1.68 (t, *J* = 10.8 Hz, 1H), 1.28 (s, 3H), 0.95 (s, 3H), 0.94 (s, 3H) ppm.

8.6.10 Preparation of 12-acetoxy-6-chlorocaryophyllene 186

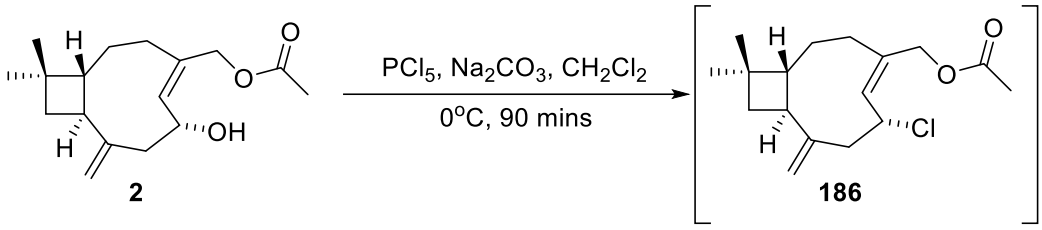

A solution of the caryophyllene acetate (34 mg, 0.12 mmol) in dry CH_2Cl_2 (5 mL) was added dropwise to a stirred slurry of PCl_5 (144 mg, 0.69 mmol) and anhydrous Na_2CO_3 (126 mg, 1.19 mmol) in dry CH_2Cl_2 (2 mL) at 0°C. Upon addition of the caryophyllene acetate **2** the reaction mixture turned bright yellow in colour. After 90 mins, the reaction mixture was filtered and the residue was washed with CH_2Cl_2. The combined filtrate and washes were concentrated under reduced pressure to afford a yellow oil (40 mg). The oil was dissolved in EtOAc (25 mL) and the solution was washed with saturated $NaHCO_3$ solution (3 x 30 mL). The organic layer was dried over anhydrous $MgSO_4$ and concentrated under reduced pressure to afford 14-acetoxy-6-chlorocaryophyllene **186** as a yellow oil (32 mg). The product was not purified further due to its instability.

8.6.11 Preparation of 12-acetoxy-6-hydroxy-Z-caryophyllene 189

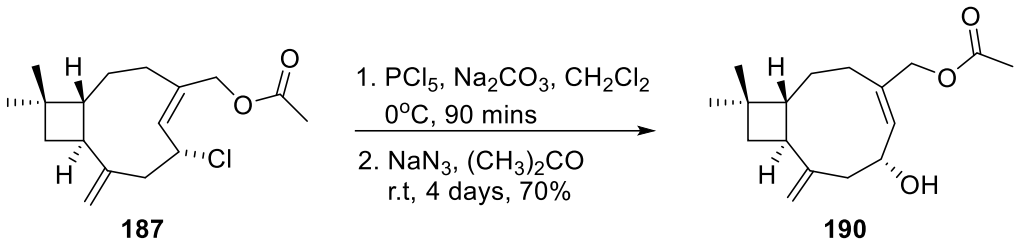

NaN_3 (23 mg, 0.35 mmol) was added to a solution of 12-acetoxy-6-chlorocaryophyllene **186** (32 mg, 0.11 mmol) in acetone (5 mL). The reaction mixture was stirred at room temperature. After 4 days, the reaction mixture was concentrated under reduced pressure to afford a white solid. The residue was diluted with deionised water (30 mL) and CH_2Cl_2 (25 mL). The organic layer was separated and the aqueous layer was further extracted with CH_2Cl_2 (2 x 25 mL). The combined organic extracts were dried over anhydrous $MgSO_4$ and concentrated under reduced pressure to afford a yellow oil (26 mg). The oil was purified by column chromatography (1:99 EtOAc/PS, silica gel) to afford 12-acetoxy-6-hydroxy-*Z*-caryophyllene **189** as a colourless oil (21 mg, 0.08 mmol, 70%).

^{1}H NMR (400 MHz, $CDCl_3$): δ 5.51 (d, *J* = 11.2 Hz, 1H), 5.08 (s, 1H), 4.94 (s, 1H), 4.72 (ddd, *J* = 6.0, 10.8, 17.2 Hz, 1H), 4.56 (d, *J* = 12.4 Hz, 1H), 4.36 (d, *J* = 12.4 Hz, 1H), 2.96 (dd, *J* = 6.0, 12.0 Hz, 1H), 2.50 (m, 1H), 2.29-2.20 (m, 2H), 2.06 (s, 3H), 1.88-1.76 (m, 2H), 1.71-1.62 (m, 2H), 1.62-1.54 (m, 1H), 1.41 (td, *J* = 2.4, 9.6 Hz, 1H), 0.98 (s, 3H), 0.97 (s, 3H) ppm.

^{13}C NMR (101 MHz, $CDCl_3$): δ 171.0 (C=O), 151.1 (C), 135.6 (C), 131.9 (CH), 114.0 (CH_2), 64.6 (CH_2), 56.4 (CH), 56.1 (CH), 51.1 (CH_2), 48.7 (CH), 42.1 (CH_2), 33.1 (C), 30.9 (CH_2), 30.3 (CH_2), 30.0 (CH_3), 21.9 (CH_3), 21.0 (CH_3) ppm.

ATR-FTIR: 3393 (OH), 3072 (vinylic CH), 2951 (aliphatic CH), 2929 (aliphatic CH), 2861 (aliphatic CH), 1738 (C=O), 1635 (C=C), 1221 (C-O) cm^{-1}.

8.6.12 Preparation of 12-acetoxy-4-hydroxycaryophyllene 190

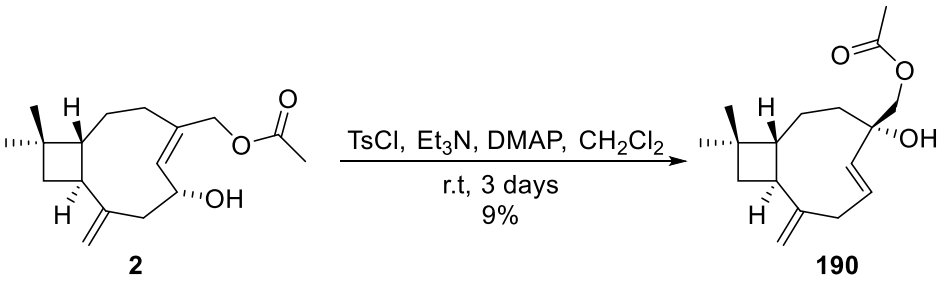

2 **190**

Et_3N (30 μL, 22 mg, 0.2 μmol) and DMAP (~1 mg) were added to a stirred solution of caryophyllene acetate **2** (27 mg, 0.10 mmol) and tosyl chloride (36 mg, 0.19 mmol) in dry CH_2Cl_2 (5 mL). The reaction mixture was stirred at room temperature. After 24 hours, tosyl chloride (26 mg, 0.14 mmol) was added to the reaction mixture and the reaction mixture was stirred at room temperature. After 2 additional days, deionised water (10 mL) was added to the reaction mixture and the reaction mixture was stirred at room temperature. After 30 mins, CH_2Cl_2 (15 mL) was added to the mixture and the organic layer was separated. The organic solution was washed with HCl solution (1M, 2 x 25 mL), followed by $NaHCO_3$ solution (5%, 2 x 25 mL). The organic layer was dried over anhydrous $MgSO_4$ and concentrated under reduced pressure to afford a yellow tinged oil (49 mg). The oil was purified by column chromatography (0:100-10:90 EtOAc/PS, silica gel) to afford impure 12-acetoxy-4-hydroxycaryophyllene **190** (8 mg). Impure 12-acetoxy-4-hydroxycaryophyllene **190** was further purified by column chromatography (0:100-50:50 CH_2Cl_2/PS, silica gel) to afford 12-acetoxy-4-hydroxycaryophyllene **190** as a colourless oil (3 mg, 9 μmol, 9%).

^{1}H NMR (400 MHz, $CDCl_3$): δ 6.03 (ddd, *J* = 4.8, 8.0, 16.0 Hz, 1H), 5.33 (dd, *J* = 2.0, 16.0 Hz, 1H), 4.88 (t, *J* = 5.6 Hz, 1H), 4.84 (s, 1H), 4.08 (d, *J* = 11.2 Hz, 1H), 3.98 (d, *J* = 11.2 Hz, 1H), 3.00 (ddd, *J* = 2.0, 4.8, 15.2 Hz, 1H), 2.76 (ddt, *J* = 2.0, 8.4, 15.6 Hz, 1H), 2.25 (app q, *J* = 9.2 Hz, 1H) 2.08 (s, 3H), 1.86 (m, 1H), 1.69 (app t, *J* = 10.8 Hz, 1H), 1.53 (dd, *J* = 8.0, 10.8 Hz, 1H), 1.45-1.39 (m, 2H), 1.31-1.26 (m, 2H), 0.95 (s, 3H), 0.94 (s, 3H) ppm.

^{13}C NMR (101 MHz, $CDCl_3$): δ 171.1 (C=O), 153.9 (C), 138.7 (CH), 125.5 (CH), 108.5 (CH_2), 75.3 (C), 70.9 (CH_2), 61.6 (CH), 45.7 (CH), 40.9 (CH_2), 38.1 (CH_2), 36.2 (CH_2), 35.3 (C), 29.9 (CH_3), 23.9 (CH_2), 22.2 (CH_3), 20.9 (CH_3) ppm.

ATR-FTIR: 3476 (OH), 2952 (aliphatic CH), 2925 (aliphatic CH), 2857 (aliphatic CH), 1739 (C=O), 1636 (C=C), 1239 (C-O) cm^{-1}.

8.6.13 Preparation of 4,5,6-trihydroxycaryophyllene aldehyde 191

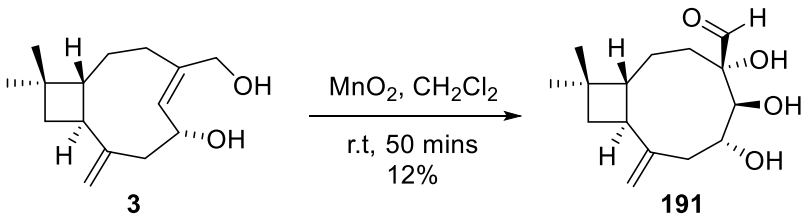

Activated MnO_2 (527 mg, 6.06 mmol) was added to a solution of the diol caryophyllene **3** (25 mg, 0.11 mmol) in dry CH_2Cl_2 (5 mL) and the reaction mixture was stirred at room temperature. After 50 mins, the reaction mixture was filtered through celite and the celite was washed with EtOAc (3 x 5 mL). The combined filtrate and washes were concentrated under reduced pressure to afford a yellow tinged oil (16 mg). The oil was purified by column chromatography (0:100-50:50 EtOAc/PS, silica gel) to afford 4,5,6-trihydroxycaryophyllene aldehyde **191** as a yellow tinged oil (3 mg, 0.01 mmol, 12%).

^{1}H NMR (400 MHz, $CDCl_3$): δ 9.18 (s, 1H), 5.01 (s, 1H), 4.96 (s, 1H), 3.86 (ddd, *J* = 6.8, 10.4, 16.8 Hz, 1H), 3.33 (d, *J* = 9.6 Hz, 1H), 2.81 (dd, *J* = 6.8, 12.4 Hz, 1H), 2.53 (dd, *J* = 2.4, 6.4 Hz, 1H), 2.27 (app q, *J* = 8.8 Hz, 1H), 2.07 (ddd, *J* = 1.2, 10.4, 12.4 Hz, 1H), 1.87 (dd, *J* = 8.4, 10.8 Hz, 1H), 1.79 (app t, *J* = 10.0 Hz, 1H), 1.67 (m, 1H), 1.55 (app t, *J* = 10.4 Hz, 1H), 1.42-1.35 (m, 2H), 1.02 (s, 3H), 0.98 (s, 3H) ppm.

^{13}C NMR (101 MHz, $CDCl_3$): δ 197.6 (C(H)=O), 146.8 (C), 115.7 (CH_2), 70.3 (CH), 64.5 (CH), 65.3 (C), 52.8 (CH), 47.5 (CH), 44.8 (CH_2), 42.5 (CH_2), 33.2 (C), 29.8 (CH_3), 27.7 (CH_2), 26.0 (CH_2), 21.7 (CH_3) ppm.

ATR-FTIR: 3415 (OH), 3072 (vinylic CH) 2953 (aliphatic CH), 2927 (aliphatic CH), 2858 (aliphatic CH), 1722 (C=O), 1637 (exocyclic C=C), 1040 (C-O) cm^{-1}.

8.6.14 Preparation of caryophyllene butenolide 192

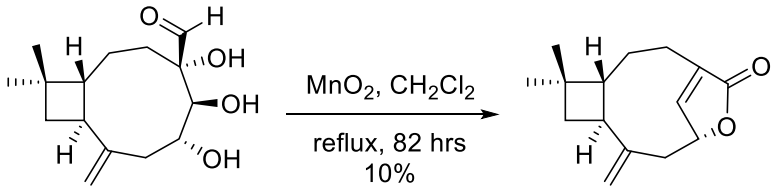

191 **192**

A mixture of activated MnO_2 (349 mg, 4.01 mmol) and aldehyde triol **191** (26 mg, 0.09 mmol) in dry CH_2Cl_2 (9 mL) was heated at reflux. After 22 hours, additional CH_2Cl_2 (10 mL) and activated MnO_2 (250 mg, 2.88 mmol) were added to the reaction mixture and reaction mixture was heated under reflux. After an additional 60 hours, the reaction mixture was diluted with CH_2Cl_2 (10 mL) and filtered through celite. The celite was washed with CH_2Cl_2 and EtOAc. The combined filtrate and washes were concentrated under reduced pressure using a weak vacuum pump to afford a yellow oil (10 mg). The oil was purified by column chromatography (0:100-10:90 EtOAc/PS, silica gel) to afford butenolide **192** as a white solid (2 mg, 0.01 mmol, 10%).

^{1}H NMR (400 MHz, $CDCl_3$): δ 6.86 (s, 1H), 5.14 (s, 1H), 5.13 (d, *J* = 6.4 Hz, 1H), 4.96 (d, *J* = 1.6 Hz, 1H), 2.79-2.52 (m, 3H), 2.19 (td, *J* = 4.4, 12.8 Hz, 1H), 2.07 (app q, *J* = 8.4 Hz, 1H), 1.95-1.86 (m, 2H), 1.69-1.58 (m, 3H), 1.04 (s, 3H), 0.94 (s, 3H) ppm.

^{13}C NMR (101 MHz, $CDCl_3$): δ 174.0 (C=O), 153.4 (C), 149.2 (CH), 132.0 (C), 114.6 (CH_2), 78.4 (CH), 57.0 (CH), 43.7 (CH_2), 40.8 (CH_2), 39.9 (CH), 31.9 (C), 30.0 (CH_3), 28.6 (CH_2), 26.2 (CH_2), 23.8 (CH_3) ppm.

ATR-FTIR: 2958 (aliphatic CH), 2924 (aliphatic CH), 2856 (aliphatic CH), 1750 (C=O), 1041 (C-O) cm^{-1}.

8.6.15 Preparation of caryophyllene enone 195

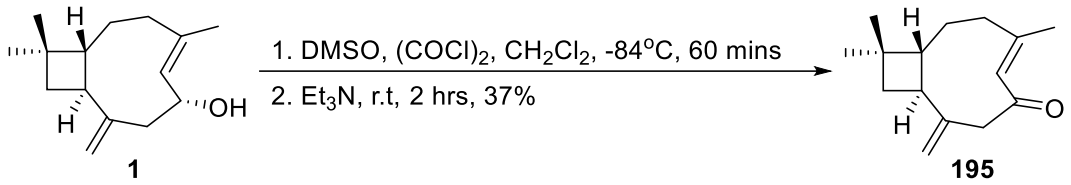

Dry DMSO (300 μL, 0.47 mmol) was added to a solution of $(COCl)_2$ (60 μL, 0.70 mmol) in dry CH_2Cl_2 (3 mL) at -84ºC and stirred. After 20 minutes a solution of 6-hydroxycaryophyllene **1** (42 mg, 0.19 mmol) in dry CH_2Cl_2 (3 mL) was added dropwise to the reaction mixture over 2 minutes and stirred at -84ºC. After 60 mins Et_3N (500 μL, 3.59 mmol) as added dropwise to the reaction mixture and stirred at -84ºC. After 2 hours, the reaction mixture was allowed to warm to room temperature and diluted with CH_2Cl_2 (30 mL). The organic solution was washed with HCl solution (1M, 2 x 30 mL), deionised water (30 mL) and brine (30 mL). The organic layer was dried over anhydrous $MgSO_4$ and concentrated under reduced pressure to afford a yellow tinged oil (56 mg). The isolated oil was purified by flash chromatography (5:95 EtOAc/PS) to give enone **195** as a yellow tinged oil (18 mg, 0.08 mmol, 37%).

^{1}H NMR (400 MHz, $CDCl_3$): δ 6.17 (s, 1H), 5.25 (s, 1H), 5.04 (s, 1H), 3.09 (d, *J* = 16.8 Hz, 1H), 2.85 (d, *J* = 16.8 Hz, 1H), 2.34 (d, *J* = 12.4 Hz, 1H), 2.22 (d, *J* = 8.8 Hz, 1H), 2.01-1.90 (m, 1H), 1.92 (dd, *J* = 8.8, 11.6 Hz, 1H), 1.79 (s, 3H), 1.78 – 1.72 (dd, *J* = 9.2, 11.6 Hz, 2H), 1.66 – 1.63 (m, 2H), 1.08 (s, 3H), 1.00 (s, 3H) ppm.

^{13}C NMR (101 MHz, $CDCl_3$): δ 202.8 (C=O), 144.7 (C), 128.9 (CH), 128.0 (C), 114.5 (CH_2), 56.8 (CH), 53.5 (br, CH_2), 43.9 (br, CH_2), 42.9 (C), 39.3 (br, CH_2), 32.8 (CH), 30.1 (CH_2), 29.0 (CH_3), 23.5 (CH_3), 18.5 (br, CH_3) ppm.

ATR-FTIR: 1716 (C=O) cm^{-1}.

***R*$_f$ =** 0.40 (5:95 EtOAc/PS, silica gel), Vanillin stain (purple).

8.6.16 Preparation of caryophyllene acetate enone 196

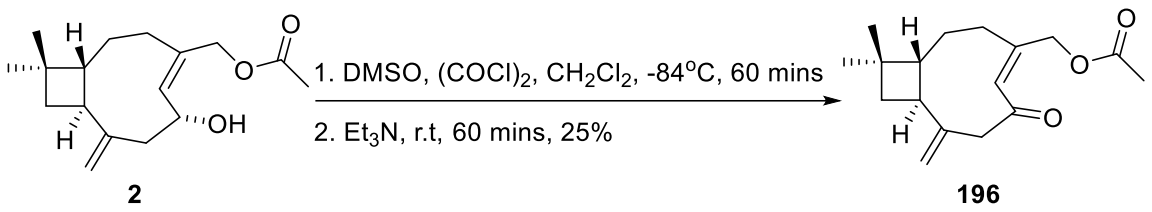

2 **196**

DMSO (290 μL, 4.08 mmol) was added to a stirred solution of $(COCl)_2$ (55 μL, 0.64 mmol) in dry CH_2Cl_2 (3 mL) at -84ºC. After 40 minutes, a solution of the caryophyllene acetate **2** (46 mg, 0.17 mmol) in dry CH_2Cl_2 (4 mL) was added to the reaction mixture at -84ºC and stirred. After 60 minutes, Et_3N (400 μL, 2.87 mmol) was added to the reaction mixture and the mixture was allowed to warm to room temperature and stirred. After 60 minutes, the reaction mixture was diluted with CH_2Cl_2 (20 mL). The organic solution was washed with HCl solution (1M, 2 x 30 mL), deionised water (30 mL) and brine (30 mL). The organic layer was dried over anhydrous $MgSO_4$ and concentrated under reduced pressure to give a yellow oil (31 mg). The oil was purified by column chromatography (50:50 CH_2Cl_2/PS, silica gel) to give the enone **196** as a colourless oil (12 mg, 0.04 mmol, 25%).

^{1}H NMR (400 MHz, $CDCl_3$): δ 6.20 (s, 1H), 5.25 (s, 1H), 5.04 (s, 1H), 4.78 – 4.61 (br m, 1H), 4.54 (d, *J* = 13.6 Hz, 1H), 3.14 (d, *J* = 16.4 Hz, 1H), 2.92 (d, *J* = 16.4 Hz, 1H), 2.46 (dt, *J* = 4.0, 13.2 Hz, 1H), 2.33 (m, 1H), 2.06 (s, 3H), 1.92 (m, *J* = 8.8, 11.6 Hz, 2H), 1.78 – 1.66 (m, 4H), 1.07 (s, 3H), 1.00 (s, 3H) ppm.

^{13}C NMR (101 MHz, $CDCl_3$): δ 202.4 (C=O), 170.6 (C=O), 139.7 (C), 131.5 (C), 130.4 (CH), 115.3 (CH_2), 63.2 (CH_2), 56.2 (CH), 54.0 (CH_2), 45.6 (CH_2), 42.8 (CH_2), 34.4 (CH), 32.9 (C), 30.1 (CH_3), 29.7 (CH_2), 23.1 (CH_3), 20.9 (CH_3) ppm.

ATR-FTIR: 3076 (vinylic CH), 2950 (aliphatic CH), 2932 (aliphatic CH), 2861 (aliphatic CH), 1742 (C=O, asym), 1703 (C=O, sym) cm^{-1}, 1634 (C=C), 1226 (C-O) cm^{-1}.

R_f = 0.16 (CH_2Cl_2, silica gel), Vanillin stain (purple).

8.6.17 Preparation of hemiacetal caryophyllene enone 197

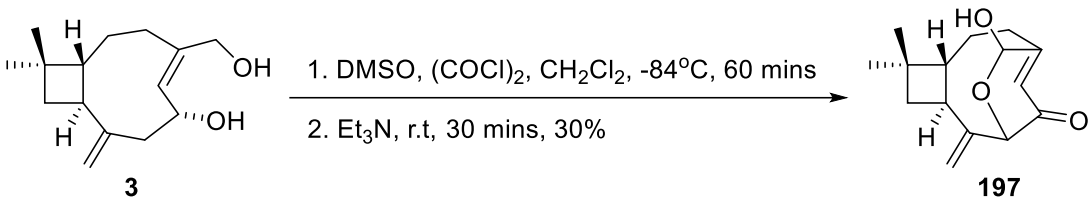

3 **197**

Dry DMSO (310 µL, 341 mg, 4.37 mmol) was added dropwise to a stirred solution of oxalyl chloride (60 µL, 89 mg, 0.70 mmol) in dry CH_2Cl_2 (2 mL) at -84ºC. After stirring for 75 mins, a solution of diol caryophyllene **3** (28 mg, 0.12 mmol) in dry CH_2Cl_2 (3 mL) was added dropwise to the reaction mixture at -84ºC. After 60 mins, Et_3N (500 µL, 363 mg, 3.59 mmol) was added to the reaction mixture at -84ºC with stirring to quench the reaction. The reaction mixture turned cloudy yellow upon addition of the Et_3N. After 30 mins, the reaction mixture was diluted with CH_2Cl_2 (20 mL). The organic solution was washed with HCl solution (1M, 2 x 20 mL), deionised water (20 mL) and brine (20 mL). The organic layer was dried over anhydrous $MgSO_4$ and concentrated under reduced pressure to afford a yellow tinged oil (21 mg). The oil was purified by column chromatography (0:100-15:85 EtOAc/PS, silica gel) to afford hemiacetal caryophyllene enone **197** as a crystalline solid (9 mg, 0.04 mmol, 30%).

^{1}H NMR (400 MHz, $CDCl_3$): δ 5.97 (dd, *J* = 1.2, 2.4 Hz, 1H), 5.13 (t, *J* = 1.6 Hz, 1H), 5.01 (t, *J* = 1.6 Hz, 1H), 4.82 (dd, *J* = 2.4, 5.2 Hz, 1H), 3.73 (d, *J* = 5.2 Hz, 1H), 2.73 (ddd, *J* = 6.8, 11.2, 18.4 Hz, 1H), 2.67 (ddd, *J* = 4.8, 11.6, 16.4 Hz, 1H), 2.22 (app q, *J* = 9.6, Hz, 1H), 2.00 (ddd, *J* = 2.8, 9.2, 12.4 Hz, 1H), 1.91 (app dquint, *J* = 2.4, 12.8 Hz, 1H), 1.79 (app t, *J* = 10.4 Hz, 1H), 1.64 (dd, *J* = 7.6, 10.4 Hz, 1H), 1.54 (dddd, *J* = 6.8, 12.4, 24.8 Hz, 1H), 0.97 (s, 3H), 0.92 (s, 3H) ppm.

^{13}C NMR (101 MHz, $CDCl_3$): δ 201.8 (C=O), 189.3 (C), 149.0 (C), 126.6 (CH), 118.1 (CH_2), 73.8 (CH), 70.3 (CH), 51.5 (CH), 42.0 (CH), 37.5 (CH_2), 35.5 (CH_2), 33.3 (C), 30.0 (CH_3), 25.6 (CH_2), 22.1 (CH_3) ppm.

ATR-FTIR: 3401 (OH), 3086 (vinylic CH), 3058 (vinylic CH), 2952 (aliphatic CH), 2829 (aliphatic CH), 2903 (aliphatic CH), 2861 (aliphatic CH), 1677 (C=O), 1113 (C-O) cm^{-1}.

HRMS (ESI): $C_{15}H_{20}O_3$ $[M+H]^+$ requires 249.1485 *m/z*, found 249.1482 *m/z*.

8.6.18 Preparation of Z-caryophyllene enone 198

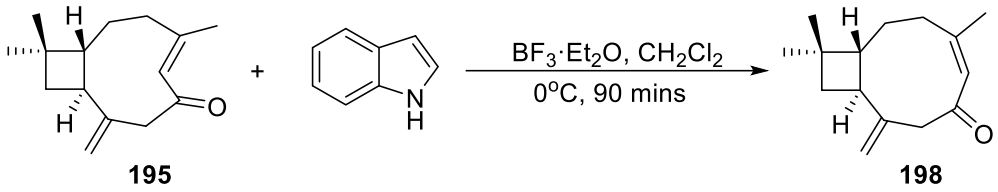

$BF_3{\cdot}Et_2O$ (20 μL, 23 mg, 0.16 mmol) was added dropwise to a stirred solution of caryophyllene enone **195** (20 mg, 0.09 mmol) and indole (12 mg, 0.10 mmol) in dry CH_2Cl_2 (4 mL) at 0ºC. The reaction mixture turned orange upon addition of the $BF_3{\cdot}Et_2O$. After 90 mins, the reaction was quenched with solid $NaHCO_3$ (56 mg, 0.67 mmol) and stirred for 20 mins. The mixture was diluted with CH_2Cl_2 (20 mL) and the organic solution was washed with saturated $NaHCO_3$ (3 x 20 mL). The organic layer was dried over anhydrous $MgSO_4$ and concentrated under reduced pressure to afford a yellow oil (23 mg). The oil was purified by column chromatography (10:90-100:0 CH_2Cl_2/PS, silica gel) to afford *Z*-caryophyllene enone **198** as a colourless oil (<1 mg). NMR spectral data matches that reported by the patent from Hiroshi *et al*.[150]

^{1}H NMR (400 MHz, $CDCl_3$): δ 5.90 (s, 1H), 5.00 (d, *J* = 1.2 Hz, 1H), 4.89 (s, 1H), 3.47 (d, *J* = 13.2 Hz, 1H), 3.42 (d, *J* = 13.2 Hz, 1H), 2.96 (m, 1H), 2.52 (app q, *J* = 8.8 Hz, 1H), 2.25 (app dt, *J* = 4.4, 13.6 Hz, 1H), 1.87 (d, *J* = 1.6 Hz, 3H), 1.79-1.73 (m, 3H), 1.69-1.62 (m, 2H), 1.03 (s, 3H), 1.00 (s, 3H) ppm.

^{13}C NMR (101 MHz, $CDCl_3$): δ 200.0 (C=O), 152.8 (C), 146.0 (C), 129.9 (CH), 113.4 (CH_2), 51.3 (CH_2), 50.4 (CH), 42.7 (CH), 37.0 (CH_2), 32.6 (C), 31.4 (CH_2), 30.5 (CH_3), 26.5 (CH_2), 25.8 (CH_3), 23.5 (CH_3) ppm.

8.6.19 Michael addition of 1,2,4-1H-triazole to caryophyllene enone 195

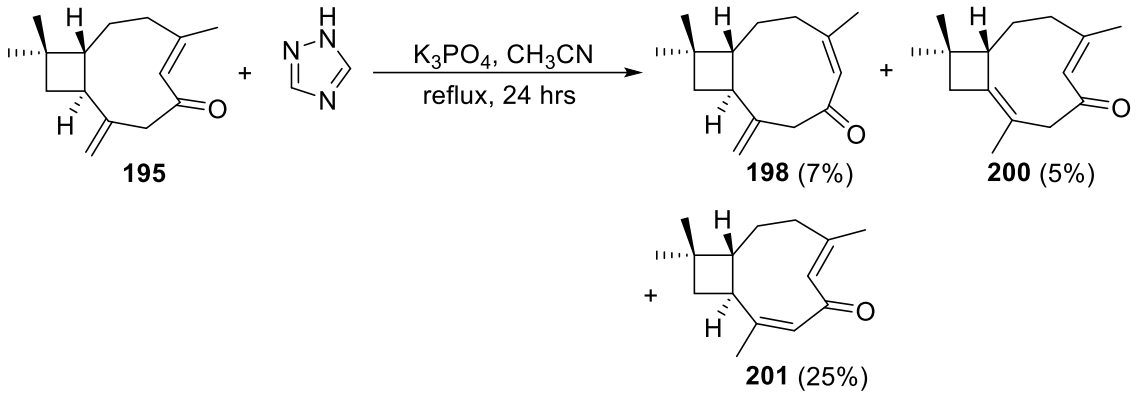

K_3PO_4 (92 mg, 0.43 mmol) was added to a solution of caryophyllene enone **195** (31 mg, 0.14 mmol) and 1,2,4-triazole (10 mg, 0.15 mmol) in dry CH_3CN (6 mL) and the reaction mixture was heated at reflux. After 24 hours, the reaction mixture was allowed to cool to room temperature. The mixture was filtered through celite and the celite was washed with CH_2Cl_2 and EtOAc. The combined filtrates and washes were concentrated under reduced pressure to afford a yellow tinged oil (27 mg). The oil was purified by column chromatography (3:97-10:90 EtOAc/PS, silica gel). Elution at 3:97 EtOAc/PS afforded *Z*-caryophyllene enone **198** as a colourless oil (2 mg, 9 μmol, 7%) and dimethyl enone **200** as a colourless oil (1 mg, 6 μmol, 5%). Elution at 10:90 EtOAc/PS afforded dienone **201** as a colourless oil (8 mg, 0.04 mmol, 25%). NMR spectral data for dienone **201** matches that reported by the patent from Hiroshi *et al*.[150]

Dimethyl enone 200

^{1}H NMR (400 MHz, $CDCl_3$): δ 5.64 (s, 1H), 3.63 (d, *J* = 13.2 Hz, 1H), 3.00 (d, *J* = 13.2 Hz, 1H), 2.60 (ddd, *J* = 1.6, 8.0, 13.6 Hz, 1H), 2.49 (d, *J* = 13.6 Hz, 1H), 2.43 (dd, *J* = 2.0, 10.8 Hz, 1H), 2.43-2.34 (m, 2H), 2.19 (d, *J* = 14.8 Hz, 1H), 1.89 (d, *J* = 1.2 Hz, 3H), 1.85-1.76 (m, 1H), 1.54-1.47 (m, 3H), 1.11 (s, 3H), 1.04 (s, 3H) ppm.

HRMS (ESI): $C_{15}H_{22}O$ $[M+H]^+$ requires 219.1743 *m/z*, found 219.1743 *m/z*.

Dienone 201

^{1}H NMR (400 MHz, $CDCl_3$): δ 6.10 (s, 1H), 6.01 (s, 1H), 3.82 (app q, *J* = 9.6 Hz, 1H), 2.87 (app t, *J* = 11.6 Hz, 1H), 2.07 (ddd, *J* = 8.0, 10.8 Hz, 1H), 1.97 (d, *J* = 1.2 Hz, 3H),

1.96 (d, *J* = 1.2 Hz, 3H), 1.90-1.81 (m, 2H), 1.69 (dd, *J* = 8.0, 13.2 Hz, 1H), 1.58 (ddd, *J* = 0.8, 8.4, 11.2 Hz, 1H), 1.53-1.46 (m, 1H), 1.06 (s, 3H), 1.00 (s, 3H) ppm.

^{13}C NMR (101 MHz, $CDCl_3$): δ 193.5 (C=O), 155.2 (C), 153.6 (C), 130.5 (CH), 128.8 (CH), 46.7 (CH), 36.4 (CH_2), 34.8 (C), 33.8 (CH), 30.3 (CH_3), 28.5 (CH_2), 25.6 (CH_3), 23.4 (CH_3), 22.7 (CH_3), 21.2 (CH_2) ppm.

ATR-FTIR: 3018 (vinylic CH), 2947 (aliphatic CH), 2938 (aliphatic CH), 2864 (aliphatic CH), 1602 (C=O) cm^{-1}.

HRMS (ESI): $C_{15}H_{22}O$ $[M+H]^+$ requires 219.1741 *m/z*, found 219.1743 *m/z*.

8.6.20 Preparation of Diels-Alder adduct 208

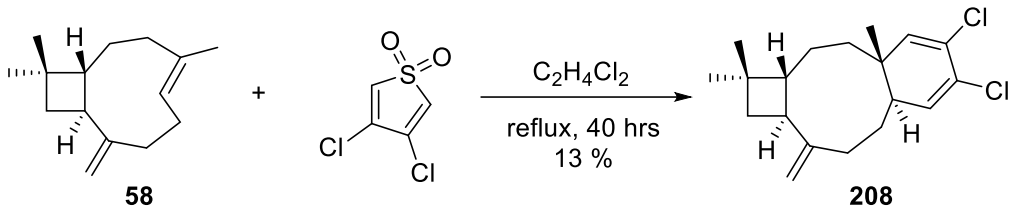

3,4-Dichlorothiophene-1,1-dioxide (59 mg, 0.32 mmol) was added to a solution of β-caryophyllene **58** (53 mg, 0.26 mmol) in 1,2-dichloroethane (6 mL) and heated at reflux. After 24 hours, the reaction mixture was allowed to cool to room temperature and concentrated under reduced pressure to afford an orange oil (110 mg). The oil was purified using column chromatography (PS, silica gel) to afford the adduct as a yellow tinged oil (33 mg). The oil was further purified using radial chromatography to afford Diels-Alder adduct **208** as a colourless oil (11 mg, 0.03 mmol, 13%).

^{1}H NMR (400 MHz, $CDCl_3$): δ 5.56 (d, *J* = 2.4 Hz, 1H), 5.53 (s, 1H), 4.95 (s, 1H), 4.86 (s, 1H), 2.60 (m, 1H), 2.42 (app q, *J* = 9.6 Hz, 1H), 2.29 (ddd, *J* = 4.0, 10.0, 14.0 Hz, 1H), 2.21 – 2.14 (m, 1H), 1.96 (m, 1H), 1.80 – 1.71 (m, 2H), 1.69 – 1.47 (m, 4H), 1.38 (dtd, *J* = 4.0, 8.0, 14.0 Hz, 1H), 1.12 – 1.02 (m, 1H), 0.99 (s, 3H), 0.98 (s, 3H), 0.92 (s, 3H) ppm.

^{13}C NMR (101 MHz, $CDCl_3$): δ 151.5 (C), 137.7 (CH), 131.3 (CH), 125.4 (C-Cl), 125.4 (C-Cl), 111.1 (CH_2), 57.6 (CH), 42.8 (CH_2), 42.0 (CH), 40.8 (C), 38.8 (CH), 36.2 (CH_2), 35.6 (CH_2), 34.4 (C), 30.1 (CH_3), 28.1 (CH_2), 23.8 (CH_2), 22.1 (CH_3), 18.6 (CH_3) ppm.

8.6.21 Preparation of formylphloroglucinol 210

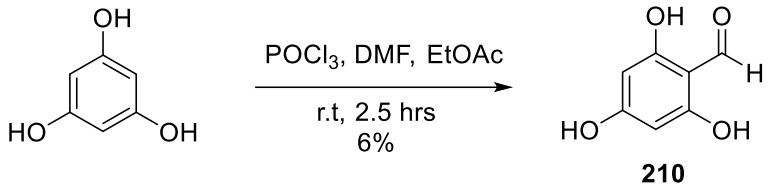

210

Phosphoryl chloride (1.28 mL, 13.7 mmol) was added to a solution of phloroglucinol (1.003 g, 7.95 mmol) and dry DMF (1.05 mL, 16.8 mmol) in dry EtOAc (16 mL). Upon addition of the phosphoryl chloride, the reaction mixture turned cloudy yellow. After 2.5 hours, deionised water (10 mL) was added to the reaction mixture and the mixture was extracted with EtOAc (3 x 30 mL). The combined organic extracts were washed with brine (2 x 100 mL) and dried over anhydrous Na_2SO_4 for 15 minutes. The dried organic extract was concentrated under reduced pressure to afford a yellow-orange solid (0.176 g). The solid was purified by flash chromatography (3:97 MeOH/CH_2Cl_2, silica gel) to afford formylphloroglucinol **210** an off-white solid (80 mg, 0.516 mol, 6%). NMR and FTIR spectral data matched that reported by Lawrence *et al*.[155]

^{1}H NMR (400 MHz, DMSO-*d*$_6$): δ 9.92 (s, 1H), 5.78 (s, 2H) ppm.
^{13}C NMR (101 MHz, DMSO-*d*$_6$): δ 190.9 (C=O), 167.3 (C), 164.1 (C), 104.5 (C), 94.1 (CH) ppm.
ATR-FTIR: 3318 (O-H, s), 1638 (C=O, asym), 1601 (C=O, sym), 1573 (ar, C=C), 1471 (ar, C=C) cm^{-1}.

8.6.22 Preparation of diformylphloroglucinol 209

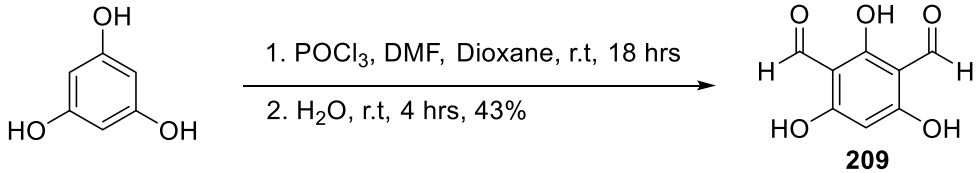

209

Phosphoryl chloride (1.6 mL, 17.1 mmol) was slowly added dropwise to stirred DMF (1.3 mL, 16.8 mmol) at room temperature. Upon addition, the reaction mixture turned pale yellow and was allowed to stir at room temperature. After 3 hours, a solution of phloroglucinol (0.999 g, 7.9 mmol) in dry dioxane (5 mL) was added dropwise to the Vilsmeier reagent over 5 minutes. Upon addition of the solution, the reaction mixture turned bright yellow. The reaction was allowed to stir at room temperature. After 18 hours,

the reaction mixture was cooled at 0ºC and poured into an ice-water slurry (100 mL) with stirring. After 2 hours a yellow precipitate was formed that gradually changed colour to orange. After an additional 2 hours, the orange precipitate was isolated and air-dried to afford diformylphloroglucinol **209** as an orange powder (626 mg, 3.43 mmol, 43%). NMR and FTIR spectral data matched that reported by Lawrence *et al*.[155]

^{1}H NMR (400 MHz, DMSO-*d*$_6$): δ 10.01 (s, 2H), 5.90 (s, 1H) ppm.

^{13}C NMR (101 MHz, DMSO-*d*$_6$): δ 191.5 (CHO), 169.5 (C), 169.1 (C), 103.8 (C), 94.1 (CH) ppm.

ATR-FTIR: 3350 (O-H, br), 1605 (C=O, br), 1508 (C=C, ar), 1433 (C=C, ar) cm^{-1}.

8.6.23 Preparation of caryophyllene ether 211

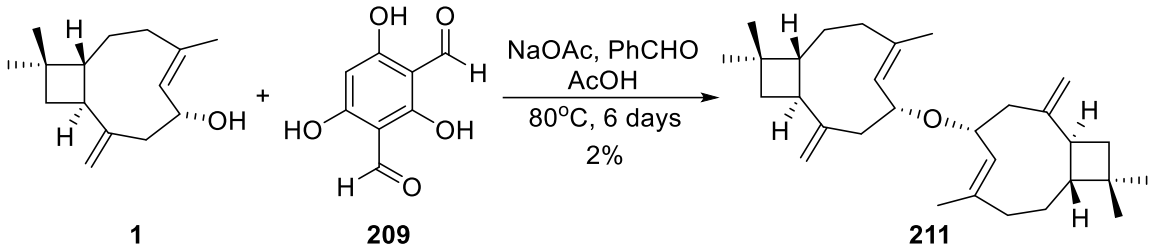

NaOAc (6 mg, 0.13 mmol) was added to a solution of benzaldehyde (60 μL, 62 mg, 0.6 μmol), diformylphloroglucincol **209** (42 mg, 0.24 mmol) and 6-hydroxycaryophyllene **1** (54 mg, 0.24 mmol) in AcOH (0.1M, 10 mL) and the reaction mixture was heated at 80ºC. After 6 days, the reaction mixture was allowed to cool to room temperature and was diluted with deionised water (20 mL) and brine (10 mL). The aqueous solution was extracted with EtOAc (3 x 30 mL). The combined organic extracts were dried over anhydrous $MgSO_4$ and concentrated under reduced pressure to afford a dark orange oil. The oil was dissolved in EtOAc (40 mL) and washed with a mixture of saturated $NaHCO_3$ solution and brine (1:1, 3 x 50 mL). The organic layer was diluted with EtOAc (20 mL) and deionised water (20 mL) and filtered through celite to remove an emulsion. A red waxy solid was trapped by the celite and the filtrate was yellow in colour. The organic layer of the filtrate was dried over anhydrous $MgSO_4$ and concentrated under reduced pressure to afford a dark orange oil (32 mg). The product was purified by column chromatography (10:90 EtOAc/PS, silica gel) to afford caryophyllene dimer **211** as a colourless oil (2 mg, 4 μmol, 2%)

^{1}H NMR (400 MHz, $CDCl_3$): δ 5.19 (d, *J* = 10.4 Hz, 2H), 4.97 (s, 2H), 4.87 (s, 2H), 4.27 (ddd, *J* = 6.8, 10.4 Hz, 2H), 2.68 (dd, *J* = 6.4, 11.6 Hz, 2H), 2.57 (br d, *J* = 13.6 Hz, 2H),

2.29 (app q, *J* = 9.2 Hz, 2H), 1.97 (app t, *J* = 10.8 Hz, 2H), 1.78 (dd, *J* = 8.0, 10.8 Hz, 2H), 1.74-1.62 (m, 2H),1.62-1.54 (m, 6H), 1.53 (s, 6H), 1.40 (app t, *J* = 9.6 Hz, 2H), 0.96 (s, 6H), 0.95 (s, 6H) ppm.

^{13}C NMR (101 MHz, $CDCl_3$): δ 150.8 (C), 138.3 (C), 127.7 (CH), 112.2 (CH_2), 75.0 (CH), 55.9 (CH), 48.9 (CH), 47.0 (CH_2), 42.5 (CH_2), 35.1 (CH_2), 32.9 (C), 31.1 (CH_2), 30.0 (CH_3), 22.7 (CH_3), 22.0 (CH_3) ppm.

HRMS (ESI): $C_{30}H_{46}O$ $[M+H]^+$ requires 423.3621 *m/z*, found 423.3621 *m/z*.

8.6.24 Preparation of 6-acetoxy-12-hydroxy-caryophyllene 212

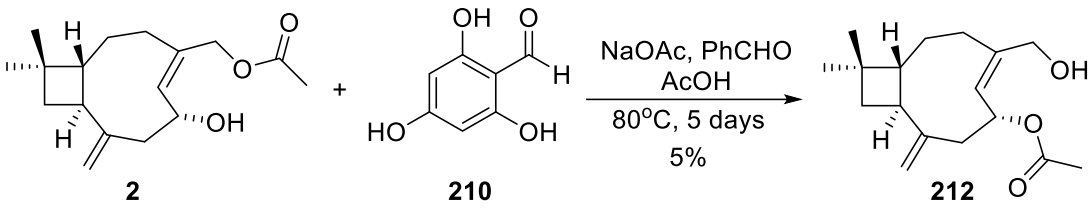

NaOAc (6 mg, 0.07 mmol) was added to a solution of benzaldehyde (30 μL, 31 mg, 0.3 μmol), formylphloroglucincol **210** (22 mg, 0.14 mmol) and caryophyllene acetate **2** (56 mg, 0.20 mmol) in AcOH (0.1M, 7 mL) and the reaction mixture was heated at 80ºC. After 5 days, the reaction mixture was allowed to cool to room temperature and was diluted with deionised water (10 mL). The aqueous solution was extracted with EtOAc (3 x 30 mL). The combined organic extracts were washed with saturated $NaHCO_3$ solution (2 x 100 mL), followed by deionised water (100 mL) and brine (100 mL). The organic layer was dried over anhydrous $MgSO_4$ and concentrated under reduced pressure to afford a yellow oil (45 mg). The oil was purified by column chromatography (0:100-3:97 MeOH/CH_2Cl_2, silica gel) to afford impure 6-acetoxy-12-hydroxycaryophyllene **212** (4 mg). The 6-acetoxy-12-hydroxycaryophyllene **212** was further purified by column chromatography (10:90-20:80 EtOAc/PS, silica gel) to afford 6-acetoxy-12-hydroxycaryophyllene **212** as a colourless oil (3 mg, 0.01 mmol, 5%).

^{1}H NMR (400 MHz, $CDCl_3$): δ 5.59 (ddd, *J* = 6.8, 10.8, 17.6 Hz, 1H), 5.29 (d, *J* = 10.4 Hz, 1H), 5.11 (s, 1H), 5.00 (s, 1H), 4.05 (s, 2H), 2.81 (dd, *J* = 6.8, 11.6 Hz, 1H), 2.51 (d, *J* = 15.6 Hz, 1H), 2.26 (app q, *J* = 9.2 Hz, 1H), 2.11-2.06 (m ,1H), 2.04 (s, 3H), 1.81 (dd, *J* = 8.0, 10.8 Hz, 1H), 1.70-1.50 (m, 3H), 1.44 (td, *J* = 1.6, 10.4 Hz, 1H), 0.98 (s, 3H), 0.97 (s, 3H) ppm.

^{13}C NMR (101 MHz, $CDCl_3$): δ 170.3 (C=O), 152.0 (C), 141.3 (C), 126.9 (CH), 113.1 (CH_2), 72.5 (CH), 63.9 (CH_2), 56.6 (CH), 48.8 (CH), 45.5 (CH_2), 42.1 (CH_2), 33.0 (C), 30.7 (CH_2), 30.4 (CH_2), 29.7 (CH_3), 21.8 (CH_3), 21.3 (CH_3) ppm.

HRMS (ESI): $C_{17}H_{26}O_3$ $[M+H]^+$ requires 279.1955 *m/z*, found 279.1949 *m/z*.

8.6.25 Preparation of N-hydroxylbenzimidoyl bromide 213

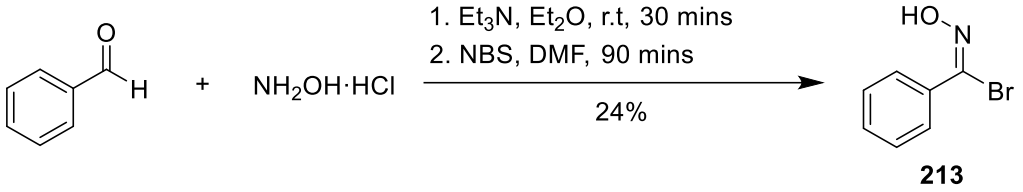

213

$NH_2OH·HCl$ (1.026 g, 14.76 mmol) was added to a stirred solution of benzaldehyde (750 μL, 0.78 g, 7.35 mmol) in Et_2O (6 mL). After 15 mins, Et_3N (4 drops) was added to the reaction mixture. After another 15 mins, the reaction mixture was dried over anhydrous $MgSO_4$ and concentrated under reduced pressure to afford a yellow oil. NBS (1.430 g, 8.03 mmol) was added to a stirred solution of the crude oil in dry DMF (9 mL). The reaction mixture turned orange upon addition of the NBS. After 90 mins, the reaction mixture was quenched with deionised water and stirred for 16 hours. The orange solution was diluted with deionised water (10 mL) and extracted with EtOAc (2 x 30 mL). The combined organic extracts were washed with deionised water (40 mL) and brine (2 x 30 mL). The organic layer was dried over anhydrous $MgSO_4$ and concentrated under reduced pressure to afford an orange solid (757 mg). For removal of residual DMF, the crude solid was dissolved in CH_2Cl_2 (50 mL) and washed with deionised water (3 x 50 mL). The organic layer was dried over anhydrous $MgSO_4$ and concentrated under reduced pressure to afford *N*-hydroxylbenzimidoyl bromide **213** as a yellow-white solid (353 mg, 1.77 mmol, 24%).

^{1}H NMR (400 MHz, $CDCl_3$): δ 8.13 (d, *J* = 7.2 Hz, 2H), 7.62 (tt, *J* = 1.2, 7.2 Hz, 1H), 7.49 (t, *J* = 7.2 Hz, 2H) ppm.

^{13}C NMR (101 MHz, $CDCl_3$): δ 171.8 (C(Br)=N-OH), 133.9 (CH), 130.4 (CH), 129.4 (C), 128.6 (CH) ppm.

Chapter 9
References

[1] A. D. Chapman, *Number of Living Species in Australia and the World, Canberra, Australian Capital Territory, Australia,* **2009**.

[2] B. Simpson, V. Bulone, S. Semple, G. Booker, R. McKinnon, P. Weinstein, *Rangel* **2016**, *38*, 467-478.

[3] C. Gutiérrez, A. Gonzalez-Coloma, J. J. Hoffmann, *Ind. Crops. Prod.* **1999**, *10*, 35-40.

[4] a) E. L. Ghisalberti, *Fitoterapia* **2004**, *75*, 429-446; b) E. Ghisalberti, *Fitoterapia* **1998**, *69*, 99-113.

[5] a) R. Carolin, D. Morrison, T. Rajput, *Australian Government Publishing Service, Canberra, Australian Capital Territory, Australia* **1992**; b) W. Elliot, D. Jones, *Encyclopaedia of Australian plants suitable for cultivation. Volume 5.* **1990**.

[6] D. G. Howarth, M. H. Gustafsson, D. A. Baum, T. J. Motley, *Am. J. Bot.* **2003**, *90*, 915-923.

[7] E. V. Lassak, *Australian medicinal plants*, Methuen Australia, **1983**.

[8] a) Z. Wang, J. Song, Z. Han, Z. Jiang, W. Zheng, J. Chen, Z. Song, S. Shang, *J. Agric. Food. Chem.* **2008**, *56*, 11361-11366; b) R. A. Dixon, *Nature* **2001**, *411*, 843-847; c) F. Chen, D. Tholl, J. C. D'Auria, A. Farooq, E. Pichersky, J. Gershenzon, *The Plant Cell* **2003**, *15*, 481-494.

[9] a) G. D. Martin, J. Narvaez, A. Marti, *J. Nat. Prod.* **2013**, *76*, 1966-1969; b) A. Zhang, A. L. Demain, *Drug Discovery and Therapeutical Medicine, New Jersey* **2005,** 382.

[10] a) E. Quinoa, Y. Kakou, P. Crews, *J. Org. Chem.* **1988**, *53*, 3642-3644; b) P. A. Wender, S. G. Hegde, R. D. Hubbard, L. Zhang, *J. Am. Chem. Soc.* **2002**, *124*, 4956-4957.

[11] Q. Wang, S. Quan, H. Xiao, *Bioresour. Bioprocess.* **2019**, *6*, 1-13.

[12] P. G. Kerr, R. B. Longmore, T. J. Betts, *Planta Med.* **1996**, *62*, 519-522.

[13] R. C. Cambie, P. S. Rutledge, K. D. Wellington, *J. Nat. Prod.* **1997**, *60*, 1303-1306.

[14] A. L. Skaltsounis, S. Sbahi, C. Demetzos, J. Pusset, *Ann. Pharm. Fr.* **1989**, *47*, 249-254.

[15] A.-L. Skaltsounis, F. Tillequin, M. Koch, J. Pusset, G. Chauvière, *Planta Med.* **1989**, *55*, 191-192.

[16] a) M. B. Majnooni, S. Fakhri, A. Smeriglio, D. Trombetta, C. R. Croley, P. Bhattacharyya, E. Sobarzo-Sánchez, M. H. Farzaei, A. Bishayee, *Molecules* **2019**, *24*, 4278; b) Y. Bansal, P. Sethi, G. Bansal, *Med. Chem. Res.* **2013**, *22*, 3049-3060; cH. Li, Y. Yao, L. Li, *J. Pharm. Pharmacol.* **2017**, *69*, 1253-1264.

[17] K. Taniguchi, M. Funasaki, A. Kishida, S. K. Sadhu, F. Ahmed, M. Ishibashi, A. Ohsaki, *Bioorg. Med. Chem. Lett.* **2018**, *28*, 1063-1066.

[18] a) F. Bohlmann, J. Jacob, M. Grenz, *Chem. Ber.* **1975**, *108*, 433-436; b) S. Yamaguchi, S. Muro, M. Kobayashi, M. Miyazawa, Y. Hirai, *J. Org. Chem.* **2003**, *68*, 6274-6278.

[19] T. Kikuchi, T. Yokoi, K. Umemoto, T, Shingu, *Yakagaku Zasshi*, **1974**, *94(12)*, 1616 .

[20] a) R. Griesbach, *Plant Breed Rev* **2005**, *25*, 89-114; b) A. Takahashi, K. Takeda, T. Ohnishi, *Plant Cell Physiol.* **1991**, *32*, 541-547.

[21] a) J. Formica, W. Regelson, *Food Chem. Toxicol.* **1995**, *33*, 1061-1080; b) A. Panche, A. Diwan, S. Chandra, *J. Nutri. Sci.* **2016**, *5*, *E47*.

[22] R. Patterson, *Syst. Bot.* **1984**, 263-265.

[23] S. F. Nobbs, *Extraction, Isolation and Structural Determination of Organic Compounds from Scaevola spiniscens R. Br., Adelaide, South Australia, Australia*, **2001**.

[24] J. Cannon, *Econ. Bot.* **1971**, *25*, 366-380.

[25] J. R. Dean, *Extraction techniques in analytical sciences, Vol. 34*, John Wiley & Sons, **2010**.

[26] A. Muruganandam, S. Bhattacharya, S. Ghosal, *Indian J. Chem.*, **2000**, 39B, 125-131.

[27] S. Sasidharan, Y. Chen, D. Saravanan, K. Sundram, L. Y. Latha, *Afr. J. Tradit. Complement. Altern. Med.* **2011**, *8, 1-10*.

[28] A. Moustafa, S. Ahmed, Z. Nabil, A. Hussein, M. Omran, *Pharm. Biol.* **2010**, *48*, 1080-1190.

[29] V. N. Moussa, B. W. Skelton, A. D. Payne, *Tetrahedron* **2016**, *72*, 7470-7480.

[30] K. M. George, D. Chatterjee, G. Gunawardana, D. Welty, J. Hayman, R. Lee, P. Small, *Science* **1999**, *283*, 854-857.

[31] a) P. P. Mitra, D. Loqué, *J. Vis. Exp.* **2014**, 87, e51381 ; b) I. Zeise, Z. Heiner, S. Holz, M. Joester, C. Büttner, J. Kneipp, *Plants* **2018**, *7(1)*, 7-23.

[32] F. Pomar, F. Merino, A. R. Barceló, *Protoplasma* **2002**, *220*, 0017-0028.

[33] G. O. Rolls, N. J. Farmer, J. B. Hall, *Artifacts in histological and cytological preparations*, Leica Microsystems' Education Series, **2008**.

[34] L. A. McDonnell, R. M. Heeren, *Mass Spectrom. Rev.* **2007**, *26*, 606-643.

[35] R. Shroff, F. Vergara, A. Muck, A. Svatoš, J. Gershenzon, *Proc. Natl. Acad. Sci. U.S.A.* **2008**, *105*, 6196-6201.

[36] A. L. Lane, L. Nyadong, A. S. Galhena, T. L. Shearer, E. P. Stout, R. M. Parry, M. Kwasnik, M. D. Wang, M. E. Hay, F. M. Fernandez, *Proc. Natl. Acad. Sci. U.S.A.* **2009**, *106*, 7314-7319.

[37] K. Saito, T. Mitsutani, T. Imai, Y. Matsushita, K. Fukushima, *Anal. Chem.* **2008**, *80*, 1552-1557.

[38] P. Larkin, *Infrared and Raman spectroscopy: principles and spectral interpretation*, USA, Elsevier, **2017**.

[39] *Vol. 2021*, ANSTO, **2021**, [online], Available at: https://www.ansto.gov.au/our-facilities/australian-synchrotron/synchrotron-beamlines/infrared-microspectroscopy.

[40] *Vol. 2021*, ANSTO, **2021**, [online], Available at: https://www.ansto.gov.au/research/facilities/australian-synchrotron/overview.

[41] H. Schulz, G. Özkan, M. Baranska, H. Krüger, M. Özcan, *Vib. Spectrosc* **2005**, *39*, 249-256.

[42] L. Sanchez, D. Baltensperger, D. Kurouski, *Anal. Chem.* **2020**, *92*, 7733-7737.

[43] M. J. Baker, J. Trevisan, P. Bassan, R. Bhargava, H. J. Butler, K. M. Dorling, P. R. Fielden, S. W. Fogarty, N. J. Fullwood, K. A. Heys, *Nat. Protoc.* **2014**, *9*, 1771-1791.

[44] K. L. Summers, N. Fimognari, A. Hollings, M. Kiernan, V. Lam, R. J. Tidy, D. Paterson, M. J. Tobin, R. Takechi, G. N. George, *Biochem.*, **2017**, *56*, 4107-4116.

[45] M. Schmidt, A. Schwartzberg, P. Perera, A. Weber-Bargioni, A. Carroll, P. Sarkar, E. Bosneaga, J. Urban, J. Song, M. Balakshin, *Planta* **2009**, *230*, 589-597.

[46] U. P. Agarwal, J. D. McSweeny, S. A. Ralph, *J. Wood Chem. Technol.* **2011**, *31*, 324-344.

[47] L. Donaldson, N. Williams, *Plants* **2018**, *7(1)*, 10-26.

[48] a) M. Clericuzio, L. Toma, G. Vidari, *Eur. J. Org. Chem.* **1999**, *1999*, 2059-2065; b) A. F. Barrero, J. Molina, J. E. Oltra, J. Altarejos, A. Barragán, A. Lara, M. Segura, *Tetrahedron* **1995**, *51*, 3813-3822; c) H. J. Williams, G. Moyna, S. B. Vinson, A. I. Scott, A. A. Bell, R. D. Stipanovic, *Nat Prod Lett* **1997**, *11*, 25-30; d) A. Zardi-Bergaoui, M. Znati, F. Harzallah-Skhiri, H. B. Jannet, *Chem. Biodivers.* **2019**, *16*, e1800483.

[49] B. M. Fraga, *Nat. Prod. Rep.* **1997**, *14*, 145-162.

[50] A. Chicca, D. Caprioglio, A. Minassi, V. Petrucci, G. Appendino, O. Taglialatela-Scafati, J. r. Gertsch, *ACS Chem. Biol.* **2014**, *9*, 1499-1507.

[51] S. Koyama, A. Purk, M. Kaur, H. A. Soini, M. V. Novotny, K. Davis, C. C. Kao, H. Matsunami, A. Mescher, *PloS one* **2019**, *14*, e0216104.

[52] a) M. Clericuzio, G. Alagona, C. Ghio, L. Toma, *J. Org. Chem.* **2000**, *65*, 6910-6916; b) M. Hübner, B. Rissom, L. Fitjer, *Helv. Chim. Acta* **1997**, *80*, 1972-1982.

[53] O. Wallach, *Justus Liebigs Ann. Chem.* **1887**, *238*, 78-89.

[54] I. G. Collado, J. R. Hanson, A. J. Macías-Sánchez, *Nat. Prod. Rep.* **1998**, *15*, 187-204.

[55] a) V. A. Barkhash, M. P. Polovinka, *Russ. Chem. Rev.* **1999**, *68*, 393-414; b) L. Fitjer, A. Malich, C. Paschke, S. Kluge, R. Gerke, B. Rissom, J. Weiser, M. Noltemeyer, *J. Am. Chem. Soc.* **1995**, *117*, 9180-9189.

[56] A. F. Cameron, C. Hannaway, J. M. Robertson, *J. Chem. Soc., Perkin Trans. 2* **1973**, 1938-1942.

[57] I. G. Collado, J. Aleu, A. J. Macías-Sánchez, R. Hernández-Galán, *J. Nat. Prod.* **1994**, *57*, 738-746.

[58] A. Tkachev, Y. V. Gatilov, I. Korobeinicheva, Z. V. Dubovenko, V. Pentegova, *Chem. Nat. Compd.* **1983**, *19*, 154-162.

[59] G. Ramage, R. Whitehead, *J. Chem. Soc. (Resumed)* **1954**, 4336-4340.

[60] I. G. Collado, J. R. Hanson, A. J. Macías-Sánchez, *Tetrahedron* **1996**, *52*, 7961-7972.

[61] C. F. Amigo, I. G. Collado, J. R. Hanson, R. Hernández-Galán, P. B. Hitchcock, A. J. Macías-Sánchez, D. J. Mobbs, *J. Org. Chem.* **2001**, *66*, 4327-4332.

[62] G. Ohloff, G. Uhde, K. Schulte-Elte, *Helv. Chim. Acta* **1967**, *50*, 561-570.

[63] a) L. D. Pennington, D. T. Moustakas, *J. Med. Chem.* **2017**, *60*, 3552-3579; b) S. Pathania, R. K. Narang, R. K. Rawal, *Eur. J. Med. Chem.* **2019**, *180*, 486-508.

[64] R. R. Karimov, A. Sharma, J. F. Hartwig, *ACS Cent. Sci.* **2016**, *2*, 715-724.

[65] Y. V. Gyrdymova, S. Rubtsova, P. Slepukhin, *Chem. Nat. Compd.* **2021**, *57*, 72-78.

[66] L. Saiz-Urra, J. C. Racero, A. J. Macias-Sanchez, R. Hernandez-Galan, J. R. Hanson, M. Perez-Gonzalez, I. G. Collado, *J. Agric. Food. Chem.* **2009**, *57*, 2420-2428.

[67] Y. V. Gyrdymova, D. Sudarikov, S. Rubtsova, A. Kuchin, *Chem. Nat. Compd.* **2017**, *53*, 66-71.

[68] H. C. Lam, J. T. Spence, J. H. George, *Angew. Chem.* **2016**, *128*, 10524-10527.

[69] Y. Wu, J. Hu, C. Sun, Y. Cao, Y. Li, F. Xie, T. Zeng, B. Zhou, J. Du, Y. Tang, *Bioconjugate Chem.* **2018**, *29*, 2287-2295.

[70] H. Schulz, M. Baranska, *Vib. Spectrosc* **2007**, *43*, 13-25.

[71] G. Paczkowska, *Scaevola nitida R. Br., Vol. 2021*, Florabase, **1996**, [online], Available at: https://florabase.dpaw.wa.gov.au/browse/profile/7626.

[72] R. M. Labib, S. S. Ebada, F. S. Youssef, M. L. Ashour, S. A. Ross, *Pharmacog. Mag.* **2016**, *12*, 319.

[73] C. I. Cerceau, L. C. Barbosa, E. S. Alvarenga, A. G. Ferreira, S. S. Thomasi, *Talanta* **2016**, *161*, 71-79.

[74] M. Piochon, J. Legault, C. Gauthier, A. Pichette, *Phytochemistry* **2009**, *70*, 228-236.

[75] a) B. Shao, G. Qin, R. Xu, H. Wu, K. Ma, *Phytochemistry* **1995**, *38*, 1473-1479; b) M.-K. Wang, F.-E. Wu, Y.-Z. Chen, *Phytochemistry* **1997**, *44*, 333-335; c) M.-K. Wang, F.-E. Wu, Y.-Z. Chen, *Phytochemistry* **1993**, *34*, 1395-1397.

[76] A. Spooner, *Scaevola striata R. Br., Vol. 2021*, Florabase, **1999**, [online], Available at: https://florabase.dpaw.wa.gov.au/browse/profile/7646.

[77] G. Paczkowska, *Scaevola Calliptera Benth., Vol. 2021*, Florabase, **1996,** [online], Available at: https://florabase.dpaw.wa.gov.au/browse/profile/7602.

[78] A. Khathi, M. R. Serumula, R. B. Myburg, F. R. Van Heerden, C. T. Musabayane, *PLoS One* **2013**, *8*, e81632.

[79] a) E. Gudoityte, O. Arandarcikaite, I. Mazeikiene, V. Bendokas, J. Liobikas, *Int. J. Mol. Sci.* **2021**, *22*, 4599; b) D. Palu, A. Bighelli, J. Casanova, M. Paoli, *Molecules* **2019**, *24*, 4413.

[80] A. Spooner, *Scaevola aemula R. Br., Vol. 2021*, Florabase, **2001**, [online], Available at: https://florabase.dpaw.wa.gov.au/browse/profile/7594.

[81] *Scaevola aemula f. white, Vol. 2021*, The Royal Botanic Garden Sydney, **2021,** [online], Available at: https://rbgsydney.gardenexplorer.org/taxon-204804.aspx.

[82] G. Paczkowska, *Goodenia varia R. Br., Vol. 2021*, Florabase, **1996**, [online], Available at: https://florabase.dpaw.wa.gov.au/browse/profile/7559.

[83] D. Quaglio, S. Corradi, S. Erazo, V. Vergine, S. Berardozzi, F. Sciubba, F. Cappiello, M. E. Crestoni, F. Ascenzioni, F. Imperi, *ACS Med. Chem. Lett.* **2020**, *11*, 760-765.

[84] A. Abad, C. Agulló, M. Arnó, M. L. Marín, R. J. Zaragozá, *J. Chem. Soc., Perkin Trans. 1* **1994**, 2987-2991.

[85] T. S. G. Tennakoon, G. K. B. Gunaherath, K. T. D. De Silva, C. Padumadasa, D. S. A. Wijesundara, A. M. Abeysekera, *BMC Chem.* **2020**, *14*, 1-12.

[86] S. Santi, S. Grisan, A. Pierasco, F. De Marco, R. Musetti, *Plant Cell Environ.* **2013**, *36*, 343-355.

[87] E. C. T. Yeung, C. Stasolla, M. J. Sumner, B. Q. Huang, *Plant microtechniques and protocols*,USA, Springer, **2015**.

[88] K. L. McDonald, *Microsc. Microanal.* **2014**, *20*, 152-163.

[89] *Tissue-Tek O.C.T Compound Safety Data Sheet*, Sakura, **2008**, p. 3.

[90] R. S. Pearce, *Ann. Bot.* **2001**, *87*, 417-424.

[91] *Sectioning unembedded plant tissues*, CSIRO, **2020**.

[92] a) A. Ng, M. L. Parker, A. J. Parr, P. K. Saunders, A. C. Smith, K. W. Waldron, *J. Agric. Food. Chem.* **2000**, *48*, 5612-5617; b) Q. He, J. Yang, O. A. Zabotina, C. Yu, *PloS One* **2021**, *16*, e0250650; c) M. Espina Palanco, K. B. Mogensen, K. Kneipp, *J Raman Spectrosc.* **2016**, *47*, 156-161.

[93] J. Yabuzaki, *Database*, **2017**, *2017(1)*, bax004.

[94] T. Kim, R. S. Assary, L. A. Curtiss, C. L. Marshall, P. C. Stair, *J. Raman Spectrosc.* **2011**, *42*, 2069-2076.

[95] a) R. L. Lindroth, P. A. Koss, *J. Chem. Ecol.* **1996**, *22*, 765-771; b) S. Luo, H. Tai, B. Zebarth, X.-Q. Li, P. Millard, D. De Koeyer, X. Xiong, *Plant Mol. Biol. Rep.* **2011**, *29*, 369-378.

[96] L. Taiz, E. Zeiger, I. M. Møller, A. Murphy, *Plant Physiol. Develop.*, USA, Sinauer Associates Incorporated, **2015**.

[97] S. Dinant, N. Wolff, F. De Marco, F. Vilaine, L. Gissot, E. Aubry, C. Sandt, C. Bellini, R. Le Hir, *J. Exp. Bot.* **2019**, *70*, 871-884.

[98] C. Albenne, H. Canut, L. Hoffmann, E. Jamet, *Proteomes* **2014**, *2*, 224-242.

[99] B. S. Simpson, D. J. Claudie, N. M. Smith, R. A. McKinnon, S. J. Semple, *Phytochemistry* **2012**, *84*, 141-146.

[100] R. Atkinson, H. Gunosewoyo, A. Payne, *Unpublished Work*, Curtin University, Perth, **2019**.

[101] C. Kallepitis, M. S. Bergholt, M. M. Mazo, V. Leonardo, S. C. Skaalure, S. A. Maynard, M. M. Stevens, *Nat. Commun.* **2017**, *8*, 1-9.

[102] K. Majzner, A. Kaczor, N. Kachamakova-Trojanowska, A. Fedorowicz, S. Chlopicki, M. Baranska, *Analyst* **2013**, *138*, 603-610.

[103] L.-Q. Chu, R. Masyuko, J. V. Sweedler, P. W. Bohn, *Bioresour. Technol.* **2010**, *101*, 4919-4925.

[104] A. Boto, L. Alvarez, *Heterocycles in natural product synthesis*, **2011**, 97-152, John Wiley and Sons.

[105] a) H.-M. Niu, D.-Q. Zeng, C.-L. Long, Y.-H. Peng, Y.-H. Wang, J.-F. Luo, H.-S. Wang, Y.-N. Shi, G.-H. Tang, F.-W. Zhao, *J. Asian Nat. Prod. Res.* **2010**, *12*, 7-14; b) W. J. Olivier, N. L. Kilah, J. Horne, A. C. Bissember, J. A. Smith, *J. Nat. Prod.* **2016**, *79*, 3117-3126.

[106] A. H. J. Cross, S. G. E. Stevens, T. H. E. Watts, *J. Appl. Chem.* **1957**, *7*, 562-565.

[107] X. Tan, K. Li, Z. Wang, K. Zhu, X. Tan, J. Cao, *Plants* **2019**, *8*, 327-338.

[108] a) M. Regvar, D. Eichert, B. Kaulich, A. Gianoncelli, P. Pongrac, K. Vogel-Mikuš, I. Kreft, *J. Exp. Bot.* **2011**, *62*, 3929-3939; b) T. S. Withana-Gamage, D. D. Hegedus, X. Qiu, P. Yu, T. May, D. Lydiate, J. P. Wanasundara, *J. Agric. Food Chem.* **2013**, *61*, 901-912.

[109] M. Park, S. J. Kim, A. Vitale, I. Hwang, *Plant Physiol.* **2004**, *134*, 625-639.

[110] S. Gattolin, M. Sorieul, P. R. Hunter, R. H. Khonsari, L. Frigerio, *BMC Plant Biol.* **2009**, *9*, 1-9.

[111] G. Paczkowska, *Scaevola crassifolia Labill.*, *Vol. 2021*, Florabase, **1996**, [online], Available at: https://florabase.dpaw.wa.gov.au/browse/profile/7606.

[112] a) L. Yang, K.-S. Wen, X. Ruan, Y.-X. Zhao, F. Wei, Q. Wang, *Molecules* **2018**, *23*, 762; b) J. Radušienė, B. Karpavičienė, Ž. Stanius, *Bot. Lith.* **2012**, *18*, 101-108.

[113] F. Bohlmann, C. Zdero, R. M. King, H. Robinson, *Phytochemistry* **1979**, *18*, 1246-1247.

[114] K. Kajiyana, S. Demizu, Y. Hiraga, K. Kinoshita, K. Koyama, K. Takahashi, Y. Tamura, K. Okada, T. Kinoshita, *J. Nat. Prod.* **1992**, *55*, 1197-1203.

[115] R. C. Bansal, M. Goyal, *Activated carbon adsorption*, Boca Raton, CRC press, **2005**, 520.

[116] a) K. D. Klika, B. Demirci, J. P. Salminen, V. V. Ovcharenko, S. Vuorela, K. H. Can Başer, K. Pihlaja, *Eur. J. Org. Chem.* **2004**, *2004*, 2627-2635; b) T. Hirokawa, S. Kuwahara, *Eur. J. Org. Chem.* **2013**, *2013*, 2780-2782.

[117] a) A. Orav, E. Arak, T. Boikova, A. Raal, *Biochem. Syst. Ecol.* **2011**, *39*, 744-748; b) V. A. Isidorov, L. Szczepaniak, S. Bakier, *Food Chem.* **2014**, *142*, 101-106; c) K. H. C. Başer, B. Demirci, *Arkivoc* **2007**, *7*, 348; d) V. A. Isidorov, M. Stocki, L. Vetchinikova, *Trees* **2019**, *33*, 1329-1344; e) V. Isidorov, Ł. Szoka, J. Nazaruk, *PloS one* **2018**, *13*, e0201949.

[118] D. Vedernikov, V. Roshchin, *Russ. J. Bioorg. Chem.* **2010**, *36*, 899-908.

[119] A. W. Lutz, E. B. Reid, *J. Chem. Soc. (Resumed)* **1954**, 2265-2274.

[120] D. Vedernikov, N. Shabanova, *Khim Rastit Syr*, **2010**, *36(7)*, 899-908.

[121] M. Sköld, A.-T. Karlberg, M. Matura, A. Börje, *Food Chem. Toxicol.* **2006**, *44*, 538-545.

[122] K. Surendra, E. Corey, *J. Am. Chem. Soc.* **2008**, *130*, 8865-8869.

[123] D. Vedernikov, V. Roshchin, *uss. J. Bioorg. Chem.* **2012**, *38*, 753-761.

[124] G. Ohloff, W. Giersch, *Angew. Chem. Int. Ed.* **1973**, *12*, 401-402.

[125] a) A. Potapovich, V. Kostyuk, *Biochemistry (Moscow)* **2003**, *68*, 514-519; b) C. Rice-Evans, N. Miller, G. Paganga, *Trends Plant Sci.* **1997**, *2*, 152-159; c) A. Martínez-Sánchez, A. Gil-Izquierdo, M. I. Gil, F. Ferreres, *J. Agric. Food. Chem.* **2008**, *56*, 2330-2340.

[126] W. A. Yehye, N. A. Rahman, A. Ariffin, S. B. Abd Hamid, A. A. Alhadi, F. A. Kadir, M. Yaeghoobi, *Eur. J. Med. Chem.* **2015**, *101*, 295-312.

[127] A. Boumendjel, A. Di Pietro, C. Dumontet, D. Barron, *Med. Res. Rev.* **2002**, *22*, 512-529.

[128] F. Ververidis, E. Trantas, C. Douglas, G. Vollmer, G. Kretzschmar, N. Panopoulos, *Biotechnol. J. Health. Nutri. Tech.* **2007**, *2*, 1214-1234.

[129] T. Fukai, T. Nomura, *Heterocycles (Sendai)* **1990**, *31*, 1861-1872.

[130] J. Shen, Y. Cui, J. Gu, Y. Li, L. Li, *Comb. Chem. High Throughput Screen.* **2014**, *17*, 162-172.

[131] J. M. Jez, J. P. Noel, *J. Biol. Chem.* **2002**, *277*, 1361-1369.

[132] D. H. Jung, Y. R. Lee, S. H. Kim, *Helv. Chim. Acta* **2010**, *93*, 635-647.

[133] a) Y. Yao, H. Zhang, Z.-S. Li, *J. Mol. Model.* **2013**, *19*, 4753-4761; b) J. Li, R. Chen, R. Wang, X. Liu, K. Xie, D. Chen, J. Dai, *Acta Pharm. Sin.* **2018**, *8*, 678-686.

[134] U. Olsher, R. M. Izatt, J. S. Bradshaw, N. K. Dalley, *Chem. Rev.* **1991**, *91*, 137-164.

[135] a) S. Lee, C. J. Lim, S. Kim, R. Subramaniam, J. Zimmerman, M. P. Sibi, *Org. Lett.* **2006**, *8*, 4311-4313; b) M. P. Sibi, P. Liu, J. Ji, S. Hajra, J.-x. Chen, *J. Org. Chem.* **2002**, *67*, 1738-1745; c) H.-S. Yoon, X.-H. Ho, J. Jang, H.-J. Lee, S.-J. Kim, H.-Y. Jang, *Org. Lett.* **2012**, *14*, 3272-3275.

[136] A. Muthukaruppan, H. Arumugam, S. Krishnan, K. Kannan, M. Chavali, *J Polym. Res.* **2018**, *25*, 1-11.

[137] T.-L. Shih, H.-Y. Li, M.-S. Ke, W.-S. Kuo, *Synth. Commun.* **2008**, *38*, 4139-4149.

[138] H. C. Kolb, M. S. VanNieuwenhze, K. B. Sharpless, *Chem. Rev.* **1994**, *94*, 2483-2547.

[139] T. Harayama, O. Sakurai, H. Fukushi, Y. Tezuka, F. Yoneda, *J. Chem. Soc., Perkin Trans. 1* **1988**, 2335-2337.

[140] G. Sabitha, R. S. Babu, M. Rajkumar, J. Yadav, *Org. Lett.* **2002**, *4*, 343-345.

[141] C. Prévost, *C. R. Chim.* **1933**, *196*, 1129-1131.

[142] L. Emmanuvel, T. M. A. Shaikh, A. Sudalai, *Org. Lett.* **2005**, *7*, 5071-5074.

[143] R. A. Shenvi, E. Corey, *Org. Lett.* **2010**, *12*, 3548-3551.

[144] V. Isidorov, L. Szczepaniak, A. Wróblewska, E. Pirożnikow, L. Vetchinnikova, *Biochem. Syst. Ecol.* **2014**, *52*, 41-48.

[145] Y. Kanda, H. Nakamura, S. Umemiya, R. K. Puthukanoori, V. R. Murthy Appala, G. K. Gaddamanugu, B. R. Paraselli, P. S. Baran, *J. Am. Chem. Soc.* **2020**, *142*, 10526-10533.

[146] K. Gollnick, G. Schade, *Tetrahedron Lett.* **1968**, *9*, 689-695.

[147] R. M. Ghalib, R. Hashim, O. Sulaiman, S. H. Mehdi, A. Valkonen, K. Rissanen, S. R. Trifunović, M. B. K. Ahamed, A. M. S. A. Majid, F. Kawamura, *Eur. J. Med. Chem.* **2012**, *47*, 601-607.

[148] G. R. Flematti, E. L. Ghisalberti, K. W. Dixon, R. D. Trengove, *Science* **2004**, *305*, 977-977.

[149] A. Swetha, M. R. Reddy, B. M. Babu, H. Meshram, *Tetrahedron Lett.* **2017**, *58*, 4427-4431.

[150] K. N. Ishii Hiroshi, Morimoto Ikuko, Watanabe Sadamoto, [Patent], *Vol. JP2514916B2*, Takasago Perfumery Co Ltd, Japan, **1991**.

[151] X. Hou, H. Hemit, J. Yong, L. Nie, H. A. Aisa, *Synth. Commun.* **2010**, *40*, 973-979.

[152] A. F. Abdel-Magid, K. G. Carson, B. D. Harris, C. A. Maryanoff, R. D. Shah, *J. Org. Chem.* **1996**, *61*, 3849-3862.

[153] L. Lv, Y. Li, Y. Zhang, Z. Xie, *Tetrahedron* **2017**, *73*, 3691-3695.

[154] K.-i. Takao, S. Noguchi, S. Sakamoto, M. Kimura, K. Yoshida, K.-i. Tadano, *J. Am. Chem. Soc.* **2015**, *137*, 15971-15977.

[155] A. L. Lawrence, R. M. Adlington, J. E. Baldwin, V. Lee, J. A. Kershaw, A. L. Thompson, *Org. Lett.* **2010**, *12*, 1676-1679.

[156] S. B. Bharate, I. P. Singh, *Tetrahedron Lett.* **2006**, *47*, 7021-7024.

[157] C. Dittmer, G. Raabe, L. Hintermann, *Eur. J. Org. Chem.* **2007**, *2007*, 5886-5898.

[158] T. A. King, H. L. Stewart, K. T. Mortensen, A. J. North, H. F. Sore, D. R. Spring, *Eur. J Org. Chem.* **2019**, *2019*, 5219.

Chapter 10

Appendix A

Supplementary Raman figures

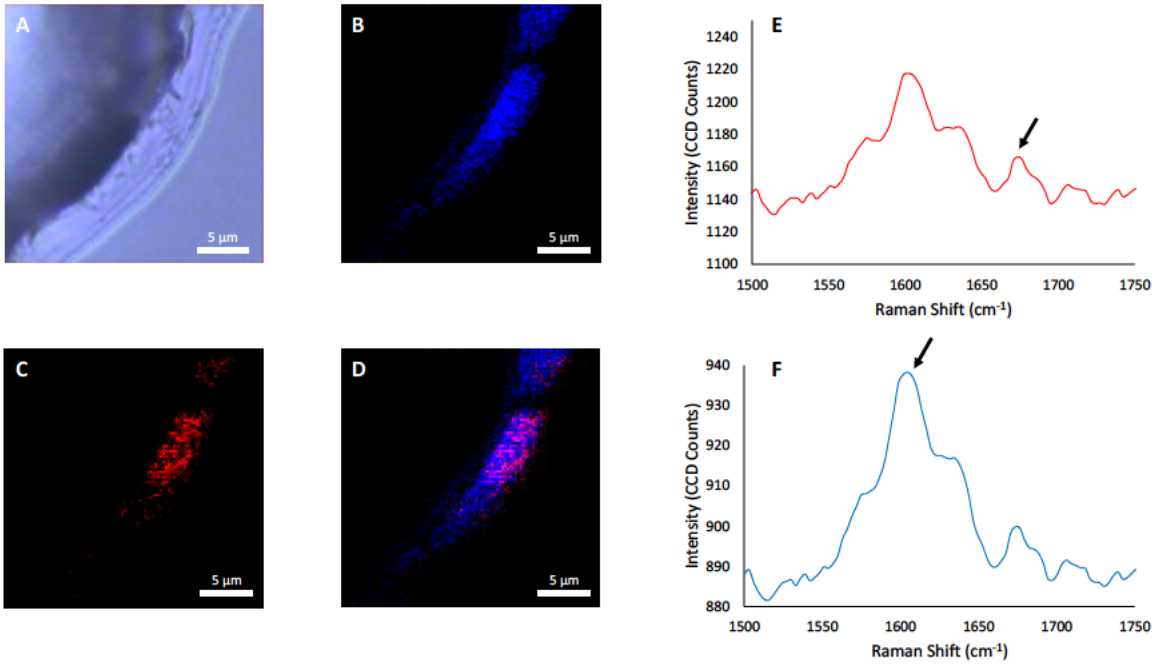

Figure A1.1. *Raman spectroscopic imaging (A-F) of S. crassifolia leaf resin. (A) Bright field image of a S. crassifolia plant cell, and the surface leaf resin (indicated by the white arrow) (B) Raman spectroscopic map of the phenol distribution with the surface leaf resin indicated by the white arrow (area under the curve aromatic C = C stretching bands, centred at 1606 cm^{-1}), (C) Raman spectroscopic map of the caryophyllene distribution (area under the curve strained C = C stretching band centred at 1678 cm^{-1}), (D) Composite Raman spectroscopic map of caryophyllene and phenol distribution, (E) representative Raman spectrum of caryophyllene distribution, (F) representative Raman spectrum of phenolic distribution. Black arrows indicate key peaks. Scale bars are 5 µm.*

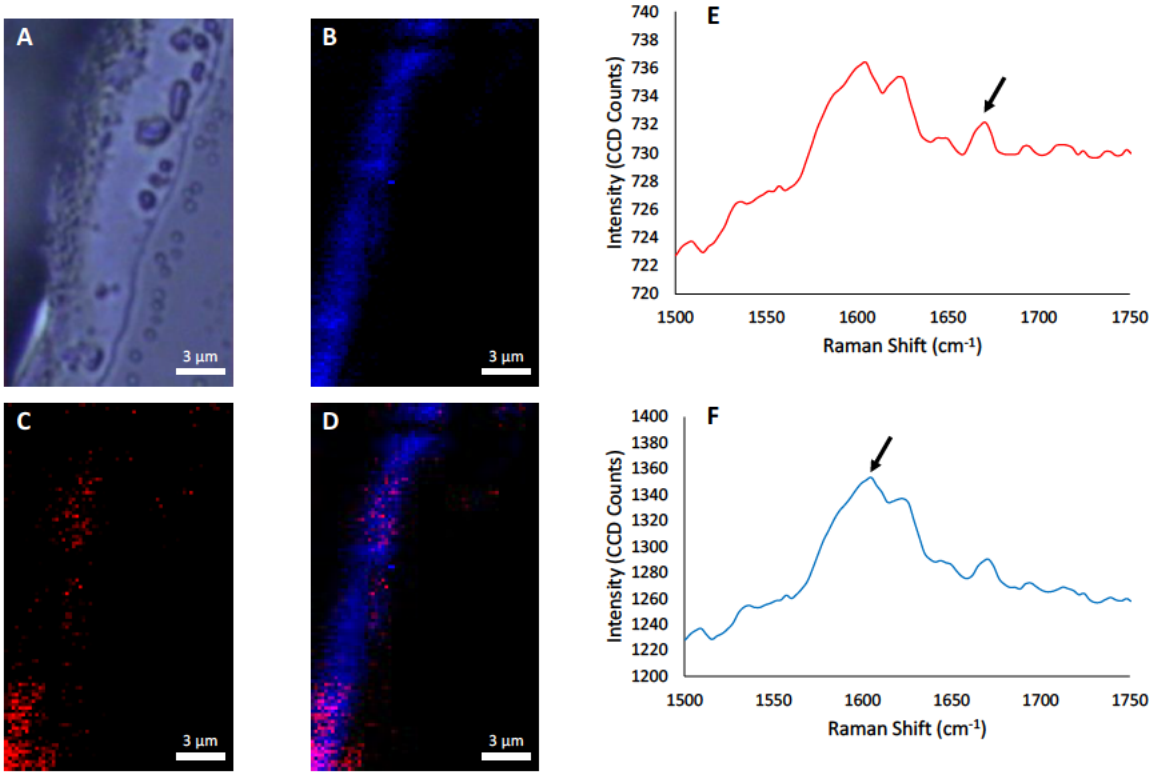

Figure A1.2. *Raman spectroscopic imaging (A-F) of S. crassifolia leaf resin. (A) Bright field image of a S. crassifolia plant cell, and the surface leaf resin (indicated by the white arrow) (B) Raman spectroscopic map of the phenol distribution with the surface leaf resin indicated by the white arrow (area under the curve aromatic C = C stretching bands, centred at 1606 cm^{-1}), (C) Raman spectroscopic map of the caryophyllene distribution (area under the curve strained C = C stretching band centred at 1667 cm^{-1}), (D) Composite Raman spectroscopic map of caryophyllene and phenol distribution, (E) representative Raman spectrum of caryophyllene distribution, (F) representative Raman spectrum of phenolic distribution. Black arrows indicate key peaks. Scale bars are 5 µm.*

Appendix B

NMR Spectra

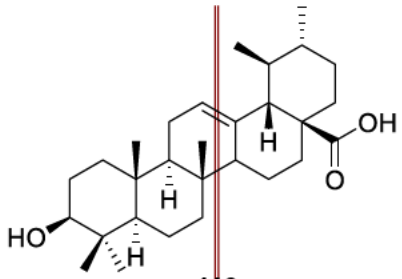

110

^{1}H NMR Spectrum
(400 MHz, C_5D_5N)

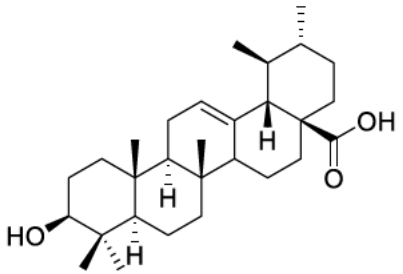

110

^{13}C NMR Spectrum
(101 MHz, C_5D_5N)

180.461
139.780
126.176
78.677
56.349
54.081
48.580
43.028
40.494
40.015
39.933
39.904
39.612
37.977
37.805
34.102
31.597
29.342
29.212
28.618
25.440
24.443
23.460
21.939
19.309
18.050
17.994
17.109
16.204

288

230 220 210 200 190 180 170 160 150 140 130 120 110 100 90 80 70 60 50 40 30 20 10 0 -1
f1 (ppm)

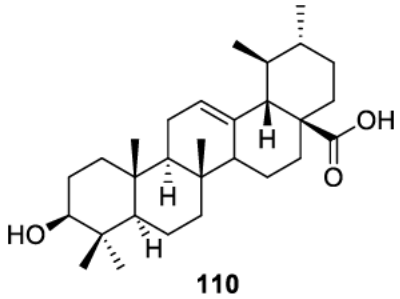

110

^{1}H NMR Spectrum
(400 MHz, $CDCl_3$)

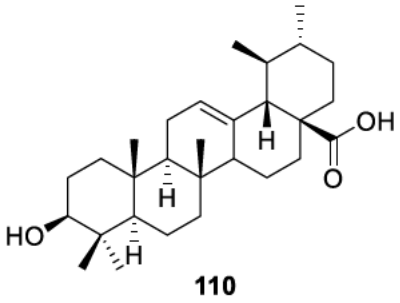

110

^{1}H NMR Spectrum
(400 MHz, $CDCl_3$)

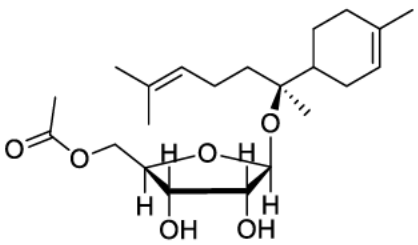

111

^{1}H NMR Spectrum
(400 MHz, $CDCl_3$)

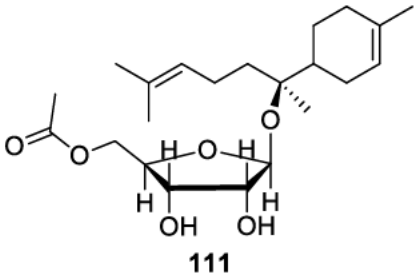

111

^{13}C NMR Spectrum
(101 MHz, $CDCl_3$)

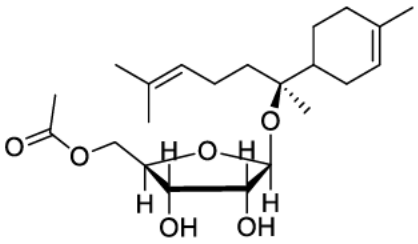

111

DEPT135 NMR Spectrum
(101 MHz, $CDCl_3$)

111
COSY NMR Spectrum
($CDCl_3$)

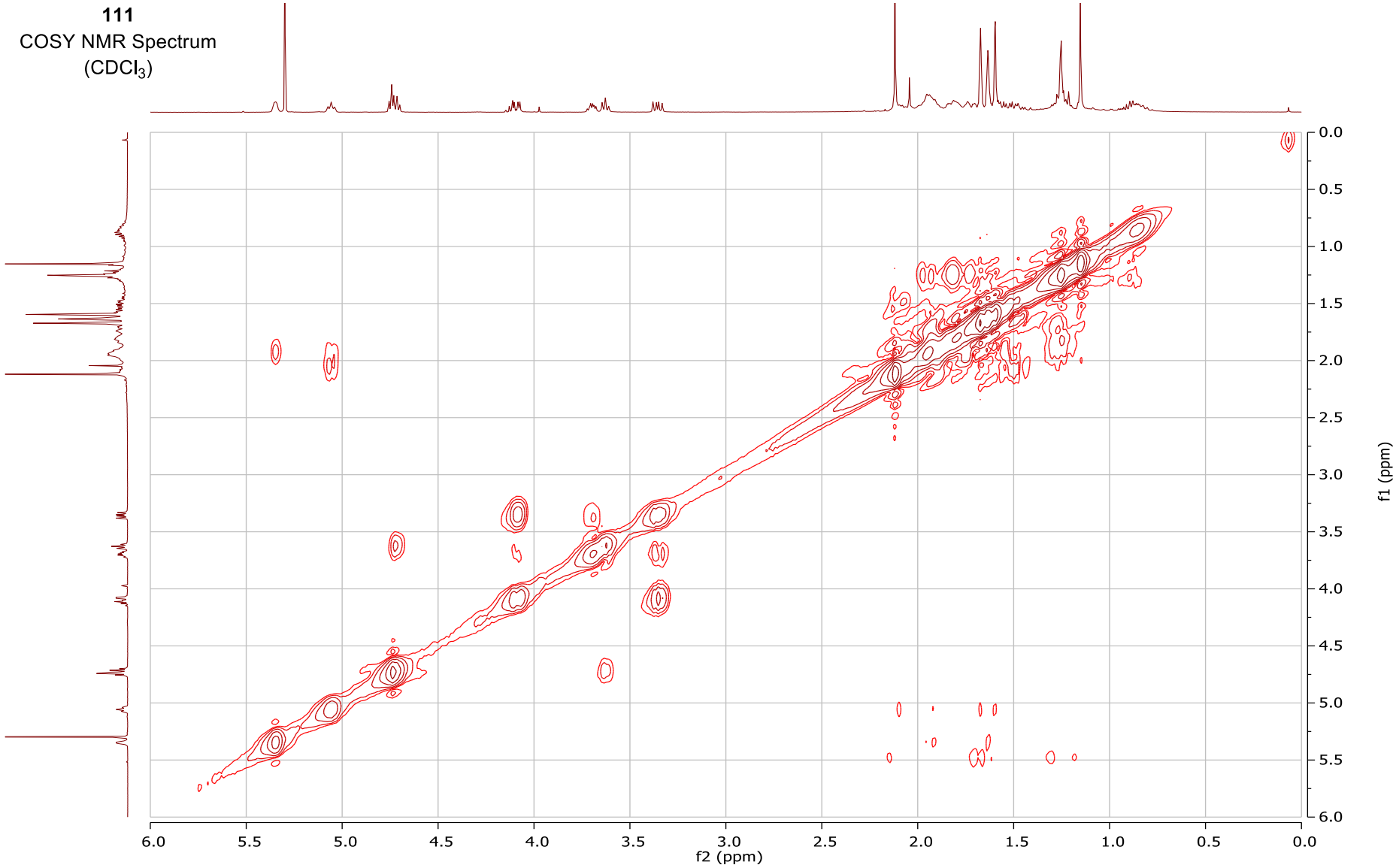

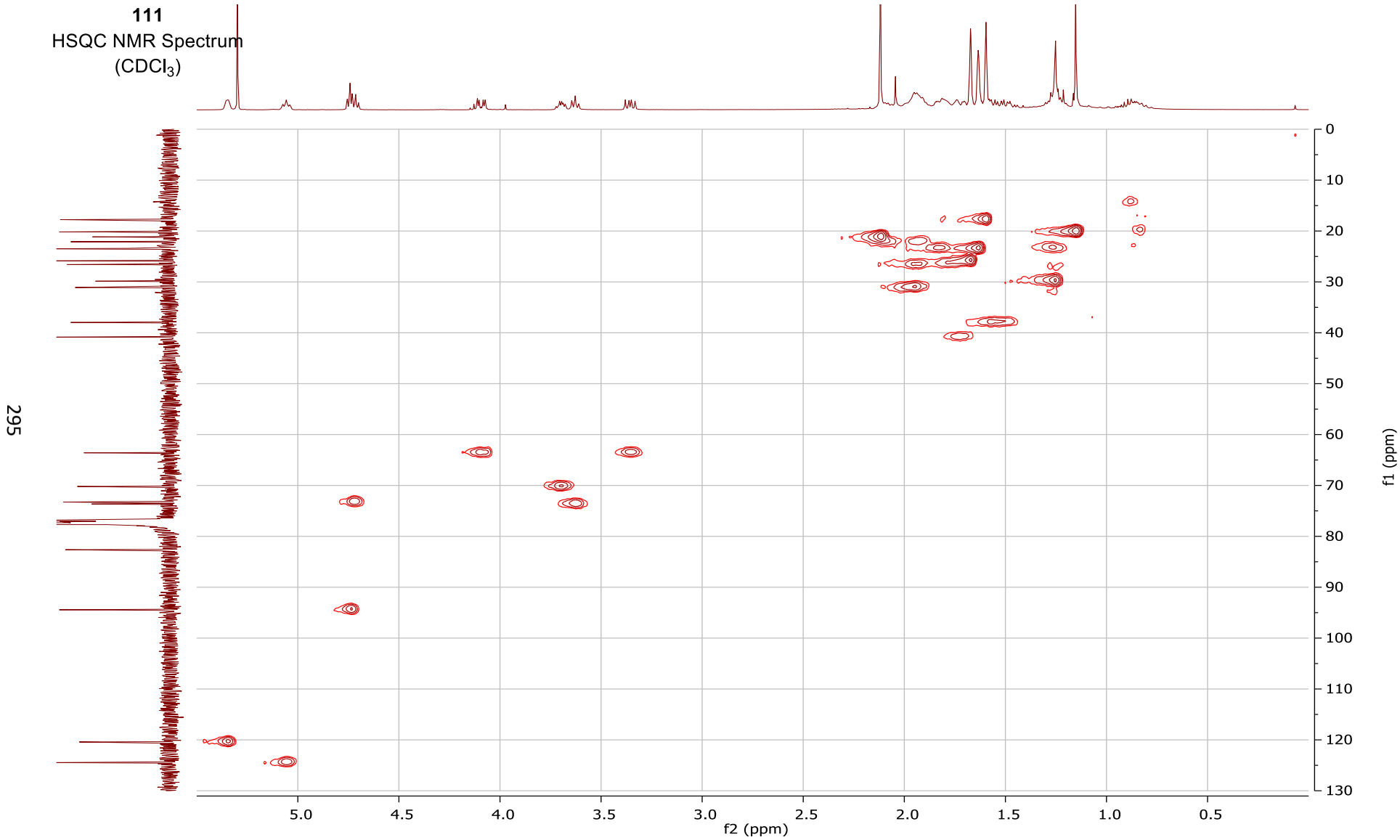
111
HSQC NMR Spectrum
(CDCl3)
295
f2 (ppm)
f1 (ppm)
5.0
4.5
4.0
3.5
3.0
2.5
2.0
1.5
1.0
0.5
0
10
20
30
40
50
60
70
80
90
100
110
120
130

111

HMBC NMR Spectrum

($CDCl_3$)

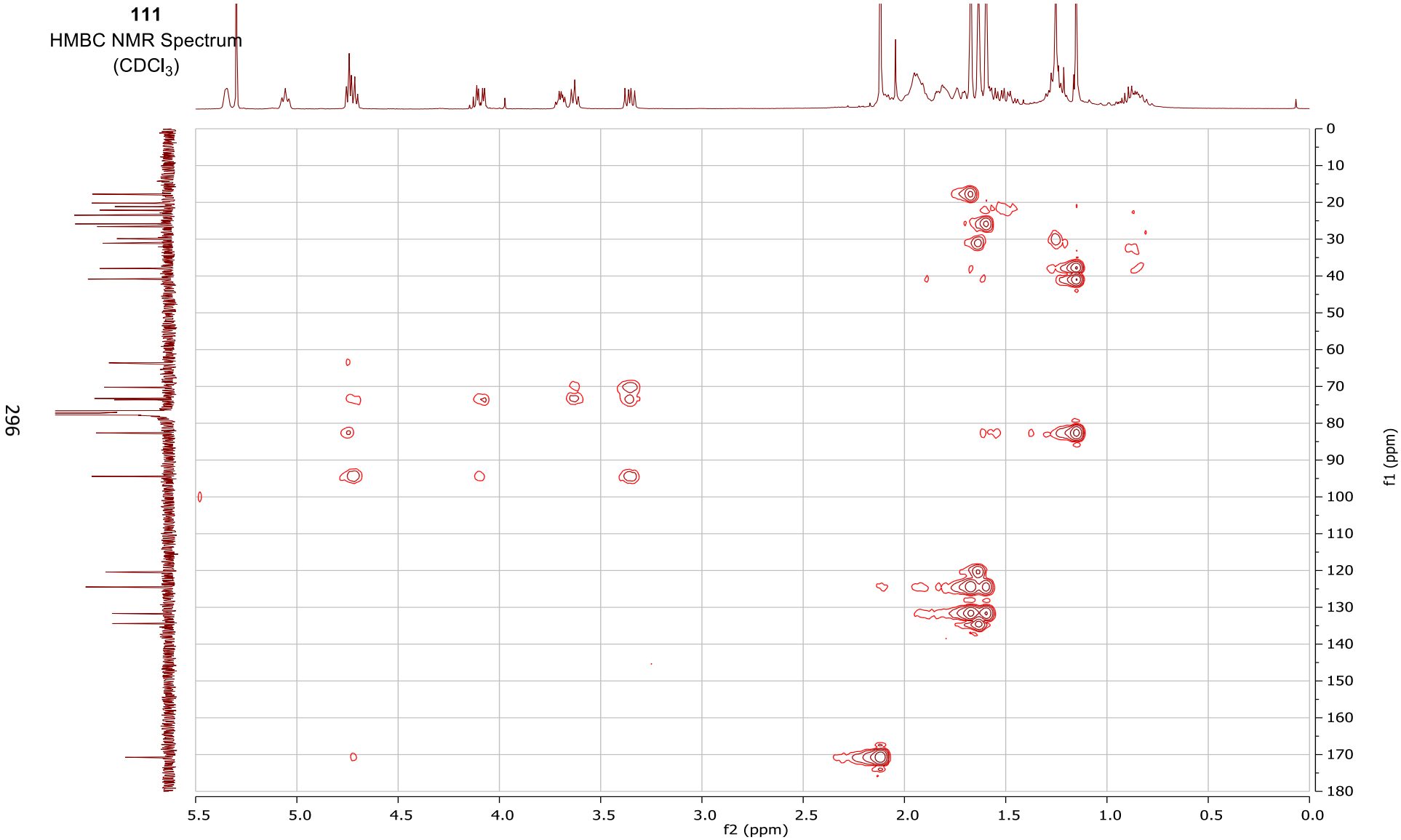

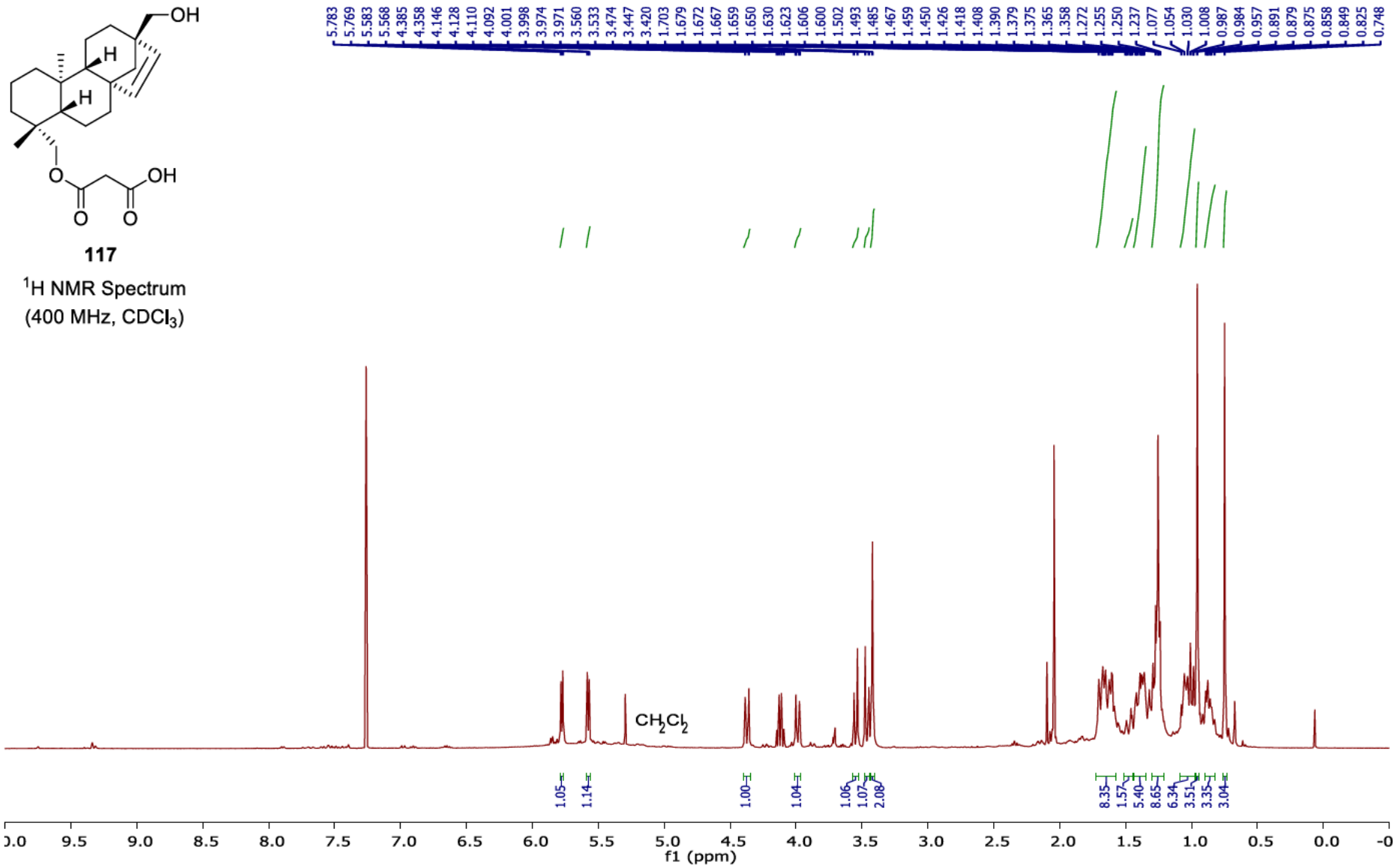

117

^{1}H NMR Spectrum
(400 MHz, $CDCl_3$)

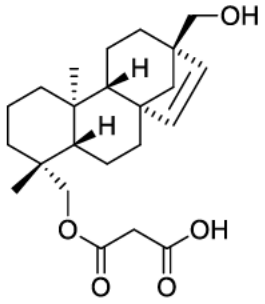

117

^{13}C NMR Spectrum
(101 MHz, $CDCl_3$)

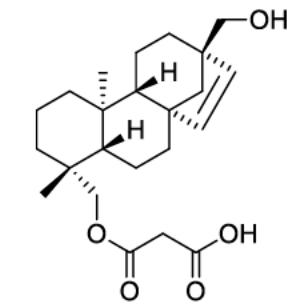

117

DEPT135 NMR Spectrum
(101 MHz, $CDCl_3$)

117

COSY NMR Spectrum

($CDCl_3$)

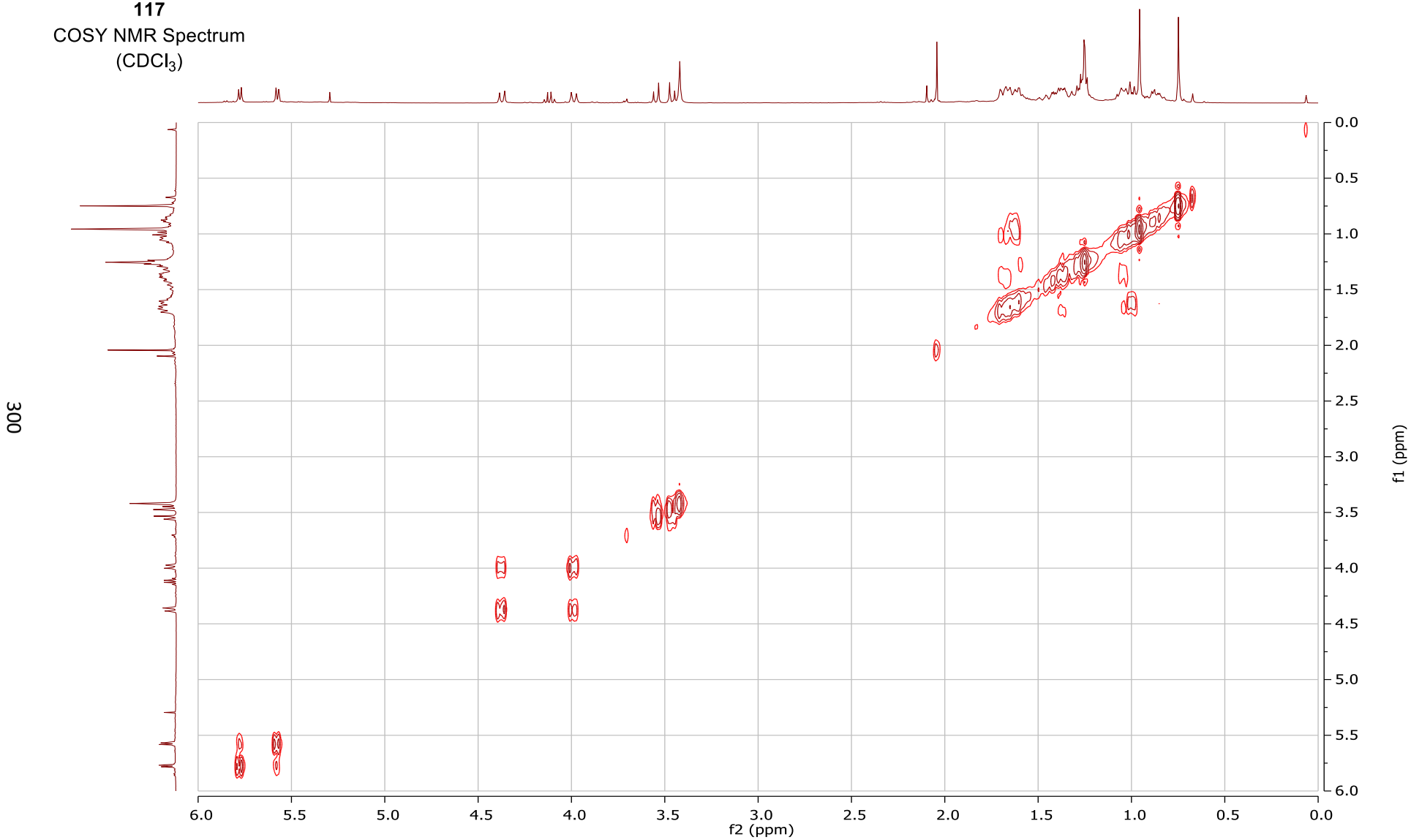

117

HSQC NMR Spectrum

($CDCl_3$)

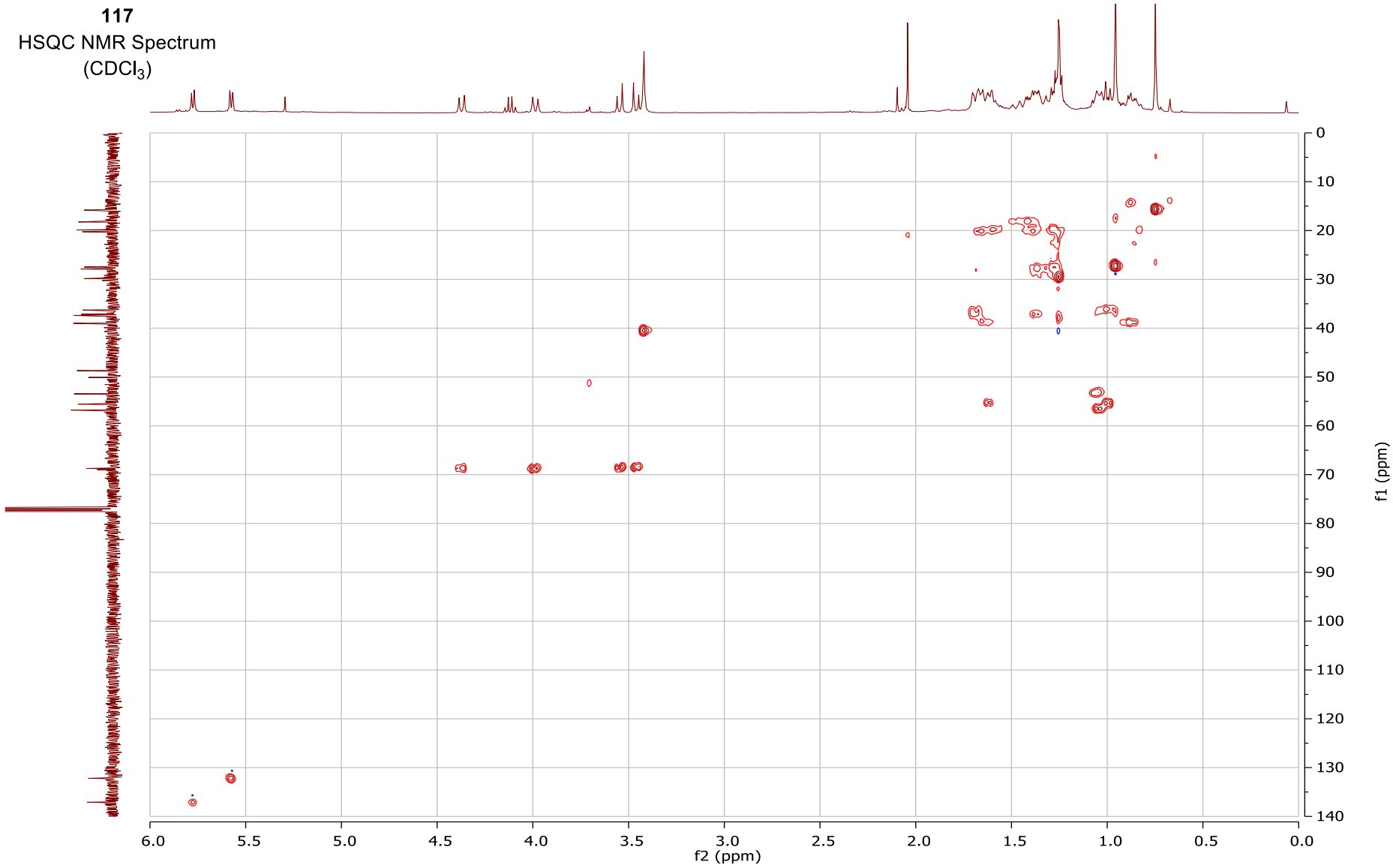

117

HMBC NMR Spectrum

($CDCl_3$)

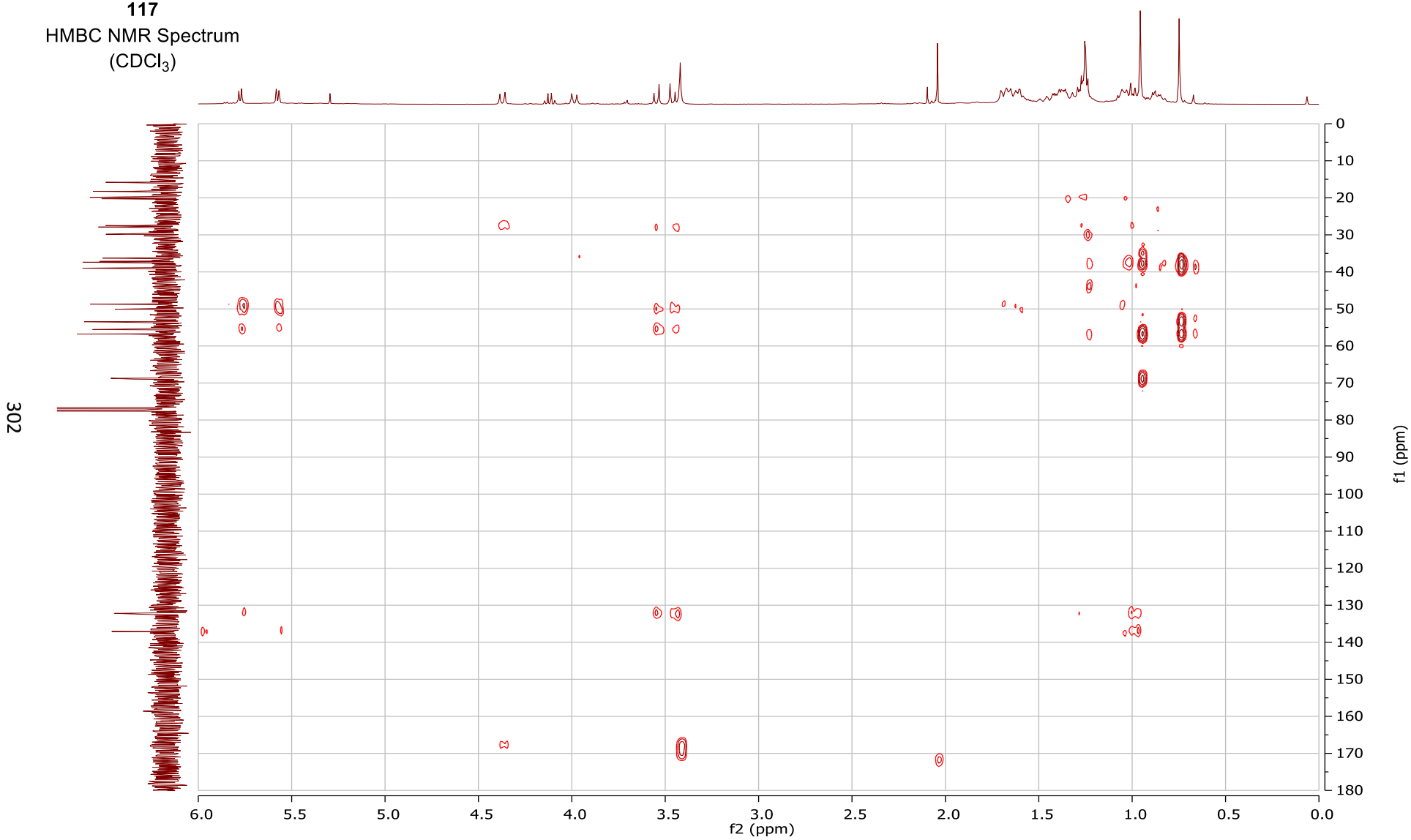

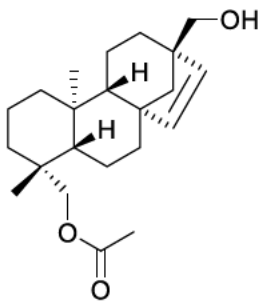

120

^{1}H NMR Spectrum
(400 MHz, $CDCl_3$)

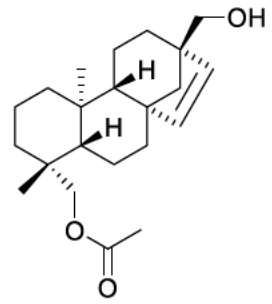

120

^{13}C NMR Spectrum

(101 MHz, $CDCl_3$)

171.592
137.110
132.153
68.718
67.222
56.810
55.587
53.480
50.089
48.689
39.067
37.465
37.366
37.031
36.316
27.896
27.597
21.142
20.237
19.853
18.286
15.829

f1 (ppm)

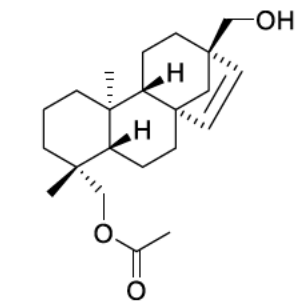

120

DEPT135 NMR Spectrum
(101 MHz, $CDCl_3$)

120

COSY NMR spectrum

($CDCl_3$)

120

HSQC NMR spectrum

($CDCl_3$)

307

120

HMBC NMR spectrum

($CDCl_3$)

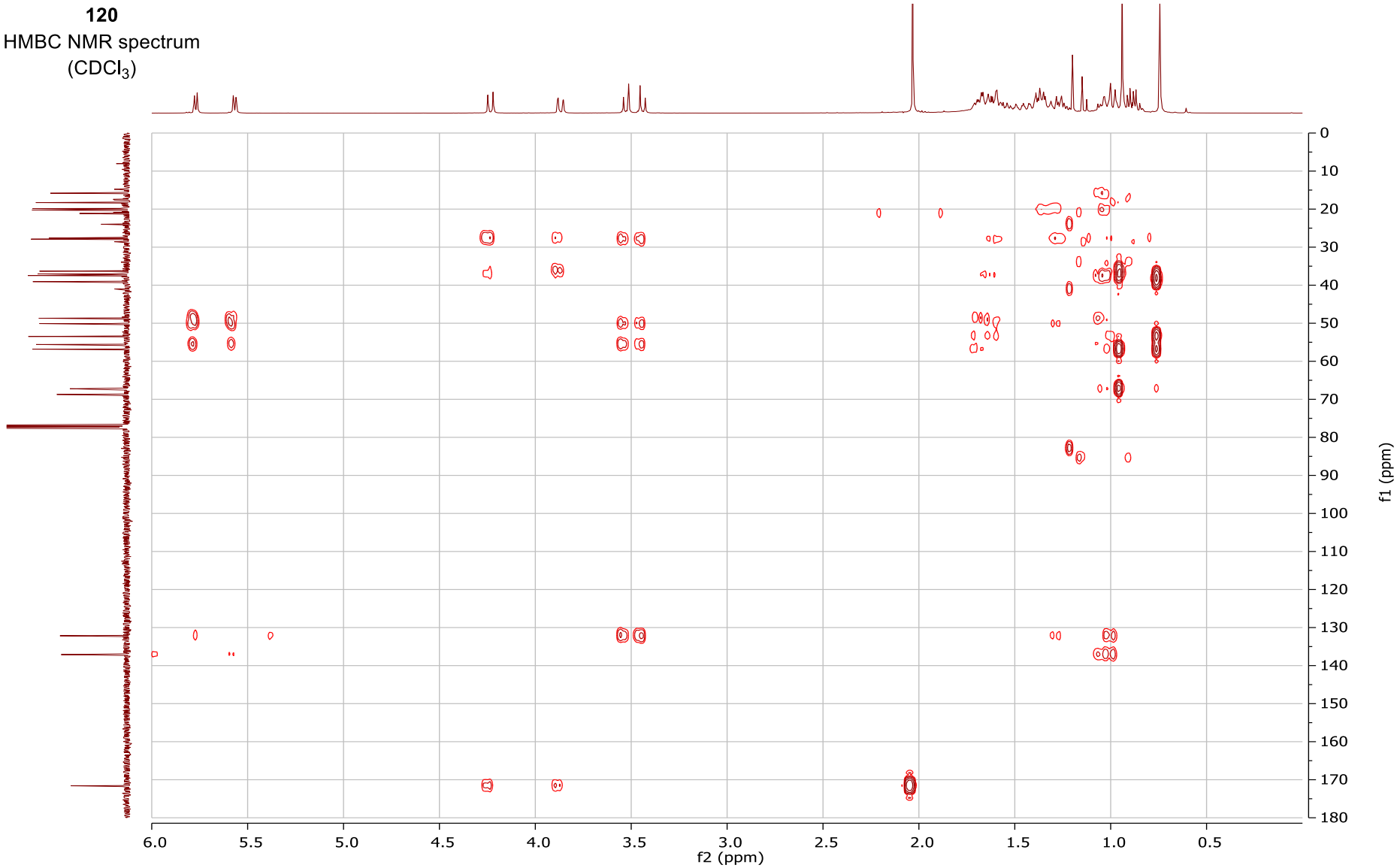

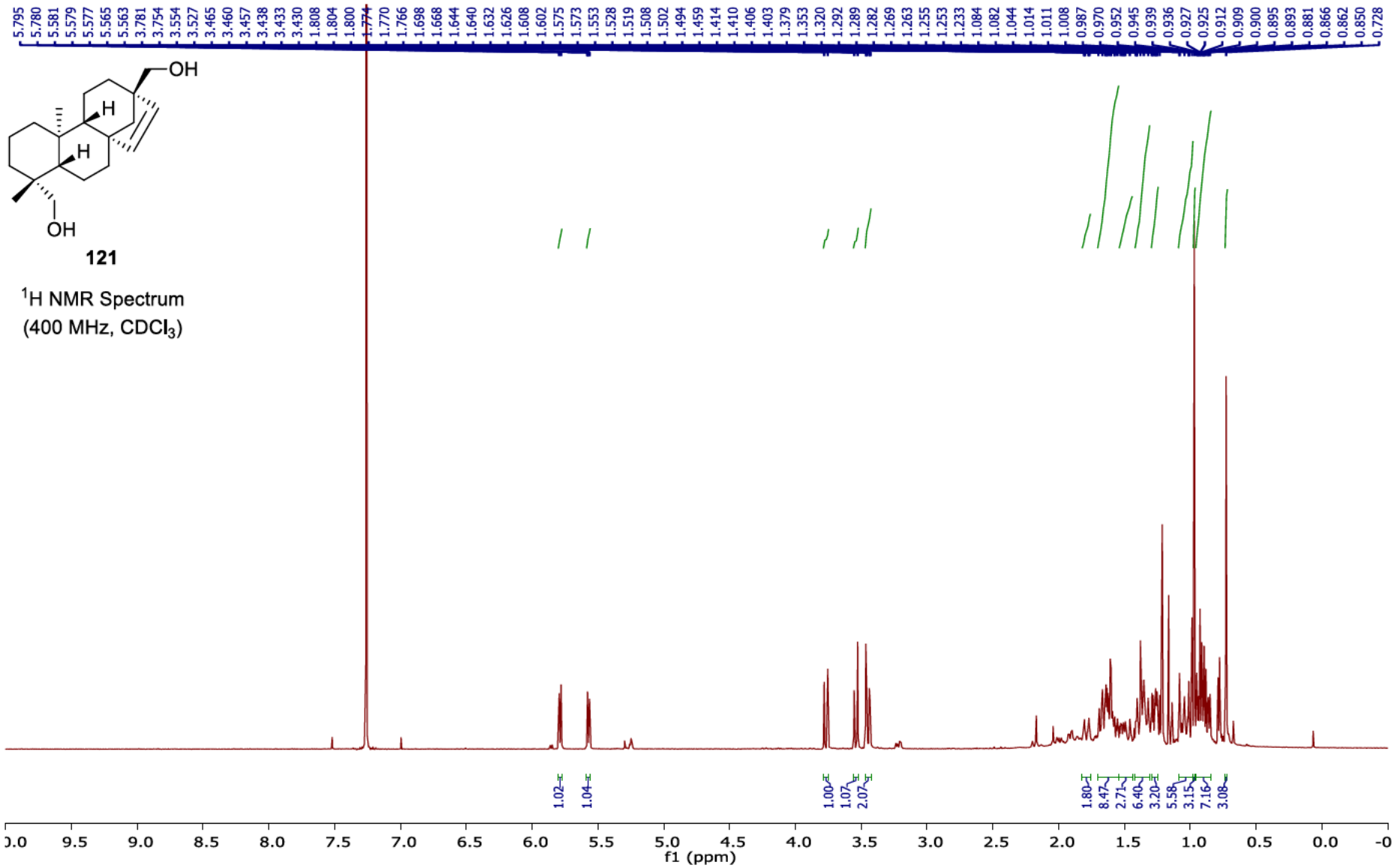
OH
H
H
OH
121
1H NMR Spectrum
(400 MHz, CDCl3)
f1 (ppm)

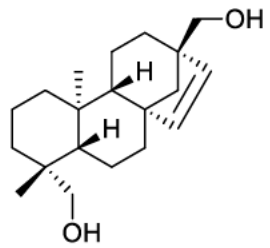

121

^{13}C NMR Spectrum
(101 MHz, $CDCl_3$)

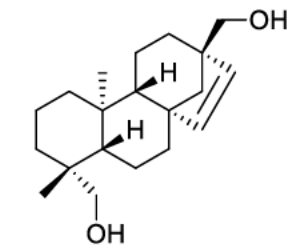

121

DEPT135 NMR Spectrum
(101 MHz, $CDCl_3$)

121

COSY NMR spectrum

($CDCl_3$)

121

HSQC NMR spectrum

($CDCl_3$)

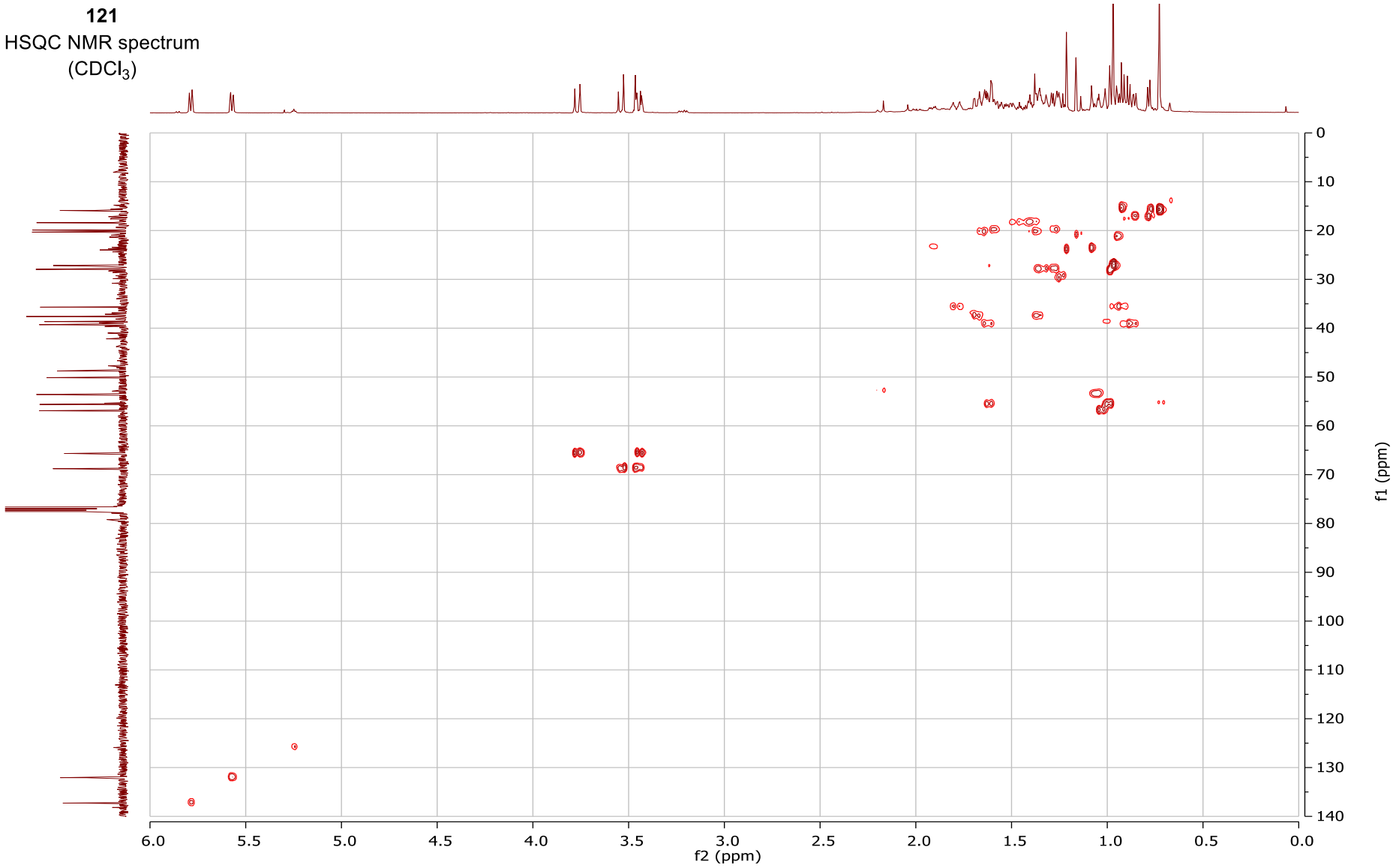

121

HMBC NMR spectrum

($CDCl_3$)

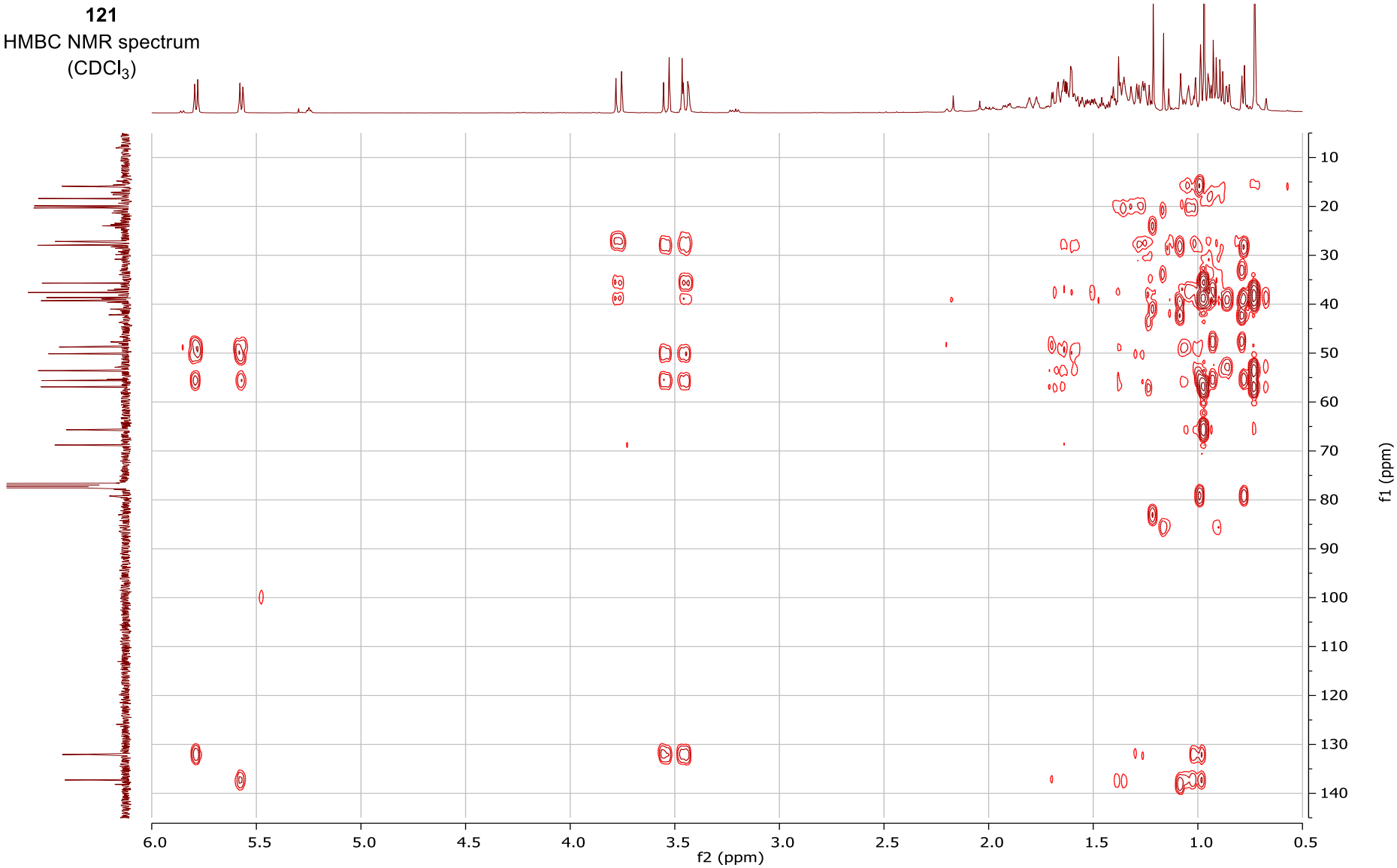

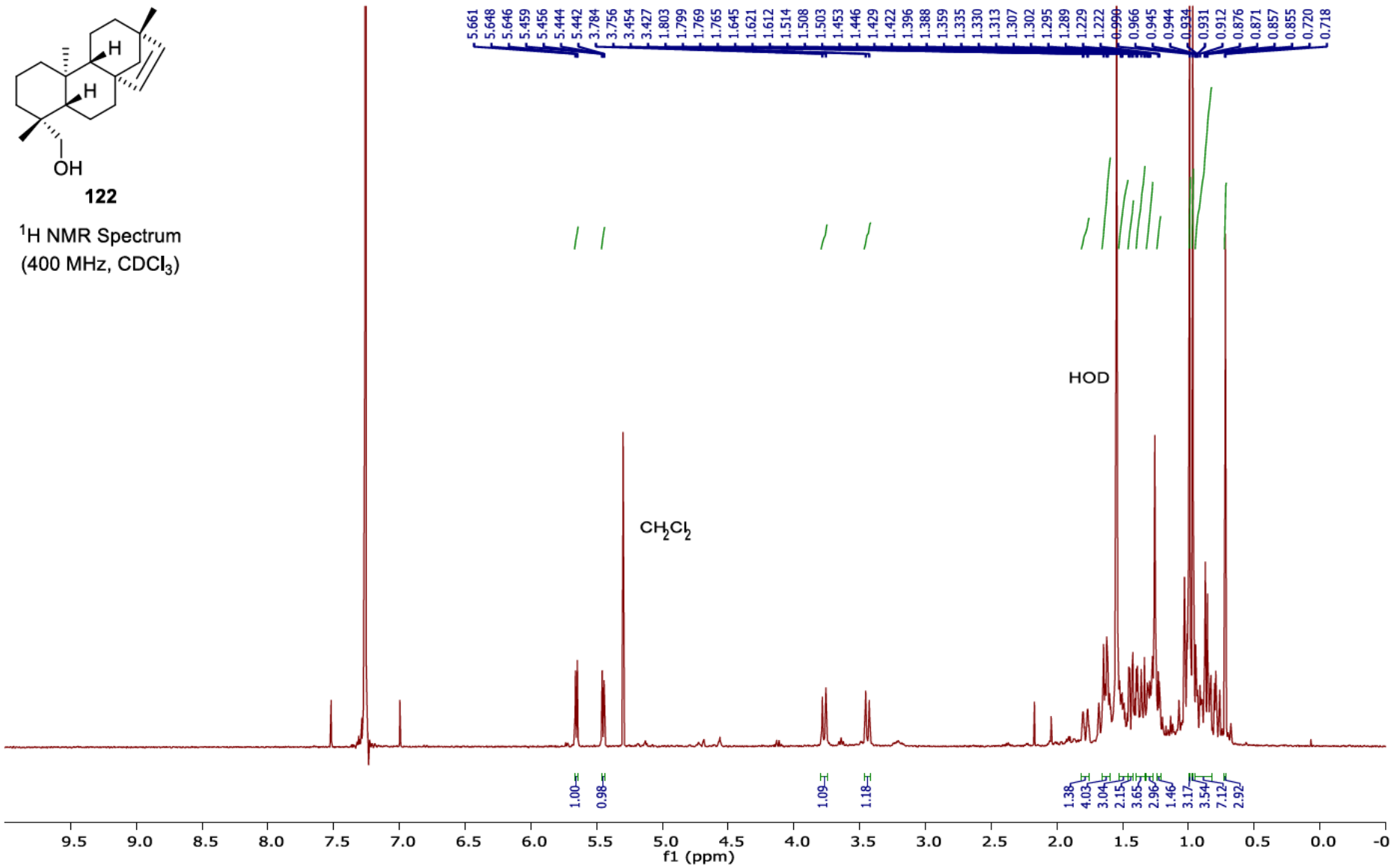
H
H
OH
122
1H NMR Spectrum
(400 MHz, CDCl3)
5.661
5.648
5.646
5.459
5.456
5.444
5.442
3.784
3.756
3.454
3.427
1.803
1.799
1.769
1.765
1.645
1.621
1.612
1.514
1.508
1.503
1.453
1.446
1.429
1.422
1.396
1.388
1.359
1.335
1.330
1.313
1.307
1.302
1.295
1.289
1.229
1.222
0.990
0.966
0.945
0.944
0.934
0.931
0.912
0.876
0.871
0.857
0.855
0.720
0.718
HOD
CH2Cl2
1.00
0.98
1.09
1.18
1.38
4.03
3.04
2.15
3.65
2.96
1.46
3.17
3.54
7.12
2.92
9.5
9.0
8.5
8.0
7.5
7.0
6.5
6.0
5.5
5.0
4.5
4.0
3.5
3.0
2.5
2.0
1.5
1.0
0.5
0.0
-0
f1 (ppm)

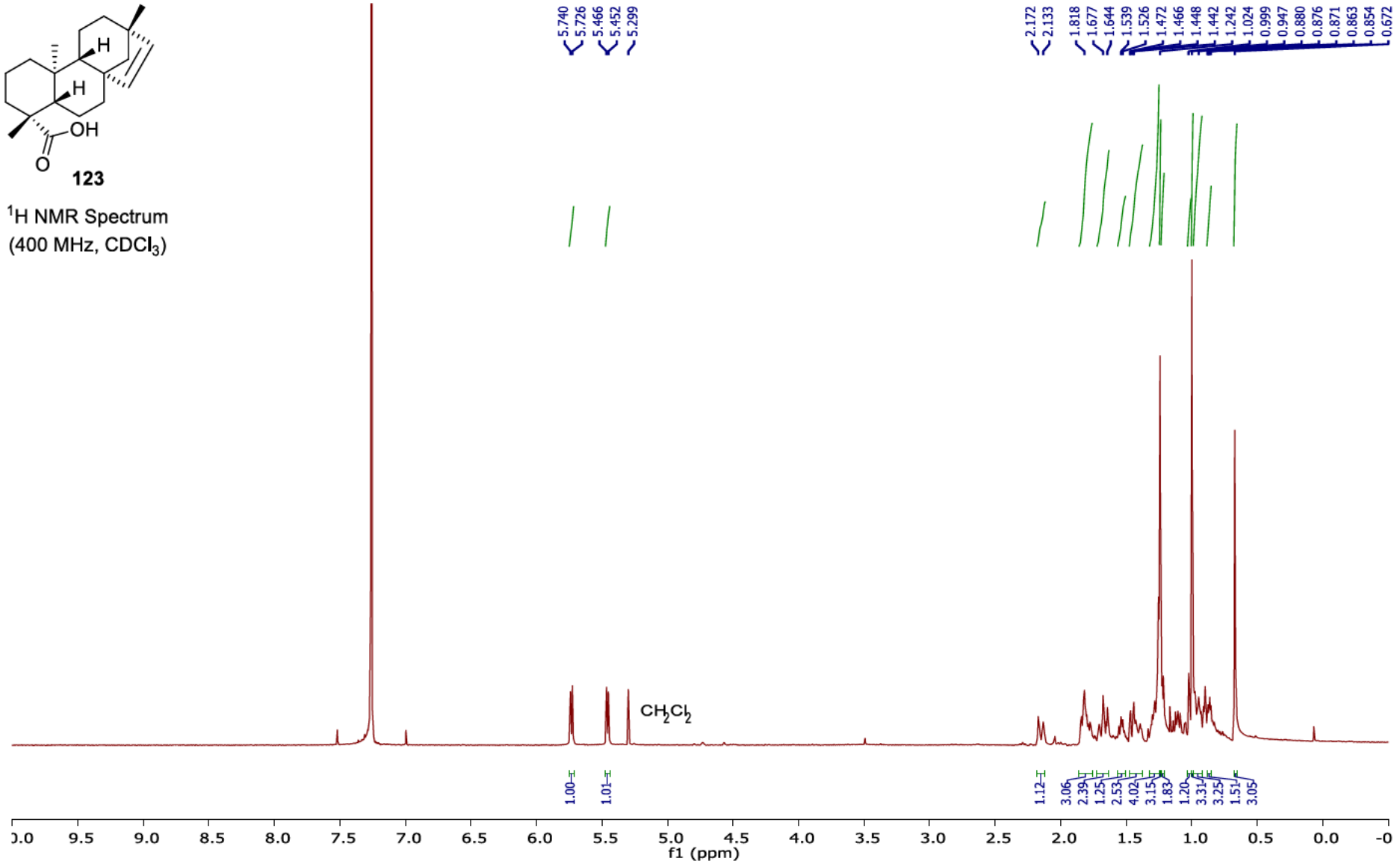
H
H
OH
O
123
1H NMR Spectrum
(400 MHz, CDCl3)
5.740
5.726
5.466
5.452
5.299
2.172
2.133
1.818
1.677
1.644
1.539
1.526
1.472
1.466
1.448
1.442
1.242
1.024
0.999
0.947
0.880
0.876
0.871
0.863
0.854
0.672
CH2Cl2
1.00
1.01
1.12
3.06
2.39
1.25
2.53
4.02
3.15
1.83
1.20
3.31
3.25
1.51
3.05
f1 (ppm)

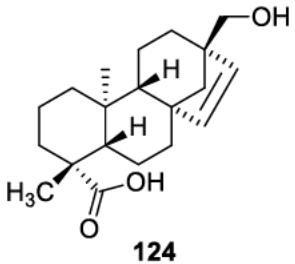

124

^{1}H NMR Spectrum
(400 MHz, $CDCl_3$)

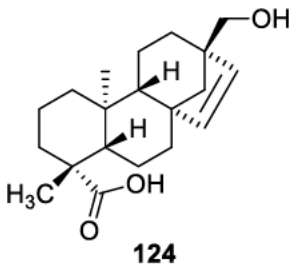

124

^{13}C NMR Spectrum
(101 MHz, $CDCl_3$)

183.692
137.039
132.062
68.781
57.062
55.531
52.871
50.152
48.865
43.887
39.606
38.140
38.039
37.515
29.258
27.834
23.978
21.678
19.984
19.323
13.941

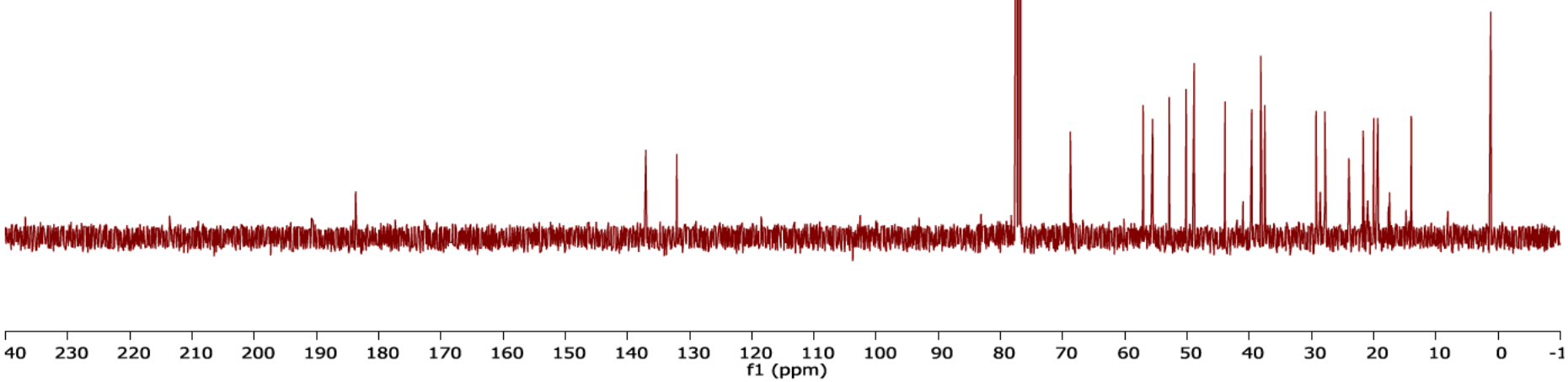

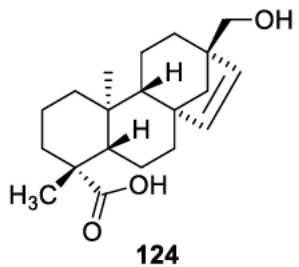

124

DEPT135 NMR Spectrum
(101 MHz, $CDCl_3$)

124

COSY NMR spectrum

($CDCl_3$)

124

HSQC NMR spectrum

($CDCl_3$)

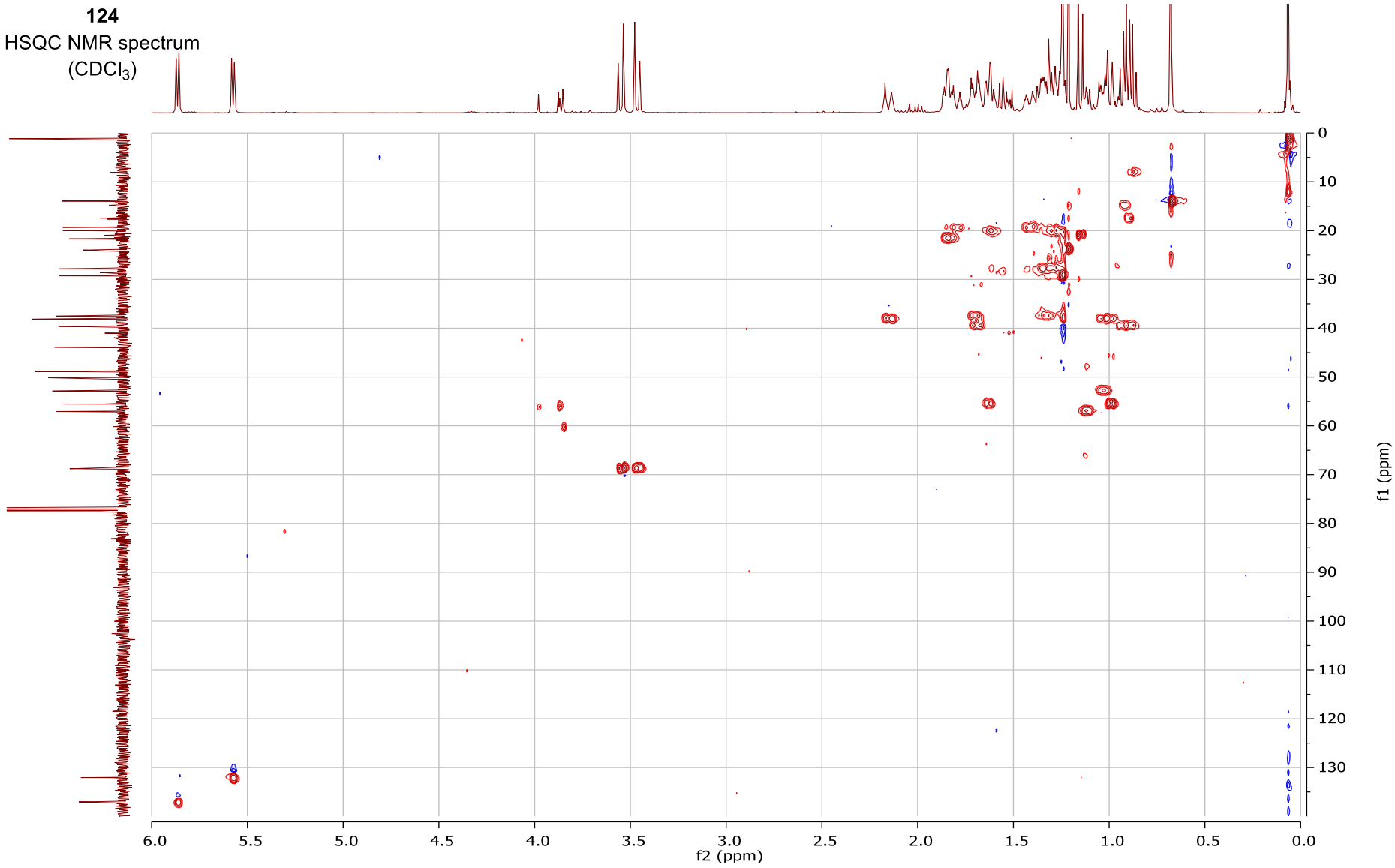

124

HMBC NMR spectrum

($CDCl_3$)

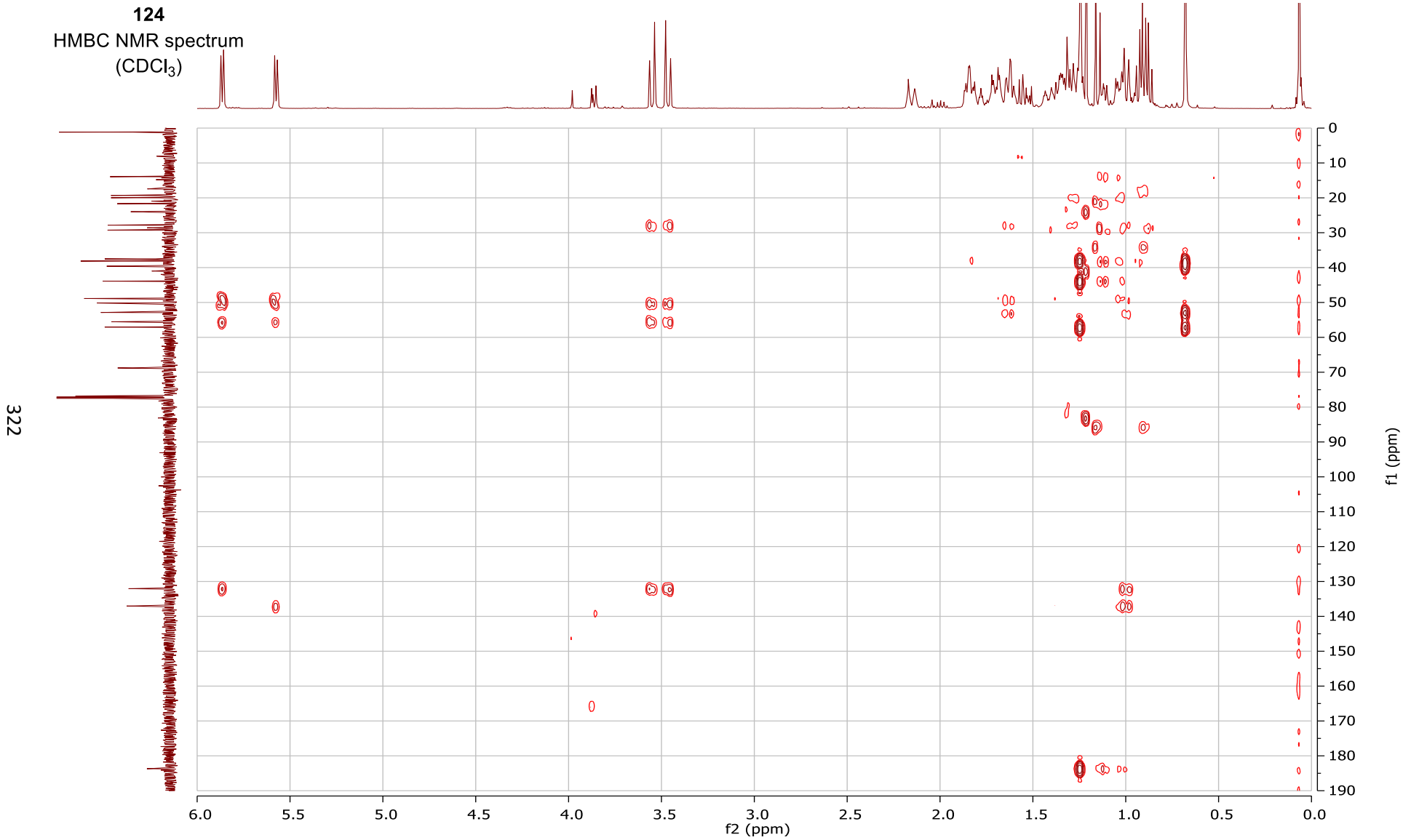

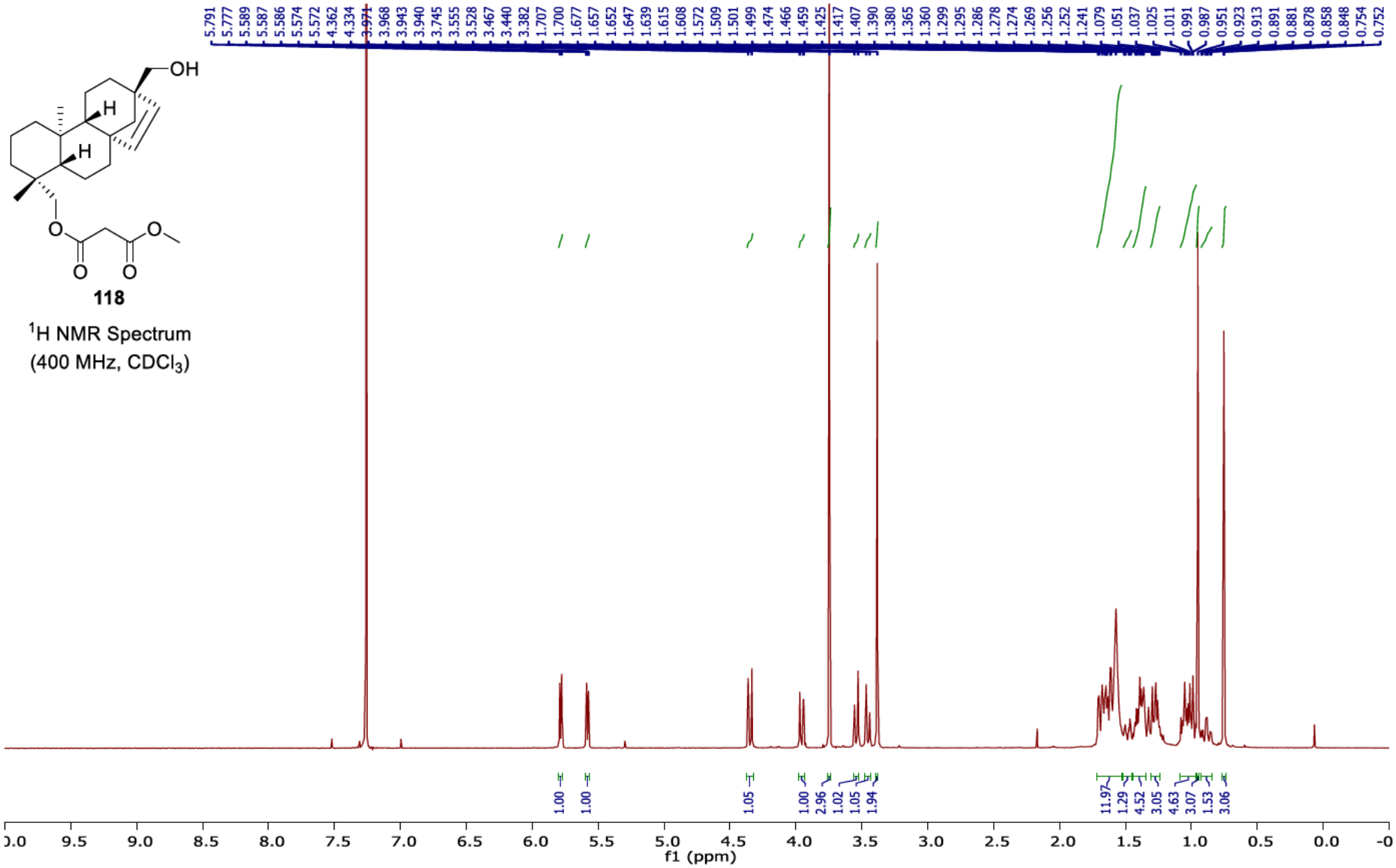
OH
H
H
O
O
O
O
118
1H NMR Spectrum
(400 MHz, CDCl3)
f1 (ppm)

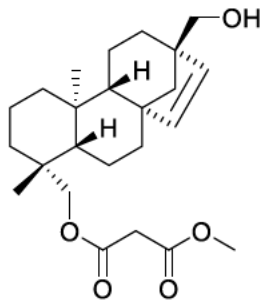

118

^{13}C NMR Spectrum
(101 MHz, $CDCl_3$)

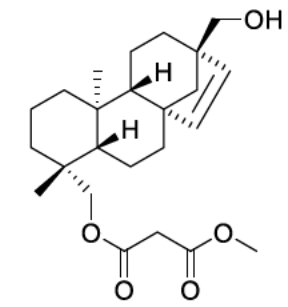

118

DEPT135 NMR Spectrum
(101 MHz, $CDCl_3$)

118

COSY NMR spectrum

($CDCl_3$)

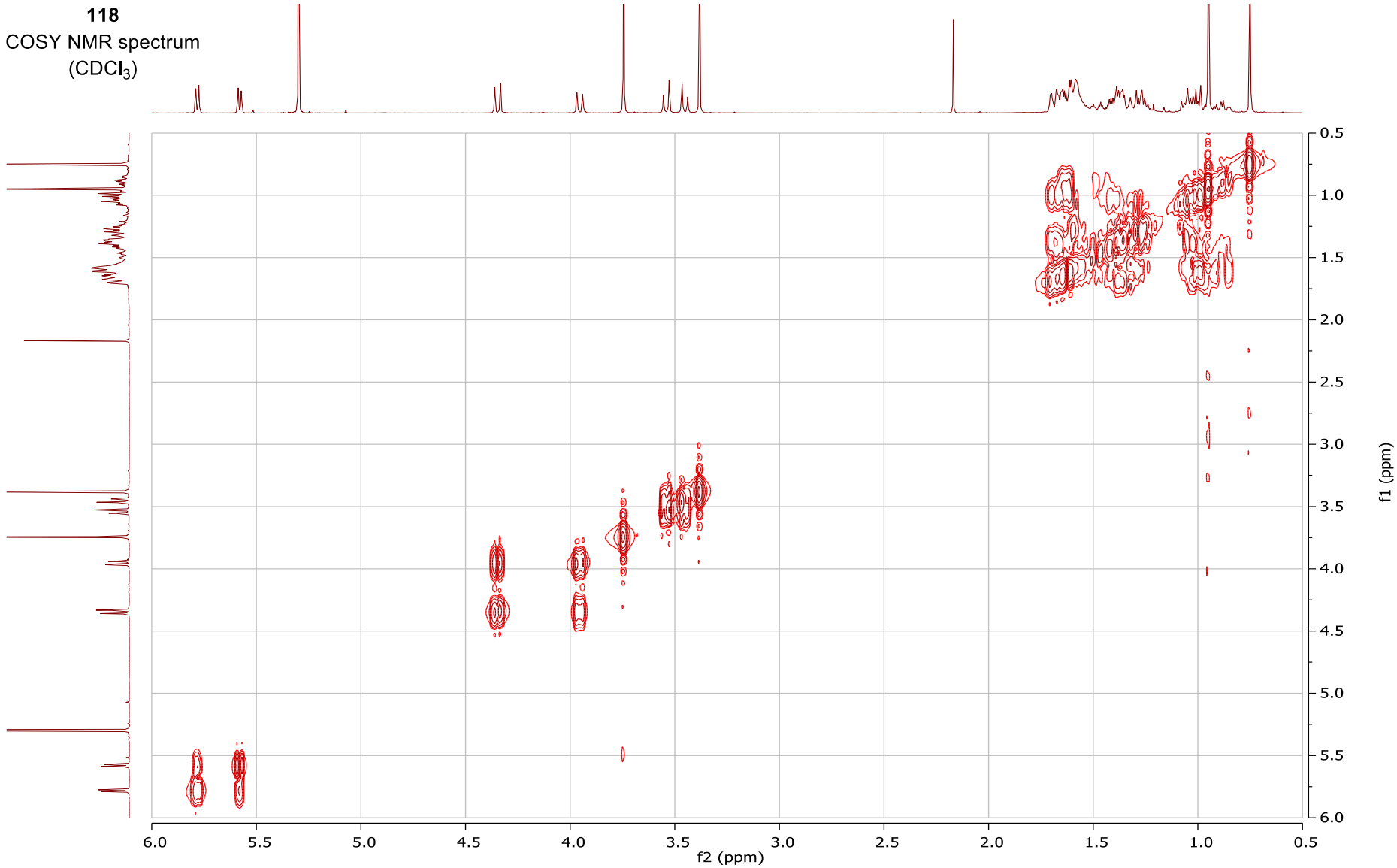

118

HSQC NMR spectrum

($CDCl_3$)

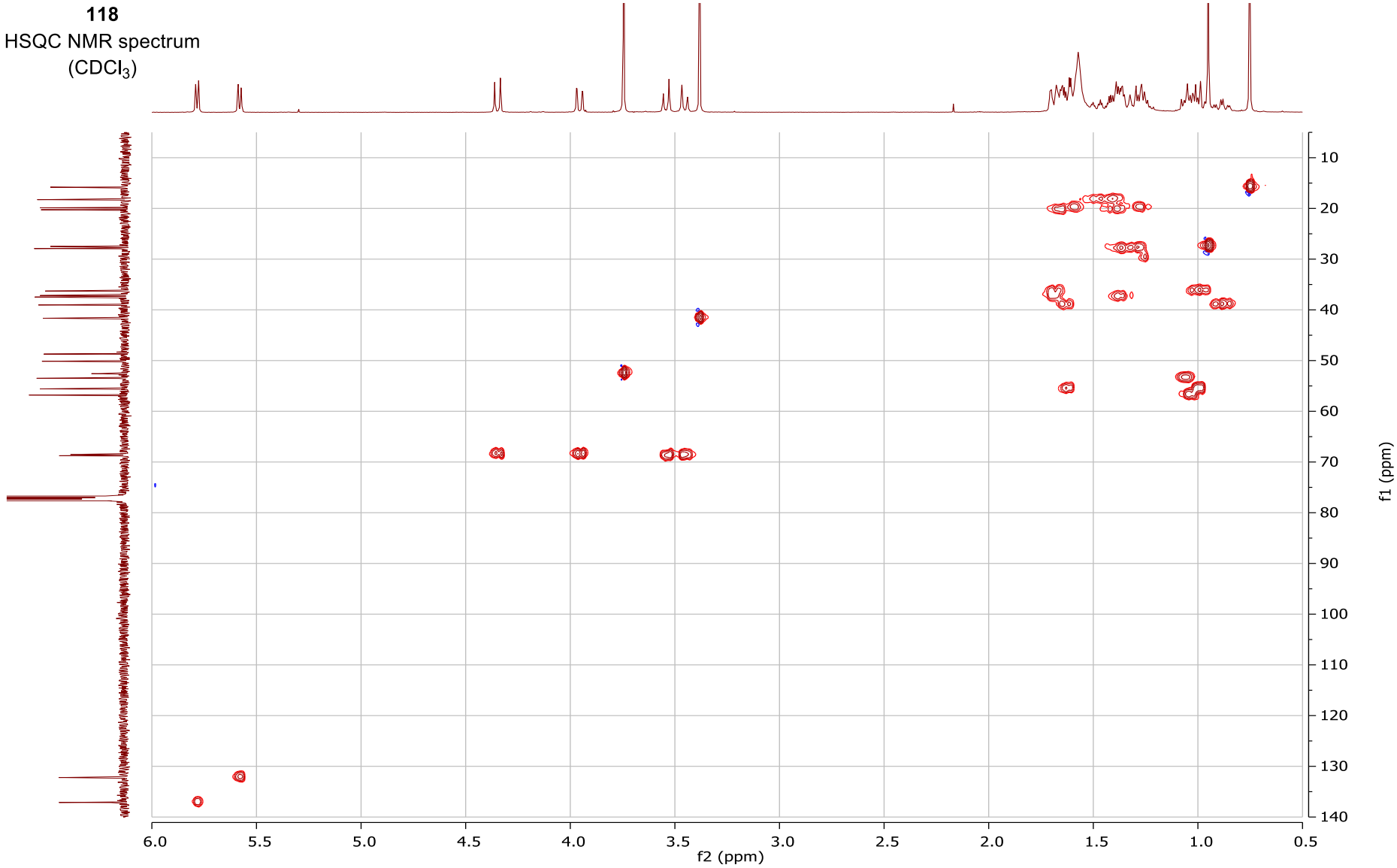

327

118

HMBC NMR spectrum

($CDCl_3$)

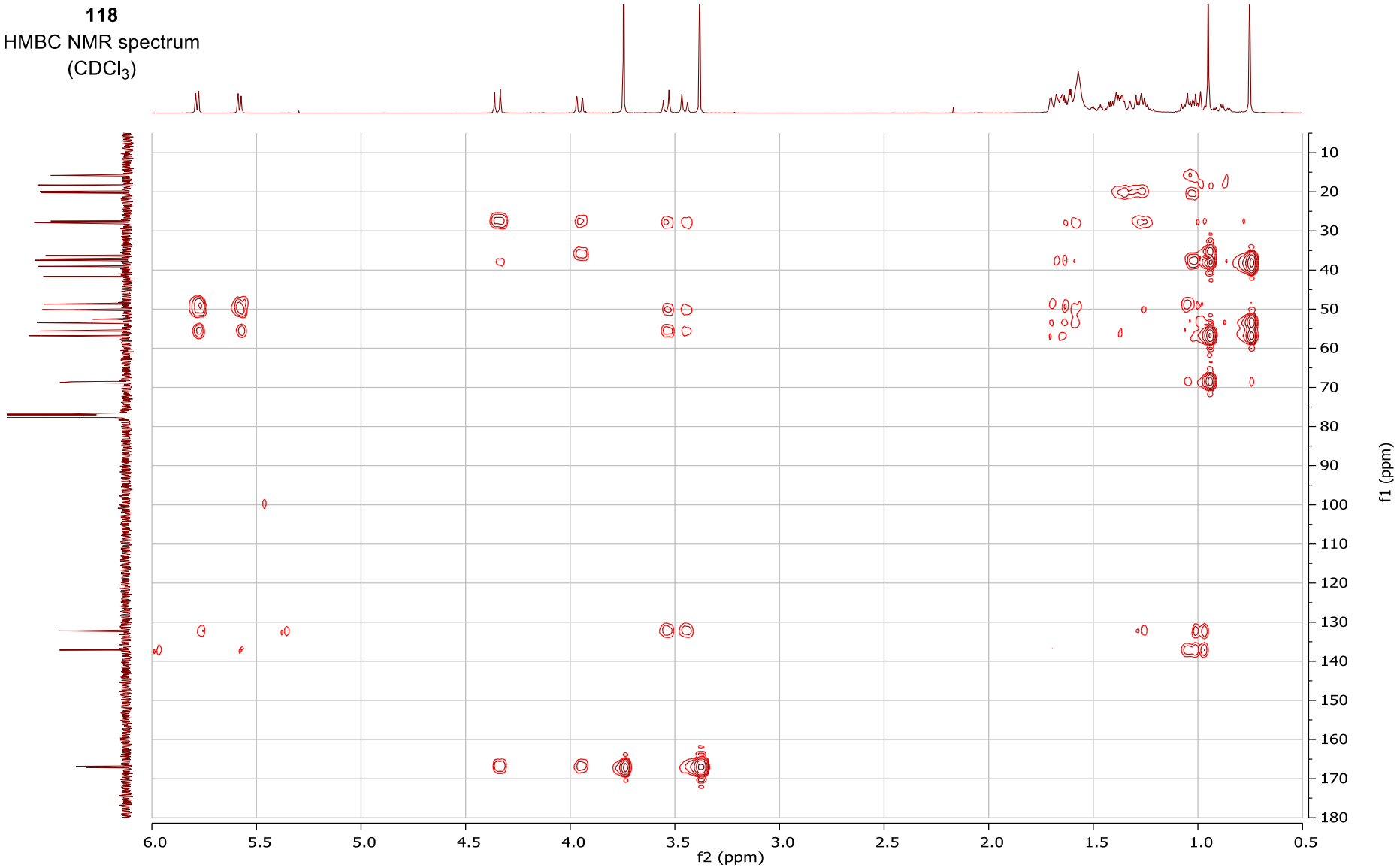

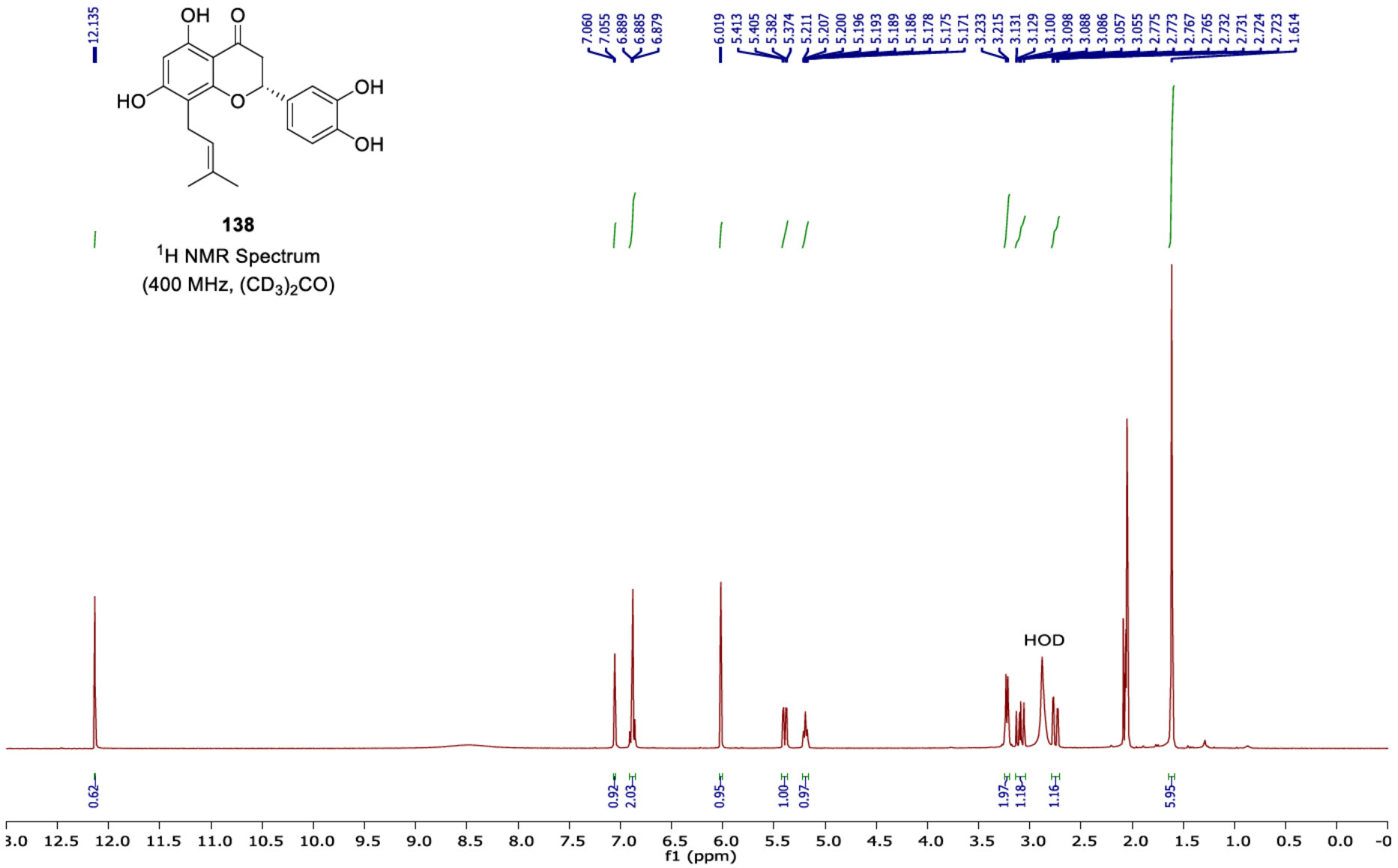

138

^{1}H NMR Spectrum

(400 MHz, $(CD_3)_2CO$)

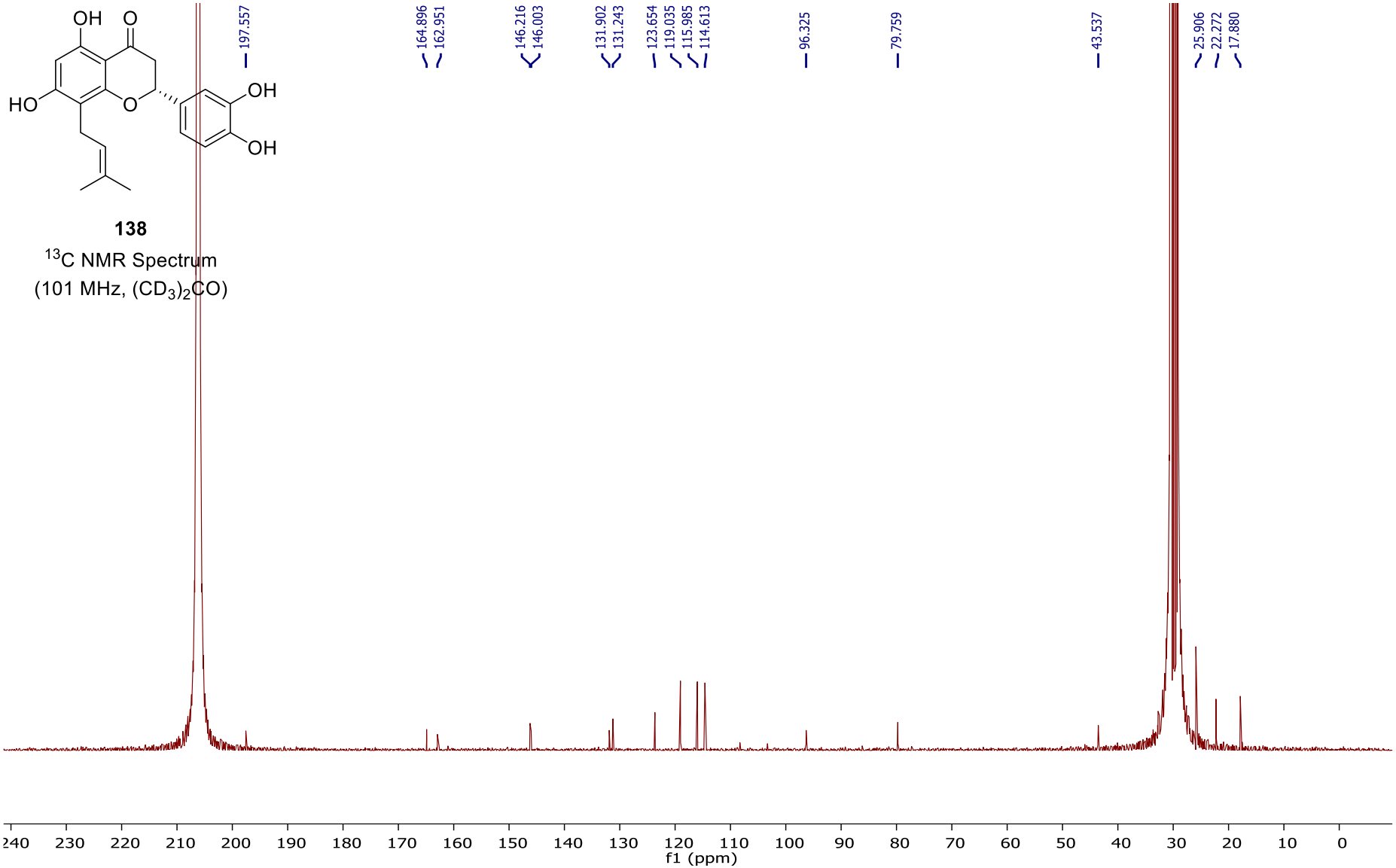

138

^{13}C NMR Spectrum

(101 MHz, $(CD_3)_2CO$)

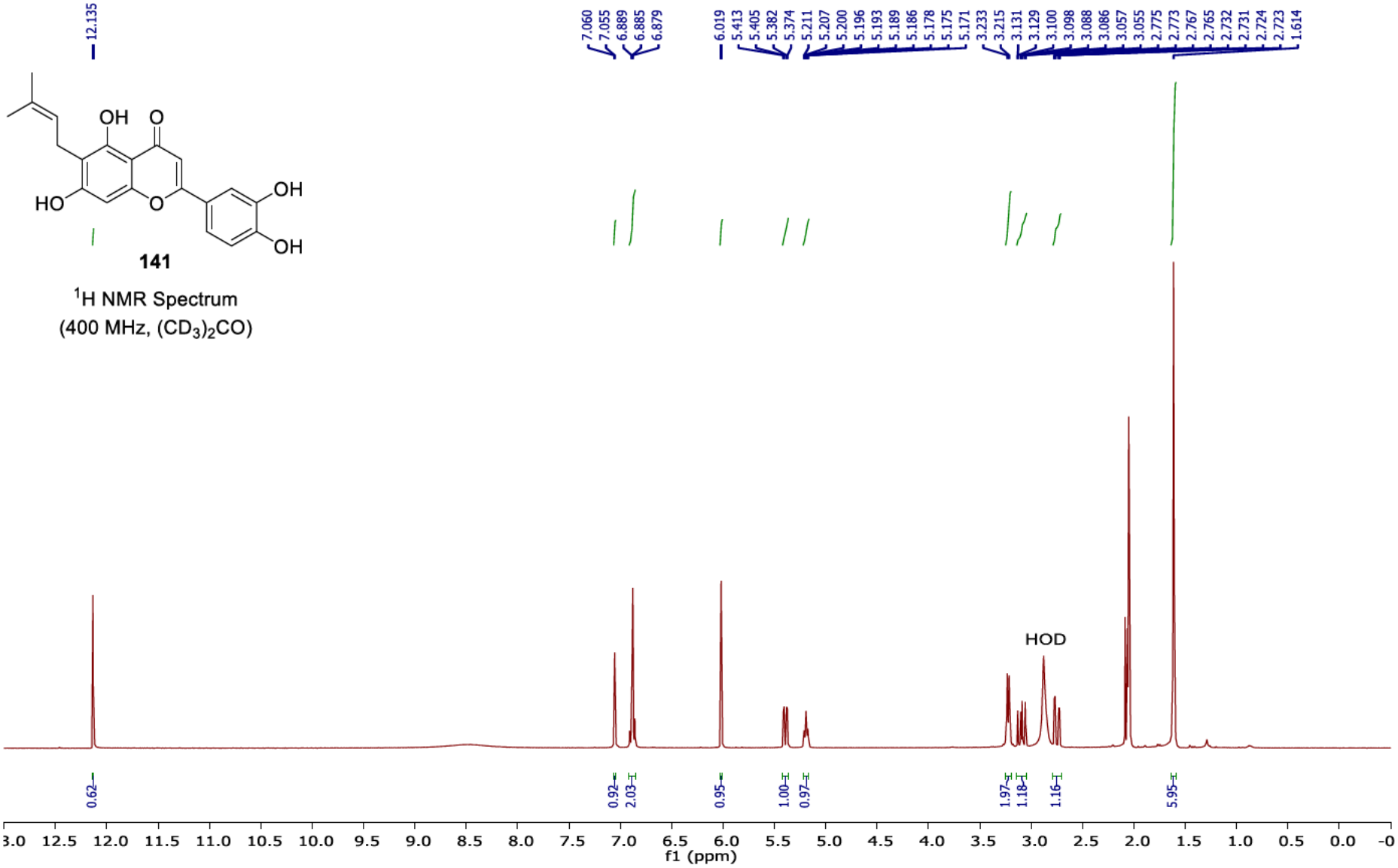

141

^{1}H NMR Spectrum
(400 MHz, $(CD_3)_2CO$)

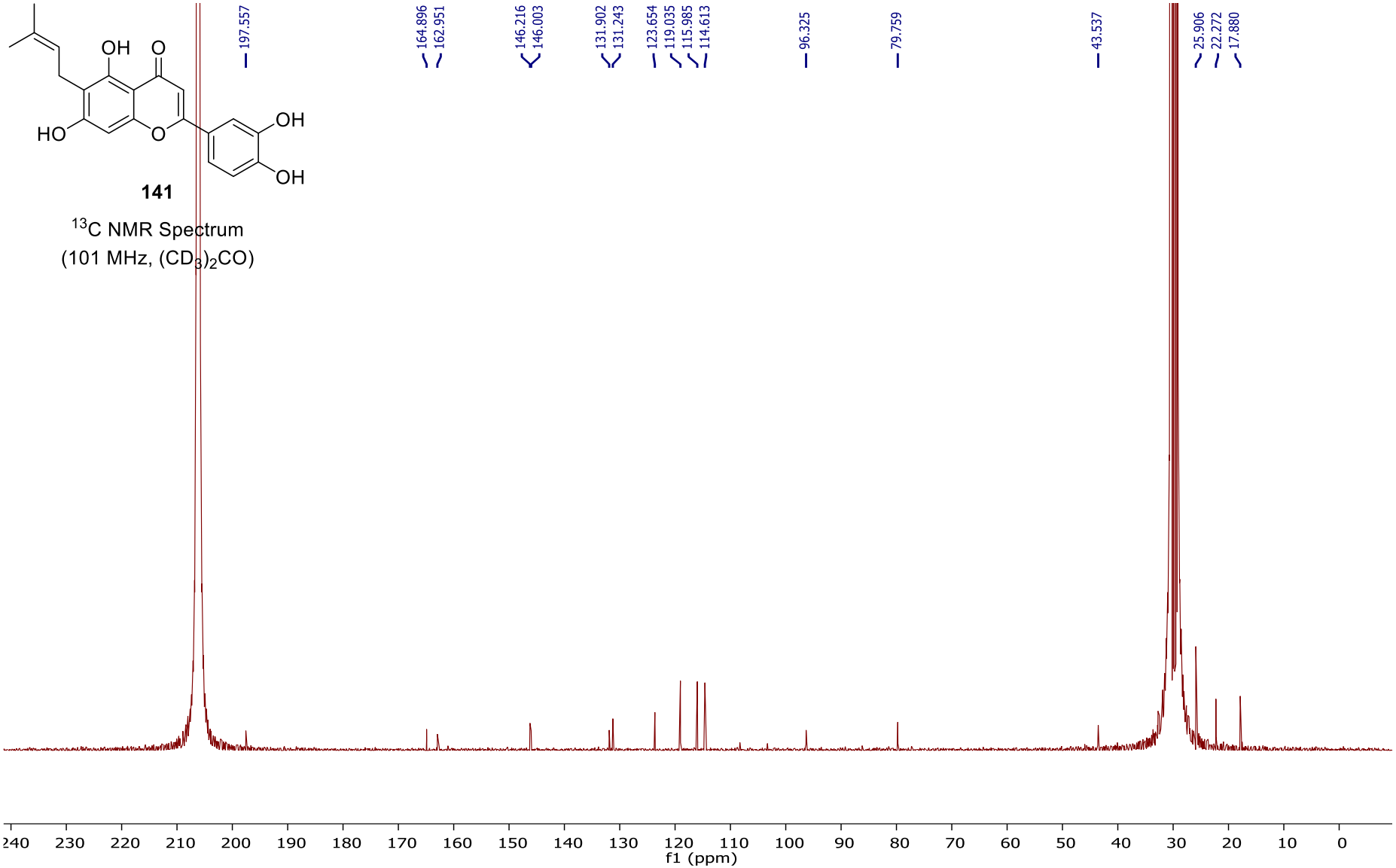

141

^{13}C NMR Spectrum
(101 MHz, $(CD_3)_2CO$)

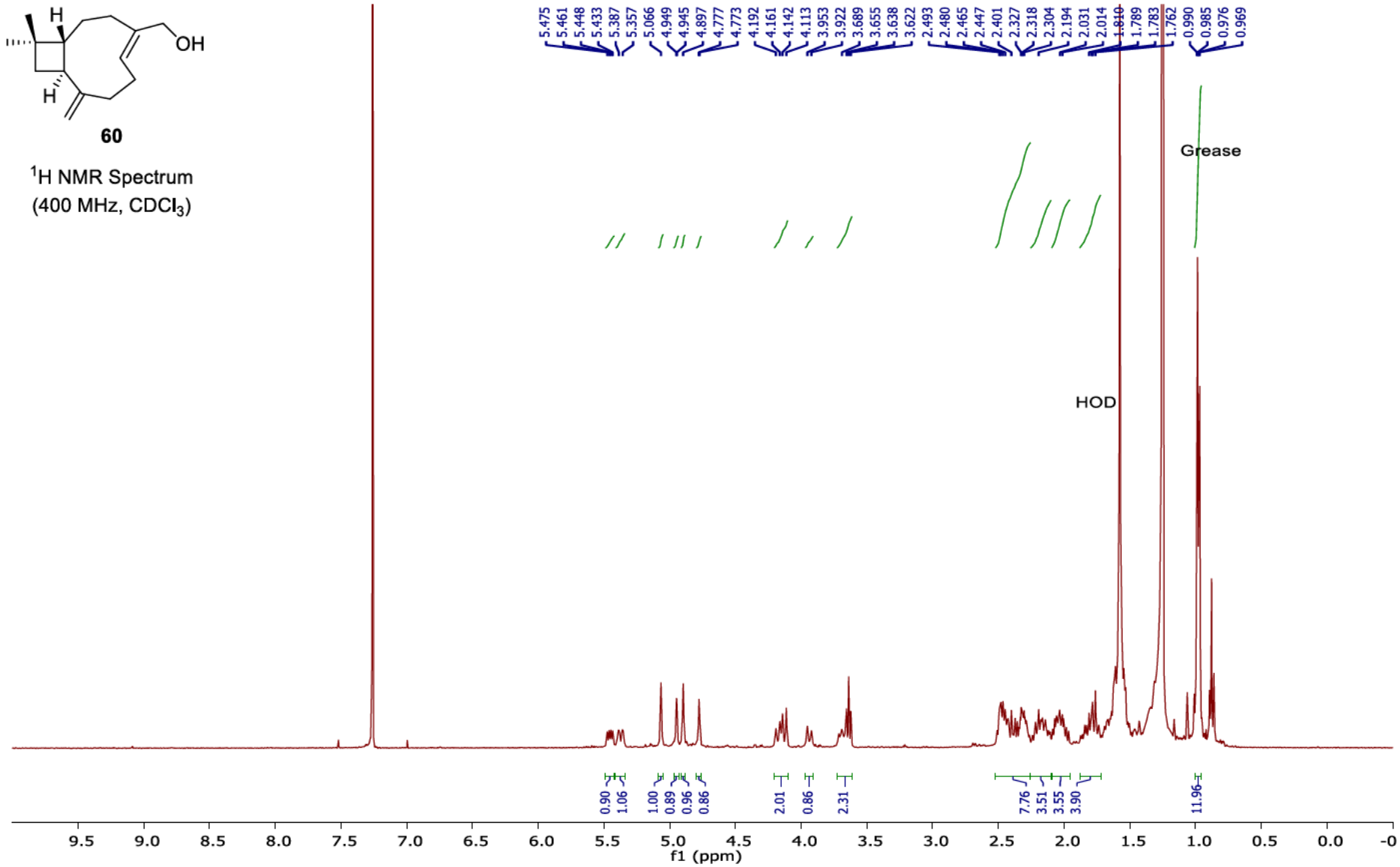
H
OH
H
60
1H NMR Spectrum
(400 MHz, CDCl3)
5.475
5.461
5.448
5.433
5.387
5.357
5.066
4.949
4.945
4.897
4.777
4.773
4.192
4.161
4.142
4.113
3.953
3.922
3.689
3.655
3.638
3.622
2.493
2.480
2.465
2.447
2.401
2.327
2.318
2.304
2.194
2.031
2.014
1.810
1.789
1.783
1.762
0.990
0.985
0.976
0.969
Grease
HOD
0.90
1.06
1.00
0.89
0.96
0.86
2.01
0.86
2.31
7.76
3.51
3.55
3.90
11.96
9.5
9.0
8.5
8.0
7.5
7.0
6.5
6.0
5.5
5.0
4.5
4.0
3.5
3.0
2.5
2.0
1.5
1.0
0.5
0.0
-0
f1 (ppm)

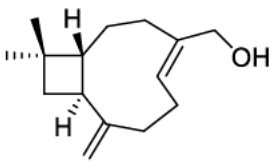

60

^{1}H NMR Spectrum
(101 MHz, $CDCl_3$)

158.973
153.997
138.010
137.756
129.602
128.912
113.175
110.233
63.228
62.075
60.272
56.963
50.433
49.833
49.171
42.666
40.743
40.428
34.980
33.872
33.047
32.957
30.642
30.158
30.097
29.320
22.215
21.999

Grease

334

40 230 220 210 200 190 180 170 160 150 140 130 120 110 100 90 80 70 60 50 40 30 20 10 0 -1
f1 (ppm)

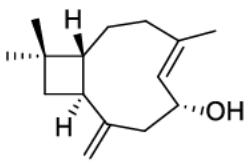

1

^{1}H NMR spectrum
(400 MHz, $CDCl_3$)

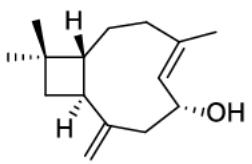

1

^{13}C NMR spectrum
(101 MHz, $CDCl_3$)

150.19
136.99
128.00
112.53
70.80
55.60
49.31
49.05
42.35
34.86
32.86
31.34
29.97
23.09
21.97

336

240 230 220 210 200 190 180 170 160 150 140 130 120 110 100 90 80 70 60 50 40 30 20 10 0 -1
f1 (ppm)

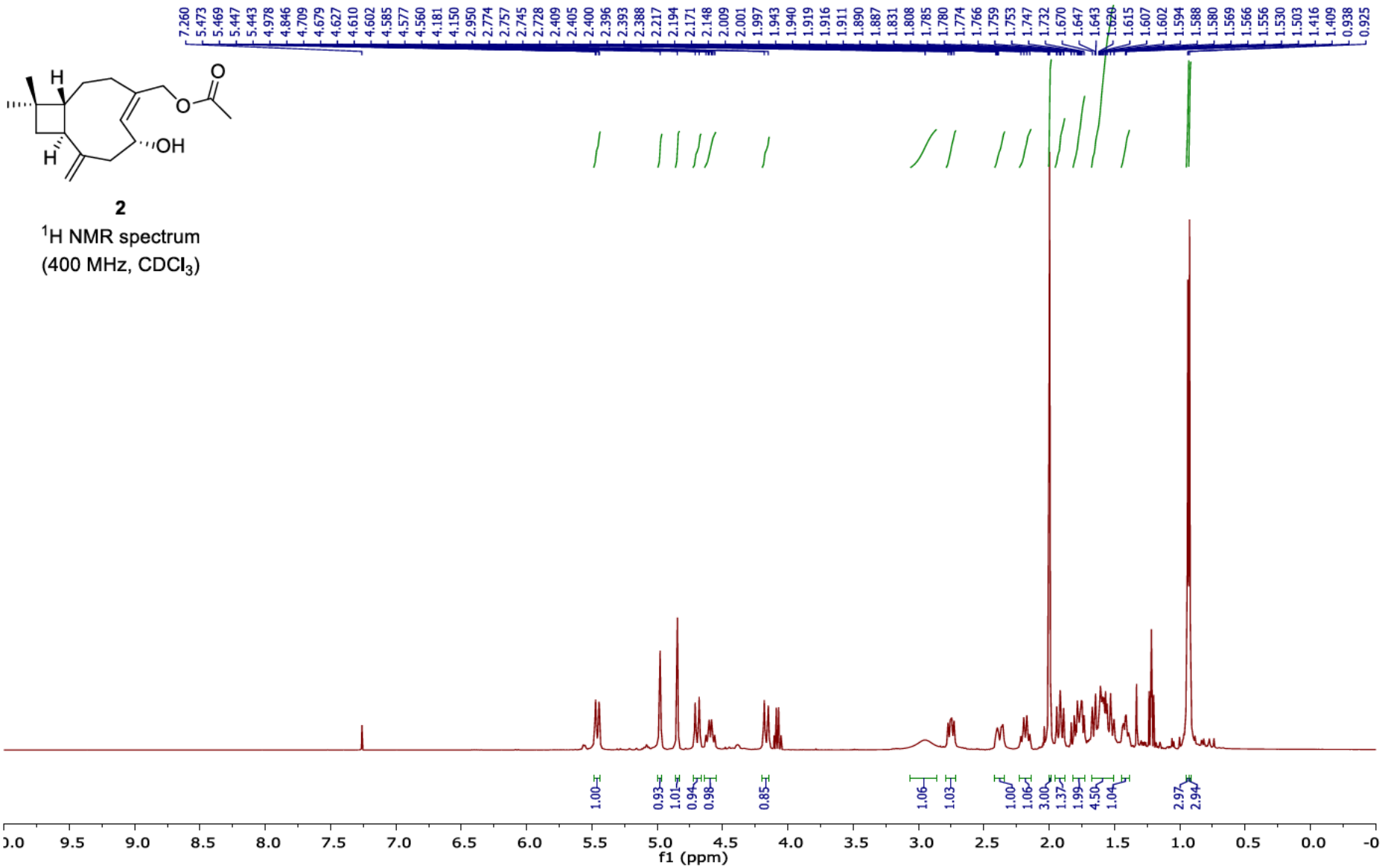

2

^{1}H NMR spectrum
(400 MHz, $CDCl_3$)

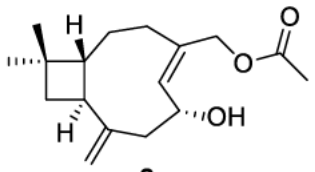

2

^{13}C NMR spectrum
(101 MHz, $CDCl_3$)

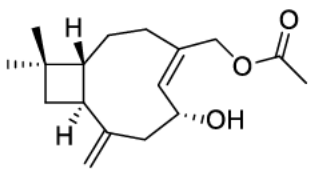

2

DEPT135 NMR spectrum
(101 MHz, $CDCl_3$)

2

COSY NMR spectrum

($CDCl_3$)

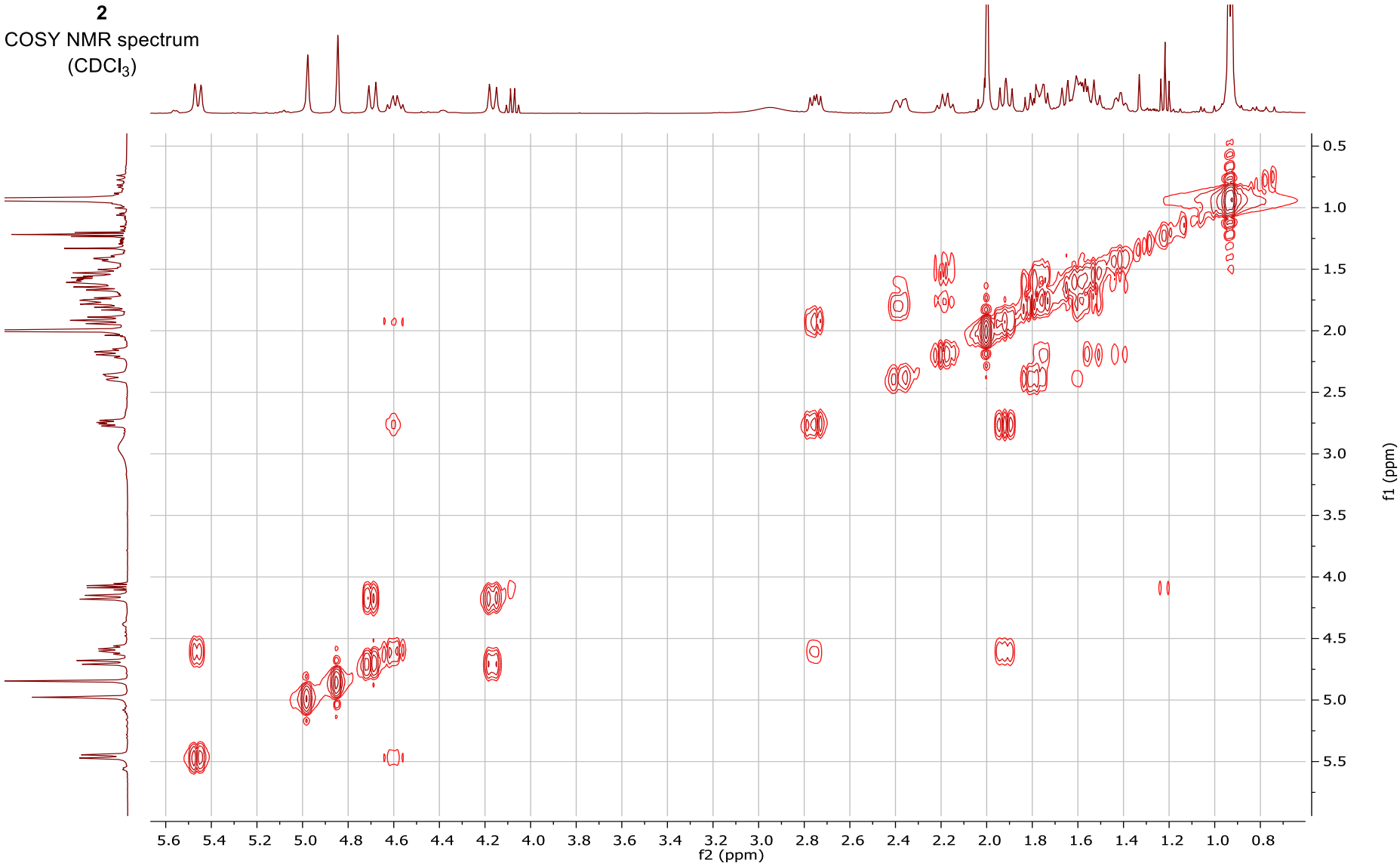

2

HSQC NMR spectrum

($CDCl_3$)

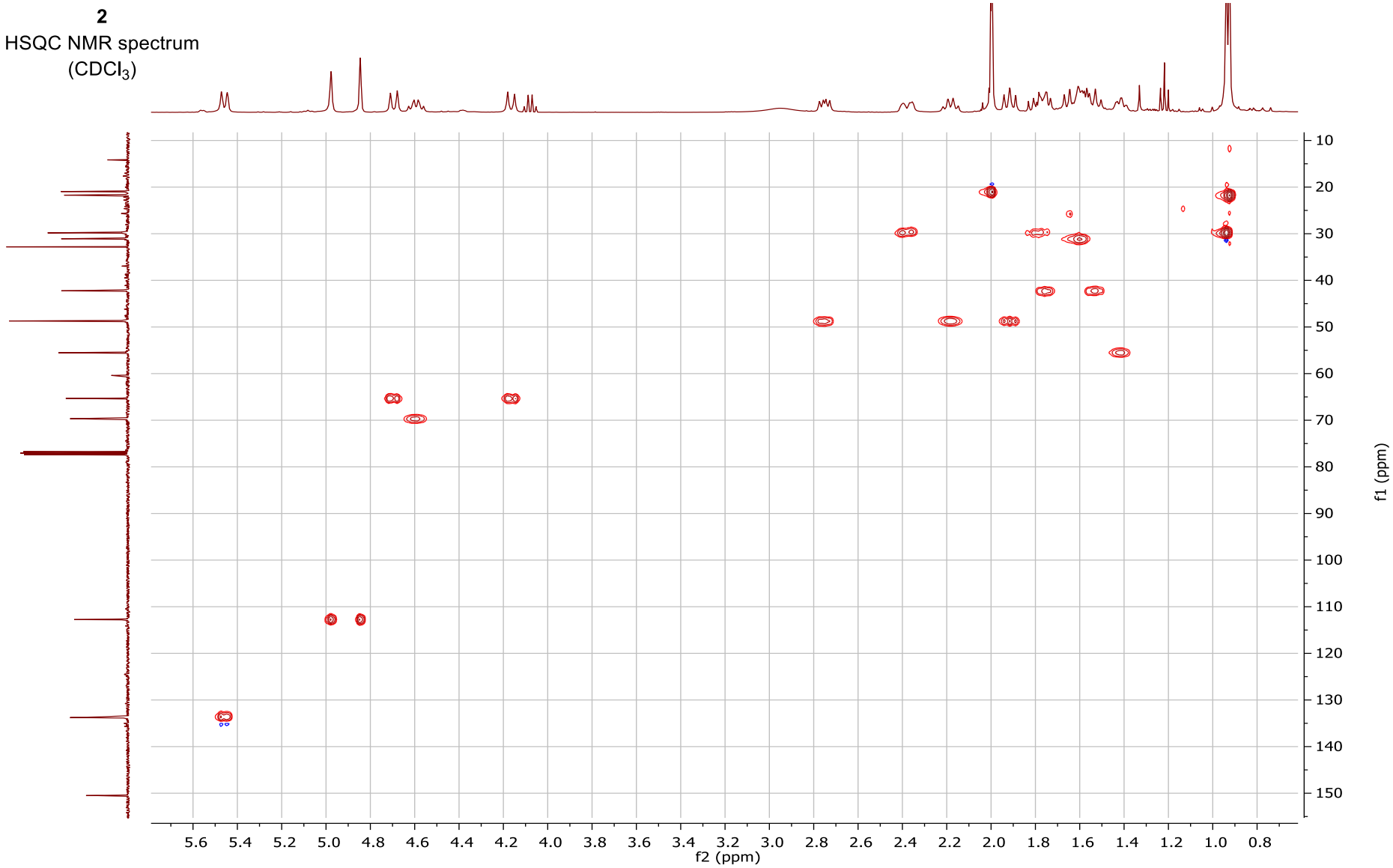

2

HMBC NMR spectrum

($CDCl_3$)

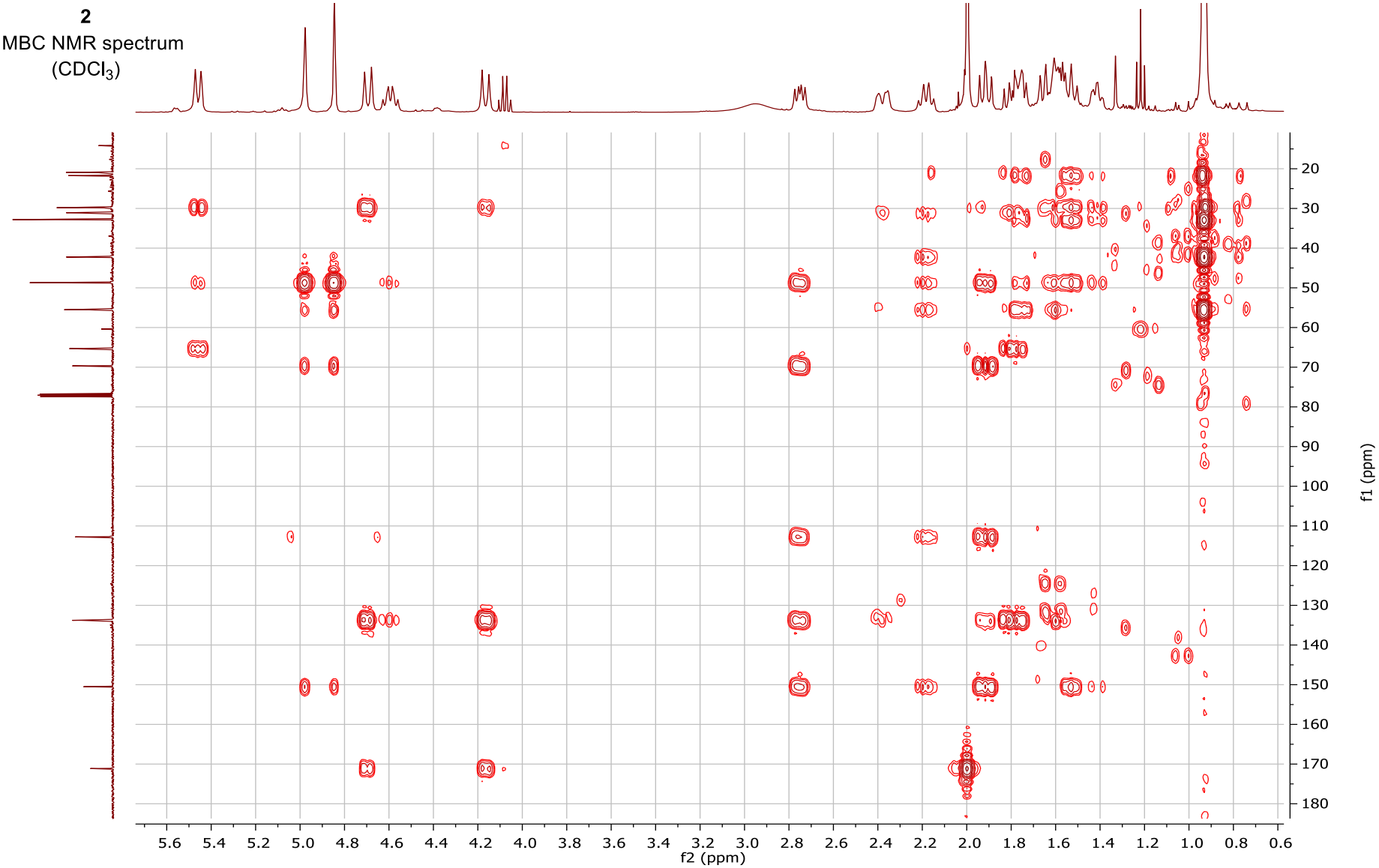

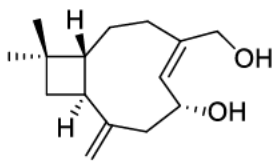

3

^{1}H NMR spectrum
(400 MHz, $CDCl_3$)

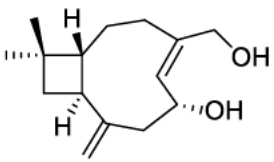

3

^{13}C NMR spectrum
(101 MHz, $CDCl_3$)

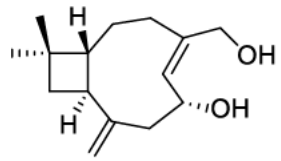

3

DEPT135 NMR spectrum
(101 MHz, $CDCl_3$)

3

COSY NMR spectrum

($CDCl_3$)

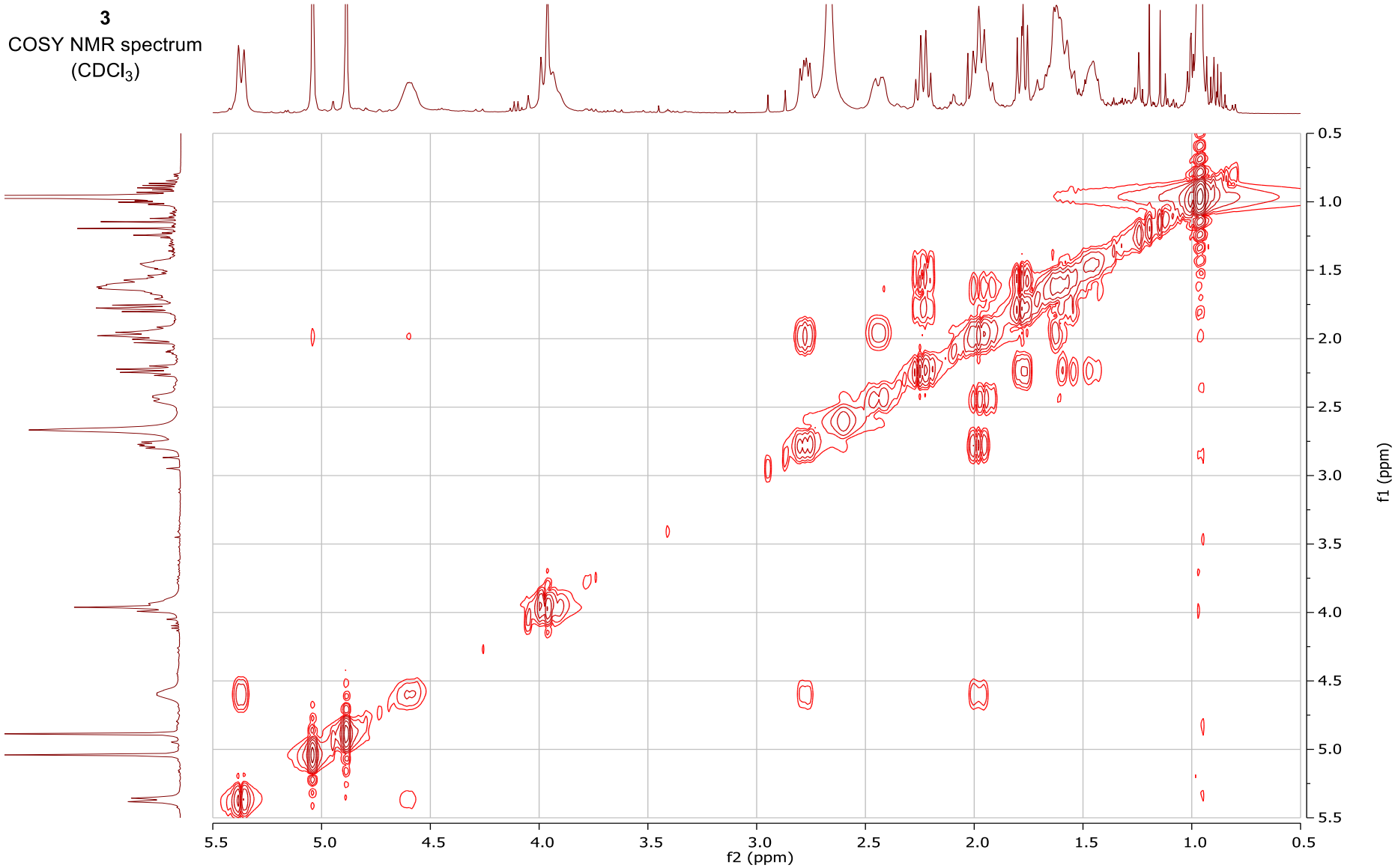

3

HSQC NMR spectrum

($CDCl_3$)

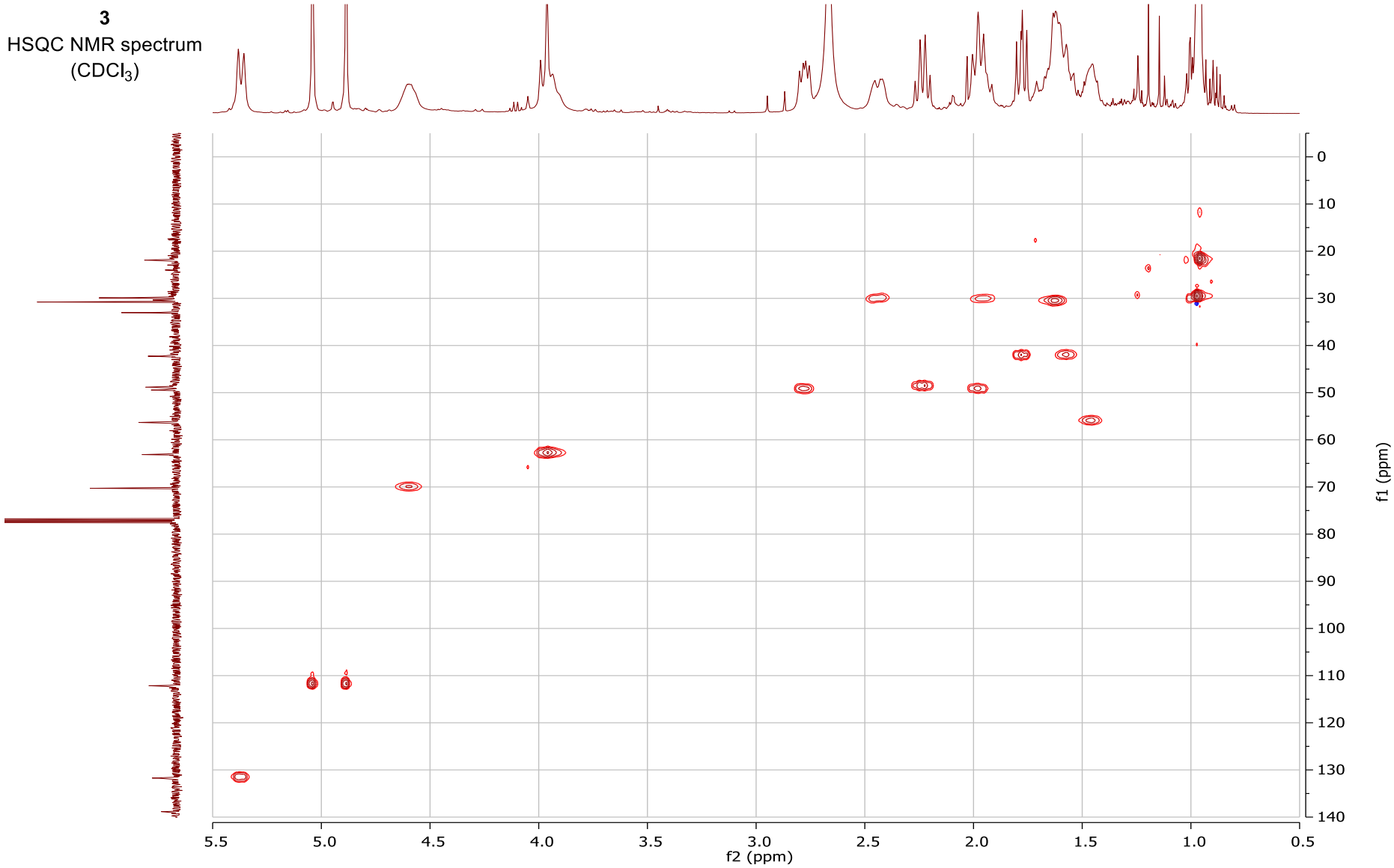

3

HMBC NMR spectrum

($CDCl_3$)

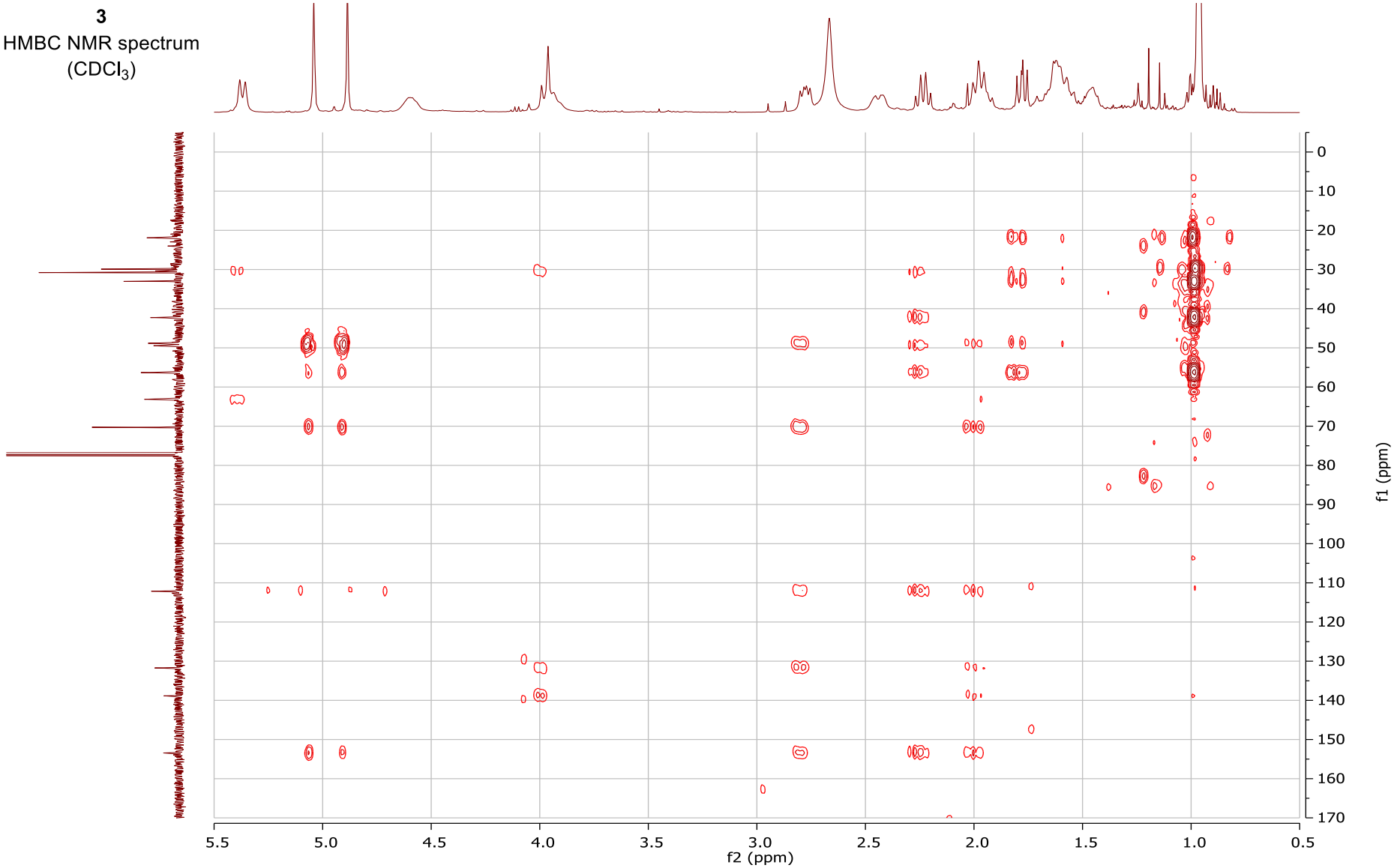

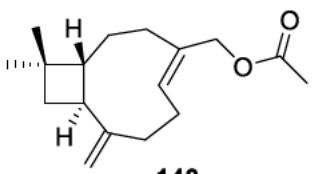

140

^{1}H NMR spectrum
(400 MHz, $CDCl_3$)

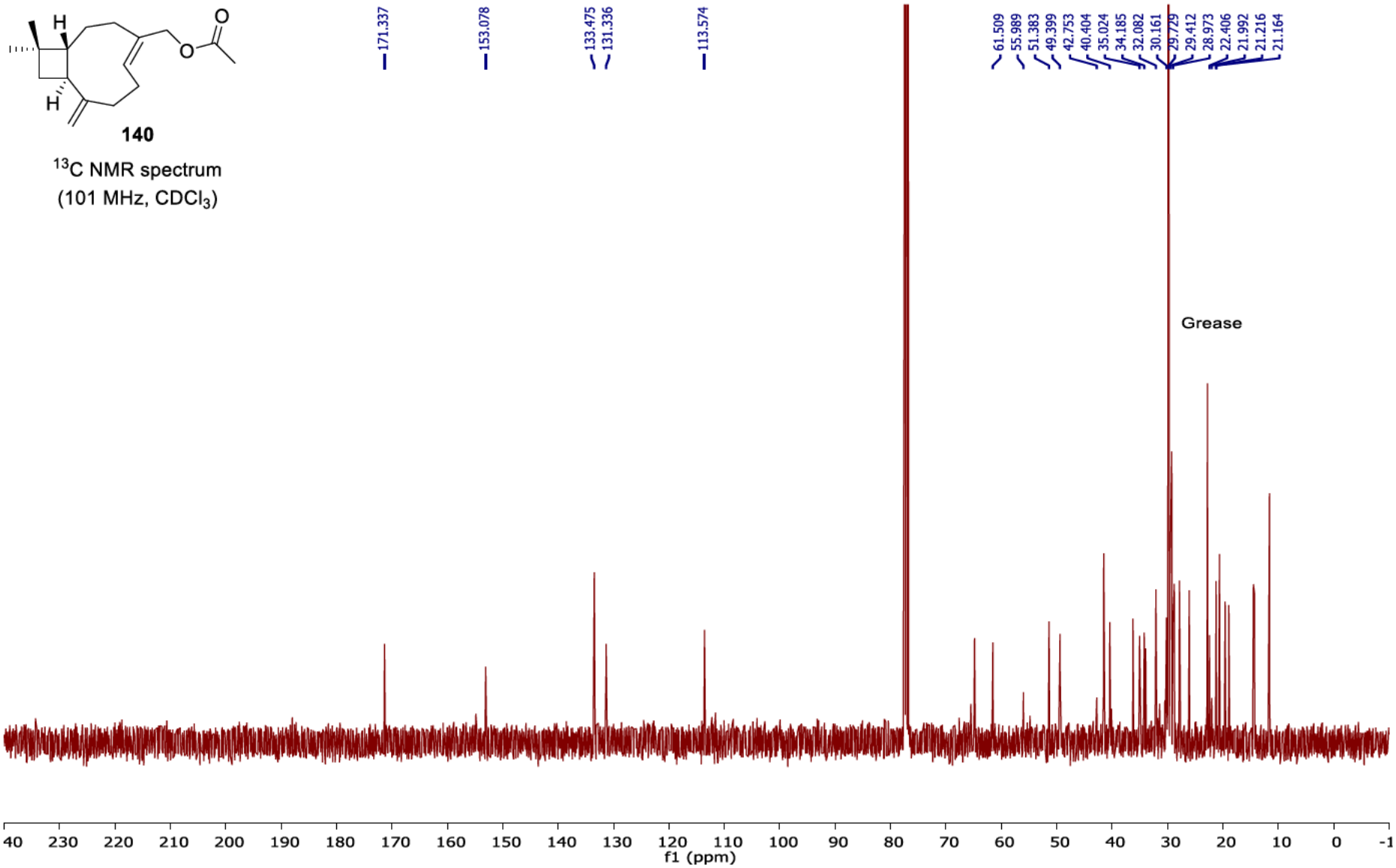
H
H
O
O
140
^{13}C NMR spectrum
(101 MHz, $CDCl_3$)
171.337
153.078
133.475
131.336
113.574
61.509
55.989
51.383
49.399
42.753
40.404
35.024
34.185
32.082
30.161
29.729
29.412
28.973
22.406
21.992
21.216
21.164
Grease
350
40 230 220 210 200 190 180 170 160 150 140 130 120 110 100 90 80 70 60 50 40 30 20 10 0 -1
f1 (ppm)

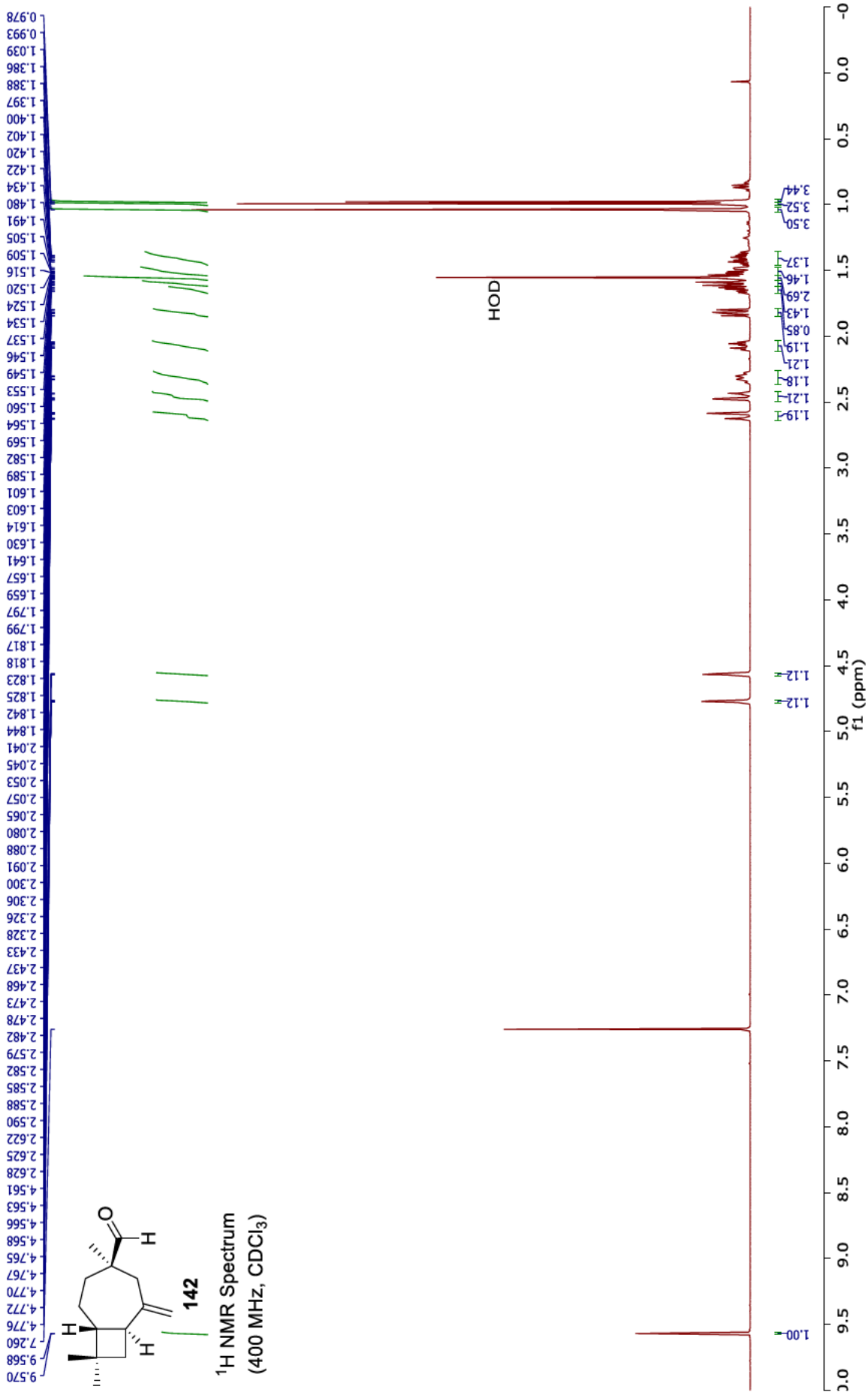

142

^{1}H NMR Spectrum
(400 MHz, $CDCl_3$)

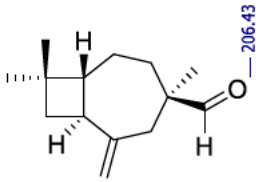

142

^{13}C NMR Spectrum
(101 MHz, $CDCl_3$)

206.43
150.56
107.38
50.59
48.87
44.65
40.90
38.57
36.32
34.71
30.41
25.65
25.03
22.05

40 230 220 210 200 190 180 170 160 150 140 130 120 110 100 90 80 70 60 50 40 30 20 10 0 -1
f1 (ppm)

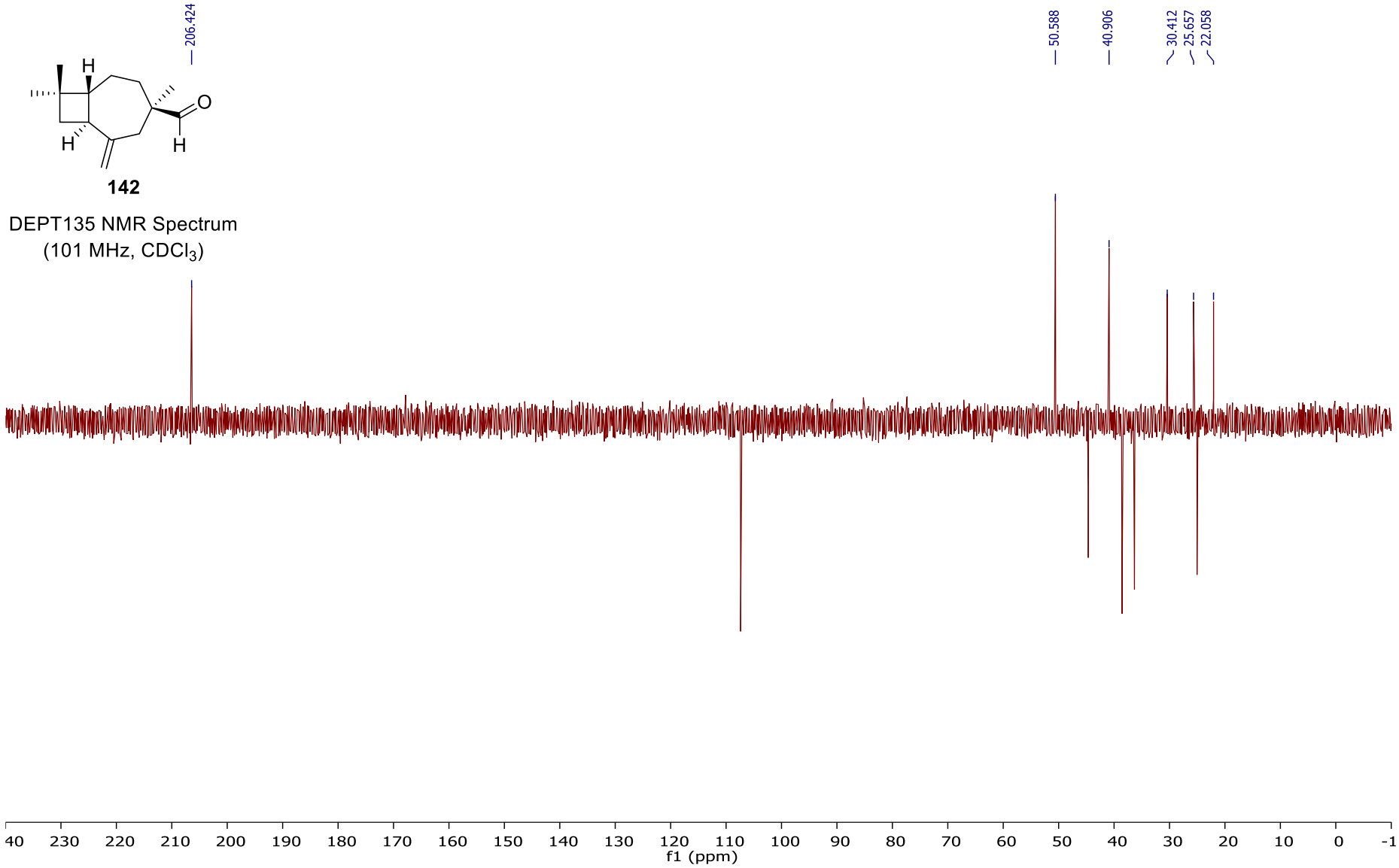
206.424
50.588
40.906
30.412
25.657
22.058
H
H
H
O
142
DEPT135 NMR Spectrum
(101 MHz, CDCl3)
353
40 230 220 210 200 190 180 170 160 150 140 130 120 110 100 90 80 70 60 50 40 30 20 10 0 -1
f1 (ppm)

142

COSY NMR spectrum

($CDCl_3$)

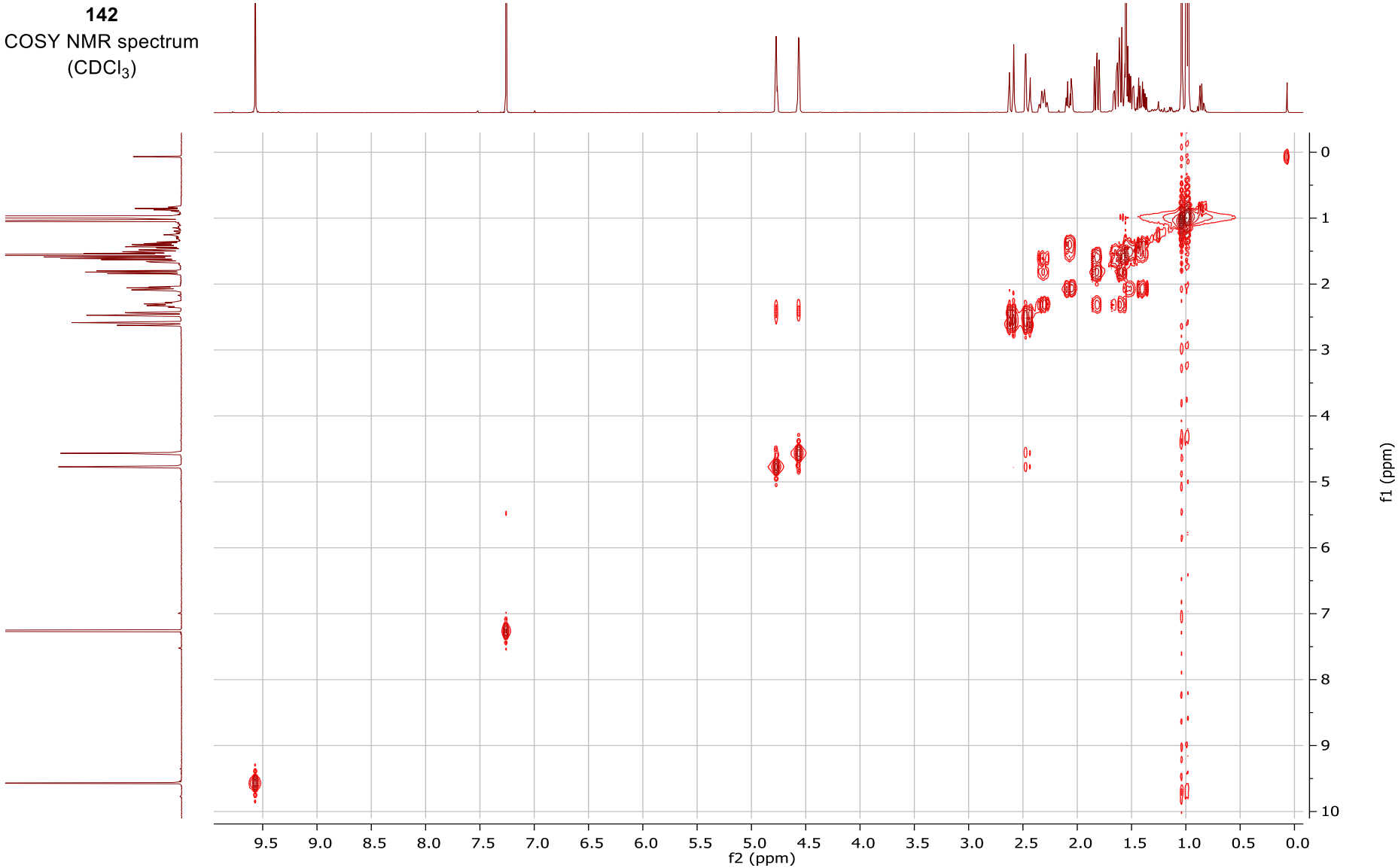

354

142

HSQC NMR spectrum

($CDCl_3$)

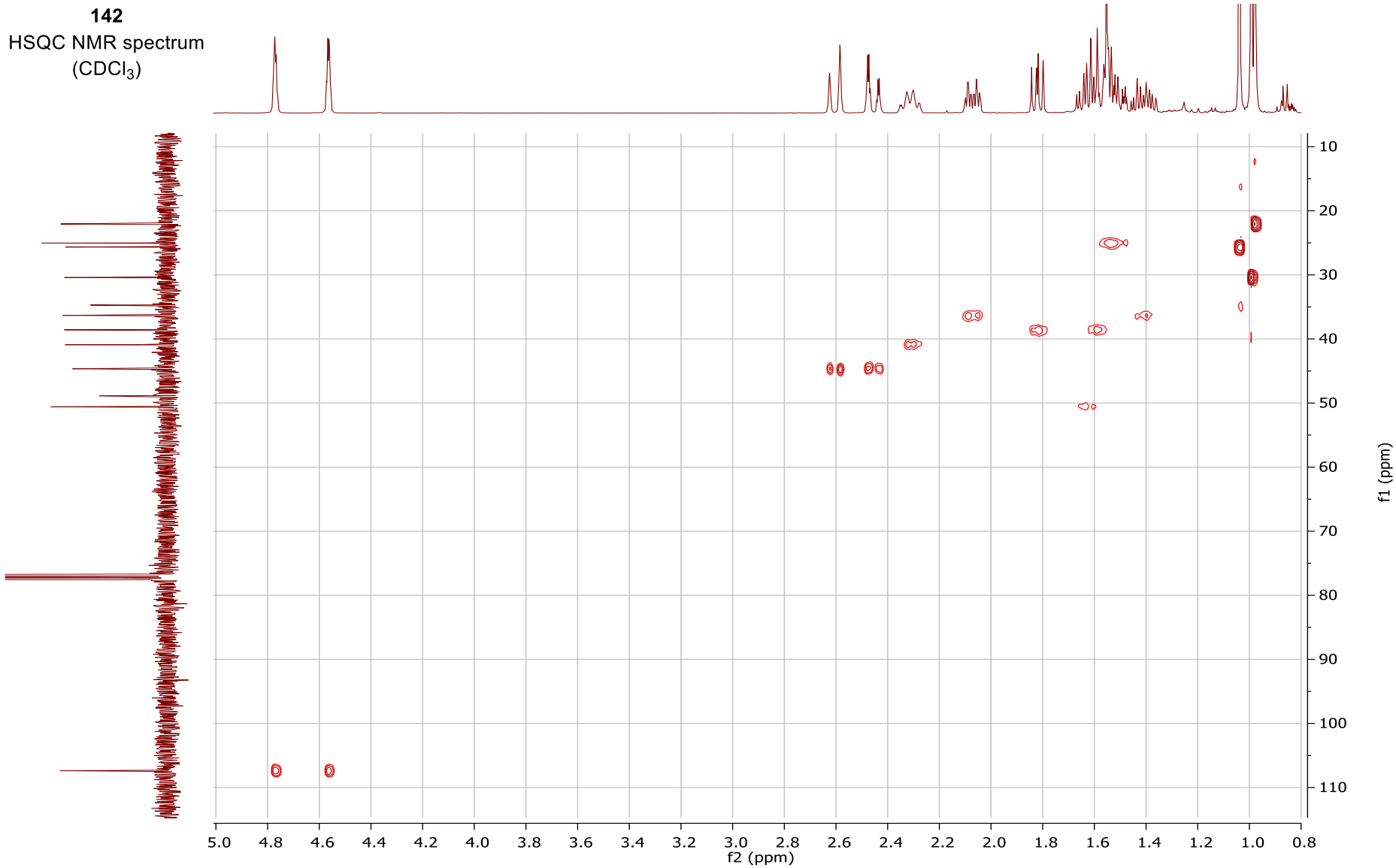

142

HMBC NMR spectrum

($CDCl_3$)

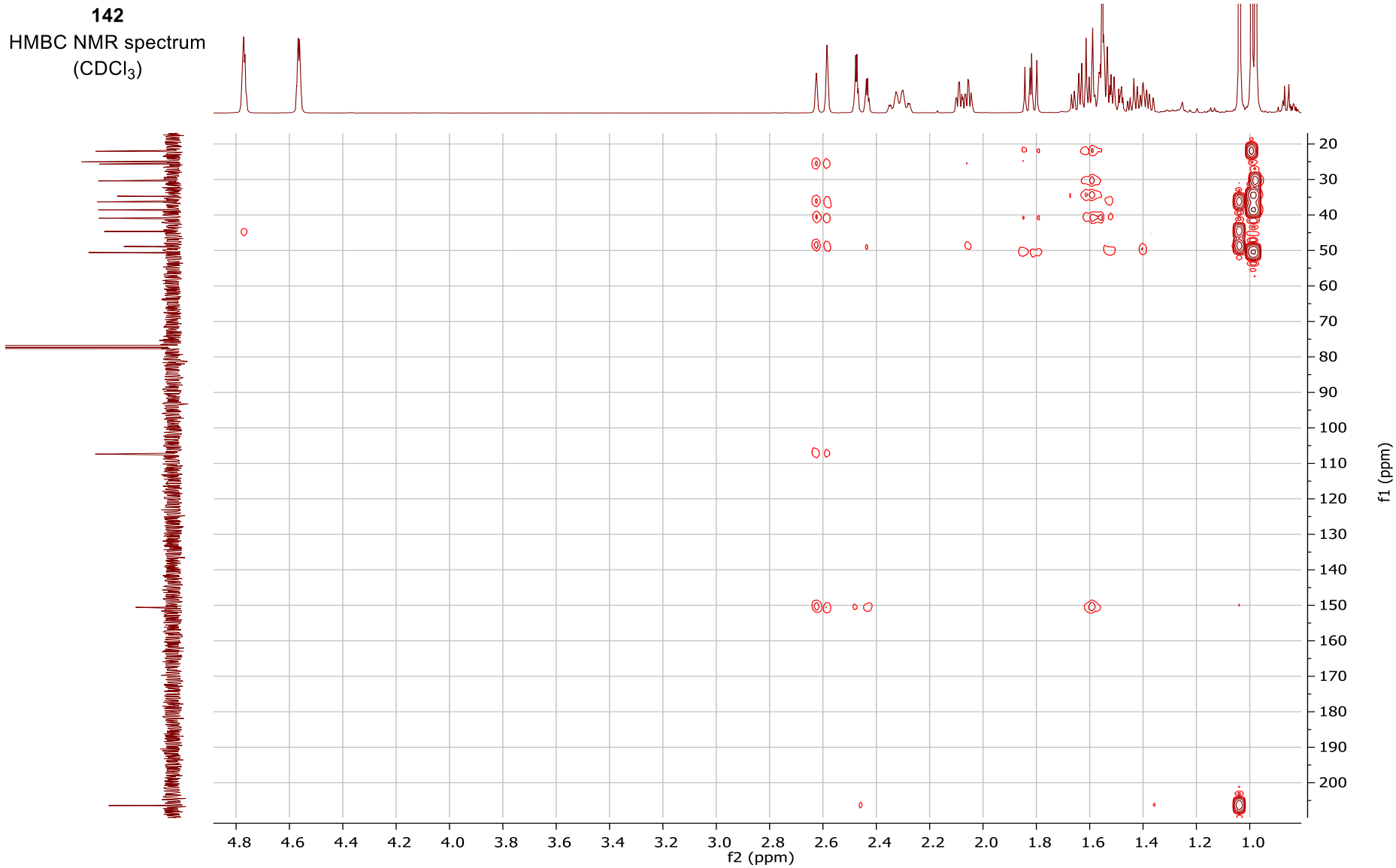

356

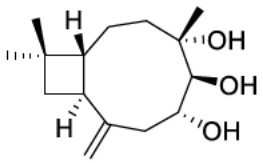

146

^{1}H NMR Spectrum
(400 MHz, $CDCl_3$)

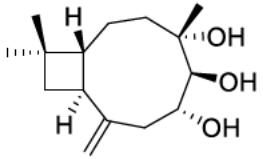

146

^{13}C NMR Spectrum
(101 MHz, $CDCl_3$)

146

COSY NMR Spectrum

($CDCl_3$)

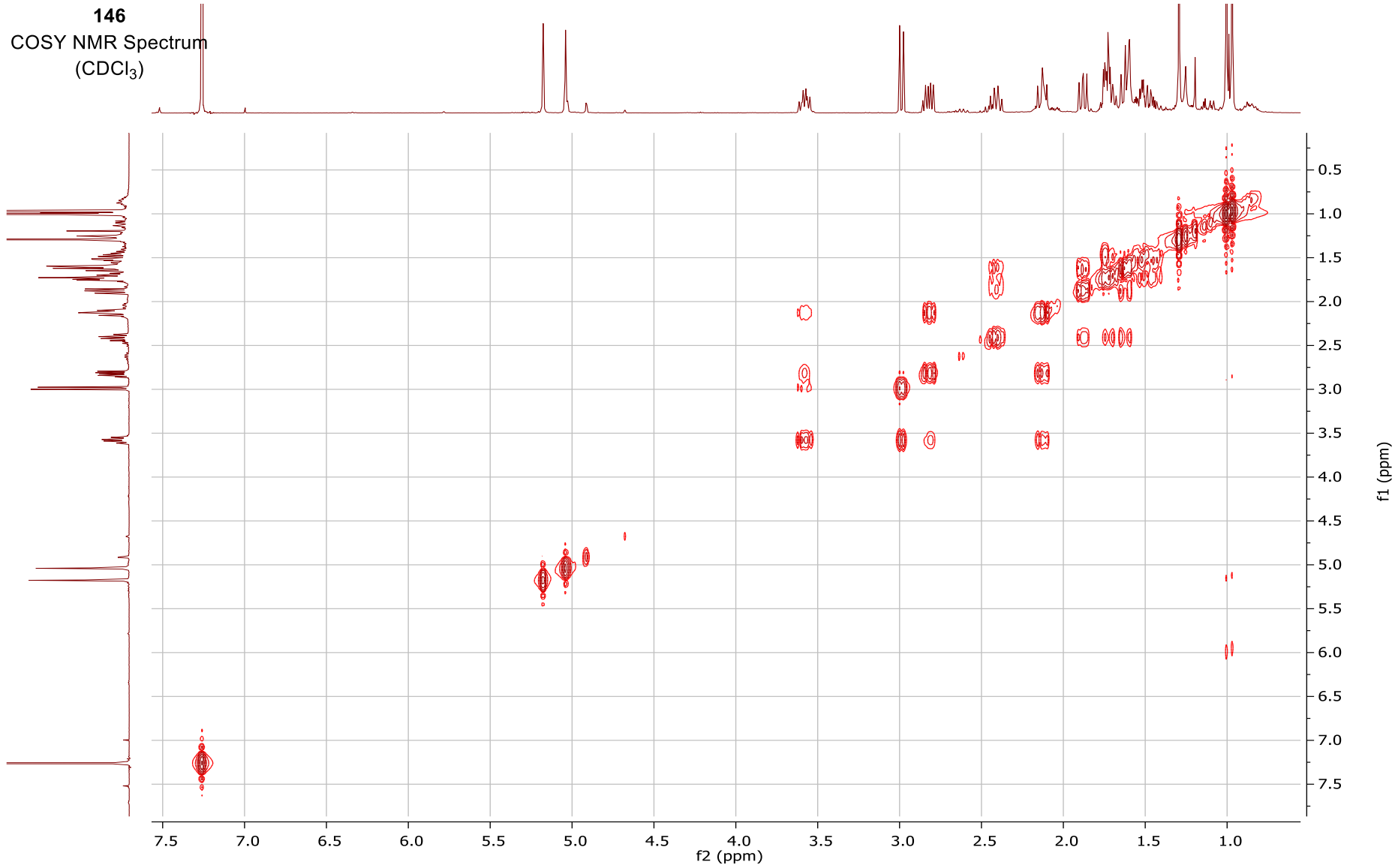

359

146

NOESY NMR Spectrum

($CDCl_3$)

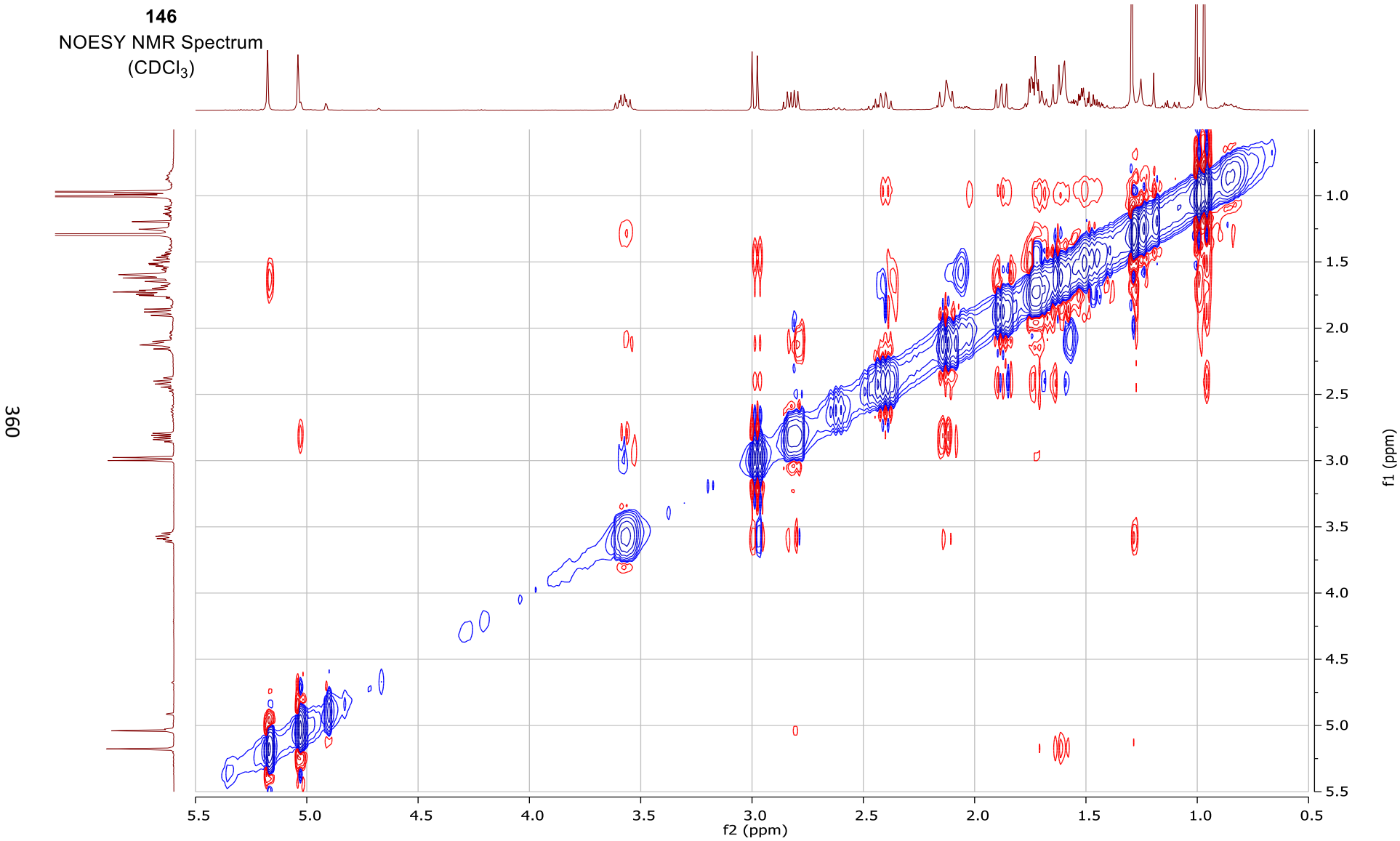

146

HSQC NMR Spectrum

($CDCl_3$)

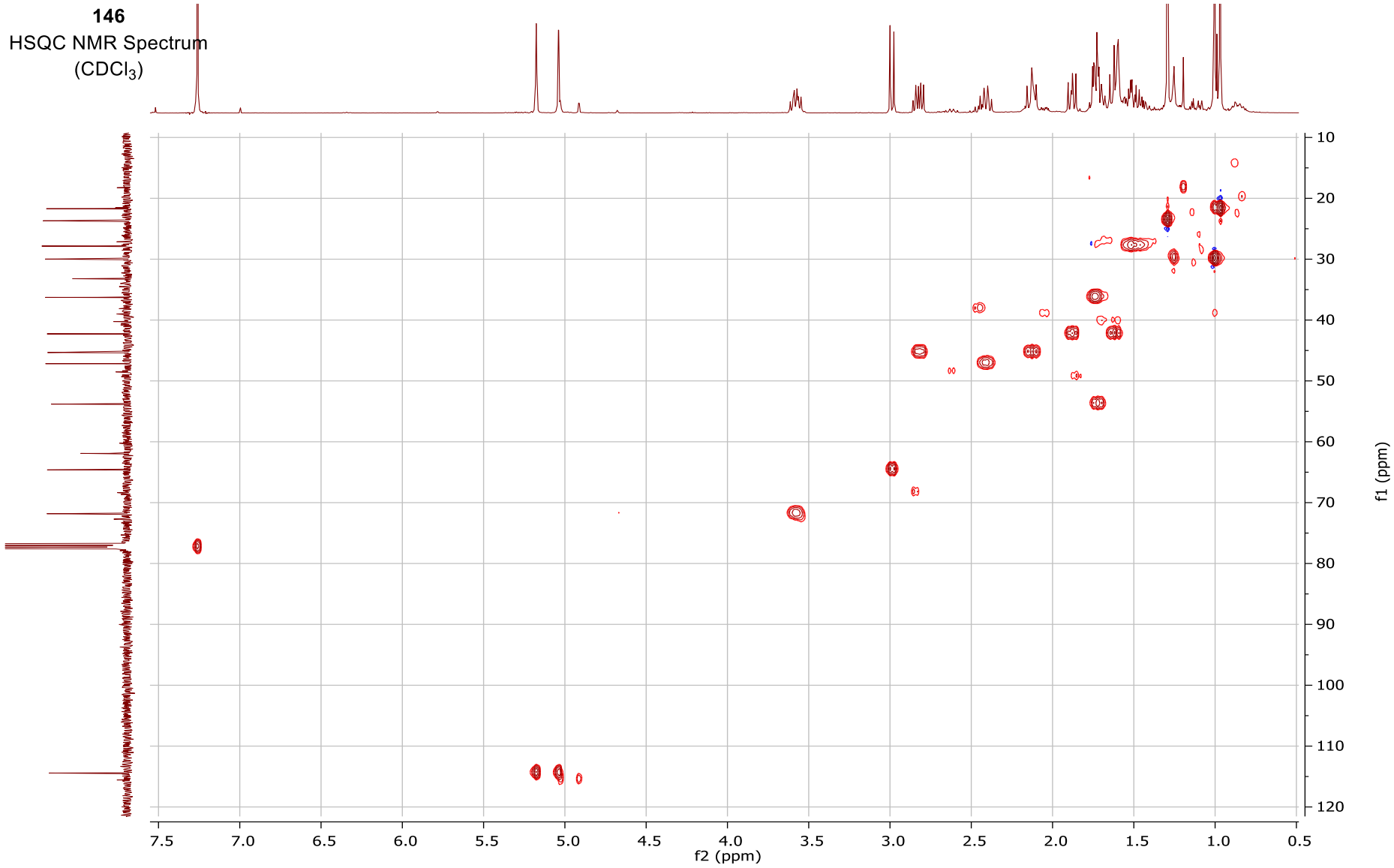

361

146

HMBC NMR Spectrum

($CDCl_3$)

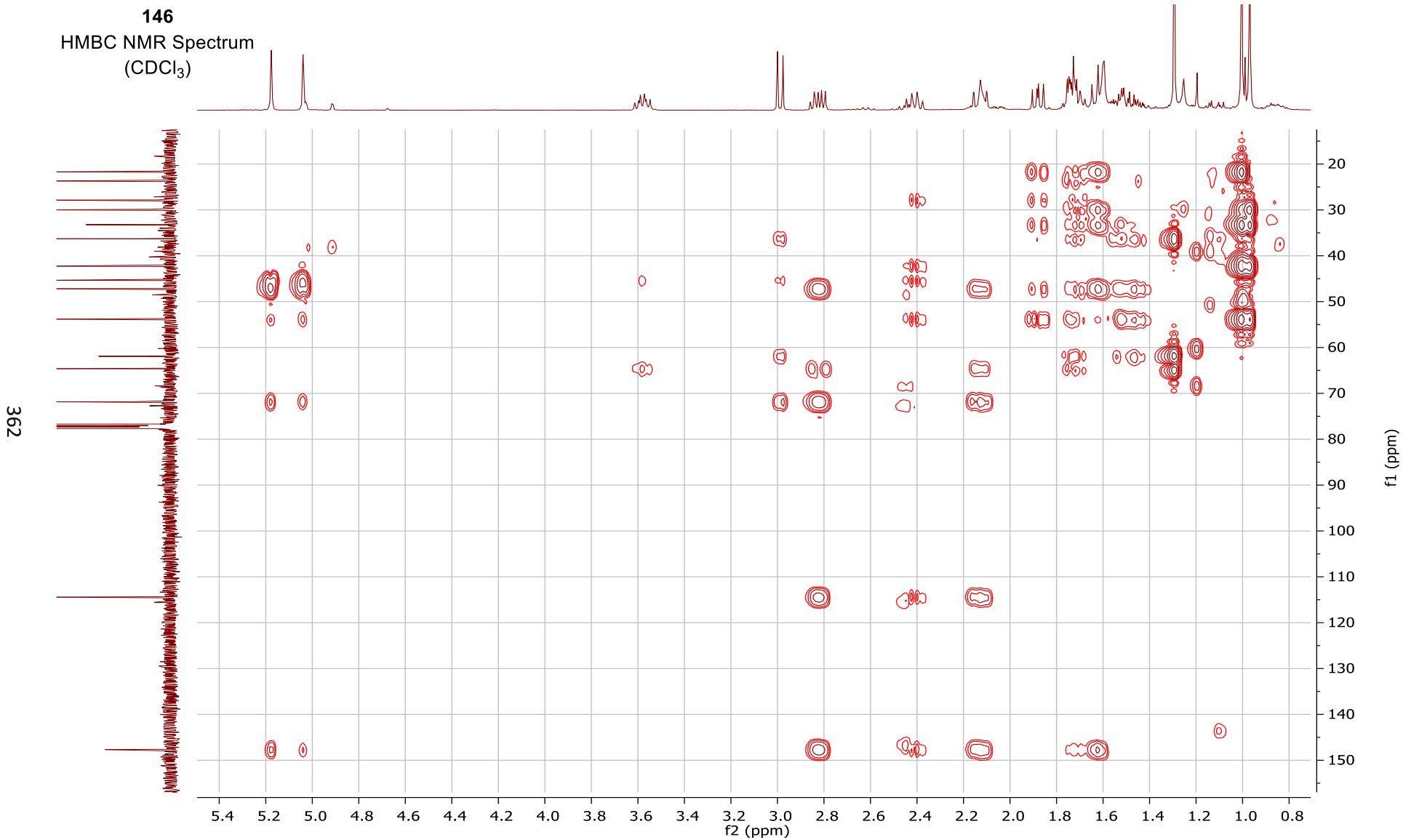

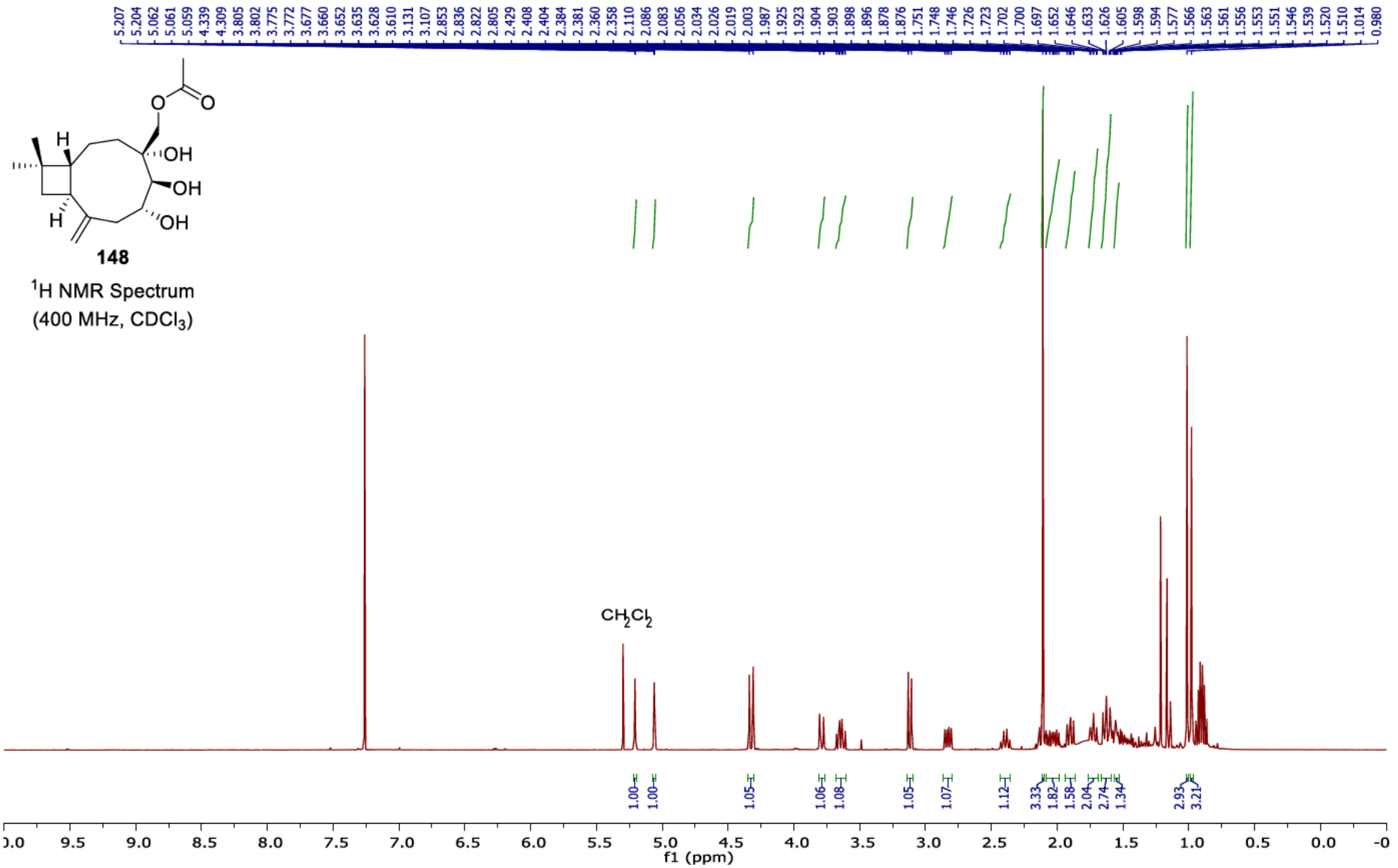
5.207 5.204 5.062 5.061 5.059 4.339 4.309 3.805 3.802 3.775 3.772 3.677 3.660 3.652 3.635 3.628 3.610 3.131 3.107 2.853 2.836 2.822 2.805 2.429 2.408 2.404 2.384 2.381 2.360 2.358 2.110 2.086 2.083 2.056 2.034 2.026 2.019 2.003 1.987 1.925 1.923 1.904 1.903 1.898 1.896 1.878 1.876 1.751 1.748 1.746 1.726 1.723 1.702 1.700 1.697 1.652 1.646 1.633 1.626 1.605 1.598 1.594 1.577 1.566 1.563 1.561 1.556 1.553 1.551 1.546 1.539 1.520 1.510 1.014 0.980
O
O
H
OH
OH
H
OH
148
^{1}H NMR Spectrum
(400 MHz, $CDCl_3$)
CH_2Cl_2
1.00 1.00 1.05 1.06 1.08 1.05 1.07 1.12 3.33 1.82 1.58 2.04 2.74 1.34 2.93 3.21
9.5 9.0 8.5 8.0 7.5 7.0 6.5 6.0 5.5 5.0 4.5 4.0 3.5 3.0 2.5 2.0 1.5 1.0 0.5 0.0
f1 (ppm)

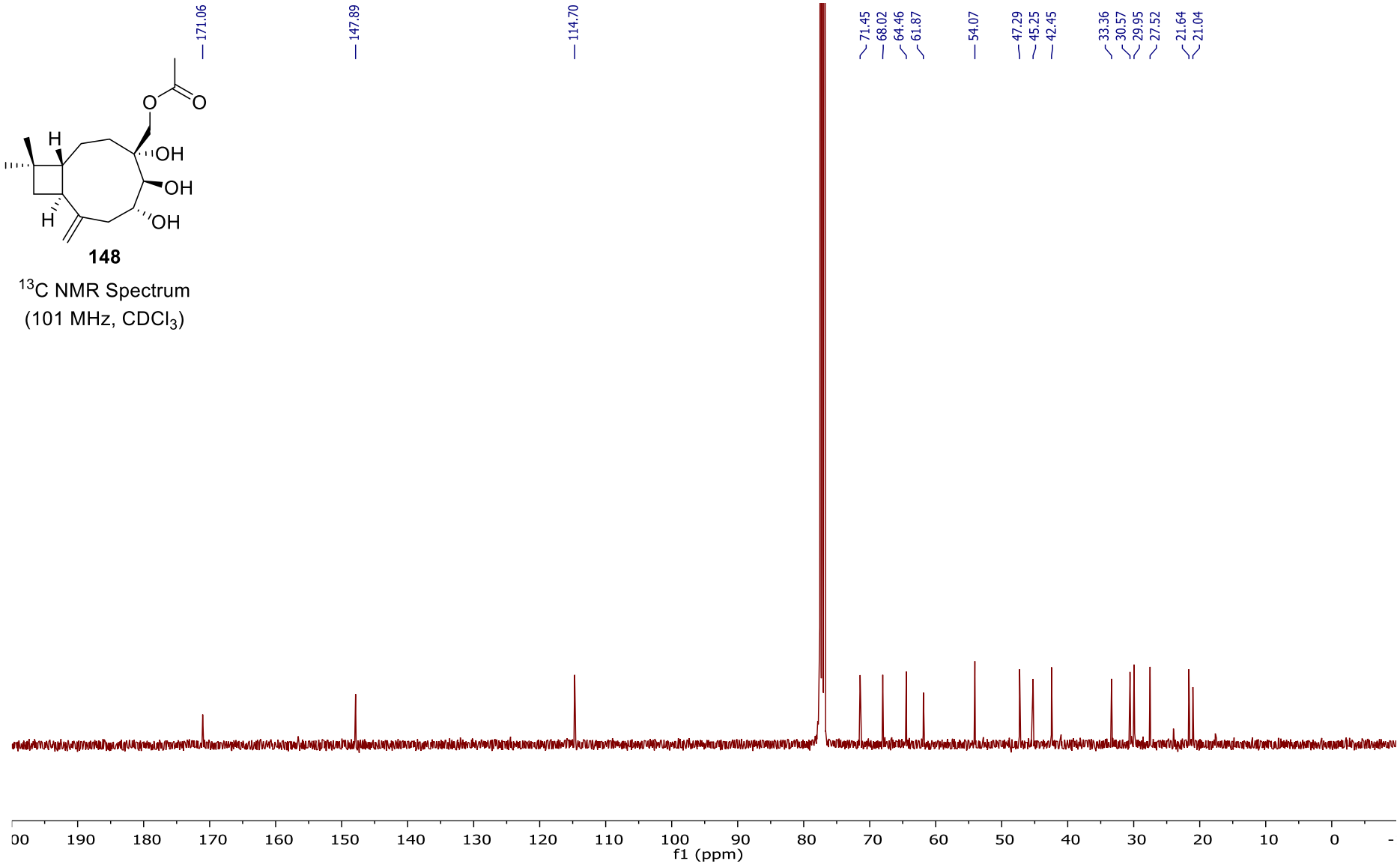
171.06
147.89
114.70
71.45
68.02
64.46
61.87
54.07
47.29
45.25
42.45
33.36
30.57
29.95
27.52
21.64
21.04
O
O
H
OH
OH
H
OH
148
13C NMR Spectrum
(101 MHz, CDCl3)
f1 (ppm)

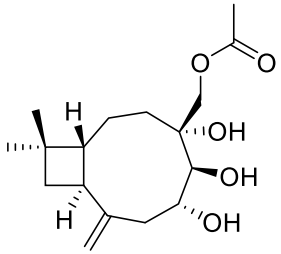

148

DEPT135 NMR Spectrum
(101 MHz, $CDCl_3$)

148
COSY NMR Spectrum
($CDCl_3$)

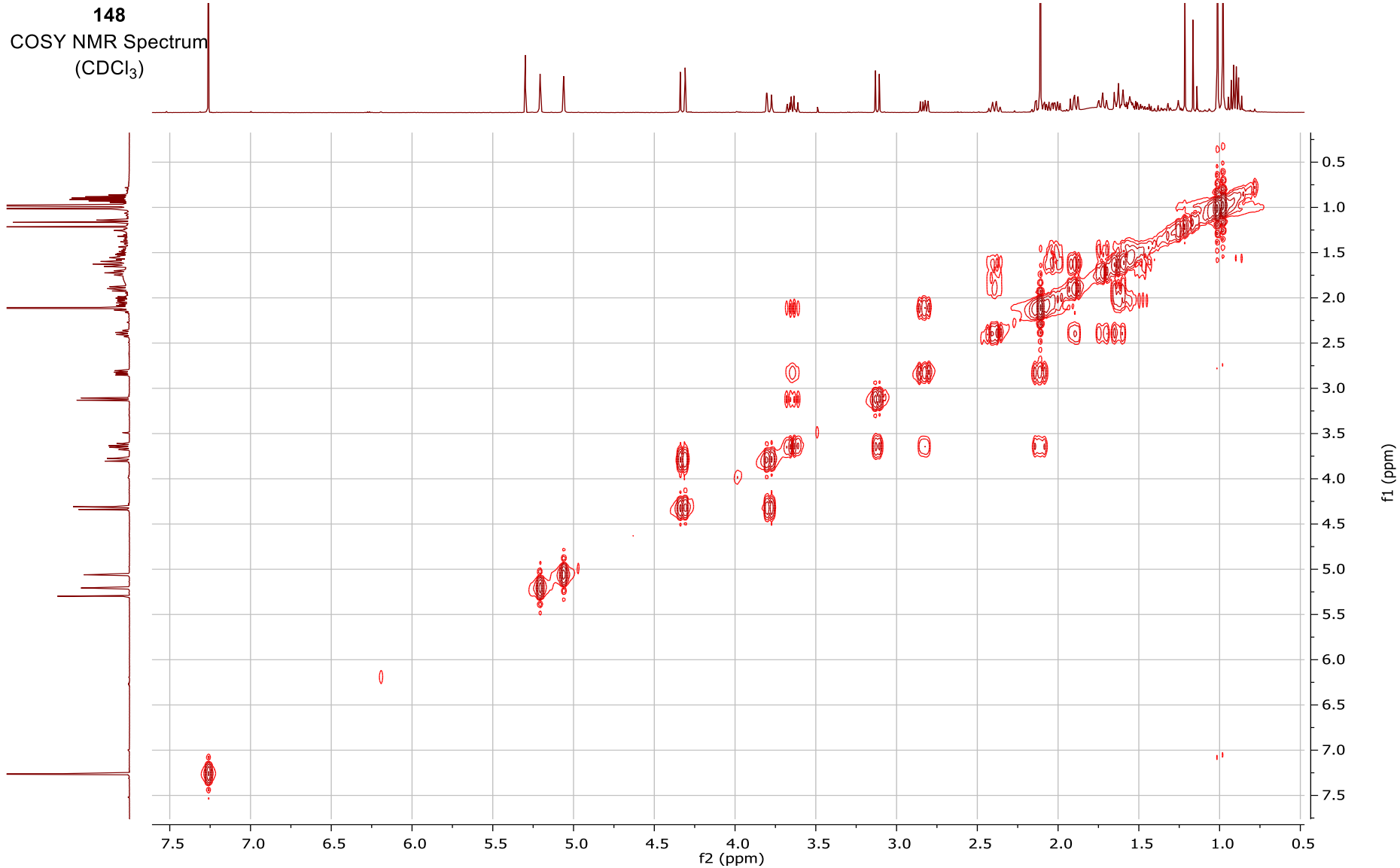

148

NOESY NMR Spectrum

($CDCl_3$)

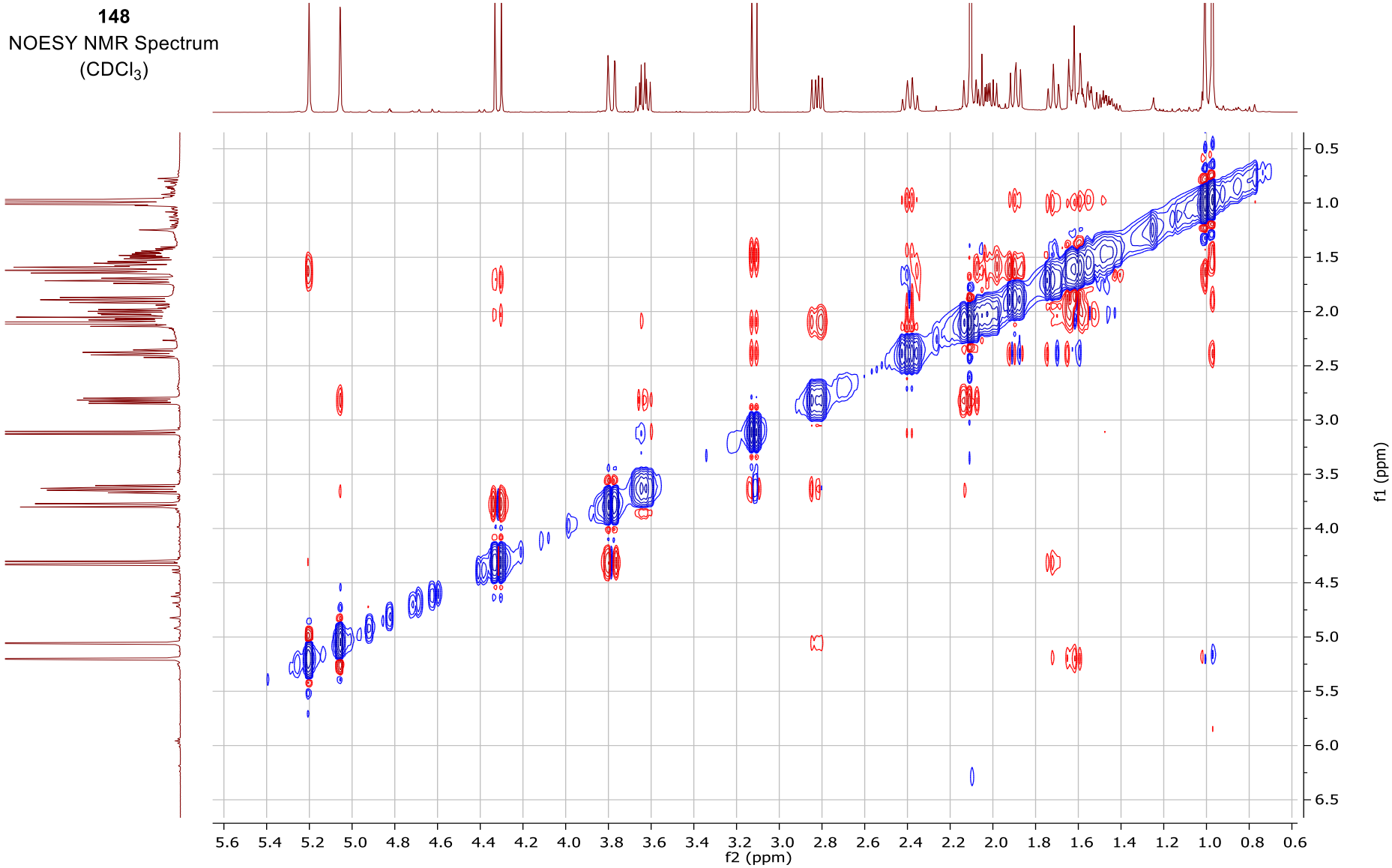

148

HSQC NMR Spectrum

($CDCl_3$)

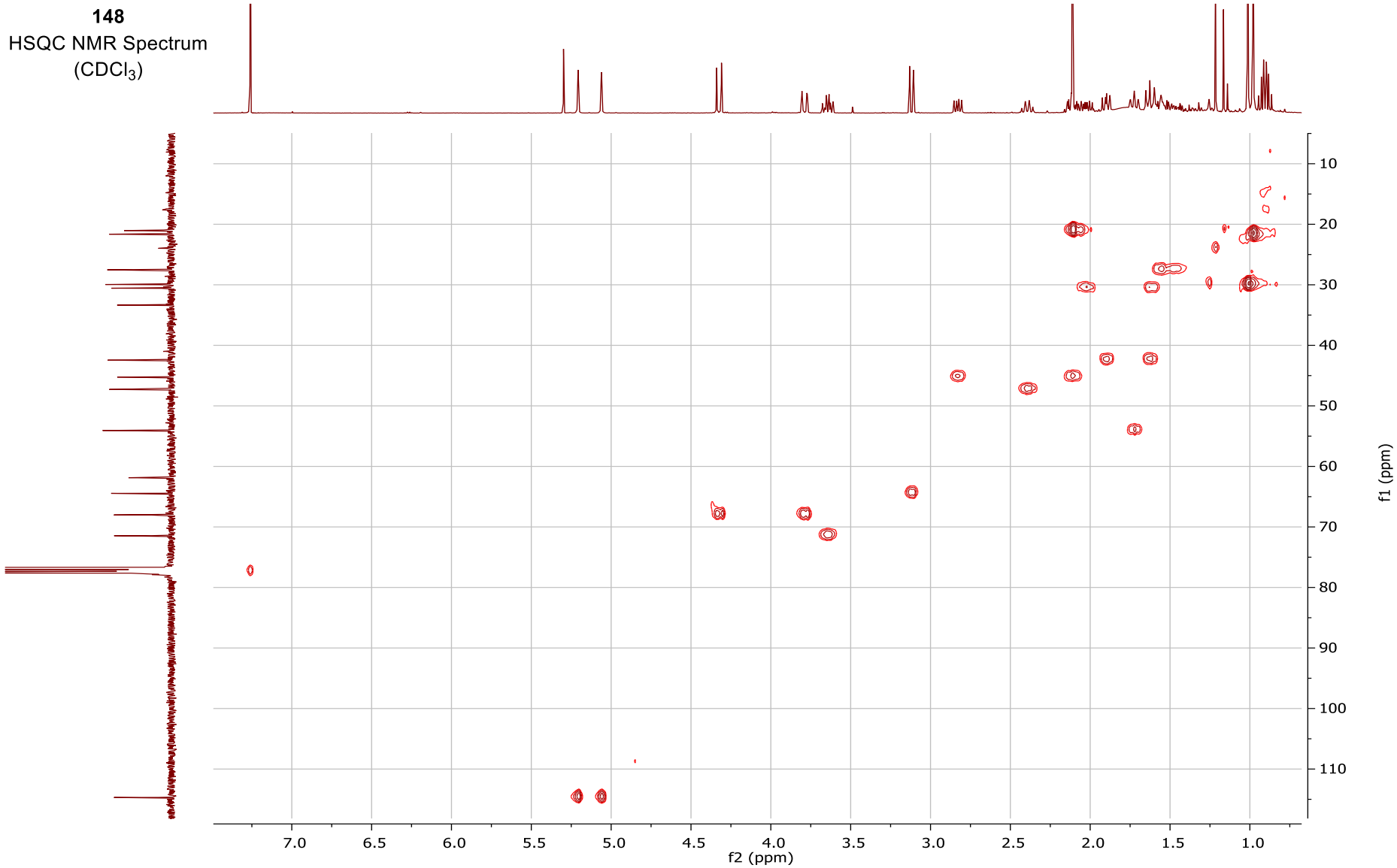

148

HMBC NMR Spectrum

($CDCl_3$)

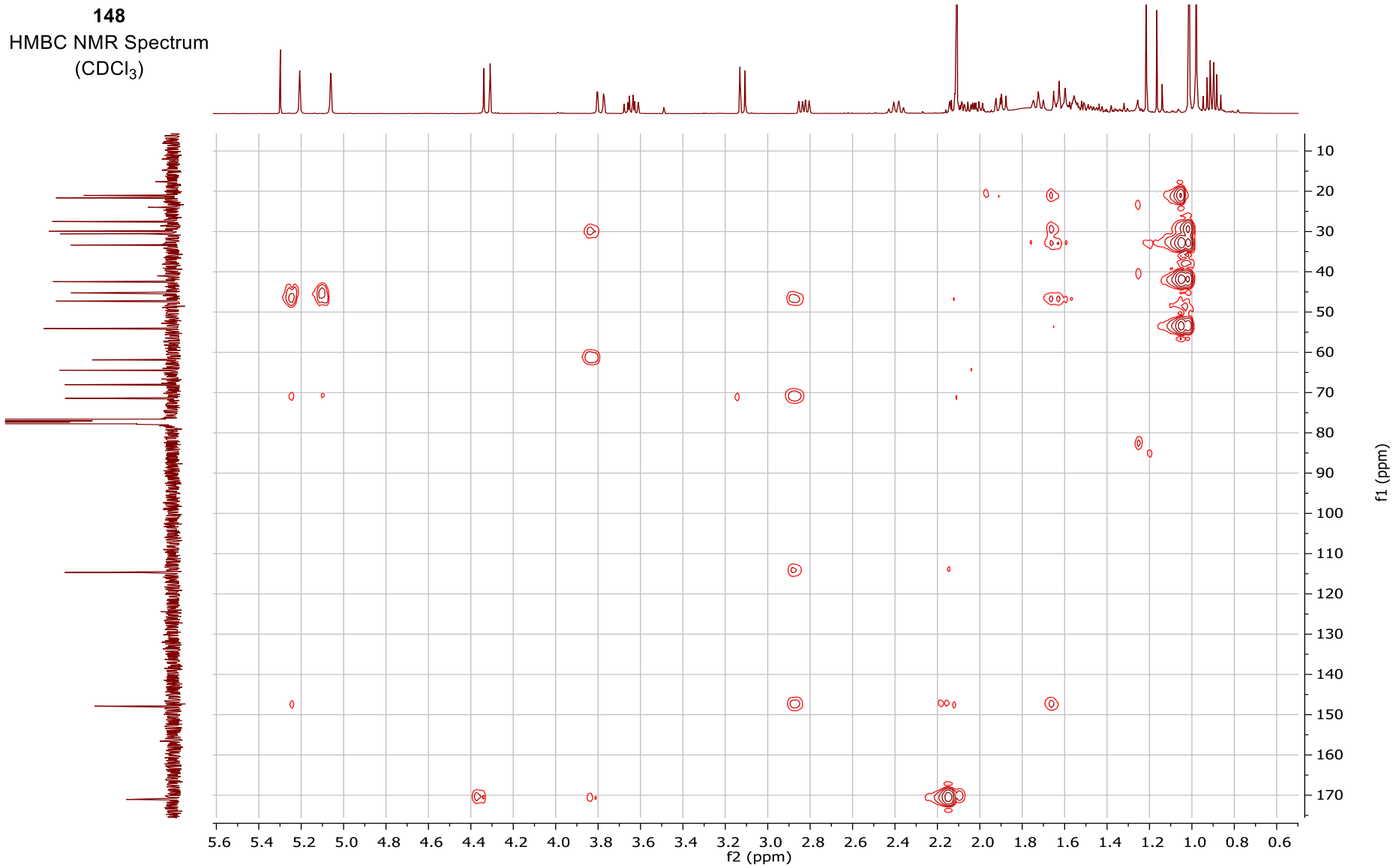

369

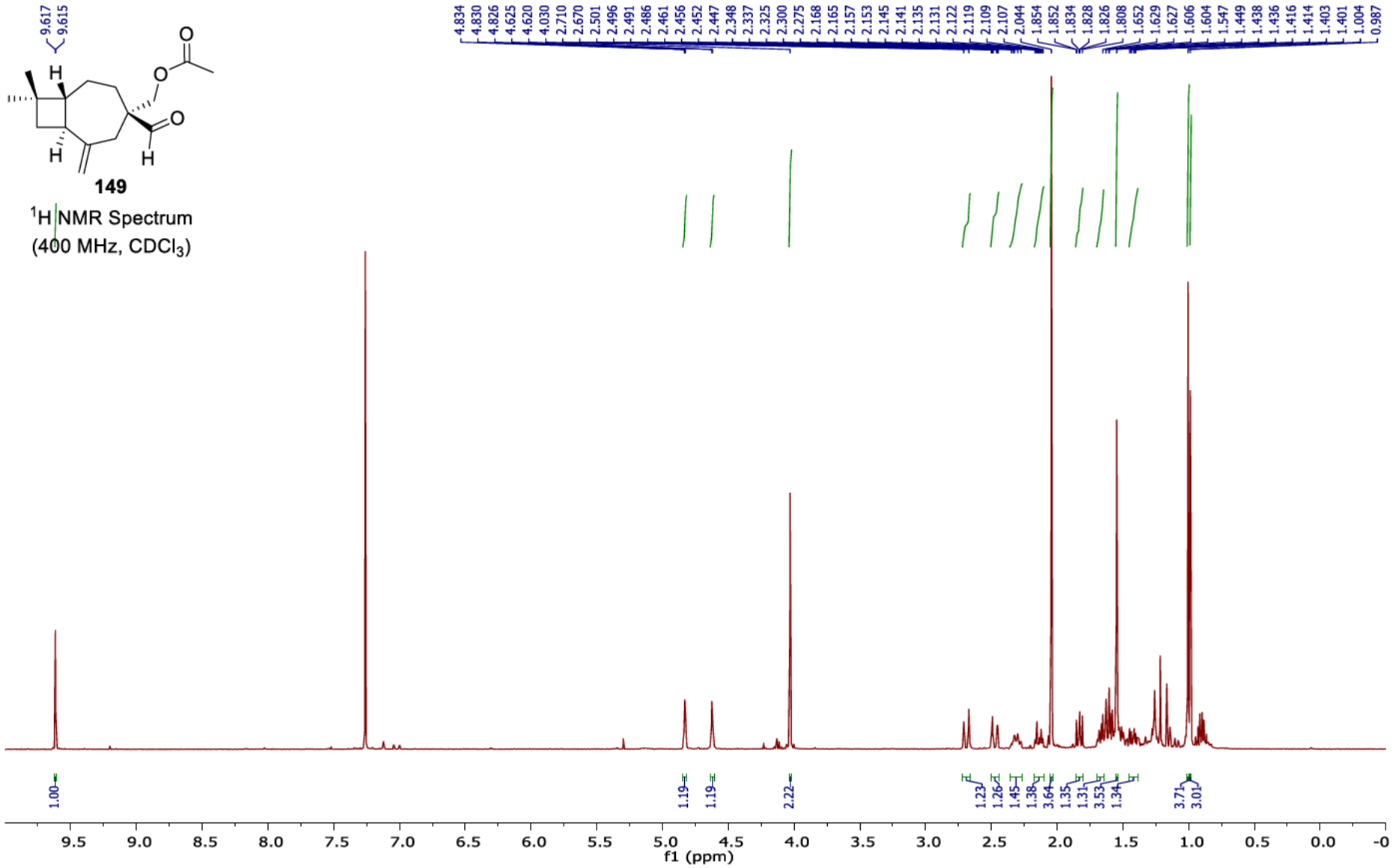
9.617
9.615
H
O
O
O
H
H
149
^{1}H NMR Spectrum
(400 MHz, $CDCl_3$)
4.834 4.830 4.826 4.625 4.620 4.030 2.710 2.670 2.501 2.496 2.491 2.486 2.461 2.456 2.452 2.447 2.348 2.337 2.325 2.300 2.275 2.168 2.165 2.157 2.153 2.145 2.141 2.135 2.131 2.122 2.119 2.109 2.107 2.044 1.854 1.852 1.834 1.828 1.826 1.808 1.652 1.629 1.627 1.606 1.604 1.547 1.449 1.438 1.436 1.416 1.414 1.403 1.401 1.004 0.987
1.00 1.19 1.19 2.22 1.23 1.26 1.45 1.38 3.64 1.35 1.31 3.53 1.34 3.71 3.01
9.5 9.0 8.5 8.0 7.5 7.0 6.5 6.0 5.5 5.0 4.5 4.0 3.5 3.0 2.5 2.0 1.5 1.0 0.5 0.0 -0
f1 (ppm)

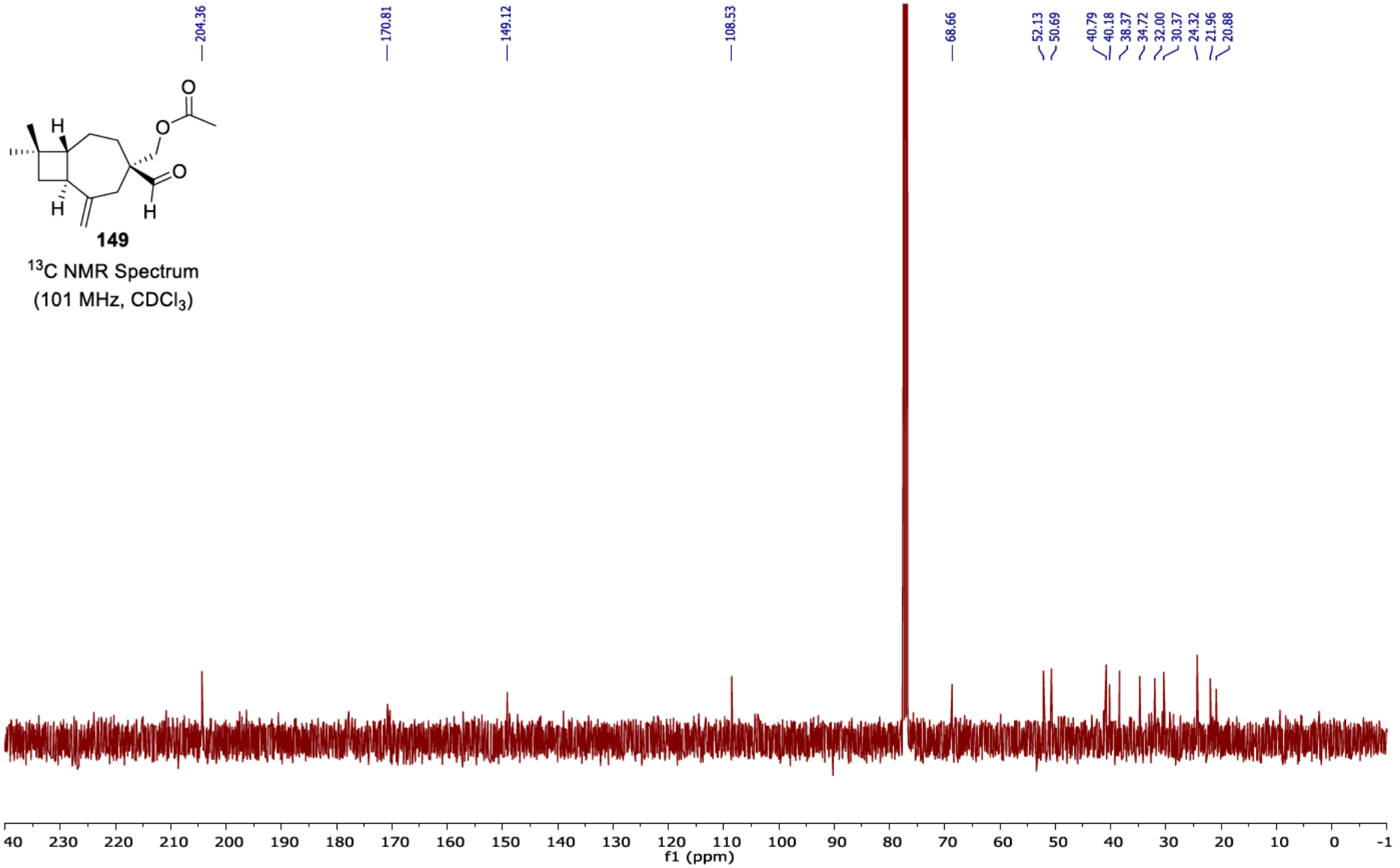
204.36
170.81
149.12
108.53
68.66
52.13
50.69
40.79
40.18
38.37
34.72
32.00
30.37
24.32
21.96
20.88
O
O
O
H
H
H
149
^{13}C NMR Spectrum
(101 MHz, $CDCl_3$)
40 230 220 210 200 190 180 170 160 150 140 130 120 110 100 90 80 70 60 50 40 30 20 10 0 -1
f1 (ppm)

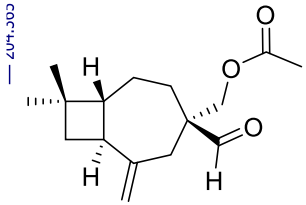

149

DEPT135 NMR Spectrum
(101 MHz, $CDCl_3$)

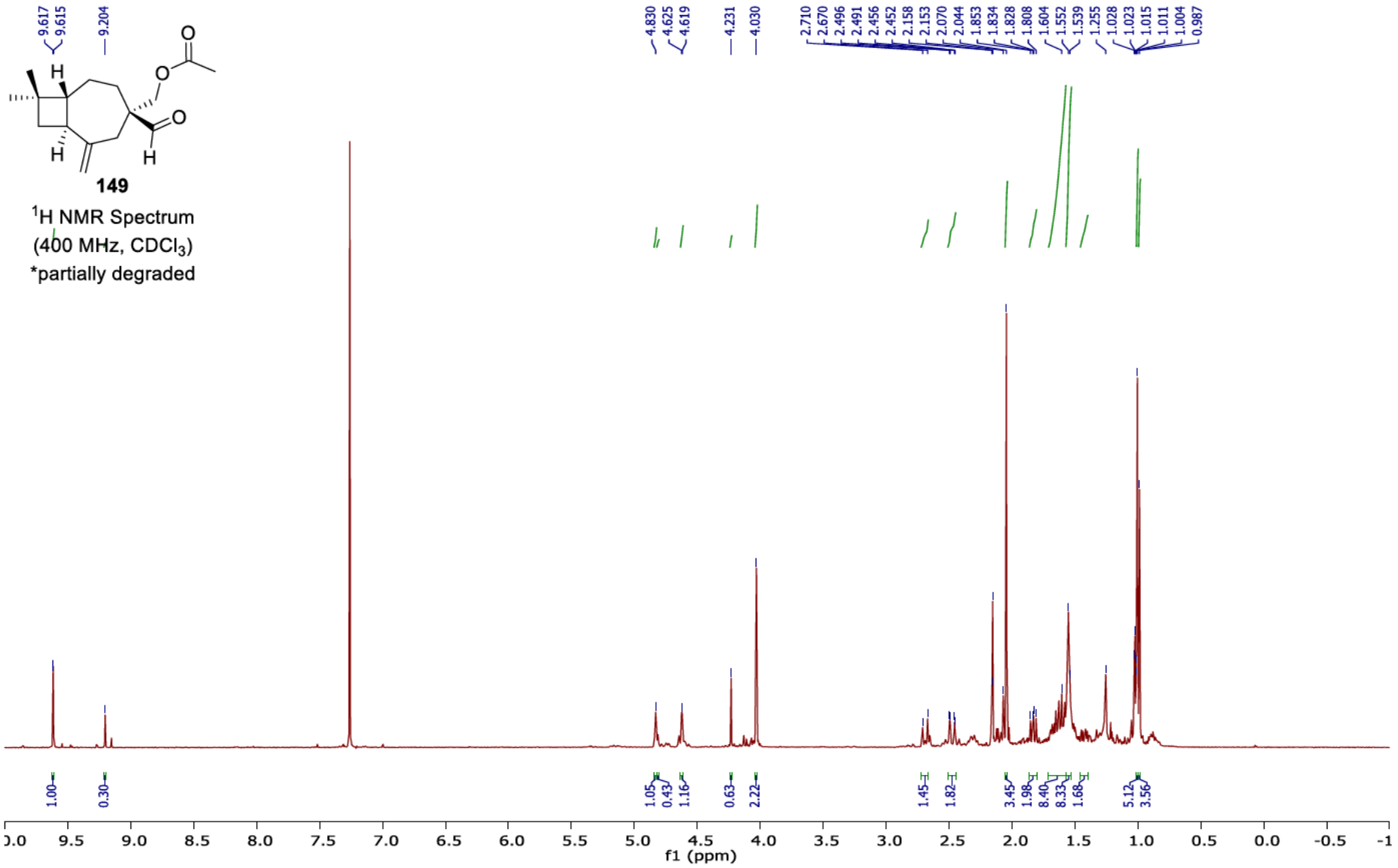
9.617
9.615
9.204
4.830
4.625
4.619
4.231
4.030
2.710
2.670
2.496
2.491
2.456
2.452
2.158
2.153
2.070
2.044
1.853
1.834
1.828
1.808
1.604
1.552
1.539
1.255
1.028
1.023
1.015
1.011
1.004
0.987
O
O
O
H
H
H
149
1H NMR Spectrum
(400 MHz, CDCl3)
*partially degraded
1.00
0.30
1.05
0.43
1.16
0.63
2.22
1.45
1.82
3.45
1.98
8.40
8.33
1.68
5.12
3.56
f1 (ppm)

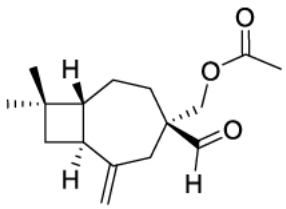

149

^{13}C NMR Spectrum
(101 MHz, $CDCl_3$)
*partially degraded

149
COSY NMR Spectrum
($CDCl_3$)
*partially degraded

149
HSQC NMR Spectrum
($CDCl_3$)
*partially degraded

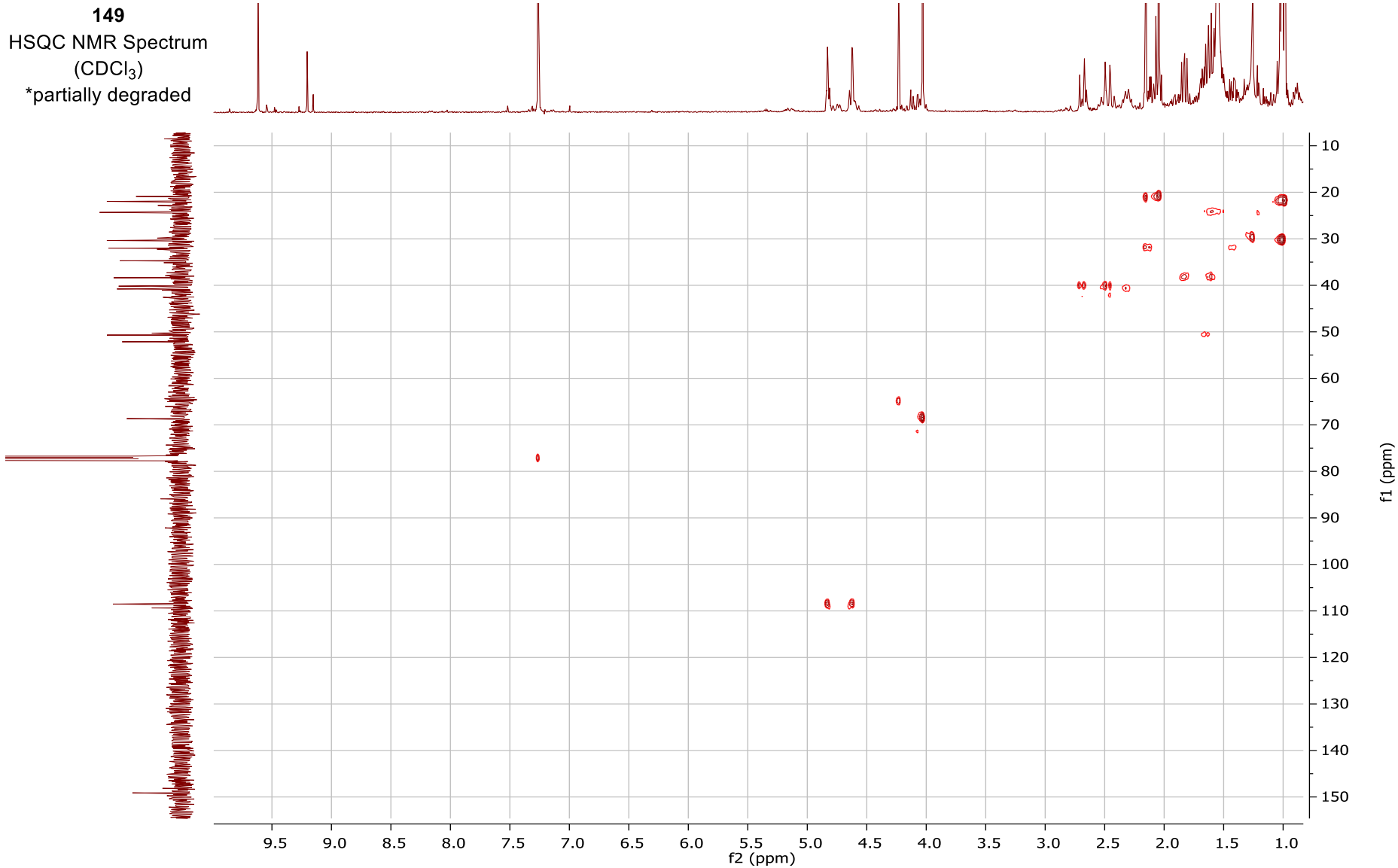

149

HMBC NMR Spectrum

($CDCl_3$)

*partially degraded

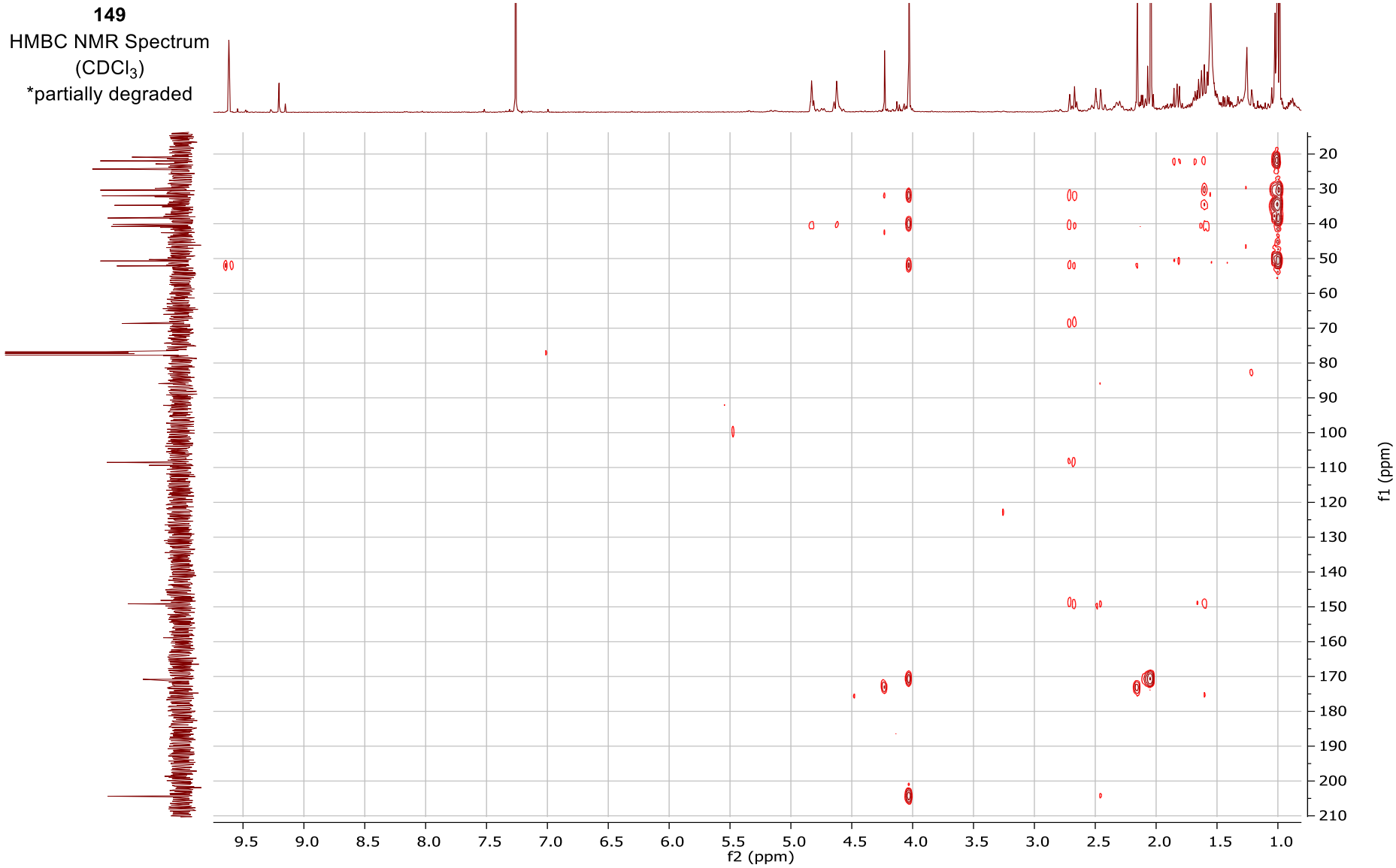

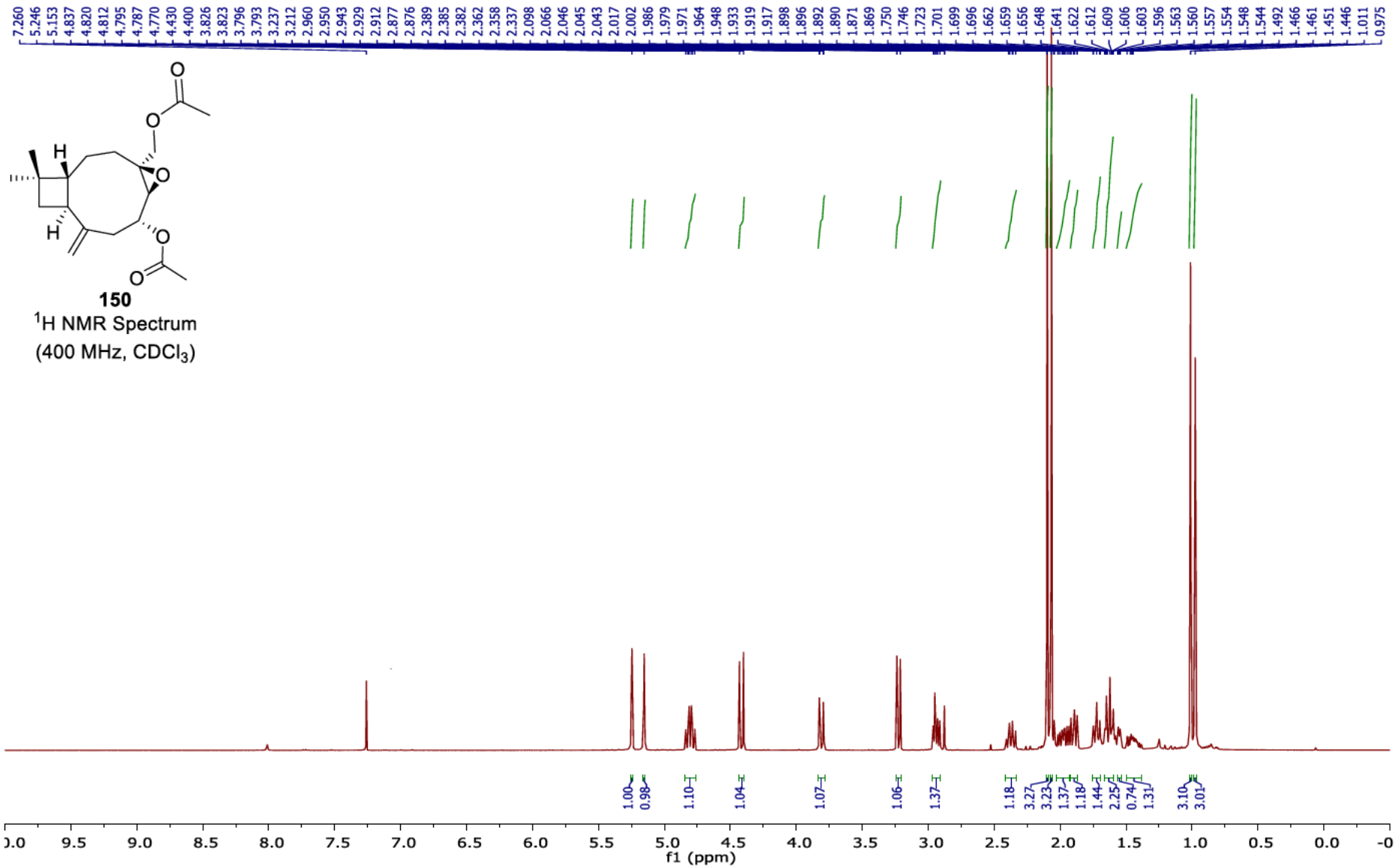

150

^{1}H NMR Spectrum

(400 MHz, $CDCl_3$)

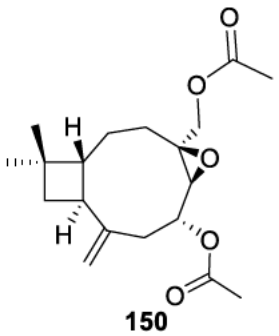

150

^{13}C NMR Spectrum
(101 MHz, $CDCl_3$)

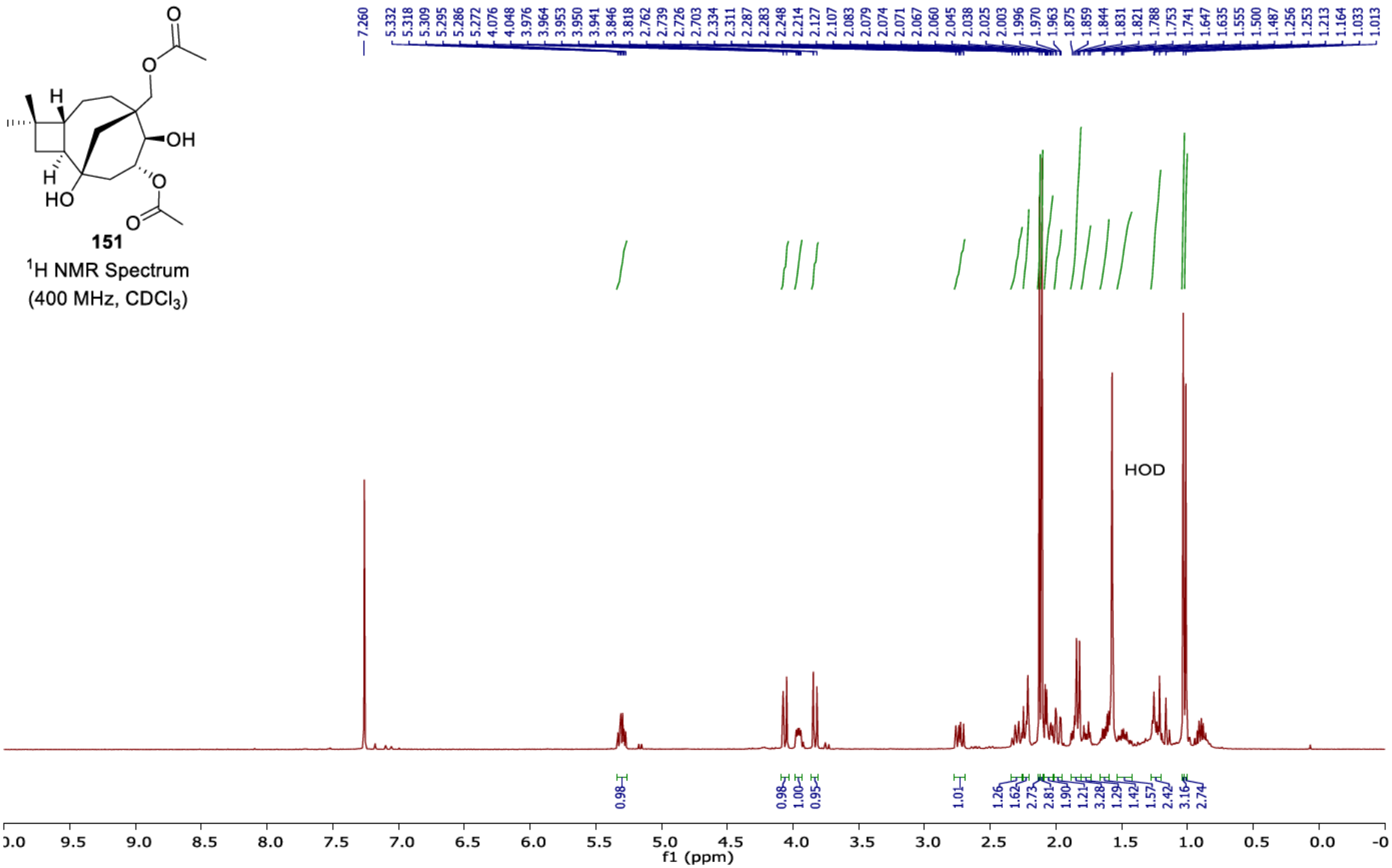
O
O
H
OH
H
HO
O
O
151
1H NMR Spectrum
(400 MHz, CDCl3)
7.260
5.332
5.318
5.309
5.295
5.286
5.272
4.076
4.048
3.976
3.964
3.953
3.950
3.941
3.846
3.818
2.762
2.739
2.726
2.703
2.334
2.311
2.287
2.283
2.248
2.214
2.127
2.107
2.083
2.079
2.074
2.071
2.067
2.060
2.045
2.038
2.025
2.003
1.996
1.970
1.963
1.875
1.859
1.844
1.831
1.821
1.788
1.753
1.741
1.647
1.635
1.555
1.500
1.487
1.256
1.253
1.213
1.164
1.033
1.013
HOD
0.98
0.98
1.00
0.95
1.01
1.26
1.62
2.73
2.81
1.90
1.21
3.28
1.29
1.42
1.57
2.42
3.16
2.74
f1 (ppm)

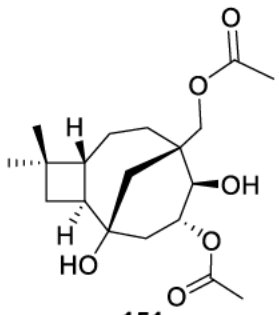

151

^{13}C NMR Spectrum
(101 MHz, $CDCl_3$)

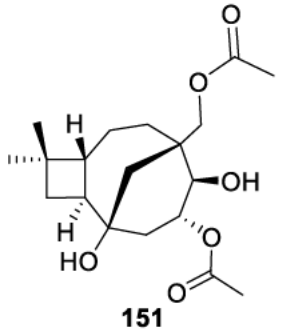

151

DEPT135 NMR Spectrum
(101 MHz, $CDCl_3$)

151

COSY NMR Spectrum

($CDCl_3$)

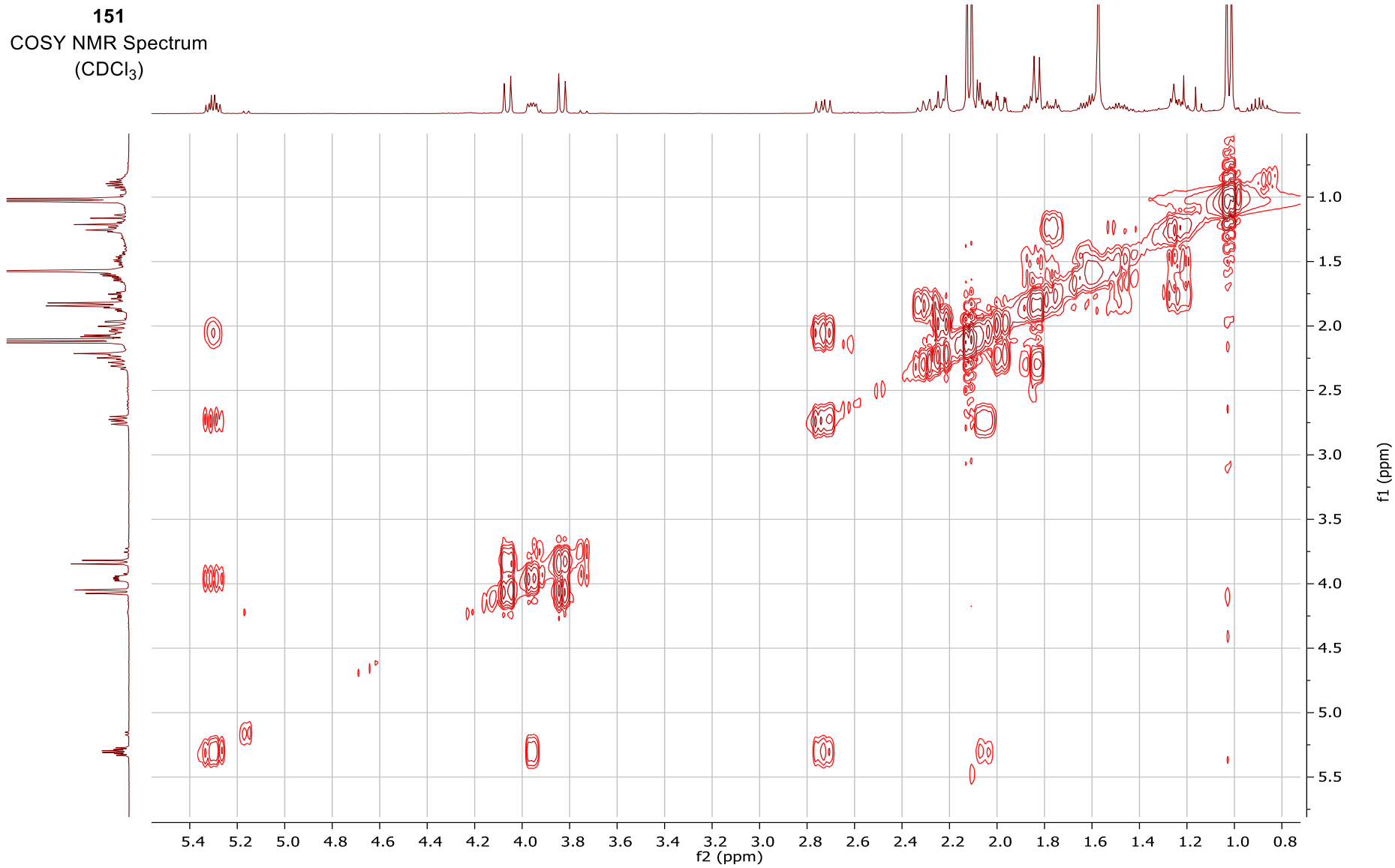

151

HSQC NMR Spectrum

($CDCl_3$)

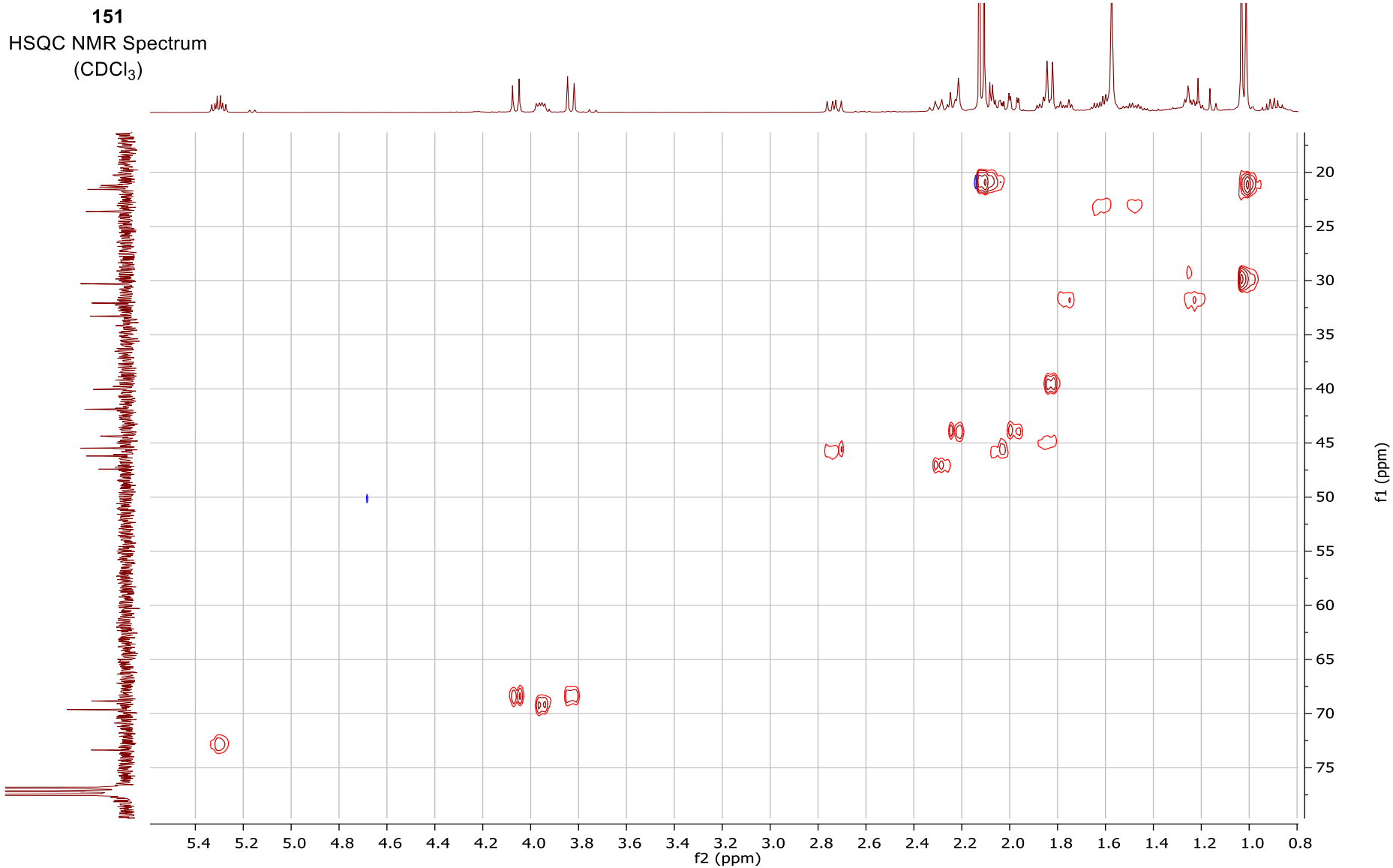

151

HMBC NMR Spectrum

($CDCl_3$)

385

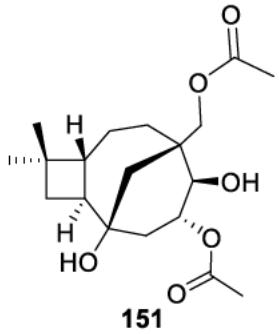

151

^{1}H NMR Spectrum
(400 MHz, $(CD_3)_2CO$)

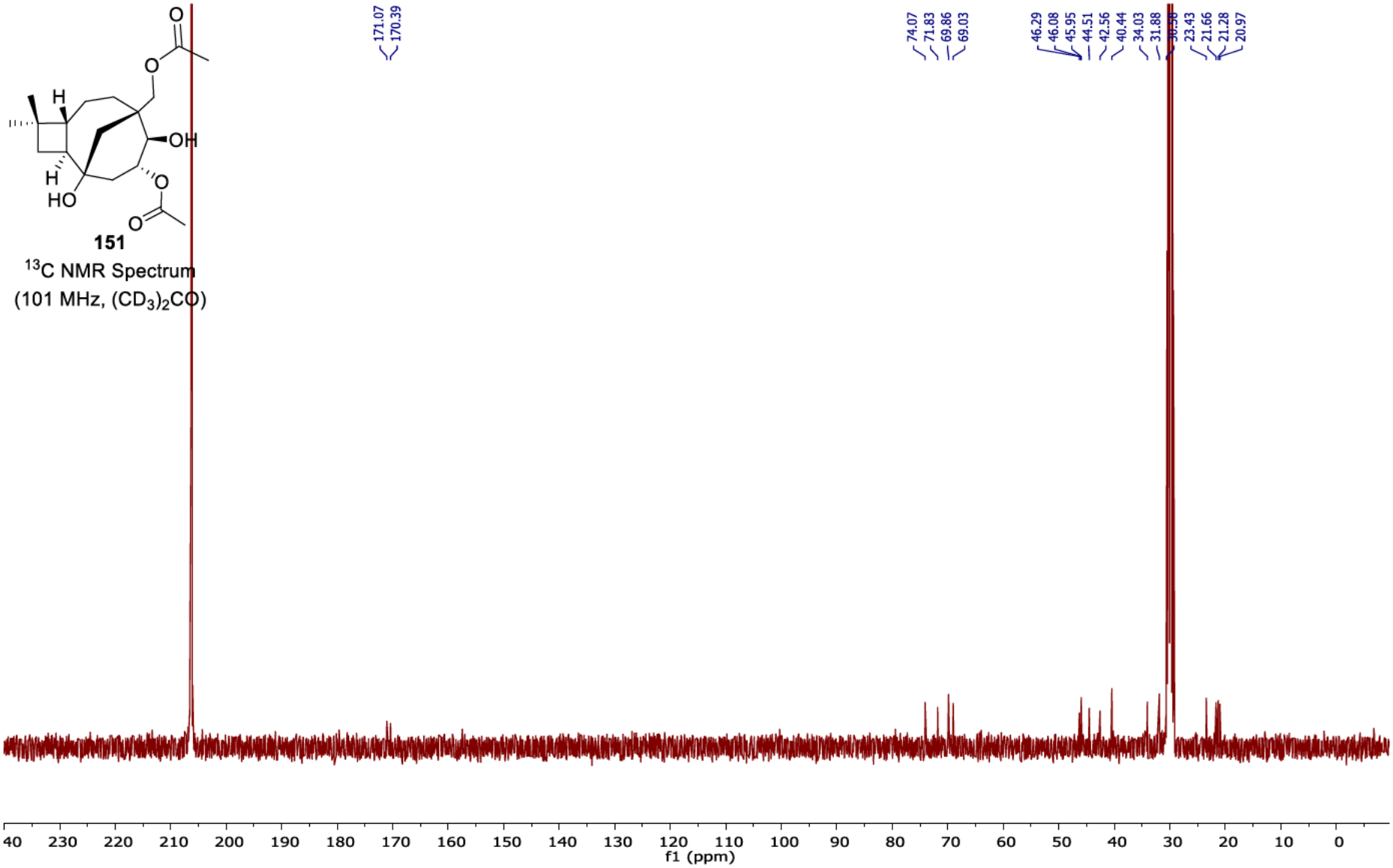
171.07
170.39
74.07
71.83
69.86
69.03
46.29
46.08
45.95
44.51
42.56
40.44
34.03
31.88
30.58
23.43
21.66
21.28
20.97
O
O
H
OH
H
HO
O
O
151
13C NMR Spectrum
(101 MHz, (CD3)2CO)
f1 (ppm)

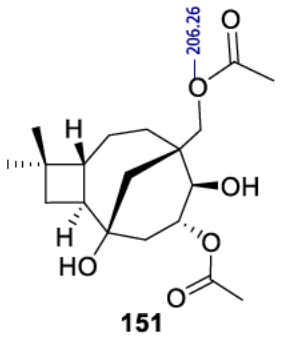

151

DEPT135 NMR Spectrum
(101 MHz, $(CD_3)_2CO$)

151
COSY NMR Spectrum
$((CD_3)_2CO)$

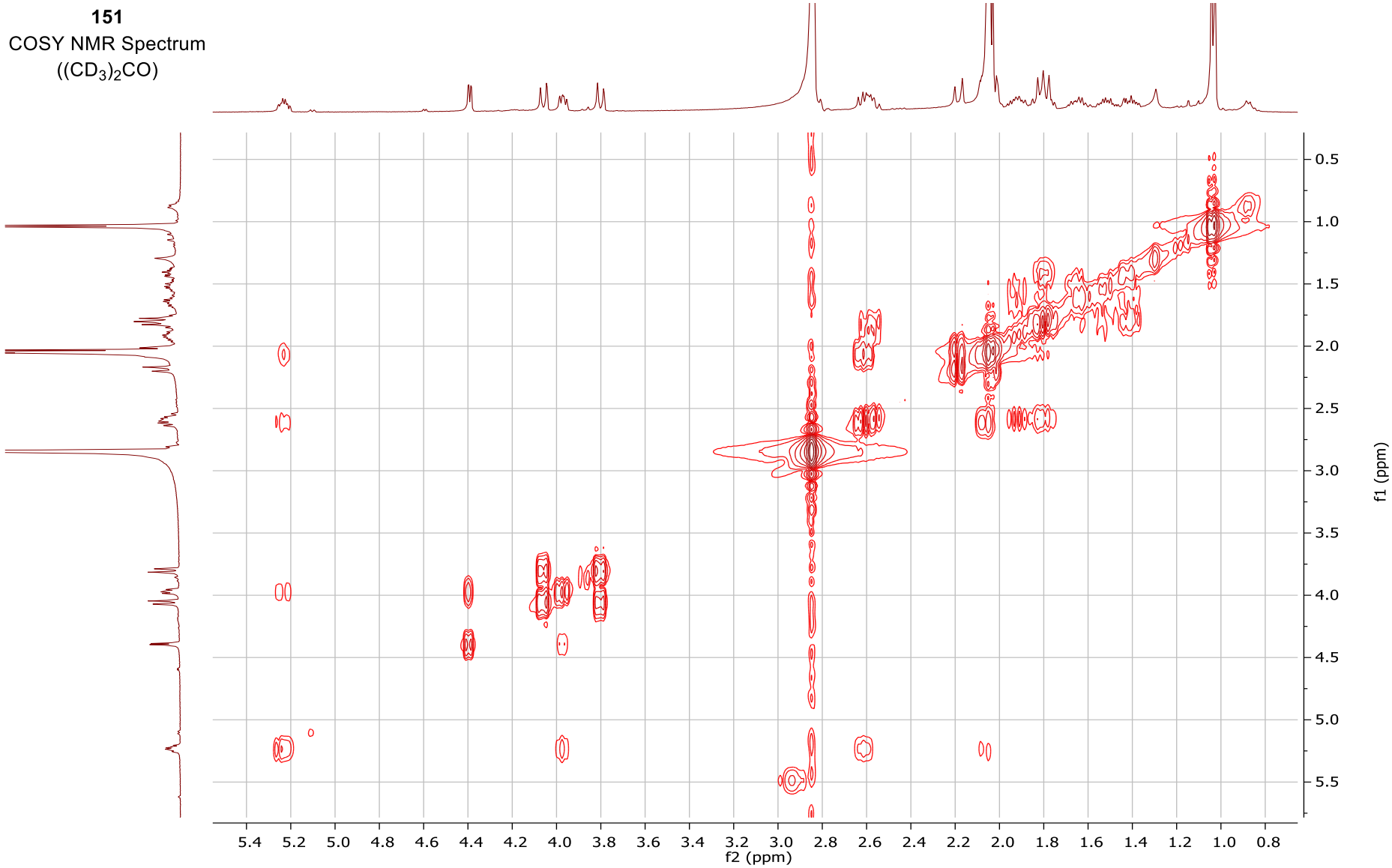

151

HSQC NMR Spectrum

($(CD_3)_2CO$)

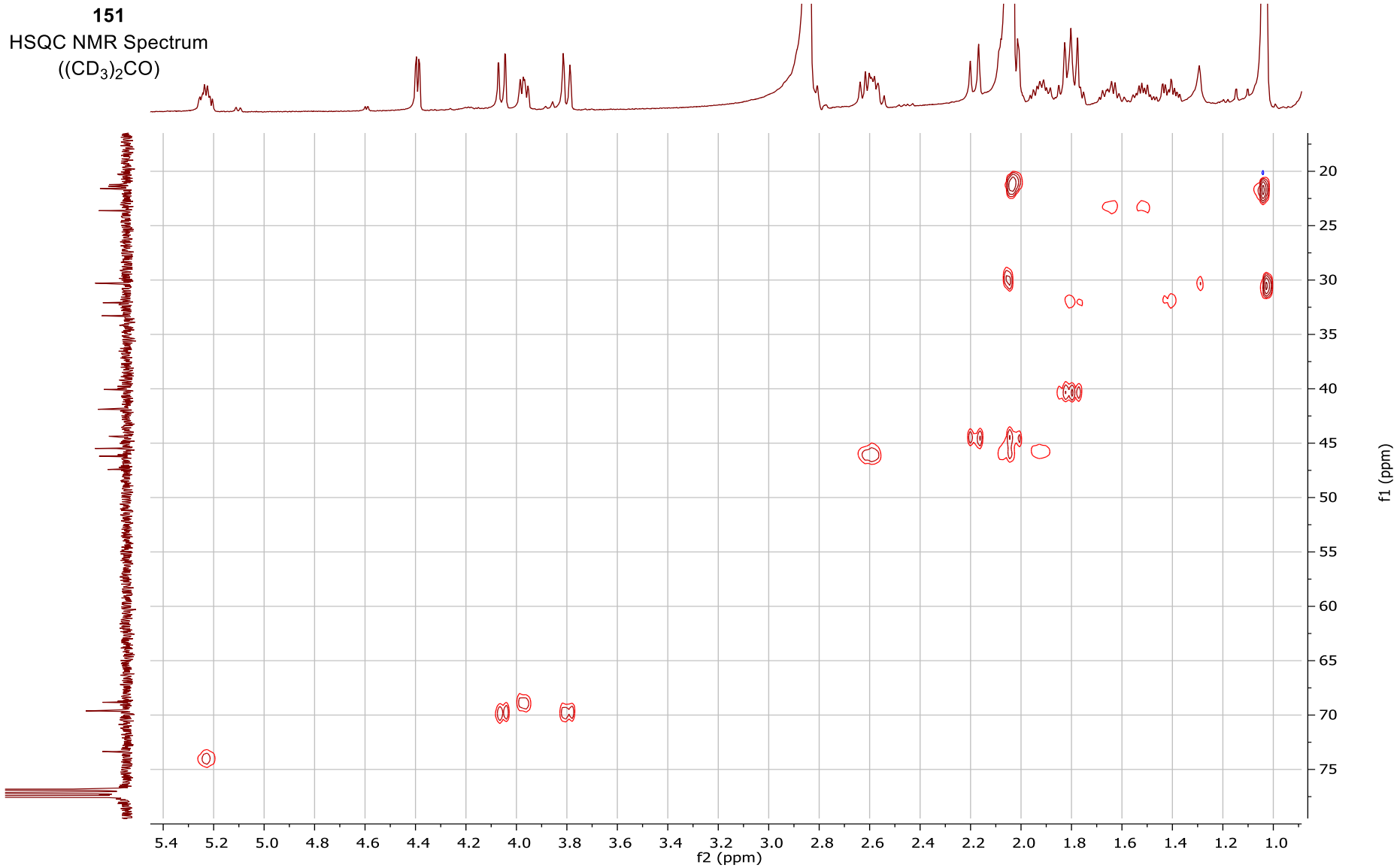

151

HMBC NMR Spectrum

($(CD_3)_2CO$)

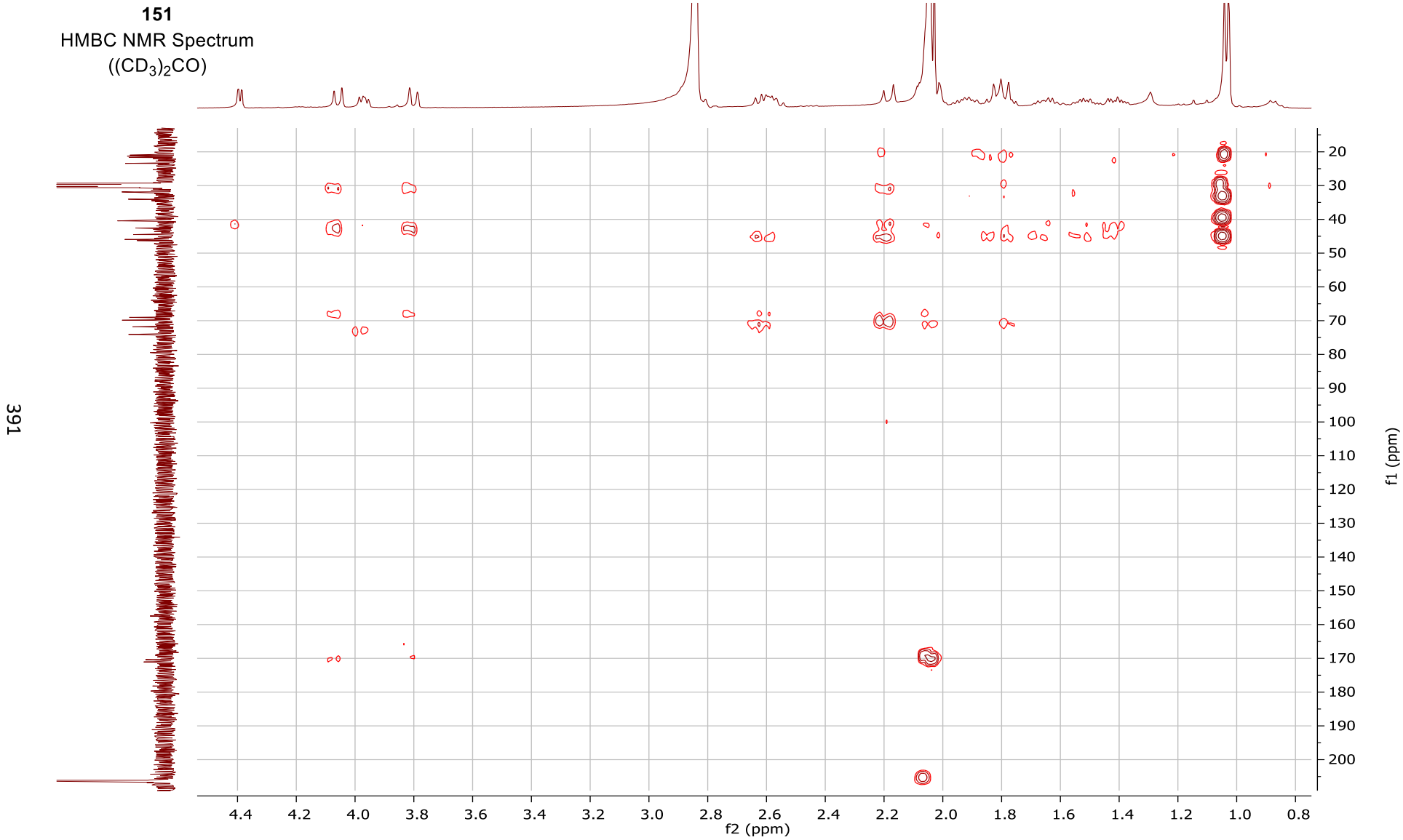

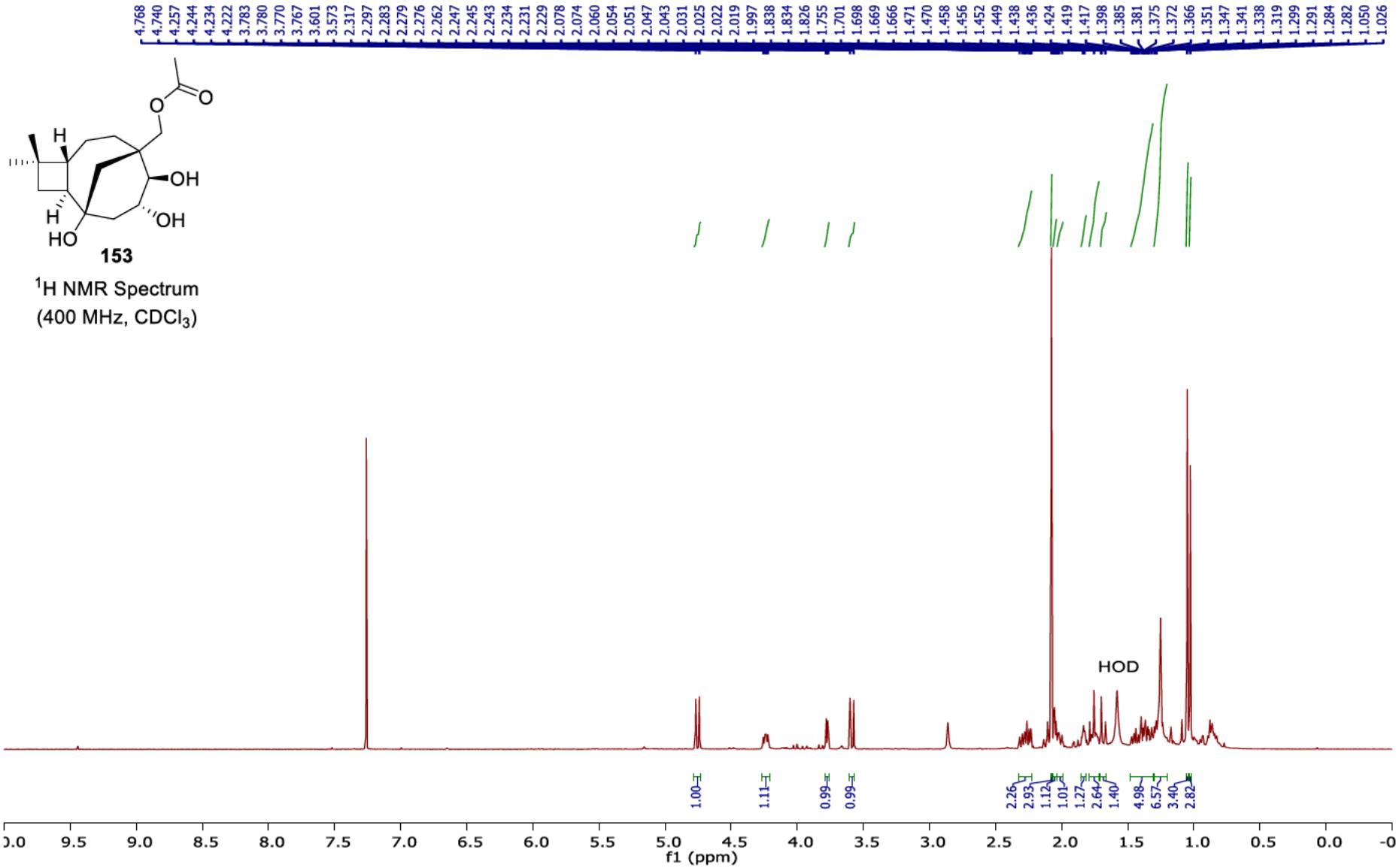
4.768 4.740 4.257 4.244 4.234 4.222 3.783 3.780 3.770 3.767 3.601 3.573 2.317 2.297 2.283 2.279 2.276 2.262 2.247 2.245 2.243 2.234 2.231 2.229 2.078 2.074 2.060 2.054 2.051 2.047 2.043 2.031 2.025 2.022 2.019 1.997 1.838 1.834 1.826 1.755 1.701 1.698 1.669 1.666 1.471 1.470 1.458 1.456 1.452 1.449 1.438 1.436 1.424 1.419 1.417 1.398 1.385 1.381 1.375 1.372 1.366 1.351 1.347 1.341 1.338 1.319 1.299 1.291 1.284 1.282 1.050 1.026
O
O
H
OH
H
OH
HO
153
1H NMR Spectrum
(400 MHz, CDCl3)
HOD
1.00 1.11 0.99 0.99 2.26 2.93 1.12 1.01 1.27 2.64 1.40 4.98 6.57 3.40 2.82
9.5 9.0 8.5 8.0 7.5 7.0 6.5 6.0 5.5 5.0 4.5 4.0 3.5 3.0 2.5 2.0 1.5 1.0 0.5 0.0
f1 (ppm)

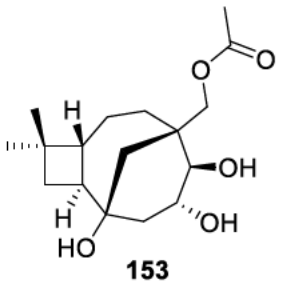

153

^{13}C NMR Spectrum
(101 MHz, $CDCl_3$)

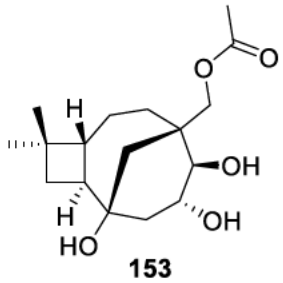

153

DEPT135 NMR Spectrum
(101 MHz, $CDCl_3$)

153

COSY NMR Spectrum

($CDCl_3$)

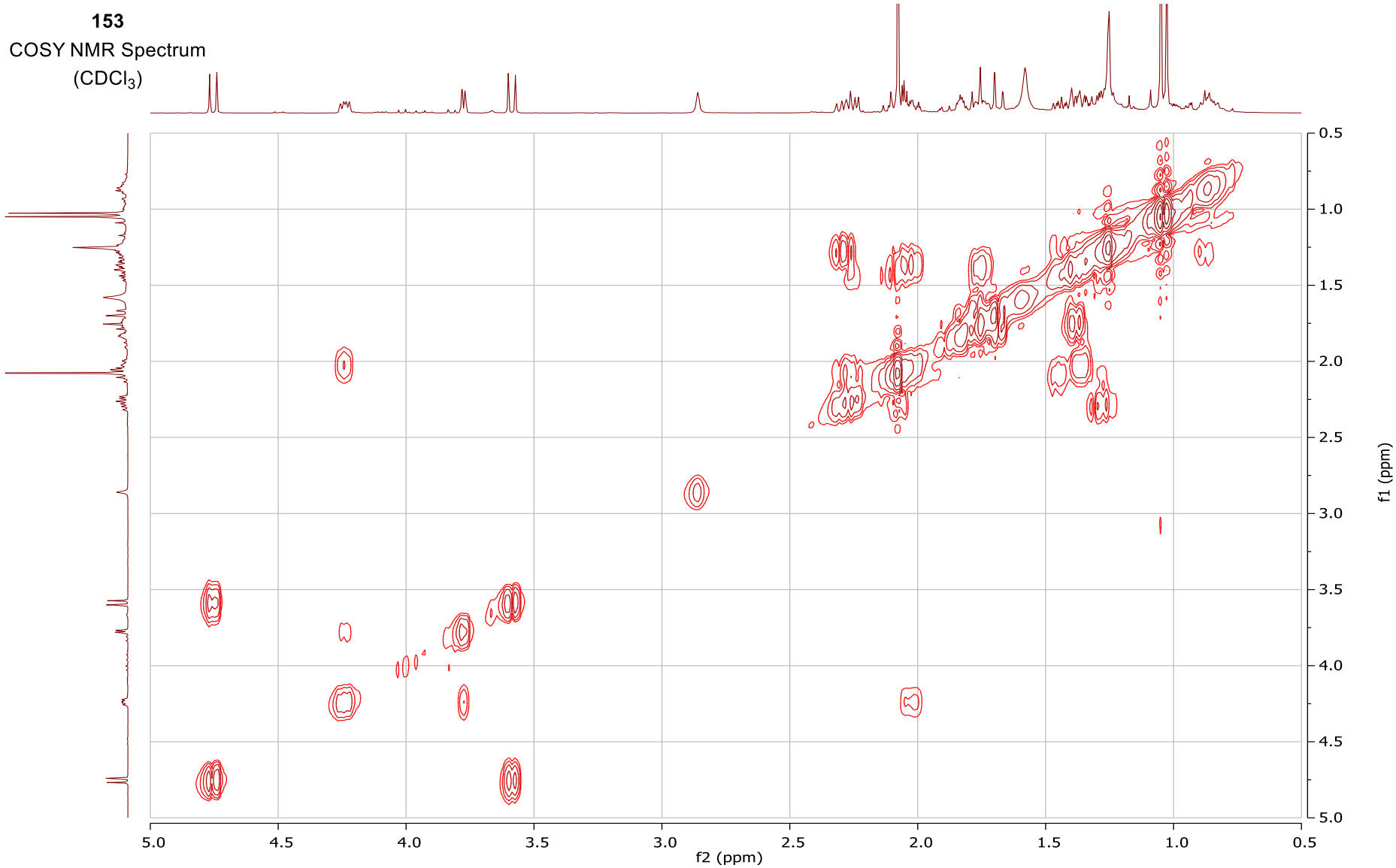

153

HSQC NMR Spectrum

($CDCl_3$)

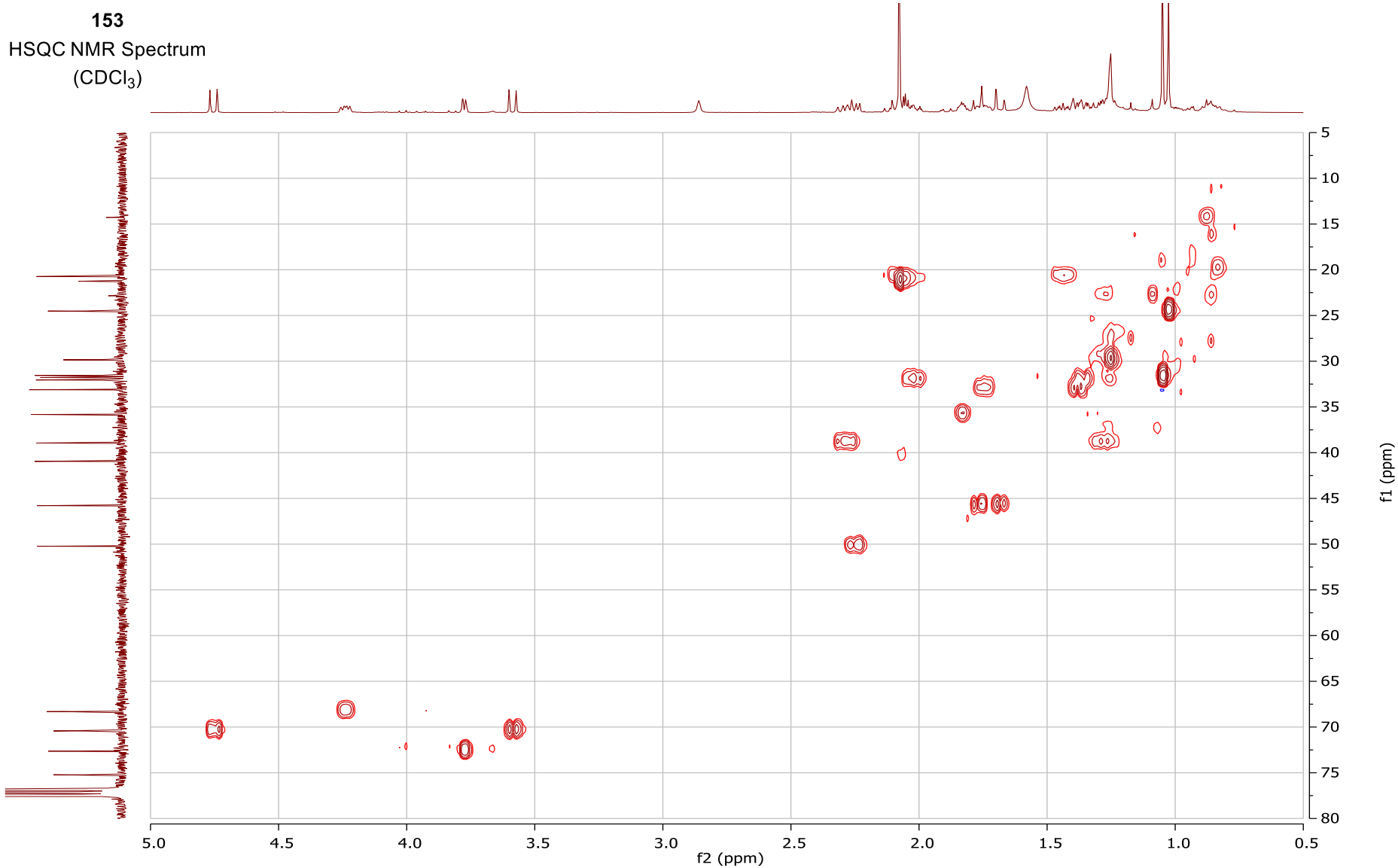

153

HMBC NMR Spectrum

($CDCl_3$)

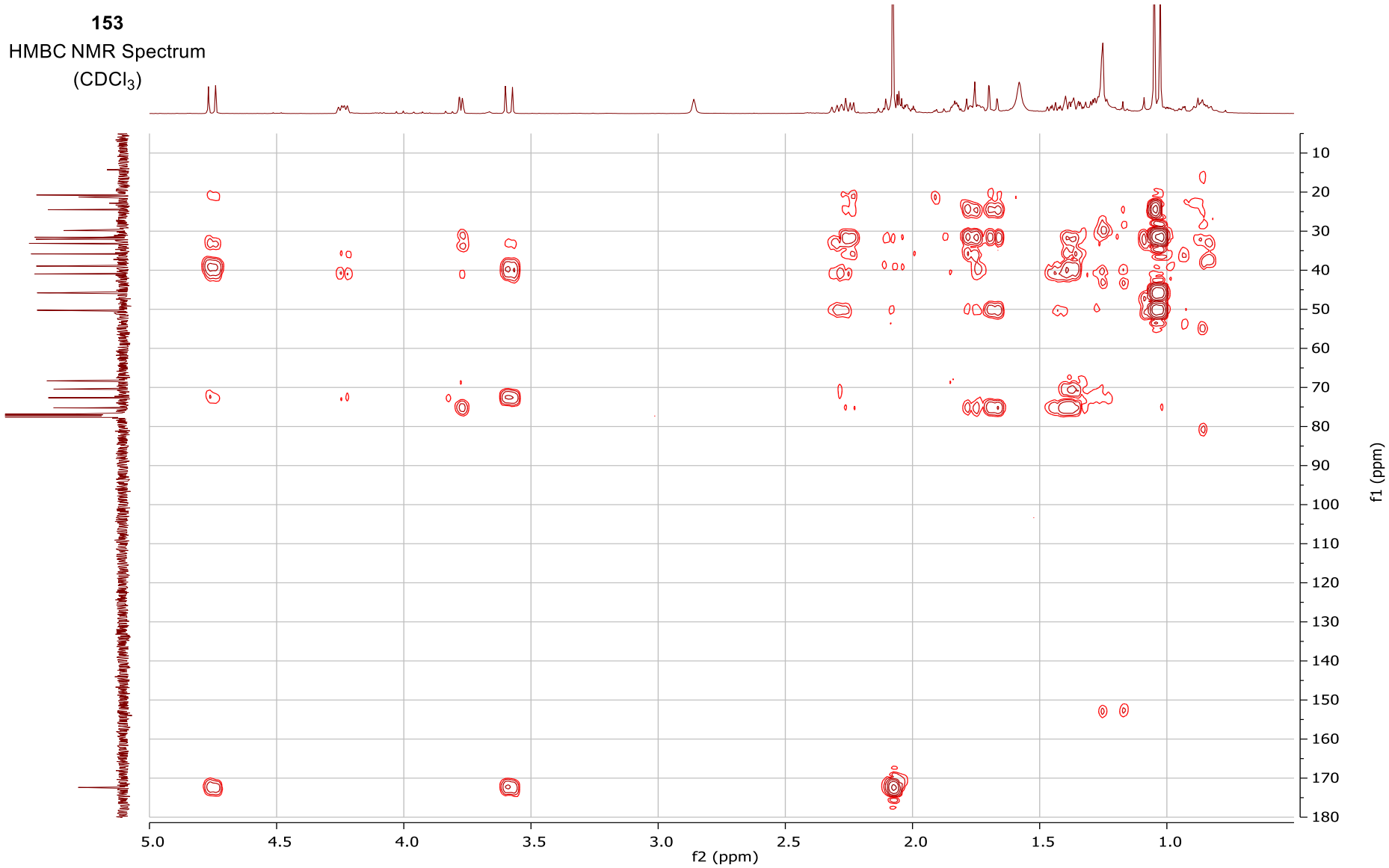

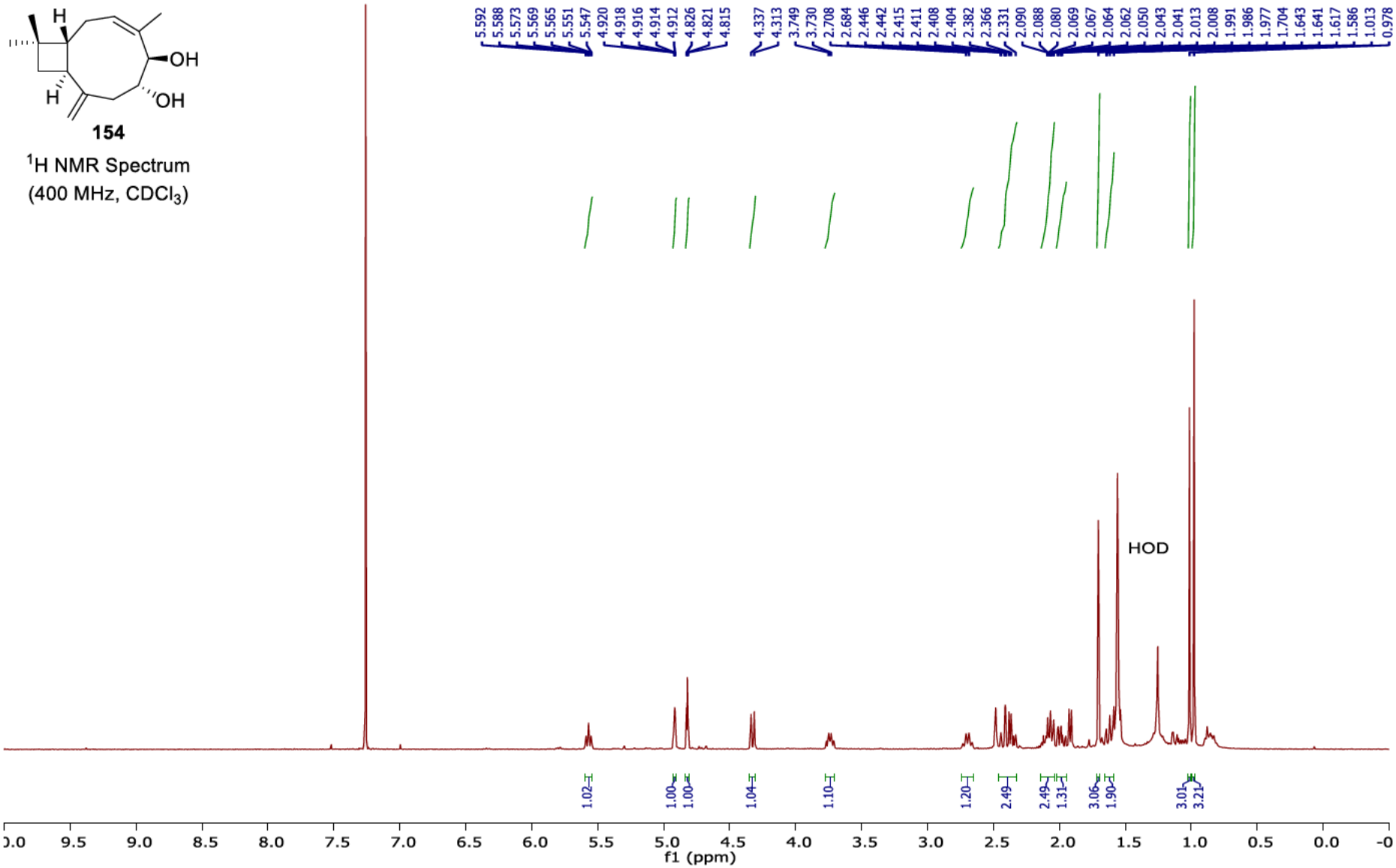
H
OH
H
OH
154
1H NMR Spectrum
(400 MHz, CDCl3)
5.592
5.588
5.573
5.569
5.565
5.551
5.547
4.920
4.918
4.916
4.914
4.912
4.826
4.821
4.815
4.337
4.313
3.749
3.730
2.708
2.684
2.446
2.442
2.415
2.411
2.408
2.404
2.382
2.366
2.331
2.090
2.088
2.080
2.069
2.067
2.064
2.062
2.050
2.043
2.041
2.013
2.008
1.991
1.986
1.977
1.704
1.643
1.641
1.617
1.586
1.013
0.978
HOD
1.02
1.00
1.00
1.04
1.10
1.20
2.49
2.49
1.31
3.06
1.90
3.01
3.21
f1 (ppm)

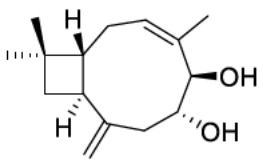

154

^{13}C NMR Spectrum
(101 MHz, $CDCl_3$)

148.214
136.896
127.158
115.646
74.165
71.155
49.404
43.052
40.555
38.059
33.330
30.033
28.916
22.591
17.144

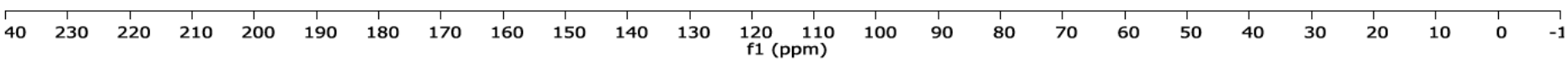

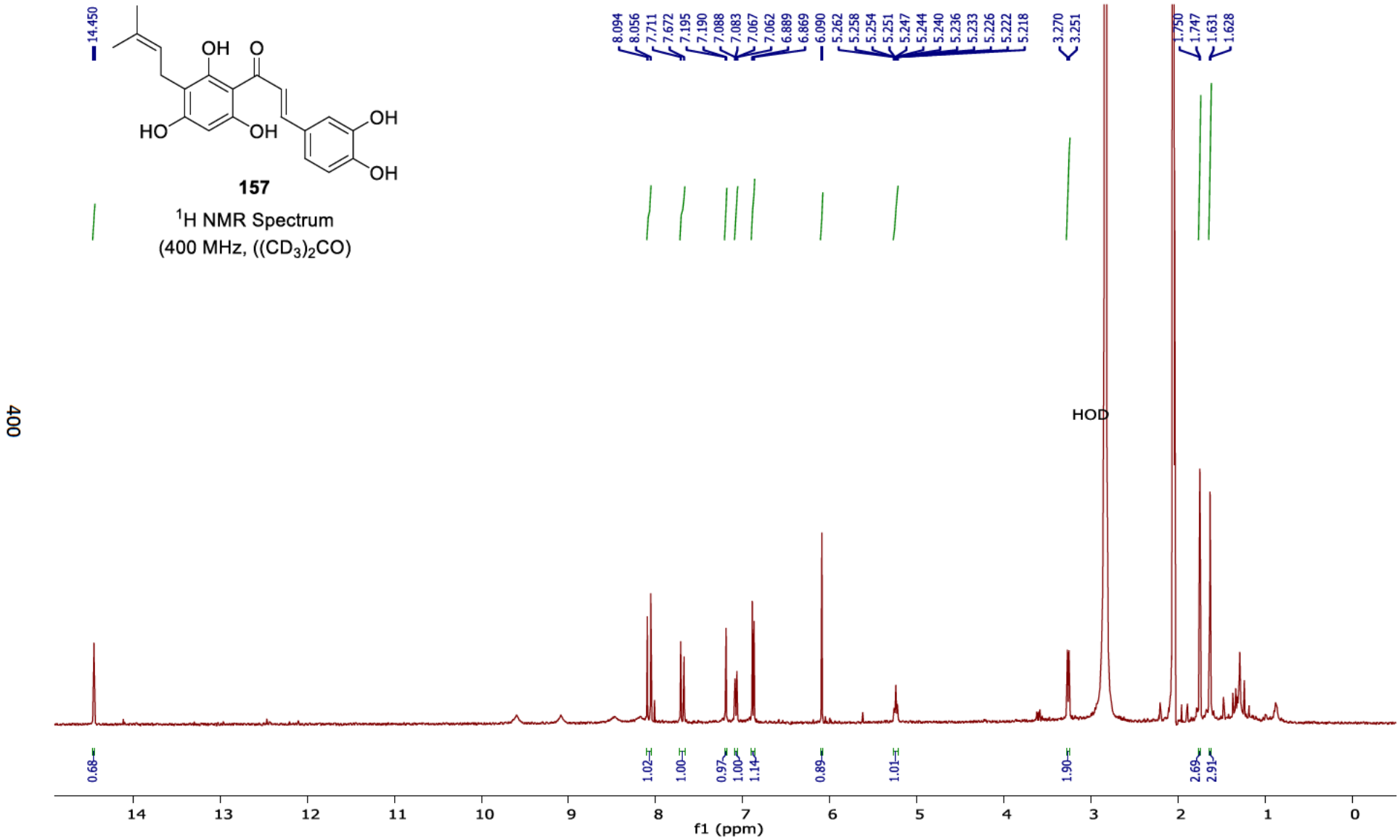
14.450
OH
O
HO
OH
OH
OH
157
1H NMR Spectrum
(400 MHz, ((CD3)2CO)
8.094
8.056
7.711
7.672
7.195
7.190
7.088
7.083
7.067
7.062
6.889
6.869
6.090
5.262
5.258
5.254
5.251
5.247
5.244
5.240
5.236
5.233
5.226
5.222
5.218
3.270
3.251
1.750
1.747
1.631
1.628
HOD
400
0.68
1.02
1.00
0.97
1.00
1.14
0.89
1.01
1.90
2.69
2.91
14
13
12
11
10
9
8
7
6
5
4
3
2
1
0
f1 (ppm)

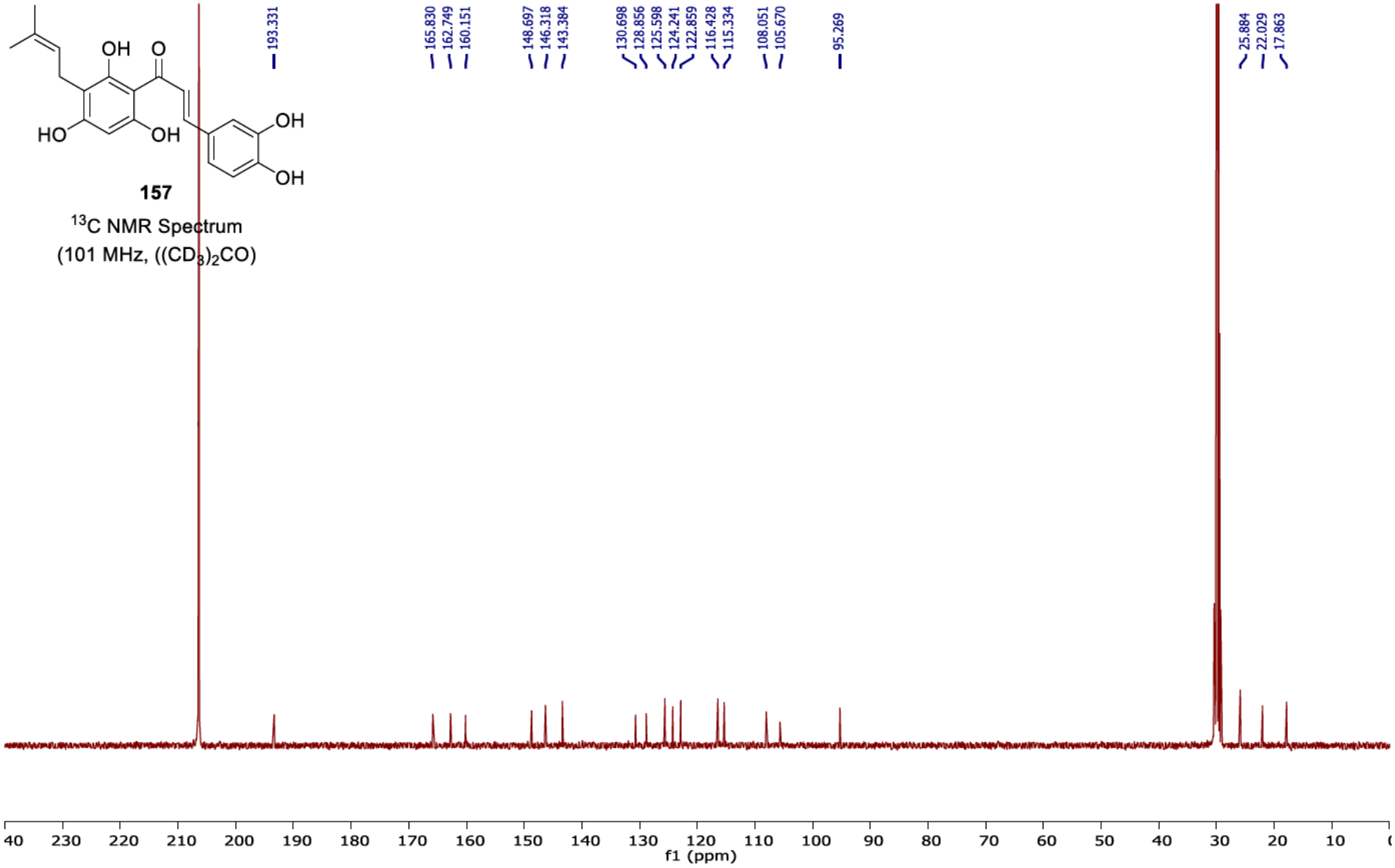

157

^{13}C NMR Spectrum

(101 MHz, $((CD_3)_2CO)$

401

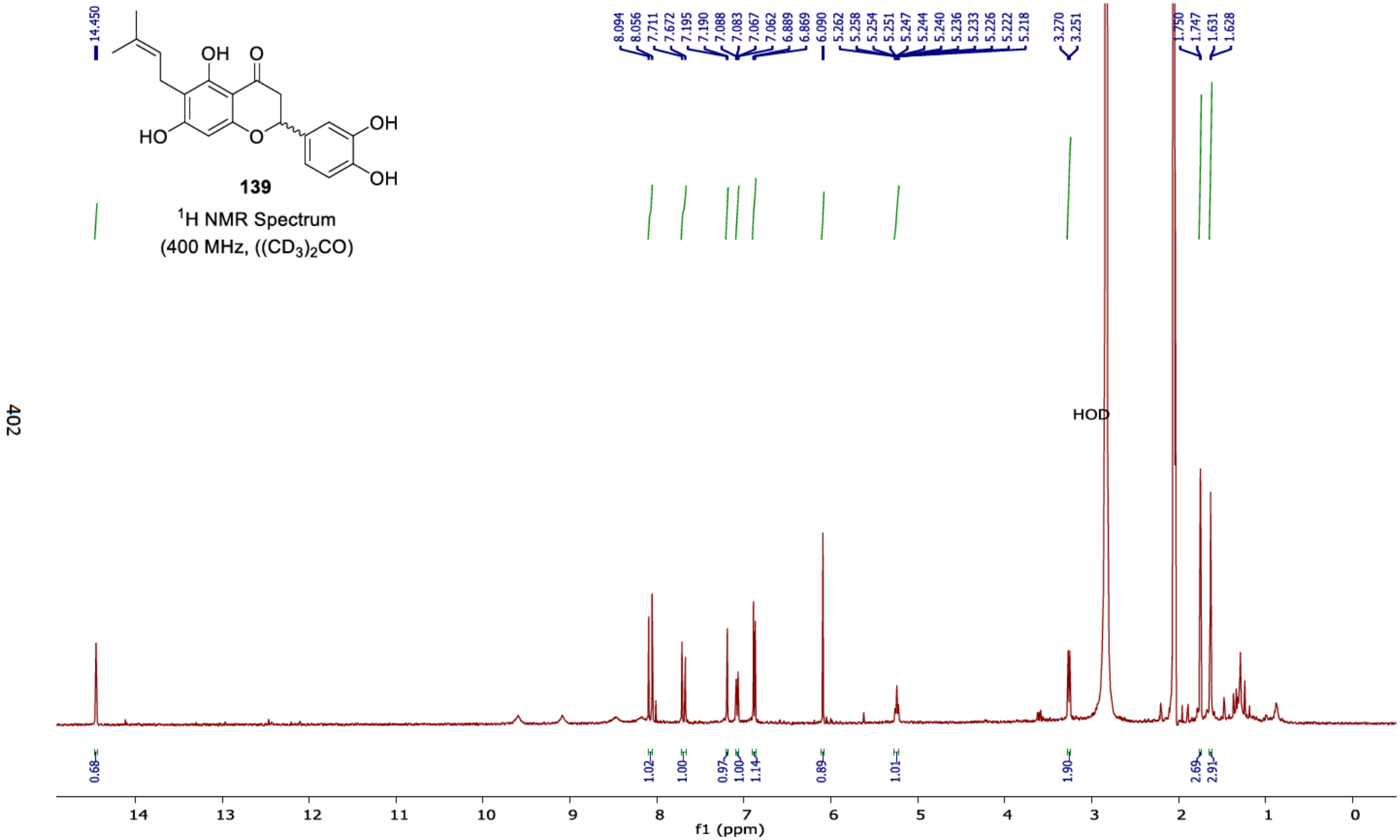
OH
O
HO
O
OH
OH
139
1H NMR Spectrum
(400 MHz, ((CD3)2CO)
14.450
8.094
8.056
7.711
7.672
7.195
7.190
7.088
7.083
7.067
7.062
6.889
6.869
6.090
5.262
5.258
5.254
5.251
5.247
5.244
5.240
5.236
5.233
5.226
5.222
5.218
3.270
3.251
1.750
1.747
1.631
1.628
HOD
0.68
1.02
1.00
0.97
1.00
1.14
0.89
1.01
1.90
2.69
2.91
14
13
12
11
10
9
8
7
6
5
4
3
2
1
0
f1 (ppm)

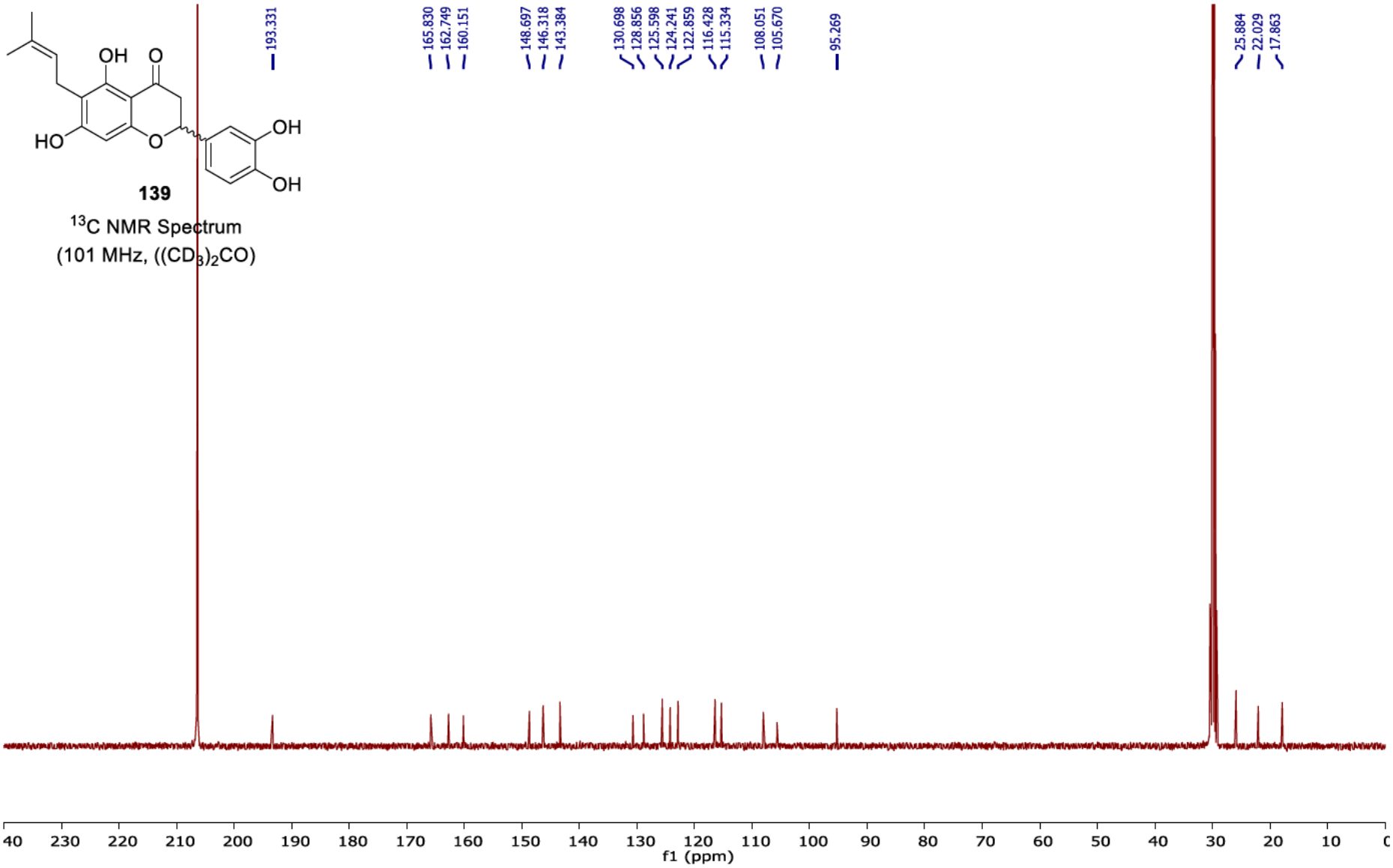

^{13}C NMR Spectrum
(101 MHz, $((CD_3)_2CO)$

403

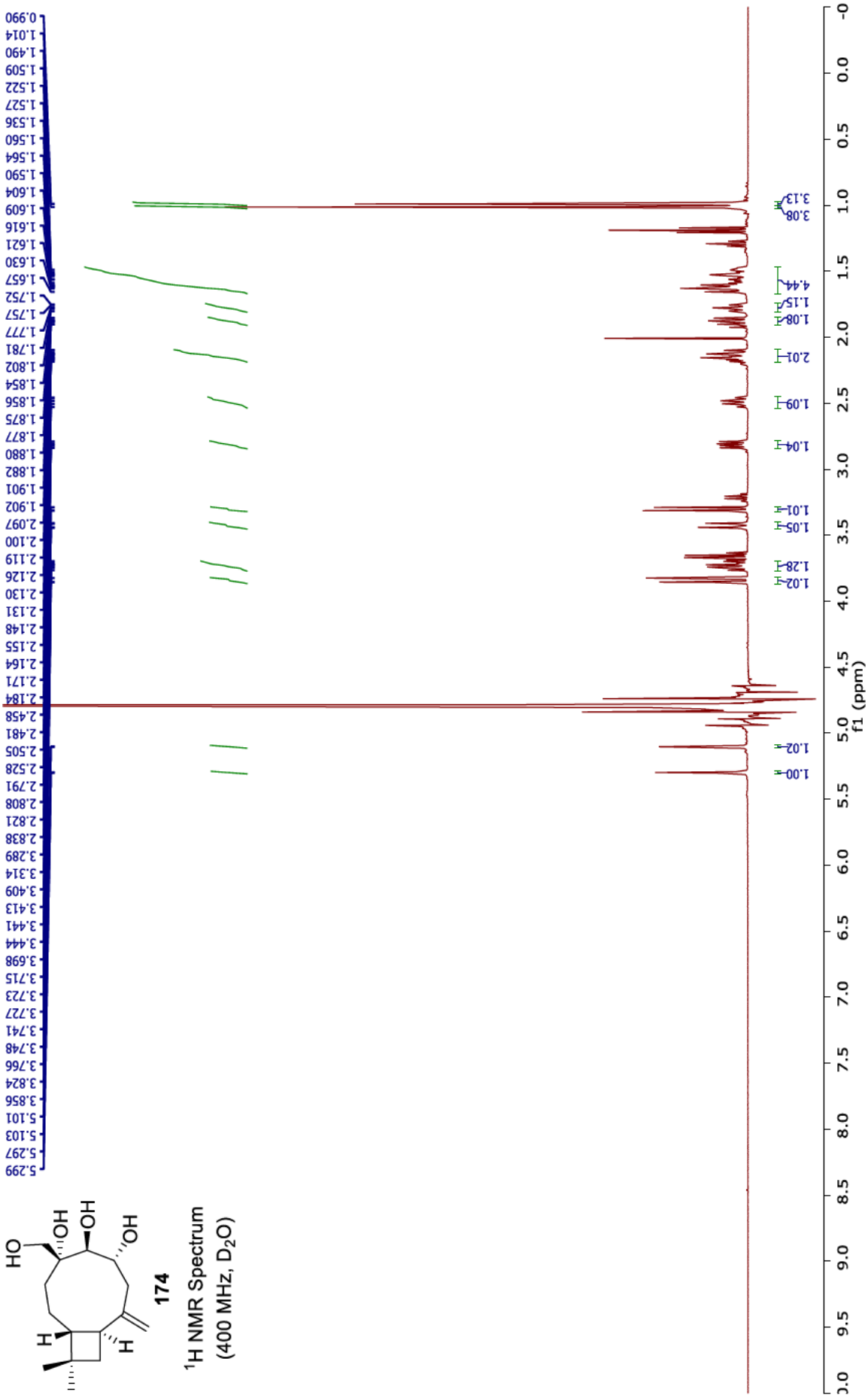
HO
OH
OH
OH
H
H
174
^{1}H NMR Spectrum
(400 MHz, D_2O)
f1 (ppm)

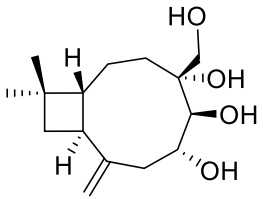

174

^{13}C NMR Spectrum
(101 MHz, D_2O)

148.253
114.183
70.455
65.361
65.169
64.646
53.078
46.208
44.601
41.722
32.469
29.475
28.720
26.457
20.586

405

40 230 220 210 200 190 180 170 160 150 140 130 120 110 100 90 80 70 60 50 40 30 20 10 0 -1

f1 (ppm)

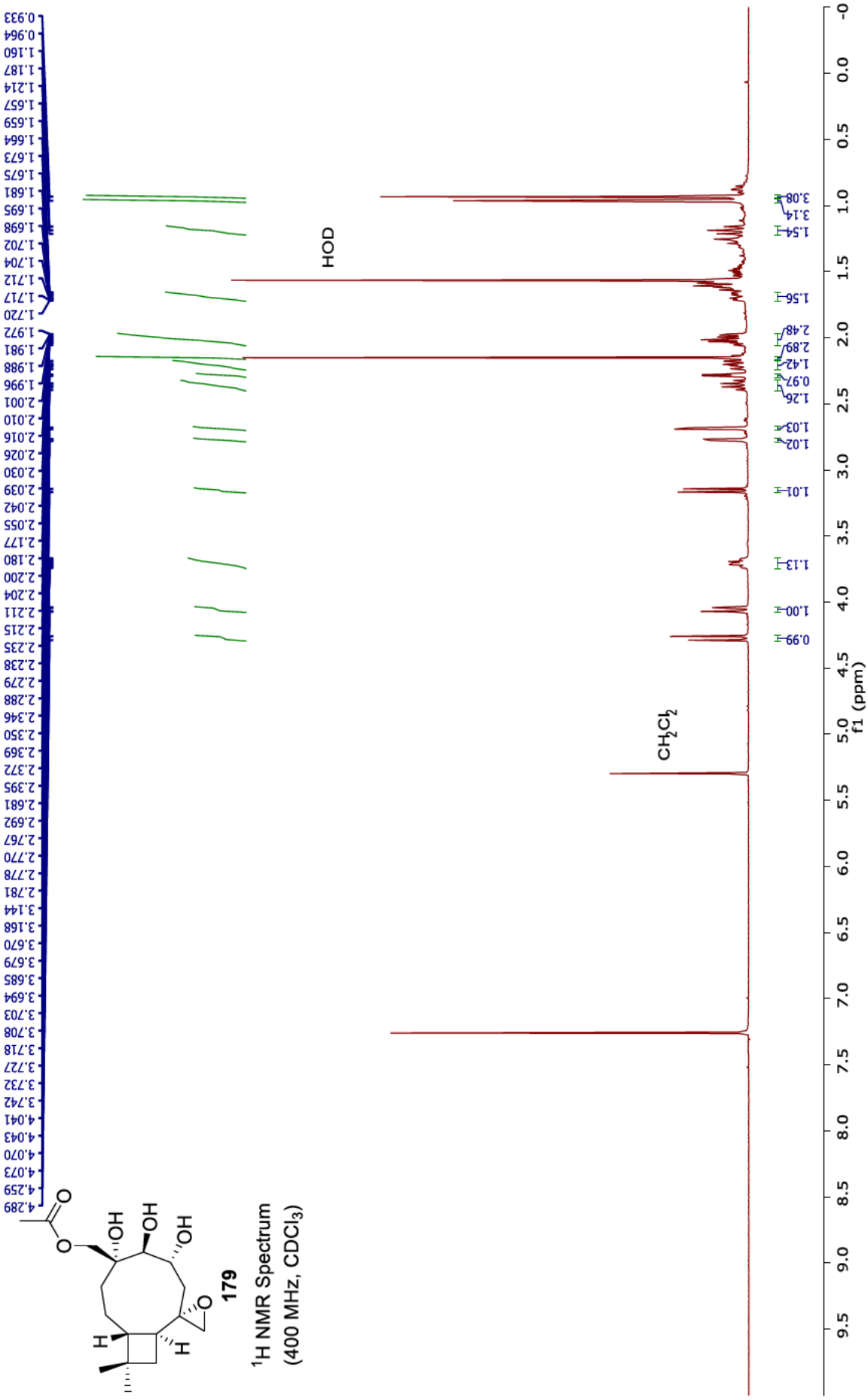
HOD
CH_2Cl_2
f1 (ppm)
179
^{1}H NMR Spectrum
(400 MHz, $CDCl_3$)

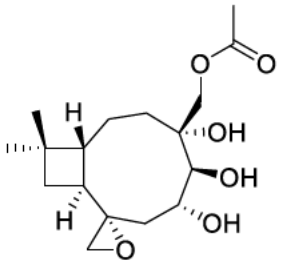

179

^{13}C NMR Spectrum
(101 MHz, $CDCl_3$)

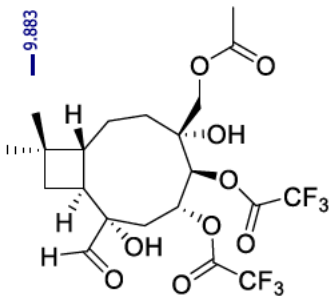

180

^{1}H NMR Spectrum
(400 MHz, $CDCl_3$)

180
COSY NMR Spectrum
($CDCl_3$)

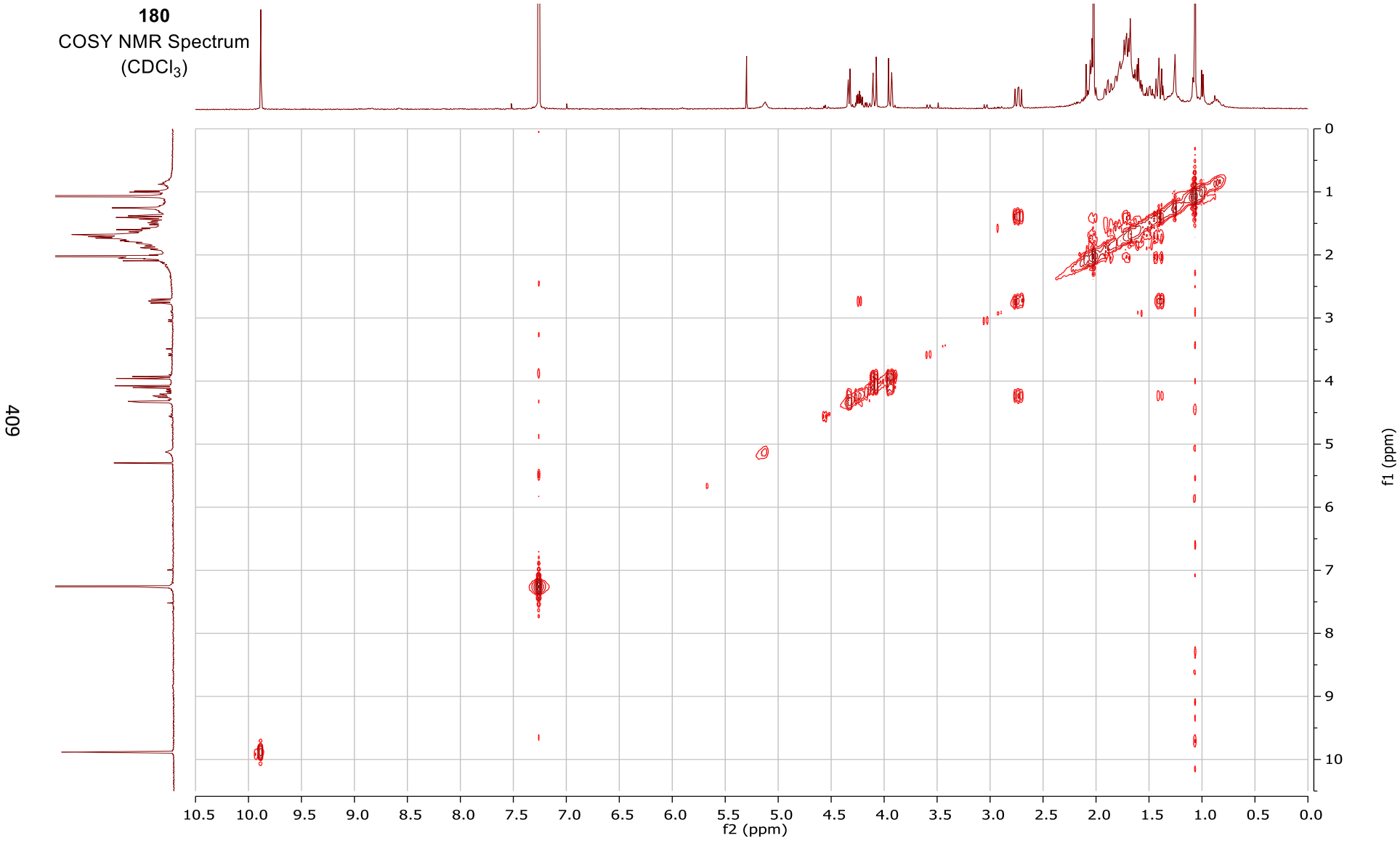

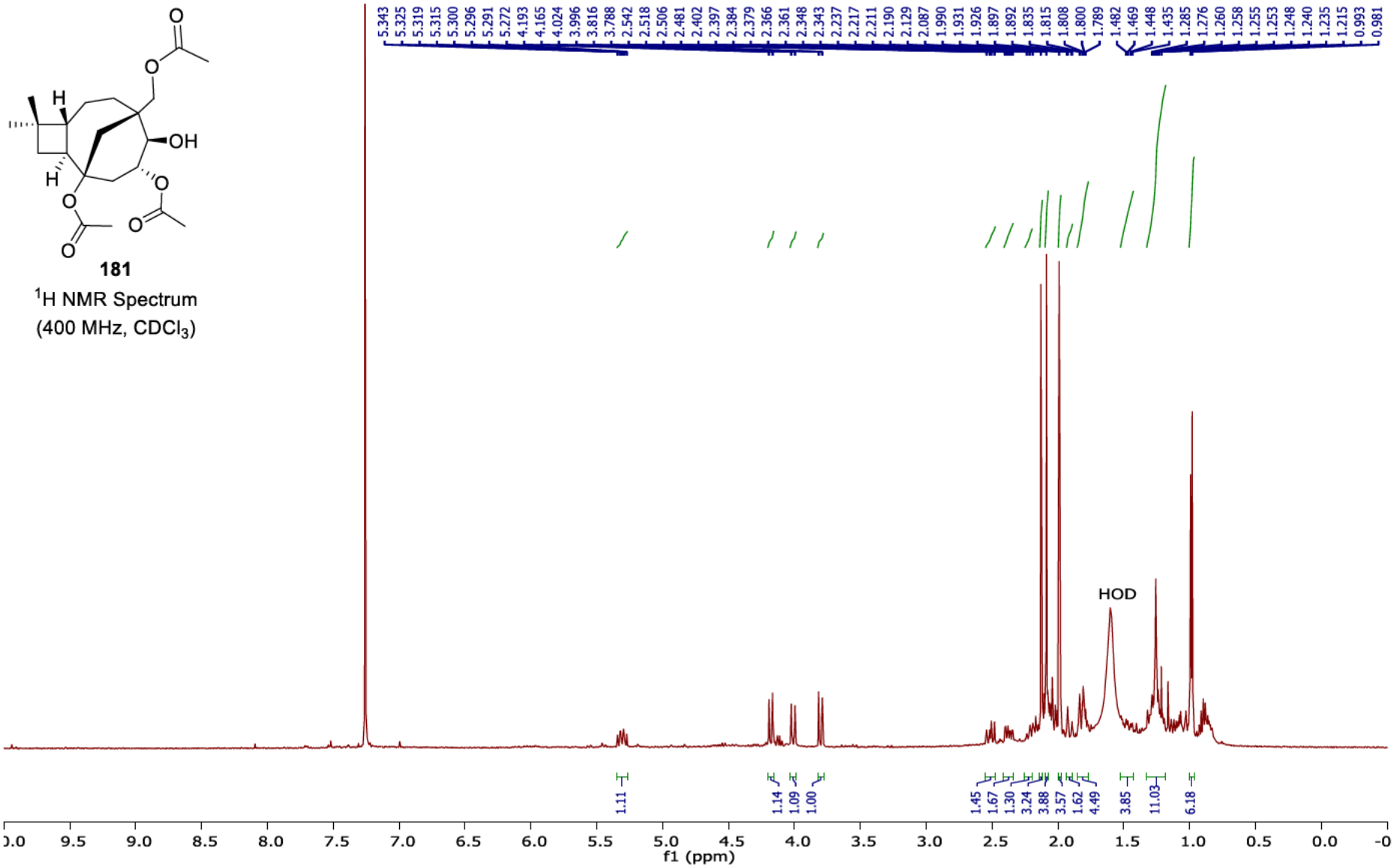
181
^{1}H NMR Spectrum
(400 MHz, $CDCl_3$)
HOD
f1 (ppm)

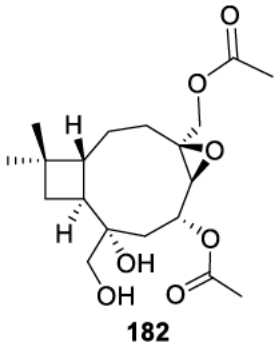

182

^{1}H NMR Spectrum
(400 MHz, $CDCl_3$)

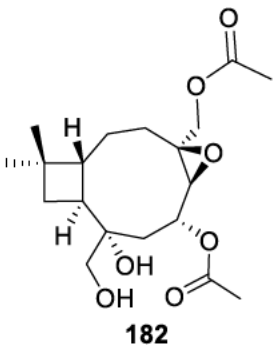

182

^{13}C NMR Spectrum
(101 MHz, $CDCl_3$)

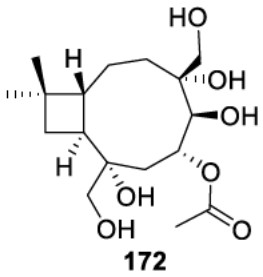

172

^{1}H NMR Spectrum
(400 MHz, D_2O)

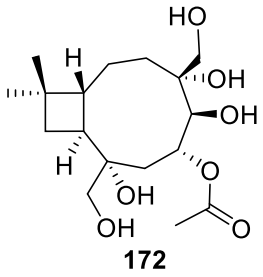

172

^{13}C NMR Spectrum
(101 MHz, D_2O)

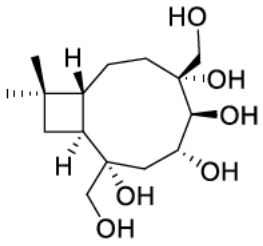

173

^{1}H NMR Spectrum
(400 MHz, D_2O)

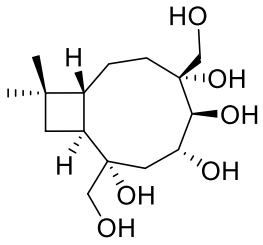

173

^{13}C NMR Spectrum
(101 MHz, D_2O)

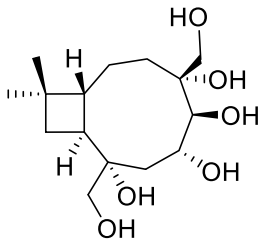

173

DEPT135 NMR Spectrum
(101 MHz, D_2O)

173
COSY NMR Spectrum
(D_2O)

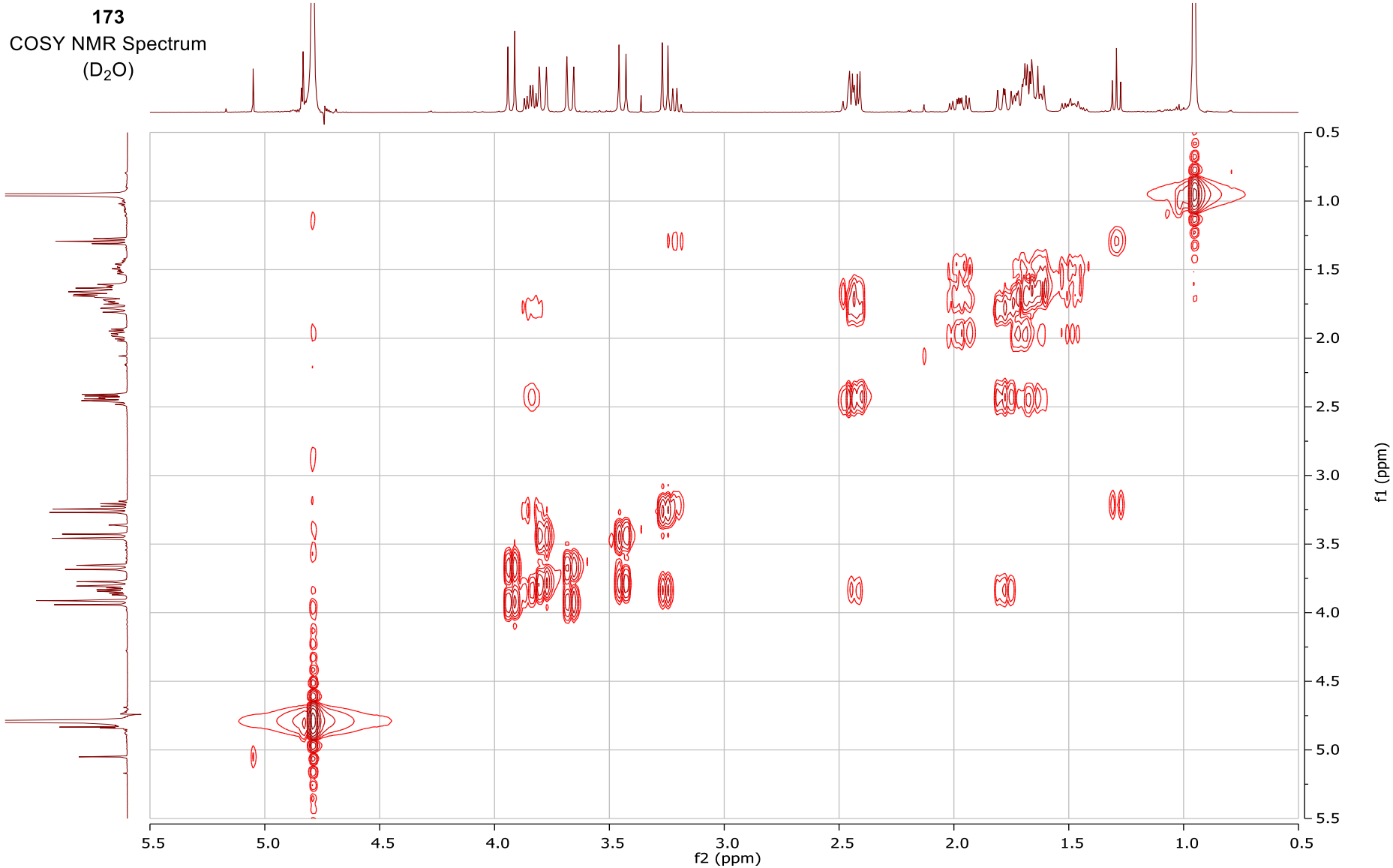

418

173

HSQC NMR Spectrum

(D_2O)

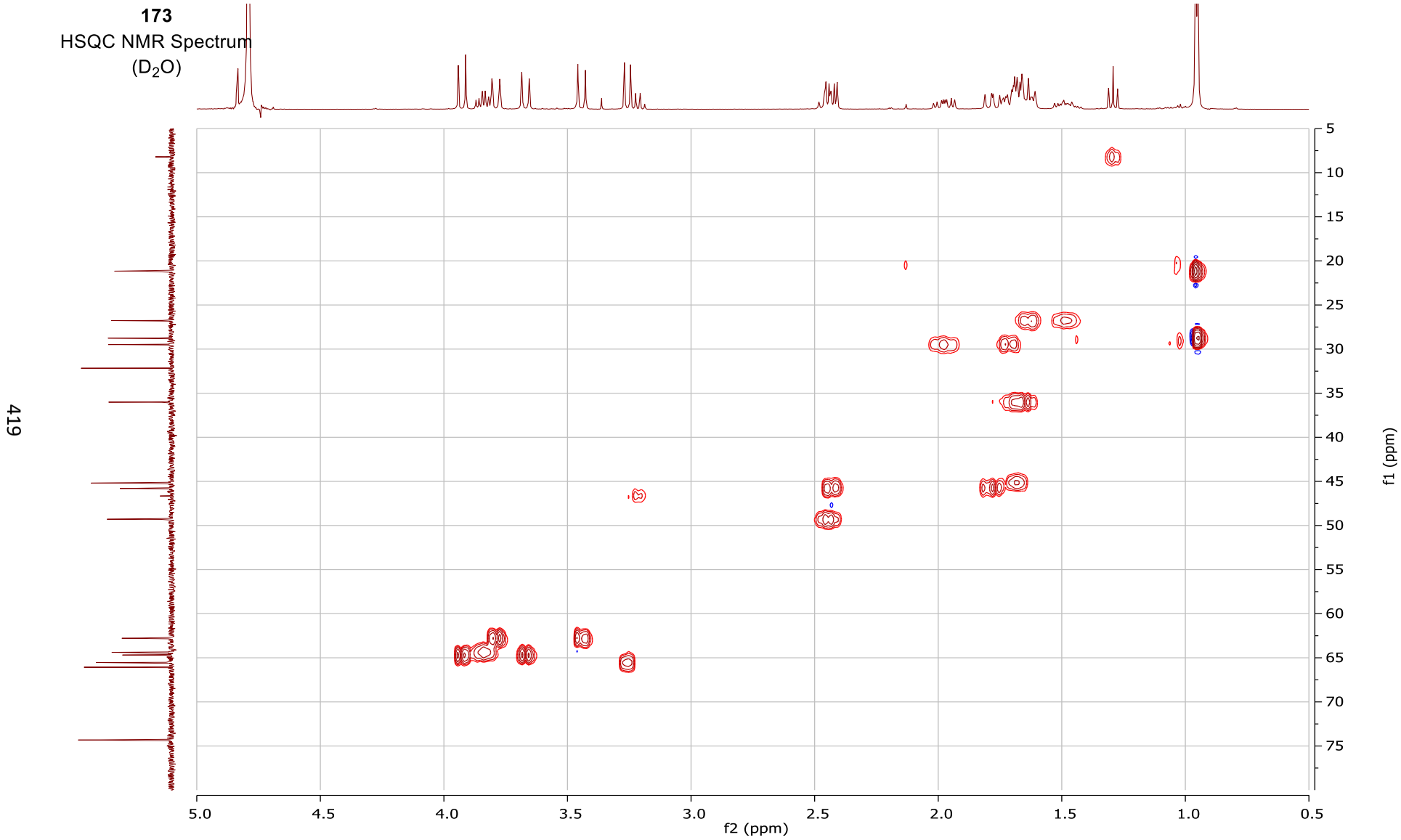

173

HMBC NMR Spectrum

(D_2O)

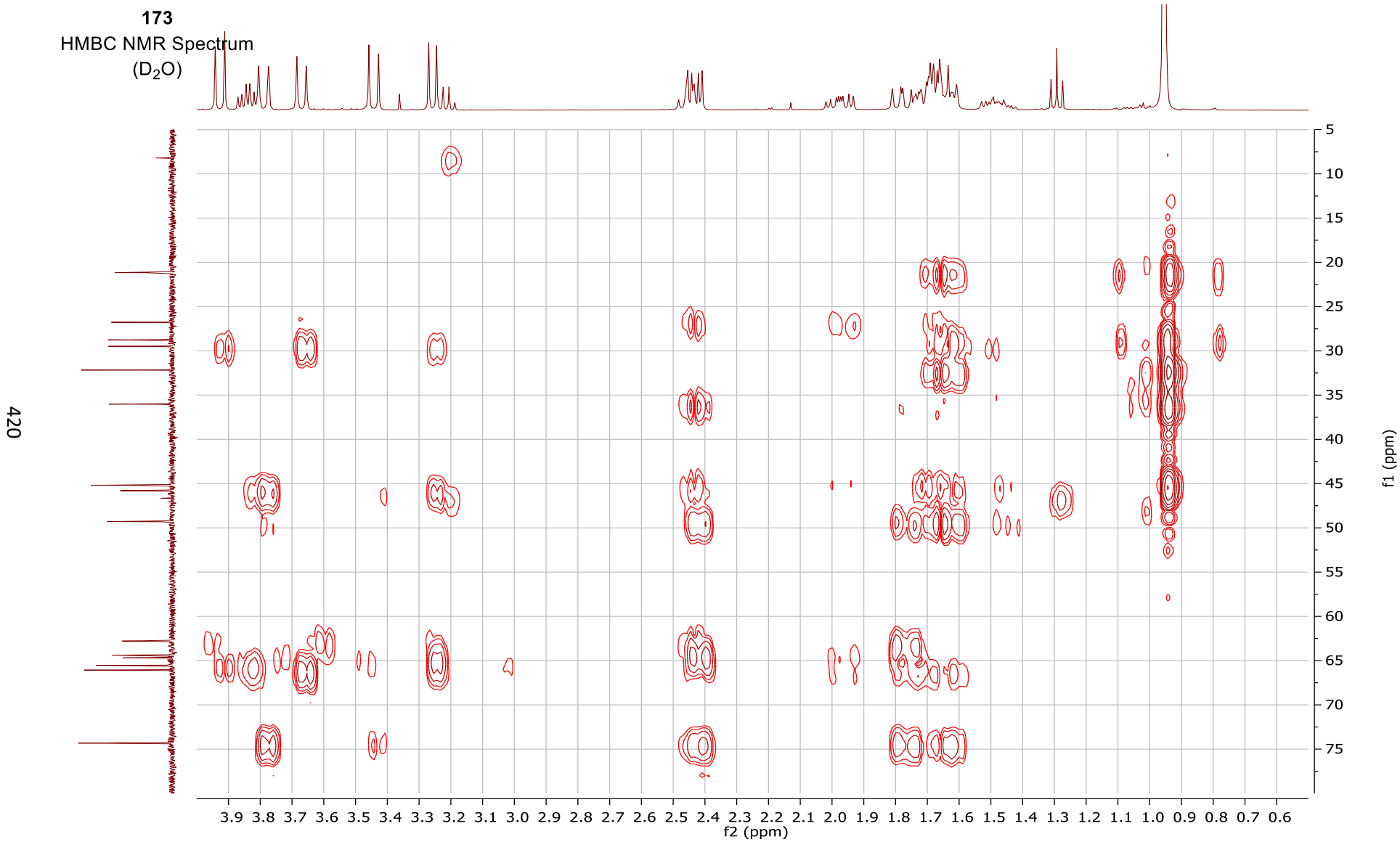

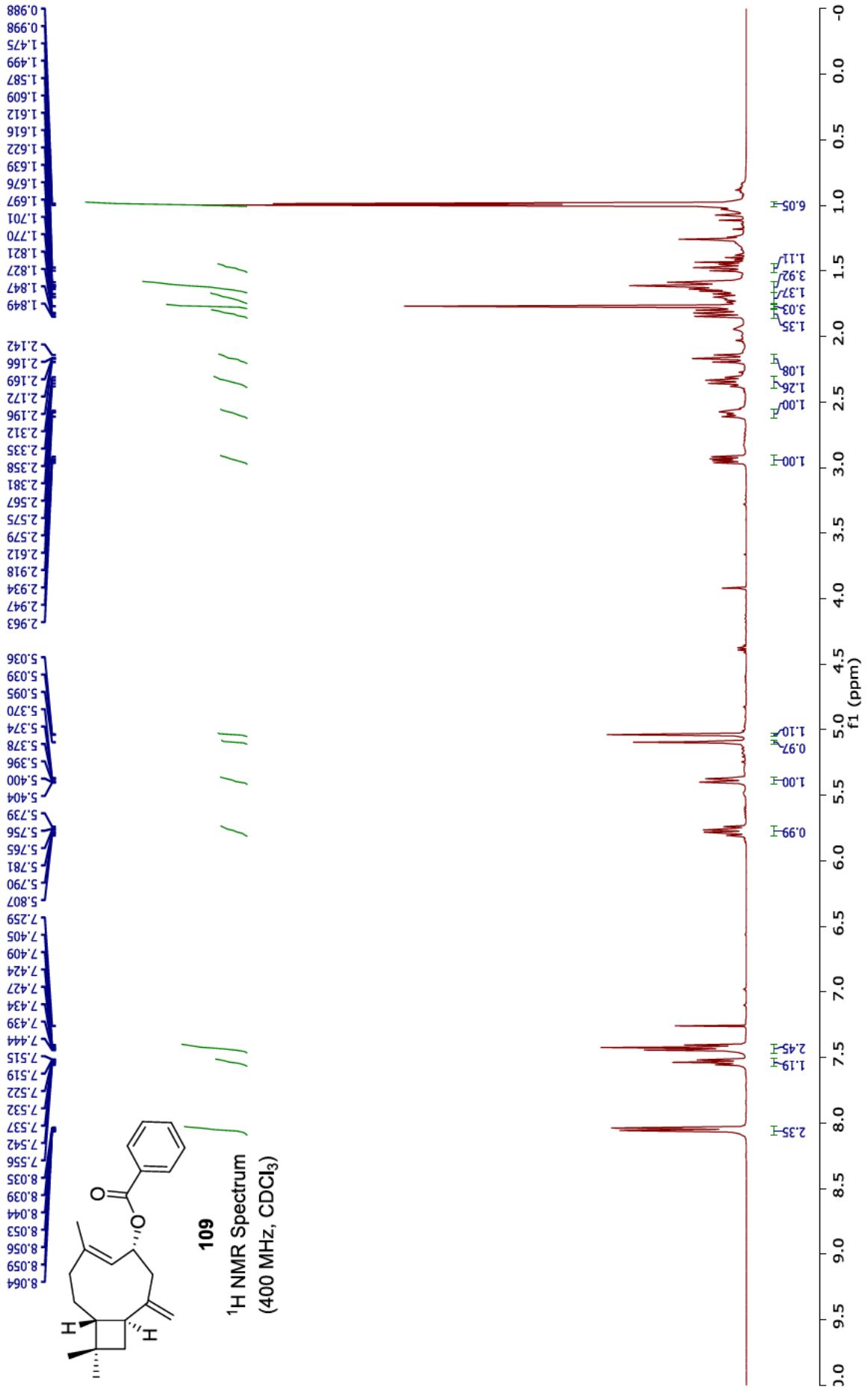
109
^{1}H NMR Spectrum
(400 MHz, $CDCl_3$)
f1 (ppm)

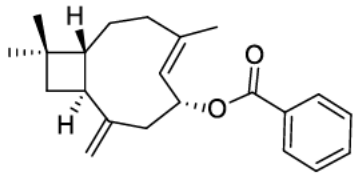

109

^{13}C NMR Spectrum

(101 MHz, $CDCl_3$)

166.273
149.451
139.142
132.843
130.880
129.687
128.382
124.202
113.625
73.540
55.910
49.085
45.624
42.419
34.988
32.930
31.212
29.956
23.018
21.993

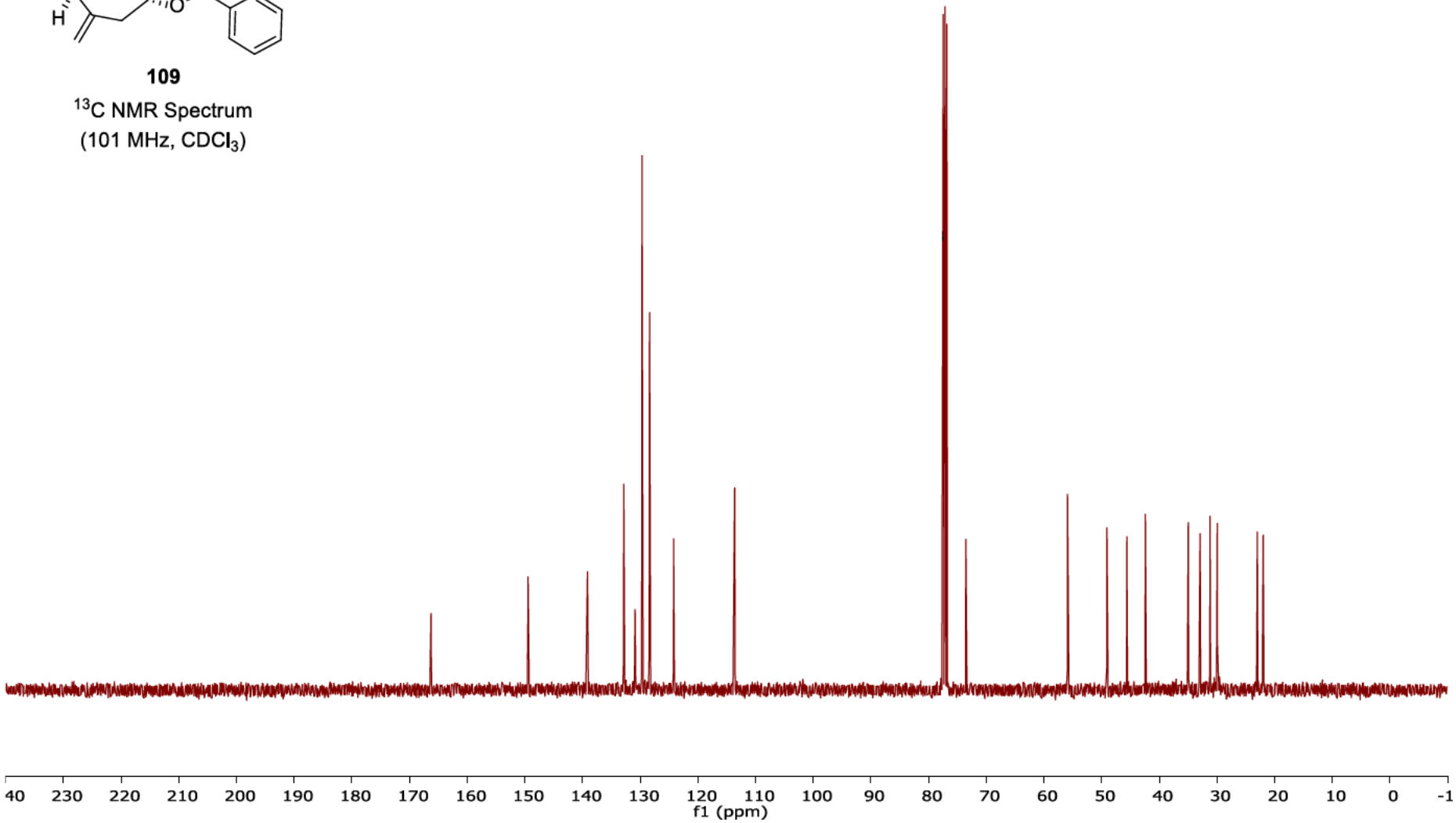

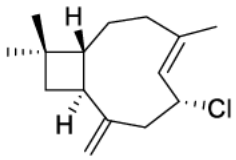

184

^{1}H NMR Spectrum
(400 MHz, $CDCl_3$)

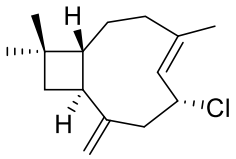

184

^{13}C NMR Spectrum

(101 MHz, $CDCl_3$)

150.959
138.264
126.961
113.512
58.146
55.960
51.292
48.786
42.142
34.809
32.939
31.077
29.943
29.840
22.608
21.954

40 230 220 210 200 190 180 170 160 150 140 130 120 110 100 90 80 70 60 50 40 30 20 10 0 -1

f1 (ppm)

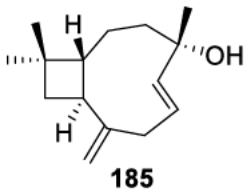

185

^{1}H NMR Spectrum
(400 MHz, $CDCl_3$)

425

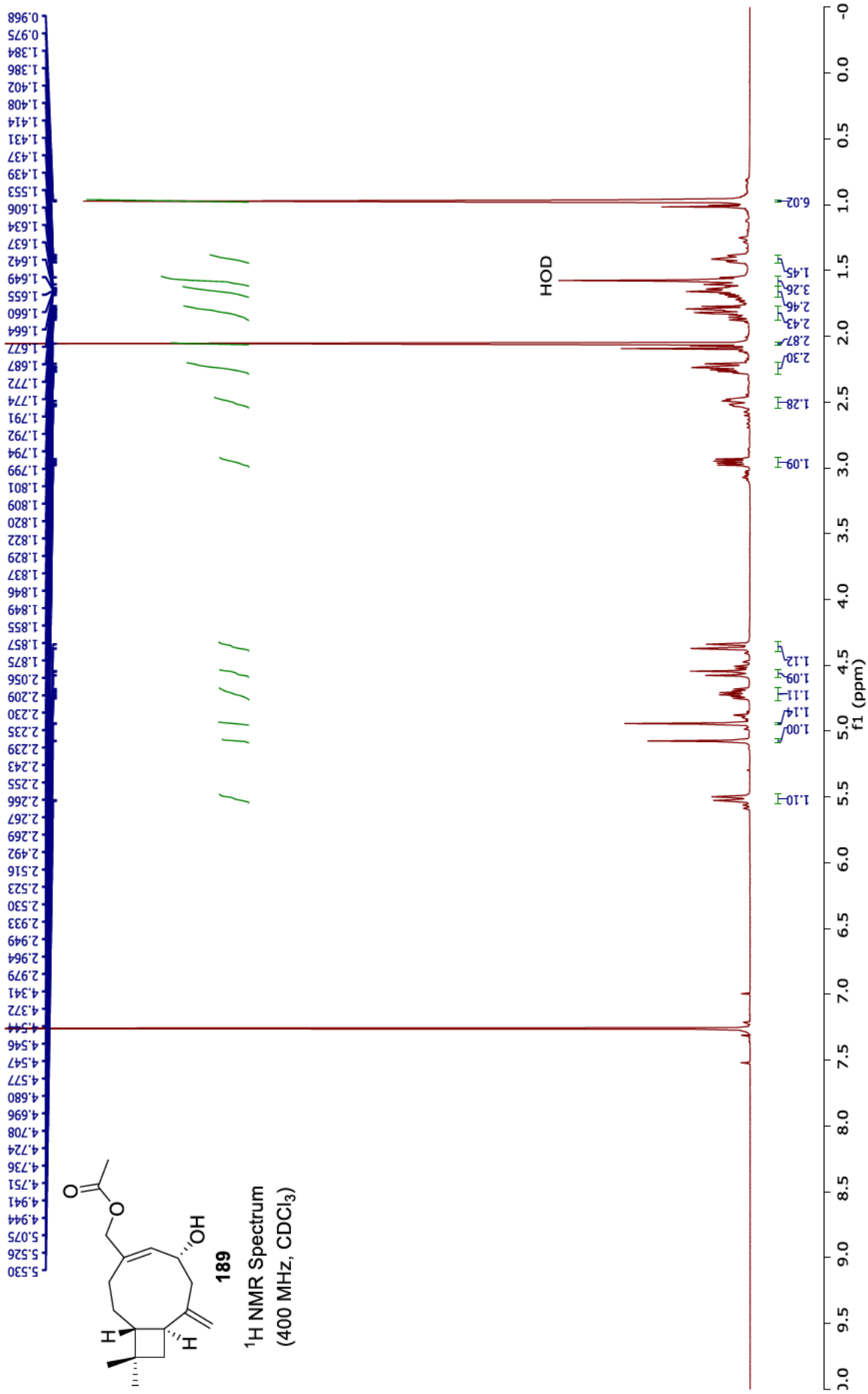

189

^{1}H NMR Spectrum
(400 MHz, $CDCl_3$)

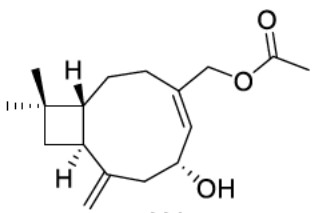

189

^{13}C NMR Spectrum
(101 MHz, $CDCl_3$)

170.968
151.060
135.635
131.901
114.053
64.643
56.408
56.145
51.059
48.673
42.146
33.063
30.861
30.290
29.965
21.904
21.048

40 230 220 210 200 190 180 170 160 150 140 130 120 110 100 90 80 70 60 50 40 30 20 10 0 -1
f1 (ppm)

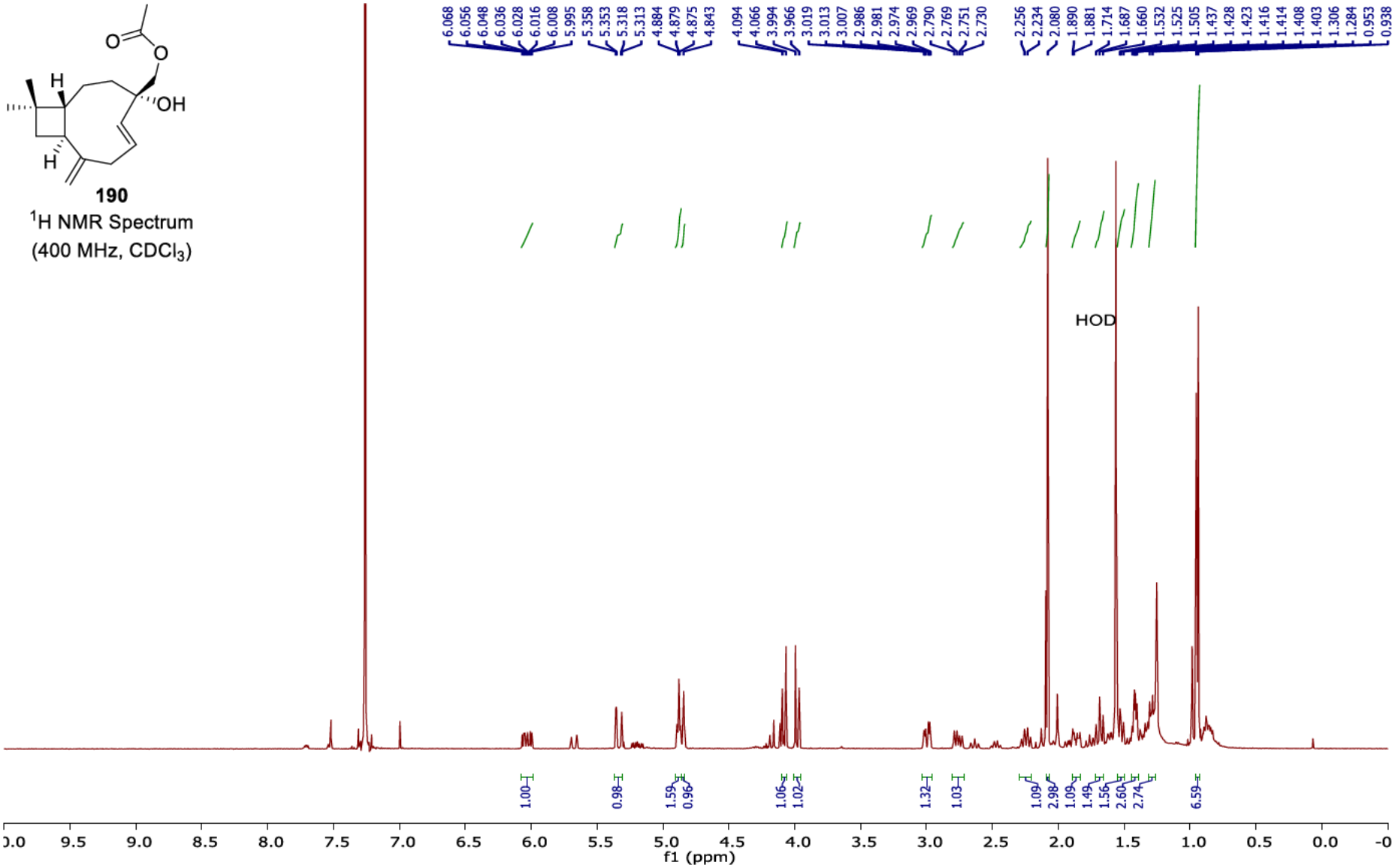
O
O
H
OH
H
190
1H NMR Spectrum
(400 MHz, CDCl3)
6.068
6.056
6.048
6.036
6.028
6.016
6.008
5.995
5.358
5.353
5.318
5.313
4.884
4.879
4.875
4.843
4.094
4.066
3.994
3.966
3.019
3.013
3.007
2.986
2.981
2.974
2.969
2.790
2.769
2.751
2.730
2.256
2.234
2.080
1.890
1.881
1.714
1.687
1.660
1.532
1.525
1.505
1.437
1.428
1.423
1.416
1.414
1.408
1.403
1.306
1.284
0.953
0.938
HOD
1.00
0.98
1.59
0.96
1.06
1.02
1.32
1.03
1.09
2.98
1.09
1.49
1.56
2.60
2.74
6.59
f1 (ppm)

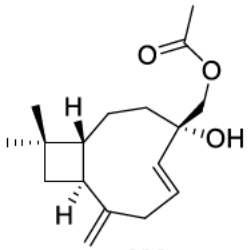

190

^{13}C NMR Spectrum

(101 MHz, $CDCl_3$)

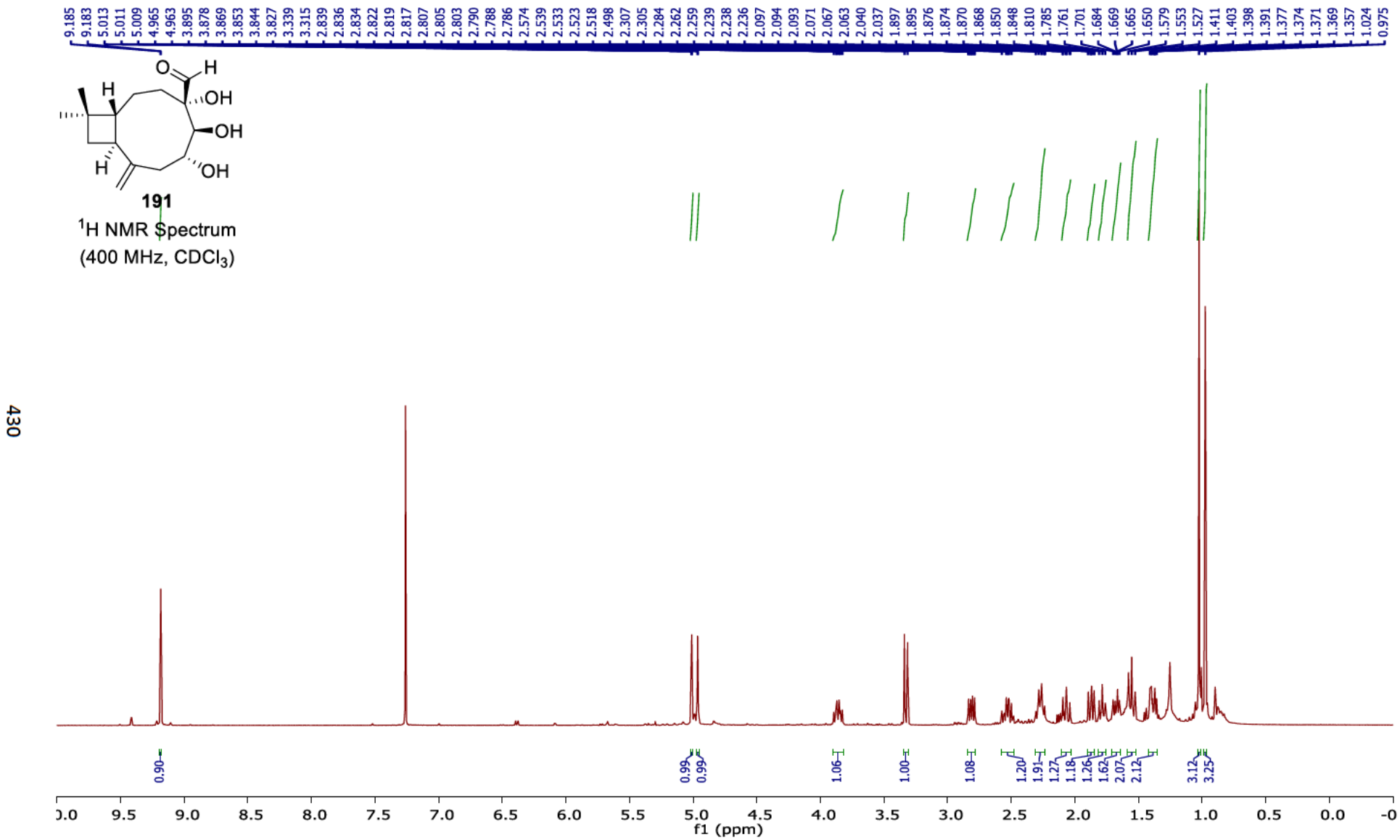
9.185 9.183 5.013 5.011 5.009 4.965 4.963 3.895 3.878 3.869 3.853 3.844 3.827 3.339 3.315 2.839 2.836 2.834 2.822 2.819 2.817 2.807 2.805 2.803 2.790 2.788 2.786 2.574 2.539 2.533 2.523 2.518 2.498 2.307 2.305 2.284 2.262 2.259 2.239 2.238 2.236 2.097 2.094 2.093 2.071 2.067 2.063 2.040 2.037 1.897 1.895 1.876 1.874 1.870 1.868 1.850 1.848 1.810 1.785 1.761 1.701 1.684 1.669 1.665 1.650 1.579 1.553 1.527 1.411 1.403 1.398 1.391 1.377 1.374 1.371 1.369 1.357 1.024 0.975
O
H
H
OH
OH
H
OH
191
1H NMR Spectrum
(400 MHz, CDCl3)
430
0.90
0.99
0.99
1.06
1.00
1.08
1.20
1.91
1.27
1.18
1.26
1.62
2.07
2.12
3.12
3.25
9.5 9.0 8.5 8.0 7.5 7.0 6.5 6.0 5.5 5.0 4.5 4.0 3.5 3.0 2.5 2.0 1.5 1.0 0.5 0.0
f1 (ppm)

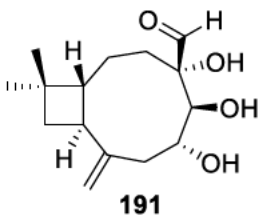

191

^{13}C NMR Spectrum
(101 MHz, $CDCl_3$)

197.654
146.842
115.671
70.332
65.499
65.335
52.837
47.506
44.813
42.554
33.247
29.837
27.684
26.010
21.689

40 230 220 210 200 190 180 170 160 150 140 130 120 110 100 90 80 70 60 50 40 30 20 10 0 -1
f1 (ppm)

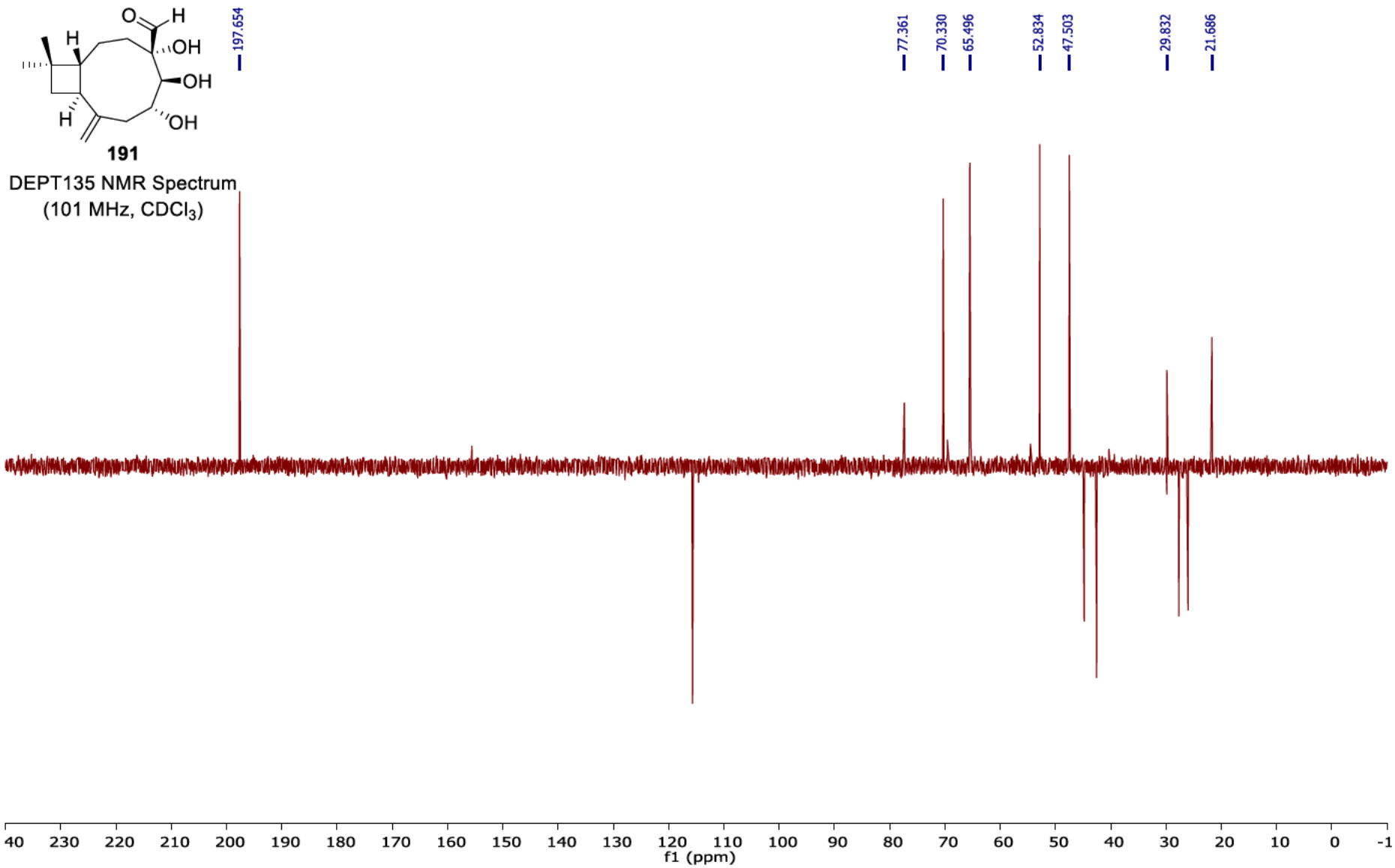
O
H
H
OH
OH
H
OH
191
DEPT135 NMR Spectrum
(101 MHz, CDCl3)
197.654
77.361
70.330
65.496
52.834
47.503
29.832
21.686
432
40 230 220 210 200 190 180 170 160 150 140 130 120 110 100 90 80 70 60 50 40 30 20 10 0 -1
f1 (ppm)

191
COSY NMR Spectrum
($CDCl_3$)

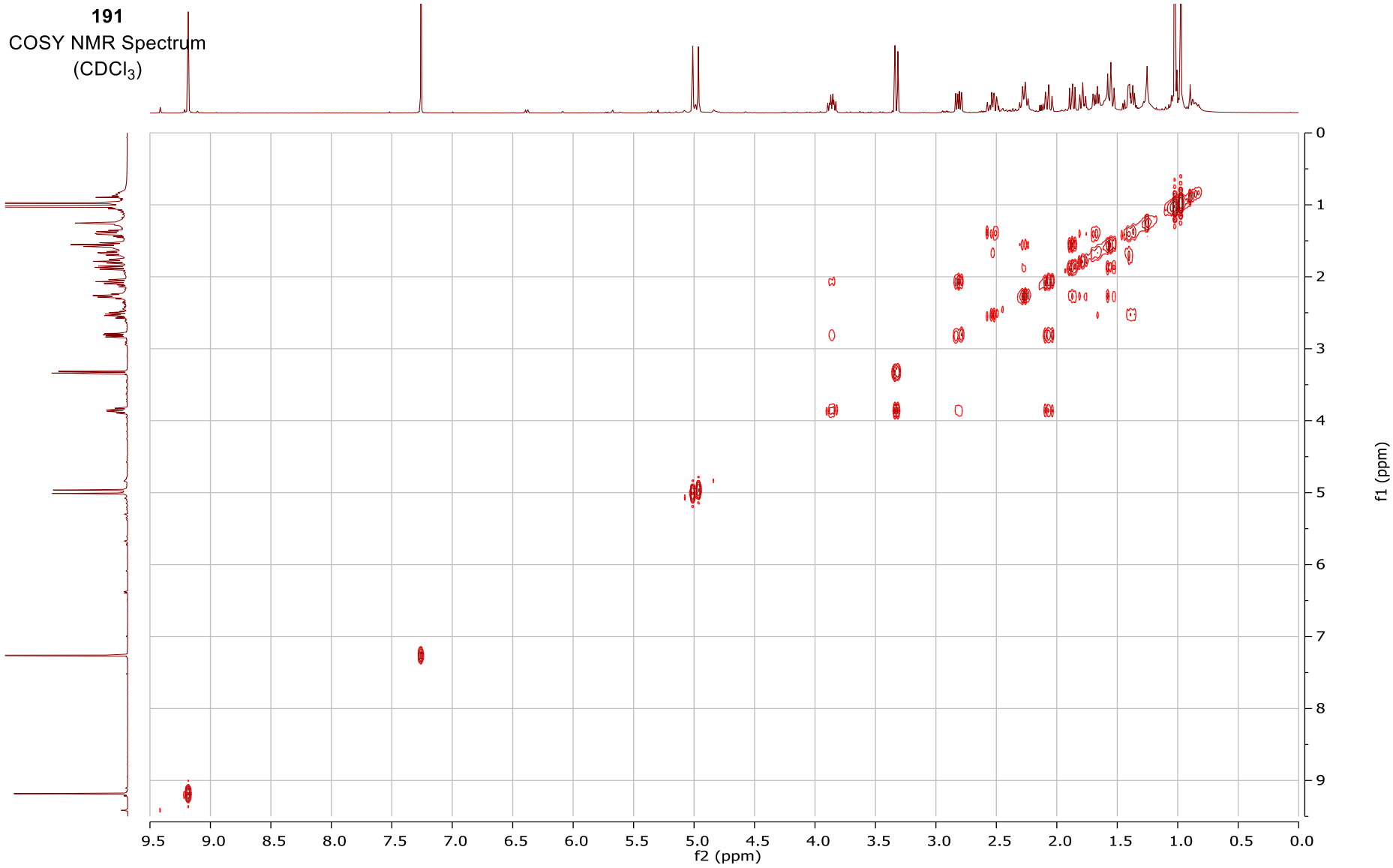

191

HSQC NMR Spectrum

($CDCl_3$)

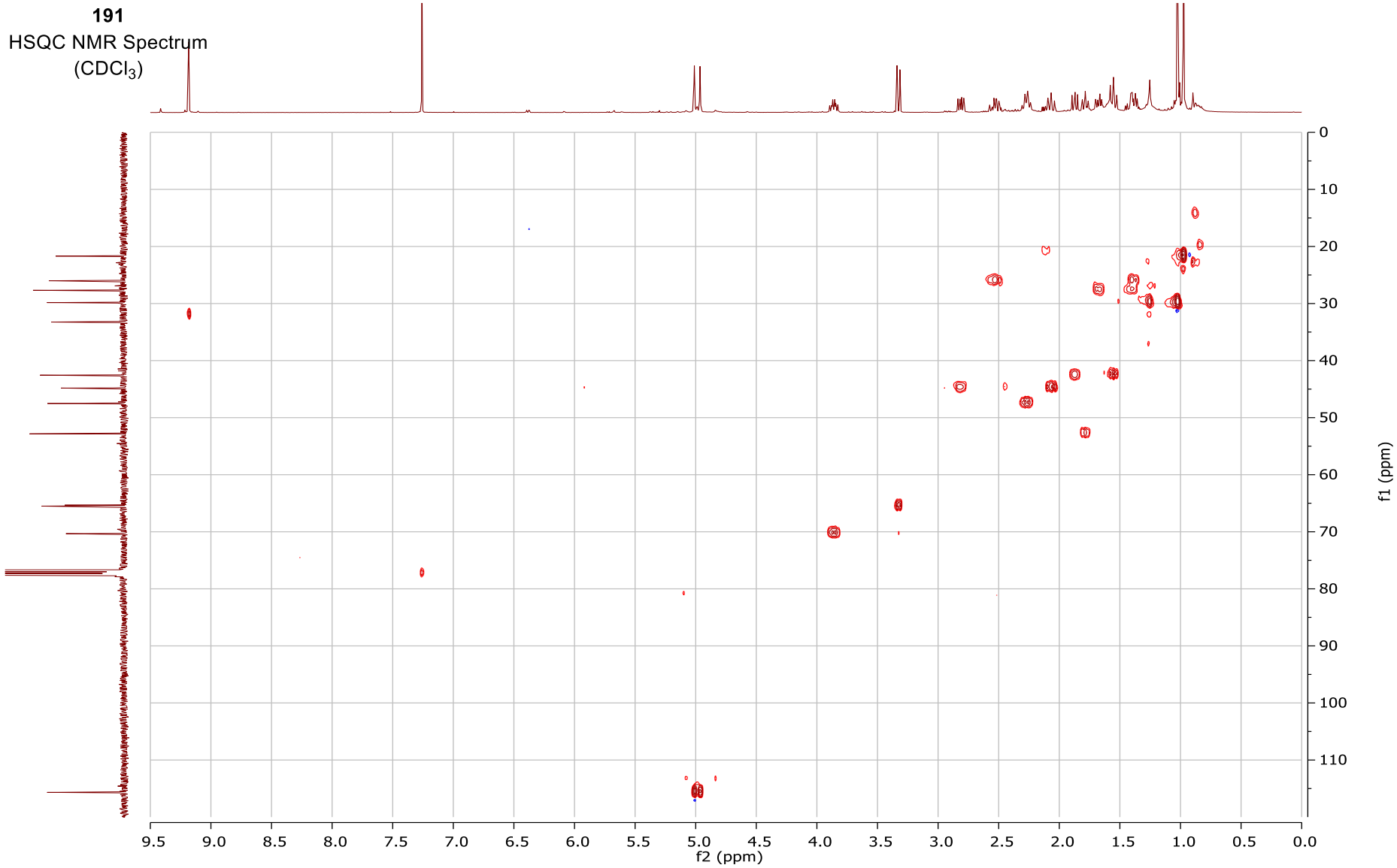

191

HMBC NMR Spectrum

($CDCl_3$)

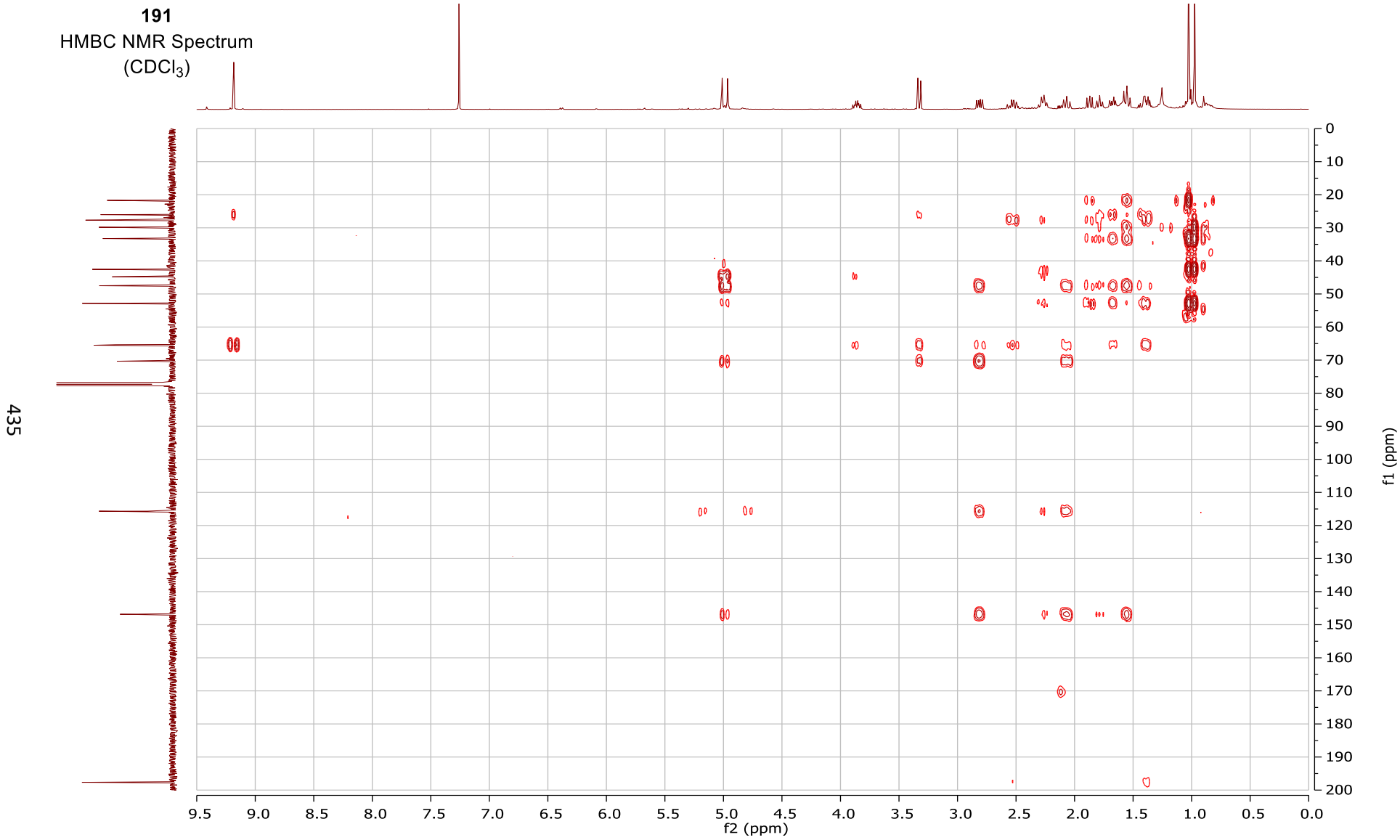

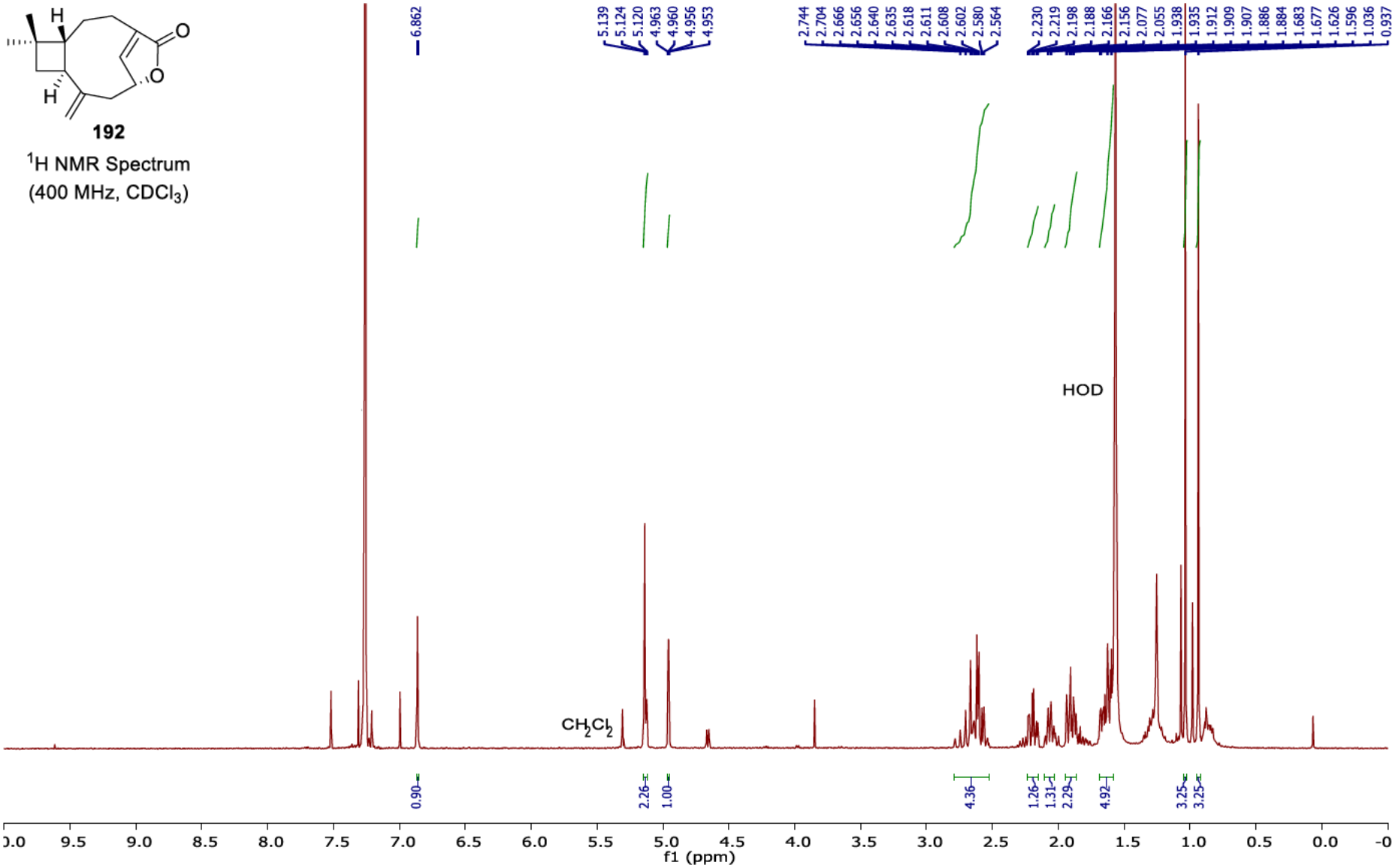
H
O
O
H
192
1H NMR Spectrum
(400 MHz, CDCl3)
6.862
5.139
5.124
5.120
4.963
4.960
4.956
4.953
2.744
2.704
2.666
2.656
2.640
2.635
2.618
2.611
2.608
2.602
2.580
2.564
2.230
2.219
2.198
2.188
2.166
2.156
2.077
2.055
1.938
1.935
1.912
1.909
1.907
1.886
1.884
1.683
1.677
1.626
1.596
1.036
0.937
HOD
CH2Cl2
0.90
2.26
1.00
4.36
1.26
1.31
2.29
4.92
3.25
3.25
f1 (ppm)

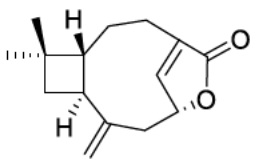

192

^{13}C NMR Spectrum
(101 MHz, $CDCl_3$)

171.233
154.052
138.866
125.706
108.618
75.469
71.035
61.802
45.877
41.054
38.304
36.324
35.479
30.038
24.020
22.353
21.047

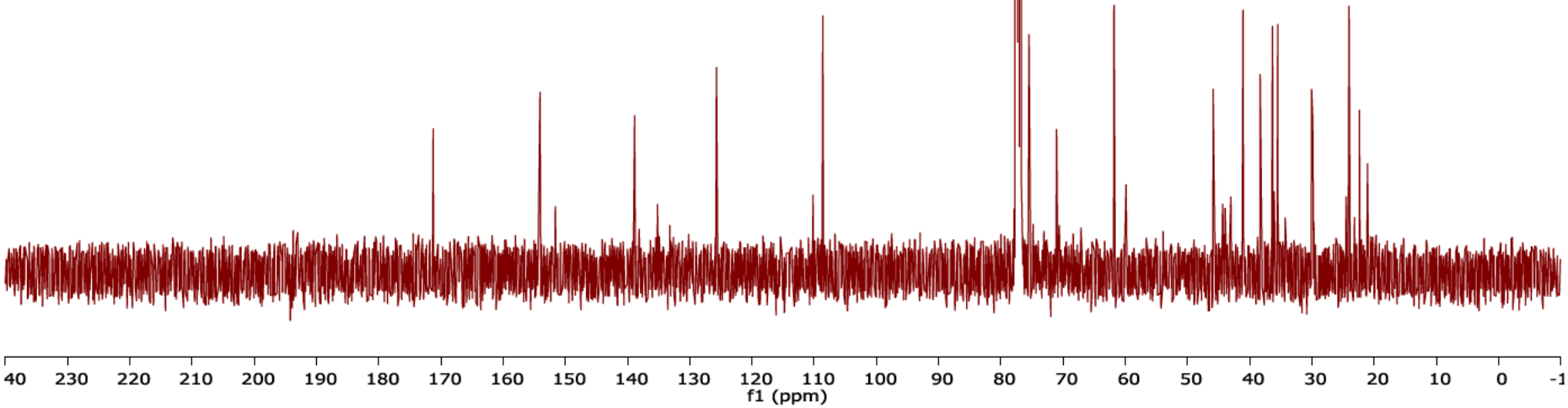

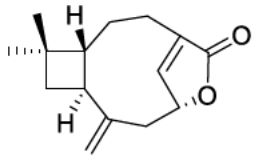

192

DEPT135 NMR Spectrum
(101 MHz, $CDCl_3$)

192

COSY NMR Spectrum

($CDCl_3$)

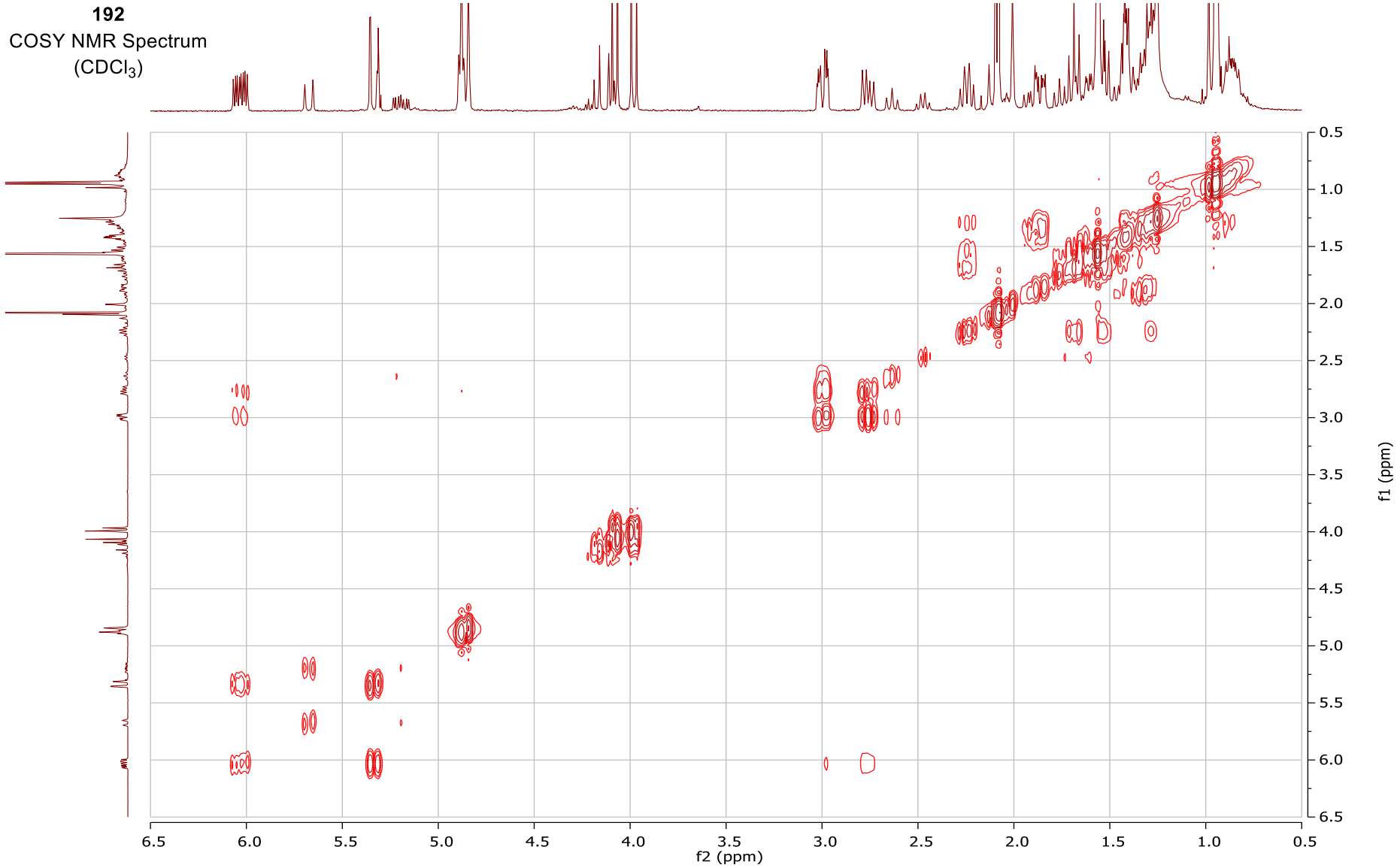

192

HSQC NMR Spectrum

($CDCl_3$)

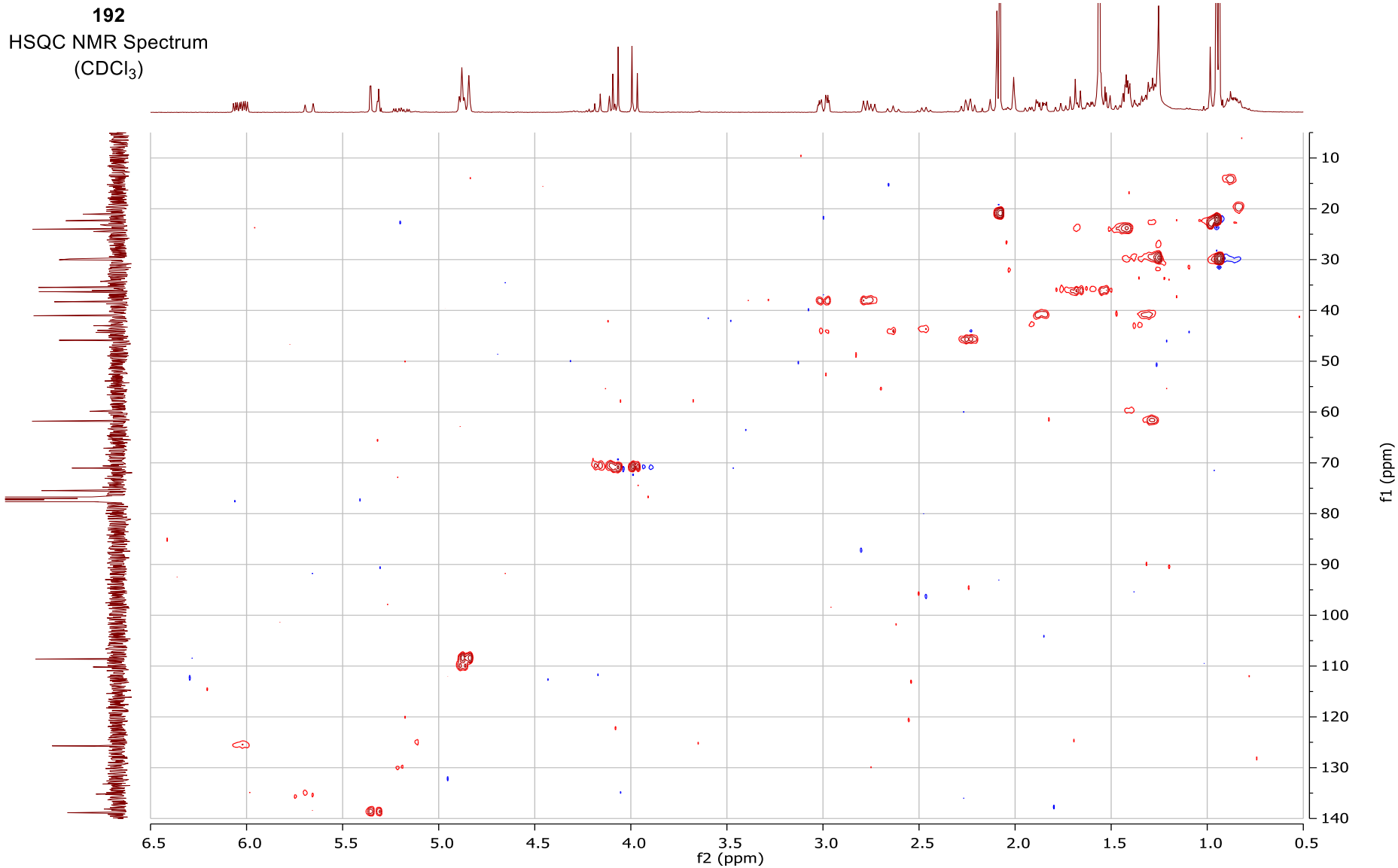

192

HMBC NMR Spectrum

($CDCl_3$)

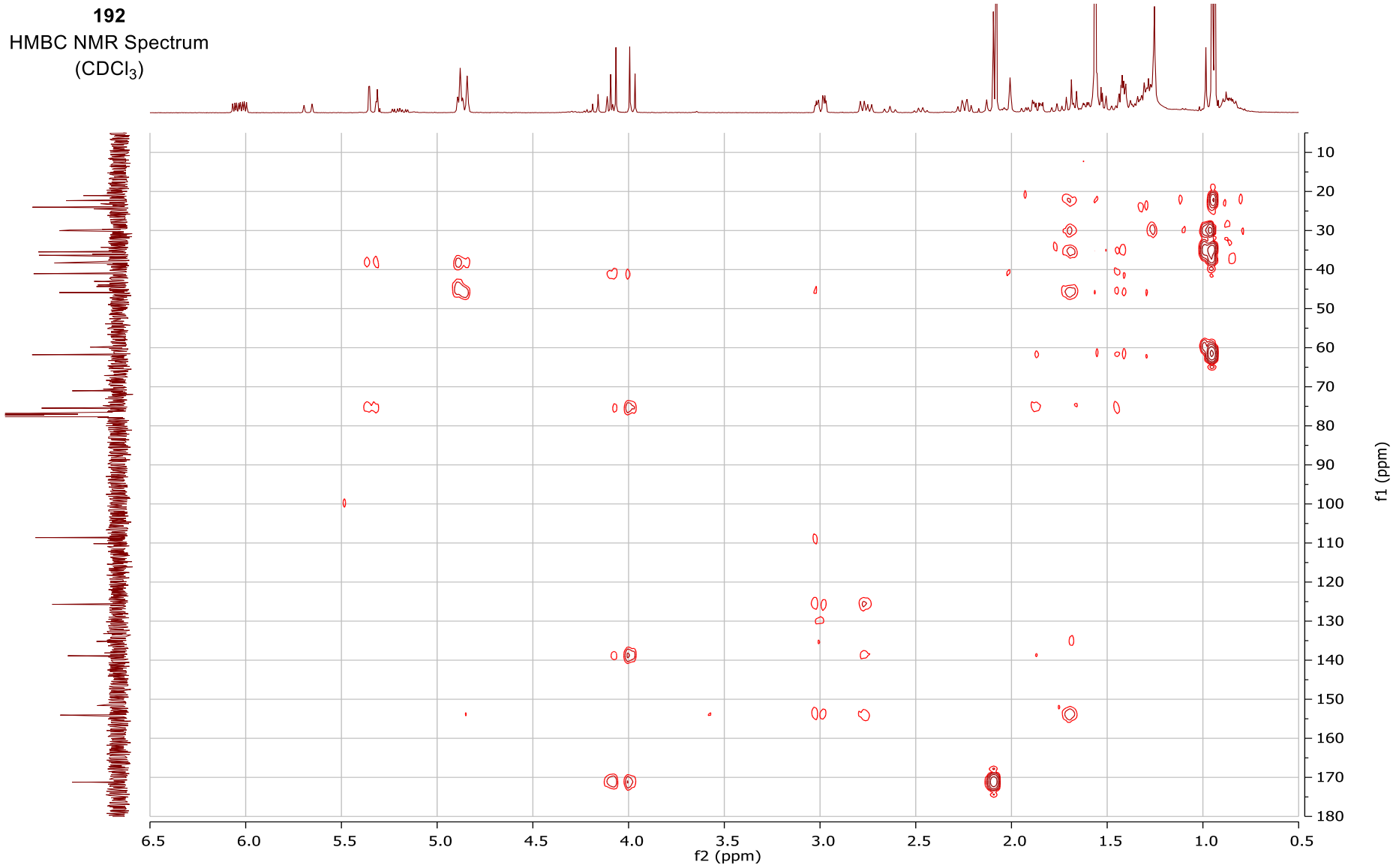

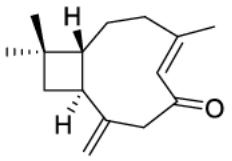

195

^{1}H NMR Spectrum
(400 MHz, $CDCl_3$)

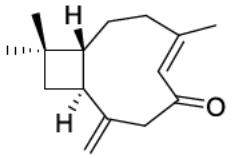

195

^{13}C NMR Spectrum
(101 MHz, $CDCl_3$)

202.793
144.732
128.893
114.531
56.817
42.903
32.769
30.078
28.973
23.462

40 230 220 210 200 190 180 170 160 150 140 130 120 110 100 90 80 70 60 50 40 30 20 10 0 -1
f1 (ppm)

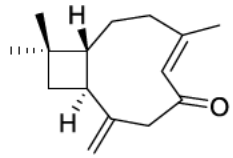

195

^{13}C NMR Spectrum
(101 MHz, $CDCl_3$)
*apodization = 20 Hz

202.791
144.743
128.897
114.544
56.822
53.426
43.947
42.906
39.272
32.766
30.074
28.962
23.462
18.512

444

240 230 220 210 200 190 180 170 160 150 140 130 120 110 100 90 80 70 60 50 40 30 20 10 0 -1
f1 (ppm)

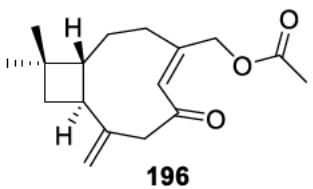

196

^{1}H NMR Spectrum
(400 MHz, $CDCl_3$)

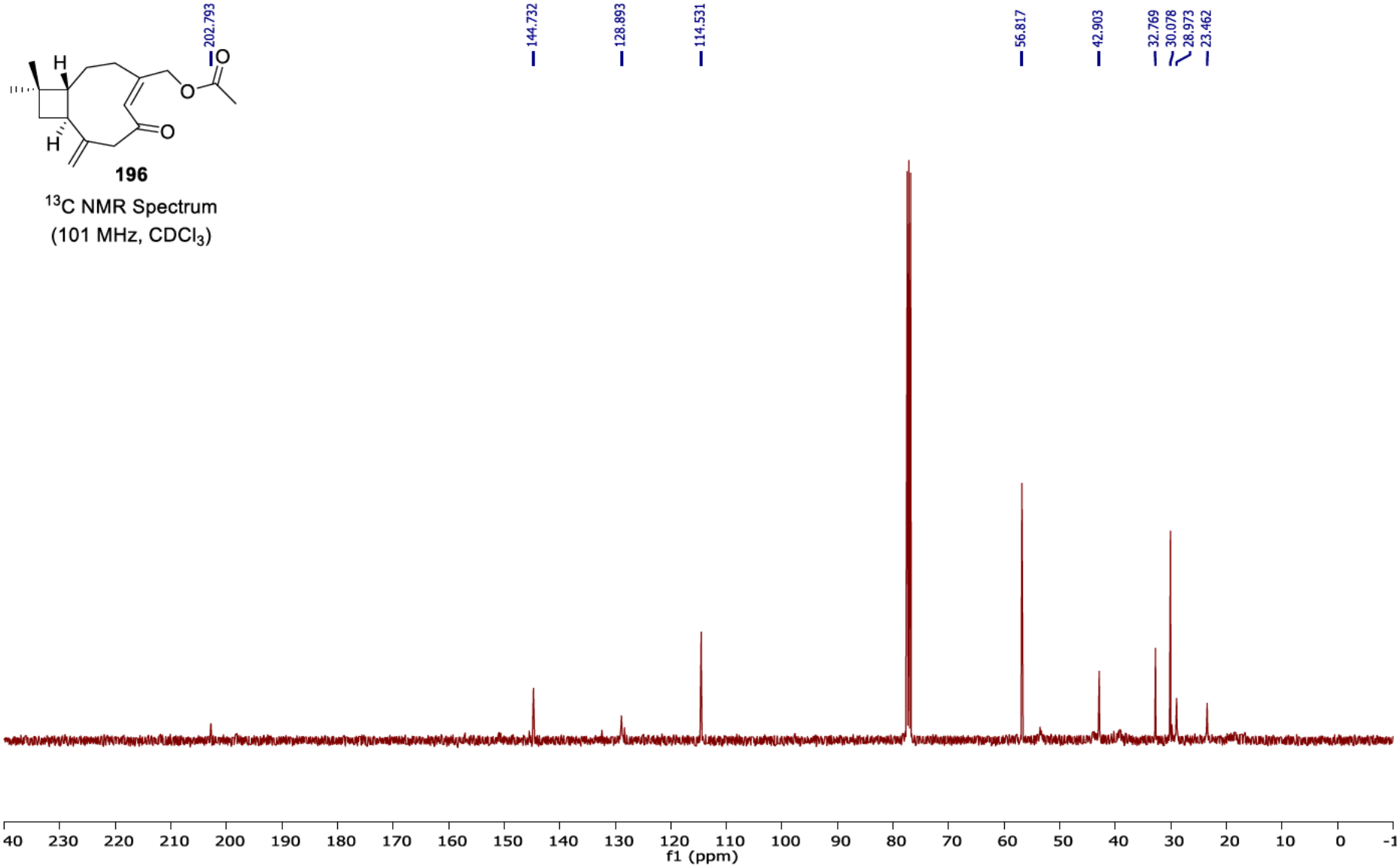
202.793
144.732
128.893
114.531
56.817
42.903
32.769
30.078
28.973
23.462
O
O
O
H
H
196
^{13}C NMR Spectrum
(101 MHz, $CDCl_3$)
446
40 230 220 210 200 190 180 170 160 150 140 130 120 110 100 90 80 70 60 50 40 30 20 10 0 -1
f1 (ppm)

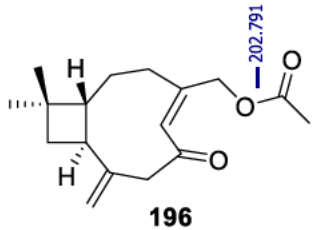

196

^{13}C NMR Spectrum
(101 MHz, $CDCl_3$)
*apodization = 20 Hz

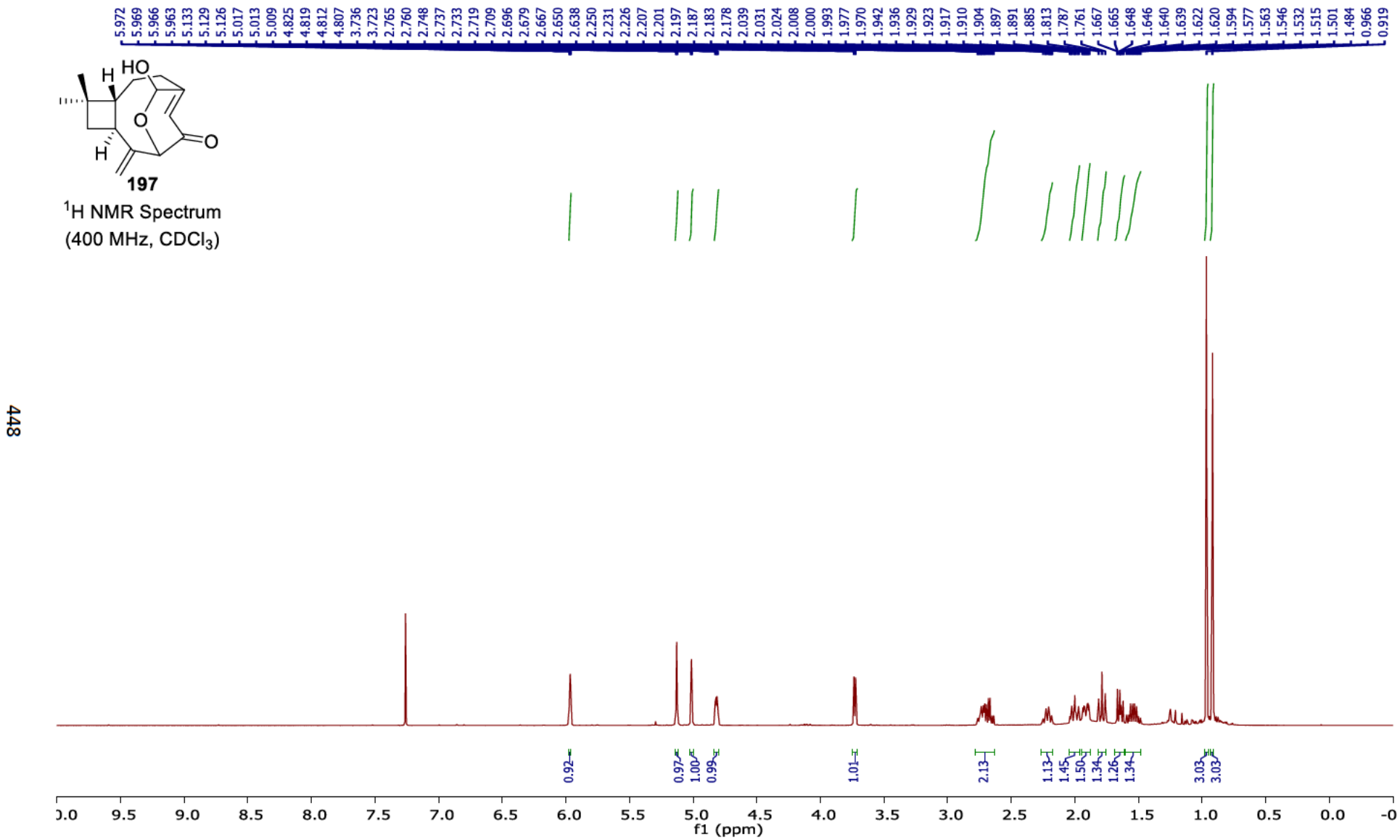
5.972 5.969 5.966 5.963 5.133 5.129 5.126 5.017 5.013 5.009 4.825 4.819 4.812 4.807 3.736 3.723 2.765 2.760 2.748 2.737 2.733 2.719 2.709 2.696 2.679 2.667 2.650 2.638 2.250 2.231 2.226 2.207 2.201 2.197 2.187 2.183 2.178 2.039 2.031 2.024 2.008 2.000 1.993 1.977 1.970 1.942 1.936 1.929 1.923 1.917 1.910 1.904 1.897 1.891 1.885 1.813 1.787 1.761 1.667 1.665 1.648 1.646 1.640 1.639 1.622 1.620 1.594 1.577 1.563 1.546 1.532 1.515 1.501 1.484 0.966 0.919
HO
H
O
O
H
197
^{1}H NMR Spectrum
(400 MHz, $CDCl_3$)
448
0.92 0.97 1.00 0.99 1.01 2.13 1.13 1.45 1.50 1.34 1.26 1.34 3.03 3.03
9.5 9.0 8.5 8.0 7.5 7.0 6.5 6.0 5.5 5.0 4.5 4.0 3.5 3.0 2.5 2.0 1.5 1.0 0.5 0.0
f1 (ppm)

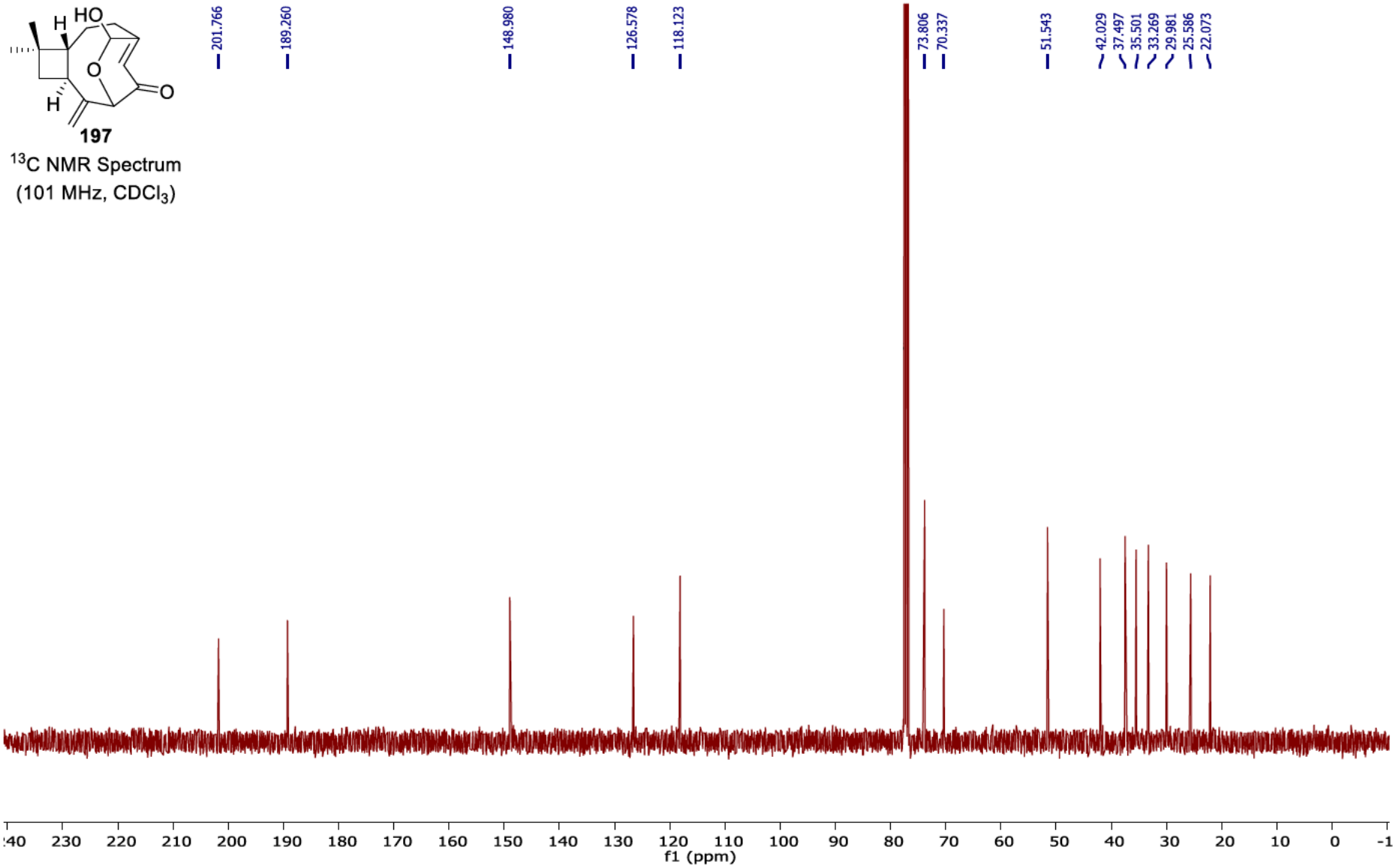
HO
H
O
O
H
197
13C NMR Spectrum
(101 MHz, CDCl3)
201.766
189.260
148.980
126.578
118.123
73.806
70.337
51.543
42.029
37.497
35.501
33.269
29.981
25.586
22.073
f1 (ppm)

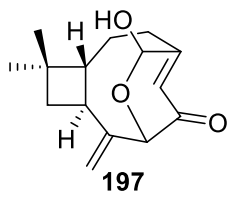

197

DEPT135 NMR Spectrum
(101 MHz, $CDCl_3$)

197

COSY NMR Spectrum

($CDCl_3$)

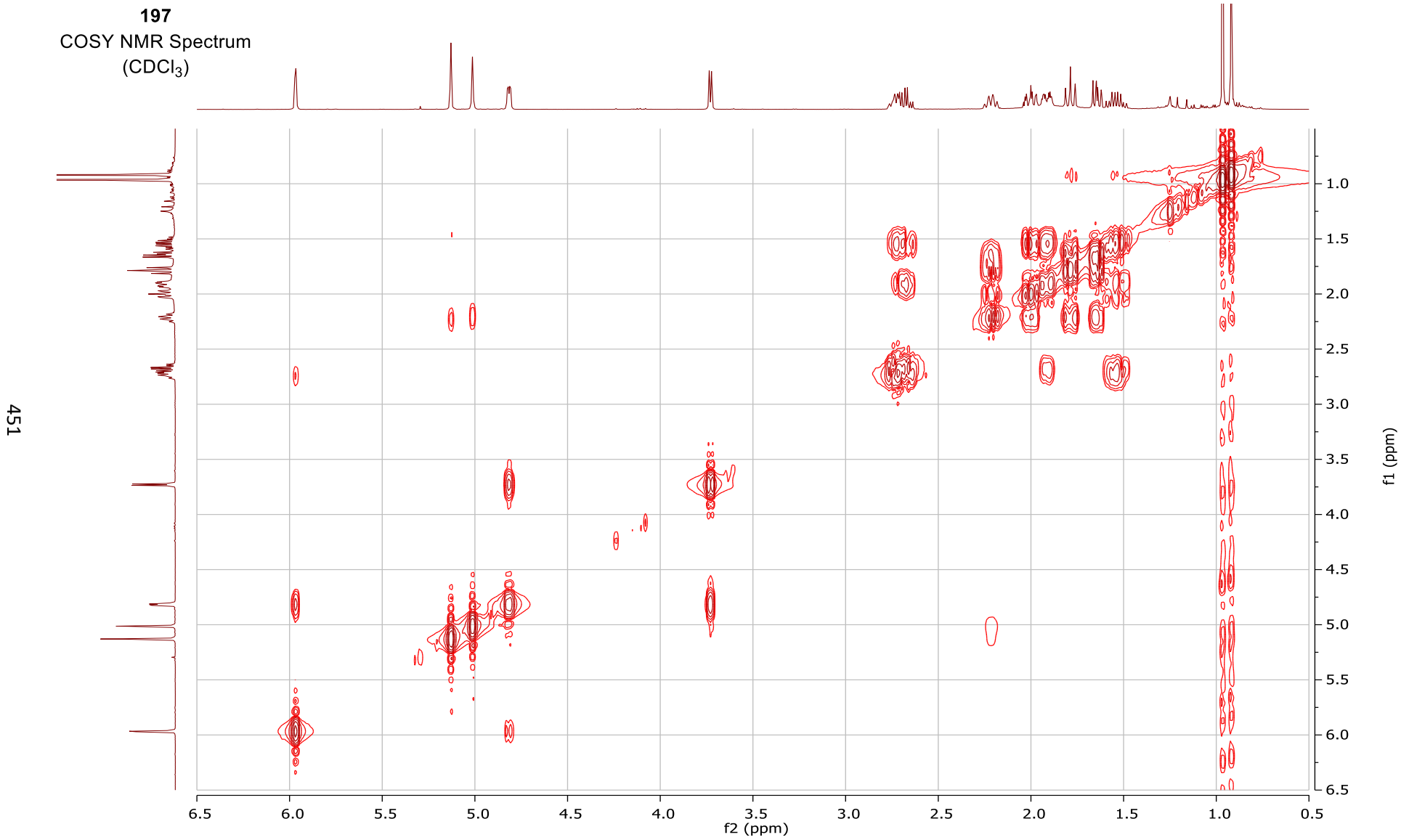

451

197

HSQC NMR Spectrum

($CDCl_3$)

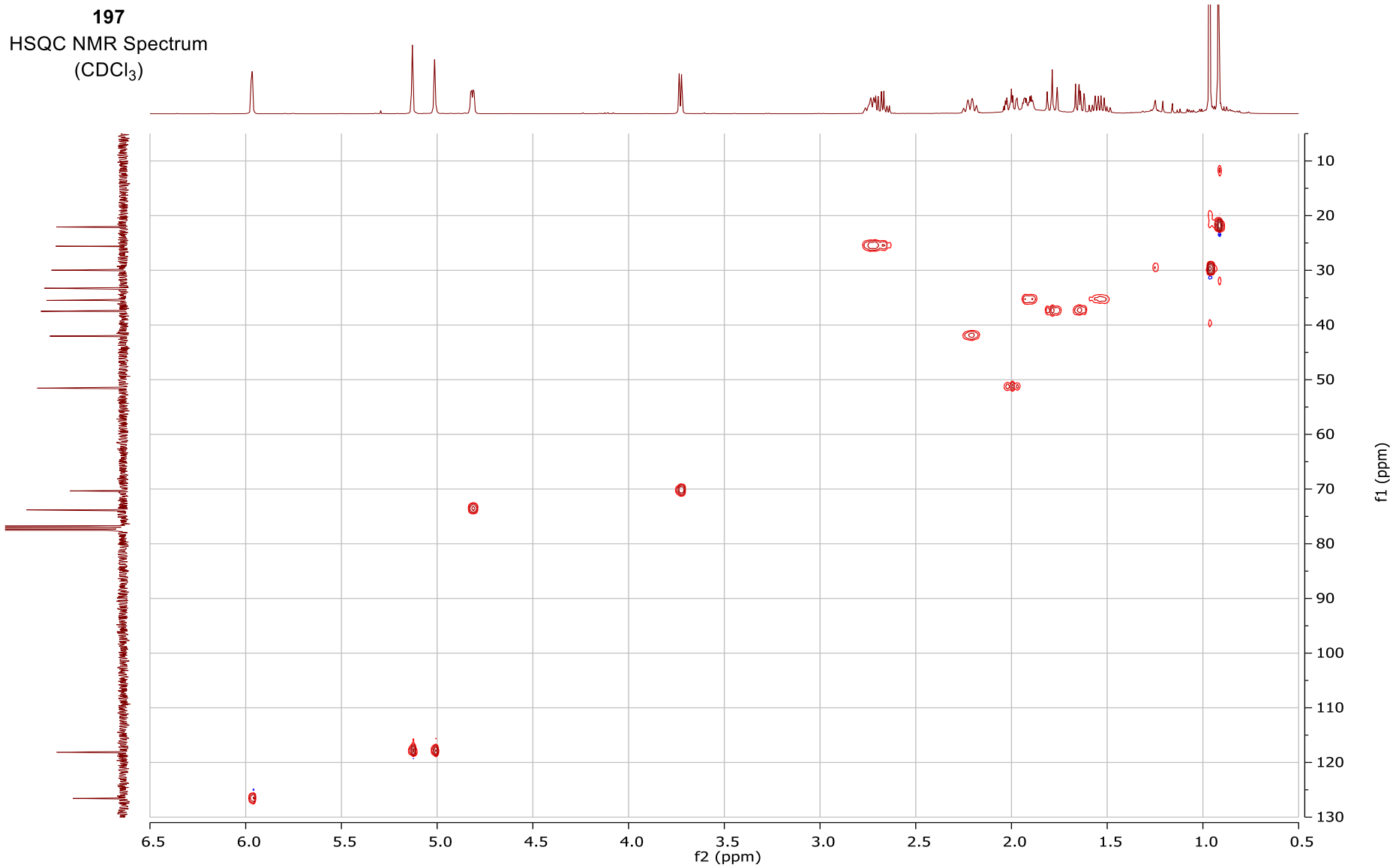

197

HMBC NMR Spectrum

($CDCl_3$)

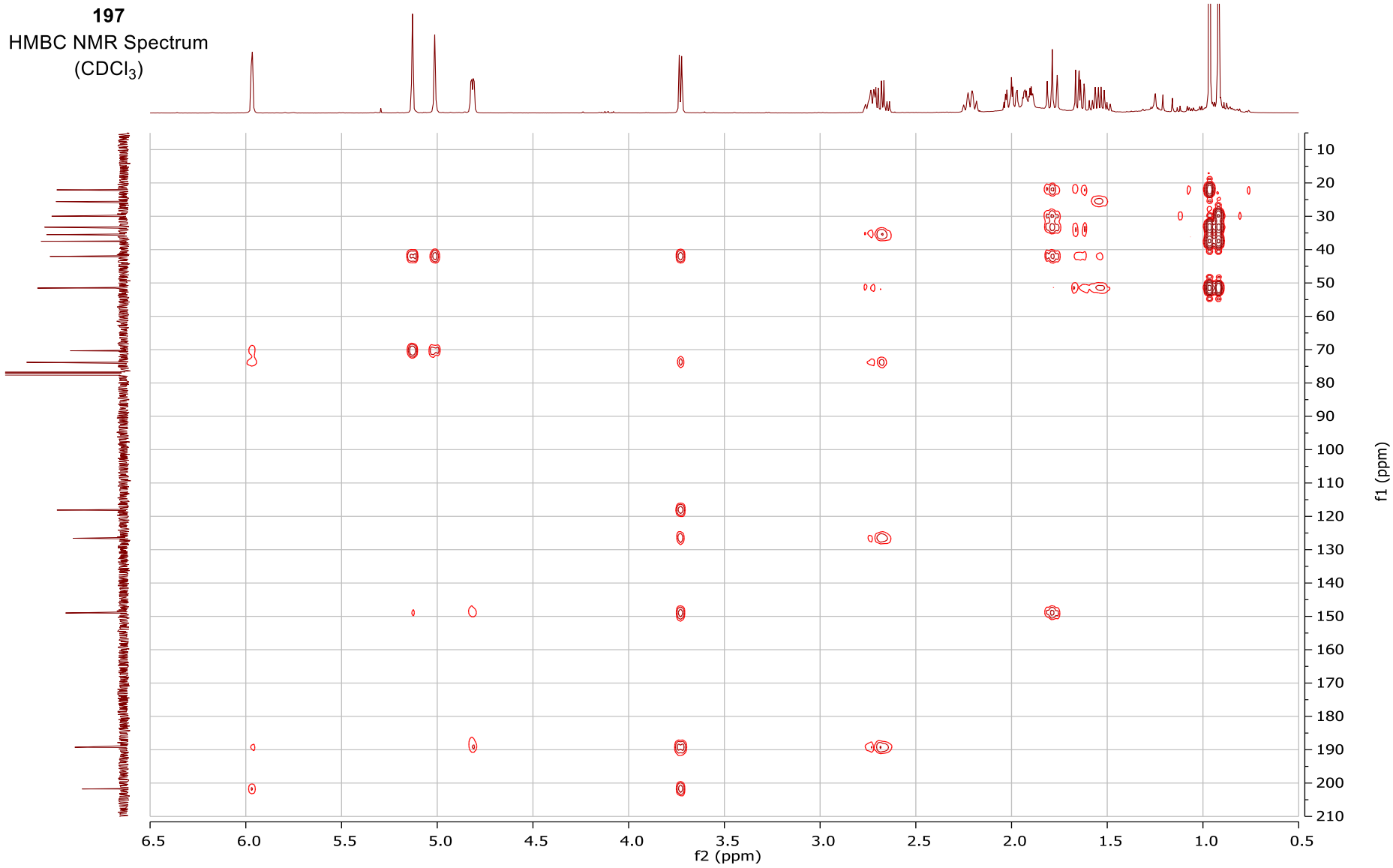

453

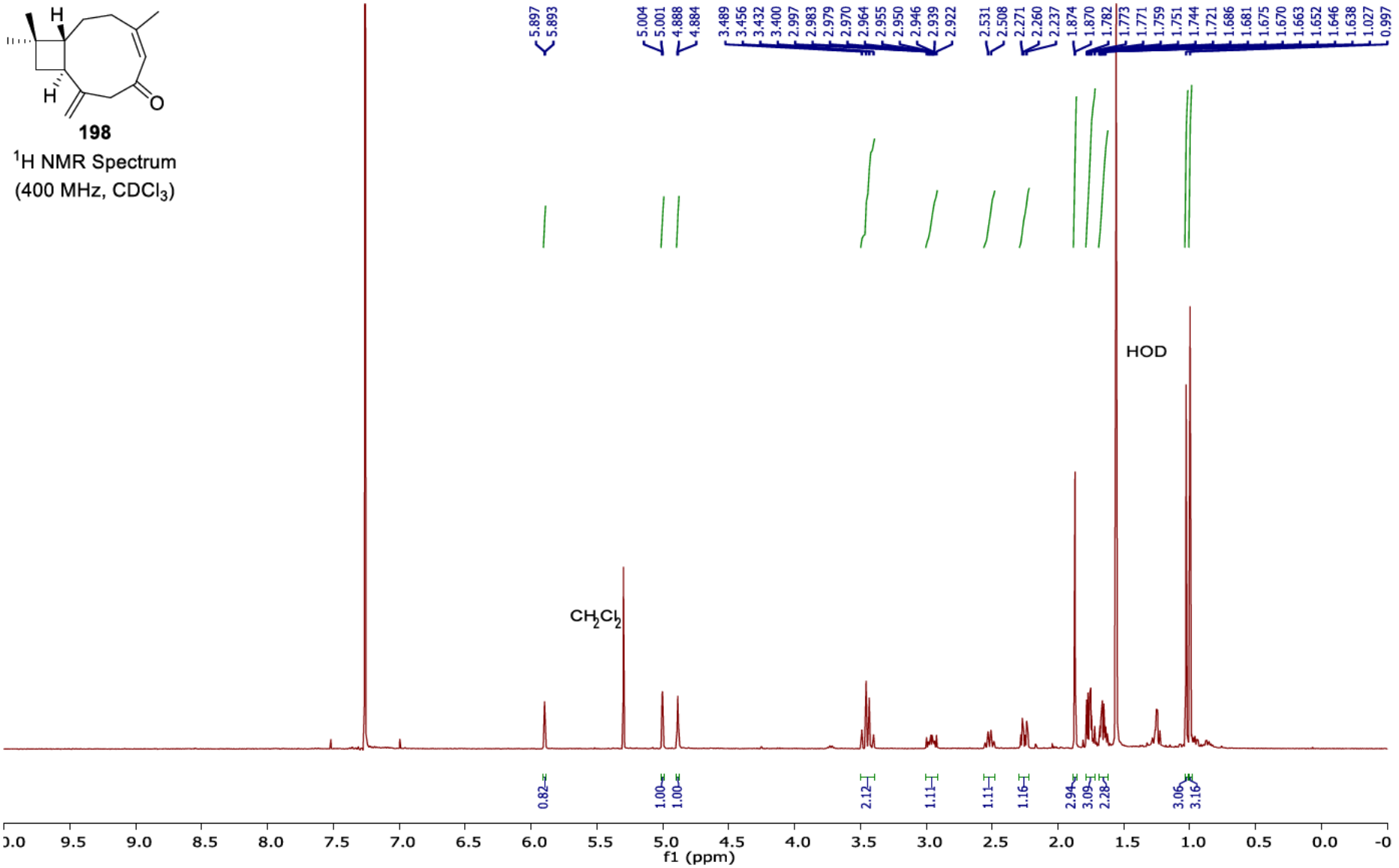
198
^{1}H NMR Spectrum
(400 MHz, $CDCl_3$)
5.897
5.893
5.004
5.001
4.888
4.884
3.489
3.456
3.432
3.400
2.997
2.983
2.979
2.970
2.964
2.955
2.950
2.946
2.939
2.922
2.531
2.508
2.271
2.260
2.237
1.874
1.870
1.782
1.773
1.771
1.759
1.751
1.744
1.721
1.686
1.681
1.675
1.670
1.663
1.652
1.646
1.638
1.027
0.997
HOD
CH_2Cl_2
0.82
1.00
1.00
2.12
1.11
1.11
1.16
2.94
3.09
2.28
3.06
3.16
f1 (ppm)

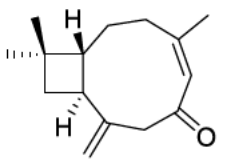

198

^{13}C NMR Spectrum

(101 MHz, $CDCl_3$)

200.050
152.816
146.026
129.920
113.356
51.315
50.434
42.685
37.025
32.632
31.370
30.455
26.486
25.847
23.537

40 230 220 210 200 190 180 170 160 150 140 130 120 110 100 90 80 70 60 50 40 30 20 10 0 -1

f1 (ppm)

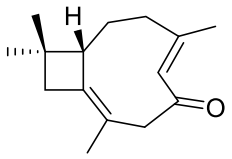

200

^{1}H NMR Spectrum

(400 MHz, $CDCl_3$)

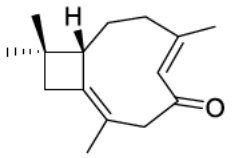

200

^{13}C NMR Spectrum

(101 MHz, $CDCl_3$)

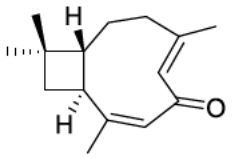

201

^{1}H NMR Spectrum
(400 MHz, $CDCl_3$)

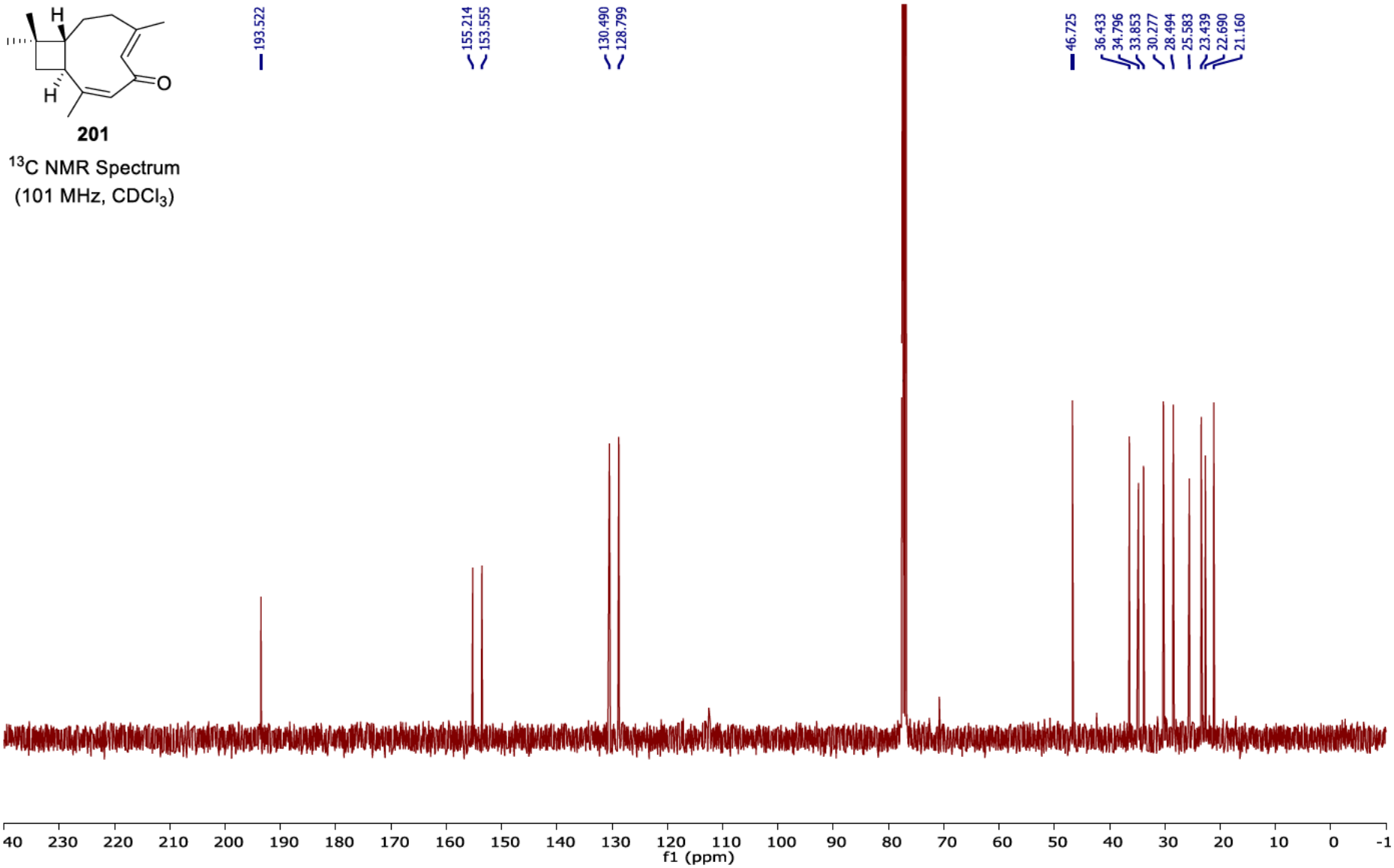

^{13}C NMR Spectrum
(101 MHz, $CDCl_3$)

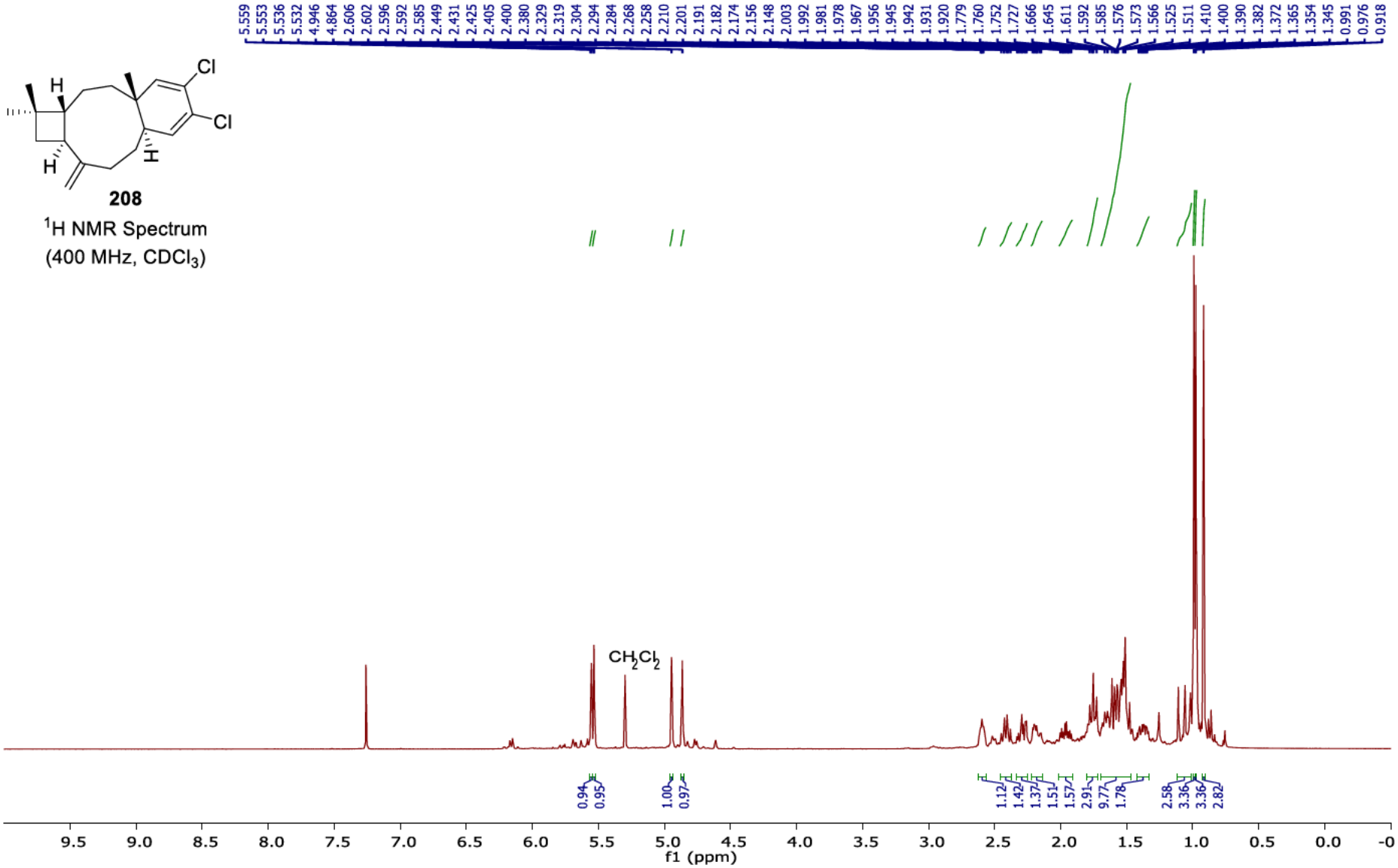
Cl
Cl
H
H
H
208
1H NMR Spectrum
(400 MHz, CDCl3)
460
CH2Cl2
f1 (ppm)

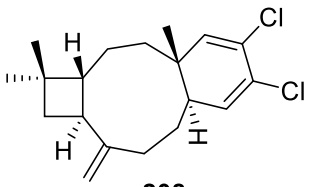

208

^{13}C NMR Spectrum

(101 MHz, $CDCl_3$)

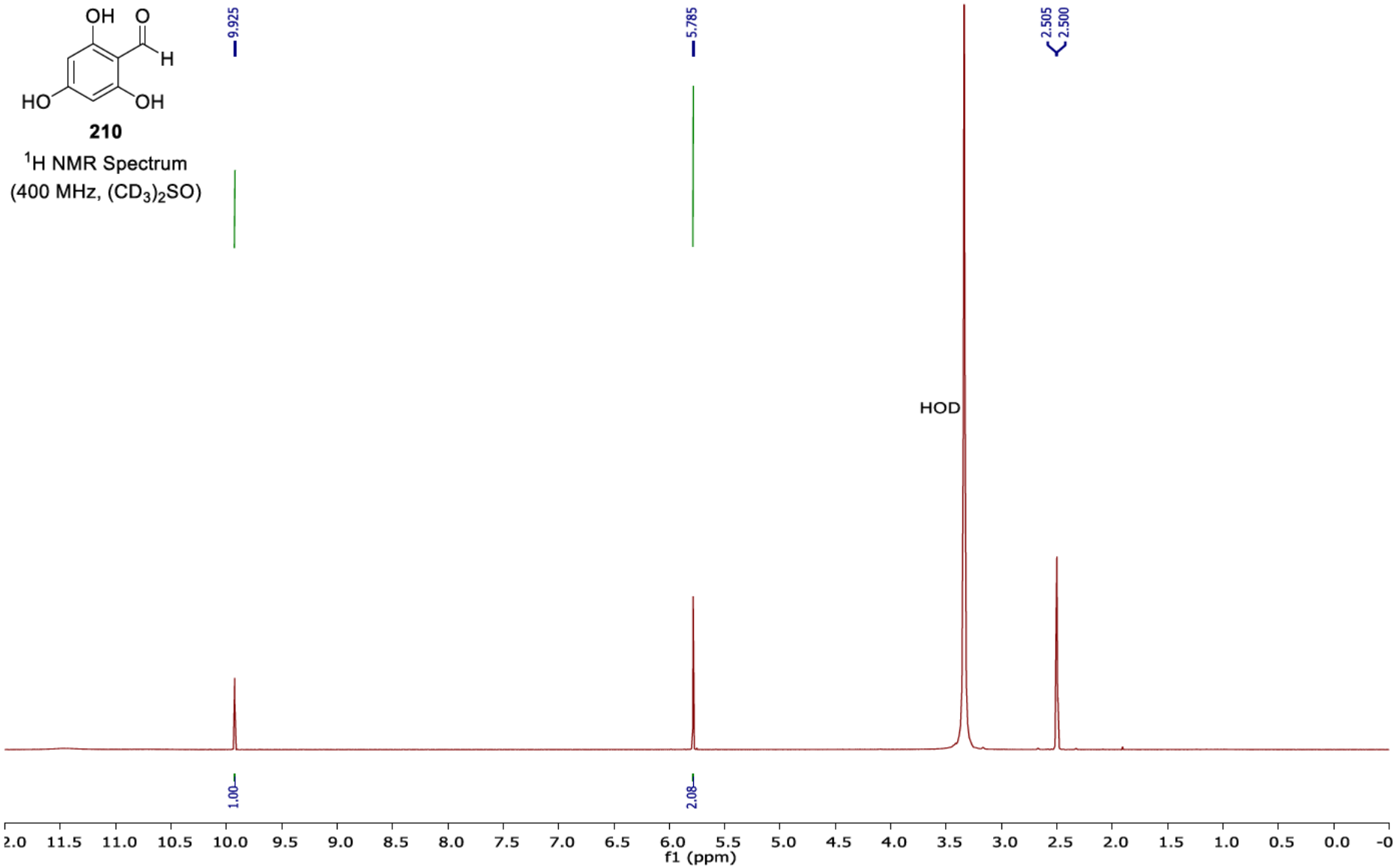
OH
O
H
HO
OH
210
1H NMR Spectrum
(400 MHz, (CD3)2SO)
9.925
5.785
2.505
2.500
HOD
1.00
2.08
f1 (ppm)

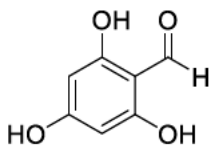

210

^{13}C NMR Spectrum

(101 MHz, $(CD_3)_2SO$)

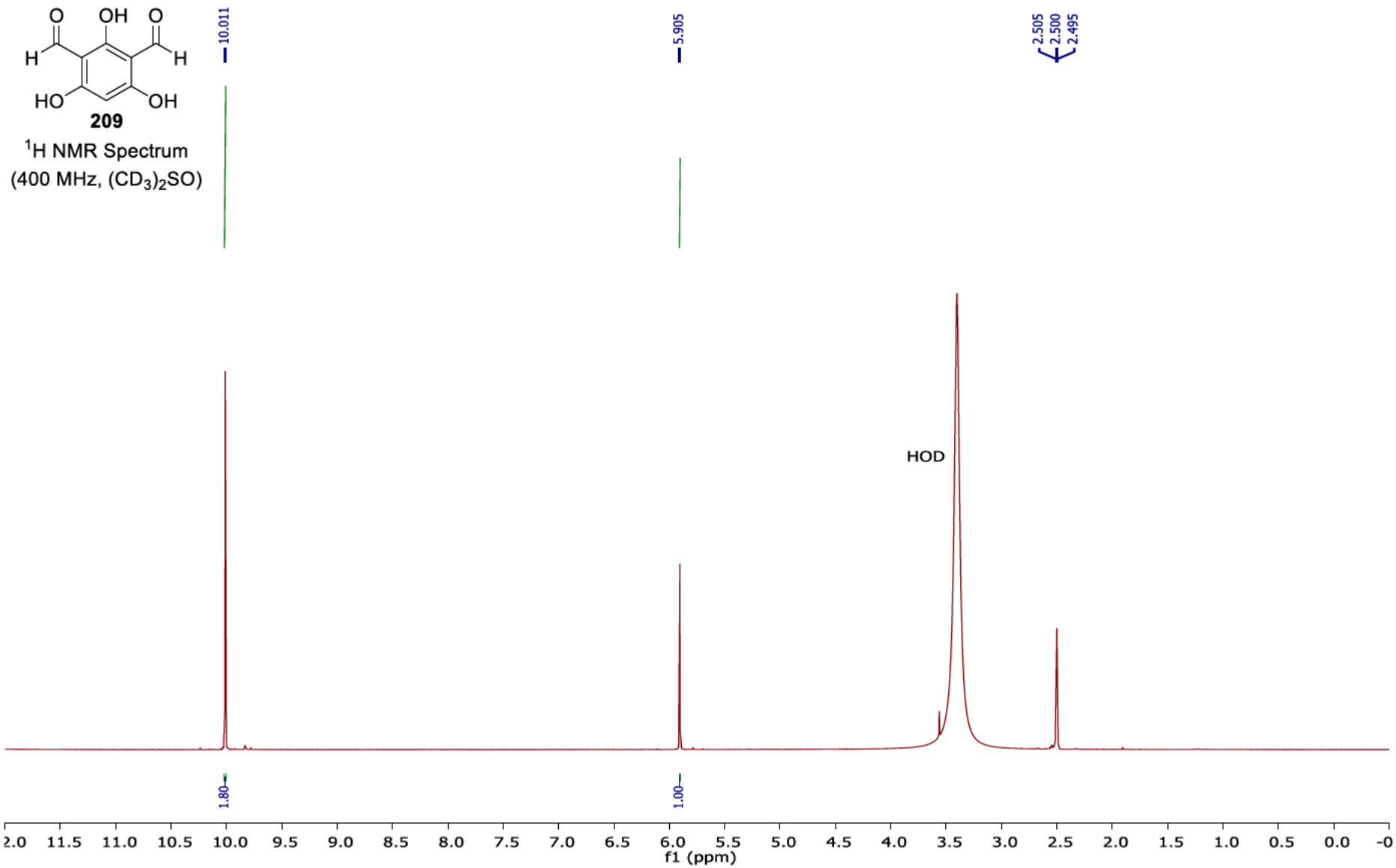
O
OH
O
H
H
HO
OH
209
^{1}H NMR Spectrum
(400 MHz, $(CD_3)_2SO$)
10.011
5.905
2.505
2.500
2.495
HOD
1.80
1.00
f1 (ppm)

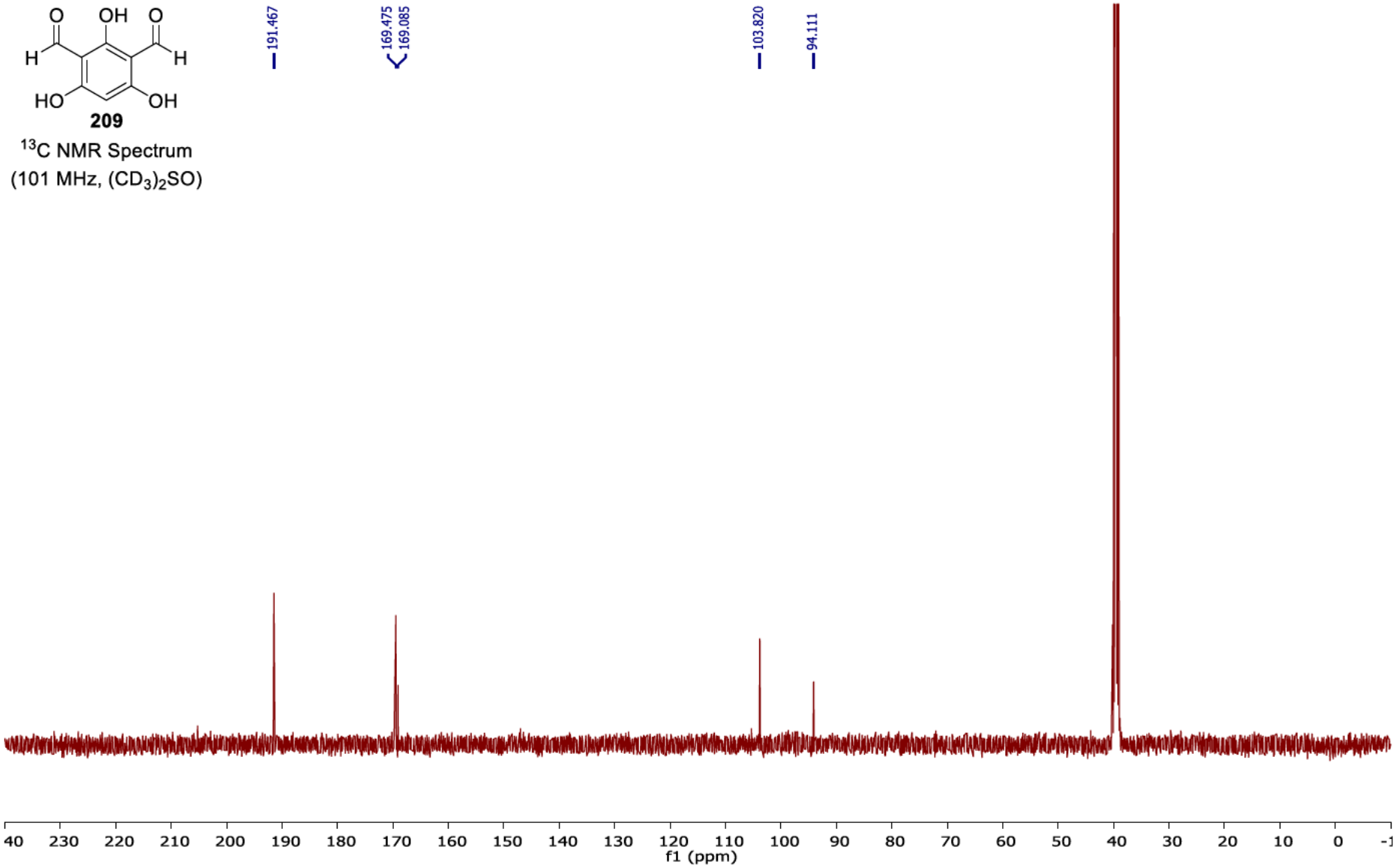
O
OH
O
H
H
HO
OH
209
191.467
169.475
169.085
103.820
94.111
^{13}C NMR Spectrum
(101 MHz, $(CD_3)_2SO$)
465
40 230 220 210 200 190 180 170 160 150 140 130 120 110 100 90 80 70 60 50 40 30 20 10 0 -1
f1 (ppm)

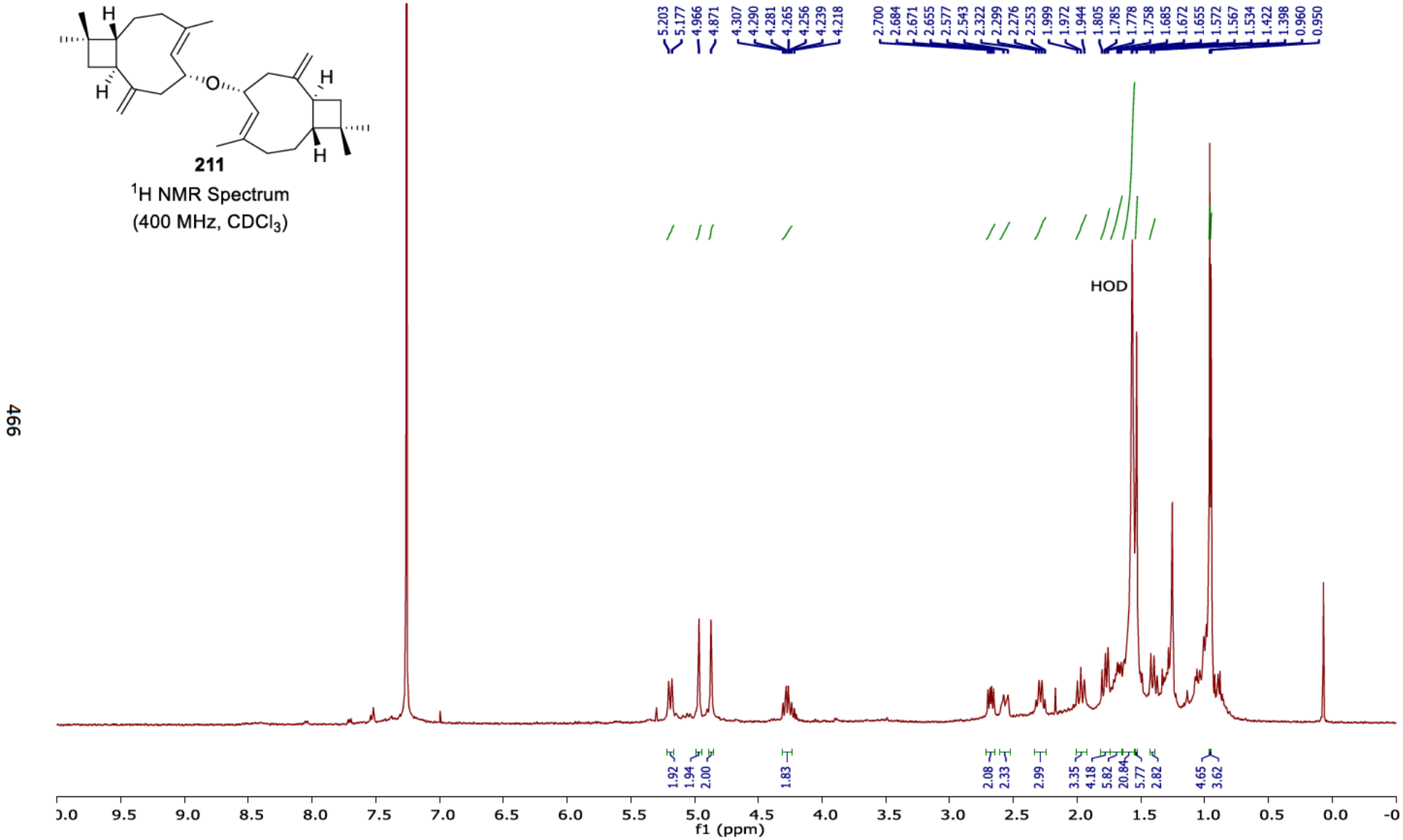
211
^{1}H NMR Spectrum
(400 MHz, $CDCl_3$)
HOD
f1 (ppm)

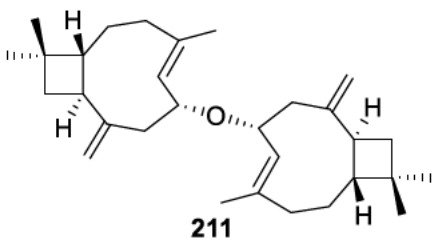

211

^{13}C NMR Spectrum
(101 MHz, $CDCl_3$)

150.836
138.291
127.719
112.218
74.974
55.931
48.926
46.958
42.497
35.105
32.860
31.129
29.955
22.736
22.007

467

40 230 220 210 200 190 180 170 160 150 140 130 120 110 100 90 80 70 60 50 40 30 20 10 0 -1
f1 (ppm)

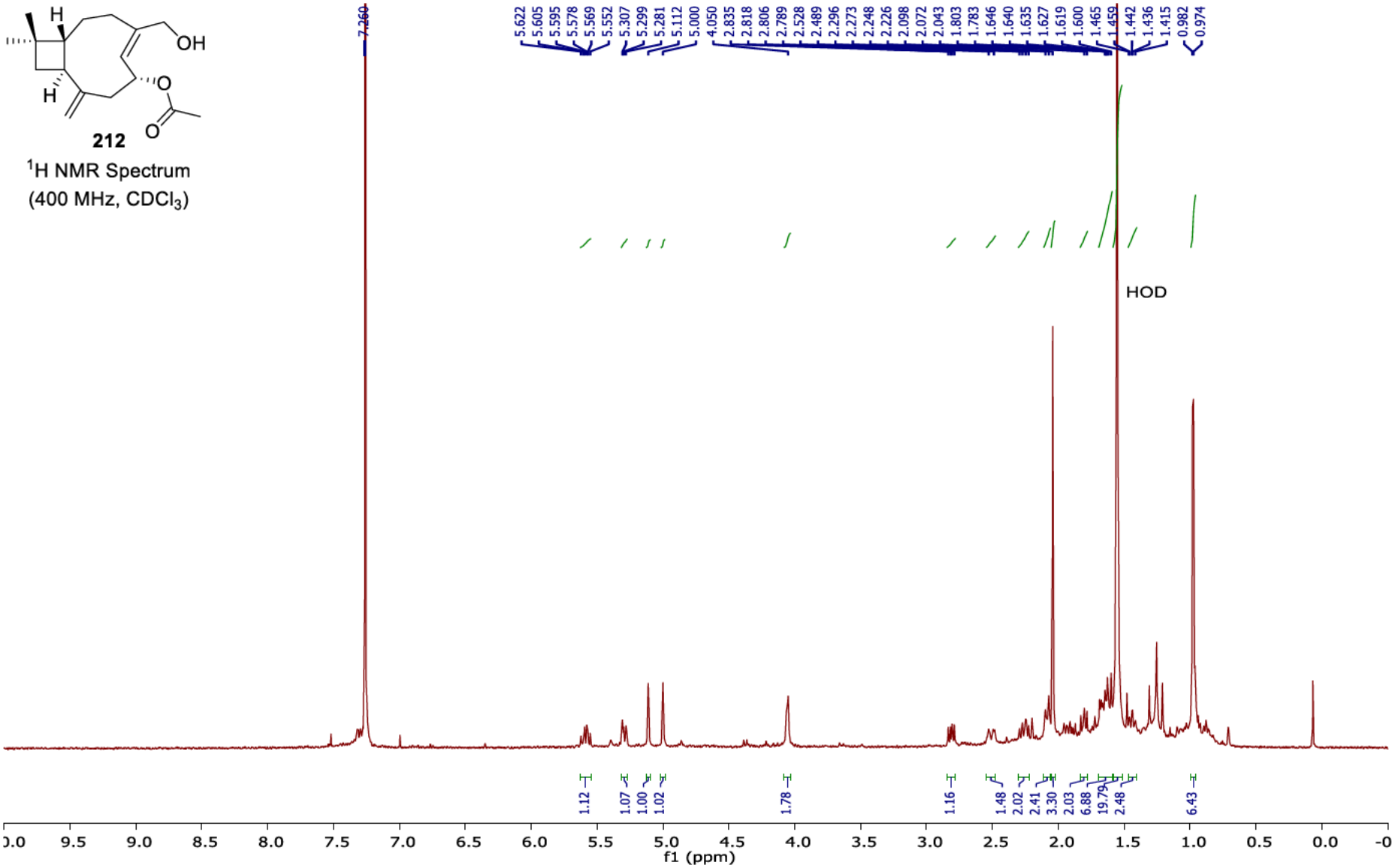
H
OH
H
O
O
212
1H NMR Spectrum
(400 MHz, CDCl3)
HOD
f1 (ppm)

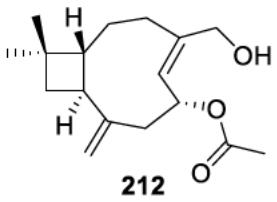

212

^{13}C NMR Spectrum
(101 MHz, $CDCl_3$)

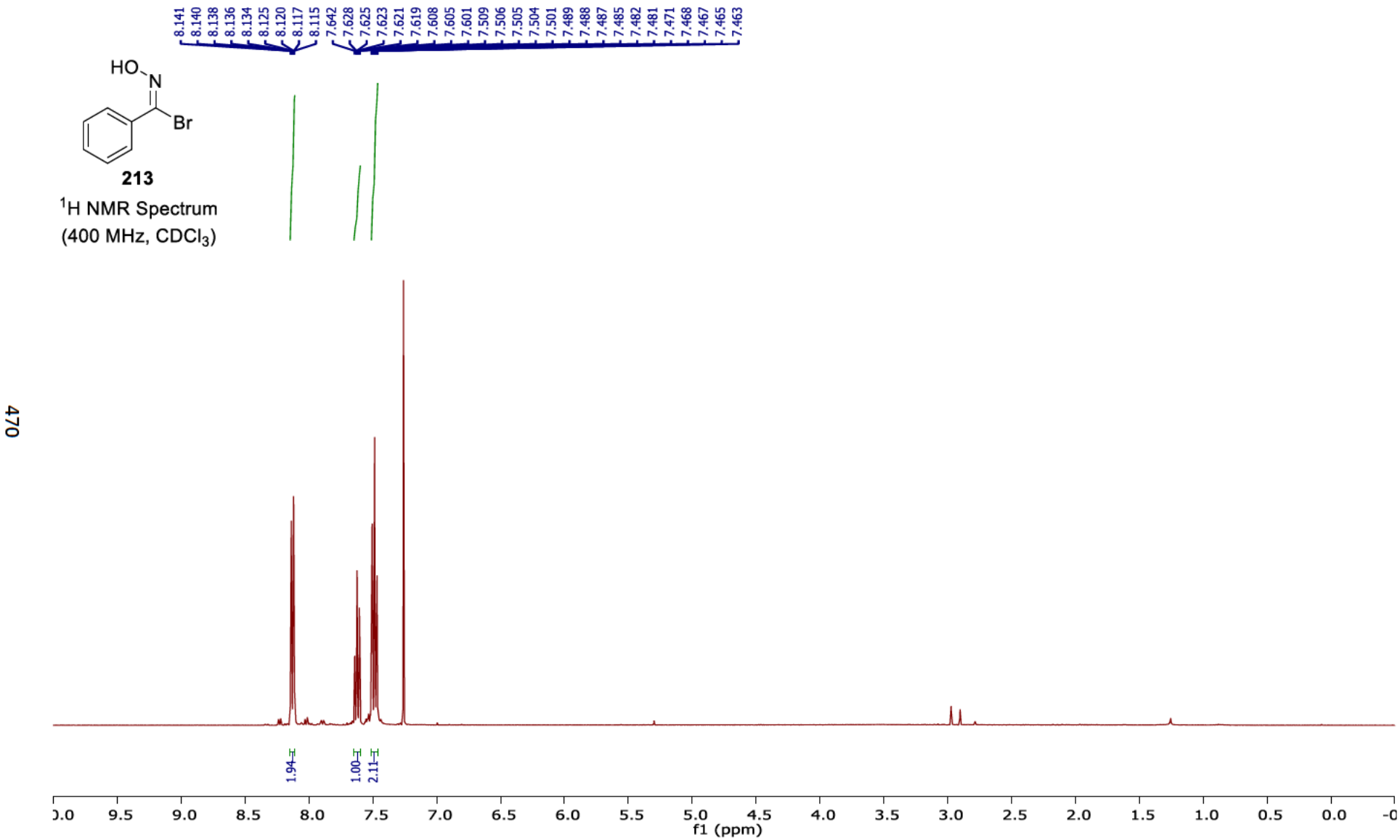
8.141
8.140
8.138
8.136
8.134
8.125
8.120
8.117
8.115
7.642
7.628
7.625
7.623
7.621
7.619
7.608
7.605
7.601
7.509
7.506
7.505
7.504
7.501
7.489
7.488
7.487
7.485
7.482
7.481
7.471
7.468
7.467
7.465
7.463
HO
N
Br
213
1H NMR Spectrum
(400 MHz, CDCl3)
470
1.94
1.00
2.11
9.5
9.0
8.5
8.0
7.5
7.0
6.5
6.0
5.5
5.0
4.5
4.0
3.5
3.0
2.5
2.0
1.5
1.0
0.5
0.0
f1 (ppm)

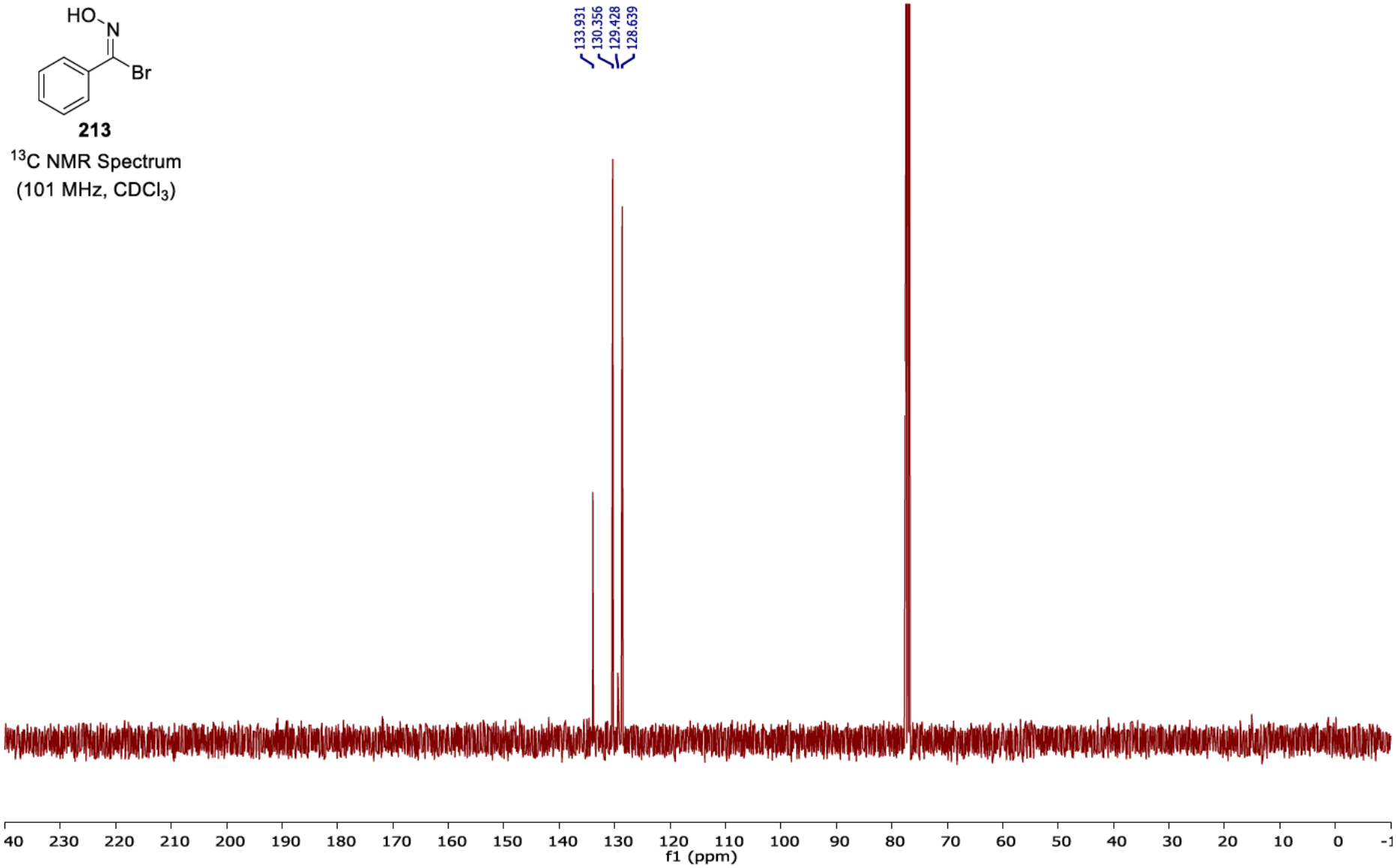
HO
N
Br
213
^{13}C NMR Spectrum
(101 MHz, $CDCl_3$)
133.931
130.356
129.428
128.639
471
40 230 220 210 200 190 180 170 160 150 140 130 120 110 100 90 80 70 60 50 40 30 20 10 0 -1
f1 (ppm)

To whom it may concern

I, **Aswin Rajagopalan**, contributed conceptualization, investigation, methodology, visualization, writing-original draft, writing-review & editing to the following paper:

Aswin Rajagopalan, Mark J. Hackett and Alan D. Payne

In situ *confocal Raman imaging of caryophyllenes on the leaves of* Scaevola crassifolia *and a revised biosynthesis of birkenal.* Draft publication.

Development of three-dimensional Raman imaging methods for mapping of mammalian and plant tissue. Draft publication.

I as a Co-Author, endorse that this level of contribution by the candidate indicated above is appropriate.

Mark J. Hackett **Alan D. Payne**